

PREDICTIVE MODELLING OF MULTI-PERIOD GEOARCHAEOLOGICAL RESOURCES AT A RIVER CONFLUENCE

Phase II Report (PNUM 3357)

A. G. Brown¹, C. Carey¹, K. Challis², A. Howard³, M. Kinsey², E. Tetlow⁵ & L. Cooper⁴

¹ School of Geography, Archaeology & Earth Resources, Amory Building, Rennes Drive,
University of Exeter EX4 4RJ

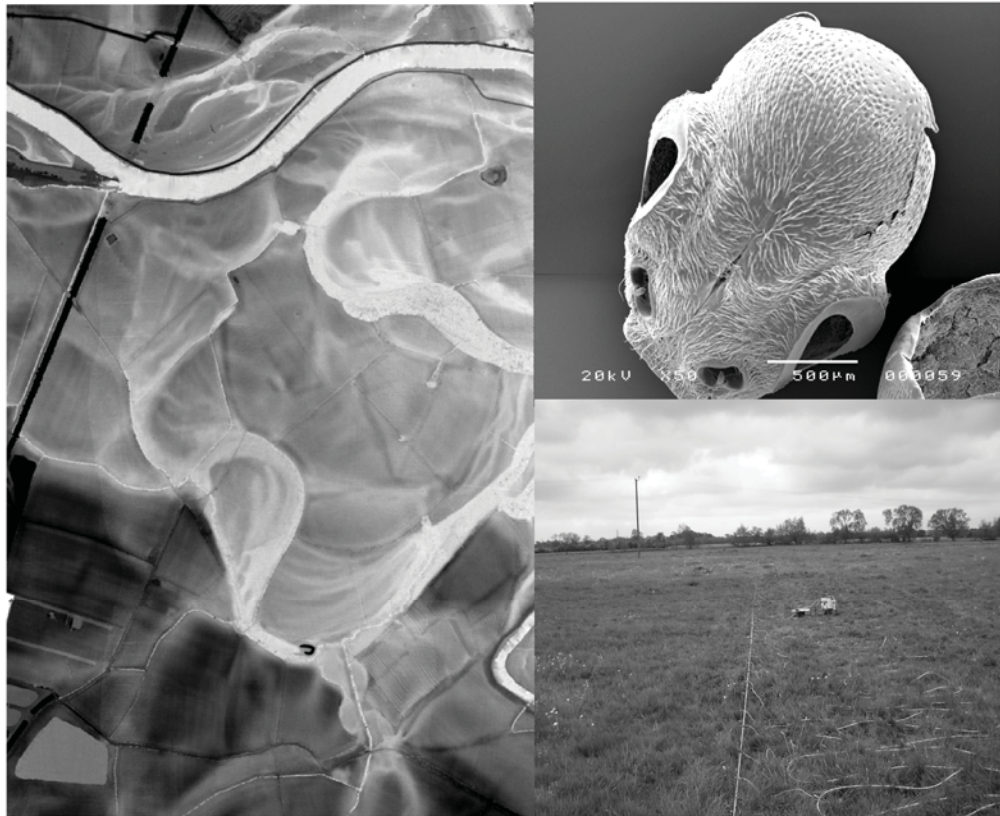
² Institute of Antiquity and Archaeology, University of Birmingham

³ Birmingham Archaeology & HP Visual & Spatial Technology Centre

⁴ University of Leicester Archaeological Services (ULAS)

⁵ Birmingham Archaeology Environmental, University of Birmingham

With contributions from P. Toms (University of Gloucester) and D. Hamilton (English Heritage)



February 2007

I Executive summary

This report of Phase II of Predictive Modelling of Multi-period Geoarchaeological Resources at a River Confluence” follows a Phase I report (Brown *et al.* 2005). Phase I has contained the creation of a LiDAR model, geomorphological survey, an archaeological assessment, hand coring, ground penetration radar transects and relative chronostratigraphic modelling. The second phase involved further fieldwork and analyses. The fieldwork included; electrical resistivity survey (ER), ground near infra red (NIR) intensity measurement, mechanical coring and sampling for palaeoecological assessments and dating purposes. The collection of subsurface data by coring was serendipitously augmented by the exposure of several palaeochannels in the La Farge aggregate pit (Warren Farm Quarry) located in the south east of the study area. The analyses included in this report include: ER modelling, analysis of the NIR intensity ground imaging, core analyses, palaeoecological assessments and dating. The palaeoecological assessments included beetles and pollen and the dating included ¹⁴C (AMS), dendrochronology and optically stimulated luminescence (OSL).

The ER profiles were run on or close to the GPR and hand coring transects undertaken in Phase I. They showed the normal trade-off between depth and resolution but in general successfully demarcated the channel edges, base and some elements of internal stratigraphy. As suspected ER was not as efficacious as GPR at revealing any intra-gravel stratigraphy and it is suggested that in order to get as full a stratigraphic cross-section as possible across a palaeochannel in gravels both methods should be employed. The ground radar imaging experiments conducted had the aim of trying to quantify and explain variations in LiDAR intensity, which appeared to be systematic (see Phase I).

Mechanical coring with a Geoprobe corer proved to be both efficient and reasonably fast. The collection of samples for OSL also appears to have been successful as none showed signs of post extraction exposure. The stratigraphy of the cores related well to standard analyses including loss on ignition (to measure organic and carbonate contents) and magnetic susceptibility. Stratigraphic modeling of both borehole/core data and exposure/quarry data using ROCKWORKS is then outlined and approaches to integrating quarry face and borehole data discussed. The analysis of cores (organic content, carbonate content & magnetic susceptibility) suggests that several of the channels had been reoccupied by river flow creating hiatuses in their sedimentary sequences. Pollen and spore samples were processed from a representative selection of cores and the Warren Farm Quarry faces. Concentrations were extremely variable (<1->50,000 grains ml⁻¹) with as expected greater variability in the cores than in the exposures. There was not a consistent relationship with any variables other than a weak and probably partial correlation with pH. Bulk samples recovered directly from the quarry face with a standard volume of 10 litres produced abundant, well-preserved and incredibly diverse beetle assemblages except in the case of a Lateglacial channel. Otherwise preservation was more variable but the role of sample size and the importance of having large quantities (5l – 10l/3 kg), which will provide a representative assemblage, cannot be underestimated.

The dating program showed that the different techniques produced different date frequencies as expected, due to a combination of sampling design and the spatial chronology of the confluence zone. The dendrochronological dates are all clustered around 4.5-4.8 Kyr BP, whereas the ¹⁴C dates ranged from 0.1-7.3 Kyr BP (excluding the Lateglacial channel) and most fell into the range 1-4.1 Kyr BP and the OSL dates ranged from 0.9-7.1 Kyr BP. A definite oral clustering is evident caused by the pattern of channel change and sedimentation.

The chronostratigraphic model constructed in Phase I is then compared with the results of the luminescence (OSL) and radiocarbon dating. Using the stratigraphic, core, dating, LiDAR and geophysical data an evolutionary /diachronic geoarchaeological model of the Trent-Soar confluence zone is proposed. This model places heavy emphasis on a avulsion, the re-occupation of channels and levee and overbank sedimentation as the key processes that pattern the geoarchaeological record and not meander migration, lateral erosion and aggradation that are normally seen as the patterning processes. This has important implications for similar high-energy floodplains as well as the lower sedimentary fills of lowland floodplains, in that it constrains and patterns the distribution of archaeological artefact and structure survival. The report concludes with the main conclusions of the techniques used in Phase II and presents new research directions and presents a methodological statement for geoarchaeological surveys of similar floodplain confluence zones.

II Acknowledgements

This report has been written with the considerable support and help from many individuals. Technical and cartographic advice is acknowledged from S. Rouillard, H. Jones and D. Fraser. The landowners of the target area must be thanked for access and in particular Lafarge Aggregates Ltd. for both access and the provision of data. The project is also grateful to staff of the HP Visualization Centre at Birmingham University and University of Leicester Archaeological Services. English Heritage is acknowledged as the funding body through the ALSF.

III Report Contents
I. Executive Summary
II. Acknowledgements
III. Contents
IV. List of figures
V. List of tables

III Contents

Chapter 1: Introduction

- 1.1 Introduction to the study
- 1.2 Summary of objectives
- 1.3 The study area
- 1.4 Project background
- 1.5 Previous work

Chapter 2: Archaeological Assessment of the Study Area and its Environs

- 2.1 Lower-Middle Palaeolithic
- 2.2 Upper Palaeolithic
- 2.3 Mesolithic
- 2.4 Neolithic – Mid Bronze Age
- 2.5 Late Bronze Age – Iron Age
- 2.6 Romano-British
- 2.7 Anglo-Saxon
- 2.8 Medieval
- 2.9 Post-medieval
- 2.10 Geomorphology and the archaeological resource
- 2.11 Conclusions

Chapter 3: Materials and methods

- 3.1 OSL sampling
 - 3.1.1 *Optical dating: Mechanisms and principles*
 - 3.1.2 *Sample Collection and Preparation*
 - 3.1.3 *Acquisition and accuracy of D_e value*
 - 3.1.4 *Laboratory Factors*
 - 3.1.4.1 Feldspar contamination
 - 3.1.4.2 Preheating
 - 3.1.4.3 Irradiation
 - 3.1.4.3 Internal consistency
 - 3.1.5 *Environmental factors*
 - 3.1.5.1 Incomplete zeroing
 - 3.1.5.2 Turbation
 - 3.1.6 *Acquisition and accuracy of D_f value*
 - 3.1.7 *Estimation of Age*

- 3.1.8 *Analytical uncertainty*
- 3.1.9 *Intrinsic Assessment of Reliability*
- 3.2 Radiocarbon and pollen sample collection**
- 3.2.1 *Tin collection Warren Farm Quarry*
- 3.2.2 *Gouge core sampling*
- 3.2.3 *Pollen sample methods*
- 3.2.4 *Radiocarbon sample methods*
- 3.2.4.1 Sampling**
- 3.2.4.2 *Macrofossils*
- 3.2.4.3 *Sediment*
- 3.3 Dendrochronological dating**
- 3.4 Core stratigraphy, physical and chemical parameters**
- 3.4.1 *Organic content*
- 3.4.2 *Carbonate content*
- 3.4.3 *Magnetic susceptibility*
- 3.4.4 *Eh*
- 3.4.5 *pH*
- 3.4.6 *Geochemistry*
- 3.4.7 *Grain size*
- 3.4.8 *Tin/core sediment stratigraphy*
- 3.4.9 *Data ordering and analysis methods*
- 3.5 Pollen and Spore Assessment**
- 3.6 Coleopteran Assessment**
- 3.6.1 *Processing and Identification*
- 3.6.1.1 *Processing – The Paraffin Flotation Technique*
- 3.6.1.1 *Sorting and Identification*
- 3.6.2 *The objective analysis, quantification and presentation of palaeoentomology as an environmental indicator*
- 3.6.3 *Difficulties with environmental interpretation using palaeoentomology*
- 3.6.4 *A solution to problems of interpretation*
- 3.6.5 *Visual Presentation of Data*
- 3.7 Field survey**
- 3.7.1 *Section recording*
- 3.7.2 *Field survey*
- 3.8 Electrical resistivity (ER) materials and methods**
- 3.8.1 *Geoprospection within alluvial environments*
- 3.8.2 *GPR prospection within alluvial environments – a resume*
- 3.8.3 *ER prospection within alluvial environments*
- 3.8.4 *An introduction to ER survey*
- 3.8.3.1 *Electrical resistivity and sediment stratigraphy*
- 3.8.4 *ER materials and methods*
- 3.8.4.1 *Instrumentation and data collection parameters*
- 3.8.4.2 *Field methodology*
- 3.8.4.3 *Data download and pseudosection viewing*
- 3.8.4.4 *Data inversion*
- 3.8.4.5 *Data interpretation*
- 3.8.6 *The aims of ER survey within this study*
- 3.9 Standardised keys for stratigraphy descriptions**
- 3.10 LiDAR intensity ground scanning**
- 3.10.1 *Introduction*

- 3.10.2 *Aims and Objectives*
- 3.10.3 *Method Statement*
- 3.10.3.1 *Toposil Moisture and Intensity: Broad Area Survey*
- 3.10.3.2 *Topsoil Moisture, Organic Content and Intensity: Detailed Study*
- 3.11 Data archive and query**
- 3.12 Ground penetrating radar materials and methods**

Chapter 4: stratigraphic modelling

4.1 Stratigraphic overview of the study area

4.1.1 Introduction to the study area

4.1.1.1 Geology

4.1.1.2 Topography

4.1.1.3 Stratigraphy

4.1.1.4 Terrace 2 (Devensian) stratigraphy

4.1.1.5 Terrace 1 (Holocene) stratigraphy

4.1.1.6 Modern floodplain stratigraphy

4.2 Three-dimensional stratigraphic modelling of the study area using existing data sets

4.2.1 Outline

4.2.2 Methodology of wider area 3D stratigraphic model

4.3.3 Summary of modelling

Chapter 5: Chronostratigraphy

5.1 Original chronostratigraphic model

5.2 RC dating of palaeochannels

5.3 OSL dating of intervening valley floor

5.4 Dendrochronological dating of trees

5.5 Summary

Chapter 6: Palaeoenvironmental analysis and taphonomy

6.1 Palaeoenvironmental sample stratigraphy

6.1.1 Core MFC2

6.1.2 Core TIC7

6.1.3 Core TIC10

6.1.4 Core TIC12

6.1.5 Core TIC14

6.1.6 Core TFGC14

6.1.7 WQFC1

6.1.8 WQFC2

6.1.9 WQFC3

6.1.10 WQFC5

6.1.11 Comparison of palaeoenvironmental samples organic contents

6.2 Coleopteran analysis

6.2.1 Preservation

6.2.2 Coleopteran analysis: palaeoecology

6.2.3 Discussion

6.1.4 Palaeochannel Relationships

- 6.1.5 *Conclusions*
- 6.2 Pollen and Spore Assessment**
- 6.3 Map of palaeoenvironmental potential over the study area**
- 6.4 Summary**

Chapter 7: Investigating backscattered intensity of Airborne LiDAR

7.1 Topsoil Moisture and Intensity: Broad Area Survey

7.1.1 Discussion

7.2 Topsoil Moisture, Organic Content and Intensity: Detailed Study

7.2.1 AREA FF

7.2.2 AREA MTF

7.2.3 AREA MF

7.3 Conclusions

Chapter 8: Electrical resistivity survey

8.3 Terrace 2 ER surveys

8.3.1.1 Transect T2A

8.4 Terrace 1 ER surveys

8.4.1 Transect T1A

8.4.2 Transect T1B

8.4.3 Transect T1C and T1D: comparison of electrode spacing

8.4.3.1 Transect T1C

8.4.3.2 Transect T1D

8.4.3.3 A comparison between ER transects T1C and T1D

8.4.4 Transect T1E

8.4.5 ER transect T1F

8.4.6 ER transect T1G

8.4.7 ER transect T1H

8.4.8 ER transect T1J

8.4.9 ER transect T1K

8.5 Modern Floodplain ER surveys

8.5.1 ER Transect MFA 1m electrode spacing

8.5.2 ER transect MFB 0.5m electrode spacing

8.5.3 Comparing 1m and 0.5m electrode spacing on the Modern Floodplain

8.6 Methodological considerations of using ER

8.6.1 Relationship of ER data to electrode spacing

8.6.2 Relationship of ER data to stratigraphy

8.6.3 Relationship of ER data to GPR data

8.7 Ranking palaeochannels by biotaphonomic potential based on ER resistivity values

8.8 Overview and summary

Chapter 9. A geoarchaeological model of the Trent-Soar Confluence Zone

9.1 Generalising and modelling the chronostratigraphy

9.2 Development of a valley floor evolution model

Chapter 10. Conclusions and methodological Implications

10.1 Conclusions

10.2 New research directions

10.3 Methodological Statement for Archaeological Prospection in Confluence Zones

11 Bibliography

12 Appendices

Appendix A. ¹⁴C report (Dr. Hamilton)

Appendix B. OSL Report (Dr. P. Toms)

Appendix C. Dendrochronology (Dr. R Howard)

IV. List of figures.

Chapter 1

Fig 1.1: The location of the study area.

Chapter 2

Fig 2.1: The study area mapped by geological stage.

Fig 2.2: The archaeological resource plotted by its method of investigation, against the LiDAR last pulse DTM.

Fig 2.3: The archaeological resource plotted by period.

Fig 2.4: The 'Lockington Villa' complex within the study area.

Fig 2.5: The cropmark enclosure on terrace 1.

Chapter 3

Fig 3.1: The Geoprobe coring rig, about to commence a drive.

Fig 3.2: A sample recovered from the Geoprobe.

Fig 3.3: The locations of the palaeoenvironmental samples.

Fig 3.4: The location of the palaeochannels sampled in the quarry and the exposed section that were drawn.

Fig 3.5: Sections 1 and 2 WFQ.

Fig 3.6: Sections 3 and 4 WFQ.

Fig 3.7: Palaeochannel WFQ C1 during sampling.

Fig 3.7: Palaeochannel WFQ C2 during sampling, with the tins *in-situ* before removal.

Fig 3.8: Palaeochannel WQFC3.

Fig 3.9: The basis of a resistivity measurement.

Fig 3.10: The Wenner and Schlumberger arrays.

Fig 3.11: The data collection points on the 0.5m electrode spacing first transect.

Fig 3.12: The data collection points on the 0.5m second and subsequent transects.

Fig 3.13: The data collection points on the 1m electrode spacing first transect.

Fig 3.14: The data collection points on the 1m electrode spacing second and subsequent transects.

Fig 3.15: The data collection points on the 1m electrode spacing first transect.

Fig 3.16: ER transect running across a palaeochannel on the lower floodplain.

Fig 3.17: Recording the position of the ER transect T1F using dGPS.

Fig 3.18: Modified Troel Smith key for sediment descriptions.

Fig 3.19: Air-photographic, LiDAR elevation and LiDAR intensity data for a part of the Hemington Terrace unit at Lockington.

Fig 3.20: LiDAR elevation (bottom) and Intensity (Top) data for the Lockington study area.

Fig 3.21: Graph showing the measured reflectance of sediments of differing moisture organic content and particle size across the spectrum.

Fig 3.22: Sample locations for soil moisture/intensity comparison.

Fig 3.23: Lockington study area. LiDAR LPG elevation data with detailed LiDAR intensity study areas highlighted in red.

Fig 3.24: Lockington. Field collection of volumetric soil moisture data at regular grid intervals using a Delta T Devices Theta Probe.

Fig 3.25: Lockington. Field collection sediment samples for organic content analysis.

Chapter 4

Fig 4.1: Location of data points for the 3D stratigraphic modelling (map by permission of OS).

Fig 4.2: Location of stratigraphic fence diagrams (map by permission of OS).

Fig 4.3: ArcScene visualisation of study area stratigraphic fence diagrams below lidar elevation model.

Fig 4.4: ArcScene visualisation of Terrace 1 stratigraphic fence diagrams below lidar elevation model.

Fig 4.5: Interpolated surface showing base of alluvium across the study area (map by permission of OS).

Fig 4.6: Location of Warren Farm Quarry and the active extraction area (map by permission of OS).

Chapter 5

Fig 5.1: The ¹⁴C dates plotted at core/sample locations.

- Fig 5.2:** A plot of the cores with basal dates against surface height OD.
Fig 5.3: The OSL dates plotted at sample locations.
Fig 5.4: The OSL dates plotted by height.
Fig 5.5: Photograph of the tree trunks from Warrens Farm Quarry that were dendrochronologically dated.

Chapter 6

- Fig 6.1:** The location of the palaeoenvironmental samples and their basal dates ascertained through radiocarbon dating.
Fig 6.2: Core MFC2 stratigraphy shown against organic content, carbonate content and magnetic susceptibility.
Fig 6.3: Core MFC2 stratigraphy with pollen sample points and radiocarbon dates.
Fig 6.4: Core TIC7 stratigraphy shown against organic content, carbonate content and magnetic susceptibility.
Fig 6.5: Core TIC7 stratigraphy with pollen sample points and radiocarbon dates.
Fig 6.6: Core TIC10 stratigraphy shown against organic content, carbonate content and magnetic susceptibility.
Fig 6.7: Core TIC7 stratigraphy with pollen sample points and radiocarbon dates.
Fig 6.8: Core TIC12 stratigraphy shown against organic content, carbonate content and magnetic susceptibility.
Fig 6.9: Core TIC12 stratigraphy with pollen sample points and radiocarbon dates.
Fig 6.10: Core TIC14 stratigraphy shown against organic content, carbonate content and magnetic susceptibility.
Fig 6.11: Core TIC14 stratigraphy with pollen sample points and radiocarbon dates.
Fig 6.12: Core TFGC14 stratigraphy shown against organic content, carbonate content and magnetic susceptibility.
Fig 6.13: Core TFGC14 stratigraphy with pollen sample points and radiocarbon dates.
Fig 6.14: Core WQFC1 stratigraphy shown against organic content, carbonate content, magnetic susceptibility Eh and Ph.
Fig 6.15: WQFC1 stratigraphy with pollen sample points and radiocarbon dates.
Fig 6.16: WQFC2 stratigraphy shown against organic content, carbonate content, magnetic susceptibility Eh and pH.
Fig 6.17: WQFC2 stratigraphy with pollen sample points and radiocarbon dates.
Fig 6.18: WQFC3 stratigraphy shown against organic content, carbonate content, magnetic susceptibility Eh and pH.
Fig 6.19: WQFC3 stratigraphy with pollen sample points and radiocarbon dates.
Fig 6.20: WQFC5 stratigraphy shown against organic content, carbonate content, magnetic susceptibility Eh and pH.
Fig 6.21: WQFC5 stratigraphy with pollen sample points and radiocarbon dates.
Fig 6.22: The palaeoenvironmental samples shown by mean organic content.
Fig 6.23: Warren Farm Quarry species ecological groups.
Fig 6.24: Variation of % damaged (grains) with depth all data.
Fig 6.25: Variation of % damaged (grains) with depth cores only.
Fig 6.26: Mean concentration of pollen and spores against mean core pH.

Chapter 7

- Fig 7.1:** Lockington study area. LiDAR LPG elevation data with detailed LiDAR intensity study areas highlighted in red.
Fig 7.2: Scatter plot of LiDAR intensity and volumetric soil moisture for study area.
Fig 7.3: Scatter plot of LiDAR intensity and volumetric soil moisture for Hemington Terrace only.
Fig 7.4: Scatter plot of LiDAR intensity and volumetric soil moisture for alluvium only.
Fig 7.5: Lockington, selected sample locations.
Fig 7.6: Scatter plot of LiDAR intensity and volumetric soil moisture for selected area.
Fig 7.7: Lockington study area FF.
Fig 7.8: Lockington area FF showing left airborne LiDAR DSM and right airborne LiDAR intensity.
Fig 7.9: Lockington area FF showing left topsoil organic content and right volumetric soil moisture of topsoil.
Fig 7.10: Lockington area FF showing topsoil organic content.
Fig 7.11: Lockington area FF scatter plot showing topsoil organic content and LiDAR intensity.
Fig 7.12: Lockington area FF showing topsoil volumetric soil moisture.
Fig 7.13: Lockington area FF scatter plot showing topsoil volumetric soil moisture and LiDAR intensity.
Fig 7.14: Lockington, FF study area - Volumetric soil moisture and statistics.
Fig 7.15: Lockington, FF study area - Topsoil organic content and statistics.
Fig 7.16: Lockington area MTF: Left, LiDAR elevation data and right LiDAR intensity values.

- Fig 7.17:** Lockington area MTF: Left, LiDAR intensity values and right intensity with interpolated volumetric soil moisture for each study area superimposed.
- Fig 7.18:** Lockington area MTF1: Scatter plot of LiDAR intensity and volumetric soil moisture.
- Fig 7.19:** Lockington area MTF2: Scatter plot of LiDAR intensity and volumetric soil moisture.
- Fig 7.20:** Lockington MTF1 study area - Volumetric soil moisture statistics.
- Fig 7.21:** Lockington, MTF2 study area - Volumetric soil moisture (%) statistics.
- Fig 7.22:** Lockington study area MF showing channel (left) and bar feature (right).
- Fig 7.23:** Lockington study area MF LiDAR elevation (left) and intensity (right).
- Fig 7.24:** Lockington study area MF volumetric soil moisture (left) and topsoil organic content (right).
- Fig 7.25:** Lockington study area MF topsoil organic content.
- Fig 7.26:** Lockington study area MF scatter plot of LiDAR intensity and topsoil organic content.
- Fig 7.27:** Lockington study area MF volumetric soil.
- Fig 7.28:** Lockington study area MF scatter plot of LiDAR intensity and volumetric soil.
- Fig 7.29:** Lockington, MF study area - Volumetric soil moisture statistics.
- Fig 7.30:** Lockington, MF study area - Topsoil organic content.

Chapter 8

- Fig 8.1:** The location of T2A on the upper Devensian Holme Pierrepont terrace 2.
- Fig 8.2:** Transect T2A ER section.
- Fig 8.3:** The location of transects T1A and T1B, at the junction between terrace 2 and terrace 1.
- Fig 8.4:** The stratigraphy of transects T1A and T1B.
- Fig 8.5:** ER transect T1A.
- Fig 8.6:** ER transect T1B. The palaeochannel in the section is an obvious feature.
- Fig 8.7:** The location of ER transects T1C and T1D.
- Fig 8.8:** The ER transect T1C.
- Fig 8.9:** The ER transect T1D.
- Fig 8.10:** The location of ER transect T1E, placed on the LiDAR LP DTM.
- Fig 8.11:** ER transect T1E placed on the LiDAR intensity survey.
- Fig 8.12:** Earth resistance survey over the same area as T1E.
- Fig 8.13:** ER transect T1E.
- Fig 8.14:** Photograph of ER transect T1F
- Fig 8.15:** Location of the ER transect T1F.
- Fig 8.16:** ER transect T1F.
- Fig 8.17:** Location of ER transect T1G.
- Fig 8.18:** The ER transect T1G.
- Fig 8.19:** Location of transect T1H on terrace 1.
- Fig 8.20:** ER transect T1H.
- Fig 8.21:** The location of transect T1J.
- Fig 8.22:** The ER transect T1J, gouge core stratigraphy combined with GPR and ER sections.
- Fig 8.23:** The ER transect T1J with interpretation.
- Fig 8.24:** Location of ER transect T1K, on the same transect line as T1A.
- Fig 8.25:** ER transect T1K, raw data (top) and with gouge core stratigraphy (bottom).
- Fig 8.26:** ER section T1K with interpretation.
- Fig 8.27:** Comparison of the ER sections T1K and T1A, comparing the 2m and 1m electrode spacings.
- Fig 8.28:** The location of transects MFA and MFB.
- Fig 8.29:** ER transect MFA.
- Fig 8.30:** ER transect MFB.
- Fig 8.31:** Combined visualisation of GPR and ER data, with the ER section at 80% transparency.
- Fig 8.32:** Combined visualisation of GPR and ER data, with the ER section at 60% transparency.
- Fig 8.33:** Combined visualisation of GPR and ER data, with the ER section at 40% transparency.
- Fig 8.34:** Combined visualisation of GPR and ER data, with the ER section at 20% transparency.

Chapter 9

- Fig 9.1:** Re-zoned study area using basal radiocarbon and OSL dates (left) and chronostratigraphic model (right).
- Fig 9.2:** The chronostratigraphic model with OSL dates shown.
- Fig 9.3:** The chronostratigraphic model with OSL dates shown.
- Fig 9.4:** Neolithic channels flowing approximately S-N and depositing terrace 1.
- Fig 9.5:** Bronze Age channels trending SE-NW abandoned on terrace 1.

- Fig 9.6:** Iron-Age-early Post Roman. Note older Neolithic – Bronze Age core within meander loop.
Fig 9.7: New Soar channel location Romano-British – Medieval.
Fig 9.8: Medieval-early Historic abandonment of loop and channel shift to the NE.
Fig 9.9: Post Medieval northward migration of Trent channel and establishment of the present junction.

V. List of tables

Chapter 3

- Tab 3.1:** Sites used for environmental sampling with number of pollen samples taken for assessment.
Tab 3.2: Species ecological groups.
Tab 3.3: General resistivity and conductivity values of some rocks and soils.
Tab 3.4: Table of predicted resistivity ranking of sediment units within the study area, on a *pre-hoc* basis before survey.
Tab 3.5: ER surveys undertaken.

Chapter 5

- Tab 5.1:** Details of samples from Lockington Quarry on the river Trent in Leicestershire.
Tab 5.2: Results of the cross-matching of site chronology LOKQS Q01 and relevant reference chronologies when first ring date is 2928 BC and last ring date is 2629 BC.
Tab 5.3: Results of the cross-matching of sample LOK-Q06 and relevant reference chronologies when first ring date is 2623 BC and last ring date is 22519 BC.

Chapter 6

- Tab 6.1:** Preservation of insect sclera from the Warrens Farm Quarry cores.
Tab 6.2: Pollen and spore concentrations and descriptive classes.
Tab 6.3: Summary statistics for pollen and spore assessment.
Tab 6.4: Correlation matrix for sediment, pollen and environmental variables.
Tab 6.5: Correlation matrix for sediment, pollen and environmental variables, core samples only.
Tab 6.6: Mean values for pollen taphonomic variables against mean core pH and Eh.
Tab 6.7: Ranks of the palaeoenvironmental (pollen and spore) potential of the cores.

Chapter 8

- Tab 8.1:** Summary of field considerations of using different electrode spacings.
Tab 8.2: Summary of the data capture properties of different electrode intervals.
Tab 8.3: Ranking of biotaphonomic potential of palaeochannels based on resistivity values.

Chapter 9

- Tab. 9.1:** Correspondance (confusion) of matrix of chronostratigraphic model with observed dates.

Chapter 1: Introduction

1.1 Introduction to the study

This project has been framed to address the core ALSF theme of developing capacity to manage aggregate extraction landscapes in the future (English Heritage 2004). In addition it addresses several objective two ALSF themes, namely:

- 1) Characterising the [archaeological] resource and developing evaluation frameworks, predictive tools and mitigation strategies.
- 2) Development [of] remote sensing and predictive techniques and mitigation strategies.
- 3) Training and professional development and to raise awareness of issues and to improve the quality of historic environment work undertaken in response to aggregate extraction.
- 4) Development of advanced visualisation and immersive three-dimensional models of landscape development, largely part of phase 2 of the project, has the potential to address the theme of interpretation and outreach to the community of the knowledge gained from work related to aggregate extraction.

1.2 Summary of objectives

The full detail of objectives are given in the original Project Design (PNUM3357, phase II PD). The principal aim of this project is to predictively model the landscape of a major river confluence over a time-scale of millennia and at a spatial scale appropriate for archaeological management. The overall purpose is:

- 1) To establish a rigorous research model for the future development of predetermination designs for site evaluation.
- 2) To assess the effectiveness of various airborne and ground based remote sensing methods in alluvial environments.
- 3) To derive relationships between pre-extraction site survey data and likely chronostratigraphic and environmental data as part of archaeological assessment.

This research will assist regulatory bodies (i.e. County Councils) in demanding and specifying rapid evaluations of geoarchaeological potential as part of the implementation of PPG16. The novelty of the approach lies in the integration of high-resolution topographical, archaeological and geological (three-dimensional sub-surface) data within a Geographical Information System (GIS). The technical innovation will be the combination of Interferometric Synthetic Aperture Radar (IFSAR), Airborne Laser Altimetry (LiDAR), CW Differential GPS (DGPS), Ground Penetrating Radar (GPR) and other ground based remote sensing techniques. This research will contribute to the framework for management of the archaeological resource in the Trent Valley developed through Trent Valley GeoArchaeology (Bishop *et al.* 2002) and provide a transferable model for the geoarchaeological investigation and management of valley floor archaeology.

1.3 The study area

The study area is a block of the Trent/Soar confluence landscape approximately 2 by 4 km (Fig. 1.1; East Midlands, U.K). The area abuts the main area of Trent Valley GeoArchaeology (TVG) interest and is close to but not overlapping sites of continuing research by University of Leicester Archaeological Services (ULAS). The area is not zoned for aggregate extraction although the area to the west is.

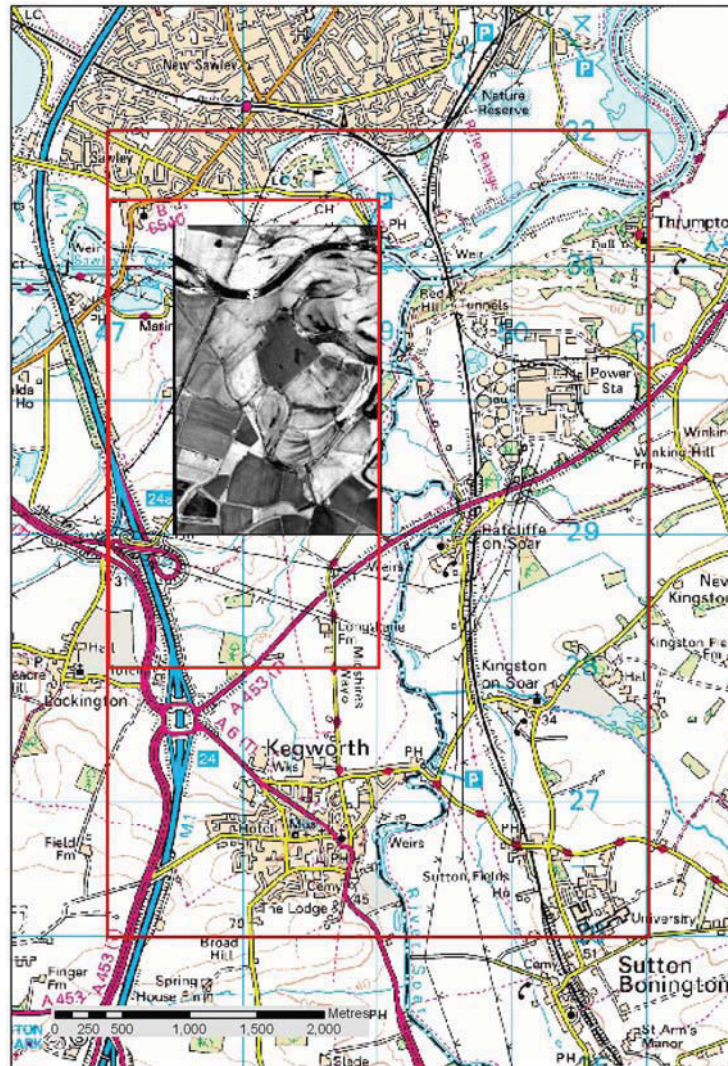


Fig 1.1: The study area over the 1:50,000 Ordnance Survey map (by permission of OS).

1.4 Project background

Recent archaeological work on the Thames and other British floodplains suggests that river confluences have been the foci of settlement and human activity since the earliest post-glacial periods. At confluences the high density of palaeochannels provides an opportunity to determine records of past environmental change. Migration of rivers channels also provides an environment with high potential for the burial and preservation *in situ* of cultural and environmental materials. Unfortunately this potential is generally only realised during the destruction of the land surface by development and subsequent 'rescue' archaeological investigation. It is the nature of the archaeological record of floodplains that there is a direct link between the geomorphology, including the nature and distribution of channels, levees, gravel bars, terrace remnants, etc. and the distribution and nature of archaeological materials, from flint scatters to structures. Therefore there is a predictive capability in the subsurface geomorphology, stratigraphy and buried land surfaces.

1.5 Previous work

The Middle Trent is one of the archaeologically richest stretches of alluvial landscape in the UK. Finds include medieval bridges (the Hemington Bridges excavations, funded by English Heritage), a Norman milldam, fishweirs and dugout canoes (Salisbury *et al.*, 1984; Cooper, 2003). The study area (a block of floodplain 8 km²) is centred on the Lockington Marshes at the confluence of the Trent and Soar. This area is rich in cultural archaeology lying immediately east of the nationally significant prehistoric ritual landscape of the Derbyshire Trent Valley (Riley, 1987). Recent finds from a Bronze Age barrow cemetery (Hughes, 2000) strongly suggests that this prehistoric ritual landscape extends into the area. In the Romano-British period the area lies in the hinterland of a villa complex at Lockington and a small town, possibly a centre of ritual/religion at Red Hill, Ratcliffe on Soar (Elsdon, 1982). The area, although not threatened with imminent destruction, is earmarked for longer-term development. Pilot studies indicate the high buried archaeological potential of the locality (Ripper, 1997), which combined with a high density of sites suitable for palaeoenvironmental studies (Howard, 1997) provide an ideal zone for detailed modelling. Work by Trent Valley GeoArchaeology (Knight and Howard, 2004) has done much to provide a regional framework for the cultural, landscape and environmental archaeology of the Trent Valley. The present proposal provides an opportunity to build constructively on that framework through detailed consideration of a significant confluence zone, targeted fieldwork and innovative use of GIS and allied technologies.

Chapter 2: Archaeological Assessment of the Study Area and its Environs

*And of the British floods, though but the third I be,
Yet Thames and Severne both in this come short of me,
For that I am the mere of England, that divides
The north part from the south, on my so either sides, that reckoning how these
tracts in compasse be extent,
Men bound them on the north, or on the south of Trent*

Michael Drayton, *Poly-Olbion*, The Sixe and Twentieth Song, 1622

The environs for the study area is taken as a transect along the Trent floodplain from Swarkestone to the west of the study area, and Attenborough to the east. The wider environs allows consideration of the Trent's confluence zone with the Derwent and Soar, an area where significant archaeological discoveries spanning the Lower Palaeolithic to the Post-Medieval period have occurred. It is suggested below that the rich archaeological resource of this area is partly due to the confluence zone being an important communications node.

The information included in the report is derived from an SMR search for the eight square kilometre study area (Leicestershire and Derbyshire), a review of published and unpublished reports from the study area and a general search of published data for the environs. The regional and national significance of the sites and monuments in the study area is gauged against the recent regional research frameworks initiative (N.J. Cooper 2006).

The recognition of the archaeological resource in the Trent-Soar-Derwent confluence zone was initially linked with aggregates extraction. Palaeolithic handaxes were recovered from quarries in the Beeston area in the 1920s while occasional finds of Bronze and Iron Age metalwork from the Trent produced the first glimpses of the later prehistoric period (Scurfield 1997; Watkin *et al.* 1996). Aerial photography from the 1940s first began to reveal the hidden past landscapes represented by cropmark evidence on the gravel terraces. The first of the Lockington barrows was located by St Joseph in 1947 and subject to survey and trial excavation in 1954 (Posnansky 1955). Aerial reconnaissance within the study area from the 1960s led to the discovery of further barrows (Pickering and Hartley 1985) and the Lockington Iron Age and Romano-British settlement and villa (St Joseph 1961 and 1968, Frere and St Joseph 1983, Pickering and Hartley 1985), both now Scheduled Ancient Monuments. Follow-up fieldwalking survey of the two cropmarks produced both Iron Age and Romano-British pottery (Clay 1985).

Since the early 1990s the study area and immediate environs has seen much archaeological activity in relation to aggregates extraction, road schemes and proposed developments, all under the remit of PPG16. An area of the barrow cemetery was subject to evaluative and mitigative excavation in advance of the Derby Southern Bypass scheme and associated works (Hughes 2000). Noteworthy was the near-complete excavation of Barrow VI which revealed a multi-phased monument and a spectacular pit deposit of metalwork and ceramics. Two possible ring ditches seen as very faint cropmarks were confirmed by trial trenching in the same field. More recently desk-based survey, geophysical survey, field survey and evaluation have increased the size of the Lockington barrow cemetery area and the Iron Age/Romano-British settlement and associated field systems (Clark 1995; Ripper and Butler 1999).

Perhaps one of the most significant developments in recent years has been the discovery of waterlogged archaeological remains in the palaeochannels in the Derwent-Soar-Trent confluence zone. Hemington Quarry immediately west of the study area has revealed palaeochannels going back as far as the Late Glacial period. These have produced highly significant palaeoenvironmental data while the medieval channels of 9th-14th century date have preserved unique structural evidence for fisheries, bridges and river management.

2.1 Lower-Middle Palaeolithic

Although no finds of this date have been reported from the study area several artefacts have been recovered from the environs, all from gravel pits at Beeston and Stapleford parish. Wymer (1999) records 20 handaxes from the Beeston Sand and Gravel (OIS 4), one from Hemington Terrace Deposits (OIS 1-2) and one from alluvium. Some 16 handaxes and several flakes were recovered from the Tottle Brook pit (Smith 1928; Posnansky 1963). It remains uncertain whether the finds from the Beeston terrace are Devensian or earlier in date (Wymer 1999, 115). Posnansky (ibid) noted the fresh condition of some of the material from Tottle Brook pit, which might suggest that some is of Devensian age, while other pieces were rolled and would seem to be secondary deposits. The mapped Soar-Trent terraces across the study area are probably of OIS 1-2 date and have some potential for derived Lower-Middle Palaeolithic artefacts.

River confluences were favoured places for Lower and Middle Palaeolithic hunter-gatherers (Wymer 1999) and, given the finds from the Beeston terrace, it is suggested that the study area has some potential for the preservation of artefactual and ecofactual evidence for this period. The finds from the environs are among some of the more northerly European Lower Palaeolithic finds and may help to address questions of colonisation and population dynamics (Graf 2002).

2.2 Upper Palaeolithic

Early Upper Palaeolithic evidence is absent from the Trent valley, but this is not surprising as such sites are rare at the national level. While this partly reflects low population densities there is also a problem in recognising sites of this period. Early Upper Palaeolithic sites are identified on the basis of limited lithic typology, in the finding and recognition of leaf points, Font Robert points or Aurignacian type fossils (Jacobi 1980; Barton 1997). An Early Upper Palaeolithic presence in the region is well attested at Creswell Crags (Jacobi 1980), while the recently investigated site at Glaston, Leics. demonstrates the considerable potential for open-air sites in the East Midlands (Thomas and Jacobi 2001; Cooper 2001). While open sites are likely to have been detrimentally affected by periglacial conditions, these can also present some chance for preservation. Ice wedges, which were frequently seen at Hemington Quarry and on aerial photographs of the local terraces, can be repositories for early sites as demonstrated locally on the Wing to Whatborough pipeline (Graf 2002; Cooper 2002b). While only a single flake was recovered from the latter site, remarkable lithics and faunal assemblages have been reported from similar contexts e.g. Wilczyce, Poland (Fiedieczuk and Schild 2002).

The onset of the Dimlington Stadial led to the abandonment of Britain for some 10,000 years. After the climatic amelioration of the Lake Windermere Interstadial Britain was re-colonised, but this was probably not a continuous process being affected by rapid fluctuations in climate and environment. Radiocarbon dating and distinct typological and technological differences in material culture (lithics and organic tools) suggests that the process was punctuated between 13,000 and 10,000 Cal. BP. Conventionally the material culture of this period is divided into the Late and Final Upper Palaeolithic (Barton 1997). The evidence for occupation of the Trent valley during this period is more compelling with a number of

reported later Upper Palaeolithic findspots and sites. Indeed the cluster of findspots within the East Midlands is one of the densest across the country (Jacobi 2004).

The earliest re-colonisation of Britain is associated with the Creswellian culture, dating to *c.* 12,900-12,000 BP (Barton et al. 2003), named after the cave sites at Creswell Crags on the Nottinghamshire/Derbyshire border; Mother Grundy's Parlour cave being the type site (Garrod 1926). The type fossil for this period is now seen as the Cheddar point, a trapezoidal backed blade (Jacobi 1991). A Cheddar point and possibly contemporary blades were recovered by fieldwalking from a field immediately west of the study area at SK 4662 2832, Lockington-Hemington (Cooper and Jacobi 2001). The findspot adds to the growing number of Creswellian sites in the Trent valley located by fieldwalking (Jacobi et al. 2001) including the nationally significant open-air site at Farndon (Garton 1993).

The pollen record of Northern Europe shows a change to a more wooded environment around 12,000 BP, the beginning of the *Allerod* chronozone. The distinctive lithics associated with this phase are the *federmesser* (convex backed blades) including a variant, the penknife point (shouldered, convex backed blade). *Federmesser* technologies appear across much of northern Europe and are probably linked to Azilian industries from southern Europe (Schwabedissen 1954). A *federmesser* from Castle Donington, Leics. (Cooper and Jacobi 2001) is the only certain Final Upper Palaeolithic finds from the study area environs, although other findspots are known within the Trent Basin (Jacobi *et al.* 2001).

The study area has great potential for Late Devensian palaeochannels. At Hemington Quarry eastern extension a truncated channel base produced radiocarbon dates of $11,735 \pm 75$, $10,960 \pm 110$, $11,725 \pm 80$ and $11,775 \pm 80$ Cal. BP (Cooper and Ripper 2001; Greenwood et al. 2003, 648). Another Late-glacial channel at Hemington Quarry (western extension) has produced similar dates (Cooper and Ripper 2001, 141; M. Greenwood, pers. comm.). The latter channel was of note in having a surface expression. The silted palaeochannels contained well-preserved organic remains including cold-climate caddis fly larvae and Greenwood *et al.* (2003) have demonstrated their usefulness as proxy climatic indicators in local and regional palaeo-environmental reconstructions. While there is an absence of Upper Palaeolithic finds from the study area there is considerable potential for their survival on the terrace deposits. Should any such sites have been preserved by alluvium they would be regarded as nationally significant.

2.3 Mesolithic

Mesolithic material is reported from several flint scatters within the study area (LE 4714, 7095, 7096, 7097, 7120), though none of the scatters have been as large as those seen at local upland sites. However, it should be noted that the identifications are based upon technological criteria; there are no typological identifications. Furthermore, the Leicestershire SMR has a tendency to record blade-like flakes as of a general Late Mesolithic – Early Neolithic date e.g. LE 7120. Repeat fieldwalking of the area has further sampled the scatters and the author has reported on this material. There are some Mesolithic debitage pieces in the collections, i.e. showing bladelet technology, but the evidence is slight. However, the fieldwalking within the study area was undertaken at 20m intervals a method not conducive to the location of small scatters.

A remarkable find of a Late Mesolithic antler harpoon from just north of the study area at Long Eaton, Derbs. or Thrumpton, Notts. (Knight and Howard 2004, 38) hints at the likely lost valley bottom sites. Systematic fieldwalking elsewhere in the Trent Valley has shown a widespread occurrence of sparse Late Mesolithic material, but Early Mesolithic material was apparently absent. However, an Early Mesolithic assemblage was reported from excavations at Swarkestone Lowes and, when considered within the Trent Valley context, was described as a rare resource (Jacobi and Garton 1999).

Palaeochannels of early Holocene date within the environs have been sampled. The potential for channels being archaeological repositories is highlighted by the recovery of a Late Mesolithic human femur from Staythorpe, Notts., a find that has allowed some real consideration of Mesolithic economy in the Midlands; stable isotope analysis showed that the female had subsisted on a diet rich in animal protein but lacking evidence for consumption of fish and marine food (Cooper, 2004).

2.4 Neolithic – Mid Bronze Age

The Middle Trent has a remarkable Neolithic ceremonial landscape within the confluence zone between the Dove and the Erewash¹. Early Neolithic monuments are generally sparse but possibly occur in the environs of the study area at Barton in Fabis where an interrupted ditch system, a likely causewayed enclosure, is juxtaposed with a possible henge site (interpreted by Harding with Lee 1987, 221; repeated in Deegan 1999). Neither the causewayed enclosure nor henge have been subject to scientific dating, but it is suggested that the causewayed enclosure dates to the Neolithic and the henge to the Mid to Late Neolithic. However, in the absence excavation and dating this interpretation is speculative. Another cropmark site is the probable henge at Round Hill, Twyford and Stenson (Harding with Lee 1987, 116).

Middle Neolithic monuments closer to the study area include the cursus monument at Aston, Derbs, first identified by aerial photography in 1966 (St Joseph 1966). The monument incorporated an earlier ring ditch (round barrow) along its western side while other associated ring ditches might be later additions (Gibson and Loveday 1979). The excavations of Aston I confirmed this to be an Early Bronze Age monument though earlier Neolithic features and artefacts were revealed beneath the mound (Reaney 1968). The NE-SW alignment of the monument is a common trait with cursus and similar monuments such as long mortuary enclosures. Such alignment has been claimed to represent positioning with respect to the solar calendar (Field 1999), although reference to other elements of the natural environment may have also occurred (Brophy 1999; McOmish 2003).

Some 70m west of the study area there is an enigmatic cropmark at the Lockington barrow cemetery (Rookery Lane) that plausibly could be a cursus terminal, or part of a long mortuary enclosure. This was first reported by Pickering and Hartley (1985, 37, fig 2), although the feature was not assigned to a particular monument class². The faint cropmark comprised two parallel ditches some aligned NE-SW with a rounded terminus at its southern end. There is another possible cropmark that deserves mention; just to the west of the study area, near to the barrow excavated by Posnansky (1953), is a possible concentric pit circle (though slightly oval in plan). Pit circles have been recorded at Rearsby and Oakham, the latter excavated by Clay (1998) revealing a multi-phased monument of Late Neolithic and Early Bronze Age date. Both of these features are potentially significant additions to the ceremonial landscape at Lockington-Hemington and both urgently require further work to clarify their character and date.

The Lockington barrow cemetery just extends into the western edge of the study area. Posnansky (1953) partially excavated the first known barrow showing that it had a remnant mound. A central cremation burial had grave goods that included a bronze knife, bronze awl, a barbed and tanged arrowhead and three plano-convex knives (ibid). It is of some interest that the flintwork was all heat damaged.

Subsequent aerial survey recorded further ring ditches; Pickering and Hartley (1985) recorded seven examples including one enclosing a pit circle, and a concentric monument. Barrow VI was subject to an evaluation ahead of works associated with the Derby Southern Bypass and eventually full excavation

¹ A wider environs is considered necessary here to provide the landscape context of the study area.

² The feature could not be seen on the aerial photographs searched by the author. The feature is plotted in slightly different locations by Pickering and Hartley (1985) and Meek (2003).

(Hughes 2000). This revealed a remarkably complex monument: initially the site was demarcated with a palisade. An adjacent pit contained a remarkable group of deposits including substantial parts of two beaker vessels, a large copper dagger and two gold bracelets (ibid). Organic residues on the dagger produced radiocarbon dates of 2580-2200 and 2190-1880 Cal. BC, the latter date best fitting the typology of the dagger. Pre-mound activity has been interpreted as a pyre site but there was no evidence for burials associated with the pit deposits or the mound. The site identified as Barrow V by Pickering and Hartley (1985) was also subject to full excavation, revealing a pit group rather than a ring ditch (J. Meek in Hughes 2000).

The extent of this Late Neolithic - Bronze Age ceremonial landscape has greatly increased in recent years following more intensive assessment of aerial photographs, geophysical survey and fieldwork. Meek (2003) identified 27 possible Neolithic-Bronze Age monuments³ while the present study adds a further four ring ditches and the afore-mentioned possible concentric pit circle. The 23 known or probable ring ditches are widely distributed, three km east-west by two kilometers north-south, and might be classified as an 'area cemetery'. However, there is distinct clustering of Lockington sites 1-10, with a sub-group of seven aligned WSW-ENE⁴. The more northerly barrows also appear to be a distinct cluster and might better be termed the Hemington barrow cemetery. However, as much of the area between the two groups has been quarried this might be more apparent than real. A more systematic search of the older air photographs might be useful to assess the areas lost to gravel extraction and the construction of the M1.

Perhaps the most significant result of the recent fieldwork has been to demonstrate the survival of some barrows and associated features beneath alluvial cover (Ripper and Butler 1999). In contrast to the examples revealed by aerial survey, where long term ploughing has levelled and truncated monuments, the sub-alluvial barrows have excellent preservation potential. Deeper cut features such as graves, pits, shafts and enclosing ditches may well preserve organic remains. The location of the sub-alluvial monuments in and adjacent to the study area should be a priority for future research. The excavations at West Cotton, Raunds highlights how nationally significant monument complexes can be masked by alluvium (Windell 1989).

While the conspicuous Neolithic and Early Bronze Age monuments have gradually been revealed in recent years, there has been little evidence of Mid-Late Bronze Age cemeteries. It would be surprising if these did not exist. While many secondary cremation burials in barrows may have perished with the plough, some flat cemeteries can be anticipated. At Eye Kettleby, on the river Wreake, almost 100 cremations were recovered in a flat cemetery (N. Finn pers. comm.). There are numerous small cropmark features in the field containing the barrow excavated by Posnansky (1953) and it is quite plausible that these might be later cremation burials. The 1756 Gentleman's Magazine reported the discovery in Kegworth of ten earthen pots containing bones which fell to pieces when touched (Meek 1999).

As well as the fine metalwork deposited in and around barrows there is an increase in deposition in watery places in the study area environs (Scurfield 1997), mirroring a national picture of depositional translocation during the Bronze Age. The Middle Trent has provided several loci for Bronze Age metalwork clusters recovered from old channels or dredging of the modern Trent (Scurfield 1997). The study area lies between two such clusters at Attenborough (ibid) and Aston on Trent (Salisbury 2004). The Attenborough finds include Early and Late Bronze Age bronze artefacts, but the majority are Mid Bronze Age in date. A sword of this date was recovered from the Trent at Ratcliffe on Soar immediately east of the study area (Scurfield 1997, 54)

³ 'Ring ditch' sites 26 and 27 are now known to have been infilled ponds while the 'henge' site 25 appears to be a palaeochannel.

⁴ Four ring ditches exactly aligned, the remaining three very closely.

The Aston on Trent site has been very prolific producing 12 bronze artefacts from probable lake deposits including rapiers and axes dating from the Mid to Late Bronze Age (Salisbury 2004). A stone and timber structure, possibly a causeway, has also been dated to the Middle Bronze Age. The structure was at least 12 x 50m and comprised irregular rows of oak piles (250-300 in total) stabilised by brushwood and quarried Mercia mudstone blocks, probably from outcrops at Weston Cliff or Kings Mill, some 2km upstream. The structure might be compared with similar structures at Flag Fen, Peterborough and in the Witham Valley (Salisbury 2004). Two Middle Bronze Age logboats have also been recovered from the Aston Lakes, one of which contained a cargo of quarried stone blocks. Another metalwork cluster recovered from the Trent at Clifton in the 1930s included 22 bronze artefacts. The site also produced many wooden piles, boats and human skulls, all undated but quite feasibly associated (Scurfield 1997).

While the monumental archaeology is rich in the study area and environs, any evidence for contemporary settlement is sparse, mirroring the national picture. Several flint scatters from the study area and environs have produced diagnostic Late Neolithic - Early Bronze Age artefacts (LE 4657, 4714, 4724, 7625, 8053 & 9715). Of these the larger scatters with wider ranges of tool forms might be the best indicators for settlement. A large pit containing Peterborough Ware was located during an evaluation at Warren Farm (Ripper and Butler 1999) while other Late Neolithic features have been recorded in the environs at Castle Donington .

Late Neolithic palaeochannels at Hemington Quarry (eastern extension) provided palaeoenvironmental indicators of a cleared floodplain with evidence for use as pasture (Beamish *et al.* 2002). Nearby woodland was mixed oak and hazel, while lime and elm probably occurred on the higher ground. Rising up the profile were indications of further clearance and increasing cereal cultivation. A slightly later palaeochannel produced further evidence for an open environment of grassland. A section of wattle panel, interpreted as a fishweir fragment, produced a date of c. 3600-3300 Cal. BC, making it the earliest known in Britain⁵ (Clay and Salisbury 1990).

Many Neolithic channels in the Middle Trent have produced so-called ‘bog oaks’, often providing the dating and locational evidence for the channels (Salisbury *et al.* 1984). These have been seen as indicative of clearance of the wildwood from the valley, that is the result of soil erosion (Knight and Howard 2004, 51). An example was observed in the Warren Farm pit during the fieldwork stage of this project.

2.5 Late Bronze Age – Iron Age

The later prehistoric period sees a rise in the archaeology of settlement across the Middle Trent area, with a trajectory away from the previous ceremonial landscape and ‘towards an enclosed landscape’ (Knight and Howard 2004). The large corpus of archaeological data from this period in the study area environs allows some generalisation for this landscape development (*ibid*; Clay 2002; Willis forthcoming). At the start of this period open settlements, often just single buildings, occur in a landscape that has started to be ‘marked out’ by pit alignments. The earlier ceremonial monuments are often referenced by the pit alignments showing that they still played an important role defining the physical landscape. From the Middle Iron Age settlements start to be bounded by small enclosures while by the beginning of the first millennium AD the landscape has been fully enclosed (Willis forthcoming).

Late Bronze Age – Early Iron Age structures have been recorded from the environs at Swarkestone Lowes (Guilbert and Elliott 1999), Willows Farm, Castle Donington and Hemington Quarry, Castle

⁵ However, there may have been problems with the radiocarbon date nb the Current Arch article on the ‘Bronze Age’ date for the Hemington mill dam site, later re-dated to the medieval period.

Donington (Cooper and Ripper forthcoming). Each site has produced only single buildings, each of distinctive post-ring construction. Postholes and gullies of probable Early Iron Age date were recorded at Red Hill, Ratcliffe-on-Soar immediately east of the study area (Elsdon 1983). Later prehistoric lithic scatters have been found at Willow Farm (pers. obs.), comprising small scatters demonstrating squat flake technology and a high tool index dominated by piercers and scrapers, often with linear retouch.

Pit alignments occur across much of the environs and within the study area itself. These are dated conventionally to the later prehistoric period although a longer currency into the Roman period may occur (Deegan 1999). Knight and Howard (2004, 104-5) suggest that the dating evidence for such monuments in the Trent Valley indicates a relatively late development, concomitant with the development of an enclosed landscape. An alignment at Willows Farm, Castle Donington was undated but LBA and Iron Age pottery was recovered from features adjacent to a gap in the alignment. None of the monuments within the study area has produced dating evidence.

There is a large settlement complex within the study area that is conventionally interpreted as an Iron Age nucleated settlement (Clay 1985; Clay 2004; Liddle 1982) although essentially the complex remains undated and, arguably, much of its more regular layout may be of Romano-British date (see below). Certain earlier elements are apparent such as some of the pit alignments and the smaller enclosures that lie uncomfortably with the later settlement. The current study has allowed a re-interpretation of the latest 'phase', that is an extensive co-axial settlement flanking a major Roman road (see below).

To the north of the large settlement there are indications of Iron Age and early Romano-British settlement from a small field scatter (LE 4721). The scatter straddles the Roman road but may also be related to a faint cropmark in the field immediately to the east, which appears to represent a D-shaped enclosure with a roundhouse towards the centre. The sites provide proxy-dating evidence for the underlying channel(s).

There is some continuation of metalwork being placed in watery places into the Late Bronze Age e.g. a sword was recovered from gravel working at Church Wilne, just north-west of the study area (Hughes 1998, fig 18). These depositional practices appear to end in the Early Iron Age but there is some resumption of ritual deposition in watery contexts in the later Iron Age. The Ratcliffe-on-Soar shield was found c. 500m east of the study area and is thought to date to c. 300 BC (Watkin et al. 1996). The quality of the metalwork led to it being described as standing 'at the head of a series of British masterpieces unsurpassed in Europe' (ibid. 27). The deposition of metalwork in this area might be related to the proximity of the suspected Iron Age religious site at Red Hill, immediately east of the study area (Elsdon 1983). Of course, it may also indicate the former presence of a ford at this location (Palfreyman and Evans 2003). The Red Hill cliffs at Ratcliffe-on-Soar with their colourful striped appearance (red clay and gypsum) are a dramatic sight rising from the wide Trent floodplain and it is not too difficult to imagine how it may have been deemed a special place. There is good evidence for a Romano-British temple site at Red Hill and it has been suggested that this developed from a late Iron Age shrine site (Elsdon 1983; Palfreyman and Evans 2003).

2.6 Romano-British

There are significant Romano-British sites both within the study area and its immediate environs, that is respectively, the villa complex at Lockington and the 'small town' at Redhill, Ratcliffe-on-Soar, both having clear origins as significant Iron Age sites (Liddle 1982; Elsdon 1982). The current study has presented fresh evidence for a Roman road passing through the study area and it would appear that the co-axial elements of the so-called Iron Age settlement are actually Romano-British.

A Roman road (Margary 182) from Little Chester (Derwentio) to Sawley passes into the study area north of the modern Trent (Margary 1967, Dool 1985). The line of the road in Sawley is that of Draycott Road with a continuation beyond the modern junction with the B6540, Tamworth Road. The line would appear to turn slightly following the property boundary to Grounds Farm and the river (a slight earthwork is shown on the OS map for part of this stretch). This takes one to the Billystones ford, a known crossing point until the 18th century. While Margary (1955) believed the Derby-Sawley road terminated at the river, implying a port in the area, a crossing point and a southern continuation has been postulated (Liddle 1982; Lycett 1999; Palfreyman and Ebbins 2003).

Liddle (1982) speculated that a route existed between Redhill and Leicester and Lycett (1999) has presented a convincing case for its course, from Leicester passing through the Charnwood uplands via Anstey, Shepshed and Long Whatton into the Soar/Trent floodplain through Kegworth into the study area, i.e. Long Lane, Lockington. The Leics. SMR suggests that the route continues beyond the modern T-junction, progressing to the Soar. Immediately north of this speculative crossing point there is a report of a layer of cobbles halfway up the riverbank, feasibly the remains of a road. However, the straight route of Long Lane is that of the turnpike road; Hartley (1984) plotted the lane overlying and cutting across the grain of ridge and furrow along its course. However, it is tempting to suggest a crossing to Red Hill in this vicinity; the historical crossing of the Soar is located in this area.

A more speculative proposal for a southern route has been made by Simon Marchini (http://www.btinternet.com/~simonmarchini/History/History_Measham.htm) suggesting that the Roman road linking Tamworth and Measham might extend to Sawley. He points to the straight parish boundaries, nearly 5km long, between the villages of Diseworth, Castle Donington and Lockington-Hemington and a land parcel in Lockington called King Street plantation; such names often indicating Roman roads (Margary 1967). The parish boundary of Castle Donington and Lockington-Hemington eventually kinks to the northeast and then follows the line of the Tipnall Bank. One might speculate that this could have been the remains of a Roman road extending to the aforementioned crossing point in the study area.

The present study has presented strong evidence for a major Roman road heading north to the crossing point of the Derwentio road. The afore-mentioned King Street Plantation actually lies on the parish boundary of Lockington-Hemington and Kegworth, *between* the two postulated routes mentioned above. Meek (1999) noted that 19th century documents refer to four adjacent closes called First King Street, Far King Street, King Street and King Street. The appellation can be given to Roman roads. The parish boundary here has a relative straightness. Indeed the straight line can be traced southwards to the northern parish boundary of Belton, with one slight kink. Projected northwards the line continues into the study area and is fossilised as Warren Lane. This continues to the north as a trackway to Cliff Farm. The most convincing evidence for the route is the co-axial arrangement of the large cropmark site flanking the postulated route. The terminus is remarkably close to the aforementioned Billystones ford site, the likely crossing point of the Derwentio road, and passes through the Iron Age and Romano-British scatter of LE 4721.

The cropmark (Pickering and Hartley; Clay 1985) and geophysical survey (Ripper and Butler 1999, 102) show an extensive site flanking the postulated road, comprising co-axial trackways and field boundaries. To the east there is a parallel track some 100m from the road line, partly defined by double pit alignments and/or ditches. There are *c.* 20 roundhouses in this area, but it is uncertain if they are contemporary or represent earlier settlement. The western side of the roadside settlement, recently revealed by geophysical survey, has many small enclosures that may represent paddocks. The dating evidence for the scheduled site is limited to Iron Age and Romano-British pottery recovered from the surface. However, to the west and south, evaluation trenches have provided Roman dates for associated features. The site would appear to extend further south beyond Ratcliffe Lane but the cropmark evidence is poor, possibly due to alluvial cover. Further geophysical survey of this area could prove fruitful.

Lockington villa (SAM 140), just east of the afore-mentioned settlement, comprises the well-defined cropmark site of a corridor villa within a trapezoidal enclosure with associated buildings and structures including two large barns (Frere and St. Joseph 1983; Clay 1985; Pickering and Hartley 1985). Fieldwalking survey across the villa complex produced pottery of 2nd-4th century date, while limited excavations by Deaney produced pottery of a similar date (Clay 1985). The cropmark indicates that the walls of the complex have been robbed of masonry.

A rectangular earthwork at Sawley (SAM 228) just to the east of the Derby-Sawley road 'terminus' has been claimed as a small fort (Todd 1968). The earthwork was investigated by the Derbyshire Archaeological Society revealing a near square enclosure of 0.61 ha with a possible western entrance, but secure dating evidence was not found (Deegan 1999). The SMR records that medieval pottery was recovered from a section, but there are no details. There are two other earthworks also in the study area, the Bull Ring (LE 4719), a small rectangular raised platform with a surrounding ditch and the raised platform of Cliff Farm. These are both interpreted as later features.

2.7 Anglo-Saxon

On place name evidence it is assumed that both Hemington and Lockington were established in the late Anglo-Saxon period. Early Anglo-Saxon settlement evidence is recorded from the environs at Willows Farm and Hemington Quarry, both in Castle Donington parish. Two post-built halls and a sunken featured building were excavated at Willows Farm (Coward and Ripper 1999) while at Hemington Quarry two small, post-built structures of sub-square plan were excavated (pers. obs.). An Early Anglo-Saxon pottery vessel from an associated pit provided the only dating evidence for the latter site. Small buildings of similar form were recorded at the large Anglo-Saxon site of Eye Kettleby, Leics. where the excavator interpreted them as bothies; they occurred away from the settlement areas, as defined by numerous post-built halls, within a craft-working area. It might be speculated that the Hemington Quarry structures were used for temporary occupations such as task-specific seasonal waterside activities such as fishing or withy harvesting.

Within the study area the evidence for Early Anglo-Saxon settlement is limited to a small number of sherds recovered by fieldwalking (LE4713). A small number of Early Anglo-Saxon sherds were reported from Red Hill (Palfreyman and Ebbins 2003) and a larger assemblage has also been recovered (N. Cooper, pers. comm.).

Anglo-Saxon exploitation of the river is well documented in the Middle Trent with fishweirs recorded at Colwick, Notts. and Hemington Quarry. At the latter some 46 fishweirs have been reported, although many of the observations were limited to fragments showing in the quarry faces. However, four recent examples were subject to more controlled excavation and have provided unique evidence for fishing methods and technologies in inland Britain (Cooper 2003). Radiocarbon dating of the fishweirs shows a chronological range from the 8th-12th century (Brown and Salisbury forthcoming; Cooper 2003).

It is quite likely that there would have been a crossing point of the Trent in the vicinity of the study area. Domesday mentions a ferry at the Weston estate, one of only two along the Trent. Several Saxon cross fragments have been located in the northern part of the original Hemington Quarry and it might be speculated that these were once way-place markers for a crossing point.

2.8 Medieval

The study area lies within the prime champion landscape of the Trent Valley. Much of the area to the south of the Trent comprises part of the open field system of Lockington, the settlement focus being off the floodplain to the south of the study area. Hartley (1984, map 2) has partly mapped the field system from cropmarks and earthworks of the ridge and furrow. To the north of the Trent is the parish of Sawley and the medieval core of the settlement lies within the study area but this is mainly covered by modern development.

The SMR has few records for the study area but there is great potential for archaeological remains in medieval palaeochannels of the Trent and Soar. The Lockington estate map of AD 1849 (LRO Ti/202/1) shows that the northeastern extent of the modern parish was originally part of Sawley, reflected in the name of Sawley Cliff Farm. The palaeochannel in this vicinity would appear to be an oxbow of the old Soar. The calendar of Patent Rolls for 1402 mentions an avulsion episode for the Trent between Sawley and Lockington (Clay and Salisbury 1990), but this probably relates to the Sawley loop.

Archaeological work at Hemington quarry has demonstrated the incredible potential for preserved riverine structures from this period and some discussion of this evidence aptly demonstrates such potential. An important bridge crossing along this stretch of the Trent was located at Hemington *c.* 1km to the west of the study area (Cooper *et al.* 1994; Cooper 2003). The crossing linked Derby and the north with Leicester and the site, effectively the major route now known as the A6. Three successive bridges were excavated at Hemington Quarry between 1993-8. The earliest was a timber bridge constructed in AD 1097 and partly rebuilt *c.* AD 1111, evidently due to severe flood damage. The bridge was superseded by another timber structure in the later 12th century that in turn was replaced by a large masonry bridge in AD 1240/1. Each was built slightly upstream of its predecessor, demonstrating the importance of the crossing location. Documentary and proxy archaeological evidence suggest that the bridge crossing was redundant by *c.* AD 1311/12 when the Wilne Ferry was established, near the site of the modern crossing at Cavendish Bridge (Courtney forthcoming; Cooper 2003). The Sawley Ferry was established in AD 1321, possibly also reflecting the loss of the Hemington bridge crossing (Cooper and Ripper forthcoming). This was probably located at the site of the modern crossing of Harrison Bridge, in the northwestern corner of the study area.

Another class of monument recorded at the quarry was the 'shoot'. Salisbury (1985) described surviving 18th century 'shoots' (from the waterman vernacular) along the Trent, these being bankside works of stone and timber designed to protect the banks from erosion (their name derived from the local waterman vernacular). Up to six examples of 'shoot' structures have been recorded from the right (Leicestershire) bank of the medieval channel (Cooper & Ripper 2000; 2001) several dated to the 1320s (R. Howard, pers. comm.). It is suggested that the shoots were near-contemporary measures to protect the eroding right bank of the medieval river. The associated channel was traced for almost 500m, showing evidence for dynamic bank erosion (clasts of anaerobic clay from silted palaeochannels) and deep scouring, cutting through Devensian gravels, occasionally into the Mercian mudstone below. The evident dynamism of the channel would seem to reflect the national picture of climatic downturn seen in the period 1310-30 when severe winters caused damage to bridges almost every year (Brown *et al.* 2001) and, as suggested above, probably destroyed Hemington Bridge III and led to channel avulsion.

Hemington Quarry has also revealed rare structural and artefactual evidence for inland fishing in the form of 46 fishweir structures, numerous anchor stones and several fish traps (Salisbury 1991; Cooper 2003). A large weir structure (HL12), possibly a 'fixed engine' fishery was associated with fish baskets up to 2m long (Cooper 2003). However, the structure bears some resemblance to the 12th century mill dam excavated in 1985 (Clay and Salisbury 1990). The apparent demise of fishweirs from the 12th century may reflect the changing use of the river with water mills exacting greater control over the river.

2.9 Post-medieval

The Lockington estate has been described as old enclosure by Nichols and the open field system was likely to have been enclosed between 1601 and 1607 (Beresford 1948, 109). Warren Farm probably dates to this period (Smith and Ripper 2000) but its early status is uncertain. The early 18th century saw major investment in the road networks and much of the medieval landscape of the study area was lost to the new turnpike routes and enclosure. The study area was traversed by several major routes at this time, the Derby-Leicester road (modern A6) and the Tamworth-Sawley road (B6540). By the 18th century the respective crossings for these routes were bridges, Cavendish Bridge (AD 1758) and Harrington Bridge (AD 1788) across the Trent, each being the site of earlier ford and ferry crossings. The river crossing at Ratcliffe on Soar remained a ford until the construction of the Kegworth to Nottingham road (A453).

The 18th century also saw the rapid development of water transport with works to make the Trent navigable in the early 18th century, followed by the Soar Navigation and the Erewash Canal later in the century. There was a customs house at Cavendish Bridge and, in the study area, associated wharf development at Sawley. By the 19th century the area had several farms including Lockington Grounds Farm, Warren Farm and Long Lane Farm and, in Sawley, Grounds Farm. Warren Farm was a fine example of a model farm and was fully recorded prior to demolition (Smith and Ripper 2000). This agricultural landscape remains but has been further impinged upon by modern transport (M1 motorway, A453, A50), development (Sawley Marina) and mineral extraction.

2.10 Geomorphology and the archaeological resource

The archaeological resource within the study area has been identified through consulting the SMR databases at Leicestershire and Nottingham County Councils. This SMR search creates a 'known' archaeological resource, containing data on the location, morphology and in some cases dating evidence, of the archaeology. Conversely, the study area also has an 'unknown' archaeological resource, which is comprised of the undiscovered archaeological artefacts and sites. The known archaeological resource has been identified due to the 'visibility' of the sites and artefacts to conventional methods of archaeological detection. Such site detection methods are principally air photography and fieldwalking.

The BGS drift geology map provides the basis for describing the relationship of the archaeology to the geomorphology, labelling one area of older Devensian terrace (terrace 2), with younger Holocene drift geology making up terrace 1 and the modern floodplain (Fig. 2.1). The archaeological resource can be plotted against the LiDAR last pulse DTM to investigate patterns of the archaeological resource related to the terrace sequence (Fig. 2.2). The archaeological resource is plotted by method of investigation and two clear trends come out from the data. The 'known' archaeological resource effectively clusters on terrace 2 (Devensian – Bronze Age). On terrace 1 (Neolithic – post medieval) and the modern floodplain there are six SMR entries, compared to nineteen entries on the much smaller area of terrace 2.

The method of identification highlights a second key trend. The greater number of SMR entries located on terrace 2 have been identified through three methods. Ten sites have been identified through cropmarks, seven sites from surface finds and two sites through excavation. This can be compared to the known archaeological resource within the Holocene deposits, which have identified two sites through earthworks, three sites from surface finds and only one from cropmarks.

The geomorphology of the terrace 2 deposits provides the explanation for the distribution of the known archaeological resource. The GPR investigations on terrace 2 have shown the terrace has a thin layer of

alluvium overlying deep gravels deposits. The shallow alluvium (circa 40cm and often less) has meant the archaeological resource contained within it is visible. Much of the alluvium covering the terrace 2 gravels is within the plough zone. Therefore, archaeological structures can affect plant growth, identifying archaeology as cropmarks. The ploughing action has also disturbed artefacts allowing identification through surface survey/field walking.

The known archaeological resource in the Holocene deposits consists of one human skull as a surface deposit (SMR number 4683, terrace 1) but it is thought to be a disturbed deposit from stream dredging. The one cropmark (SMR 22595) was identified through a spectral air borne scanner. The two earthworks include a possible Roman Fort on terrace 1, although the site is more probably a post medieval enclosure (SMR 4719) and also a post medieval farmstead (SMR 4716). Of potential significance is a pottery spread of Iron Age/Romano-British (SMR 4721) located on terrace 1.

The known archaeological resource can also be plotted by the period of each site (Fig. 2.3). The Devensian terrace has a diversity of prehistoric sites and find locations, such as the Lockington Villa complex (Fig. 2.4). Whilst the terrace 1 deposits do not have such a visible archaeological record there are reasons to expect that terrace 1 has a significant archaeological resource. Terrace 1 has an Iron Age/Roman pottery scatter located on it. A second site not listed on the SMR database is visible as a cropmark (Fig. 2.5). Although there has been no dating evidence on this site its morphology (a D shaped enclosure) does suggest a Late Iron Age/Roman date. These two sites are strong evidence for later prehistoric/Roman activity and possible settlement on Terrace 1.

The reasons for the apparent invisibility of the archaeological resource on terrace 1 relates to riverine erosion and alluvial deposition on the terrace. Major channels have eroded away substantial areas of terrace 1. In this process, areas of the archaeological resource will have been destroyed. Secondly, as shown through Fig. 2.4, some archaeology has been buried by alluvial deposition. For example the GPR transect T1T1 (Phase 1) showed the alluvial deposition from TIC5 that has partially buried the D shaped enclosure.

This process of alluvial deposition on terrace 1 was also discovered through the T1G1 survey (Phase 1), on a fragment of terrace 1 adjacent to a palaeochannel. In this instance over 1.4m of alluvial deposition was discovered before the terrace 1 gravels were discovered. The quarry transect (T1QT) also demonstrated that areas of terrace 1 will have substantial levels of alluvial deposition on top of the terrace gravels. Therefore, it is suggested that specific areas of terrace 1 will have a high archaeological potential dating back at least to the later prehistoric period, due burial and preservation under more recent alluvial deposition.

The archaeological potential on the modern floodplain is likely to be lower than terrace 1. Although the date range of the modern floodplain is not known, the level of alluvial deposition onto gravels was shown to be generally shallow (survey MFG1, Phase 1). Considering this factor plus the younger age of the modern floodplain compared to terrace 1 (although neither are dated) the archaeological potential is considered to be lower. However, this does not preclude the possibility of significant archaeological remains on the modern floodplain, giving that the age of the modern floodplain has not yet been absolutely dated.

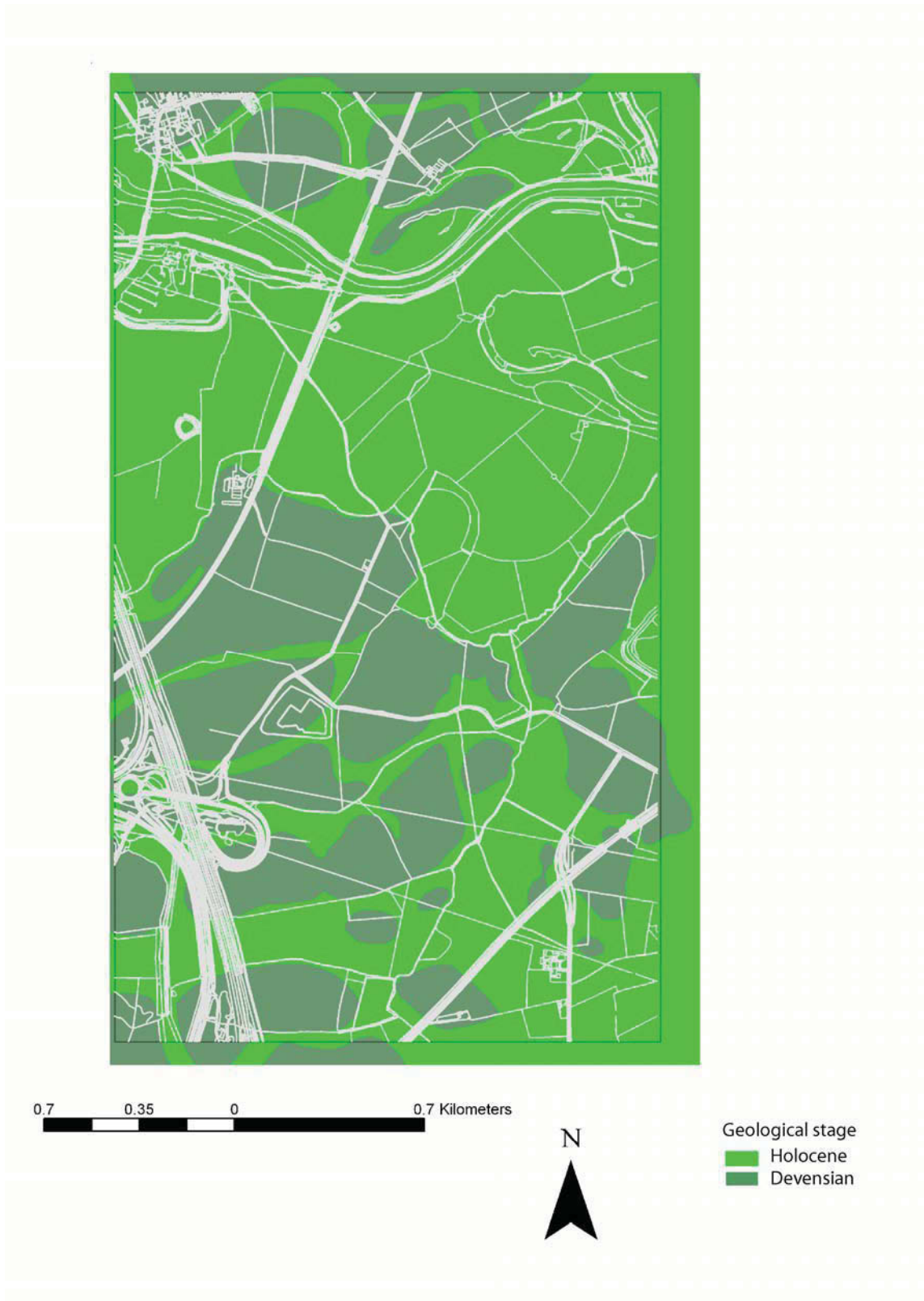


Fig 2.1: The study area mapped by geological stage.

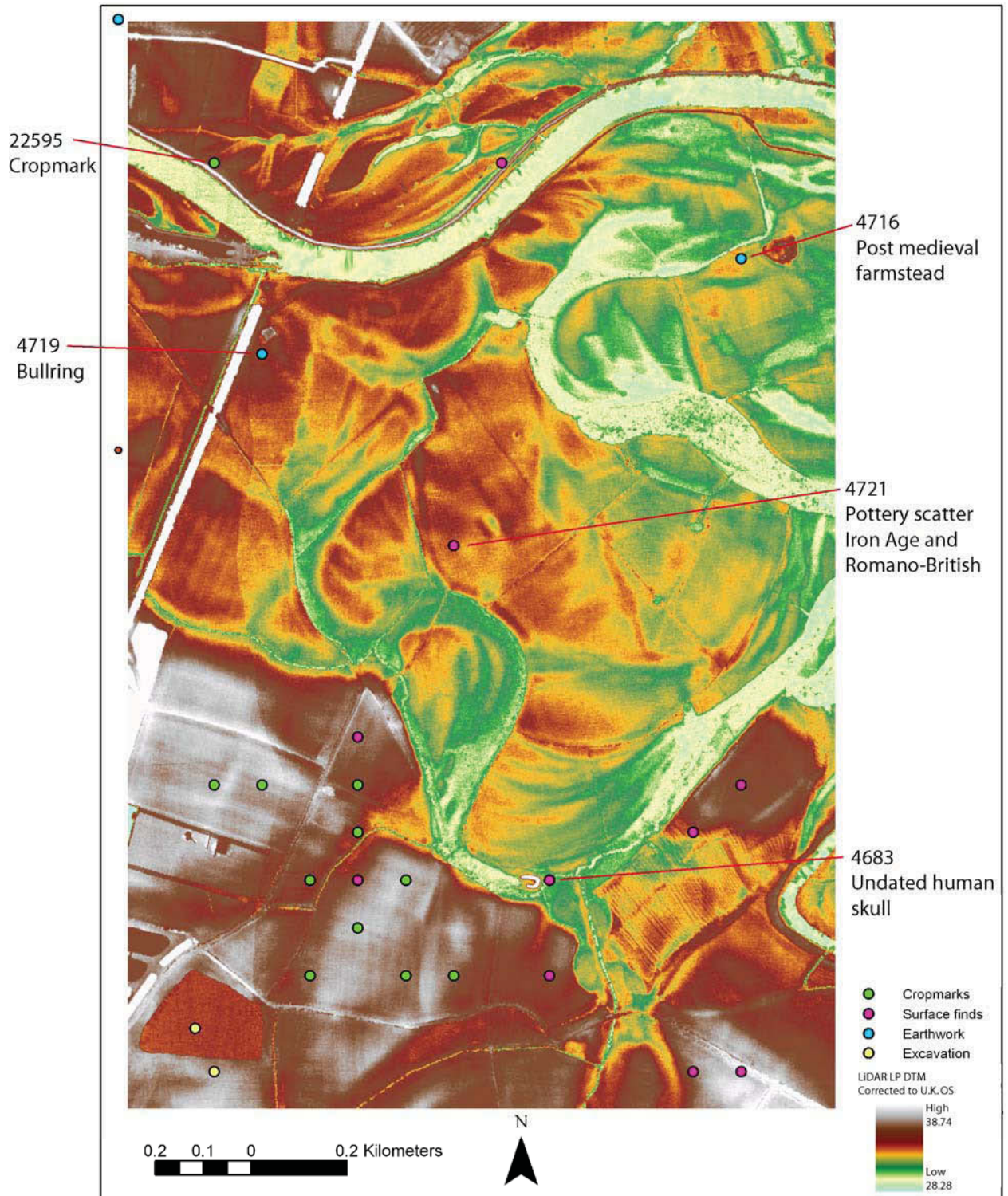


Fig 2.2: The archaeological resource plotted by its method of investigation, against the LiDAR last pulse DTM.

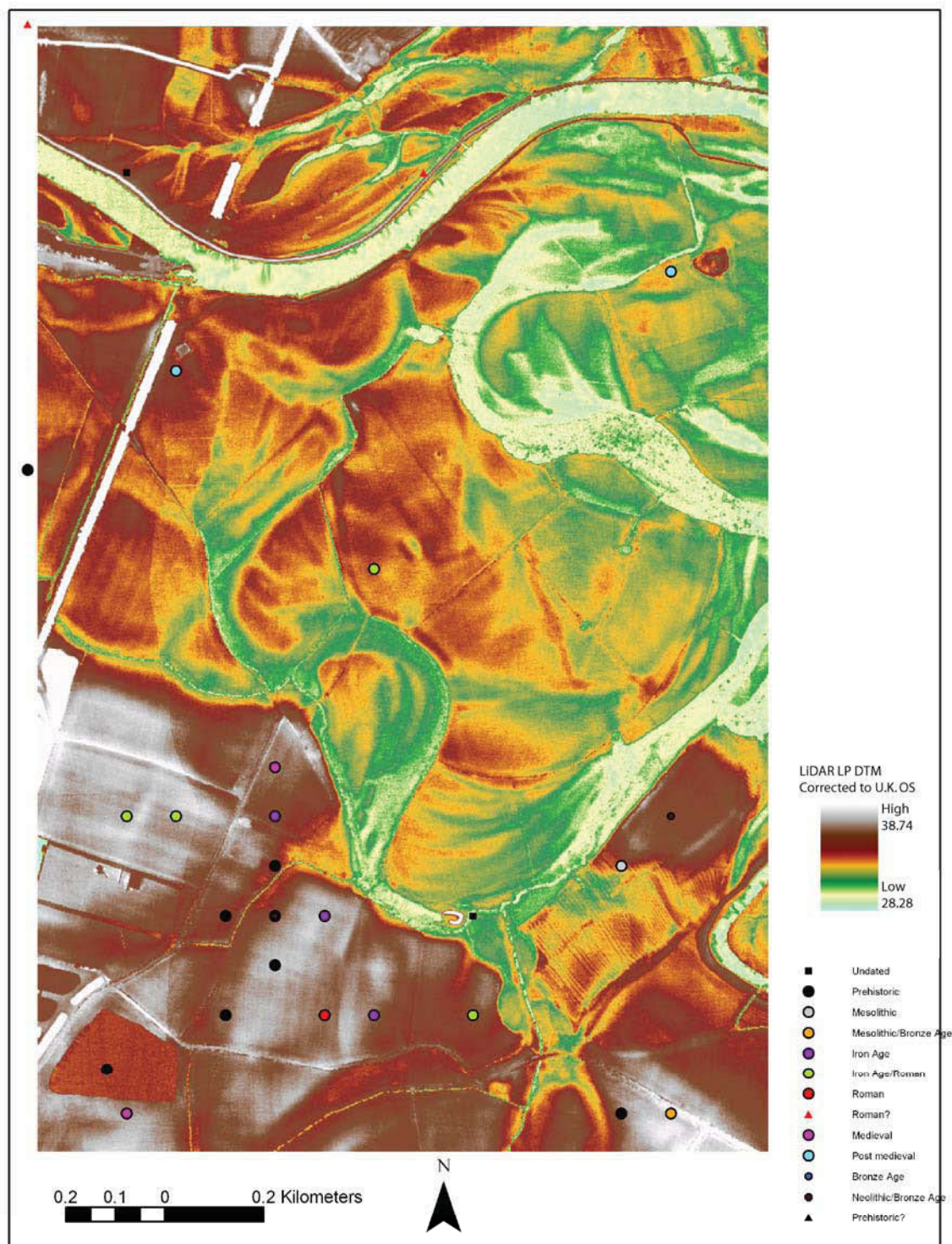


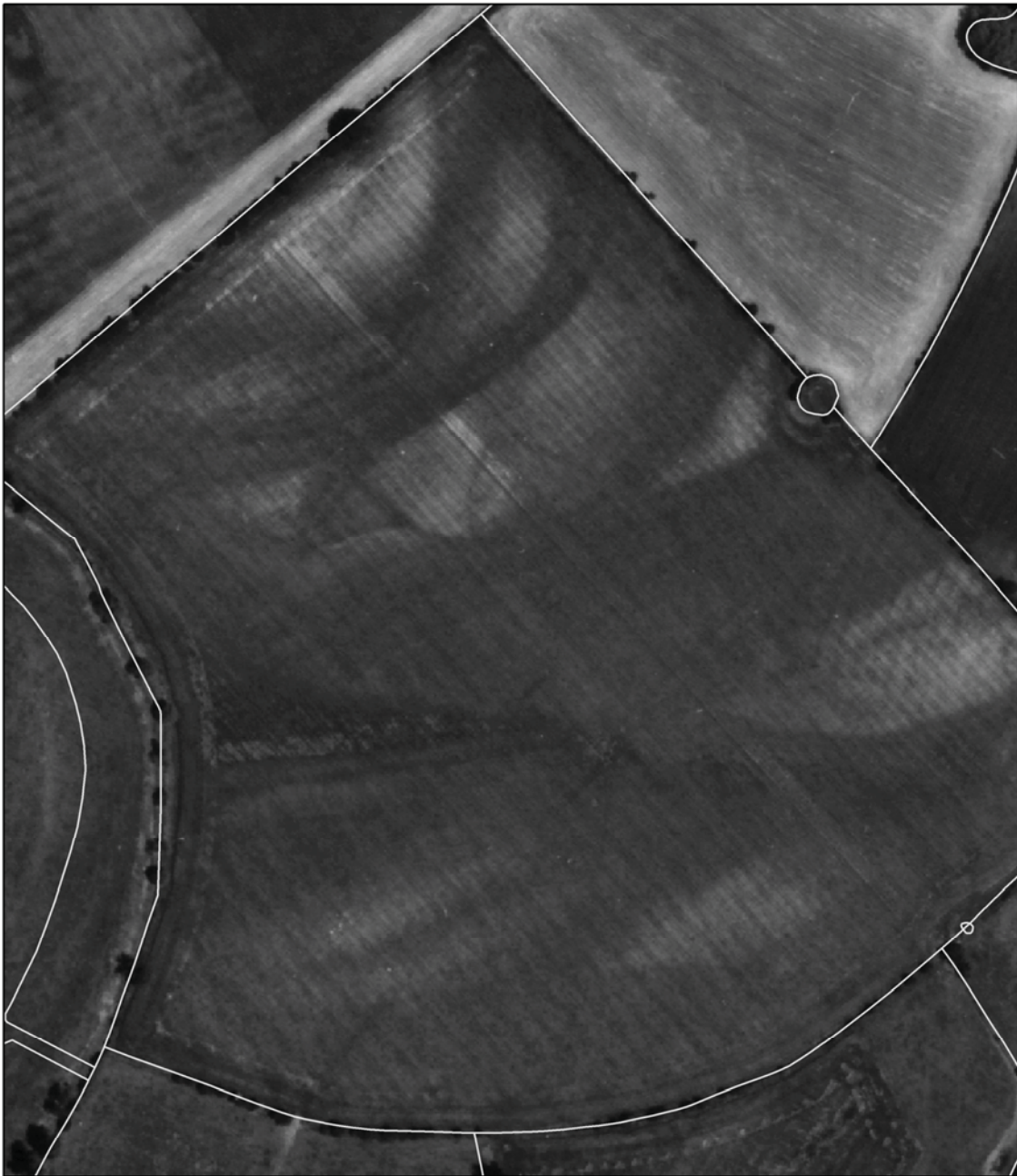
Fig 2.3: The archaeological resource plotted by period.



0.09 0.045 0 0.09 Kilometers



Fig 2.4: The 'Lockington Villa' complex within the study area. The complex contains a wealth of archaeological features, which are interpreted as dating from a range of periods, from the later prehistoric through to the Romano-British and possibly, post Romano-British periods. The complex is located on the Devensian terrace 2.



0.1 0.05 0 0.1 Kilometers



Fig 2.5: The cropmark enclosure on terrace 1. Although the enclosure is undated its morphology suggests a later prehistoric/early historic date.

2.11 Conclusions

The Trent-Derwent-Soar confluence zone, is an area with demonstrable, abundant archaeological remains from the Palaeolithic to the present while the study area encompasses significant known archaeological remains from the Mesolithic to present and great potential for remains as yet undiscovered. The cropmark evidence from the study area environs is very prolific on the terraces and new and old aerial photographs are a great resource. Indeed the present study has highlighted a number of new monuments in the study area and immediate environs including a possible pit circle, five ring ditches, a D-shaped enclosure, two pit alignments and other pre-medieval field boundaries. Further desk-based assessment has also proved fruitful in highlighting evidence for suspected Roman crossings of the Soar and Trent.

Previous geoarchaeological work in the environs has demonstrated the great mobility of the rivers in this confluence zone. This dynamism has undoubtedly truncated much archaeological evidence but has also been an agent of preservation, sealing sites under or within alluvium, such as the barrows mentioned above, and burying riverine sites within sand and gravel bars, most ably demonstrated by the discoveries at Hemington Quarry. The proximity of the latter site would suggest considerable potential for the preservation of multi-period archaeological remains within the study area.

One of the dominant themes to emerge from recent studies of the Trent Valley is the river as a physical and cultural boundary. While the river does, in a broad sense, delimit north and south, upland and lowland, possibly even different ethnic groups (Vince forthcoming), it also acts as a natural communications node along the waterways and through the valleys. The present study has presented some evidence for the importance of the study area as a central node in the regional communications network.

For the hunter-gatherers the zone would have been a crossing point for migrating animals and it is likely that the social and economic territories of the humans extended between upland and lowland. It is quite feasible that later prehistoric groups continued such movements in a transhumant economy (involving the annual migration of people with livestock). An appreciation of past communications and transport can be gained by examining the distribution of products and raw materials in the region. Loveday (2004) draws attention to the cluster of Charnwood Group XX axes around the Arbor Low henge environs. He has pointed to the 'exceptional potential' of the Middle Trent in understanding wider cultural and material connections in the Neolithic and Bronze Age. The ceremonial landscape of the study area and environs, in particular the cursus monuments, are seen to mediate these relations. Charnwood grano-diorite tempered pottery of Iron Age date has been widely recognised north of the Trent (Knight *et al.* 2003). In the Roman period Palfreyman and Ebbins (2003) have examined the role of the Red Hill site in the distribution of commodities and raw materials including iron, lead, coal, pottery, gypsum and salt. Similar distribution networks can be envisaged for the medieval period where there is a proliferation of markets around the Middle Trent. Courtney (forthcoming) has shown that the Trent was a very permeable barrier and that in the medieval and post-medieval period one would rarely have to travel over 2km to a crossing point. The major crossings such as Hemington, just outside the study area, formed part of the national infrastructure of roads while the Sawley crossing would have served these local markets and link to the larger network.

Chapter 3: Materials and methods

The materials and methods used within this study area are given, as are the standardised units and keys used in the sediment descriptions.

3.1 OSL sampling

Samples for OSL dating were collected using a Geoprobe coring rig (Fig. 3.1). After an area was selected that for dating, e.g. a block of terrace, a series of thin gouge cores were recorded to interpret the stratigraphy of the terrace and assess the basal sand unit for sample collection. If a basal sand lense of 20cm or greater was encountered then sample collection proceeded.

The Geoprobe was driven around the study area in a trailer hitched to a Landrover; meaning vehicular access was required to any sample location. The Geoprobe uses a closed chamber to collect sample cores. The chamber is 1.22m in length, with a plastic tube held inside that is 3cm in diameter (Fig. 3.2). The plastic tubes were made opaque through numerous coats of black paint applied to their exterior. A metal cutter is attached to the bottom of the collection chamber and the core is inserted into the ground. As much of the sampling as possible was done through pressure driving to minimise sample disturbance. However, hammer (percussion) drives had to be used in specific instance to get through high resistance sediment units.

Once the stratigraphy of the sample area had been ascertained a tube collected a depth to c. 25cm into the gravel body; e.g. if a 2.22m sequence to gravels was recorded the first 1.22m would be sample and discarded. A collection tube would then be inserted into the closed chamber and a second drive of 1.22m – 2.44m would be collected. This would allow the basal sands to be sampled in the tube and be capped by 22cm of gravel. The stratigraphy and depth to the basal sands was carefully noted on each sample tube. The ends were stopped and the tube was wrapped in silver foil to stop any post sampling light contamination.

3.1.1 *Optical dating: Mechanisms and principles*

Upon exposure to ionising radiation, electrons within the crystal lattice of insulating minerals are displaced from their atomic orbits. Whilst this dislocation is momentary for most electrons, a portion of charge is redistributed to meta-stable sites (traps) within the crystal lattice. In the absence of significant optical and thermal stimuli, this charge can be stored for extensive periods. The quantity of charge relocation and storage relates to the magnitude and period of irradiation. When the lattice is optically or thermally stimulated, charge is evicted from traps and may return to a vacant orbit position (hole). Upon recombination with a hole, an electron's energy can be dissipated in the form of light generating crystal luminescence providing a measure of dose absorption.

In this study quartz was segregated for dating. The utility of this minerogenic dosimeter lies in the stability of its datable signal over the mid to late Quaternary period, predicted through isothermal decay studies (e.g. Smith *et al.*, 1990; retention lifetime 630 Ma at 20°C) and evidenced by optical age estimates concordant with independent chronological controls (e.g. Murray and Olley, 2002) This stability is in contrast to the anomalous fading of comparable

signals commonly observed for other ubiquitous sedimentary minerals such as feldspar and zircon (Wintle, 1973; Templer, 1985; Spooner, 1993).

Optical age estimates of sedimentation (Huntley *et al.*, 1985) are premised upon reduction of the minerogenic time dependent signal (Optically Stimulated Luminescence, OSL) to zero through exposure to sunlight and, once buried, signal reformulation by absorption of litho- and cosmogenic radiation. The signal accumulated post burial acts as a dosimeter recording total dose absorption, converting to a chronometer by estimating the rate of dose absorption quantified through the assay of radioactivity in the surrounding lithology and streaming from the cosmos.

$$\text{Age} = \frac{\text{Mean Equivalent Dose (D}_e\text{, Gy)}}{\text{Mean Dose Rate (D}_r\text{, Gy.ka}^{-1}\text{)}}$$

Aitken (1998) and Bøtter-Jensen *et al.* (2003) offer a detailed review of optical dating.

3.1.2 Sample Collection and Preparation

Twenty one conventional sediment samples – those located within matrix-supported units composed predominantly of sand and silt - were collected within opaque plastic tubing from either sections by means of tubing (150x45 mm) forced into each face (samples GL06005 to GL06009) or from boreholes excavated by a Geoprobe (in tubing 1000x45 mm). Each sample location marked the deepest points of palaeochannels within the study area. Each tube was wrapped in cellophane and parcel tape in order to preserve moisture content and integrity until ready for laboratory preparation. To preclude optical erosion of the datable signal prior to measurement, all samples were prepared under controlled laboratory illumination provided by Encapsulite RB-10 (red) filters. To isolate that material potentially exposed to daylight during sampling or that which had been relocated by the process of coring, sediment located within the outer 5 mm of each sample was removed.

The remaining sample was dried and then sieved. Quartz within the fine sand (125-180 μm or 180-250 μm) fraction was then segregated. Samples were subjected to acid and alkali digestion (10% HCl, 15% H₂O₂) to attain removal of carbonate and organic components respectively.

A further acid digestion in HF (40%, 60 minutes) was used to etch the outer 10-15 μm layer affected by α radiation and degrade each samples' feldspar content. During HF treatment, continuous magnetic stirring was used to effect isotropic etching of grains. 10% HCl was then added to remove acid soluble fluorides. Each sample was dried, resieved and quartz isolated from the remaining heavy mineral fraction using a sodium polytungstate density separation at 2.68g.cm⁻³. Where sufficient datable mass existed, 24 multi-grain aliquots (c. 3-6 mg) of quartz from each sample were then mounted on aluminium discs to establish optimum, average measurement conditions for single grain aliquots. Around 2400 sand grains from each sample were located individually in 200 mm (diameter and depth) holes drilled as a 10x10 grid into anodised aluminium discs (Duller *et al.*, 1999) to gain a measure of inter-grain D_e distribution.

All drying was conducted at 40°C to prevent thermal erosion of the signal. All acids and alkalis were Analar grade. All dilutions (removing toxic-corrosive and non-minerogenic,

luminescence-bearing substances) were conducted with distilled water to prevent signal contamination by extraneous particles.

3.1.3 Acquisition and accuracy of D_e value

All minerals naturally exhibit marked inter-sample variability in luminescence per unit dose (sensitivity). Therefore, the estimation of D_e acquired since burial requires calibration of the natural signal using known amounts of laboratory dose. D_e values were quantified using a single-aliquot regenerative-dose (SAR) protocol (Murray and Wintle 2000; 2003) facilitated by a Risø TL-DA-15 irradiation-stimulation-detection system (Markey *et al.*, 1997; Bøtter-Jensen *et al.*, 1999; Duller *et al.*, 1999). Within this apparatus, optical signal stimulation of multi-grain aliquots was provided by an assembly of blue diodes (5 packs of 6 Nichia NSPB500S), filtered to 470 ± 80 nm conveying $15 \text{ mW}\cdot\text{cm}^{-2}$ using a 3 mm Schott GG420 positioned in front of each diode pack. Optical stimulation of single grain aliquots emanated from a focussed solid state 532 nm (green), 10 mW stabilised laser (Laser 2000 LCL-LCM-T-11ccs) scanned across grains by means of mirrors mounted on and moved by motorised linear stages. Infrared (IR) stimulation, provided by 6 IR diodes (Telefunken TSHA 6203) stimulating at 875 ± 80 nm delivering $\sim 5 \text{ mW}\cdot\text{cm}^{-2}$, was used to indicate the presence of contaminant feldspars (Duller, 2003). Stimulated photon emissions from quartz aliquots are in the ultraviolet (UV) range and were filtered from stimulating photons by 7.5 mm HOYA U-340 glass and detected by an EMI 9235QA photomultiplier fitted with a blue-green sensitive bialkali photocathode. Aliquot irradiation was conducted using a 1.48 GBq $^{90}\text{Sr}/^{90}\text{Y}$ β source calibrated for single and multi-grain aliquots of each isolated quartz fraction against the 'Hotspot 800' ^{60}Co γ source located at the National Physical Laboratory (NPL), UK. In calibrating single sand grain aliquots, no significant spatial variation in dose rate from the β source was found.

SAR by definition evaluates D_e through measuring the natural signal of a single aliquot and then regenerating that aliquot's signal by using known laboratory doses to enable calibration. For each aliquot, at least 4 different regenerative-doses were administered so as to image dose response. D_e values for each aliquot were then interpolated, and associated counting and fitting errors calculated, by way of exponential or exponential plus linear regression. The accuracy with which D_e equates to total absorbed dose and that dose absorbed since burial is assessed. The former can be considered a function of laboratory factors, the latter, one of environmental issues. Diagnostics were deployed to estimate the influence of these factors and criteria instituted to optimise the accuracy of D_e values.

3.1.4 Laboratory Factors

3.1.4.1 Feldspar contamination

The propensity of feldspar signals to fade and underestimate age, coupled with their higher sensitivity relative to quartz makes it imperative to quantify feldspar contamination. At room temperature, feldspars generate a signal (IRSL) upon exposure to IR whereas quartz does not. The signal from feldspars contributing to OSL can be depleted by prior exposure to IR. For all aliquots the contribution of any remaining feldspars was estimated from the OSL IR depletion ratio (Duller, 2003). If the addition to OSL by feldspars is insignificant, then the

repeat dose ratio of OSL to post-IR OSL should be statistically consistent with unity. Any aliquots that did not fulfil this criterion were rejected.

3.1.4.2 Preheating

Preheating aliquots between irradiation and optical stimulation is necessary to ensure comparability between natural and laboratory-induced signals. However, the multiple irradiation and preheating steps that are required to define single-aliquot regenerative-dose response leads to signal sensitisation, rendering calibration of the natural signal inaccurate. The SAR protocol (Murray and Wintle, 2000; 2003) enables this sensitisation to be monitored and corrected using a test dose, here set at c 5 Gy preheated to 220°C for 10s, to track signal sensitivity between irradiation-preheat steps. However, the accuracy of sensitisation correction for both natural and laboratory signals can be preheat dependent. Three diagnostics were used to assess the optimal preheat temperature for accurate correction and calibration.

Irradiation-preheat cycling quantifies the preheat dependence of sensitisation correction for laboratory-induced signals. If sensitisation is accurately corrected, then the same regenerative-dose should yield an equivalent sensitivity corrected value irrespective of the number of times it is applied and its associated signal measured. The ratio of subsequent to initial corrected regenerative-dose signals should be statistically concordant with unity. Alternatively, this ratio may differ from unity yet attain consistency after one or more cycles evidencing accurate sensitivity correction exists if the sample is primed by irradiation-preheat cycles. For this diagnostic, and where sufficient material was available, 18 multi-grain aliquots were divided into sets of 3 and assigned a 10 s preheat between 180°C and 280°C.

D_e preheat dependence quantifies the combined effects of thermal transfer and sensitisation on the natural signal. Insignificant adjustment in D_e values in response to differing preheats may reflect limited influence of these effects. Samples generating D_e values <10Gy and exhibiting a systematic, statistically significant adjustment in D_e value with increasing preheat temperature may indicate the presence of significant thermal transfer; in such instances low temperature (<220°C) preheats may provide the apposite measure of D_e . For this diagnostic, the D_e value of each of the same 18 multi-grain aliquots and their assigned preheat was assessed.

Dose Recovery attempts to replicate the above diagnostic, yet provide improved resolution of thermal effects through removal of variability induced by heterogeneous dose absorption in the environment, using a precise laboratory dose to simulate natural dose. The ratio between the applied dose and recovered D_e value should be statistically concordant with unity. For this diagnostic, a further 6 multi-grain aliquots were each assigned a 10 s preheat between 180°C and 280°C.

That preheat treatment fulfilling the criterion of accuracy for all three diagnostics was selected to refine the final D_e value for 2400 single grain aliquots. Further thermal treatments, prescribed by Murray and Wintle (2000; 2003), were applied to optimise accuracy and precision. Optical stimulation occurred at 125°C in order to minimise effects associated with photo-transferred thermoluminescence and maximise signal to noise ratios. Inter-cycle optical stimulation was conducted at 280°C to minimise recuperation.

3.4.1.3 Irradiation

Laboratory irradiation effects may evolve from the contrasting rates of natural dose exposure and the calibrating laboratory dose, the latter delivered to each aliquot at 9 orders of magnitude faster than the former. Bailey (2004) has suggested that for doses in excess of ~40 Gy an overestimation of age may arise due to competing mechanisms of signal accumulation within the crystal lattice of quartz. Only one sample (GL06009) generated single grain D_e values >40 Gy. These accounted for the minority of D_e values obtained for GL06009 and therefore laboratory irradiation effects were not considered significant in this study.

3.1.4.3 Internal consistency

Radial plots (Fig. 5; cf Galbraith, 1990) are used to illustrate inter-aliquot D_e variability for natural and regenerated signals. D_e values are standardised relative to the central D_e value (Galbraith *et al.*, 1999) for natural signals and applied dose for regenerated signals. D_e values are described as over dispersed when >5% lie beyond $\pm 2\sigma$ of the standardising value; resulting from a heterogeneous absorption of burial dose and/or response to the SAR protocol. Over dispersion for natural signals does not necessarily imply inaccuracy. However where over dispersion is observed for regenerated signals, the age estimate from that sample should be accepted tentatively.

3.1.5 *Environmental factors*

3.1.5.1 Incomplete zeroing

Post-burial OSL signals residual of pre-burial dose absorption can result where pre-burial sunlight exposure is limited in spectrum, intensity and/or period, leading to age overestimation. This effect is particularly acute for material eroded and redeposited sub-aqueously (Olley *et al.*, 1998, 1999; Wallinga, 2002) and exposed to a burial dose of <20 Gy (e.g. Olley *et al.*, 2004). It can have some influence in sub-aerial contexts but is rarely of consequence where aerial transport has occurred. Optical dating of dominantly Holocene fluvial sands within this study warrants that this environmental effect be addressed.

Within single-aliquot regenerative-dose optical dating there are two diagnostics of partial resetting (or bleaching); signal analysis (Agersnap-Larsen *et al.*, 2000; Bailey *et al.*, 2003) and inter-aliquot D_e distribution studies (Murray *et al.*, 1995).

Within this study the latter has been used, taking aliquots of single sand grains to quantify inter-grain D_e distribution. At present, it is contended that asymmetric inter-grain D_e distributions are symptomatic of partial bleaching and/or pedoturbation (Murray *et al.*, 1995; Olley *et al.*, 1999; Olley *et al.*, 2004; Bateman *et al.*, 2003). For partial bleaching at least, it is further contended that the D_e acquired during burial is located in the minimum region of such ranges. The Minimum Age Model (Galbraith and Laslett, 1993) is the most regularly applied statistical approach in quantifying the breadth of minimum dose regions. Olley *et al.* (2004) recommend this model for Holocene fluvial samples based upon its agreement with independent age controls for a number of samples. Yet such models have been found to underestimate post-burial D_e values owing to post depositional turbation (Roberts *et al.*,

1998) or as a product of a minority of outlying low D_e values (Rodnight, 2006). The Finite Mixture Model (Galbraith and Green, 1990) offers an alternative statistical method by which to compute the minimum dose region reflecting post-burial D_e . It identifies the number of dose components within an inter-grain D_e distribution along with the mean D_e and proportion of grains in each component. In the Finite Mixture Model each component is assumed to have an equivalent level of over dispersion (σ , herein set at 0.10; Jacobs et al., 2006; Rodnight et al., 2006). Rodnight et al. (2006) advocate use of the youngest component unless it comprises less than 10% of aliquots, whereupon the next youngest component is taken to reflect post-burial D_e . However, the mean and breadth of this minimum region in all models is the subject of current debate, as it is additionally influenced by heterogeneity in microdosimetry, variable inter-grain response to SAR and residual to post-burial signal ratios. The Central Age Model (Galbraith et al., 1999) assumes all inter-grain D_e variation is forced by spatial variations in dose rate and natural irradiation effects that can be accurately replicated by laboratory irradiation, and thus the mean D_e value coupled with the mean D_r value will generate an accurate age estimate of burial. At present, it is clear that age defined by the D_e interval delimited by the Minimum and Central Age Models will be accurate but have limited precision (Table 1). In this study, the Finite Mixture Model has been adopted to produce a more refined estimate of age (Table 1) based on the success of its implementation by Rodnight et al. (2006) in sediments equivalent in age and genus to those in this study.

3.1.5.2 Turbation

The accuracy of sedimentation ages can further be controlled by post-burial trans-strata grain movements forced by pedo- or cryoturbation. Berger (2003) contends pedogenesis prompts a reduction in the apparent sedimentation age of parent material through bioturbation and illuviation of younger material from above and/or by biological recycling and resetting of the datable signal of surface material. Berger (2003) proposes that the chronological products of this remobilisation are A-horizon age estimates reflecting the cessation of pedogenic activity, Bc/C-horizon ages delimiting the maximum age for the initiation of pedogenesis with estimates obtained from Bt-horizons providing an intermediate age ‘close to the age of cessation of soil development’. Singhvi et al. (2001), in contrast, suggest that B and C-horizons closely approximate the age of the parent material, the A-horizon, that of the ‘soil forming episode’. At present there is no post-sampling mechanism for the direct detection of and correction for post-burial sediment remobilisation. However, intervals of palaeosol evolution can be delimited by a maximum age derived from parent material and a minimum age obtained from a unit overlying the palaeosol. Pedogenic effects are not considered significant within this study owing to the lack of visible soil development. Inaccuracy forced by cryoturbation may be bidirectional, heaving older material upwards or drawing younger material downwards into the level to be dated. However, only one sample (GL06009) was retrieved from a section of sediments likely dating to the last glacial stage; no evidence was observed of cryogenic deformation.

3.1.6 Acquisition and accuracy of D_r value

Lithogenic D_r values were defined through measurement of U, Th and K radionuclide concentration and conversion of these quantities into β and γ D_r values. β contributions were estimated from sub-samples by Neutron Activation Analysis (NAA) delivered by Becquerel

Canada. γ dose rates were estimated for samples GL06005 to GL06009 from in situ NaI γ spectrometry. Where direct measurements of γ dose rate were not possible, laboratory-based Ge γ spectrometry was conducted on sub-samples composed of material at intervals within 300 mm above and below the centre of each sample within each core (weighted by relative γ contributions; Aitken, 1985). In situ measurements were conducted using an EG&G μ Nomad portable NaI γ spectrometer (calibrated using the block standards at RLHA, University of Oxford); these reduce uncertainty relating to potential heterogeneity in the γ dose field surrounding each sample. Laboratory-based γ spectrometry was conducted using an Ortec GEM-S high purity Ge coaxial detector system, calibrated using certified reference materials supplied by CANMET. Estimates of radionuclide concentration were converted into D_r values (Adamiec and Aitken, 1998), accounting for D_r modulation forced by grain size (Mejdahl, 1979) and present moisture content (Zimmerman, 1971). Cosmogenic D_r values are calculated on the basis of sample depth, geographical position and matrix density (Prescott and Hutton, 1994).

The spatiotemporal validity of D_r values can be considered as a function of five variables. Firstly, age estimates devoid of in situ γ spectrometry data should be accepted tentatively if the sampled unit is heterogeneous in texture or if the sample is located within 300 mm of strata consisting of differing texture and/or mineralogy. However, where samples are obtained throughout a vertical profile, consistent values of γD_r based solely on, for example, NAA may evidence the homogeneity of the γ field and hence accuracy of γD_r values. Secondly, disequilibrium can force temporal instability in U and Th emissions. In this study, the potential for long-term instability in D_r values forced by U disequilibrium has been considered. The impact of this infrequent phenomenon (Olley et al., 1996) upon age estimates is usually insignificant given their associated margins of error, however this effect is pronounced for at least two samples in this study (>50% disequilibrium between ^{238}U and ^{226}Ra , samples GL06014 & GL06025). Thirdly, pedogenically-induced variations in matrix composition of B and C-horizons, such as radionuclide and/or mineral remobilisation, may alter the rate of energy emission and/or absorption. If D_r is invariant through a dated profile and samples encompass primary parent material, then element mobility is likely limited in effect. In this study, there is limited evidence of pedogenesis in any unit sampled. Fourthly, spatiotemporal deviations from present moisture content are difficult to assess directly, requiring knowledge of the magnitude and timing of differing contents. However, the maximum influence of moisture content variations can be delimited by recalculating D_r for minimum (zero) and maximum (saturation) content. Finally, temporal alteration in the thickness of overburden alters cosmic D_r values. Cosmic D_r often forms a negligible portion of total D_r . It is possible to quantify the maximum influence of overburden flux by recalculating D_r for minimum (zero) and maximum (surface sample) cosmic D_r .

3.1.7 Estimation of Age

Age estimates provide an estimate of sediment burial period based on mean D_r values and D_e values derived from Minimum, Finite Mixture and Central Age Models, along with associated analytical uncertainties. Uncertainty in Finite Mixture age estimates is reported as a product of systematic and experimental errors, with the magnitude of experimental errors alone shown in parenthesis. Probability distributions indicate the inter-aliquot variability in age. The maximum influence of temporal variations in D_r forced by minima-maxima variation in moisture content and overburden thickness, coupled with Finite Mixture D_e

values. Where uncertainty in these parameters exists this age range may prove instructive, however the combined extremes represented should not be construed as preferred age estimates.

3.1.8 Analytical uncertainty

All errors are based upon analytical uncertainty and quoted at 1σ confidence. Error calculations account for the propagation of systematic and/or experimental (random) errors associated with D_e and D_f values.

For D_e values, systematic errors are confined to laboratory β source calibration. Uncertainty in this respect is that combined from the delivery of the calibrating γ dose (1.2%; NPL, pers. comm.), the conversion of this dose for SiO_2 using the respective mass energy-absorption coefficient (2%; Hubbell, 1982), reproducibility in laser positioning (3.5%; Truscott *et al.*, 2000) and experimental error, totalling 4.3%. Mass attenuation and bremsstrahlung losses during γ dose delivery are considered negligible. Experimental errors relate to D_e interpolation using sensitisation corrected dose responses. Natural and regenerated sensitisation corrected dose points (S_i) are quantified by,

$$S_i = (D_i - x.L_i) / (d_i - x.L_i)$$

Eq.1

where D_i = Natural or regenerated OSL, initial 0.2 s
 L_i = Background natural or regenerated OSL, final 5 s
 d_i = Test dose OSL, initial 0.2 s
 x = Scaling factor, 0.08

The error on each signal parameter is based on counting statistics, reflected by the square-root of measured values. The propagation of these errors within Eq. 1 generating σS_i follows the general formula given in Eq. 2. σS_i are then used to define fitting and interpolation errors within linear or exponential regressions (Green and Margerison, 1978; Ixaru *et al.*, 2004).

For D_f values, systematic errors accommodate uncertainty in radionuclide conversion factors (5%), β attenuation coefficients (5%), matrix density (0.20 g.cm^{-3}), vertical thickness of sampled section (specific to sample collection device), saturation moisture content (3%), moisture content attenuation (2%), burial moisture content (25% relative, unless direct evidence exists of the magnitude and period of differing content), NaI gamma spectrometer calibration (3%) and/or NAA (2%). Experimental errors are associated with radionuclide quantification for each sample by γ spectrometry and/or NAA.

The propagation of these errors through to age calculation is quantified using the expression,

$$\sigma_y (\delta y / \delta x) = (\sum ((\delta y / \delta x_n) \cdot \sigma_{x_n})^2)^{1/2}$$

Eq. 2

where y is a value equivalent to that function comprising terms x_n and where σ_y and σ_{x_n} are associated uncertainties.

Errors on age estimates based on the Finite Mixture Model are presented as combined systematic and experimental errors and experimental errors alone. The former (combined) error should be considered when comparing luminescence ages herein with independent chronometric controls. The latter assumes systematic errors are common to luminescence age estimates generated by means equal to those detailed herein and enable direct comparison with those estimates.

3.1.9 Intrinsic Assessment of Reliability

In this study, intrinsic assessment of reliability is restricted to analytical acceptability. Other indexes of reliability in Optical dating can be drawn by inference. Intra-site stratigraphic consistency of ages, quantified by Bayesian modelling, and the convergence of age estimates from stratigraphically equivalent units of divergent dosimetry are key intrinsic measures of reliability (Toms *et al.*, 2005). However, the low sampling density per dated level and ambiguity in inter-core relative stratigraphic position of samples precluded the use of these inferential methods.



Fig 3.1: The Geoprobe coring rig, about to commence a drive. The closed metal chamber is seen at the front of the rig, with a plastic sample collection tube located within it.



Fig 3.2: A sample recovered from the Geoprobe. The sample collection tube is shown coming out of the closed metal sampling chamber. The sample collection tubes used for OSL sampling were black opaque tubes.

3.2 Radiocarbon and pollen sample collection

A series of palaeochannels across the study area were selected for pollen sample collection and associated radiocarbon dating. Two strategies were employed to retrieve these samples: tin collection (Warren Farm Quarry) and gouge core collection (general study area). The location of all samples was recorded using differential GPS. The location of all the sample locations is given (Fig. 3.3).

3.2.1 Tin collection Warren Farm Quarry

The opportunity to record the exposed sections in Warren Farm Quarry, allowed a series of targeted samples to be collected. The location of the recorded sections and palaeochannels is given for the quarry (Fig. 3.4). The associated section drawings are also given, along with a photograph of each palaeochannel sampled (Fig 3.5 and 3.6).

Sampling used 50cm long, 10cm deep collection tins that were hammered into the sections. The tins were prized away from the section using a spade and immediately wrapped with cling film (to prevent water loss) and silver foil. The orientation and sample number was recorded on each tin. In total four palaeochannels within the quarry were selected for pollen assessment and are summarised as:

WFQ C1: 3 tins were recovered from the exposed palaeochannel, giving a total sample depth of 124cm (Figs 3.5 and 3.7).

WFQ C2: 3 tins were recovered from the exposed palaeochannel, giving a total sample depth of 1.23m (Figs. 3.5 and 3.8).

WFQ C3: 1 tin was recovered from the exposed palaeochannel, giving a sample depth of 50cm (Figs. 3.6 and 3.7).

WFQ C5: 1 tin was recovered from the exposed palaeochannel, giving a sample depth of 50cm (Fig. 3.6).

‘Bulk samples collected for Coleopteran evaluation were adjacent to the tin samples collected for pollen. Thus a depth of WQFC5 10cm, is the same for both pollen and Coleopteran evaluations’.

3.2.2 Gouge core sampling

A series of palaeochannels were sampled across the general study area for pollen. Assessment of suitable sampling locations had to be made using LiDAR, after the GPR proved ineffective at penetrating palaeochannel fills (Phase 1). Palaeochannels were initially cored using a thin 2cm gouge, to assess the sediment stratigraphy. After assessment either the section of palaeochannel was abandoned or sample collection proceeded using an 8cm diameter gouge core. Retrieved samples were wrapped in cling film and placed in plastic guttering lengths of 1m each. Sample labels and depths were recorded on each gutter before wrapping in silver foil.

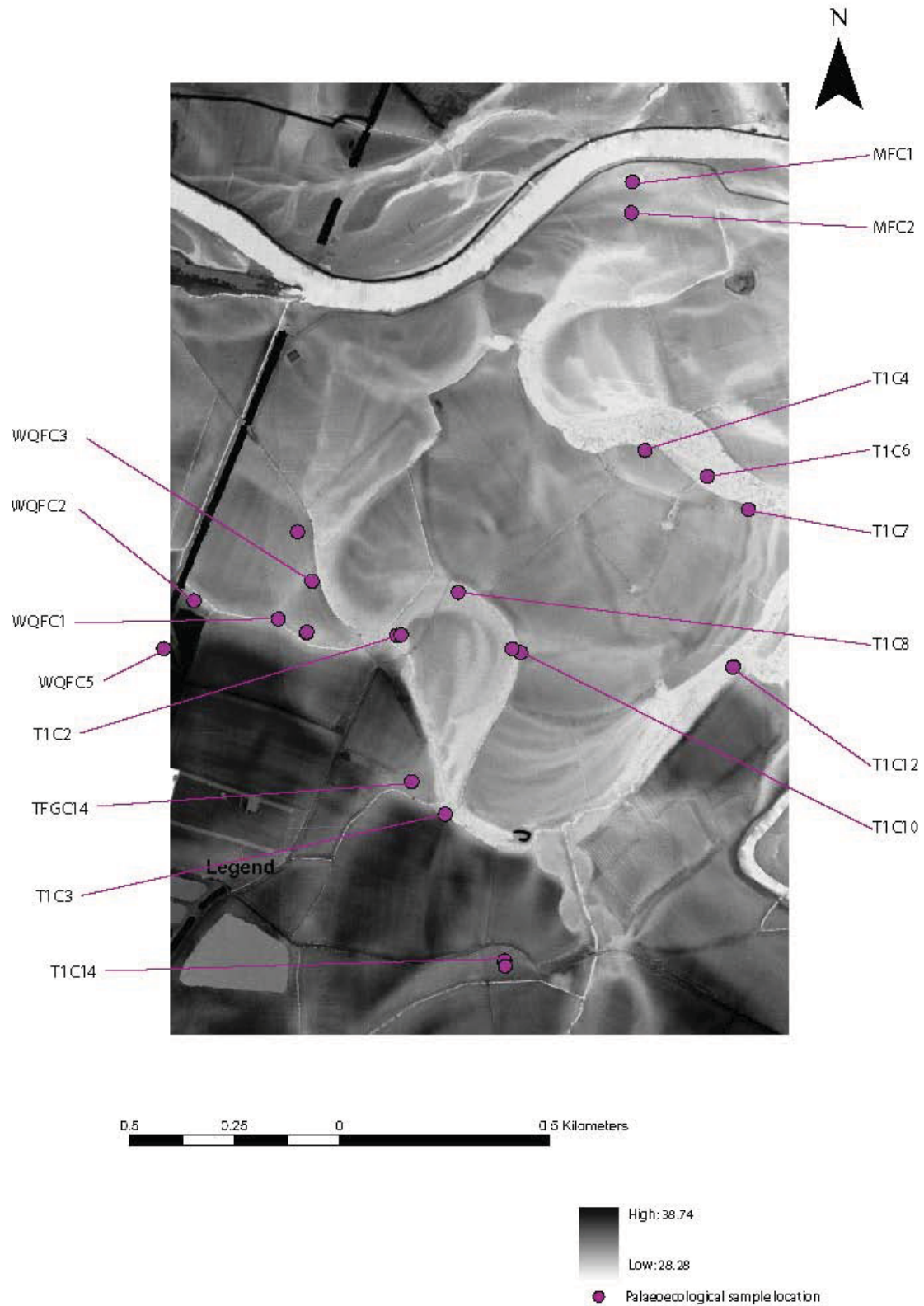


Fig 3.3: The locations of the palaeoenvironmental samples.

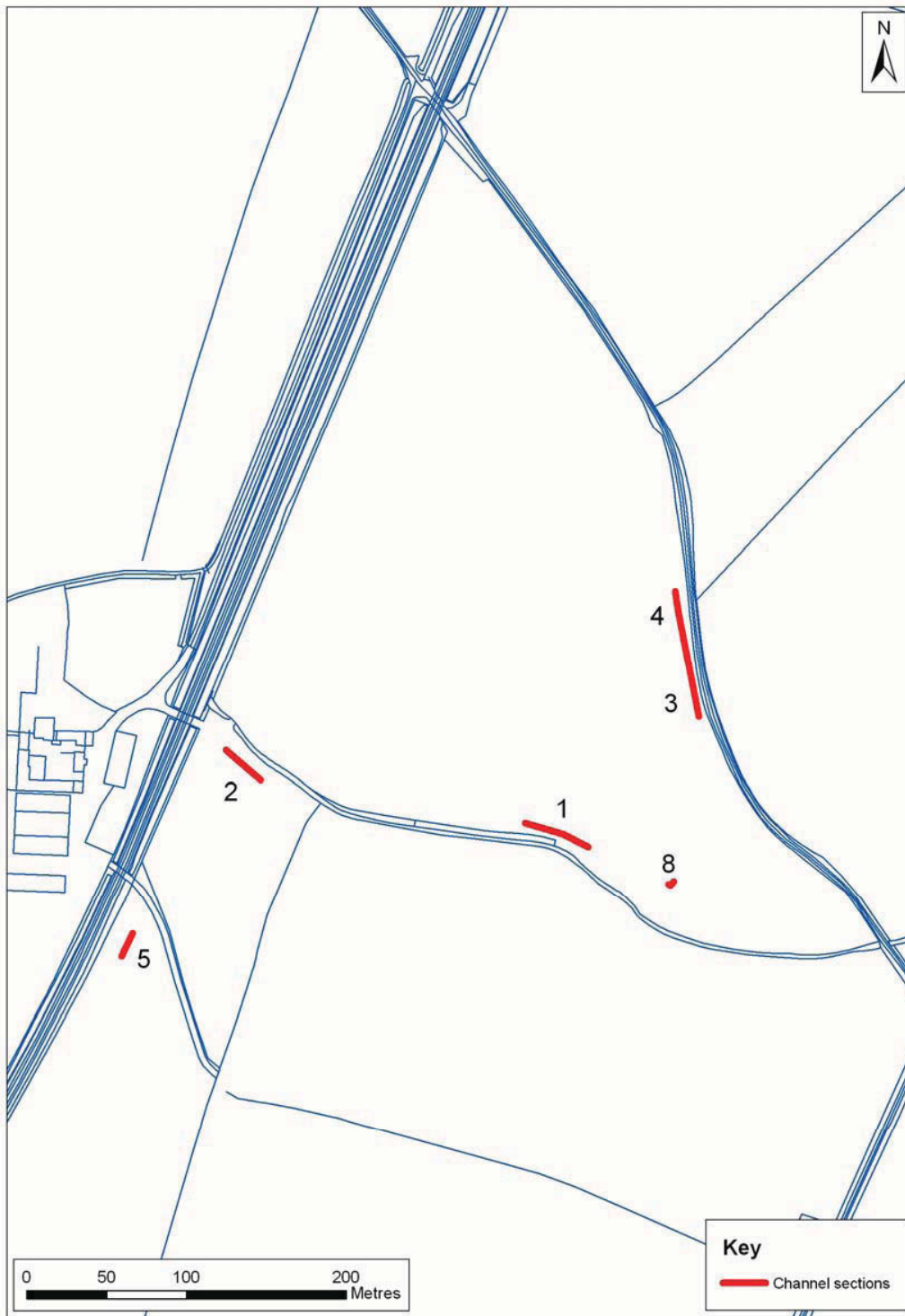
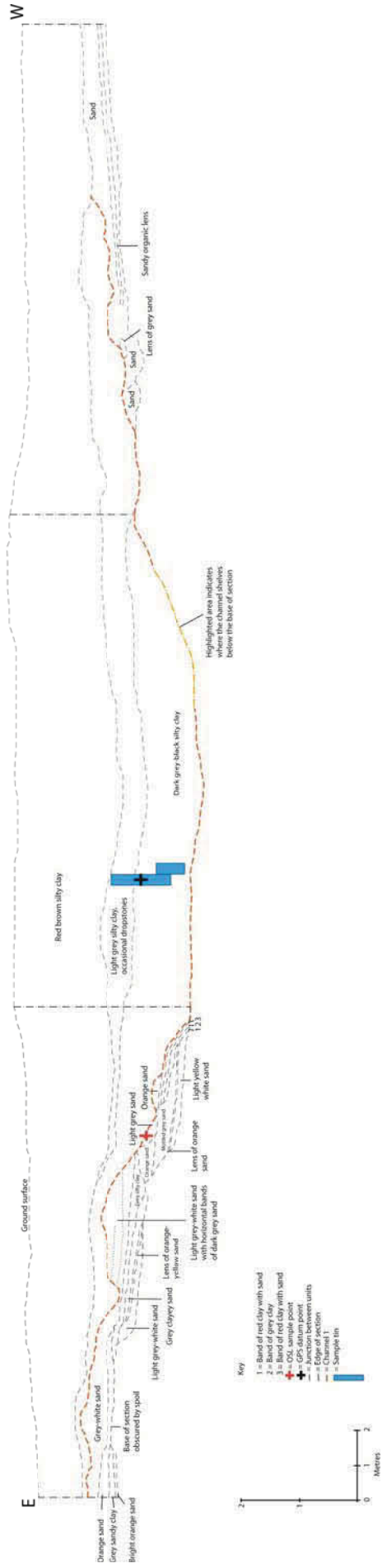


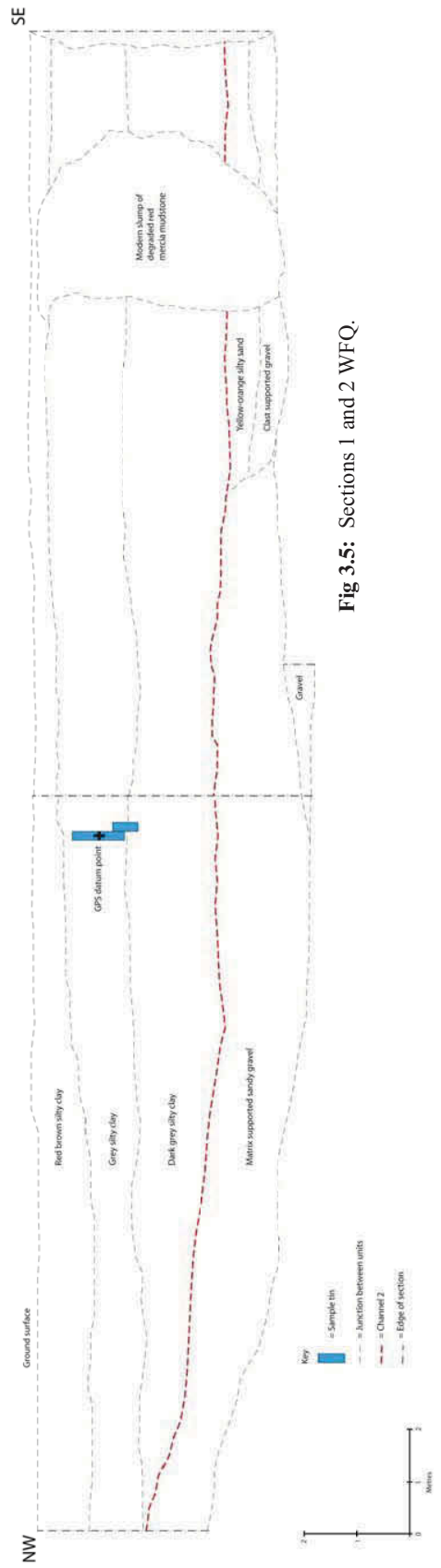
Fig 3.4: The location of the palaeochannels sampled in the quarry and the exposed section that were drawn.

Trent-Soar
Warren Farm Quarry
Channel 1
North facing section



- Key
- 1 = Band of red clay with sand
 - 2 = Band of grey clay
 - 3 = Band of red clay with sand
 - 4 = Junction between units
 - 5 = GPS datum point
 - 6 = Channel 1
 - 7 = Channel 2
 - 8 = Sample tin

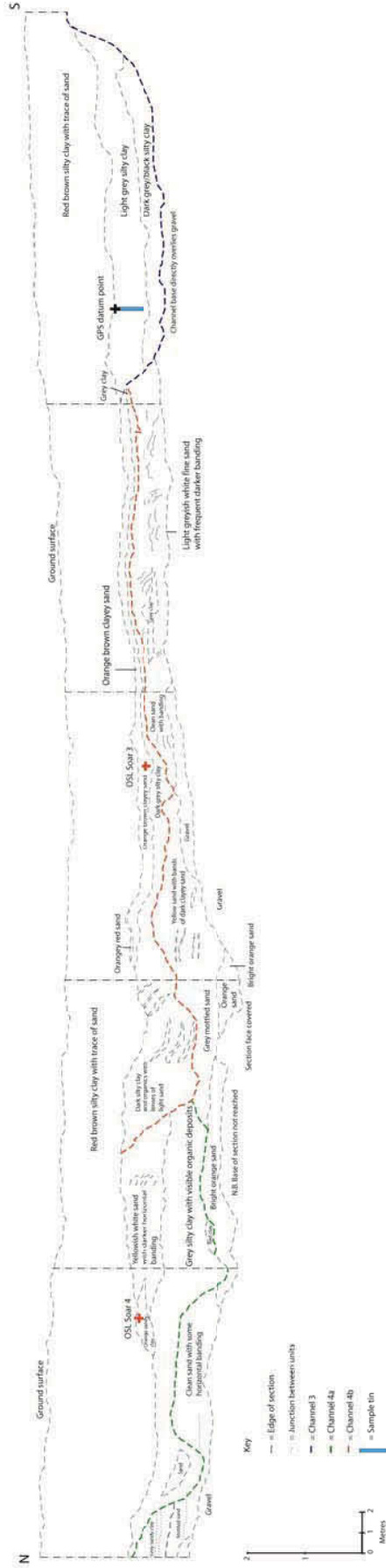
Trent-Soar
Warren Farm Quarry
Channel 2
Southwest facing section



- Key
- 9 = Sample tin
 - 10 = Junction between units
 - 11 = Channel 2
 - 12 = Edge of section

Fig 3.5: Sections 1 and 2 WFQ.

Trent-Soar
Warren Farm Quarry
Channels 3 and 4
West facing section



Trent-Soar
Warren Farm Quarry
Channel 5
Southeast facing section

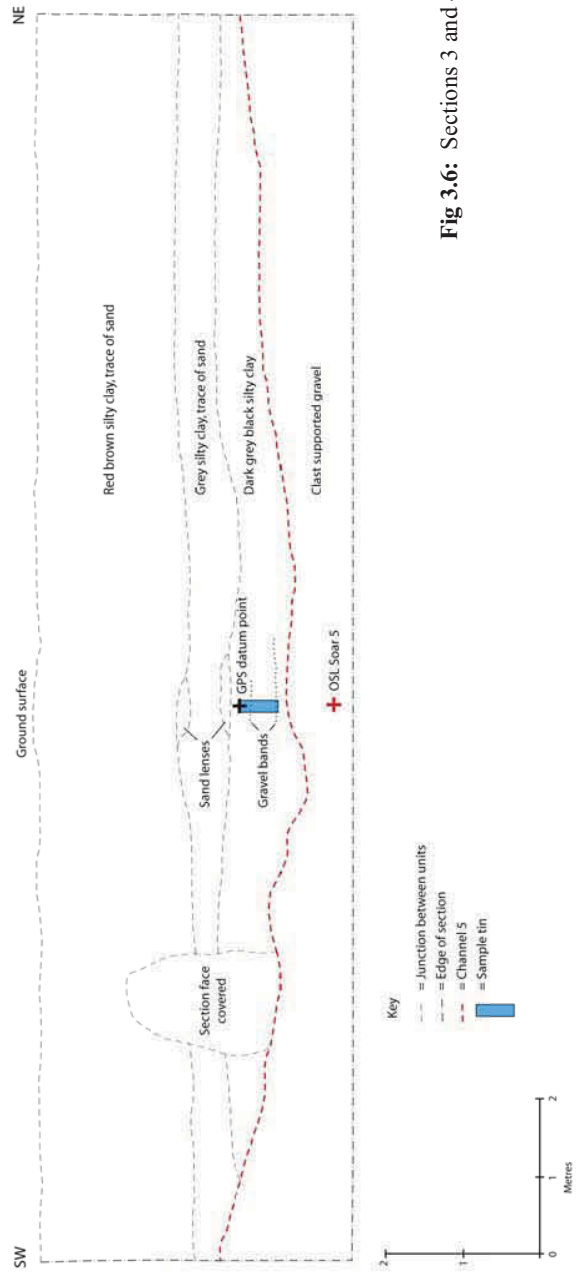


Fig 3.6: Sections 3 and 4 WFQ.



Fig 3.7: Palaeochannel WFQ C1 during sampling.



Fig 3.7: Palaeochannel WFQ C2 during sampling, with the tins *in-situ* before removal. The stratigraphy drawn in the section of red-brown silty clay above a grey silty clay, above a dark grey silty clay is clearly visible.



Fig 3.8: Palaeochannel WQFC3.

3.2.3 Pollen sample methods

Once back in the laboratory the cores and tins were cleaned back, removing material from their outer surfaces. All of the tins and specific cores were selected for detailed analysis. Pollen samples were collected at 14cm intervals, removed from the core/tin using a clean scalpel and spatula. The samples were placed in plastic bags in cold storage for sample digestion. Pollen and spore extraction used the standard chemical processing method using hydrofluoric acid digestion followed by acetolysis (Moore *et al.* 1991). Triple sieving was employed using 200 μ m and 70 μ m sieves. A standard volume was used of 1 ml of sediment. This chemical method was preferred over differential density separation (Takeshi 1998) as it is the most commonly used method and provides a standard reference with most published studies. Pollen concentrations were determined by the addition of *Lycopodium clavatum* tablets containing a known number of spores (Stockmarr, 1971). Pollen identification routinely used x 400 magnification with x 1000 magnification for small and difficult types with reference to standard keys (Andrew, 1984; Faegri and Iversen, 1989; Moore *et al.*, 1991) and the Exeter University Pollen and Spore reference collection. Pollen and spore nomenclature follows Bennett *et al.* (1994).

3.2.4 Radiocarbon sample methods

The collection of radiocarbon samples aimed to provide a basal date on all cores and tins. Cores and tins selected for pollen analysis had additional samples removed for radiocarbon dating at 50cm intervals. The removed sediment was placed in a 2mm

stainless steel sieve. Hot water was run over the sample to break up the soil matrix (mainly clay particulates) and reveal the organic matter. Organic samples were removed from the sieve using tweezers and placed in distilled water. This organic component was viewed under a light microscope to look at the integrity of the samples, for factors such as evidence of rolling, whether the sample is a rootlet that had penetrated from higher levels, etc, and for a basic identification. The best elements of the organic fraction were selected for dating and dried for several days at 50°C. A dry weight was then measured on this component. In cases where a sample did not provide sufficient organic material a second sample was selected. If this again failed to produce an organic component of sufficient quality a bulk sediment sample was used for RC dating.

A total of 37 samples were submitted for radiocarbon dating by Accelerator Mass Spectrometry (AMS), producing a total of 39 results, to the Oxford Radiocarbon Accelerator Unit (ORAU) and the Centre for Isotope Study, the University of Groningen, The Netherlands. These consisted of two waterlogged twigs, 19 Monocotyledon samples, and 15 sediment samples.

The samples submitted to ORAU were prepared according to methods given in Hedges *et al* (1989) and measured as described in Bronk Ramsey *et al* (2004). Those submitted to Groningen were processed and measured as described by Aerts-Bijma *et al* (1997; 2001) and van der Plicht *et al* (2000). Both laboratories maintain continual programmes of quality assurance procedures, in addition to participation in international inter-comparisons (Scott 2003). These tests indicate no laboratory offsets and demonstrate the validity of the measurements quoted.

The results are presented as conventional radiocarbon ages (Stuiver and Polach 1977), and are quoted in accordance with the international standard known as the Trondheim convention (Stuiver and Kra 1986). The calibrations of these results, relating the radiocarbon measurements directly to calendar dates, have been calculated using the calibration curve of Reimer *et al* (2004) and the computer program OxCal (v3.10) (Bronk Ramsey 1995; 1998; 2001). The calibrated date ranges for these samples are given in Table 1 and have been calculated using the maximum intercept method (Stuiver and Reimer 1986). They are quoted in the form recommended by Mook (1986), with the end points rounded outwards to 10 years. The graphical distributions of the calibrated dates, given in outline in Figures 1–4, are derived from the probability method (Stuiver and Reimer 1993).

3.2.4.1 Sampling

The dating of environmental cores and monoliths can present various problems, most of which can be investigated through a rigorous programme of radiocarbon dating and sample selection.

3.2.4.2 Macrofossils

Although macrofossils are now often preferred as samples from environmental cores, as they can be identified as short-lived material, care must be taken when they come from aqueous environments (*e.g.* fluvial, alluvial, estuarine, etc). In these instances there is some possibility that the macrofossils were in-washed. While in-washing is more likely to bring in material that is of an older, rather than younger, date, wet-dry cycles and invasive reeds, such as *Phragmites*, present the possibility of younger material being brought down through the sediment column. Because of these potential problems, the radiocarbon programme employed is one with consistency as its foremost aim.

Consistency can be demonstrated in two ways. The first is through good overall agreement between the radiocarbon measurements and the core sequence. The second is through the replication of results from a specific level in the core. The replication of results is why it is preferred to have two macrofossils submitted from any given level, it is also part of the reasoning behind dating multiple fractions of peats, soils, and sediment, which are dealt with in the next section. If the resultant measurements are statistically consistent (*i.e.* $T' < 3.8$, $v=1$) then it is probable that the two dates correctly date that level. When the two dates are not statistically consistent, the data need to be re-evaluated.

3.2.4.3 Sediment

The second type of material submitted for radiocarbon dating consisted of sediment. The dating of sediment and the reliability of the resultant dates from various fractions (*e.g.* humins, humic acids, etc) has been a topic of contention in the literature (see Blaauw *et al* 2004; Kilian *et al* 1995; 2000; and Shore *et al* 1995). The two most commonly dated fractions from these samples are the humins (*i.e.* alkali and acid insoluble organic detritus) and the humic acids (*i.e.* alkali soluble and acid insoluble matter). A third fraction that is sometime dated consists of the fulvic acids (*i.e.* the acid soluble fraction). Finally, if there is not enough available material to date the separate fractions then the bulk sediment can be dated (*i.e.* humin and humic fractions combined).

As the humin fraction is composed of the actual organic detritus, the resultant date from measuring this fraction is subject to many of the same processes that affect the dating of macrofossils in the same type of environment. Firstly, organic material that forms all or part of the humin fraction could be in-washed, which would result in a date that is too old. Contamination of this material by geological age carbon (*e.g.* coal, hard-water error) would have the same effect. The humin fraction can also be too young, if for example the environment is prone to wet-dry episodes or bioturbation, allowing intrusive material to work its way down the sediment column. Therefore, the humin fraction is not necessarily homogenous, and so it might be best to avoid dating this fraction by AMS as the smallest contamination would greatly affect the resultant measurement. Humins may better be dated through conventional radiocarbon dating techniques, as it is unlikely that a sufficient volume of such contamination would be present to bias such results significantly.

The second fraction that is often dated is the humic acids, which are the *in situ* products of plant decay. Although they are produced *in situ* and imply a stability to the ground surface, it has been shown that they can be mobile in groundwater, both vertically and horizontally (Shore *et al* 1995), but that their mobility is probably limited. Therefore, humic acids cannot be relied upon to always correctly date the level from which they were collected either. However, unlike the humin fraction, humic acids are homogenous, as they are alkali soluble, and therefore can be more reliably dated through AMS.

Fulvic acids are acid soluble and therefore can be suspended in a homogenous solution. Shore *et al* (1995) have shown that fulvic acids are nearly always the youngest fraction within a sediment profile. However, they also show that in a few cases they are by far the oldest of the three dated fractions at a level. They go on to suggest that this is likely due to the fact that fulvic acids are soluble in water and therefore are highly mobile, moving up and down with the water table and laterally within the subterranean drainage patterns.

In some cases, when there is not enough material for dating of separate fractions, the humic acid and humin fractions can be bulked together to provide an average date for all the organic material in that level. As stated earlier however, it is preferable to have the dates on the two fractions as this provides the data necessary for using replication as a measure of consistency. When the dates on two fractions are obtained, if they are statistically consistent, a weighted average can be taken before calibration as described in Ward and Wilson (1978). In most cases this creates a date that is more reliable. However, if the two results are not in agreement then the data need to be re-evaluated, in an attempt to determine which sample more reliably relates to the date of the level under consideration.

3.3 Dendrochronological dating

In total, 8 wood samples were collected for dendrochronological analysis from 6 large tree trunks recorded at Warren Farm Quarry, Lockington. The trees were interbedded within the sands and gravels, which on the basis of both geological geomorphological field mapping and analysis of LiDAR were assumed to be part of T1 (Hemington Terrace), aggraded during the mid Holocene. It is likely that all the tree trunks had been moved slightly during mineral extraction, though it appears from the available evidence that the majority were originally within 1-2m of the Mercia Mudstone rockhead. All the recorded trunks had intact root boles and none showed evidence for anthropogenic modification (e.g. tool marks), which suggests that they were incorporated into the channel through natural processes of riverbank erosion and tree throw on the floodplain. None of the sampled trunks were more than 50m apart. Samples were sent to the University of Nottingham for analysis.

3.4 Core stratigraphy, physical and chemical parameters

The palaeochannel cores and tins were subject to a rigorous scientific quantification of their physical and chemical parameters. The following parameters were measured:

3.4.1 Organic content

All cores and tins were sampled at 1cm contiguous samples along their entire length. Sediment from each sample was transferred to a labelled sample bag and freeze dried. After freeze drying samples were sieved in a 2mm stainless steel sieve. Crucibles were dried overnight at 109^oC to remove any excess moisture. The crucibles were weighed (a) and then approximately 1g of the ≤2mm soil fraction was added to each crucible. The crucibles were again dried overnight at 109^oC to remove any moisture from the sediment. The crucibles and samples were weighed (b) and then placed in a muffle furnace at 450^oC for 4 hours. The crucibles and soil sample were then weighed again (c). The % organic matter of the soil was then calculated using the formula:

$$\% \text{ Organic matter} = \frac{(a - c)}{(a - b)} * 100$$

3.4.2 Carbonate content

After the organic content had been burned off the samples, the crucibles were returned to the muffle furnace at 800^oC for a further hour. The crucibles were again weighed (d). The carbonate content of the sample was calculated through the formula:

$$\% \text{ carbonate content} = \frac{(c - d)}{(b - a)} * 100$$

3.4.3 Magnetic susceptibility

The magnetic susceptibility of the samples was measured through a Bartington MSII. A 10ml pot was then weighed (d), filled with the ≤2mm of sediment, then reweighed (e). The Bartington MSII was switched on for 30 minutes to warm up. Each sample was measured three times in the following sequence: Measurement of air (a), measurement of sample (b), measurement of air (c). The timing for each sample measurement was set at 30 seconds. The measurement of air samples allowed for the calibration of drift of the instrument.

From this data the average of the three readings was calculated for each sample via the calculation:

$$e - d = f$$

$$b1 - (a1 + c1) = g1$$

$$b2 - (a2 + c2) = g2$$

$$b3 - (a3 + c3) = g3$$

$$\frac{(g1 + g2 + g3)}{3} = h$$

$$\frac{h}{f} = \text{magnetic susceptibility units } (10^{-8} \text{m}^3 \text{Kg}^{-1})$$

3.4.4 *Eh*

The Eh of the samples was measured using an Alpha 500 contact probe. The instrument was switched on for 30 minutes to warm up. The contact probe was calibrated through immersion in a series of standard buffers at pH 4 and pH 7, whilst measuring the temperature of the buffer solution. Eh readings were made at 5cm intervals along the cores and tins through placing the probe into the sediment. The contact probe was washed thoroughly between readings. All Eh readings are given in millivolts.

3.4.5 *pH*

The pH of the samples was measured using an Alpha 500 contact probe. The instrument was switched on for 30 minutes to warm up. The contact probe was calibrated through immersion in a series of standard buffers at pH 4 and pH 7, whilst measuring the temperature of the buffer solution. pH readings were made at 5cm intervals along the cores and tins through placing the probe into the sediment. The contact probe was washed thoroughly between readings.

3.4.6 *Geochemistry*

Approximately 2g of the freeze dried $\leq 2\text{mm}$ fraction of sediment was accurately measured into a 100ml beaker. Three ml of concentrated Nitric Acid is added and the beakers warmed to dryness on a hotplate. The samples are removed and a further 3ml of concentrated Nitric Acid and 0.5ml of concentrated Hydrochloric Acid is added. The samples are replaced onto a hotplate and removed on the appearance of brown nitrous oxide fumes.

The contents of the beakers were transferred to centrifuge tubes using distilled water and the tubes were centrifuged for 20 minutes at 2500 rpm. The supernatants were transferred into 25ml volumetric flasks, and the beakers were cleaned again with distilled water and the contents removed to the centrifuge tubes, which were then centrifuged at 2500 rpm for a further 20 minutes. The supernatants were added to the 25ml volumetric flasks and the pellets from the tubes discarded. The volumetric flasks were made up to 25ml using distilled water and the samples transferred to 30ml plastic labelled sample tubes. The concentration of the element cat-ions was made through Inductively Coupled Plasma Mass Spectrometry (Thermo elemental X Series). Each sample had its concentration measured 3 times and an average produced of the results. The average concentration for each element on each sample was converted to mg/Kg, though dividing the concentration by the sample mass.

3.4.7 Grain size

From the freeze dried ≤ 2 mm fraction between 2 – 10g (depending on estimated sand content) was accurately weighed into a clean dry beaker. The soil is dried overnight at 90°C. and then re-weighed to give the oven-dry weight. 10 ml of water is added to each sample with 5 ml of the hydrogen peroxide. 4. After 2 – 3 hours a further 5 ml of hydrogen peroxide is added and the sample allowed to stand overnight. The beakers were warmed on a hotplate (starting at 80°C and gradually increasing the temperature to 100°C) until the reaction is complete and there is a clear supernatant above the sample.

The beaker contents were carefully transferred to a weighed centrifuge tube, using a policeman rod to clean the sides of the beaker. The tubes are centrifuged at 2500 rpm for 1 hour. The centrifuge tube is dried overnight at 90°C before being reweighed. Approximately 30 ml of the 0.4% sodium hexametaphosphate solution are added to each tube and initially disaggregated with a spatula. The soil suspension is screened through a 63µm sieve collecting the screened fraction in a 125 ml bottle. The centrifuge tube is washed with a small amount of the sodium hexametaphosphate and this is also passed through the sieve. The residue (>63 µm or >1000 µm) and centrifuge tube were then washed with water, passing the washings through the sieve. The residue on that sieve was then washed until no more fines are washed through and all the sodium hexametaphosphate has been washed away. The residue is washed into a weighed dry 60 ml bottle with distilled water and dried overnight. This is then reweighed (and stored for sand fractionation if >63 µm). The screened suspension was placed in an ultrasonic bath where it is treated for 5 minutes before being run on the MasterSizer (<63 µm) or Digisizer (<1000 µm).

3.4.8 *Tin/core sediment stratigraphy*

In addition to the quantification of the various chemical and physical parameters, selected cores/tins were subject to a qualitative assessment of their sediment stratigraphy. After cleaning each core had its stratigraphy recorded along its length. The recording of each sediment unit involved measuring its length, describing its composition in a subjective manner, e.g. a blue grey silty clay with a trace of sand, and also in a more objective way using the Troel Smith key, noting attributes such as elasticity, degree of stratification, etc. The colour of each sediment unit was recorded on a Munsel chart. This stratigraphic description was then drawn on scaled paper and scanned into Adobe Illustrator, so the core/tin stratigraphy could be viewed against graphs physical/chemical parameters.

3.4.9 *Data ordering and analysis methods*

All of the numeric data, e.g. organic content values, were entered into Excel spreadsheets, recorded by core/tin. Limited data analysis and graph production took place within the statistical analysis package SPSS.

3.5 Pollen and Spores Assessment

This sub-project was part of the palaeoenvironmental evaluation specified in the Phase II PD (Brown *et al.* 2004) which stated “Palaeoenvironmental analysis will include determination of routine sedimentary characteristics (organic and CaCO₃ content), analysis for pollen, spores and coleoptera which can provide details of the channel conditions, degree of canopy closure, the presence of grazing animals and other indicators of human presence.” This aimed to provide a systematic evaluation of the differential preservation of pollen and spores in this typical area of exploitable floodplain aggregate.

Samples were taken from a spectrum of cores from palaeochannels chosen to represent the variation in age, position and environmental conditions within the study area. A list of the cores (Tab 3.1) and their locations are shown (Fig. 3.3).

Core Number	Total depth (m)	No. of samples	Estimated Age based on chrono-stratigraphic model	Determined age (base) Cal BC/AD Oldest used	Environment
MFC2		13	Post Medieval	800-510 BC	Low swale-like palaeochannel, below watertable, regularly flooded
T1C7	2.25	16	Late Prehistoric	840-780 BC	Large Soar palaeochannel in the middle of the regularly flooded area, under woodland, watertable maintained high as SSSI site
T1C12	2.14	13	Late Prehistoric	AD 890-1120	Large Soar palaeochannel in the middle of the regularly flooded area, under woodland, watertable maintained high as SSSI site
T1C10	1.88	13	Late Prehistoric	3030-2890 BC	Palaeochannel of the Soar at the edge of the modern floodplain and the regularly flooded, under grassland
TFGC14 (GCTF14)	3.8	9	Early-Mid Holocene	3640-3370 BC	Edge of the modern floodplain but associated with a channel crossing from low terrace into modern floodplain, under grassland
T1C14	0.9	6	Early-Mid Holocene	1390-1120 BC	Palaeochannel on low terrace
WFQC1 +	0.5	4	Early-Mid Holocene	1940-1740 BC	Warren Farm Quarry exposed palaeochannel on low terrace, at top of gravels
WFQCH1	0.74	2	Early-Mid Holocene	1940-1740 BC	Warren Farm Quarry exposed palaeochannel on low terrace, at top of gravels
WFQC2M1	0.5	4	Early-Mid Holocene	1060-890 BC	Warren Farm Quarry exposed palaeochannel on low terrace, at top of gravels
WFQC2M2	0.5	4	Early-Mid Holocene	1060-890 BC	Warren Farm Quarry exposed palaeochannel on low terrace, at top of gravels

WFQCH2M3	0.5	4	Early-Mid Holocene	1060-890 BC	Warren Farm Quarry exposed palaeochannel on low terrace, at top of gravels
WFQC3	0.5	4	Early-Mid Holocene	2860-2490 BC	Warren Farm Quarry exposed palaeochannel on low terrace, at top of gravels
WFQ5	0.5	4	Devensian	14980-14180 BC	Warren Farm Quarry exposed palaeochannel within terrace gravels, most southerly of all sample locations

Tab 3.1: Sites used for environmental sampling with number of pollen samples taken for assessment.

Of particular interest in this study was the concentration and preservation of the pollen and spores. There is a large literature on pollen and spore taphonomy and several different grain classification schemes. A discussion of this research can be found in Tinsley (2004) which is based upon a similar study of the pollen preservation in the Somerset levels as part of the Monuments at Risk in Somerset Project (MARISP) and a study of the effects of peat wastage in the Somerset Levels by Brown *et. al* (2003). Pollen preservation was recorded using a three fold classification adapted from Delcourt and Delcourt (1980); corroded, degraded and mechanically damaged. Where more than one form of degradation was present only the most developed was recorded. The results were condensed to pollen concentration, % unidentified and % degraded which included a summation of the Delcourt and Delcourt (1980) categories (section 6.2).

3.6 Coleopteran Assessment

The variability in sediment architecture and often complex depositional regime of alluvial deposits necessitates a sampling strategy that considers both the archaeological and environmental development of the site. With this in mind, a ‘complete’ sampling strategy was adopted at Warren’s Farm Quarry, when recovering material for palaeoenvironmental analysis. Bulk samples (for insects) were recovered from sediments adjacent to samples collected for pollen analysis, recording the stratigraphy of the deposit locations, with the bulk sample areas being surveyed using differential GPS onto site datums. The aim was to provide a full, high resolution, environmental record at a site-specific level and elucidate *in-situ* environmental conditions during the period of alluviation and deposit formation.

Samples for palaeontomological analysis were recovered from a series of seven palaeochannels in and around the quarry at Warren’s Farm (Table 3.1). Sampling methods follow those recommended by Kenward (1978a, 1978b) and Kenward *et al.* (1980). Bulk samples of 10l were recovered from exposed palaeochannels WFQ1, 2, 3, 4, 5, and 6 within the quarry. The material was sampled at 10cm intervals from organic rich deposits overlain by sands and gravels or alluvium. Smaller samples, <500ml were also recovered from organic rich deposits using a manual auger from TFGC14 in approximately 20cm spits.

A further series of samples (Tab. 3.1), were extracted from palaeoecological cores in order to establish, if any, differential preservation of the insect remains between various palaeochannels across the study area. Bulk samples collected for Coleopteran evaluation were adjacent to the tin samples collected for pollen. Thus a depth of WQFC5 10cm, is the same for both pollen and Coleopteran evaluations.

3.6.1 Processing and Identification

The samples were processed using the standard method of paraffin flotation (Kenward *et al.* 1980, Coope and Osborne 1968). Preparation of samples for palaeoentomological analysis within the laboratory is a three-fold process. The final analysis of this material follows a series of guidelines developed, refined and disseminated over the past thirty years by Harry Kenward (e.g. 1974, 1975, 1976, 1978a, 1978b, 1982; Hall & Kenward 1990, Kenward & Hall 1995, 1997) and Mark Robinson (1981, 1983, 1993).

3.6.1.1 The Paraffin Flotation Technique

7kg/10l of each sample was placed in 15 litre plastic buckets and hot tap water was applied, where possible the material was left to soak overnight to facilitate disaggregation prior to sieving. A small amount of the sample was placed in a 300µm mesh sieve and hot tap water (40-50°C) was applied to remove the minerogenic matrix.

When washing was completed, the remaining organic detritus was allowed to drain in sieves for one hour. The sample was then returned to a clean bucket and the sample was covered with enough paraffin to produce a slurry when the paraffin was thoroughly incorporated. The material was allowed to stand for a few moments to allow the paraffin covered chitinous insect remains to float freely from the organic detritus, which are concentrated within the floating paraffin.

Fast flowing cold water was then added to the bucket, and the contents left to stand for one hour. The top twenty centimetres of the paraffin/water mixture were then poured through a clean 300µm mesh sieve. The process was repeated a total of three times at fifteen minute intervals, each time the bucket was refilled with cold water and the organic material stirred well. For the final pour, as much of the fluid was poured away as possible, before the residue in the base of the bucket is also poured into the sieve. The sample was then cleaned with domestic detergent to remove traces of paraffin from the flots. The sieve was then rinsed thoroughly until all traces of the detergent were removed. Finally, the flots were stored in airtight containers, with ethanol, to retard decomposition.

3.6.1.1 Sorting and Identification

The insect remains were then sorted from the paraffin flot and the sclerites identified under a low power binocular microscope at x10 magnification. Where possible, the insect remains were identified by comparison with specimens in the Gorham and Girling collections housed at the University of Birmingham. The taxonomy used for the Coleoptera (beetles) follows that of Lucht (1987).

3.6.2 The objective analysis, quantification and presentation of palaeoentomology as an environmental indicator

The remains of a wide variety of insects such as caddis flies (Order: Trichoptera), dragonflies (Order: Odonata), non-biting midges (Order: Diptera; Family: Chironimidae) and beetles (Order: Coleoptera) may be employed as palaeoenvironmental indicators. It is the robust remains of the beetle, however, which are currently the most commonly used, though research applying other families of insects is becoming increasingly common. Beetles are useful for several reasons:

- Their diversity.
- They are virtually ubiquitous.
- The robust character of their chitinous exoskeleton, which preserves exceptionally well.
- Distinguishing details that permit the identification of fossil material, in many cases to species level.
- Beetles, in the form in which we see them today, have been present for many millions years, as far back as the Carboniferous period.

In this instance, it is the application of beetles as ecological indicators that is of greatest importance. A great deal of ‘habitat specific’ and ‘site specific’ ecological inferences and data may be gained by examining the insect assemblages (Kenward, 1978). Species of beetle are dependent upon five criteria, which rely on species autecology and will subsequently effect species dispersal on a local scale (Elias, 1994):

- Botanical factors.
- Soil type.
- Microclimate.
- Hydrological conditions.
- Chemistry.

3.6.3 Difficulties with environmental interpretation using palaeoentomology

In many cases, the prime objective of any palaeoentomological analysis is to reconstruct the past events and ecological conditions which prevailed at a site during an episode of development and is ultimately based on the habitat requirements of the insects that are recovered (Kenward 1978).

Determining the past ecological conditions at a site is relatively easy. The species found within the sample are recorded, keys relating to the different taxa and reference books are then used to record the habitat in which this species is commonly found. This allows the establishment of the ecological conditions in the immediate vicinity of the deposit. From this it should be possible to quantify this habitat in the archaeological record e.g. one species from a particular environment = 1 area of this type of habitat being present nearby and thus the surrounding environment can be built up piece by piece. This is known as the ‘mosaic’ approach (Kenward 1978).

These simple concepts are however beset by a variety of problems that are highlighted by Kenward (1975). Further work by Kenward (1978) suggests six primary problems when interpreting archaeological material:

1. Establishing the ecological requirements and variety of habitats.
2. Gauging the number of species that have been transported some distance before any assumptions about the immediate environment are made.
3. Establishing the autochthonous fauna i.e. the component of the assemblage, which is derived from the area directly adjacent to the site.
4. Differentiating the living communities and the environments, which they inhabit, and the importance of these habitats to the overall reconstruction.
5. Establishing the importance of these habitats and their relationship to the site.
6. Establishing the age of the fauna and how/if this relates to the archaeology at the site.

Coupled with this is a series of further problems associated with species autecology and the overall ecology of the individual biome:

1. By their very nature some biomes will have a greater number of individual species associated with them than others (Kenward 1978).
2. Population densities of individual species will vary; added to this only limited information is available regarding modern population densities (Kenward 1978). This will lead to over and under-representation of both species and habitats within archaeological deposits.

It cannot be taken for granted that an assemblage is directly representative of a context over short spatial and temporal scales. It may represent weeks or even years of accumulation and represent a rapidly changing habitat (Kenward, 1978). Finally, the most significant problems lie with the basis of palaeoentomology itself, that of modern entomological study (Kenward 1978). In many cases modern work is limited and records of the modern ecological range of many species are inadequate or inaccurate. In some cases the habitats that these species dwell within are extremely broad (Kenward 1978) e.g. the entry for the Carabidae *Pterostichus strenuus* in Koch (1989a): “on loamy arable fields, meadows and weedy places; damp floodplains and woodland margins; moist turf; brick pits; wash zones on the coast. Under leaves, detritus, straw, moss and decaying vegetation; in flood debris and compost; under rotten bark; in mole nest”. This taxa, which is commonly found in palaeoentomological assemblages, is extremely cosmopolitan.

3.6.4 *A solution to problems of interpretation*

To resolve this problem, Kenward has developed several paradigms that may be used to produce a more accurate interpretation of archaeological material. The method developed by Kenward (1978) which is most pertinent to this study, is the “Whole Assemblage” approach. The assemblage is examined in its entirety and the proportional significance of the components is used to draw conclusions about the environment (Kenward 1978). This method uses the general environments suggested by the majority of the insects recovered from within the individual sample as opposed to using the individual insect to draw such conclusions (Kenward 1978). If a single individual of a species has been recovered, whilst it may intimate some aspect of the habitat not suggested by other species, its overall value as an environmental indicator is limited.

This is not however, always the case and taking this approach on face value is slightly flawed and is related to the problem of over and under-representation in a single sample. Kenward (1978) suggests that greater importance should be attached to six large ground beetles that are generally found in low population densities, than a large population of Staphylinids that are commonly found in high numbers.

3.6.5 Visual Presentation of Data

Meaningful, visual presentation of this type of data is extremely difficult. To facilitate this, each species is designated an ecological code which corresponds to the primary habitat this species is associated with. The table used in this thesis is based on the work of Kenward (1978), Kenward and Hall (1995), Robinson (1981, 1983, 1993) and more particularly Smith, Osborne and Barrett (1997, 2000).

The calculations used to visually present the data are relatively simple, the total number of species assigned to a particular ecological group is expressed as a percentage of the whole fauna. Smith *et al.* (2000) varied this method slightly and expressed the aquatic fauna as a percentage of the entire fauna and the terrestrial fauna as a percentage of the non-aquatic species after Robinson (1981, 1983, 1993). The author felt that in this case where the relative hydrological conditions are particularly important also being examined, that true representation of the aquatic fauna in relation to the terrestrial fauna was of importance. The column marked “EG” on site species lists is “ecological groups” a series of broad groupings to which individual species have been assigned by Hall & Kenward (1990), Kenward & Hall (1995, 1997), Robinson (1981, 1983, 1993) and Smith *et al.* (2000) (Tab. 3.2).

Ecological Groups	
ws	waterside
a	aquatic species
rd	species primarily associated with drier organic matter
rt	species primarily associated with rotting organic matter
rf	species primarily associated with foul organic matter, often dung
g	species associated with grassland
l	species associated with woodland
m	moorland

Tab 3.2: Species ecological groups.

3.7 Field survey

As this project required a high level of fieldwork it is worth describing the main field methodologies, not already specifically covered elsewhere.

3.7.1 Section recording

The sections recorded in the quarry had sediment units recorded every 20cm along the sections, drawn from a line level. Datums were recorded on the level via differential GPS. The drawings were made at 1:50. The drawings were scanned into Adobe Illustrator for final presentation.

3.7.2 Field survey

All field survey was recorded in XY and Z dimensions using a differential GPS, with each individual field survey being assigned a new file and tied onto existing permanent points within the study area. All permanent points had a minimum of 6 hours static observation points collected for Rinex correction of actual position.

3.8 Electrical resistivity (ER) materials and methods

3.8.1 Geoprospection within alluvial environments

Geoprospection methods are finding increasing application within geoarchaeological investigations, due to their potential to identify sediment architectures that have high geoarchaeological potentials (Carey *et al.* 2006). In contrast to shallow geophysical prospection used in conventional archaeological practice, such as gradiometer and earth resistance survey, the application of geoprospection techniques in geoarchaeological surveys is not to identify anomalies that are thought to be distinctly cultural in origin, e.g. the plan of a Romano-British Villa. Instead the techniques are applied to understand the sediment and stratigraphic sequences of different geomorphological units, in order to identify the geomorphological units/sediment architectures that have the highest geoarchaeological potential, in both palaeoecological and cultural archaeological contexts.

3.8.2 GPR prospection within alluvial environments – a resume

Although the application of geoprospection within geoarchaeological survey is still in its infancy, GPR has been employed in geoarchaeological evaluations. As discussed in Brown *et al.* 2005, the application of GPR to find areas of high palaeo-ecological and geoarchaeological potential within alluvial environments is difficult, but coherent data capture is possible to aid in geoarchaeological assessments.

Ground penetrating radar surveys use pulses of Electromagnetic (EM) radio waves directed down into the soil profile from a transmitting antenna, in order to investigate subterranean features. When discontinuities are encountered some of these radio waves are reflected back towards the surface, whilst other waves travel further down into the soil profile until they meet other discontinuities. At the surface a receiving antenna measures the reflected waves. By measuring the time taken between emission of the radar pulse and reception back at the antenna it is possible to measure the depth of a discontinuity in the soil profile. Within a floodplain context the boundaries between different geomorphological units will be seen as discontinuities, due to their different physical properties, e.g. clay and gravel.

The process of estimating the depth of discontinuities within the soil profile is complicated by different dielectric constants found within different sediment units. The electrical properties of a sedimentary unit effect the time taken for the radar pulse to travel through that unit. The dielectric permattivity is a property of an electrical insulating material (dielectric) equal to the ratio of the capacitance of a capacitor filled with the given material to the capacitance of the identical capacitor filled with air. The specific capacitance of a vacuum is $\epsilon_0 = 8.85 \times 10^{-12}$ Farads per metre. The relative dielectric constant (ϵ_r) for air is 1 and is approximately 81 for fresh water (Radan User Manual Definition 2004, GSSI, 128).

Within an alluvial context the relative dielectric permittivity (RDP) of different sediment units is critical; which is the ability of a sediment to absorb, reflect and be permeated by, the radar pulse. If there is a significant change in RDP between two different geomorphological units, such as clay and gravel, then strong reflections will result at the interface of the two units. The GPR pulse will be dissipated by materials of high conductivity. Therefore, sediments with high clay and water contents cause rapid attenuation of the GPR signal and are often impenetrable to higher frequency antennas, such as a 200MHz antenna. Jol and Bristow (2003) revise GPR applications and practices for mapping sediments. One of their conclusions is that GPR is most effective in electrically resistive materials such as sand, gravel, peat and limestone but decreases in data quality are seen in highly conductive materials such as silt, clay and calcretes. Key factors that affect the RDP of an unconsolidated material can be listed as (mainly from Ekes and Friele 2003, 90):

- Pore size
- Sediment type
- Stratification
- Grain size
- Water content

It should be emphasised that although GPR survey can be used to identify and to some degree characterise sediment architecture, the mechanisms that affect the radar wave reflections are imprecisely understood. The reflection from an unconsolidated material will be a function of its water content below saturation levels; the water content itself being a function of the sediment properties (Van Dam *et al.* 2003, 257 – 273). If GPR survey is carried out over saturated sediments penetration will be limited.

In order to correctly calibrate the electric depth model created by the GPR it is important that the dielectric properties of the soil profile can be accurately estimated. This in practice is extremely difficult, as within alluvial environments any GPR transect is likely to cross a series of different geomorphological units, each having a different RDP. Therefore, a compromise has to be reached in the dielectric constant that is used. Within this project the dielectric constant of the soil was estimated through comparison with gouge core transects, which is a common method of calibration (for example see Bridge *et al.* 1998).

The gouge core transects allowed the depth of the alluvium overlying the terrace and modern floodplain gravels to be accurately measured across a whole GPR transect. The dielectric constant was then set, which identified the interface between the alluvium and the gravels at the same depth recorded by the gouge core transect. This represents a compromise on setting the dielectric constant as the calibration is taking place within an alluvium unit, not combining the average of the alluvium and gravel units. However, the gravels are

impenetrable without powered coring equipment and thus the described compromise was reached through using gouge core data.

The identification of radar terminations is the basis for constructing a relative chronology for a sequence of sediment units (Bristow *et al.* 2005, 316). Interfaces between different geomorphological units, e.g. a silty clay unit overlying a gravel unit, represent terminal events in either deposition or erosion processes and the start of subsequent processes. Although the ages of these sediment units cannot be ascertained without absolute dating methods, relative sequences can be constructed through studying the form of the interfaces seen. This has specific importance in geoarchaeological studies of alluvial environments where erosion and deposition by channels will have both destroyed and preserved the archaeological resource.

The heterogeneity of alluvial deposits allows discontinuities to be mapped and stratigraphies to be created. This property causes special considerations for GPR survey of alluvial environments. River floodplains are heterogeneous in both X, Y and Z dimensions. Upper terraces may have gravels close to the surface, with a thin covering of alluvium, whilst modern floodplains may have a considerable degree of alluvial deposition on gravels or bedrock. Palaeochannels may have high water contents, high clay contents, with organic rich pockets. Gravel architecture can vary radically between clast to matrix supported.

For GPR survey this can be problematic, in respect of data collection and real time amplification of signal. Consider two very different units that are surveyed within the same area, such as a gravel terrace and a palaeochannel with a fill of high clay content. The gravels in the terrace will have low absorption but high reflectance properties. Conversely, the palaeochannel will have low reflectance but high absorption properties, causing rapid attenuation of signal. In such cases, which are frequently encountered in alluvial environments, the different geomorphological units require a different amplification of signal. The amplification of the radar pulse is controlled through a gain applied to the signal. The level the GPR gain (amplification) is set at will be a compromise between obtaining good penetration in a series of different sediments and collecting clipped data, where the amplification of the signal has been too great and the minimum and maximum values are not realised. When considering alluvial stratigraphy it is often the contrast between different sediment units that is most important. Therefore, relative change and difference is as important for data collection within heterogeneous environments as absolute values.

From the phase I study of Predictive Modelling of Multi-period Geoarchaeological Resources at a River Confluence, GPR was shown to be effective at mapping the depth of alluvium above the gravels, the composition of the upper gravel deposits and identifying boundaries and variation between gravels and palaeochannels on the modern floodplain, terrace 1 and terrace 2. Conversely, the GPR penetration into the palaeochannels was generally poor. When palaeochannels had high water/clay contents, GPR was ineffective at mapping sediment structure. Therefore, GPR cannot be used to investigate the stratigraphy of high water/clay content palaeochannel fills, which are likely to be the palaeochannels that have the highest palaeoenvironmental potential. However, by using this criteria, palaeochannels that cause rapid attenuation of the radar signal should be earmarked for palaeoenvironmental sampling, due to the nature of the fill causing the loss of signal.

The two and three dimensional GPR surveys recognised distinct sedimentary structures in the heterogeneous alluvium deposits. Sedimentary units were interpreted according to their

reflection pattern and interpreted shape. The reflection amplitudes that were recorded related to differences in the sedimentary architecture of different geomorphological units. However, it was not possible to unambiguously predict the physical properties of a geomorphological unit from GPR reflection data. In general it was possible to differentiate between alluvium, palaeochannels, gravel and variations within the gravel, through changes in their relative RDP and hence reflectance pattern. However, in some cases different sedimentary units gave similar patterns of reflectance, e.g. gravels were generally seen as units of high reflectance but some clay layers produced a very similar reflectance pattern.

3.8.3 *ER prospection within alluvial environments*

After assessing the results from the GPR surveys during phase I of the project, it was decided to use other deep geoprospection techniques to compliment the GPR data. Electrical resistivity (ER) was selected to investigate palaeochannel stratigraphy and act as a comparative technique to GPR. Whilst GPR survey has shown to be incapable of penetrating clay filled palaeochannels there were sound reasons for expecting that ER could be successfully used to investigate palaeochannel sediments. This said, there are fundamental differences between ER survey and GPR survey and these have to be considered when the two techniques are compared.

3.8.4 *An introduction to ER survey*

ER survey uses electrical currents injected into the soil profile from a transect of electrodes to investigate subterranean features, via the resistance of different materials to the injected current (measured as ohms.m). When discontinuities are encountered (such as adjacent sediment units) there is expected to be a difference in resistivity values, due to differences in sediment architectures affecting factors such as grain size, water content, ion content, etc, which all contribute to the ability of a sediment to conduct electrical currents. The purpose of ER surveys is to determine the subsurface resistivity distribution. Electrical resistivity surveys have been used for many decades in hydrogeological, mining and geotechnical investigations. More recently, they have been used for environmental surveys and has also found recent application in geoarchaeological surveys (Bates 2007).

The following description of electrical resistivity imaging is derived from Loke (1999) unless otherwise referenced, which provides a comprehensive overview of ER, different electrode arrays and software options. Resistivity measurements are achieved by injecting current into the ground through two current electrodes (C1 and C2), and measuring the voltage difference at two potential electrodes (P1 and P2) (Fig. 3.9).

From the current (I) and voltage (V) values, an apparent resistivity (p_a) value is calculated.

$$p_a = k V / I$$

where k is the geometric factor which depends on the arrangement of the four electrodes.

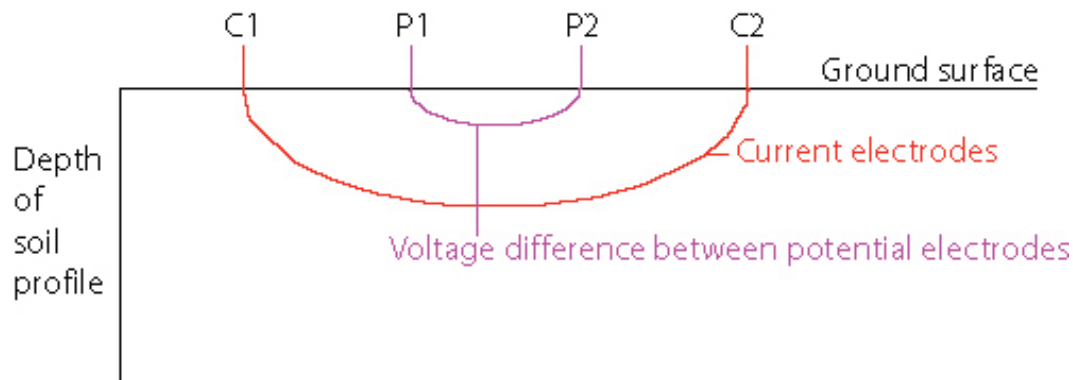


Fig 3.9: The basis of a resistivity measurement. Current is injected into the ground through C1 and C2 and the voltage difference at two potential electrodes is measured at P1 and P2.

Resistivity meters normally give a resistance value, $R = V/I$,

The apparent resistivity value is calculated by
 $\rho_a = k R$

The calculated resistivity value is not the true resistivity of the subsurface, but an “apparent” value that is the resistivity of a homogeneous ground that will give the same resistance value for the same electrode arrangement. The relationship between the “apparent” resistivity and the “true” resistivity is a complex relationship. To determine the true subsurface resistivity, an inversion of the measured apparent resistivity values needs to be undertaken.

3.8.3.1 Electrical resistivity and sediment stratigraphy

Resistivity surveys provide information on below ground sediment architectures through estimating their resistivity distributions. Whilst it is clearly not possible to assign a particular resistivity value to a particular sediment type, i.e. 53.1 ohms.m equates to an organic rich clay, understanding the resistivity values of different sediments aids in interpreting ER sections.

With GPR the RDP of a sediment unit is important in understanding how the radar pulse acts within the soil and also how to interpret the resulting GPR section. Likewise the RDP of a sediment unit will determine its ability to conduct an electrical voltage, which can be measured in ohms.m. Therefore, the RDP of a sediment unit is also crucial in interpreting ER sections and identifying different sediment units.

In a general context, igneous and metamorphic rocks typically have high resistivity values. Sedimentary rocks, which usually are more porous and have a higher water content than igneous and metamorphic rock formations, normally have intermediate resistivity values. Wet soils and fresh ground water have lower resistivity values. This is a very general rule though, as, the resistivity of rocks and soils can vary by several orders of magnitude over relatively small areas. Broad resistivity values for a variety of geological samples and some soils are

given (Tab. 3.3), which are coded as high resistance materials (red), intermediate resistance materials (green) and low resistance materials (blue).

This general classification is of limited use when considering the study area of the Trent/Soar, especially as some of the terminology is ambiguous, i.e. what is the difference between clay and alluvium? The general stratigraphy of the study area is known in both geological and pedological contexts. Therefore, it is possible rank the different sediment units as encountered within the study area on a *pre-hoc* basis, dependent on their predicted resistivity values (Tab. 3.4).

Igneous and metamorphic rocks	Resistivity range (ohm.m)	Conductivity (Siemen/m)
Granite	$5 \times 10^3 - 10^6$	$10^{-6} - 2 \times 10^{-4}$
Basalt	103 - 106	$10^{-6} - 10^{-3}$
Slate	$6 \times 10^2 - 4 \times 10^7$	$2.5 \times 10^{-8} - 1.7 \times 10^{-3}$
Quartzite	$10^2 - 2 \times 10^8$	$5 \times 10^{-9} - 10^{-2}$
Sedimentary rocks	Resistivity range (ohm.m)	Conductivity (Siemen/m)
Sandstone	$8 - 4 \times 10^3$	$2.5 \times 10^{-4} - 0.125$
Sandstone	$8 - 4 \times 10^3$	$2.5 \times 10^{-4} - 0.125$
Shale	$20 - 2 \times 10^3$	$5 \times 10^{-4} - 0.05$
Limestone	$50 - 4 \times 10^2$	$2.5 \times 10^{-3} - 0.02$
Soils and waters	Resistivity range (ohm.m)	Conductivity (Siemen/m)
Clay	1 - 100	0.01 - 1
Alluvium	10 - 800	$1.25 \times 10^{-3} - 0.1$
Groundwater (fresh)	10 - 100	0.01 - 0.1

Tab: 3.3: General resistivity and conductivity values of some rocks and soils (modified from Keller and Frischknecht, Daniels and Alberty 1966).

General sediment unit	Resistivity ranking
Clast supported gravel	<p>Highest resistivity values</p> <p>Lowest resistivity values</p>
Matrix supported gravel	
Sand	
Mercian mudstone	
Clayey sand	
Clayey silt	
Sandy clay	
Silty clay	
Clay	

Tab 3.4: Table of predicted resistivity ranking of sediment units within the study area, on a *pre-hoc* basis before survey.

This table is constructed from the principles discussed above, where sediment units with a smaller clast size and higher water contents have a lower resistivity through being more

conductive. Therefore, a waterlogged clay will have a lower resistivity value than clast supported gravel.

Within a geoarchaeological context, the actual resistivity of the sediment unit in question then starts to take on a predictive capacity. Factors that influence the preservation of organic remains in alluvial environments, both in palaeoecological and cultural contexts, produce sediments with low resistivity values. Such factors are primarily water logging and small clast/grain sizes causing low redox conditions. Conversely, areas of high resistance can indicate other sediment units, which have different geoarchaeological potentials. High resistance features can indicate sands and gravels, which in alluvial Holocene records can have high geoarchaeological potentials. For example a wealth of archaeological remains were found at Hemington within gravels features including fish dams, fish baskets and medieval bridges (Cooper 2003: Salisbury 1992). Therefore, the interpretation of different resistivity values and their relationships to different sediment units potentially has a large role to play in geoarchaeological investigations.

3.8.4 ER materials and methods

3.8.4.1 Instrumentation and data collection parameters

The IRIS Syscal junior system was the switching unit employed to automatically select the four electrodes for any single measurement. This system has a maximum capacity of 48 electrodes in any single transect, collecting measurements via two cables which can both be attached to up to 24 electrodes. The IRIS Syscal Junior was programmed through Electre II. The Wenner Schlumberger array was selected. The data collection parameters were a stack of min 3/max 6, with a measurement time of 1000ms.

Whilst there are sound theoretical reasons to expect ER to provide good data on subsurface stratigraphy, the survey parameters determine the success of any geophysical survey. When using ER there are two principle factors to consider in the instrumentation set up, being the electrode array and the electrode spacing.

The Wenner Schlumberger array was selected after considering depth of investigation and data resolution. This is a hybrid between the classical Wenner array and the Schlumberger array. This array is moderately sensitive to both vertical and horizontal structures, representing a good compromise between the Wenner and Schlumberger arrays. The Schlumberger array is commonly used in resistivity sounding surveys. A modified form of this array, so that it can be used on a system with the electrodes arranged with a constant spacing is shown in (Fig. 3.10). Note that the “*n*” factor for this array is the ratio of the distance between the C1-P1 (or P2-C2) electrodes to the spacing between the P1-P2 potential pair. The sensitivity pattern for the Schlumberger array (Fig. 3.5.2) is slightly different to the Wenner array, with a vertical curvature below the centre of the array and slightly lower sensitivity values in the regions between the C1 and P1 (and also C2 and P2) electrodes. There is a slightly greater concentration of high sensitivity values below the P1-P2 electrodes. This means that this array is moderately sensitive to both horizontal and vertical structures.

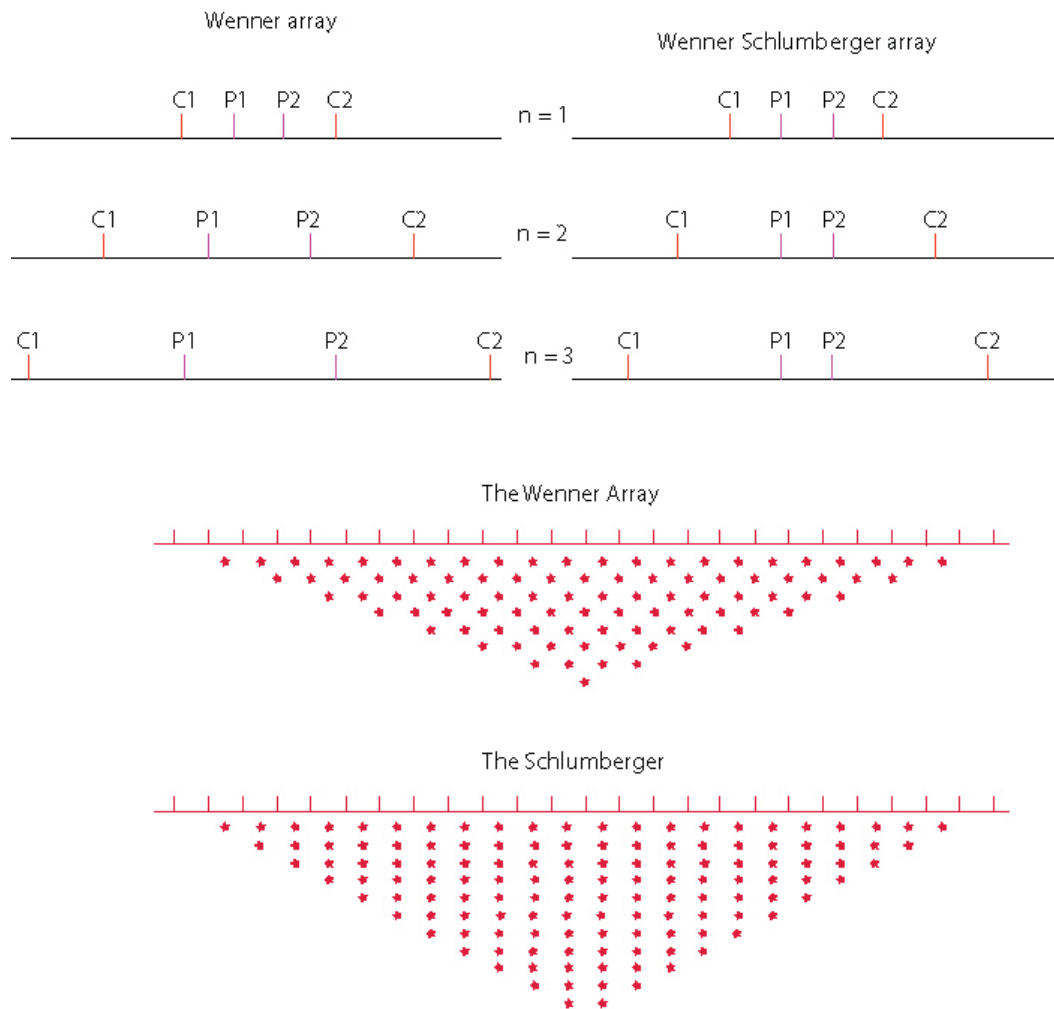


Fig 3.10: The Wenner and Schlumberger arrays.

The apparent resistivity value for the Wenner-Schlumberger array is given by

$$r = \frac{\pi n(n+1)}{a} R$$

where R is the measured resistance, a is the spacing between the $P1$ and $P2$ electrodes and n is the ratio of the distances between the $C1-P1$ and the $P1-P2$ electrodes. This array effectively becomes the Schlumberger array when the n factor is greater than 2. Thus it is actually a combination of the Wenner and Schlumberger arrays adapted for use for an arrangement with a line of electrodes with a constant spacing (as normally used in 2-D electrical imaging). Besides better horizontal coverage, the maximum depth of penetration of this array is about 15% larger than the Wenner array. Note that the normal Wenner array is actually a special case of the Wenner-Schlumberger array where the n factor is equals to 1.

The electrode spacing represents the compromise between the depth of penetration and data resolution by depth. From the borehole modelling, gouge core transects and section recording, the general stratigraphy of the study area was known. Therefore, the three electrode spacings of 0.5m, 1m and 2m were selected, keeping the number of data

measurement points equal in each. These three electrode spacings were compared in different situation across the study area to assess the effectiveness of ER in revealing alluvial sediment stratigraphy.

Using the 0.5m electrode interval 12 depth levels were used, giving 342 quadripoles (measurement points) for the first transect (Fig. 3.11). This gave a total first transect length of 23.5m. In order to avoid saw toothing and maintain depth and data resolution subsequent transects were 5.5m long, with the same 12 depth levels, that joined to the first transect of 23.5m (Fig. 3.12).

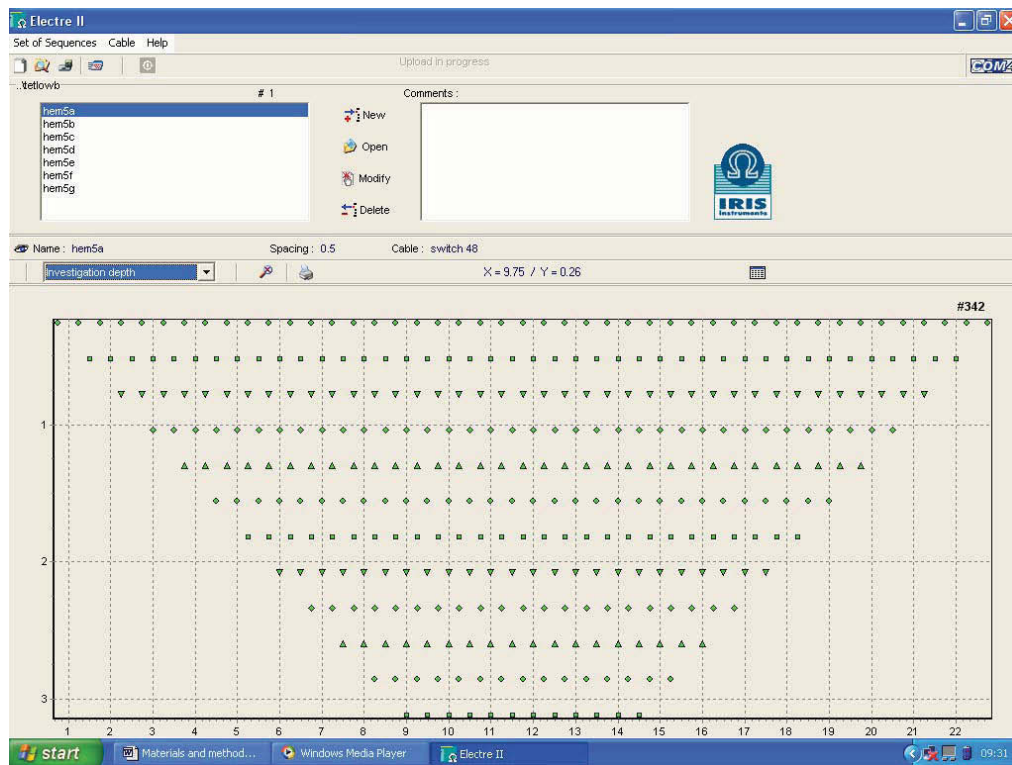


Fig 3.11: The data collection points on the 0.5m electrode spacing first transect.

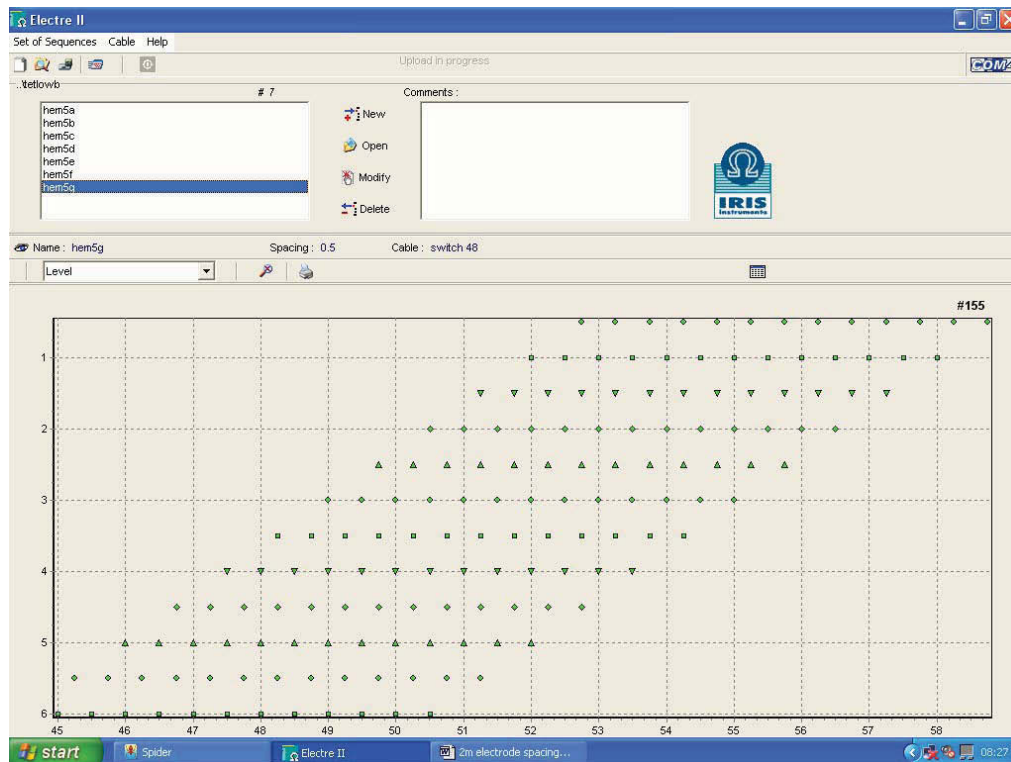


Fig 3.12: The data collection points on the 0.5m second and subsequent transects.

Using the 1m electrode interval 12 depth levels were used, giving 342 quadripoles (measurement points) for the first transect (Fig. 3.13). This gave a total first transect length of 47m. In order to avoid saw tothing and maintain depth and data resolution subsequent transects were 11m long, with the same 12 depth levels (Fig. 3.14). The same parameters were used for the 1m electrode spacing.

Using the 2m electrode interval 12 depth levels were used, giving 342 quadipoles (measurement points) for the first transect (Fig. 3.15). This gave a total first transect length of 95m. Only one 2m electrode interval transect was used in the study.

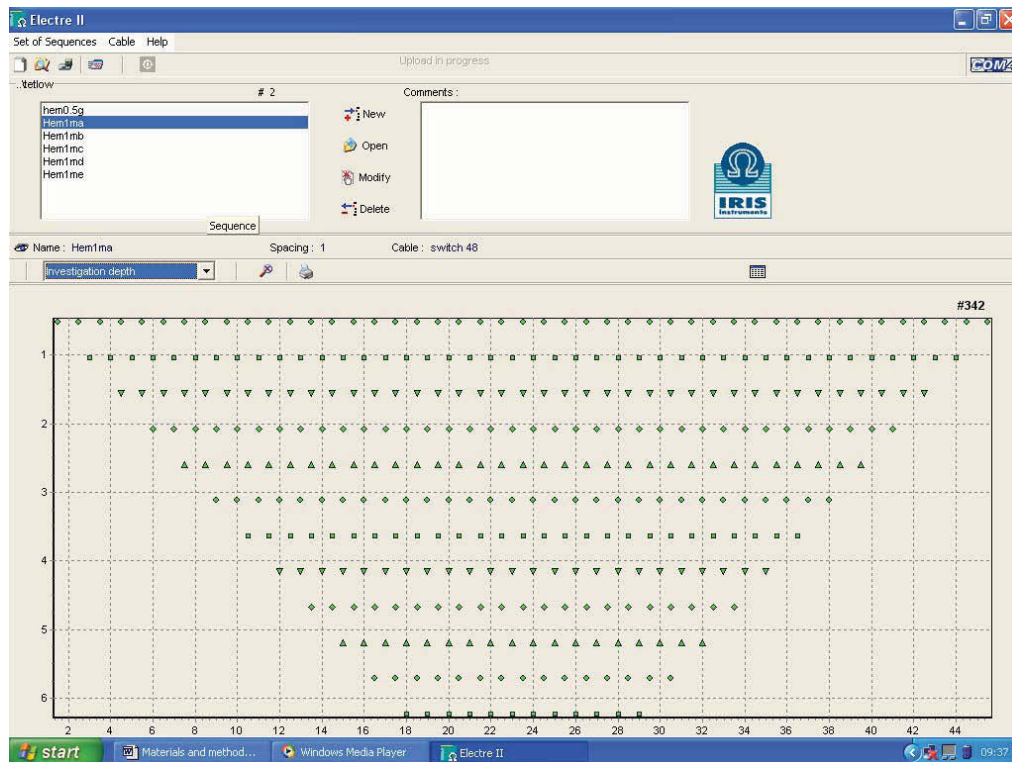


Fig 3.13: The data collection points on the 1m electrode spacing first transect.

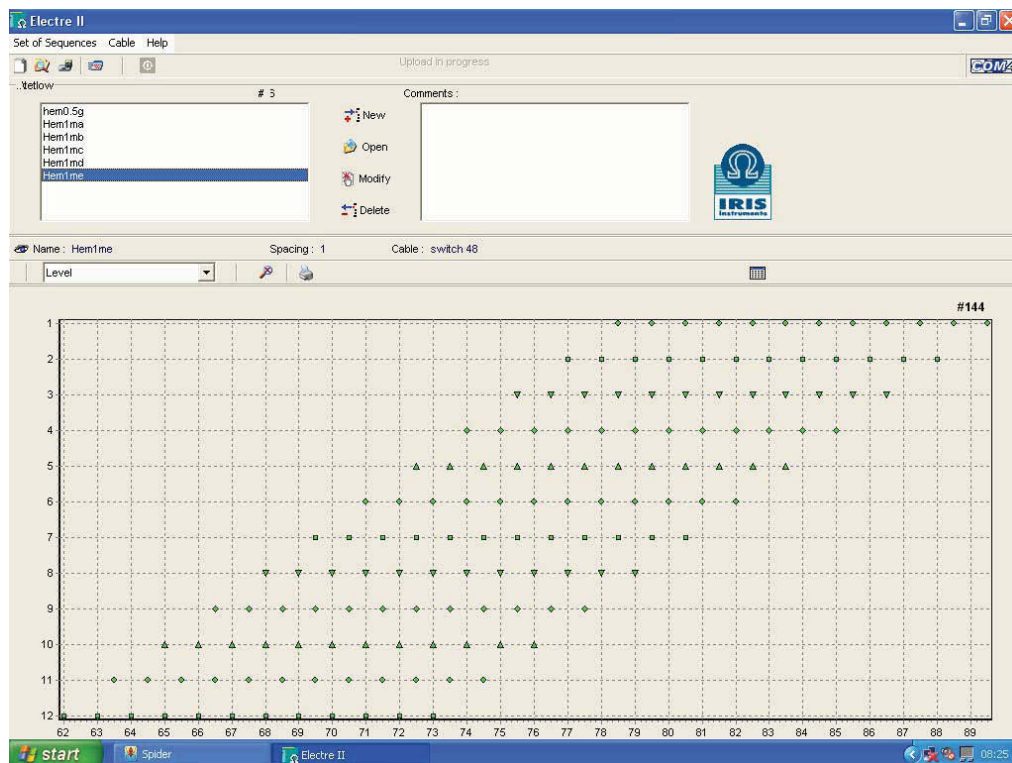


Fig 3.4: The data collection points on the 1m electrode spacing second and subsequent transects.

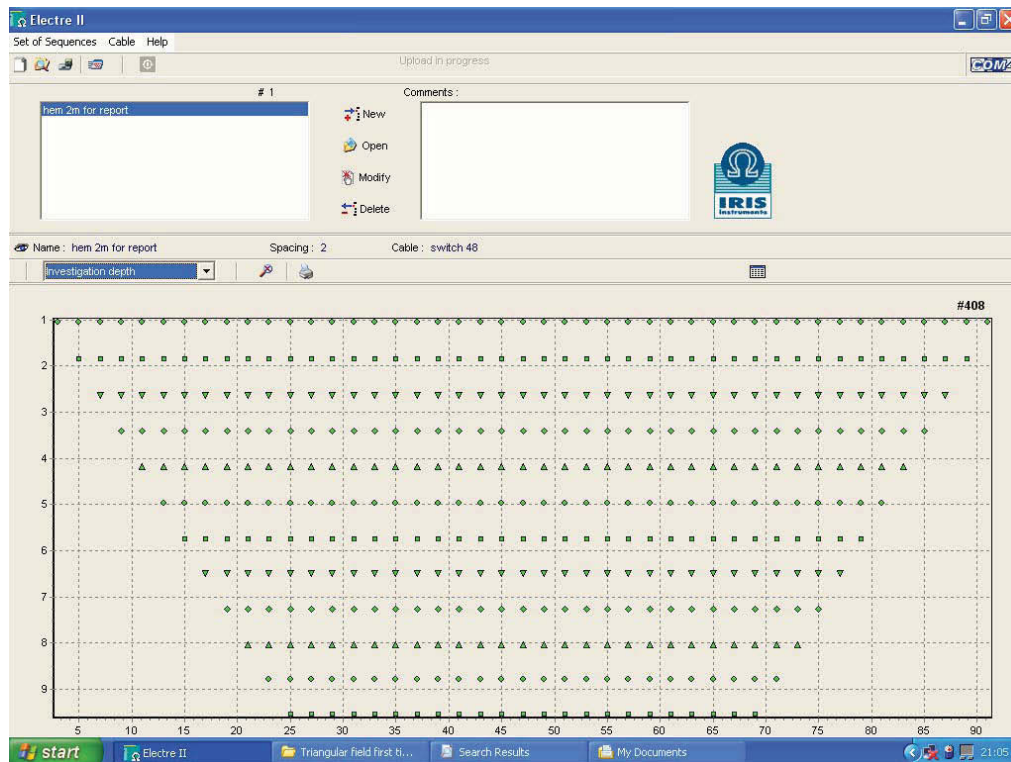


Fig 3.15: The data collection points on the 1m electrode spacing first transect.

3.8.4.2 Field methodology

The IRIS Syscal Junior was programmed directly from the PC with the files created in Electre II. Set up for the ER transects involved setting out a transect using ranging rods over selected features. Tapes were laid along the transect and then electrodes were placed at either 2m, 1m or 0.5m intervals. Two cables are employed with the Syscal Junior unit, each having 24 connections to attach to the electrodes via a wire with crocodile clips (Fig. 3.16).

On some ER sections GPR profiles were created along the same transects. Most transects had a gouge core taken at 10m intervals along the transect. The location of all ER, GPR and gouge cores were recorded using differential GPS and tied onto existing base stations within the study area. The ER sections were had their location recorded using differential GPS (Fig. 3.17).



Fig 3.16: ER transect running across a palaeochannel on the lower floodplain. The IRIS Junior unit is central between the two cables. Each cable is attached to 24 electrodes.



Fig 3.17: Recording the position of the ER transect T1F using dGPS.

3.8.4.3 Data download and pseudosection viewing

All data from the Syscal Junior was downloaded into the program Prosys II. Here the data was viewed as a pseudosection to assess data integrity and exported in a file format that could be viewed in RES2DINV. To visualise the data from a 2-D imaging survey, the pseudosection contouring method is used. The horizontal location of a point is placed at the midpoint of the set of electrodes used to make that measurement. The vertical location of the plotting point is placed at a distance that is proportional to the separation between the electrodes. The pseudosection gives an approximate picture of the true subsurface resistivity distribution. However, this picture is distorted as the shape of the contours depends on the type of array used, in addition to the true subsurface resistivity.

In order to understand the true resistivity of the subsurface there has to be inversion of the ER data. At its simplest level inversion methods try to find a model for the subsurface whose response agrees with the measured data. The inversion subroutine tries to reduce the square of the difference between the measured and calculated apparent resistivity values. Besides trying to minimise the difference between the measured and calculated apparent resistivity values, the inversion method also attempts to reduce other quantities that will produce certain desired characteristics in the resulting model. Additional constraints help to stabilise the inversion process.

3.8.4.4 Data inversion

All data inversion was undertaken in the dedicated RES2DINV program. The data was initially viewed as a line plot to visually search for erroneous data points, with these being removed from the data set. The modified file was resaved. The data inversion used the Robust constraint (section 3.8.3.4). Inversion of ER data is a subjective process, due to non-uniqueness of data. If two different constraints are applied to the same data set, two different results can be produced. For the same data set, there is a wide range of models giving rise to the same calculated apparent resistivity values. To narrow down the range of possible models, some assumptions are made concerning the nature of the subsurface that are incorporated into the inversion.

When considering the application of inversion methods to data sets collected in alluvial environments, the nature of the boundaries between sediment units is critical, as the selected constraint method will model boundaries between units in different ways. For example are gradational or sharp boundaries or both expected within an ER data set? Furthermore, are these boundaries primarily expected in horizontal, vertical or both dimensions? All of these factors will influence the decision on the inversion method used.

To undertake the data inversion a least squares inversion was used, with a 'robust constraint'. The least-squares inversion method attempts to minimise the square of difference between the measured and calculated apparent resistivity values. This method normally gives reasonable results if the data contains random or "Gaussian" noise. However if the data set contains outlier data points (where the noise comes from non-random sources such mistakes or equipment problems), this criteria is less satisfactory. Such outlier data points could have a great influence on the resulting inversion model. To reduce the effect of such outlier data points, an inversion method where the absolute difference (or the first power) between the measured and calculated apparent resistivity values is minimised can be used (Claerbout and

Muir 1973). There is a pcut-off factor which controls the degree in which this robust data constrain is used. If a value of 0.05 is used, this means the effect of data points where the differences in the measured and calculated apparent resistivity values are much greater than 5 percent will be greatly reduced.

The conventional smoothness-constrained least squares method (deGroot-Hedlin and Constable 1990) attempts to minimise the square of the changes in the model resistivity values. This will produce a model with a smooth variation in the resistivity values. This will produce a smoothed contour change, even when adjacent contours (or data points) have radically different values, such as the change between a fine clay unit and a coarse sand unit.

The robust model constrain inversion method, used on the model resistivity values, attempts to minimise the absolute changes in the resistivity values. This constraint tends to produce models with sharp interfaces between different regions with different resistivity values, but within each region the resistivity value is almost constant. This type of inversion method has clear application within alluvial environments.

Within alluvial environments there can be large differences between the measured and calculated resistivity values caused by non random sources, creating a data set with significant outliers. Such data sets that could contain a large degree of variance are where there are adjoining geomorphological units with radically different sediment architectures, such as were a silt clay palaeochannel joins terrace gravels with a shallow silty clay alluvial covering. In such examples a sharp boundary exists in resistivity relating to sediment architecture and should be modelled as discrete units.

In addition it was decided that the relative weights of the horizontal and vertical filters should not be changed. The relative weight of these filters can be changed when stratigraphy is expected to vary in only one dimension, such as temporal (depth) geological stratigraphy. In such a situation the vertical flatness filter is given a greater weight than the horizontal filter, allowing greater clarity in the stratigraphy of the section. However, geomorphological stratigraphy can vary in both X,Y (horizontal/spatial) and Z (temporal/depth) dimensions. Therefore, the relative weights of the horizontal and vertical filters were kept equal during the inversion. Finally the data was exported from RES2DINV as a bitmap and placed into Adobe Illustrator for final presentation.

3.8.4.5 Data interpretation

All ER sections had an interpretation made. Interpretation is a subjective process and in as much the identification of the geomorphological features was kept as simple as possible. Line drawing interpretations were placed on top of the ER sections, after gouge core stratigraphy and GPR sections ad been compared to the ER section.

3.8.6 *The aims of ER survey within this study*

The aims of the electrical resistivity survey can be summarised as:

- To investigate the capacity of ER to identify sediment stratigraphies on areas of terrace.

- To investigate the capacity of ER to identify sediment stratigraphies within palaeochannels.

In order to achieve these aims the following types of survey were applied.

1. ER transect compared to gouge core stratigraphy.
2. ER transect compared to GPR survey.
3. ER survey compared to both GPR and gouge core survey.
4. Assessment of ER on terrace 2.
5. Assessment of ER on terrace 1.
6. Assessment of ER on the modern floodplain.
7. Assessment of different depth penetrations of ER.

In order to achieve these aims a series of different ER transects were undertaken (Tab 3.5).

ER transect	Geomorphology	Electrode spacing	Other data on transect
T2A	Area of terrace 2, no palaeochannels visible through surface topography	1m	
T1A	Area of terrace 1, no palaeochannels visible through surface topography	1m	GPR, gouge cores, LiDAR
T1B	Area of terrace 1, no palaeochannels through surface topography	0.5m	GPR, gouge cores, LiDAR
T1C	Palaeochannel on terrace 1	1m	GPR, gouge cores, LiDAR
T1D	Palaeochannel on terrace 1	0.5m	GPR, gouge cores, LiDAR
T1E	Area of terrace 1 with palaeochannel	1m	Gouge core, earth resistance survey, LiDAR, ground based NIR scanning
T1F	Area of terrace 1 with palaeochannel	1m	
T1G	Palaeochannel marking the boundary between terrace 1 and terrace 2	0.5m	Gouge cores
T1H	Area of terrace 1 with palaeochannel	0.5m	GPR, gouge cores
T1J	Area of terrace 1 with palaeochannel	1m	GPR, gouge core
T1K	Area of terrace 1, no palaeochannels visible through surface topography	2m	GPR, gouge core
MFA	Area of modern floodplain with palaeochannels	1m	
MFB	Area of modern floodplain with palaeochannels	0.5m	

Tab 3.5: ER surveys undertaken.

3.9 Standardised keys for stratigraphy descriptions

The following key has been used throughout for sediment descriptions (Fig. 3.18).

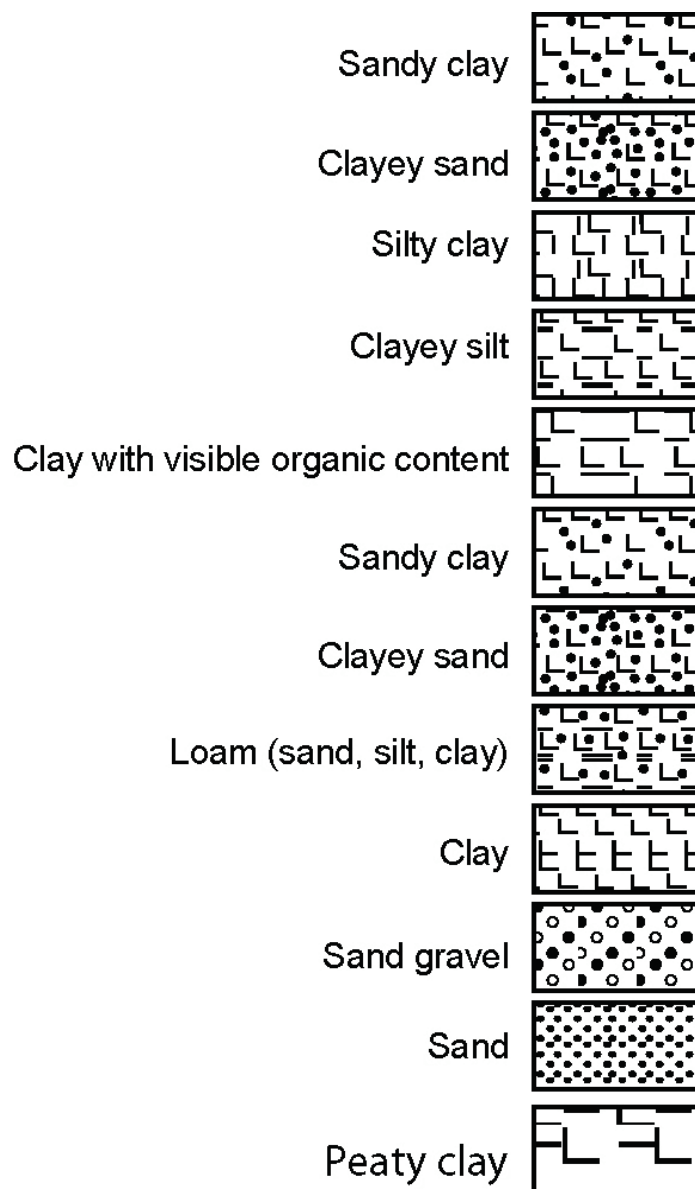


Fig 3.18: Modified Troel Smith key for sediment descriptions.

3.10 LiDAR intensity ground scanning

3.10.1 Introduction

This part of the project aimed to investigate the backscattered laser intensity data produced as a by-product of the airborne LiDAR elevation survey of the site, to determine whether soil and sediment properties might influence the reflection of the laser pulse. This chapter summarises the results of research at Lockington during 2006.

Airborne LiDAR provides access to high resolution, high accuracy terrain information and as a secondary output a laser “image” of the land surface derived from measurements of the intensity of reflection of each backscattered laser pulse. Archaeological applications of LiDAR have focused largely on its ability to provide a high resolution record of terrain variation, allowing the detection and mapping of subtle archaeological features, mapping of fluvial geomorphology and its unique ability to penetrate vegetation cover to map underlying archaeological earthworks.

Backscattered laser intensity measurements have largely escaped attention, and indeed do not form a part of the standard data product supplied by Environment Agency (EA; although intensity data is collected on each EA flight and can be accessed by reprocessing original flight data). The LiDAR system used by EA, NERC and many UK-based commercial LiDAR providers, including that used for the present project, an Optech Airborne Laser Terrain Mapper, operates in the near infra-red (NIR: 1047nm) and so backscattered intensity is in effect a record of the reflectance of earth surface materials at this wavelength.

Initial examination of backscattered laser intensity in stage one of the project suggested that a fall-off in the intensity of the reflected light corresponds with the position of sediment filled landform features such as palaeochannels (Figs. 3.19 3.20 and 3.21). Variations in the reflectivity of various earth surface materials to laser light of differing wavelength are well-documented and damp soil conditions are known to reduce reflectivity. It was therefore postulated that the increased soil-moisture associated with palaeochannels, and perhaps other associated variations in soil and vegetation properties, are responsible for the reduced reflection of the laser pulse.

Limited work in stage one of the project examined laser intensity in relation to volumetric soil moisture measured *in-situ* at topsoil and subsoil level with a theta probe. The present work extends this research to consider the relationship between intensity and topsoil moisture more extensively across the site and to investigate the relationship between intensity, topsoil moisture and topsoil organic content in representative geomorphological units across the study area.



Air-photo



LiDAR Elevation (LPG)



LiDAR Intensity (LPI)

Fig 3.19: Air-photographic, LiDAR elevation and LiDAR intensity data for a part of the Hemington Terrace unit at Lockington. These three images highlight the varying response of LiDAR intensity to geomorphological features.

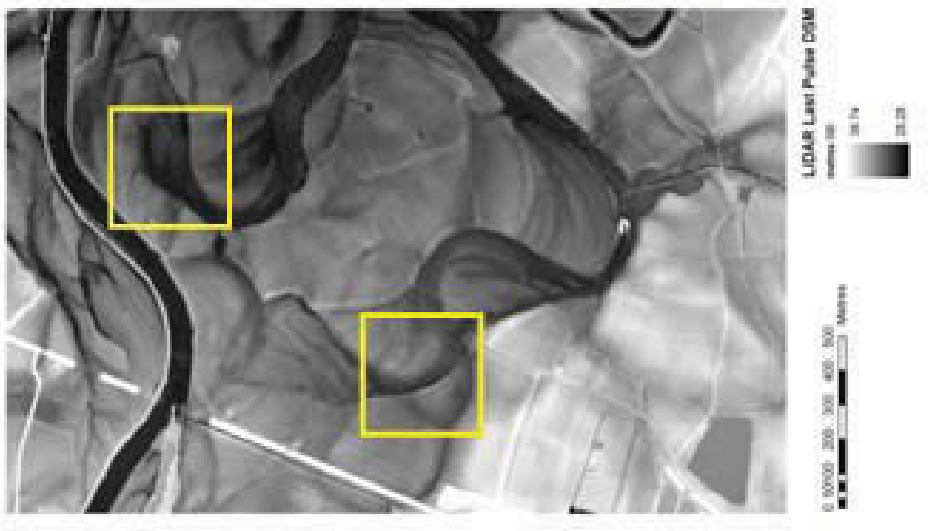
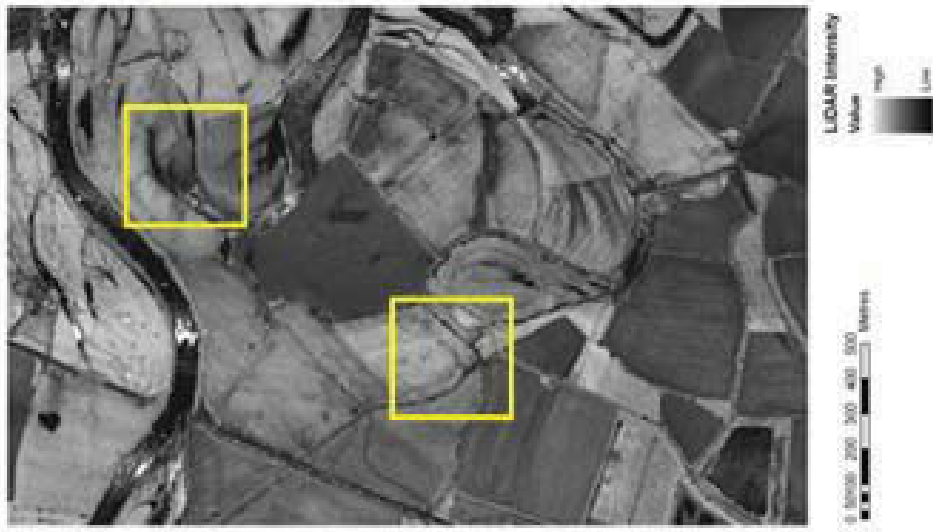


Fig 3.20: LiDAR elevation (bottom) and Intensity (Top) data for the Lockington study area. The yellow boxes highlight variations of the intensity response over palaeochannels of similar topographical character. That at the northern edge of the image produces a clear low intensity response, while that to the south is not reflected in the intensity data.

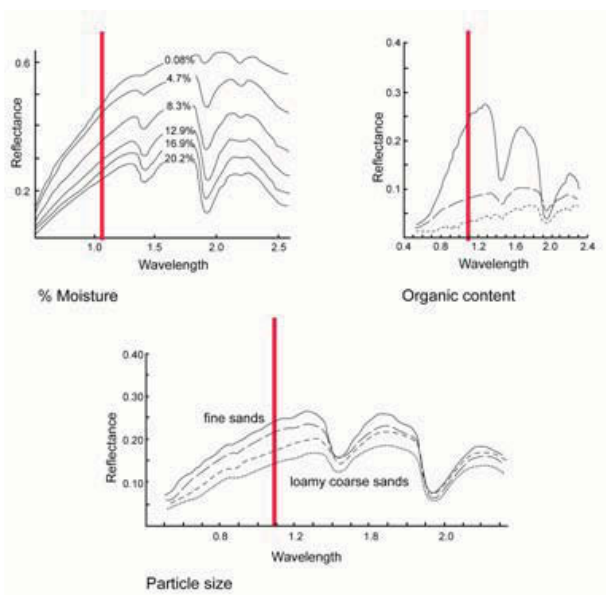


Fig 3.21: Graph showing the measured reflectance of sediments of differing moisture organic content and particle size across the spectrum. The NIR response (1047nm) is highlighted in red.

3.10.2 Aims and Objectives

The present work aimed to investigate the relationship between LiDAR backscatter laser intensity and soil and sediment properties:

- To investigate the relationship between topsoil moisture and laser intensity broadly across the study area to determine whether clearly an identifiable relationship exists between these two that holds true for different sediment types.
- To investigate in detail the relationship between topsoil moisture, laser intensity and topsoil organic content at three locations reflecting different geomorphological units across the site.

3.10.3 Method Statement

3.10.3.1 Topsoil Moisture and Intensity: Broad Area Survey

Topsoil moisture was recorded at 29 locations across the study area (Fig. 3.22) using a Delta T Devices theta probe. Sample locations were chosen deliberately to represent a variety of geomorphological and topographical settings, for which some contrast was apparent in the LiDAR intensity data. The theta probe calculates *in-situ* volumetric soil moisture, logging readings to an attached data recorder. The location of each soil moisture reading was recorded using carrier phase differential GPS. GPS co-ordinates were used within the project GIS to extract intensity values from the LiDAR data.

Intensity/soil moisture values for each location were then examined and graphed to produce scatter plots showing the data pairs. Scatter plots were produced to show all soil moisture and intensity values and to show intensity/moisture values grouped by sediment type and for spatially discrete groups.

In addition a number of permanent sample locations were established for monitoring soil moisture through the soil profile to a depth of c 1m. Hand augered holes were lined with proprietary plastic sheaths to allow insertion of a Delta T Devices profile probe, which allow logging of soil moisture at 0.2m intervals on a 1.0m column. In the event the present of dense gravely sub-soil close to the surface made the placement of permanent sample locations all but impossible. In addition the tendency of the sheath lined holes to fill with water rendered measurements of soil moisture untenable. In the event this part of the field methodology was curtailed in favour of more intensive examination of the relationship between intensity and sediment character at selected key locations.

3.10.3.2 Topsoil Moisture, Organic Content and Intensity: Detailed Study

Detailed studies of topsoil moisture and organic content were undertaken at three discrete locations across the study site on the modern floodplain (Fig. 3.23: MF), the Hemington Terrace (Fig. 3.23: FF) and the Hemington Terrace edge overlapping with a palaeochannel (Fig. 3.23: MTF). At each location topsoil moisture readings were recorded at 4m intervals within a regular grid using a theta probe (Fig. 3.24). Topsoil samples were recovered from each sample location for subsequent laboratory analysis (Fig. 3.25). Each sample location was recorded using carrier phase GPS and the coordinates of the sample locations used to extract intensity values from the LiDAR data within the project GIS. Intensity/moisture/organic content data for each sample location were used to produce scatter plots for variable pairs. In addition, discrete moisture and organic content values were interpolated to produce a continuous grid representing variations in these variables to allow visual comparison with the LiDAR intensity data.

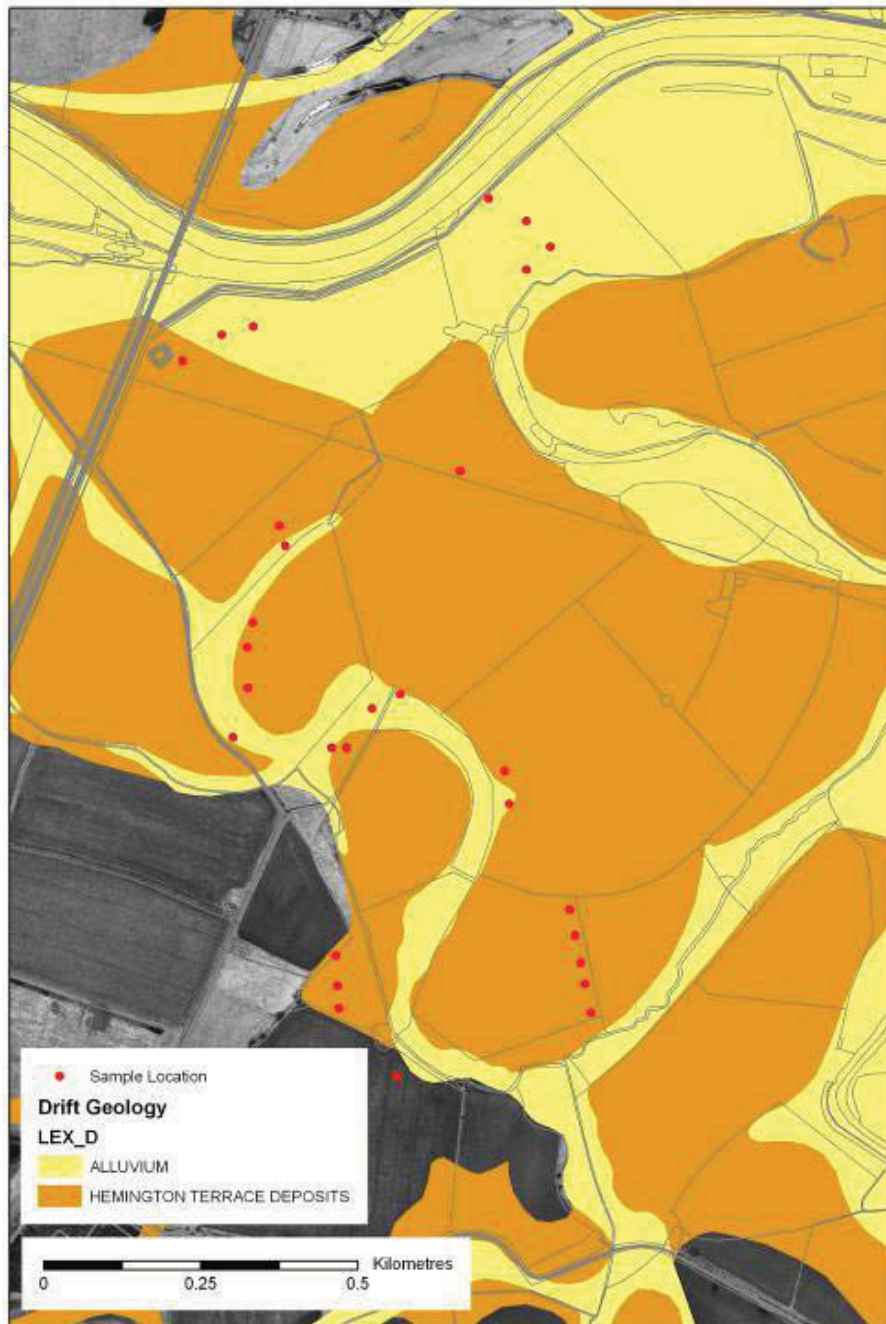


Fig 3.22: Sample locations for soil moisture/intensity comparison.

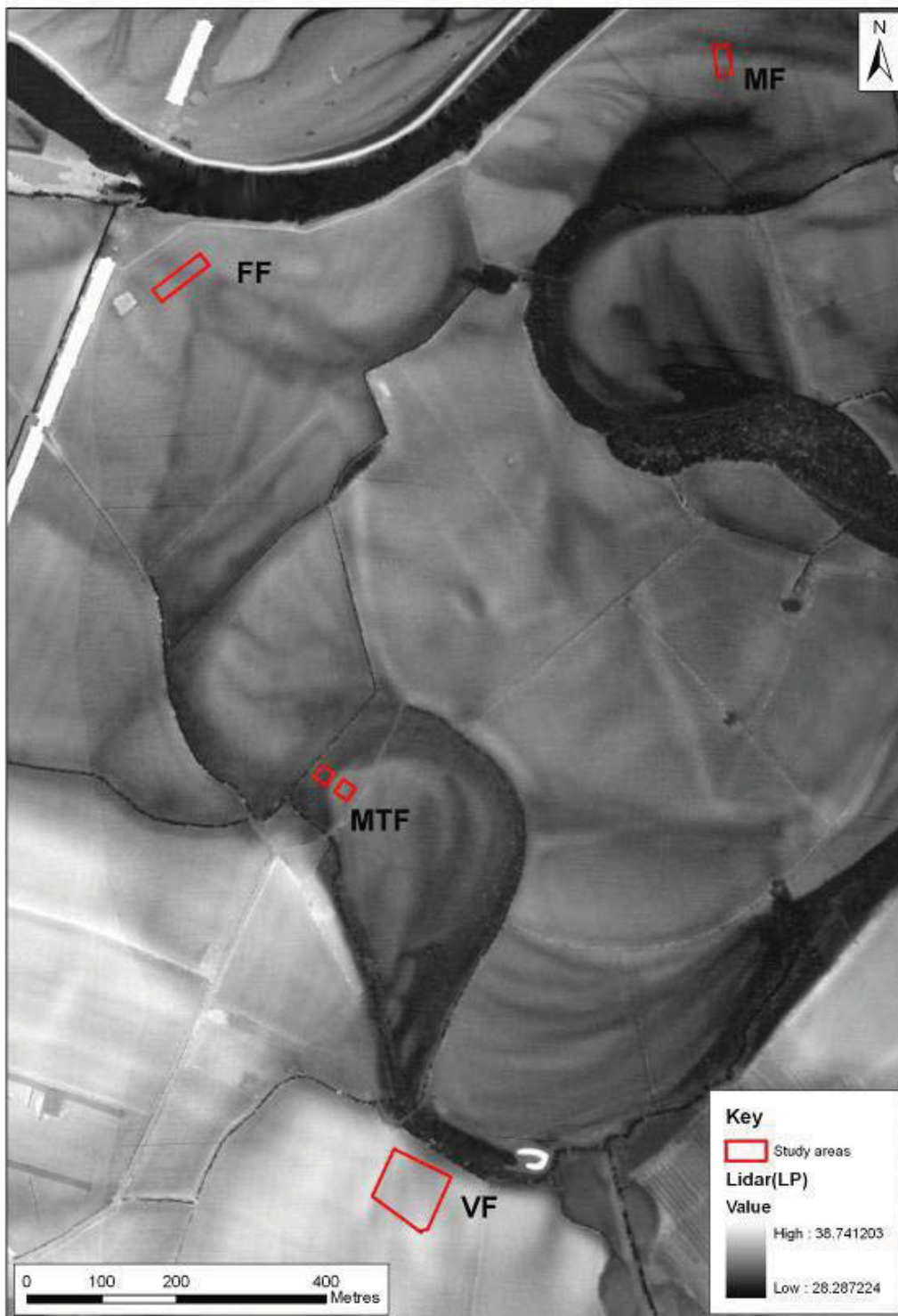


Fig 3.23: Lockington study area. LiDAR LP elevation data with detailed LiDAR intensity study areas highlighted in red.



Fig 3.24: Lockington. Field collection of volumetric soil moisture data at regular grid intervals using a Delta T Devices Theta Probe.



Fig 3.25: Lockington. Field collection sediment samples for organic content analysis.

3.11 Data archive and query

ArcGIS provided the primary database for the project. ArcGIS is a Geographical Information System (GIS), which is used for the storage and exploration of data, linking together aspects of geomorphology and archaeology, in spatial and chronological dimensions. The investigation of an area of cultural landscape requires the collection of data from a range of sources involving both field based and desk based research. These strands of information are then placed together within a GIS, allowing relationships between variables to be visualised and explored.

A GIS is a spatially referenced database. Each variable can have a large number of attributes (categories) stored with it, giving a description of that variable. Data can be stored either as point data (e.g. an archaeological site), line data (e.g. a river) or as a vector (e.g. an area of river terrace). These data can then displayed and queried as a series of layers.

The following data were entered into the ArcGIS database:

- I) Geomorphological maps, which were adapted through on screen digitisation
- II) Geology maps supplied through the BGS
- III) LiDAR intensity, DSM and DTM models
- IV) IFSAR DSM and DTM models
- V) Co-ordinates of the fieldwork survey areas
- VI) GPR transect locations
- VII) ER transect locations
- VIII) Gouge core locations
- IX) Palaeoenvironmental sample locations
- X) OSL sample locations
- XI) 1:10000 OS maps
- XII) Digitised SMR data
- XIII) Bore hole locations
- XIV) Rectified aerial photographs of the study area

ArcGIS provided the primary means of integrating the various data sources. ArcScene was also employed to allow the layering of data in a quasi-3D environment, permitting direct visual comparison between the data types.

3.12 Ground penetrating radar materials and methods

The project also utilised GPR as a ground based prospection tool, which can be effective for the investigation of sub-surface sediment stratigraphy of alluvial depositional environments (e.g. Heinz and Aigner, 2003). The surveys used a 200MHz antenna frequency, with a GSSI SIR3000 unit, collecting data with distance calibration through a survey wheel. Data was collected using 512 samples/scan, with 16 bits per sample at 64 scans per second. Field filters were set at three times the antenna frequency for the IIR vertical high pass (600MHz) and one quarter of the antenna frequency for the IIR low pass (50MHz). On site calibration of the signal amplification was made on terrace gravels.

Within a floodplain context, boundaries between geomorphological units are seen as discontinuities, due to different sediment properties. The identification of radar terminations allows a relative chronology for a sequence of sediment units to be constructed (Bristow *et al.* 2005). Interfaces between different geomorphological units represent terminal events in either deposition or erosion (erosional bounding surfaces), and the start of subsequent processes (such as palaeochannel infilling). Estimating the depth of discontinuities within floodplain sediments is complex, due to different dielectric constants found within different geomorphological units. The electrical properties of a sediment unit effect the travel time for a radar pulse.

Within an alluvial context the relative dielectric permittivity (RDP) of different sediment units is critical (the ability of sediment to absorb, reflect and be permeated by, the radar pulse). To calibrate the electric depth model created by the GPR the dielectric properties of the soil profile need to be accurately estimated. Within alluvial environments this is difficult as any GPR transect is likely to cross a series of contrasting geomorphological units, each having a different RDP. Within this project the dielectric constant of the soil was calibrated through comparison with gouge core transects drilled by the project team (Bridge *at al.* 1998). The gouge core transects allowed the depth of silty clay alluvium overlying the gravels to be accurately measured. Gouge core sampling was undertaken at 10m intervals along specific GPR transects. The depth of each sediment unit was recorded with a description of its composition before impenetrable gravel was encountered. All GPR surveys were set out and recorded using differential GPS.

The GPR data was processed through setting the correct time zero and correcting for hyperbola reflections via migration. Background removal filters, vertical high pass and vertical low pass filters were used to process the data. This is a simple processing sequence that produces good quality results in alluvial data sets. ArcGIS (© ESRI, version 8.3) was used to co-register, integrate and query the data. LiDAR data was imported as point cloud data and transformed into a TIFF image within ArcGIS. The GPR data was processed in Radan (© GSSI, version 6.0) and depth slices were exported as XYZ data. Images were produced within Surfer (© Golden software INC, version 8.02) and imported into ArcGIS as TIFF images files. The HER data was imported as point data with recorded attributes such as site name, method of identification, archaeological interventions or archaeological period, and was provided by Leicestershire and Derbyshire County Councils. Aerial photographs were imported as JPEG georectified images. The geomorphological and chronostratigraphic models were produced through the on-screen digitisation of 1:5000 field maps, using attribute encoded polygon shape files. Geological information was supplied by BGS as polygon shape files mapped at 1:50,000, with solid and drift geologies. The pseudo 3D modelling was undertaken in ArcScene (© ESRI, version 8.3).

Chapter 4: stratigraphic modelling

4.1 Stratigraphic overview of the study area

A preliminary model of stratigraphic development for the study area was created during the first phase of the project (Brown *et al* 2005: chp 9). This model was developed through a combination of data sources including BGS geology maps, airborne remote sensing, ground based remote sensing and invasive coring transects. One of the aims of the second phase of the project was to refine the phase 1 understanding of the stratigraphy of the study area through the analysis, integration and interpretation of: (1) borehole data supplied by Lafarge Aggregates Ltd; (2) Geoprobe cores drilled for OSL sampling of sediments and (3) further gouge cores used to investigate palaeochannels. The stratigraphic data from all of the various data sources was used to assess three-dimensional interpolation and modelling techniques for investigating subsurface stratigraphy and alluvial architecture. This chapter provides an overview of the stratigraphy of the study area established in phase 1, along with the results and assessment of the proposed three-dimensional modelling methodology. The stratigraphic understanding of the study area was supplemented considerably through access to record a series of exposed sediment faces within the Warren Farm Quarry (NGR SK4772330158) and so the results of this fieldwork are discussed. A final summary of the stratigraphic modelling of the study area is then provided, prior to the results of the refined chronostratigraphy and radiometric dating program being described in chapter 5.

4.1.1 Introduction to the study area

4.1.1.1 Geology

The geology of the study area has been mapped by the British Geological Survey (BGS) at 1:50,000 scale (sheet 141, 1974). Four main lithologies were identified within the study area: sand and gravel; silt and gravel; clay, silt and sand; and diamicton. The sands and gravels form the terrace deposits to the southwest and northwest of the study area, with the BGS identifying them as late Devensian (MIS 2) in age (Holme Pierrepont Sands and Gravels). The silt and gravel deposits covering much of the central part of the study area have been mapped by the BGS as Hemington Terrace deposits. These silts and gravels were probably deposited by channel migration and braiding during the early to mid Holocene and are essentially the reworking of the Devensian sediments (Brown *et al* 2005). The clay, silt and sand is concentrated along the modern channels of the Trent and Soar, as well as along the larger and topographically lower palaeochannels in the study area, and are mapped by the BGS as alluvium. These deposits are a result of overbank sedimentation in both abandoned channels and across the wider floodplain. Further to the west of the study area is an area of poorly consolidated material that has been classified by the BGS as Diamicton, a probable glacial deposit. In addition, the BGS also highlight an area of Syston Sand and Gravel on a low terrace of the River Soar to the southeast of the study area, probably resulting from an earlier Devensian aggradation (MIS 4).

4.1.1.2 Topography

The LiDAR LP DTM data provided an accurate model of the topographic variation present across the study area. In broad terms the LiDAR distinguished a general trend of decreasing elevation from north to south (i. e. towards the modern Trent channel). When compared to the stratigraphic model established in phase 1, it can be observed that this change in elevation corresponds with the tripartite division of the geomorphology of the study area into two river terraces and the modern floodplain. The Devensian terrace located to the south/southwest of the study area (Terrace 2) is evident as higher ground, with a notable decrease in elevation towards the Holocene terrace (Terrace 1) in the central part of the study area. To the north of the study area is the modern floodplain, surrounding the contemporary channel system. The elevations on the floodplain are generally significantly lower than those on the Holocene terrace to the south.

Although this general trend of decreasing elevation from south to north can be identified within the study area, there is also a considerable amount of micro-topographic variation present within each geomorphological component of the landscape. This topographic variation was clearly visible in a series of terrain profiles produced from the lidar elevation models (Brown *et. al* 2005: 7.2). The profiles were highly irregular, demonstrating significant decreases in topography where they crossed palaeochannels, as well as a tendency towards minor undulations and slopes across the terrace and floodplain surfaces themselves.

As stated in Phase 1, the LiDAR elevation profiles indicate a higher level of topographic irregularity than is generally assumed for alluvial environments. This irregular variation in height values is probably the result of the erosion of formerly flat floodplains by channels that have subsequently been abandoned, as well as reflecting the natural topographic variation of a former floodplain, which was dominated by what appear to be scroll-bars and braid-plan morphology.

4.1.1.3 Stratigraphy

The stratigraphy of the study area outlined in phase 1 was established through combined ground-penetrating radar (GPR) surveys and gouge coring transects. The transects were targeted on the various locations across the Devensian and Holocene terraces, and the modern floodplain.

4.1.1.4 Terrace 2 (Devensian) stratigraphy

The stratigraphy of the Devensian terrace was revealed most clearly through the T2T1 GPR and gouge core transect (Brown *et al* 2005:5.3). The thickness of alluvium overlying the gravel deposits on Terrace 2 was shallow, generally being between 0.3-0.4 m. The alluvium comprised a red brown clayey silt containing fine medium sand. A topographic depression partway along the survey line suggested the presence of a palaeochannel, an interpretation supported by the recognition of a yellow brown sandy clay identified during coring (this clay may represent the basal fill of an early channel). The sandy clay deposits were relatively shallow, however, and are

considered to have a low palaeoenvironmental potential. The gravels beneath the alluvium demonstrated some limited internal variation, with the GPR survey isolating four sub-units of lower reflectance within the main gravel body (Brown *et al* 2005:5.3). The bedrock was identified at a depth of c. 4 metres below the ground surface.

4.1.1.5 Terrace 1 (Holocene) stratigraphy

A series of GPR surveys and gouge core transects were carried out across the Holocene terrace during the phase 1 fieldwork, with the Terrace 1 transect 1 (T1T1) revealing the stratigraphy of the terrace with clarity. The depth of the red brown clayey silt alluvium across the terrace was found to be variable, although was generally quite shallow at c.0.40-0.50 m. The variation in the thickness in alluvium is partially due to the presence of numerous palaeochannels incised into the terrace, with some having accumulated significant quantities of alluvium onto the terrace surface. Transect T1T1 identified five palaeochannels within its 395m length. These channels were all incised into the gravel deposits of the terrace, with a relative stratigraphic relationship between the channels themselves being established where the features clearly cut across each other. The GPR surveys indicated that the gravels on Terrace 1 were heterogeneous in structure, with a broad division between stronger and weaker reflecting units (Brown *et al* 2005:5.2.1). It is unclear whether this variation is due to the weaker reflecting gravels representing earlier Devensian deposits lying beneath stronger reflecting Holocene gravels, or whether the reflectance values are showing two Holocene gravel units with differing sand and gravel ratios. It is worth noting that in the nearby Hemington gravel pit, Devensian gravels were exposed underlying the later Holocene gravels (Salisbury 1992:159). The depth to the bedrock beneath the gravels at Lockington was not established for Terrace 1.

4.1.1.6 Modern floodplain stratigraphy

The stratigraphy of the modern floodplain was found to vary considerably across the areas surveyed through GPR and gouge coring. The depth of the red brown clay alluvium ranged from shallow over gravel deposits, to much thicker within the numerous palaeochannels, which are incised into the gravel deposits underlying the modern floodplain. Considerable variation was also revealed within the gravel deposits. Distinct gravel units with higher and lower reflectance signatures were revealed by the GPR surveys, suggesting deposits with differing sediment architecture possibly suggesting different migration patterns. The depth of gravel deposits on the lower floodplain was considerable, reaching over 2 metres in places, with the contact to bedrock not determined.

4.2 Three-dimensional stratigraphic modelling of the study area using existing data sets

4.2.1 Outline

The gouge core transects and geophysical surveys conducted across the study area provided detailed information about the stratigraphic development of the particular sample locations. This information was supplemented by the provision of thirteen previously unpublished borehole logs for the study area by Lafarge Aggregates Ltd. In order to better understand the overall stratigraphy of the floodplain, these data sources were used to create a generalised model of the whole study area. It was hoped that this generalised stratigraphic model could be used as a guide to isolate areas of higher archaeological and palaeoecological potential.

4.2.2 Methodology of wider area 3D stratigraphic model

The data for constructing the three-dimensional stratigraphic model came from the interpretation of the borehole logs, the gouge core transects, the OSL sample cores and the core transects along the ground-penetrating radar (GPR) survey profiles (Fig. 4.1). Thirteen borehole logs were obtained for the project, courtesy of Lafarge Aggregates Ltd, providing detailed stratigraphic information for a series of locations across the study area. These logs provided National Grid coordinates for the borehole locations, as well as a classificatory breakdown of the main sediment units that were present. In total, there were also 248 gouge core records generated during the project, including cores taken along the GPR transects. 29 separate logs were also obtained from the cores taken to provide sedimentary samples for OSL dating. The sediment terminology was standardised across the various data sets and Excel tables were produced recording the surface elevation of each core, as well as the depth to the base of alluvium and, where possible, the depth to the base of the sands, which often form the supra bar sediments of the gravel bar cores.

An Excel table combining the stratigraphic information from all the different data sets was produced and put in to a format that was compatible with the Borehole Manager within Rockware's Rockworks software. The tabular data was imported in to the Borehole Manager in Rockworks and a series of two-dimensional logs and cross-sections, as well as three-dimensional fence diagrams and surfaces were constructed. The data was saved as Rockworks 2D ('.rkw') or 3D ('.xml') graphic image files. The stratigraphic fence diagrams were also exported from Rockworks as ESRI 3D shapefiles for integration into ArcGIS ArcScene for display in a pseudo three-dimensional environment along with other data from the project (Figs. 4.2-4.4).

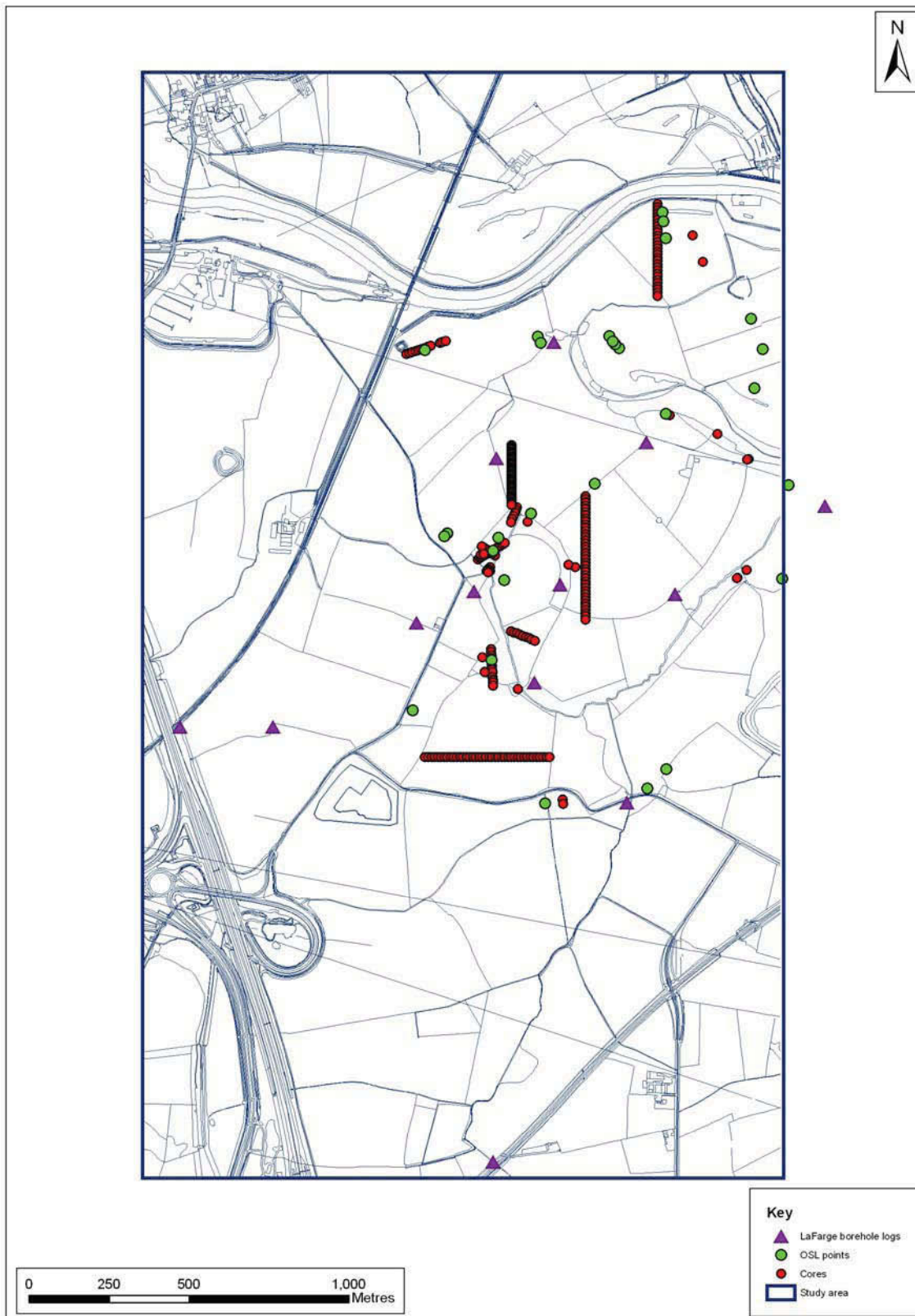


Fig 4.1: Location of data points for the 3D stratigraphic modelling (map by permission of OS).

4.3.3 Summary of modelling

The three-dimensional modelling of the wider area using the borehole and gouge core data provided mixed results in terms of resolution and interpretive information, largely due to the uneven distribution of sediment logs across the study area. In areas where a dense and regular arrangement of cores have been taken, for example where core transects followed the route of a GPR profile to allow depth calibration, an accurate and representative three-dimensional fence diagram can be produced. In these locations within the study area, the fence diagrams provide a detailed record of the depth and stratigraphic relationships of the key sediment units. However, attempting to produce fence diagrams between cores or boreholes that are widely spaced and with few intervening logs is problematic. To assess the methodology, fence diagrams were produced between widely spaced logs and then intervening cores were used to assess the validity of the interpolated profile. This process demonstrated that these fence diagrams showed little resemblance to the subsurface stratigraphy. In certain cases the surface topography had changed considerably, even between relatively closely spaced sediment logs, leading to the subsurface fence diagram displaying above the ground surface when viewed in a three-dimensional environment.

The attempt to use the borehole and core information to generate a subsurface Digital Elevation Model (DEM) representing the base of the alluvial deposits was equally problematic. The method was heavily dependent on the specific interpolation method employed and was only capable of creating a very coarse surface showing the general trend across the study area (Fig. 4.5). As with the fence diagrams produced from widely spaced cores, the uneven distribution and relatively small number of sample points from which the surface has been interpolated means that the model is of limited value for determining specific areas of high archaeological or palaeoenvironmental potential. Without a dense, carefully targeted and systematic distribution of sediment logs it is suggested that three-dimensional subsurface modelling be used with some degree of caution. Fence diagrams and surfaces produced from core transects or closely spaced logs were able to create accurate depictions of the stratigraphy. However, without a dense concentration of raw data, the interpolation methods required to produce three-dimensional models can result in false representations of subsurface stratigraphy.



Fig 4.2: Location of stratigraphic fence diagrams (map by permission of OS).

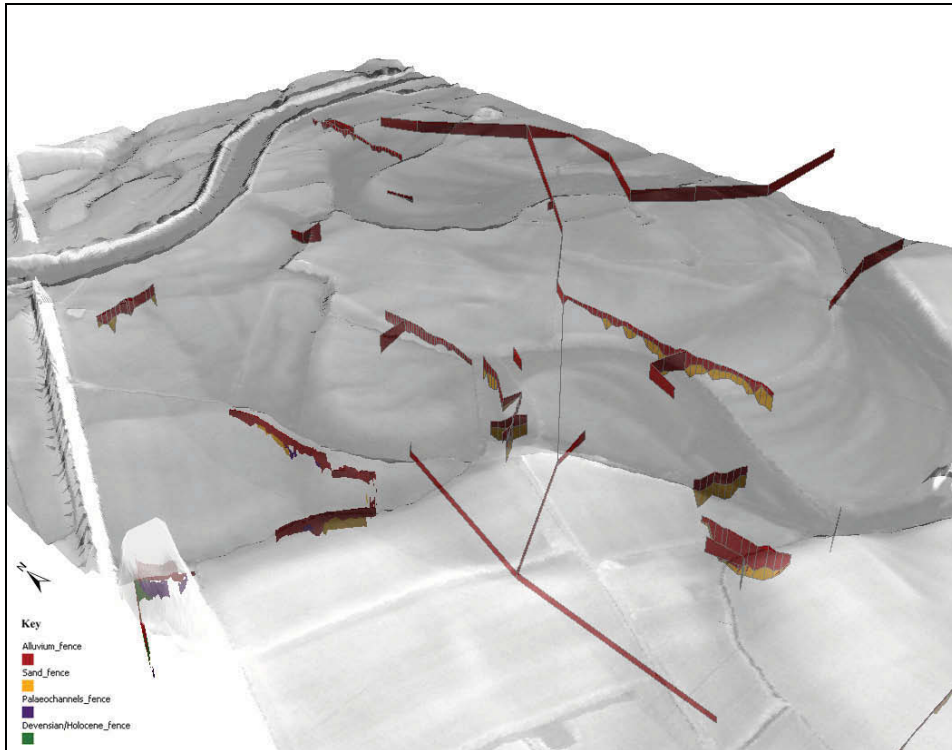


Fig 4.3: ArcScene visualisation of study area stratigraphic fence diagrams below lidar elevation model.

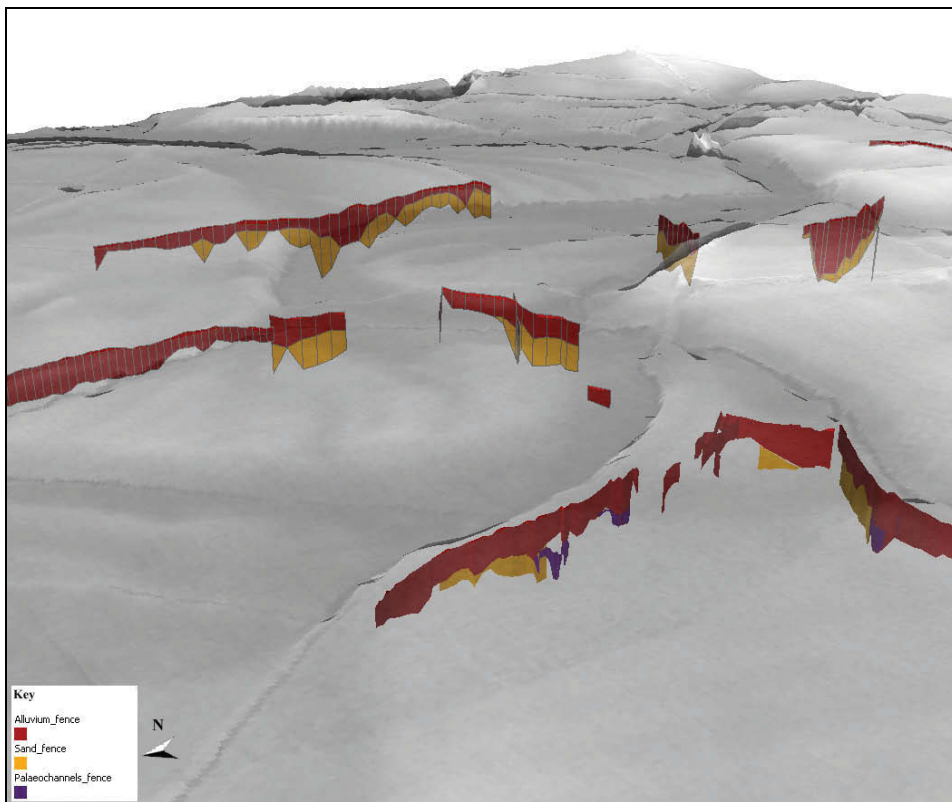


Fig 4.4: ArcScene visualisation of Terrace 1 stratigraphic fence diagrams below lidar elevation model.

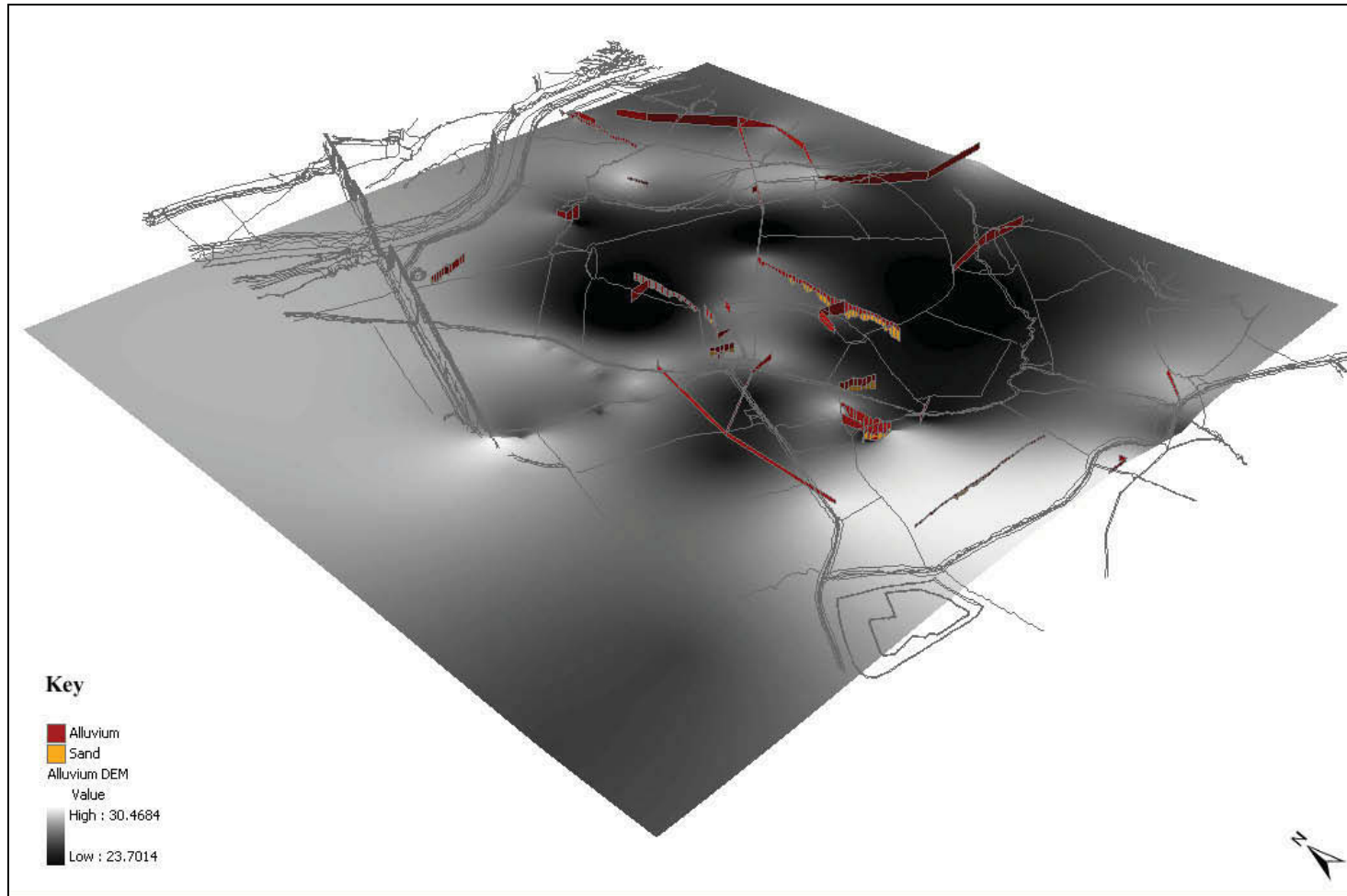


Fig 4.5: Interpolated surface showing base of alluvium across the study area (map by permission of OS).

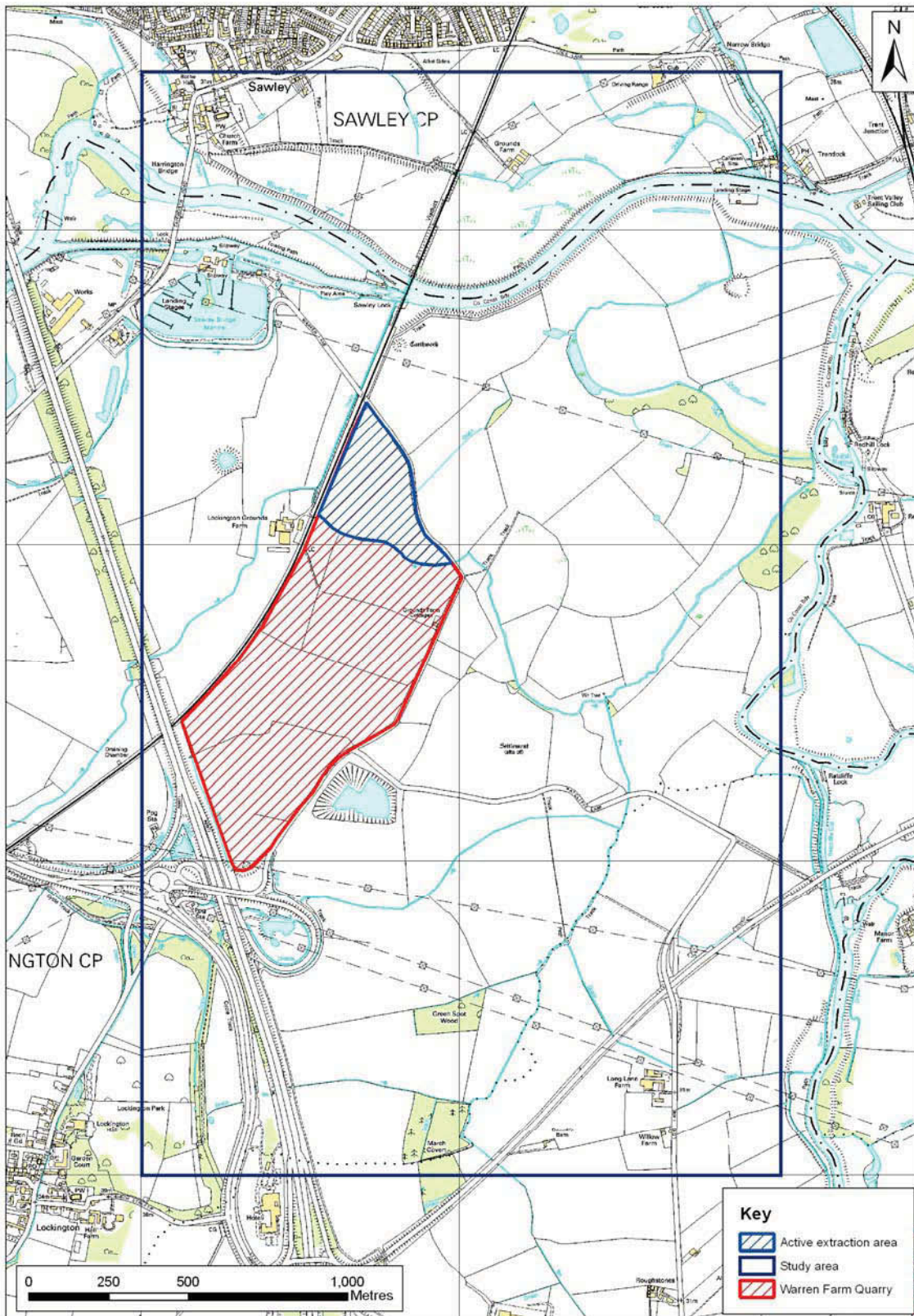


Fig 4.6: Location of Warren Farm Quarry and the active extraction area (map by permission of OS).

4.3 High resolution 3D stratigraphic modelling at Warren Farm Quarry

4.3.1 Background

During the January 2006, the opportunity arose to record a series of palaeochannels that had become exposed during the extraction of aggregates in the Warren Farm area of Lockington Quarry, owned by Lafarge Aggregates Ltd (Fig. 4.6). Consent had been granted to begin extraction at the Lockington site in 1995, with an estimated 2.77 million tonnes of sand and gravel projected to be removed by the scheduled infilling date of the quarry in late 2006 (Leics. County Council:1995). The exposure of sections within Warren Farm Quarry displaying a variety of floodplain components, such as palaeochannels and terrace deposits, afforded the opportunity to record detailed, high resolution stratigraphic information. This data could then be compared to the more general stratigraphic knowledge of the study area obtained through boreholes, coring transects and the various remote sensing techniques employed in the project. Importantly, part of the Warren Farm quarry is situated within the vicinity of the mapped interface between the Devensian and Holocene terraces and is therefore an area with considerable geoarchaeological potential. Permission to access the quarry and record the sections was kindly granted by Lafarge Aggregates Ltd, the company currently working the extraction area.

4.3.2 Methodology of stratigraphic recording

In total six channels were identified and recorded within the exposed quarry faces, numbered 1, 2, 3, 4a, 4b and 5. These channels were all located towards the northern extent of the extraction area, between Lockington Grounds Farm to the west, Grounds Farm Cottages to the south and Warren Lane to the north and east (Fig. 4.7). It was particularly fortunate that the quarry was developed since LiDAR had been flown, as this provided a comparison between quarry exposure stratigraphy and the LiDAR data. The recording of the channels was undertaken using two methods; hand-drawn recording of sedimentary sections and the digital recording of stratigraphic information (heights of boundaries, etc) using dGPS. The section drawings were produced at a scale of 1:50 using a temporary datum line positioned against the quarry face and with the datum points surveyed in using the dGPS. The drawings were produced on permatrace overlain on a gridded drawing board and using standardised sediment descriptions consistent with the stratigraphic terminology employed during coring. The position of samples removed from the quarry faces, for either radiometric dating or palaeoenvironmental assessment, were recorded on the drawings and also with dGPS. The drawings were scanned and digitised to provide digital copies of the quarry faces, allowing the vertical exaggeration of the sections where necessary for display purposes.

The recording of the sections using dGPS aimed to provide a detailed digital record of the stratigraphy of the quarry that could be used to create a three-dimensional subsurface model. The GPS recorded a series of XYZ points along the ground surface, the base of the section and any intervening stratigraphic boundaries (Fig. 4.8). The survey focused on the palaeochannels visible in the section faces and recorded the

location and outline of the channels, the thickness of alluvium, sand and gravel deposits and where the boundary between the Devensian and Holocene terrace sediments was visible. The existing survey control network already established across the study area was used to fix the survey accurately.

Rockware's Rockworks software was again used for the subsurface modelling of the stratigraphic information obtained from the GPS recording of the quarry sections. The GPS points were entered into an Excel spreadsheet in the particular format required by the Rockworks program. The table was then imported into Rockworks Borehole Manager and used to create a series of two-dimensional logs and cross-sections, as well as three-dimensional fence diagrams and surfaces. The stratigraphic fence diagrams were exported as ESRI 3D shapefiles and opened in ArcGIS ArcScene, where they could be displayed in a pseudo three-dimensional environment and compared to other data from the project, such as the lidar surfaces and palaeochannel features mapped from airborne remote sensing (Figs. 4.9 - 4.11).

4.3.3 Stratigraphic description of Warren Farm Quarry palaeochannels

4.3.3.1 Palaeochannel 1

Palaeochannel 1 was located towards the centre of the extraction area and was recorded in a north facing section of the northernmost quarry pit (Fig. 4.12). The sediment stratigraphy indicates that it is a single channel oriented in a north-northeast direction (an interpretation supported by analysis of the elevation surface from the LiDAR survey flown prior to aggregate extraction). The channel was recorded as being approximately 37 metres wide, with a maximum depth below alluvium of 2.68 metres.

The palaeochannel was incised into the Holocene sands and gravels of Terrace 1. A grey-white sand with inter-bedded horizontal bands of darker grey sand is situated immediately below the channel. Below this, to the west of the channel where the section face was deeper, a series of thin bands of orange and grey sands were revealed, interspersed with bands of red and grey sandy clay.

Two distinct sedimentary units were distinguished within the palaeochannel itself. At the base of the channel was a dark grey-black silty clay containing visible organic remains. This deposit has a maximum depth towards the centre of the profile of c. 2 metres, thinning to 0.1 metres at the eastern edge of the feature. To the west the base rises more steeply, with the silty clay deposit terminating c. 9 metres before the western edge of the channel. The upper deposit of the channel is a light grey silty clay containing occasional small clasts c. 2cm diameter. This deposit is located to the west of the channel, terminating 8.9 metres before its eastern edge. The deposit is thickest towards the western side of the channel, with a maximum depth of 1.2 metres. The channel is sealed by a covering of red brown silty clay alluvium that extends up to the modern ground surface with a maximum depth of 3.2 metres.

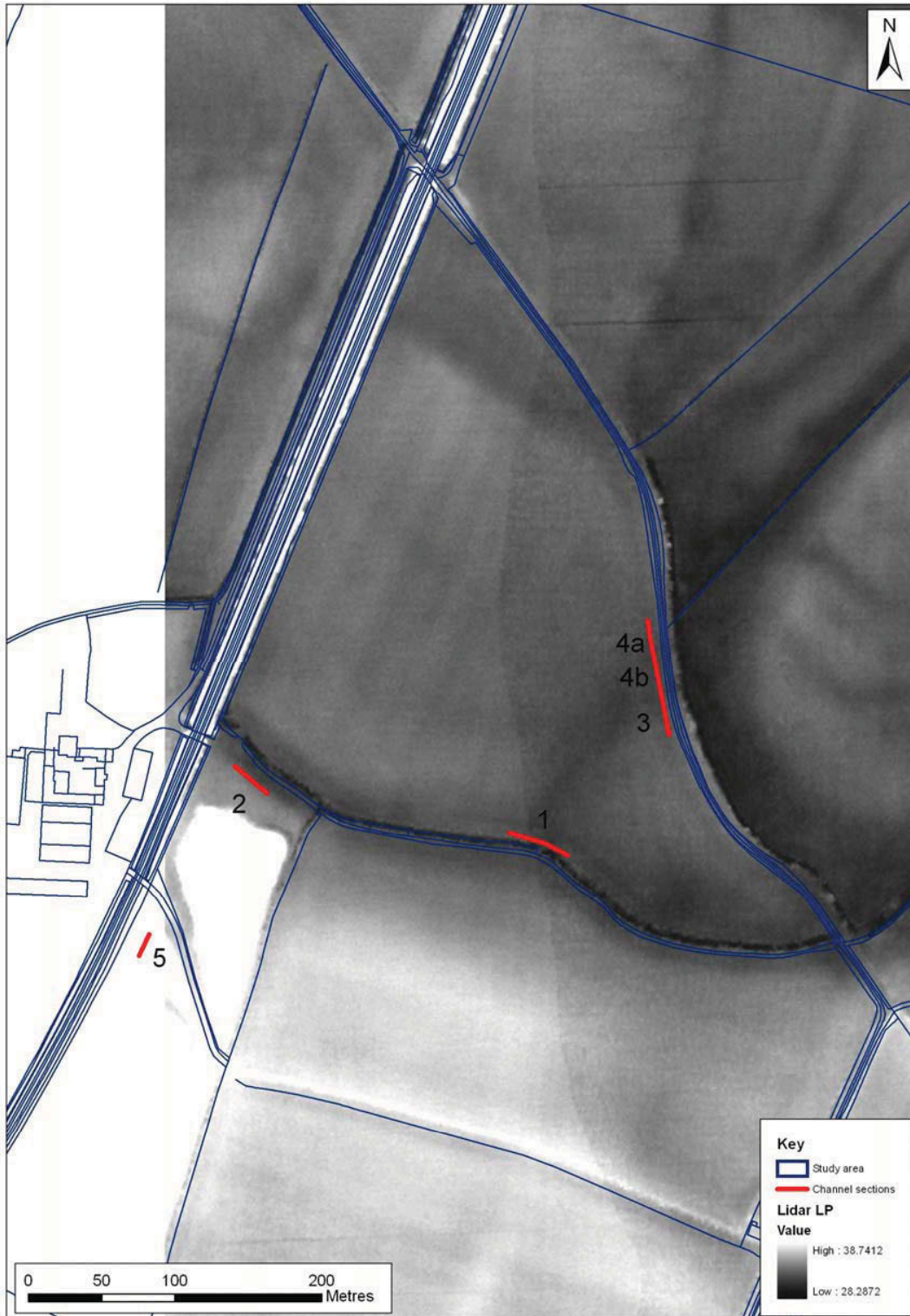


Fig 4.7: Location of sedimentary sections recorded in Warren Farm Quarry, overlain on lidar elevation model (map by permission of OS).



Fig 4.8: Location of GPS data points along visible stratigraphic boundaries in Warren Farm Quarry (map by permission of OS).

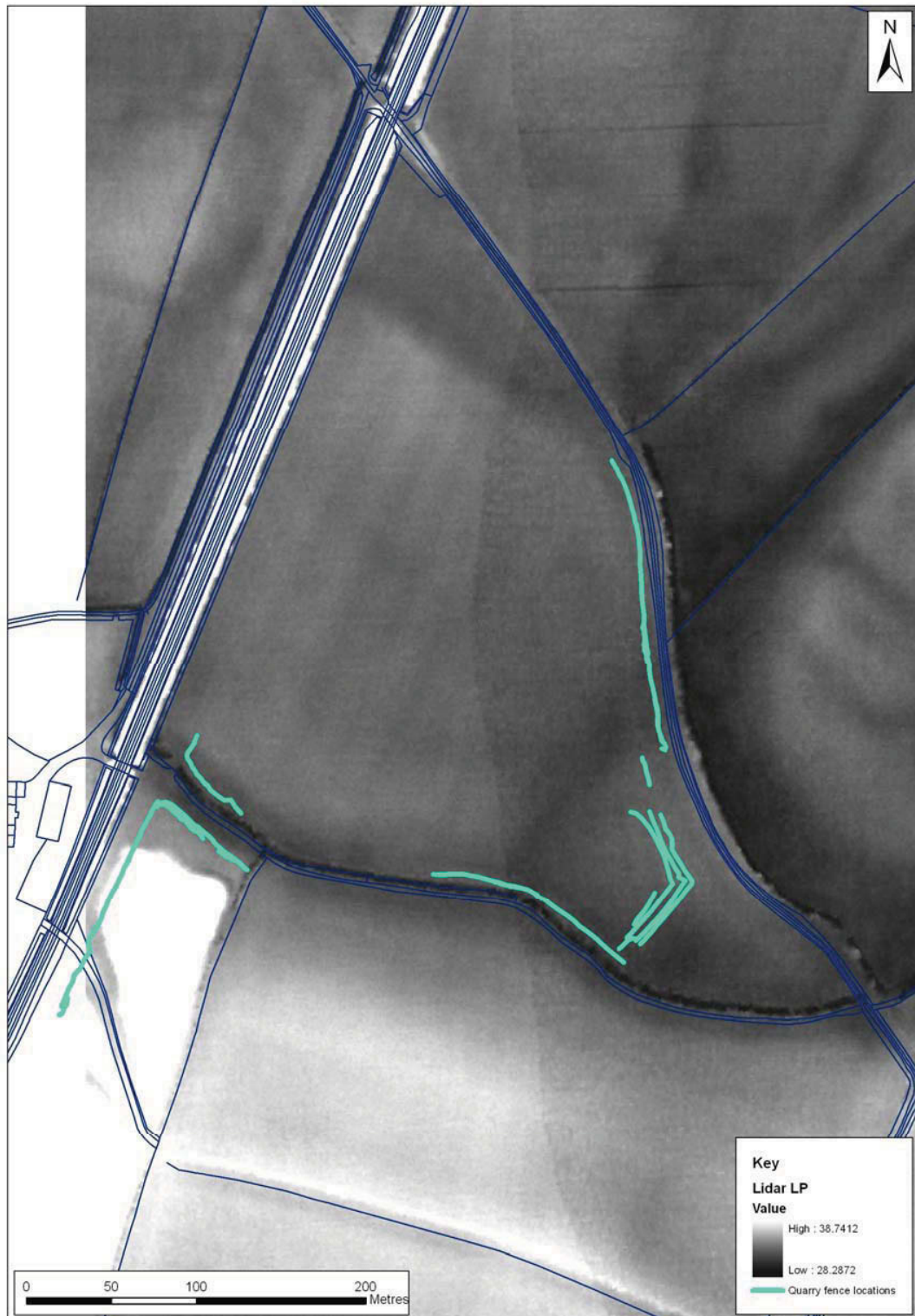


Fig 4.9: Location of stratigraphic fence diagrams within Warren Farm Quarry, overlain on lidar elevation model (map by permission of OS).

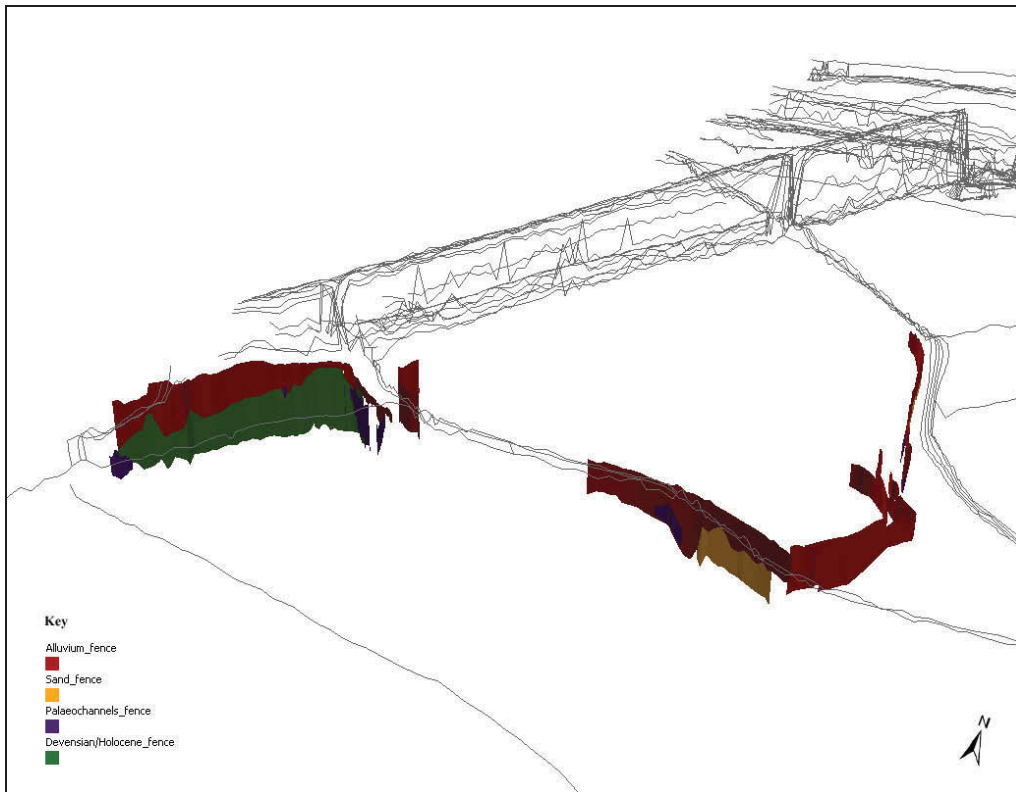


Fig 4.10: ArcScene visualisation of Warren Farm Quarry stratigraphic fence diagrams (map by permission of OS).

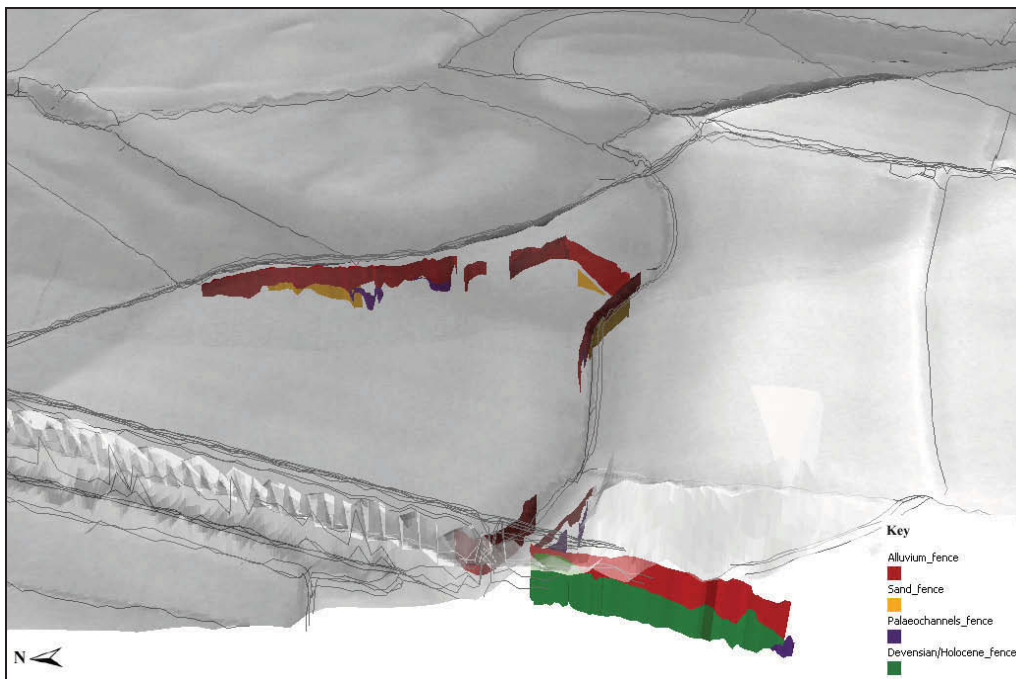


Fig 4.11: ArcScene visualisation of Warren Farm Quarry stratigraphic fence diagrams below lidar elevation model.

4.3.3.2 Palaeochannel 2

Palaeochannel 2 was located towards the western boundary of the quarry and was recorded in a southwest facing section (although the channel was also partially visible in a section face on the opposite northern side of a large access road baulk) (Fig. 4.13). The quarry face was cut obliquely across the channel, providing a section available for recording that measured c. 28.75 metres wide. The channel has a maximum depth below alluvium of 3.5 metres.

The palaeochannel was incised into the Holocene sands and gravels, with the channel extending broadly northwest-southeast trimming the boundary between the Holocene and Devensian terraces (Terraces 1 and 2 respectively). The channel has incised into a matrix supported sandy gravel along much of its profile, although with the southeastern side cutting into a yellow-orange silty sand that overlies a clast supported gravel. The matrix supported sandy gravel was exposed to a maximum thickness of 1.75 metres, but the steep slope of the section face at this point prevented the base of the deposit from being recorded.

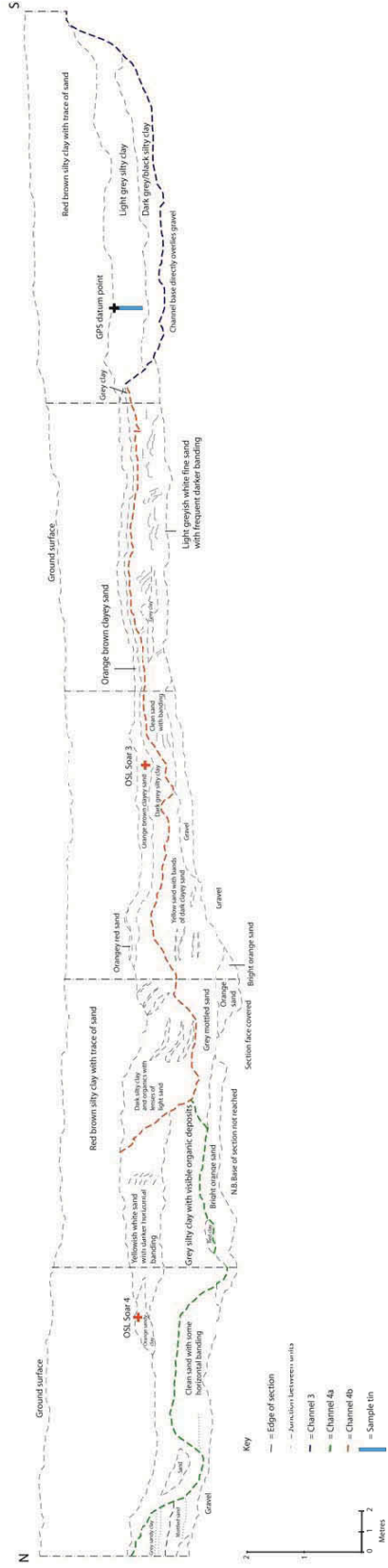
Although the section face was obscured in several places, due to modern slumping during the extraction of the sands and gravels, a considerable portion of the channel was available for recording. Two discrete sedimentary units were identified within the palaeochannel itself, showing similar stratigraphy to channel 1. At the base of the channel was a dark grey silty clay, again containing visible organic remains. The deposit extended from the edge of the channel at the northwest, gradually increasing to a maximum thickness of c. 2.10 metres in the centre. Above this basal deposit lay a lighter grey silty clay with a maximum thickness of c. 1.60 metres. The palaeochannel was sealed by a relatively thin covering of red brown silty clay alluvium, which was deepest to the northwest of the channel at c. 1 metre thick, gradually reducing to a thickness of only 0.50 metres to the southeast.

4.3.3.3 Palaeochannel 3

Palaeochannel 3 is located towards the northeast corner of the quarry and was visible in the southwest facing section, which runs parallel to the line of Warren Lane (Fig. 4.14). The channel was recorded in a c. 78 metre long section that comprised of three complexly interrelated channel units (channels 3, 4a and 4b). Channel 3 is 19.6 metres wide and has a maximum depth below alluvium of c. 1.10 metres.

The palaeochannel extends broadly southwest-northeast and is incised into the Terrace 1 Holocene sands and gravels. The northern side of the profile indicates that the channel has truncated the southern extent of the deposits filling channel 4b, making channel 3 postdate channel 4b. Below this the channel has incised through a layer of light greyish white fine sand containing frequent banding of darker sand, before reaching a layer of Holocene gravel at its base.

Trent-Soar
Warren Farm Quarry
Channels 3 and 4
West facing section



Trent-Soar
Warren Farm Quarry
Channel 5
Southeast facing section

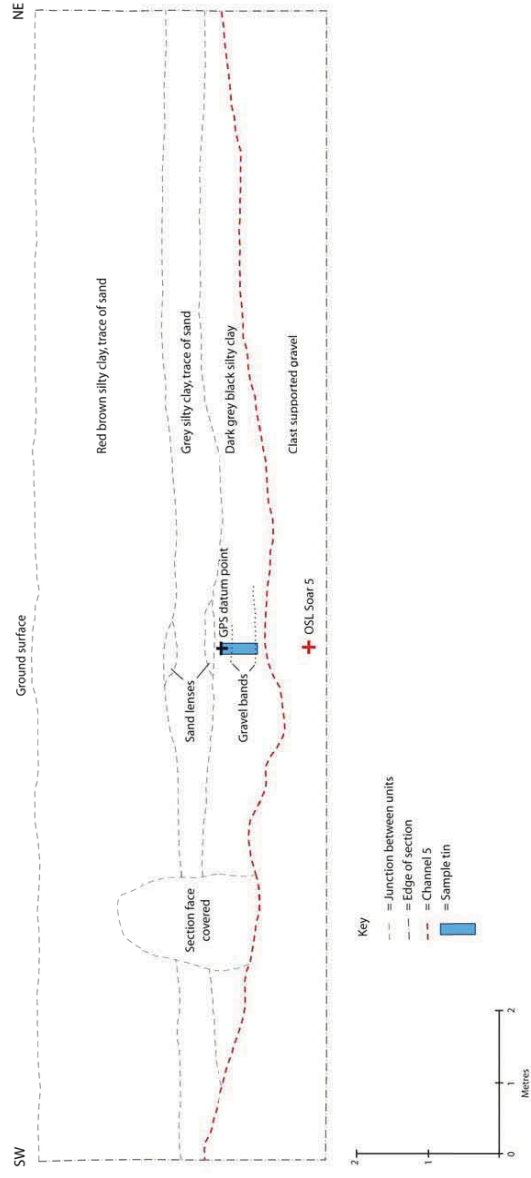


Fig 4.14 (top): Drawn stratigraphic sequence for channels 3, 4a and 4b in Warren Farm Quarry.
Fig 4.15 (bottom): Drawn stratigraphic sequence for channel 5 in Warren Farm Quarry.

Within the palaeochannel itself was a similar bipartite arrangement of sediment stratigraphy as in channels 1 and 2. A dark grey-black silty clay at the base of the channel was overlain by a lighter grey silty clay. The lower silty clay fill of the channel contained visible organics and was present to a maximum thickness of c. 0.5 metres. Above this, the grey silty clay was notably thicker, up to c. 0.8 metres towards the centre of the channel. A layer of red brown silty clay, slightly sandy in places, sealed the palaeochannel. Above channel 3 this alluvial deposit reached a maximum thickness from the ground surface to the channel fill of over 1.4 metres, although the deposit also overlay channels 4a and 4b.

4.3.3.4 Palaeochannel 4a

Palaeochannel 4a is located in the same southwest facing section running parallel to Warren Lane in which channels 3 and 4b were recorded (Fig. 4.14). The channel lies immediately north of channel 4b and extends for a length of c. 23 metres, although this is clearly only a partial width since the feature has been truncated to the south by channel 4b. The northern edge of the channel appears complete and displays a moderately steep sided channel with an undulating base. The channel has a maximum depth below the alluvial overburden of c. 1.8 metres. The channel has incised into the Holocene sand deposits of Terrace 1, with both a bright orange sand deposit and a light sand with darker banding being visible below the channel profile. To the north of the channel the Holocene gravels were visible at the base of the section.

The primary fill of the channel is a grey silty clay with visible organic deposits, which reaches a maximum thickness of c. 1.15 metres. Although this deposit is comparable to the lower fill of the other channels that have been recorded, the other deposits in channel 4a appear distinct from the in-channel sediments elsewhere in the quarry. A deposit of yellowish white sand containing darker horizontal banding is located above the grey silty clay. This deposit has a maximum depth of c. 0.8 metres and is overlain by a small pocket of orange sandy clay further to the north, measuring only c. 0.35 metres thick. To the south, deposits forming channel 4a have clearly been truncated by the incision of channel 4b, a stratigraphic relationship indicating that channel 4a predates channel 4b. Channel 4a has been sealed by the same alluvial deposit of red brown silty clay that also covers channels 3 and 4b. Above channel 4a this alluvial deposit reaches a thickness of c. 2 metres.

4.3.3.5 Palaeochannel 4b

Palaeochannel 4b is situated immediately north of channel 3 and was recorded in the same c.78 metre long section face located towards the northeast corner of the quarry (Fig. 4.14). The channel is 38.4 metres wide, with a steep sided profile to the north and a notably more gentle sloping edge to the south. The base of the channel undulates considerably at its northern end, although with a much flatter surface to the south as the slope of the profile decreases. The channel has a maximum depth below alluvium of c. 1.35 metres.

The channel is again incised into the Holocene sands and gravels of the Terrace 1 deposits. However, it is also clear that at its northern edge, the channel has incised

into the deposits filling channel 4a, indicating that channel 4b postdates channel 4a. The base of channel 4b is cut into light greyish white fine sands containing frequent mottling and bands of darker sand. Approximately halfway across the channel profile the base dips slightly to also meet the Holocene gravels that are higher at this location than elsewhere in the section.

The lower fill of the palaeochannel is a dark grey-black silty clay with traces of visible organics and containing numerous lenses of light coloured sand. This deposit has a maximum thickness of c. 1.35 metres. Overlying was a relatively thin layer of orange-brown clayey sand up to c. 0.8 metres thick. This upper layer was only located to the south of the channel, with the dark silty clay fill being overlain directly by alluvium to the north. At its southern margin, the channel has been truncated by channel 3, as mentioned above. The channel is again sealed by the same unit of red brown silty clay that sealed channel 3, although at this location the deposit is thinner, with a maximum depth over channel 4b of c.1.4 metres.

4.3.3.6 Palaeochannel 5

Palaeochannel 5 is located along the western boundary of the quarry area, to the south of channel 2 (Fig. 4.15). The channel was visible in a southeast facing section of the quarry, suggesting a single channel oriented broadly northwest-southeast. The full extent of the channel profile was not visible, but a section measuring c. 16 metres was recorded. The recorded section indicated a relatively flat channel base with only minor undulations. Although the slope to the channel sides appears slight it should be noted that neither edge of the channel was recorded and therefore the actual profile form is not fully understood. The channel has a maximum depth below alluvium of c. 1.6 metres.

Channel 5 differs from the other palaeochannels in that it is incised into the Devensian sands and gravels of Terrace 2, suggesting a much earlier date. The recorded section indicates that the channel has cut into a deposit of clast supported gravel with a maximum recorded depth of 1.65 metres (although the base of the gravel was not reached). The internal stratigraphy of the channel was divided into a lower fill of dark grey-black silty clay, overlain by grey silty clay, sandy in places. The darker silty clay had a maximum thickness of c. 1 metre towards the centre of the section, with the upper fill being shallower and reaching a maximum thickness of c. 0.65 metres. Two narrow (c. 0.15m) sand lenses were also recorded, one immediately above the dark silty clay and the second between the lighter grey silty clay and the overlying alluvium. The alluvium covering the channel was a red brown silty clay containing a trace of sand and measuring a maximum of c. 2 metres in thickness.

4.3.4 Summary

Access to the exposed faces within the Warren Farm area of Lockington Quarry has allowed the detailed recording of the stratigraphy of this part of the study area. Of the six channels visible in the quarry sections, five were found to be incised into the Holocene sands and gravels of Terrace 1, with only one being located in the Devensian deposits of Terrace 2. Although channel 5 is not visible on the LiDAR

elevation or intensity surfaces, its location at the top of the Devensian gravels is of importance in providing a maximum age for channel change in the reach. Channels 1 and 2 are cut into the Holocene sands and gravels of Terrace 1, but are located directly along the junction between this terrace and the earlier Terrace 2 formation. The LiDAR elevation surface reveals evidence of a slight depression extending along a broadly east-west orientation between channels 2 and 1, suggesting that both sections may actually be displaying the same palaeochannel.

Similarly, the LiDAR elevation model highlights another channel extending southwest-northeast between the sections covering channel 1 and channels 3, 4a and 4b. This feature suggests that a channel may have also connected the sediments of the sections drawn at these locations, although the resolution of the lidar does not allow the isolation of a single channel from the three visible in the west facing section along Warren Lane. The internal stratigraphy of channel 3 is most similar to that of channel 1, suggesting that the two may be linked to the same overall feature, but a direct relationship cannot be established. A further complication is that the channel feature visible on the LiDAR surface between channels 2 and 1 appears to continue further to the east of channel 1, with the sinuous field boundary visible on the modern OS mapping following the line of this feature. If channels 1 and 2 are part of the same feature, as well as channels 1 and 3/4a/4b being part of a connected feature, then the channel would have to divide at the location of the channel 1 section. Alternatively, these could relate to separate channels from differing periods, with the possibility that the channel 1 section was reactivated at a later date following its initial cut-off.

4.4 General study area stratigraphic summary

Based on the various data sources and methods of investigating the stratigraphy of the study area a number of general statements can be made:

- The stratigraphy of the study area can be broadly divided into four main sedimentary units:
 1. Devensian Holme Pierrepont Sands and Gravels forming the terrace deposits to the southwest and northwest of the study area. These deposits generally have a low archaeological potential, but may contain intra-gravel palaeochannels of high palaeoecological importance.
 2. Holocene Hemington Terrace silt and gravel deposits covering much of the central part of the study area. These deposits are of demonstrably higher archaeological potential and post date the terrace 2 Holme Pierrepont sands and gravels.
 3. A series of palaeochannels, which generally contain a lower fill of organic silty clay, overlain by grey silty clay. The channels are of high potential for palaeoenvironmental reconstruction and all appear to have incised into earlier gravel deposits (see chapter 5).
 4. These sediment units are generally blanketed by a red brown alluvium of variable thickness.

The construction of the three-dimensional stratigraphic model of the study area provided variable results, primarily because of the uneven spatial distribution and resolution of the sediment logs. In areas where the distribution of cores was sparse, the resulting fence diagrams and surfaces did not accurately reflect the subsurface stratigraphy. However, the method does provide a useful first approximation of the stratigraphy of an alluvial environment, and where the cores were closely spaced the resolution and potential of the resulting models was much higher.

Chapter 5: Chronostratigraphy

5.1 Original chronostratigraphic model

The chronostratigraphic model proposed in Phase I was produced based upon a number of criteria including distance from the modern channels, relative altitude, geomorphological position and correlation with adjacent area, particularly Hemington Fields. As was noted in the Phase I report “The key question of archaeological significance is the depth of the Holocene sand and gravel and whether it overlies Devensian gravels. The fundamental problem is that the Devensian and Holocene gravels are very similar in grain size, clast lithology, shape and even fabric due to the derivation of the later from the former. This means that it is rarely possible to differentiate them from borehole records. It is, however, possible to differentiate between the two from quarry faces due to the presence of archaeology, different coloration (due to Fe staining) and sometimes a different sedimentary structure. From the observations at Hemington it is hypothesized that the Devensian gravels underlie all the later phases of floodplain sedimentation with the exceptions of areas of scour near the present channel”. Despite these uncertainties the model was used for the sampling of the palaeochannels for both the analytical studies and the OSL and radiocarbon dating programmes.

The palaeochannels segment the area into a series of levels:

High	38.7m OD
Middle	34.0m OD
Low	28.2m OD

It is apparent from flood photography (Brown *et al.*, 2005) that high magnitude floods within the contemporary flood frequency-magnitude distribution can inundate both the lower and middle levels, but not the high surfaces. The high level is also seen to correlate to the south and southwest with the large area of Beeston terrace as mapped by the BGS. However, both the LiDAR and GPR show broad shallow channels excavated into the surface of the terraces and by analogy elsewhere (Fyfe *et al.* 2004) these are most likely channels formed during the final stages of gravel deposition during the Late glacial. There are, however, in this reach some deeper narrower channels, which bisect the terraces and have been shown to be of early to mid Holocene age (Brown *et al.* in press). The middle level is characterised by gravel overlain by a variable thickness of overbank sandy silts and clays. It correlates with similar floodplain parcels to the east including meander cores at Hemington. It also has later Prehistoric and Roman archaeology on its surface. It is bisected and eroded into by the southerly of the two major palaeo-Trent meander loops traversing the target area. The complex form of this palaeochannel is its significant depth of sediment and its truncation of later Roman channels, all indicating a late prehistoric age. The series of scroll bars on its inner (northerly) floodplain suggest that over time it moved in a southwesterly direction and on this basis the meander core is also ascribed to the late Prehistoric period. This palaeochannel and floodplain is truncated by the large partially water-filled Trent palaeochannel. There are many similarities in altitude, form and location between this channel and the medieval channels associated with the Old Trent at Hemington. The width of the meander belt and its sinuosity are similar to the Sawley palaeochannel that is of Roman-6th Century age, but a

correlation cannot be proven. Closer to the channel there are a number of old channels sub-parallel to the modern Trent. In some cases the connections are only severed by an artificial levee. This zone also contains engineered river sections and channels such as the Sawley Cut and straightened sections of the Soar.

The comparison between the chronostratigraphic model and the model based upon all the dating evidence is discussed in Section 9.1.

5.2 Radiocarbon dating of palaeochannels

For full details of all the individual ^{14}C dates see Appendix A. A spectrum of palaeochannels of varied age were selected for radiocarbon dating as described in Section 3.2. These have been plotted spatially (Fig. 5.1).

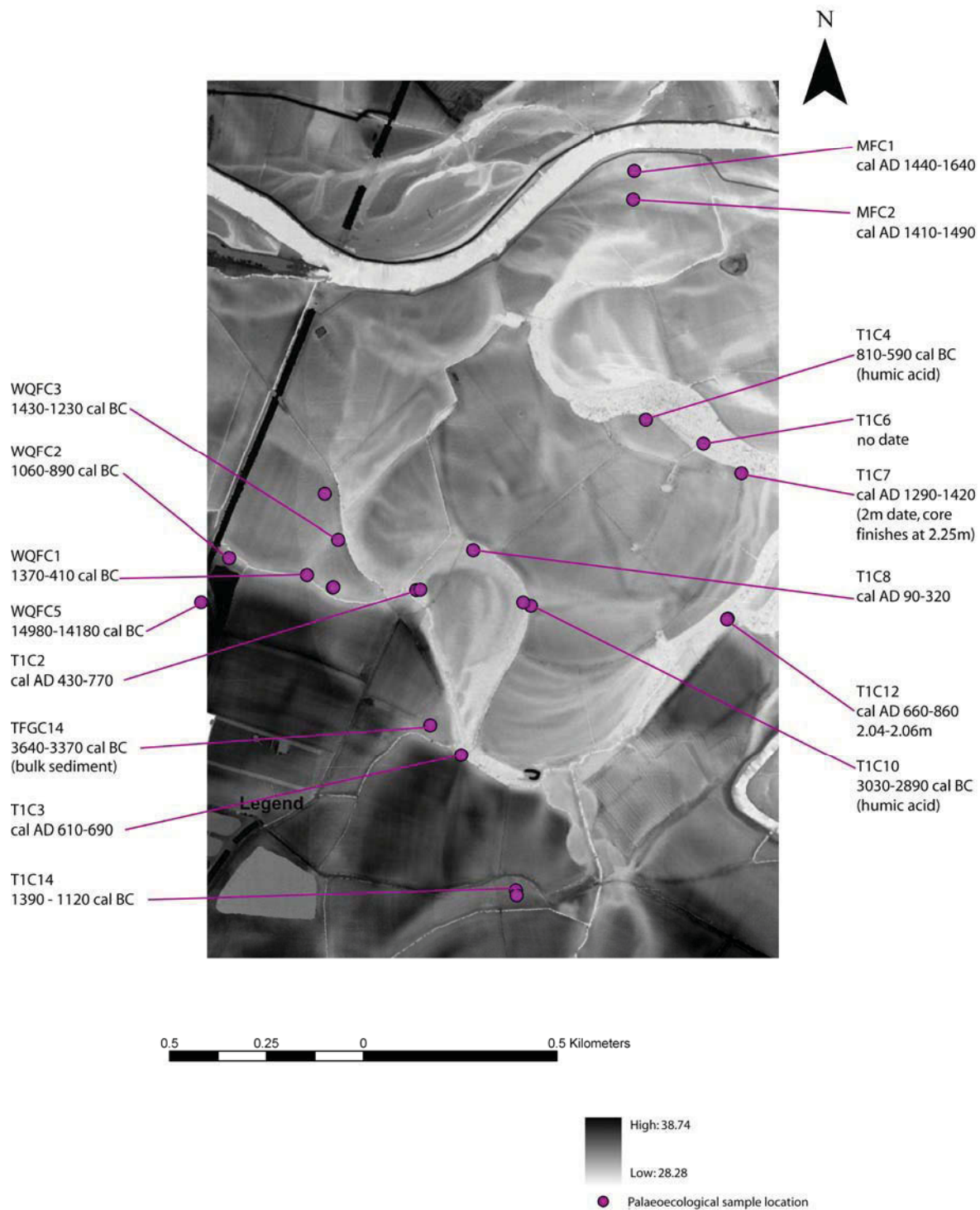


Fig. 5.1: The ^{14}C dates plotted at core/sample locations.

As can be seen from the dates there is a general tendency for the dates to be younger to the north east of the target area with the oldest (Prehistoric) dates clustered at the southern end of the area. However, there are outliers and several of the cores from adjacent palaeochannels have significantly different basal dates (e.g. T1C4 and T1C7). This suggests that there has been re-occupation of channels by main channel

water flow during the Post Roman and medieval period and that the sequence may not be as simple as had at first been envisaged (see Phase I). The general tendency is also for the dates to increase in age with increasing height OD (Fig. 5.2).

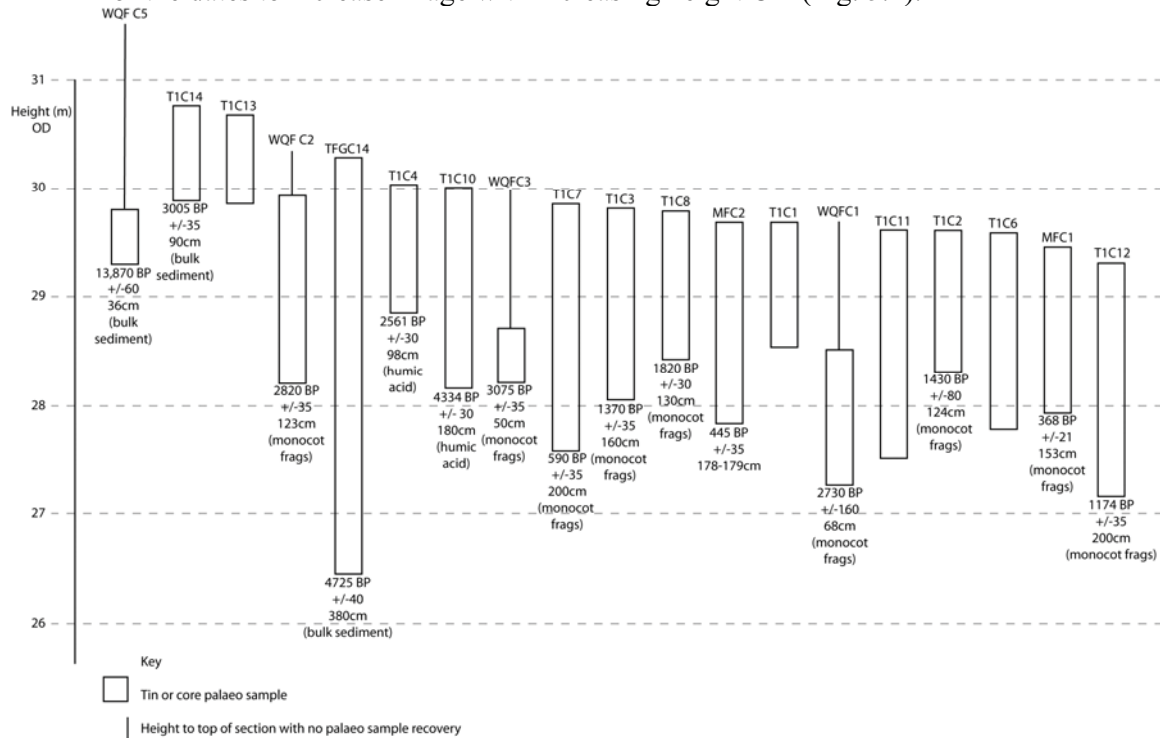


Fig 5.2: A plot of the cores with basal dates against surface height OD.

Figure 5.2 clearly shows that all the dates except one that are older than 2,500 BP occurred from sequences with surface heights of over 30 m OD. This is supportive of the notion that there was a major phase of incision in later Prehistory probably in the Late Bronze or early Iron Age.

5.3 OSL dating of intervening valley floor

The full OSL dating report is given as Appendix A. The OSL dates have been plotted at sample locations (Fig. 5.3). There is again a distinctive spatial pattern with a southeast-northwest age gradient. Here the oldest dates clustering on the southern terrace or around the most south eastern meander loop. There are, however, exceptions and most notably GEO25, which is in a meander core. This date and GEO18 suggest that the meander cores pre-dated the sediments at the base of their defining palaeochannels. This is typical of the re-occupation of meanders by later channel avulsions, which leave the old meander cores as un-eroded islands in the floodplain. The OSL dates have also been plotted against surface height OD (Fig. 5.4).

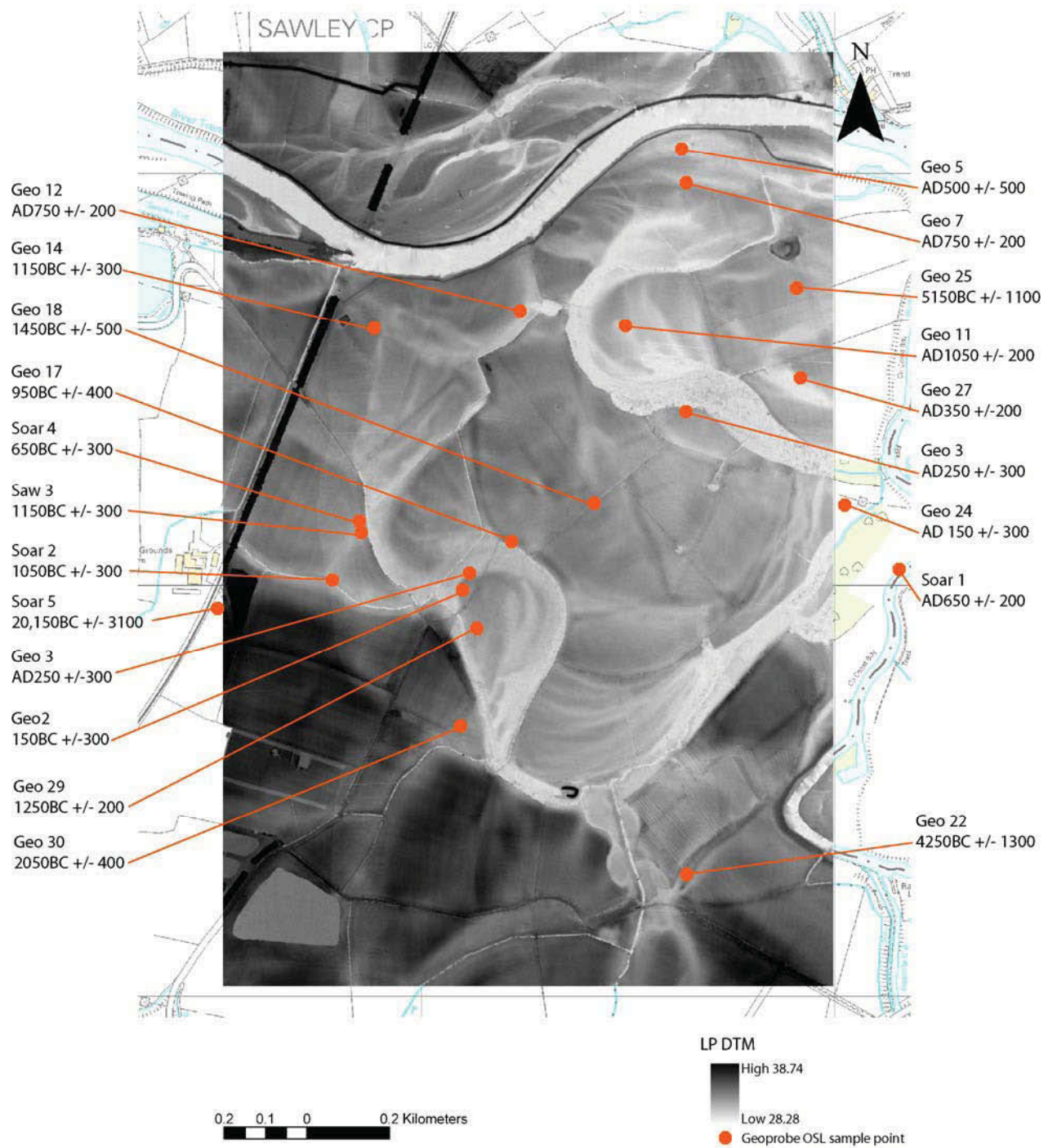


Fig 5.3: The OSL dates plotted at sample locations.

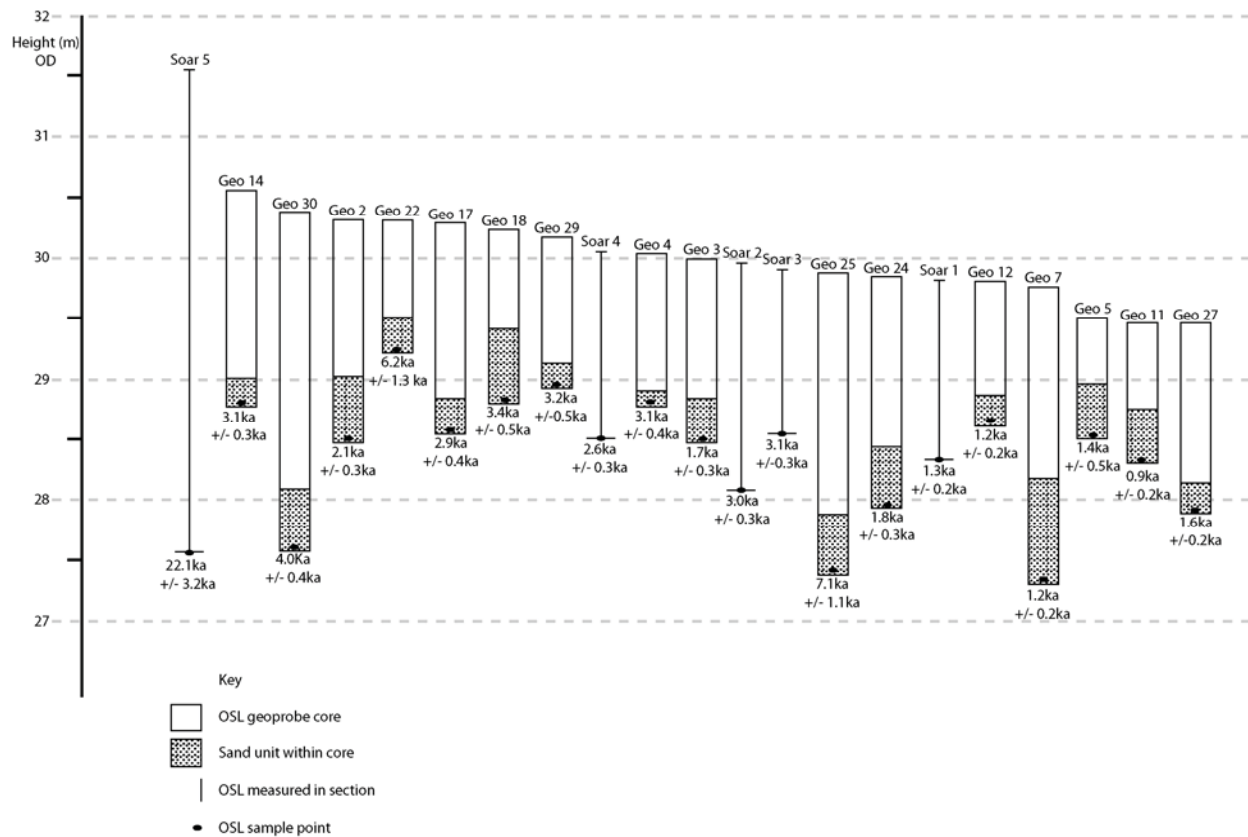


Fig 5.4: The OSL dates plotted by height.

Figure 5.4 also shows the pattern, but is less clear than for the ^{14}C dates. This is because the OSL samples come from a wider variety of geomorphological positions and not just channel fills. Several are from overbank sands sitting on gravels at the edge of channels or in meander cores. The result is an alternation of young and old dates at a variety of heights OD. This also suggests a complex model of overbank sedimentation, channel infilling, channel abandonment and re-occupation and further overbank sedimentation. In theory overbank sedimentation onto gravels could be out of phase with the channel infilling as this occurs principally when the channel has avulsed to another location. Analysis is underway to test this possibility.

5.4 Dendrochronological dating of trees

The discovery of large tree trunks and other timbers in the Warren Farm Quarry during stratigraphic investigations offered the opportunity for sampling for dendrochronological dating. In all 8 trunks all of oak (*Quercus* sp.) were sampled by Dr R. Howard and taken to the Dendrochronology Laboratory at the University of Nottingham. The trees were interbedded within the sands and gravels, which on the basis of both geological geomorphological field mapping and analysis of LiDAR were assumed to be part of T1 (Hemington Terrace), aggraded during the mid Holocene. The main group of trunks were found in the middle of the quarry (Fig. 5.5) and although it is likely that all the tree trunks had been moved slightly during mineral extraction, it appears from the available evidence that the majority were originally

within 1-2 m of the Mercia Mudstone rockhead. All the recorded trunks had intact root boles and none showed evidence for anthropogenic modification (e.g. to old marks), which suggests that they were incorporated into the channel through natural processes of river bank erosion and tree throw on the floodplain. None of the sampled trunks were more than 50m apart.



Fig 5.5: Photograph of the tree trunks from Warren Farm Quarry that were dendrochronologically dated.

Sample number	Total rings	*Sapwood rings	First measured ring date	Last heartwood ring date	Last measured ring date
LOK-Q01 84		h/s?	-----	-----	-----
LOK-Q02	202	h/s?	2871 BC	2670 BC	2670 BC
LOK-Q03	165	h/s?	2818 BC	2654 BC	2654 BC
LOK-Q04	102	h/s?	2790 BC	2689 BC	2689 BC
LOK-Q05	188	h/s?	2883 BC	2696 BC	2696 BC
LOK-Q06	105	h/s?	2623 BC	2519 BC	2519 BC
LOK-Q07	107	h/s?	2735 BC	2629 BC	2629 BC
LOK-Q08	118	no h/s	2928 BC	-----	2811 BC

**h/s? = the last ring on the sample is at or approaching the heartwood/sapwood boundary*

Tab 5.1: Details of samples from Warren Farm Quarry on the river Trent in Leicestershire.

Dendrochronological analysis indicated a high degree of cross matching of 6 of the samples. Combined, they provide a 300 year site chronology very firmly dated between 2928BC and 2629BC (Tabs. 5.1 and 5.2). In contrast, sample 1 does not date at all and suggests that it may either be of an entirely different date for which there is

no reference material; however, it may be possible to date this material in the future as more reference samples become available. Sample 6 does not cross-match with this main group of six samples, but does date independently with a last ring date of 2519BC (Tabs: 5.2 and 5.3).

Reference chronology	Span of chronology	t-value	Reference
England National	4989 - 1681 BC	12.5	(Hillam pers comm)
Shardlow Quarry, Derbys.	2942 - 2610 BC	10.9	(Tyers 2000)
East Anglia: regional	3196 - 1681 BC	9.5	(Brown pers comm)
<i>Langford Quarry, Notts.</i>	2979 - 2125 BC	7.9	(Hillam unpubl)
Colwick Hall 1	3054 - 2697 BC	6.7	(Brown pers comm)
Stourport on Severn, Worcs.	2869 - 2698 BC	6.5	(Hillam pers comm)

Tab 5.2: Results of the cross-matching of site chronology LOKQS Q01 and relevant reference chronologies when first ring date is 2928 BC and last ring date is 2629 BC.

The secure chronology from Warren Farm Quarry, Lockington, suggests a ctive sand and gravel deposition of Terrace 1 sediments during the mid-late Neolithic period. This timescale of deposition accords well with other dendrochronological analyses undertaken regionally including those at Hemington (Salisbury pers com.), Shardlow Quarry, less than 5km upstream (Garton *et al.*, 2001) and downstream at Colwick (15km downstream; Salisbury *et al.* 1984) and Langford (30 km downstream; Howard *et al.*, 1999).

Reference chronology	Span of chronology	t-value	Reference
Wootton Quarry, Isle of Wight	3463 - 2557 BC	6.0	(Hillam 1994)
England National	4989 - 1681 BC	5.8	(Hillam pers comm)
East Anglia: regional	3196 - 1681 BC	5.0	(Brown pers comm)
<i>Langford Quarry, Notts.</i>	2979 - 2125 BC	5.4	(Hillam unpubl)

Tab 5.3: Results of the cross-matching of sample LOK-Q06 and relevant reference chronologies when first ring date is 2623 BC and last ring date is 22519 BC.

The dendrochronological analyses also agree well with the OSL and radiocarbon chronologies developed for the study area. For example organic rich channels incised into the sands and gravels in the quarry have yielded Bronze Age ¹⁴C dates (e.g. WQFC1; WQFC2; WQFC3). OSL dating of supra-bar sand exposed within the quarry have also yielded age estimates of between 1050 BC ± 300 (Soar 2) and 650 BC ± 300 (Soar 4).

5.5 Summary

The core analyses, the OSL and ¹⁴C dating all show that the area has a complex set of deposits of a variety of ages but with spatial patterning. Both the distribution of dates and the complexity of some of the core sequences suggest that this may have been caused by the re-occupation of palaeochannels and complex avulsions rather than a simple migratory pattern. This spatial patterning is described in chapter 9.

Chapter 6: Palaeoenvironmental analysis and taphonomy

6.1 Palaeoenvironmental sample stratigraphy

Before a discussion can begin of the preservation and taphonomy of the environmental samples, the basic sample stratigraphies need to be summarised, in conjunction with their dating. The sample locations with their basal dates are shown (Fig. 6.1). All of the dates on these cores/tins were produced through radiocarbon dating. The stratigraphy of the samples is shown against organic content, carbonate content and magnetic susceptibility in one figure, with the pollen sample locations and the radiocarbon dates shown against stratigraphy on a second figure.

6.1.1 Core MFC2

This core was sampled in a palaeochannel on the modern floodplain. MFC2 has a dark red brown clayey silt A horizon underlain by a reddish brown silty clay. Below this at 56 – 82cm is dark grey/black silty clay, which shows elevated organic and carbonate contents and a higher magnetic susceptibility. Below this at 82 – 116cm is a red brown silty clay, underlain by a reduced grey brown silty clay. A grey brown silty sandy clay is between 151 – 163, with a black clayey sand at 163 – 172cm and a grey brown coarse sand at the base. The unit between 56 – 82cm stands out as having a higher organic content. There was no sand within this unit suggesting a very low energy depositional environment. It is also a notable break between two units of red brown clay and appears to reflect a change in depositional history (Fig. 6.2).

The pollen was evaluated at every 14cm down the core MFC2, starting at 14cm. The date near the base of MFC2 is at 178 – 179cm, which gives a date of 445±345, which is consistent with the date predicted through the original chronostratigraphic model from phase 1.

6.1.2 Core TIC7

This core was sampled in a palaeochannel of the river Soar, located on terrace 1 (Fig. 6.1). Core TIC7 has an A horizon between 0 – 6 cm, underlain between 6 – 45cm by a brown silty clay. After this point (45cm) the core is dominated by two main sediment units. Firstly, there is an upper blue grey with Fe inclusions between 45 – 140cm. Below this between 140 – 225cm is a blue grey clay with visible organic fragments. The organic content is relatively high throughout the core, but does not vary drastically or in a systematic way. The magnetic susceptibility shows a notable peak in the blue grey unit between 45 – 140cm, but this does not correspond with a recognised change in sediment composition (Fig. 6.4).

The pollen samples were taken at 14cm intervals, starting at 14cm. The original basal date for this core was shown to be unreliable (modern radiocarbon age) and further material has been sent for re-dating. Two radiocarbon dates appear coherent with

each other. The date at 90cm is 1020BP +/-35, with the date at 151cm being 1406BP +/-30 (Fig. 6.5).

6.1.3 Core TIC10

This core was taken from a palaeochannel that runs east/west through an area of terrace 1 (Fig. 6.1). This core has a brown silty clay A horizon between 0 – 22cm, underlain by a red brown loam (silt, clay with sand) between 22 – 58cm. Below this a unit extends past the redox boundary, between 58 – 142cm. The upper 58 – 100cm is red brown increasingly gleyed clay with depth. From 100 – 142cm, this unit is grey clay. Between 142 – 158cm is a dark grey clayey silt, with fine sand and heavy Fe and Mn staining. At the base is a dark grey clay with a trace of sand between 158 – 185cm. Overall the organic content through the core is low, with the carbonate content showing no systematic variation with stratigraphy. The organic content is slightly elevated in the basal dark grey clay until between 158 – 185cm. Magnetic susceptibility shows little variation, except an elevation in the A horizon and elevation in the dark grey clay basal unit (Fig. 6.6).

Pollen was sampled at 14cm intervals along the core length, starting at 14cm. The low general organic content of the core meant that finding plant macrofossils to date was problematic and only two dates were recorded on the core, both coming from direct dating of sediment. At 145cm a bulk sediment sample gave a date of 3920BP +/-35, whilst a sample dated from the humin fraction at 180cm gave a date of 4334 BP +/-30. These dates prove that this palaeochannel is considerably older than most of the other palaeochannels on terrace 1 (Fig. 6.7).

6.1.4 Core TIC12

This core was located in the palaeochannel that denotes the boundary between terrace 2 and terrace 1 (Fig. 6.1). The core stratigraphy has a 10cm A horizon of red brown clayey silty, underlain between 10 – 29cm by an organic brown black silty clay. A thin unit of reddish brown silty clay is located between 29 – 37cm. Below this is a large unit of red brown silty clay, stretching from 37 – 139cm. At 139 – 183cm a dark grey clay is encountered, with a basal unit of black grey clay between 183 – 214cm. The organic content is consistently high throughout the core, with elevated levels seen between 10 – 37cm. Magnetic susceptibility also shows elevated values between 10 – 37cm (Fig. 6.8).

Pollen was sampled at 14cm intervals along the core length, starting at 14cm. The dating of the core is not clear, with three dates that are of similar age (within 144 years of the central ages), but their chronological relationship is suspect. The depth of 193cm provides a date on monocotyledon fragments of 1174BP +/-35, whilst the depth of 214cm provides a date of 1030BP +/-40, also on monocotyledon fragments. A further sample at 204 – 206cm was dated at 1275BP +/-35, indicating that the date at 214cm is suspect (Fig. 6.9). Channel abandonment can be placed around AD 660 to AD860.

6.1.5 Core TIC14

Core TIC14 was located in a palaeochannel located on terrace 2, although the palaeochannel was suspected to date to the early Holocene in the original chronostratigraphic model produced in Phase 1 (Fig. 6.1). Core TIC14 is relatively short at 90cm, with a dark red brown AP horizon between 0 – 5cm. Below this is a dark red brown silty clay with a trace of sand between 5 – 28cm. A red brown silty clay unit is located between 28 – 54cm, with a basal blue grey clay with a trace of silt and sand, and Fe and Mn mottling between 54 – 90cm. The organic content is low throughout the core. The upper two units (0 – 5cm and 5 – 28cm) both show relatively elevated organic and magnetic susceptibility contents (Fig. 6.10).

Pollen was sampled at 14cm intervals along the core length, starting at 14cm. The date from the base of the core at 90cm is 3005BP +/-35, with a date at 45cm of 1309BP +/-28. This basal date confirms a Holocene age for the channel abandonment (Fig. 6.11).

6.1.6 Core TFGC14

This core was located on an area of terrace 1, where there was no visible expression of a palaeochannel within the field (Fig. 6.1). The most striking feature of this core is its depth, with a recovered sample to 385cm (the core stratigraphy is actually slightly longer, but there was incomplete recovery from the base of core). This core length is much greater than the cores retrieved from other palaeochannels within the study area.

The stratigraphy shows a 0 – 27cm A horizon of dark brown silt, underlain by a red brown clay with a trace of sand and occasional small clasts between 27 – 132cm. At 132 – 164cm is a grey clay with visible organic flecks and Fe mottling. Below this between 164 – 227cm is a blue grey clay with a trace of sand and visible organic matter. At 227 – 234cm is a grey clayey medium sand, underlain by olive brown peaty clay, with a trace of sand and silt, at 234 – 305cm. This unit had abundant organic material contained within its matrix and a charcoal fragment at 262cm. Below this at 305 – 318cm is an olive brown clayey sand. Below this the olive brown peaty clay unit is again evident at 318 – 319cm. At 349 – 362cm is a olive grey clayey medium sand and the basal unit is an olive brown/grey clayey medium sand (Fig. 6.12).

The organic content of the core shows a marked increase in the peaty clay unit 234 – 305cm, which confirms the field observations of the abundant organic matter within the matrix. The olive brown peaty clay at 318 – 319cm shows elevated organic values, although they are not as high as the organic values for the 234 – 305cm unit. The carbonate contents and magnetic susceptibility contents do not appear to relate to the stratigraphy in a systematic way.

The stratigraphy of this palaeochannel is interesting on two counts. First the depth of the core is much greater than other palaeochannels seen in the study area. Secondly, there are three sand units within the stratigraphy (349 – 362cm, 305 – 318cm and 227 – 234cm) interspersed with clay-dominated units. This stratigraphy suggests a

sequential process of channel re-occupation and abandonment, with 3 phases of abandonment, each represented by a clay unit above a sand unit.

This can be summarised as:

Phase 1: Unit 349 – 362cm represents channel occupation.

Phase 1: Unit 318 – 349cm represents channel abandonment.

Phase 2: Unit 305 – 318cm represents channel occupation.

Phase 2: Unit 3234 – 305cm represents channel abandonment.

Phase 3: Unit 227 – 234cm represents channel occupation.

Phase 3: Units from 164cm upwards represent channel abandonment.

Due to this palaeochannel being discovered at a relatively late phase of fieldwork, after the pollen assessment from the other palaeochannels had begun, a limited pollen evaluation was conducted with sampling starting at 266cm, and then every 14cm until 378cm (Fig 6.13).

The radiocarbon dates produce an excellent sequence for the lower portion of this core, with the following dates:

250cm 3300BP +/-40

300cm 3410BP +/-60

300cm 3880BP +/-35

380cm 4725bp +/-40

From these dates the phase 1 channel occupation can be shown to have occurred at 4725BP +/-40, and the phase 2 channel abandonment to just before 3410BP +/-60.

6.1.7 *WQFC1*

A series of three tins were taken from an exposed section in Warren Farm quarry (Fig. 6.1). The stratigraphy reveals an upper unit of light grey clay, with a trace of sand, Fe nodules and visible plant remains between 0 – 42cm. Underneath this unit at 42 – 69cm is dark grey with a trace of sand and silt, underlain by a dark grey/black clay unit between 69cm and 72cm. Below this is a dark grey clay unit with visible plant macrofossils at 72 – 117cm, with the lowest unit of dark grey clay with small clasts at 117cm. The organic content shows a spike in the dark grey unit between 69 – 72cm and generally elevated levels in the units between 42 – 69cm and 72 – 117cm (Fig. 6.14).

Pollen was sampled at 14cm intervals, starting at 14cm. Three samples were dated using radiocarbon. The first of these is a humic acid date at 75cm, which pre-dates the two dates below this at 2989BP +/-28. Both dates below this are from monocotyledon fragments and produce dates of 2580BP +/-35 at 95cm, and 2730BP +/-160 at 118cm. These two bottom dates shows some internal consistency (Fig. 6.15).

6.1.8 WQFC2

A series of three tins were taken from an exposed section in Warren Farm quarry (Fig 6.16). The stratigraphy reveals an upper grey brown clay between 0 – 47cm. Beneath this is a thin lense of red brown clay with small clasts <2cm at 47 – 50cm, underlain by grey clay with a trace of sand between 50 – 69cm. Underneath this is a dark grey/black silty clay with a trace of sand at 69 – 97cm, with a dark grey silty clay with abundant organic matter at 97 – 119cm. The lowest unit sampled is a dark grey silty clay with small clasts between 119 – 124cm. The organic content is relatively low in the units 0 – 47cm, 47 – 50 cm and 50 – 69cm. High organic contents are seen in the units at 69 – 97cm, 97 – 199cm, both of which are dark grey silty clays. The organic content decreases in the lowest unit at 119 – 124cm.

Pollen was sampled at 14cm intervals, starting at 14cm, in each of the three tins, so there is some uneven spacing of samples in the bottom tins M2 and M3, as the tins overlapped. Two samples were radiocarbon dated, giving a base date on tin M2 of 2500BP +/-35 and a base date on tin M3 of 2820BP +/-35 (Fig. 6.17), dates that agree with their relative stratigraphic order.

6.1.9 WQFC3

One tin sample was taken from this exposed palaeochannel at Warren Farm quarry (Fig. 6.1). The stratigraphy is relatively simple with a upper grey clay, with a trace of sand and Fe nodules between 0 – 31cm, a middle unit of dark grey silty clay, with some fine laminations at 31 – 46cm and a lower unit of grey brown clayey sand, with small clasts between 46 – 50cm. The organic content, carbonate content and magnetic susceptibility all display a rise in the dark grey/black silty clay unit between 31 – 46cm (Fig. 6.18). Two dates were produced at 50cm at the base of the tin. The first using the humic acid fraction, producing a date of 4078BP +/- 30, whilst the second date used monocotyledon fragments and produced a date of 3075BP +/-35. This again emphasises the difficulties of comparing humin acid dates with those from visible plant macrofossils, with humin fractions giving significantly older dates (Fig. 6.19).

6.10 WQFC5

One tin sample was taken from this exposed palaeochannel at Warren Farm quarry (Fig. 6.1). This was an extremely interesting section, as the palaeochannel WQFC5 clearly lay in a deposit just above gravels interpreted as Devensian gravels, which themselves formed a compound terrace with later Holocene gravels. The stratigraphy of the palaeochannel revealed a grey black silty clay upper unit between 0 – 21cm, with a thin black grey sand band at 21 – 22cm, possibly representing a hiatus in channel infilling and reoccupation of this channel. Below this grey black silty clay at 22 – 34cm, underlain by a grey black silty clay with small clasts and sand bands between 34 – 40cm. The lowest sampled unit is a grey black sandy clay at 40 – 50cm with small clasts. The organic content of the upper 0 – 21cm unit is elevated compared to the rest of the tin, with low values being recorded in the lower four units

(Fig. 6.20). Pollen was again sampled at every 14cm, with sampling starting at 14cm (Fig. 6.21). Two dates from the top of the tin at 0cm revealed a date from monocotyledon fragments of 11, 505BP +/- 55 and a date from bulk sediment of 12,060BP +/-50. A bulk sediment date from 36cm produced a date of 13, 870BP +/- 60.

6.11 Comparison of palaeoenvironmental samples organic contents

In order to produce an initial assessment of the palaeochannels, a bar chart was produced to show their average organic content (Fig. 6.22). Whilst this clearly represents a clear oversimplification of palaeoenvironmental potential and effectively ignores changes in stratigraphy, sediment accumulation rates and taphonomic processes, it does provide a useful means of comparison. The graph clearly shows that the palaeochannel samples from Warren Farm Quarry display elevated organic levels, with WQFC2, having the highest mean value. This is clearly a product of selective sampling of the palaeochannel fills within the quarry. Not surprisingly WQFC5 has the lowest value for the WQF series samples, a product of its early age. From the cores retrieved by gouge from the rest of the study area T1C7 and T1C12 stand out as having high mean organic contents. Both MFC2 and TFGC14 show intermediate organic content, with T1C10 and T1C14 having the lowest mean organic contents.

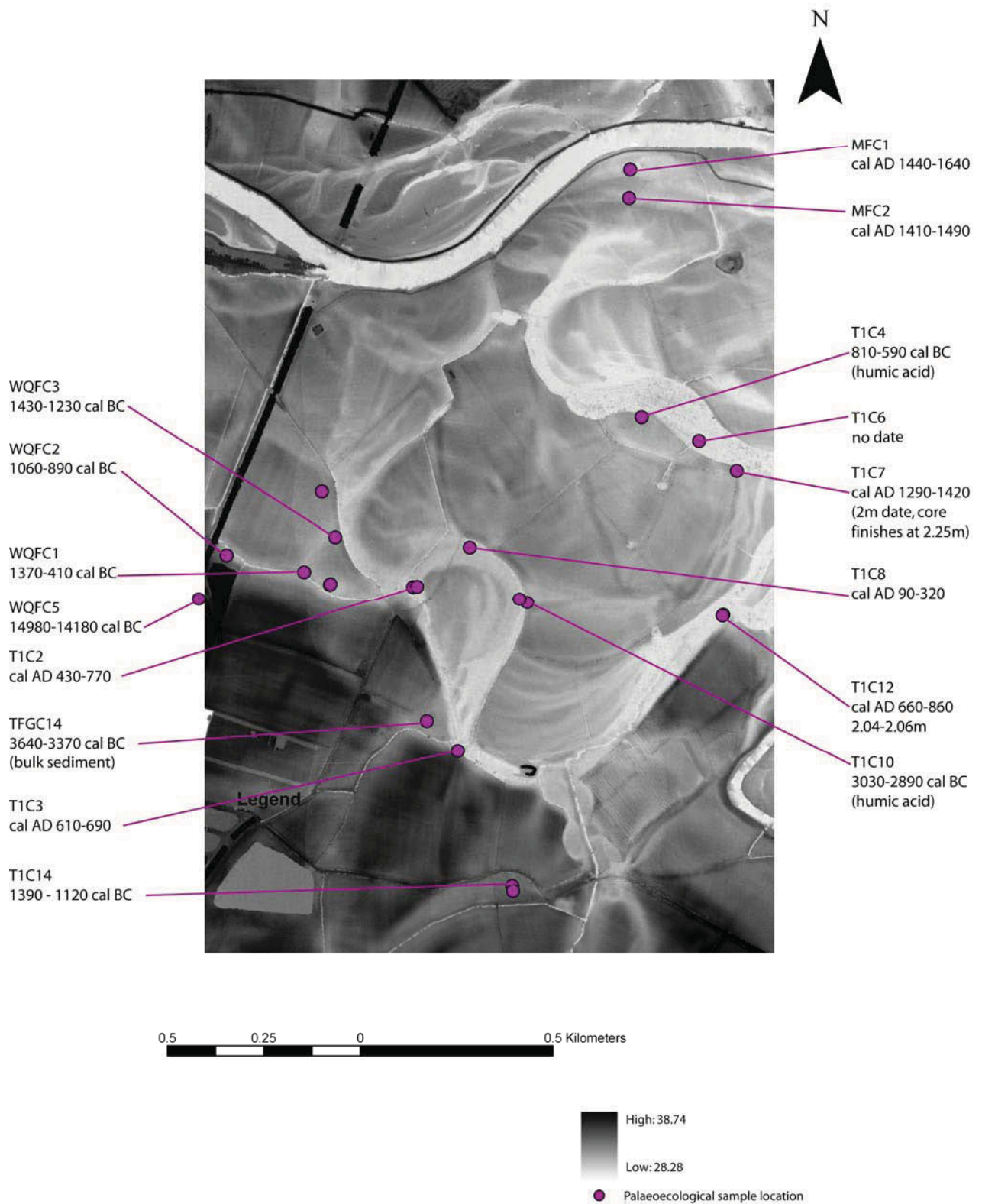


Fig 6.1: The location of the palaeoenvironmental samples and their basal dates ascertained through radiocarbon dating.

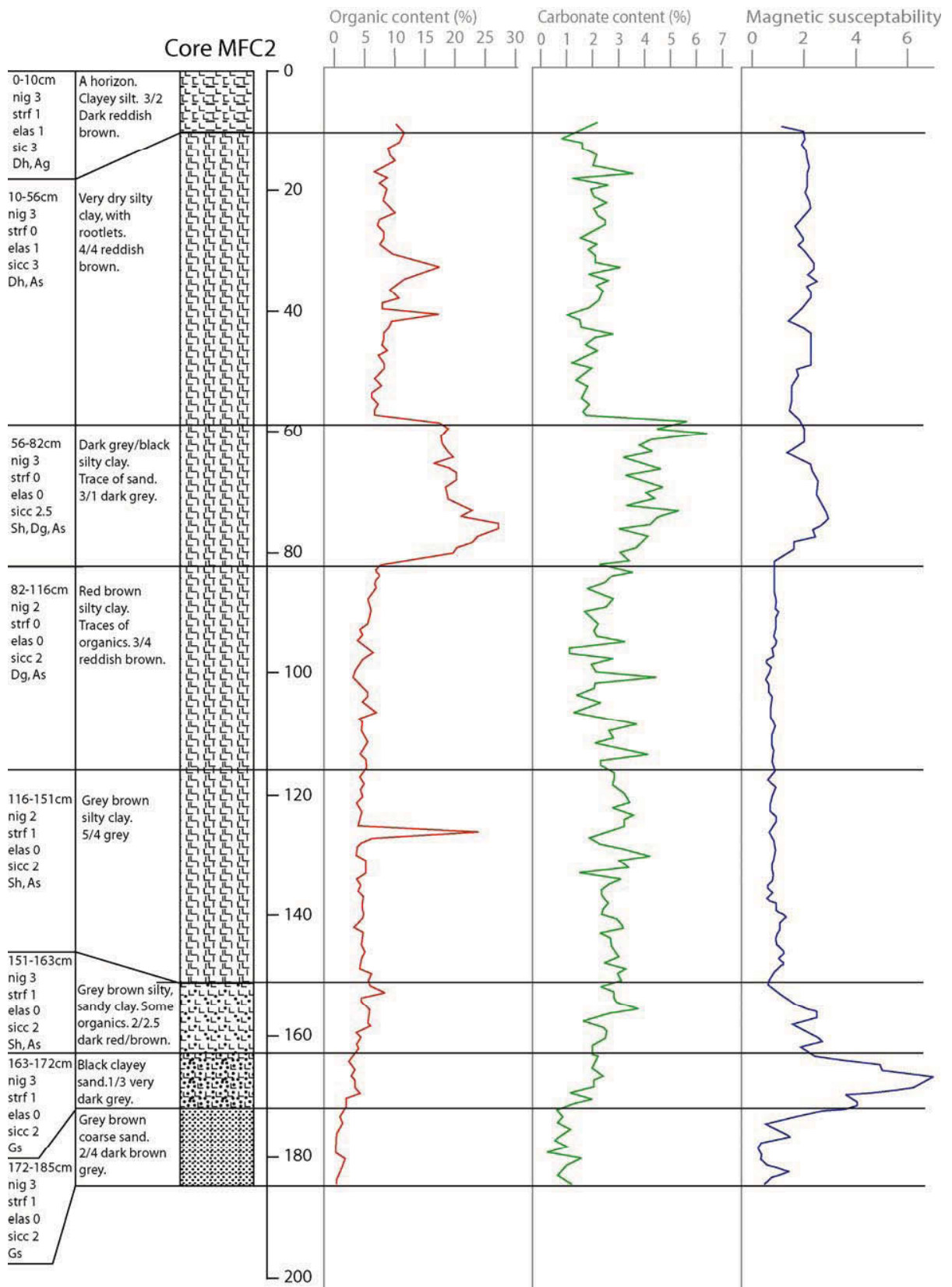


Fig 6.2: Core MFC2 stratigraphy shown against organic content, carbonate content and magnetic susceptibility.

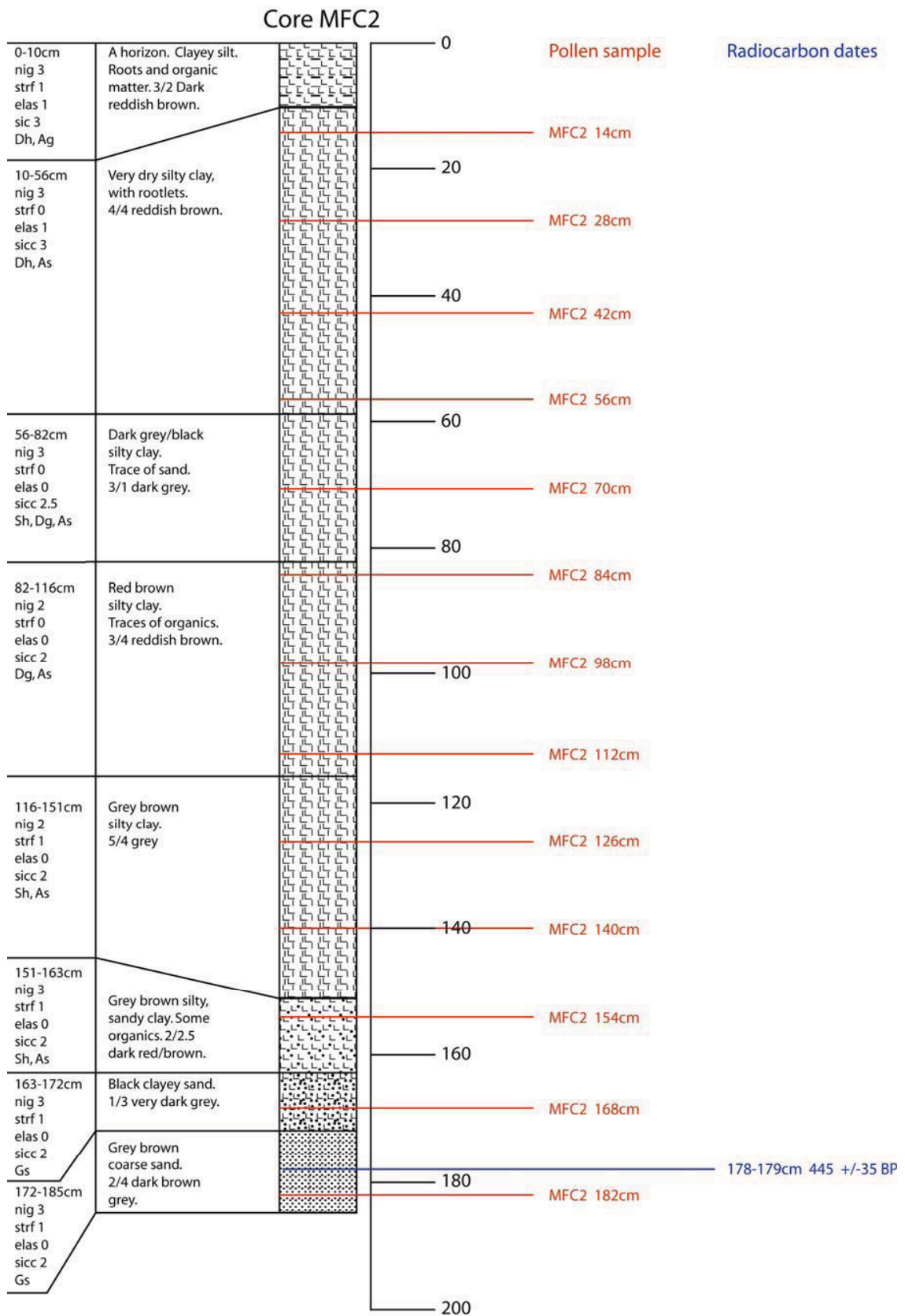


Fig 6.3: Core MFC2 stratigraphy with pollen sample points and radiocarbon dates.

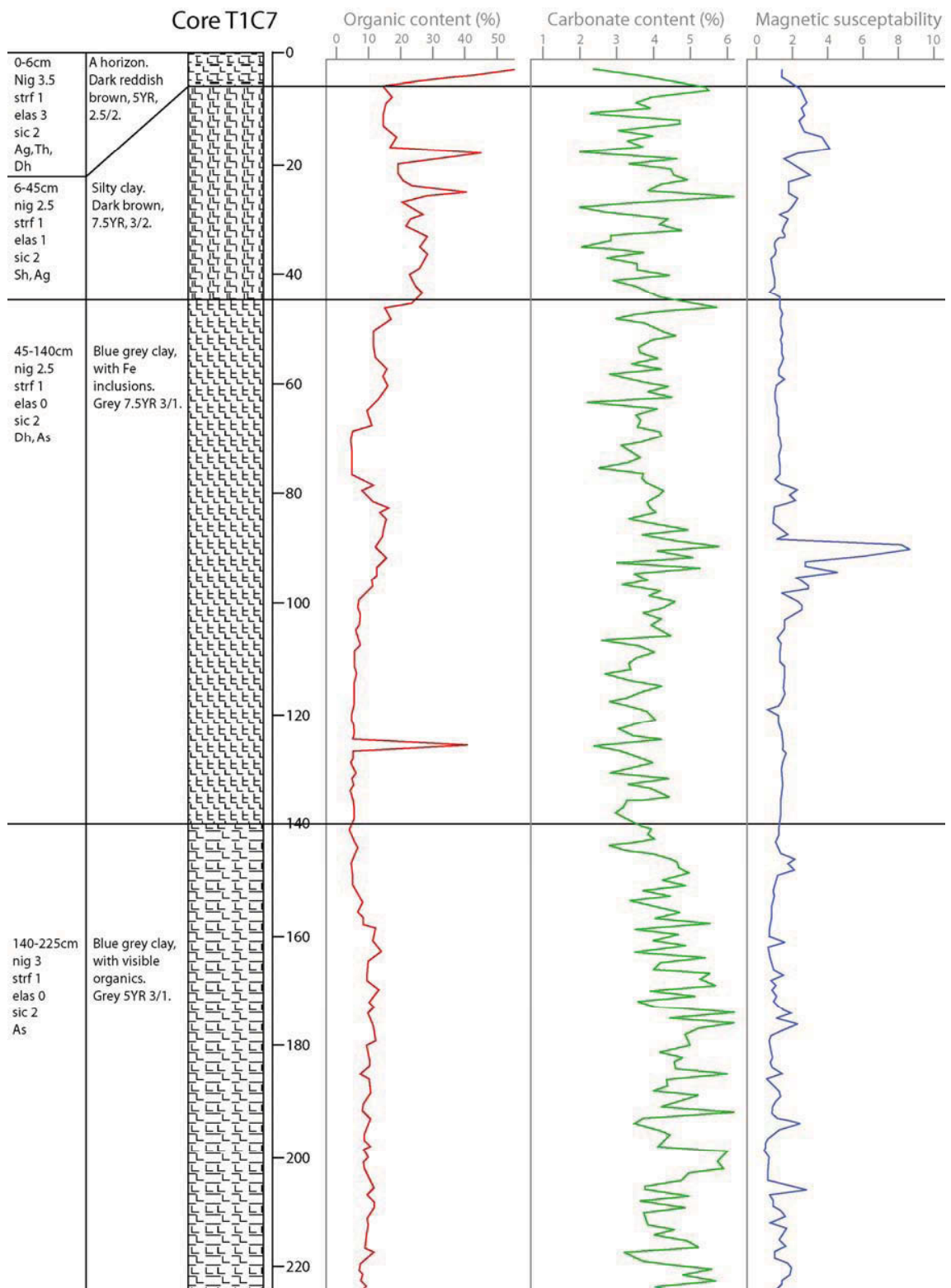


Fig 6.4: Core T1C7 stratigraphy shown against organic content, carbonate content and magnetic susceptibility.

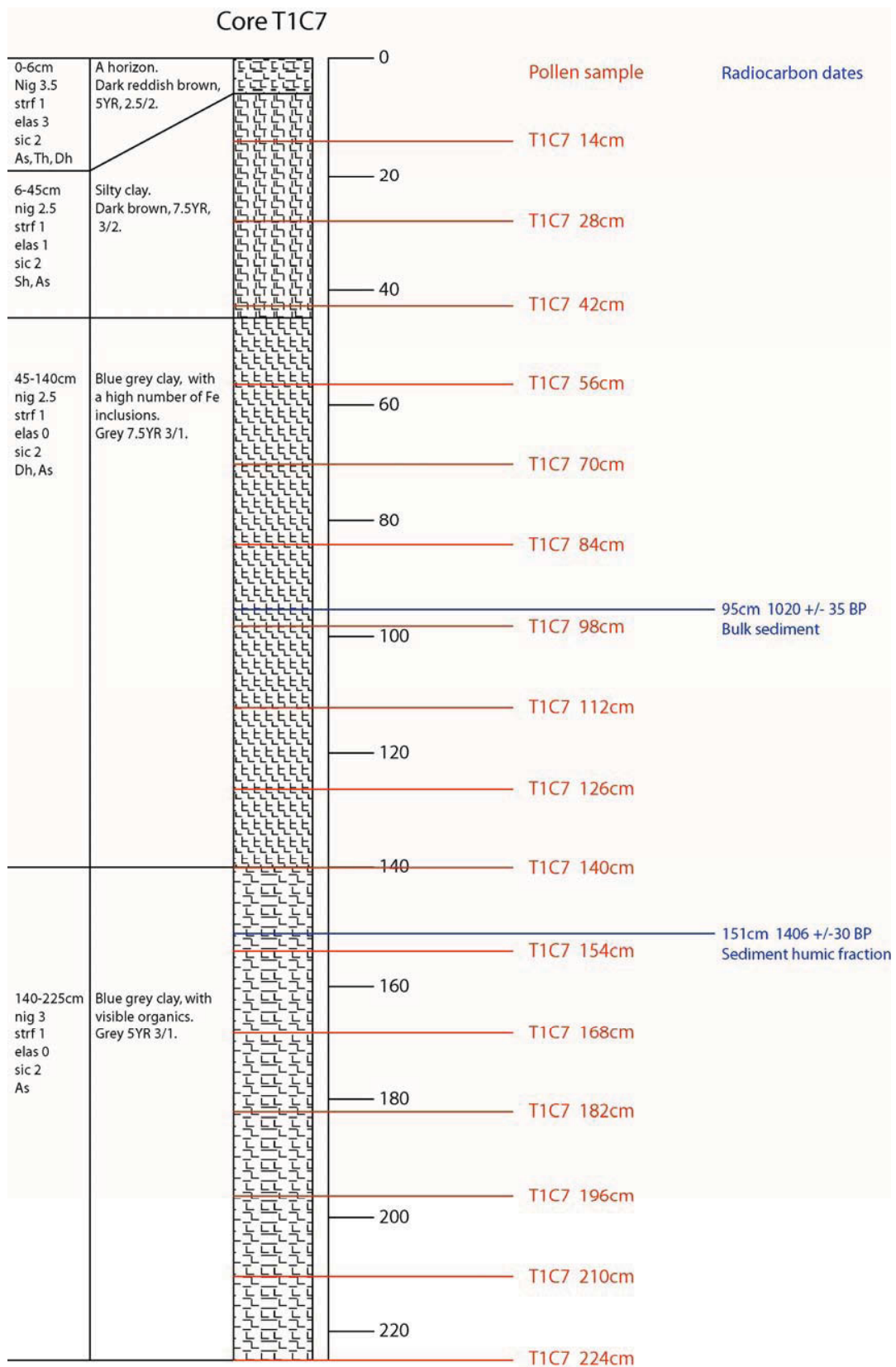


Fig 6.5: Core T1C7 stratigraphy with pollen sample points and radiocarbon dates.

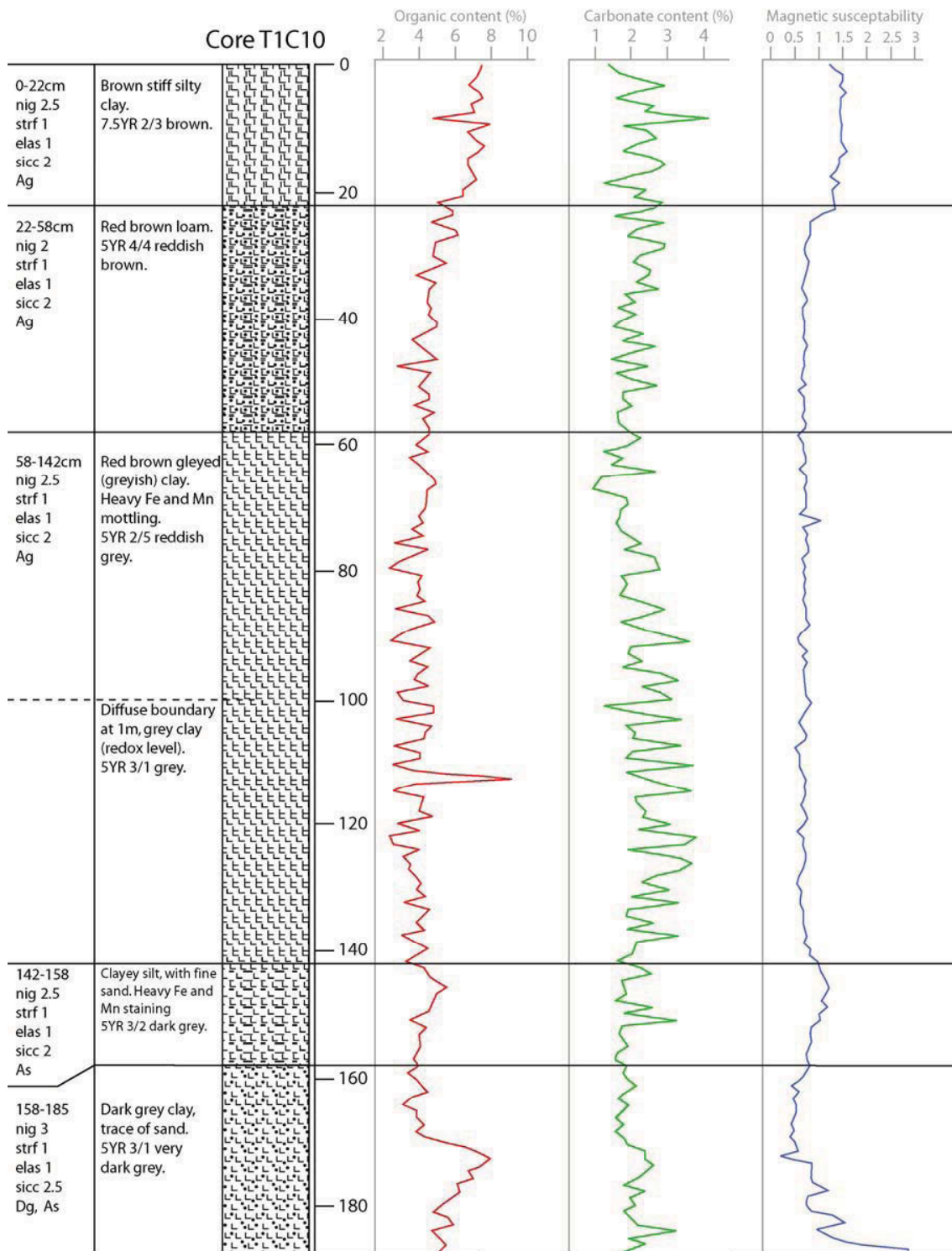


Fig 6.6: Core TIC10 stratigraphy shown against organic content, carbonate content and magnetic susceptibility.

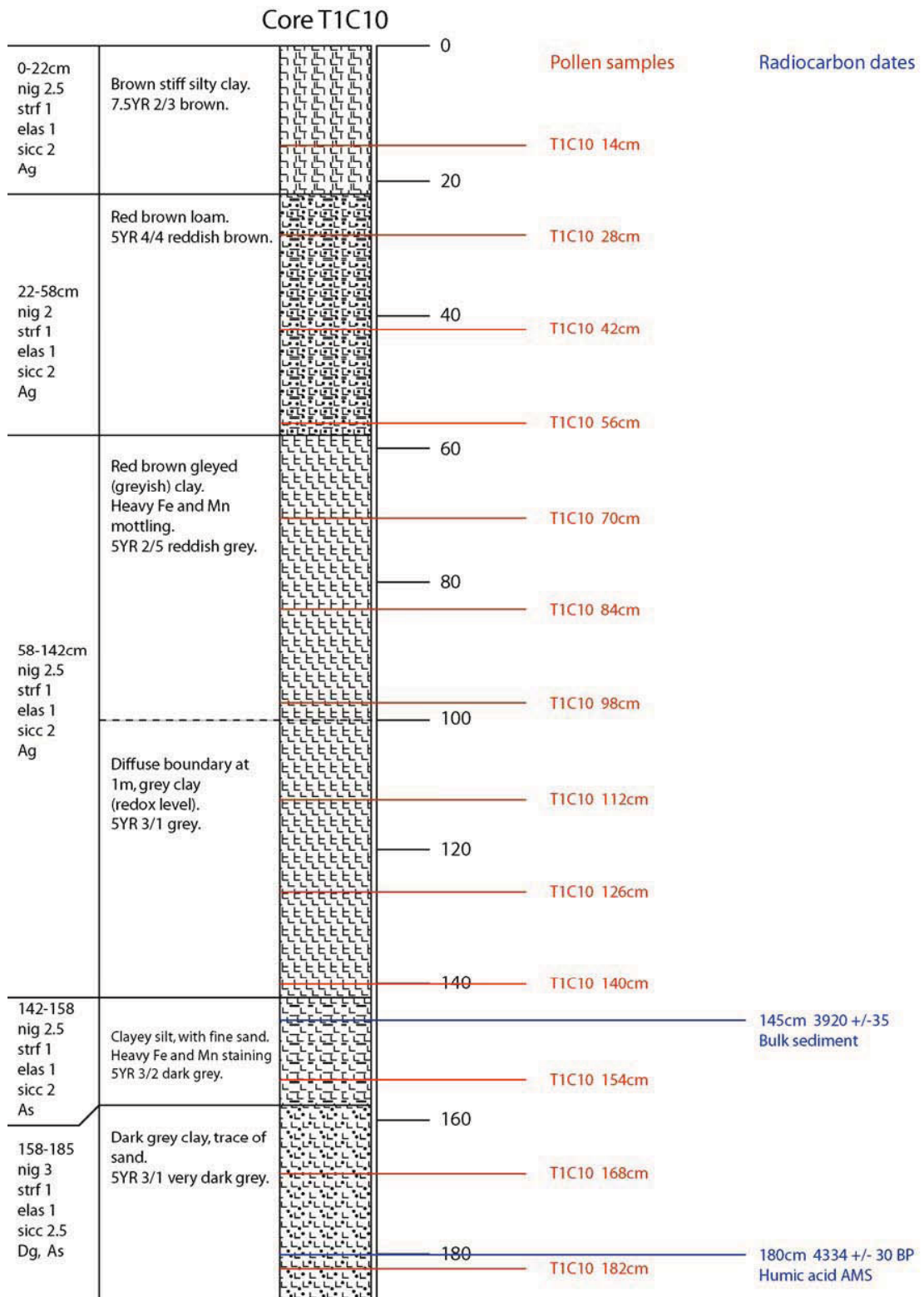


Fig 6.7: Core T1C10 stratigraphy with pollen sample points and radiocarbon dates.

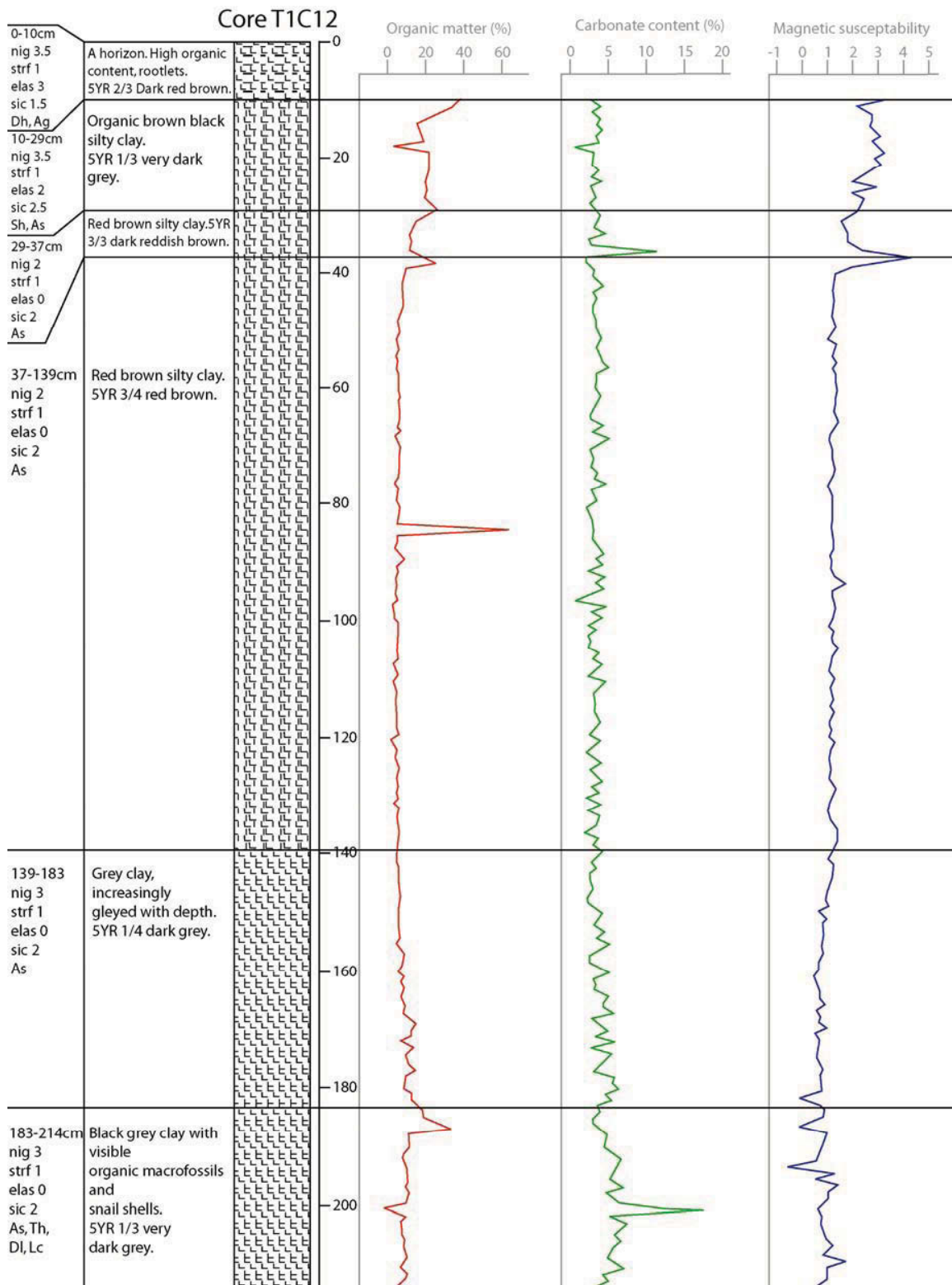


Fig 6.8: Core T1C12 stratigraphy shown against organic content, carbonate content and magnetic susceptibility.

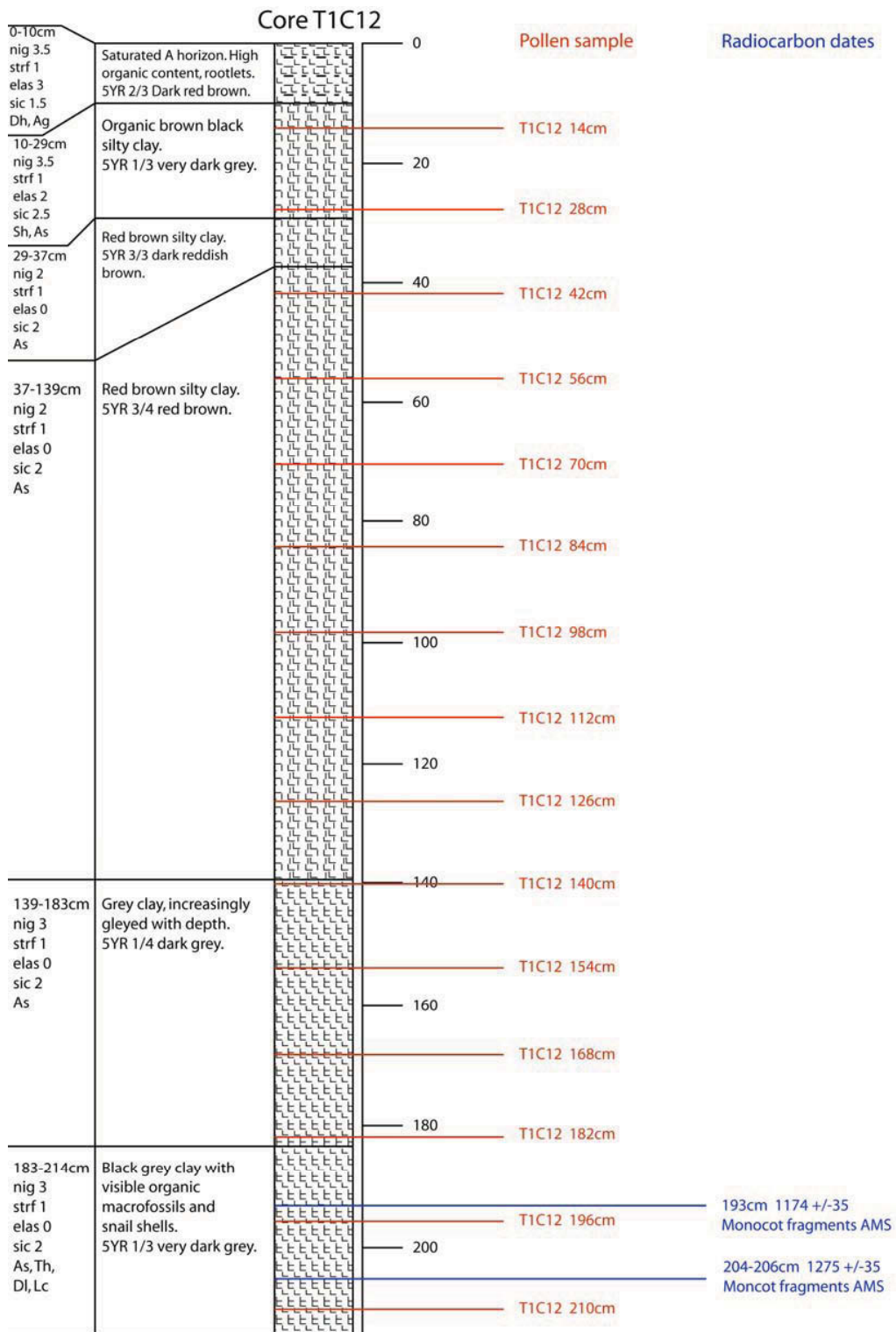


Fig 6.9: Core TIC12 stratigraphy with pollen sample points and radiocarbon dates.

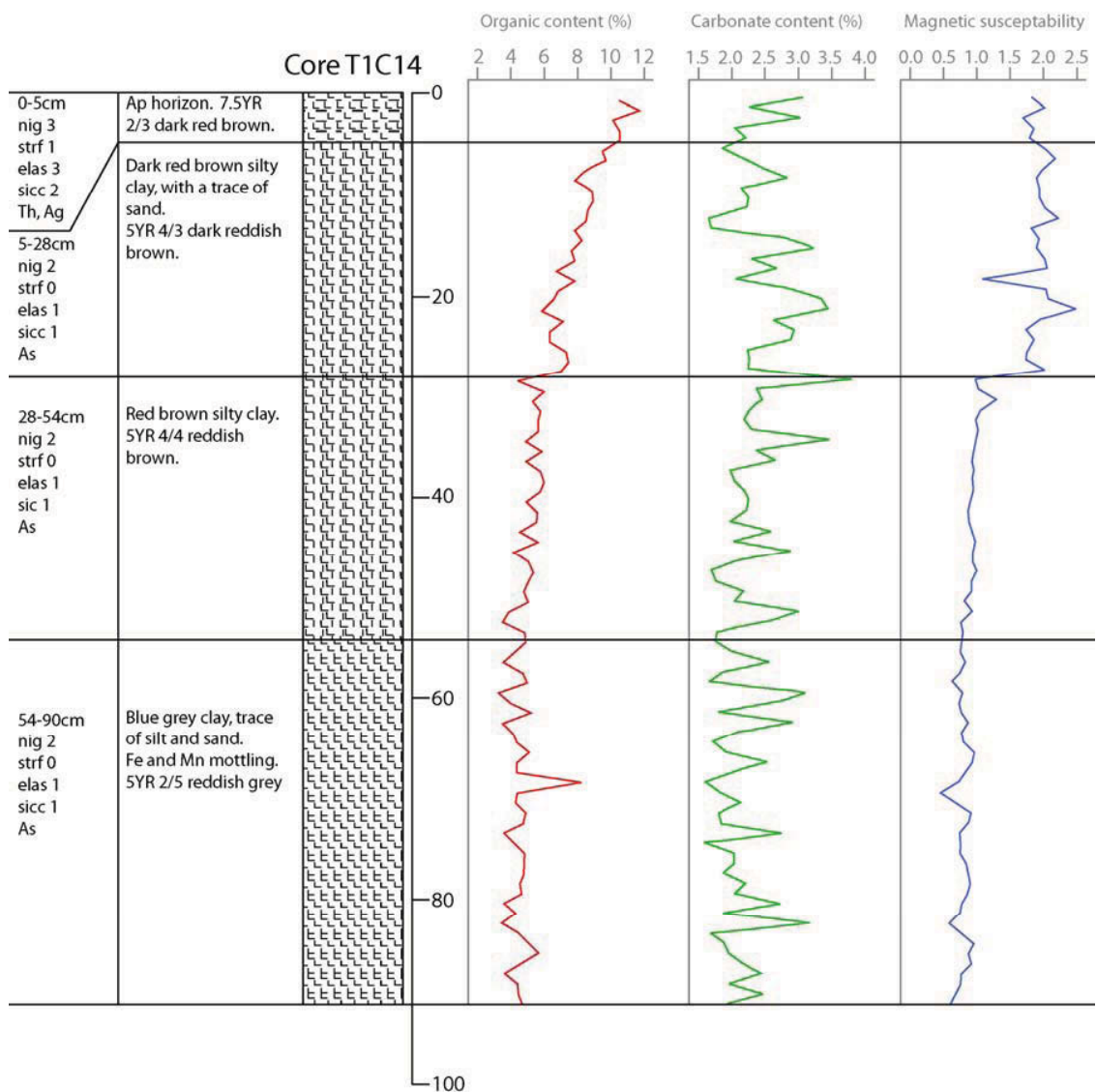


Fig 6.10: Core T1C14 stratigraphy shown against organic content, carbonate content and magnetic susceptibility.

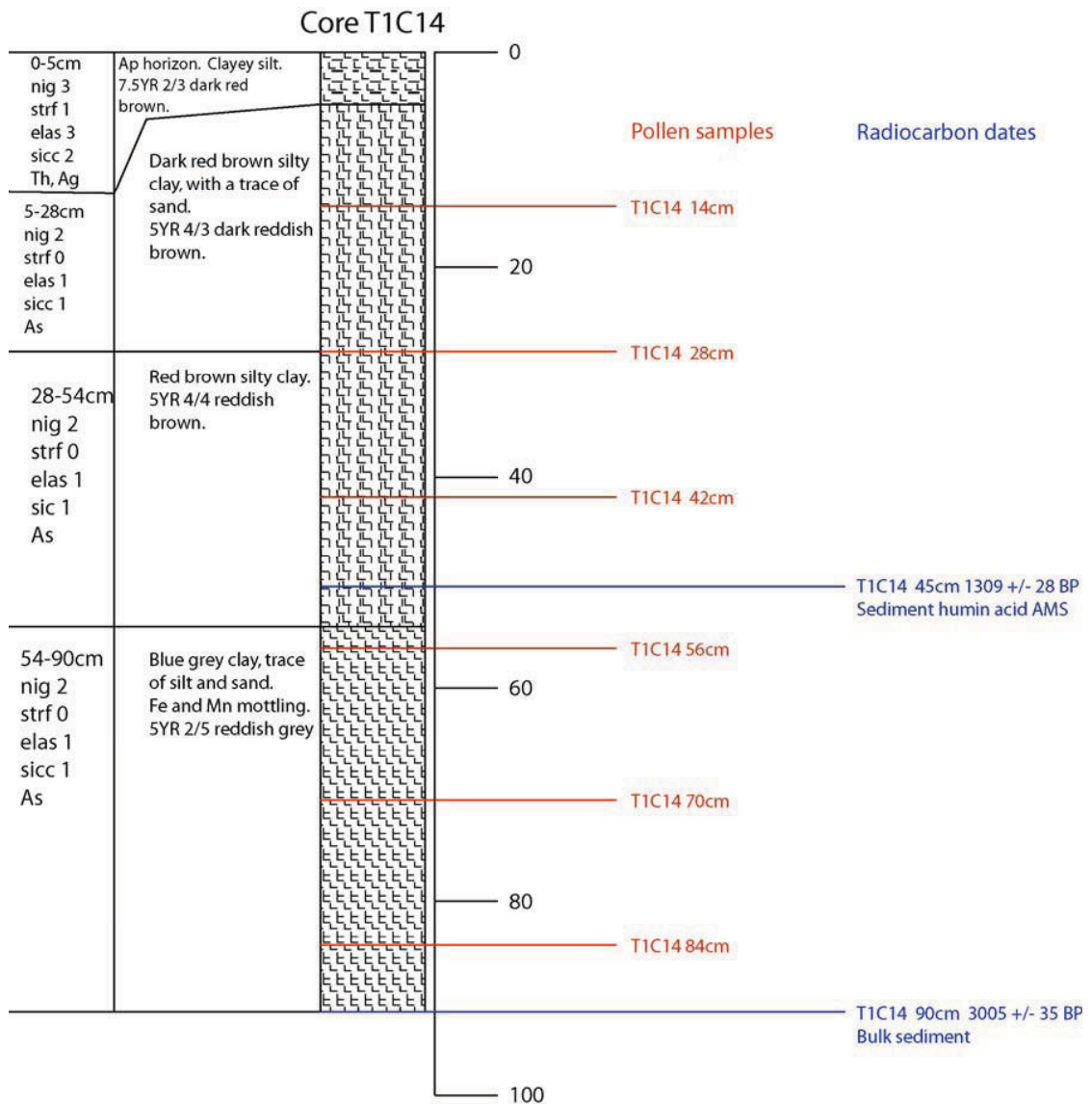


Fig 6.11: Core T1C14 stratigraphy with pollen sample points and radiocarbon dates.

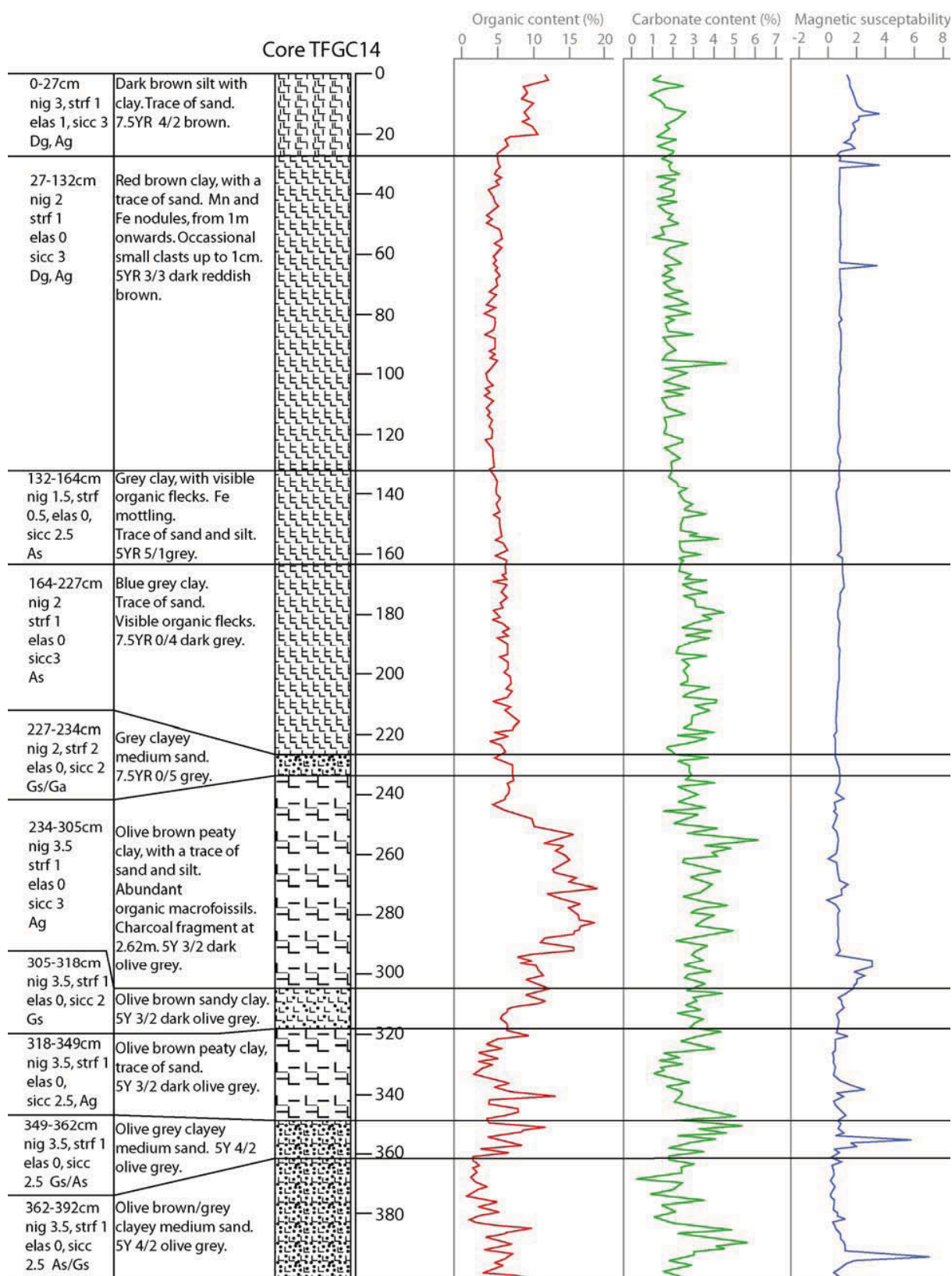


Fig 6.12: Core TFGC14 stratigraphy shown against organic content, carbonate content and magnetic susceptibility.

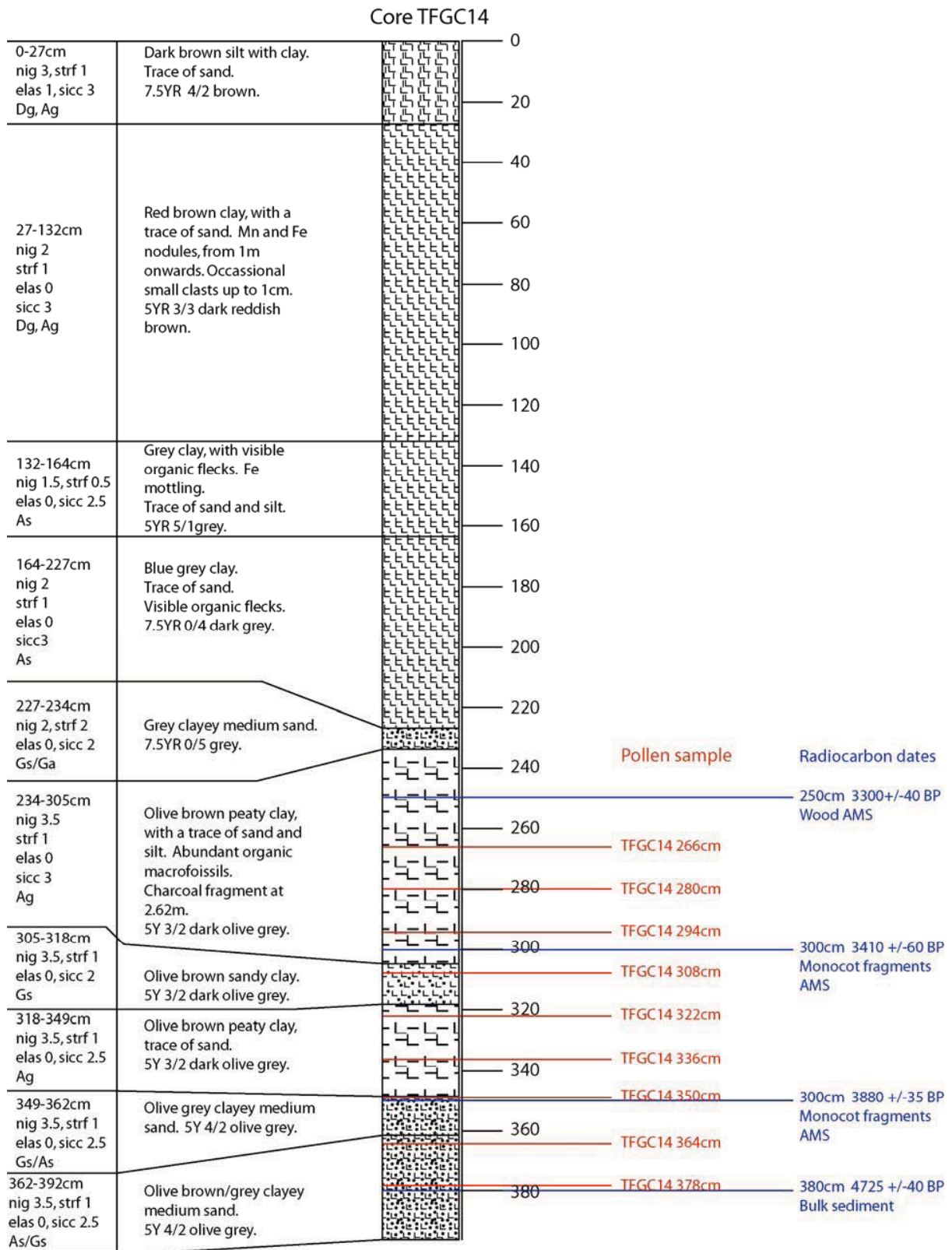


Fig 6.13: Core TFGC14 stratigraphy with pollen sample points and radiocarbon dates.

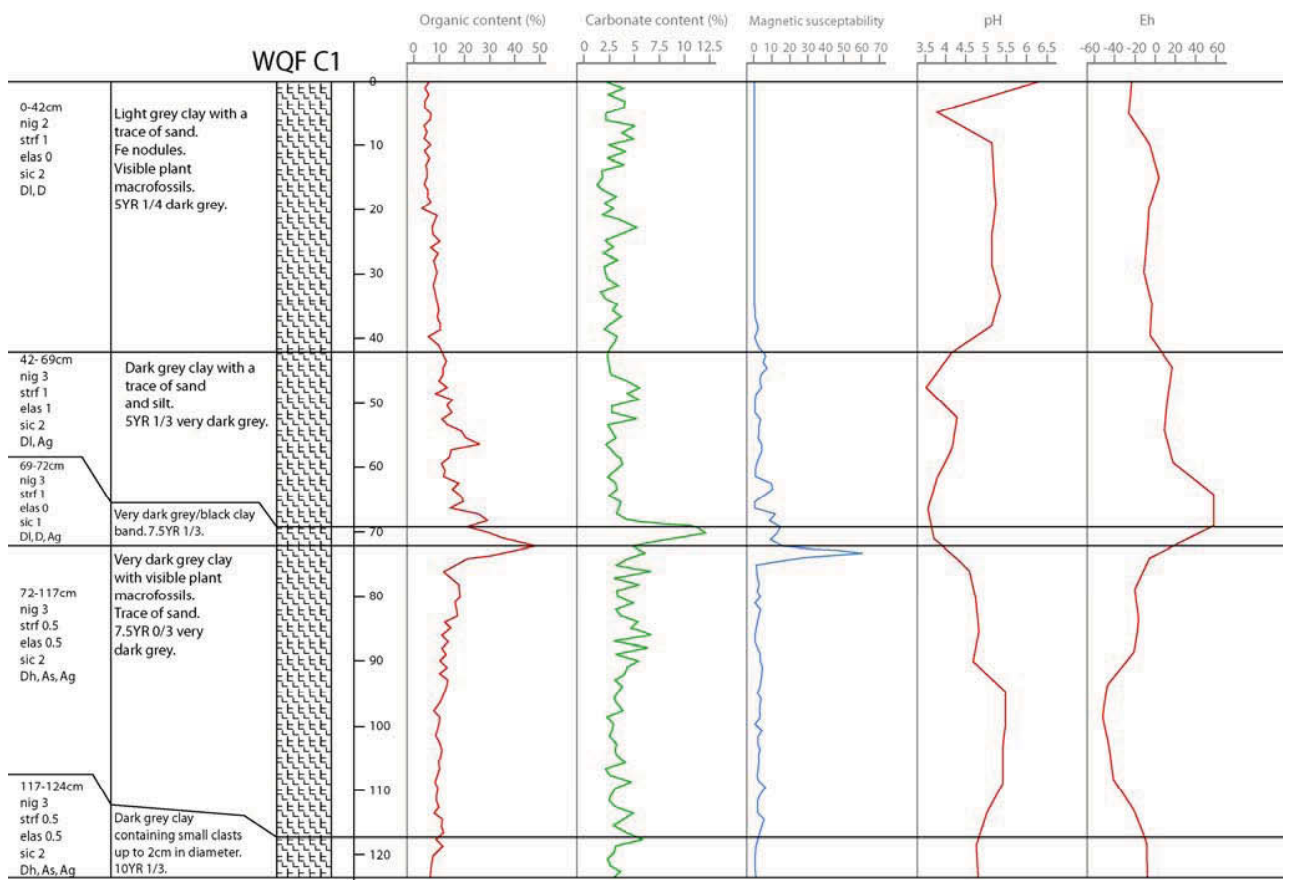


Fig 6.14: Core WQFC1 stratigraphy shown against organic content, carbonate content, magnetic susceptibility Eh and Ph.

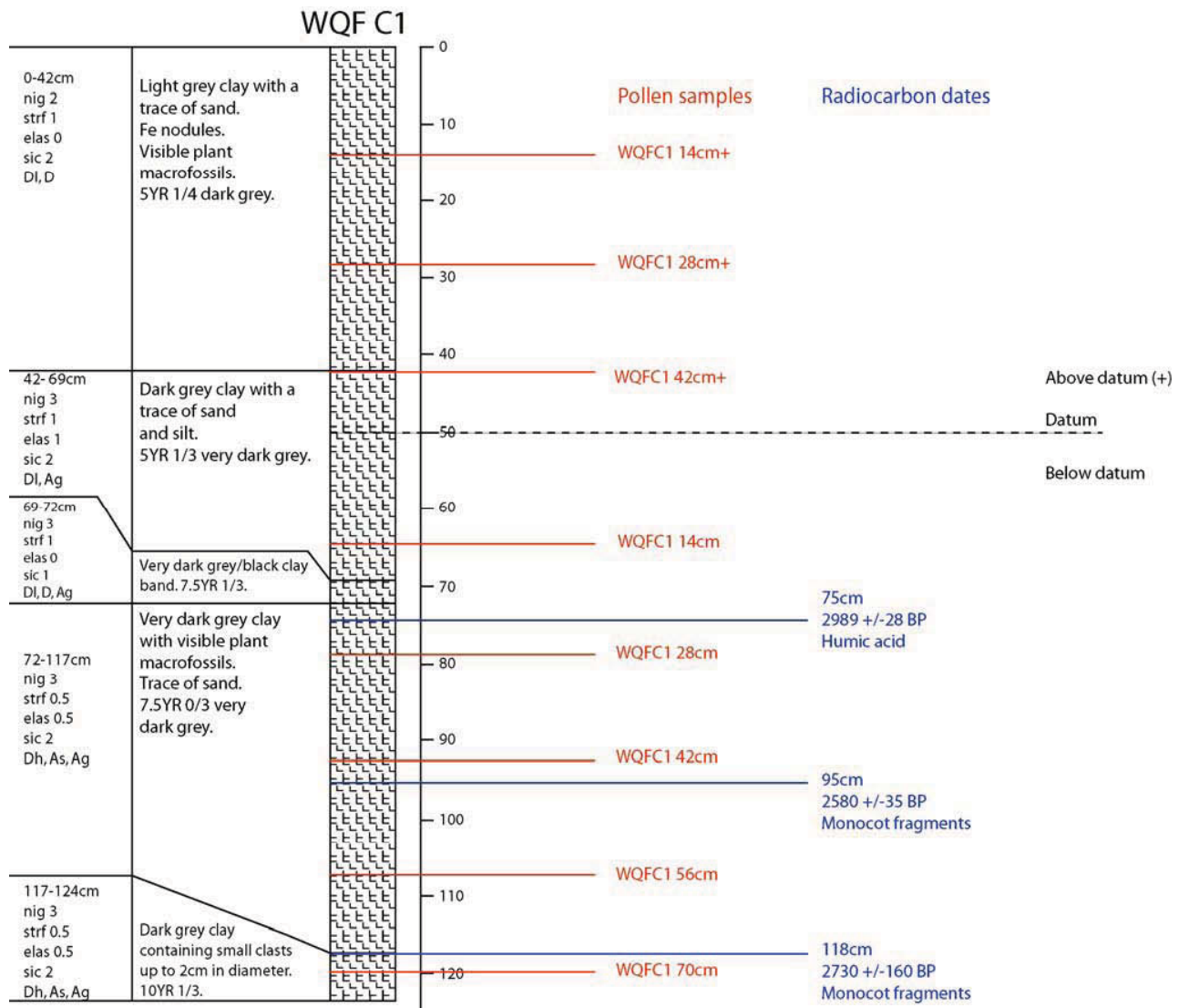


Fig 6.15: WQFC1 stratigraphy with pollen sample points and radiocarbon dates.

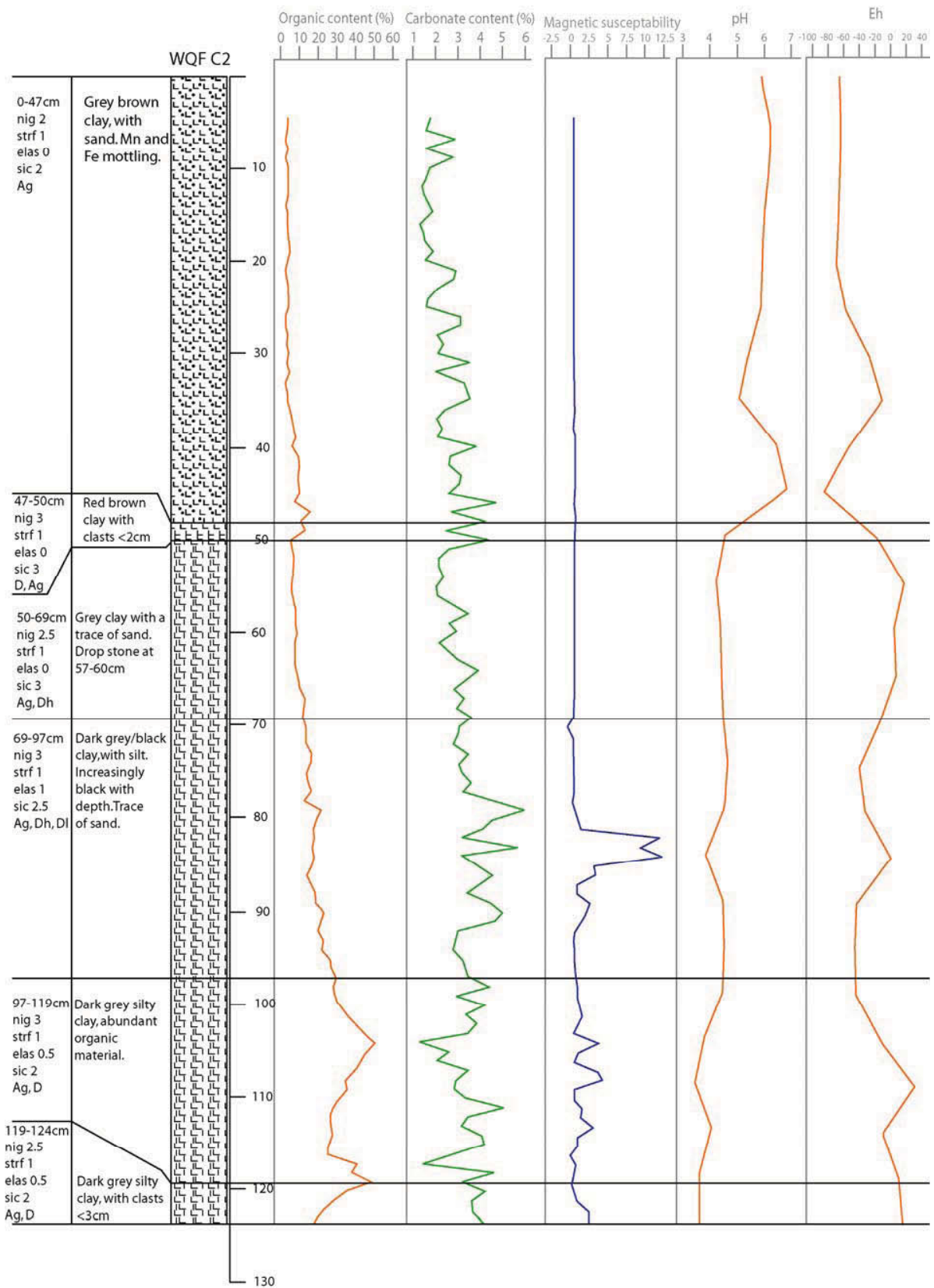


Fig 6.16: WQFC2 stratigraphy shown against organic content, carbonate content, magnetic susceptibility Eh and pH.

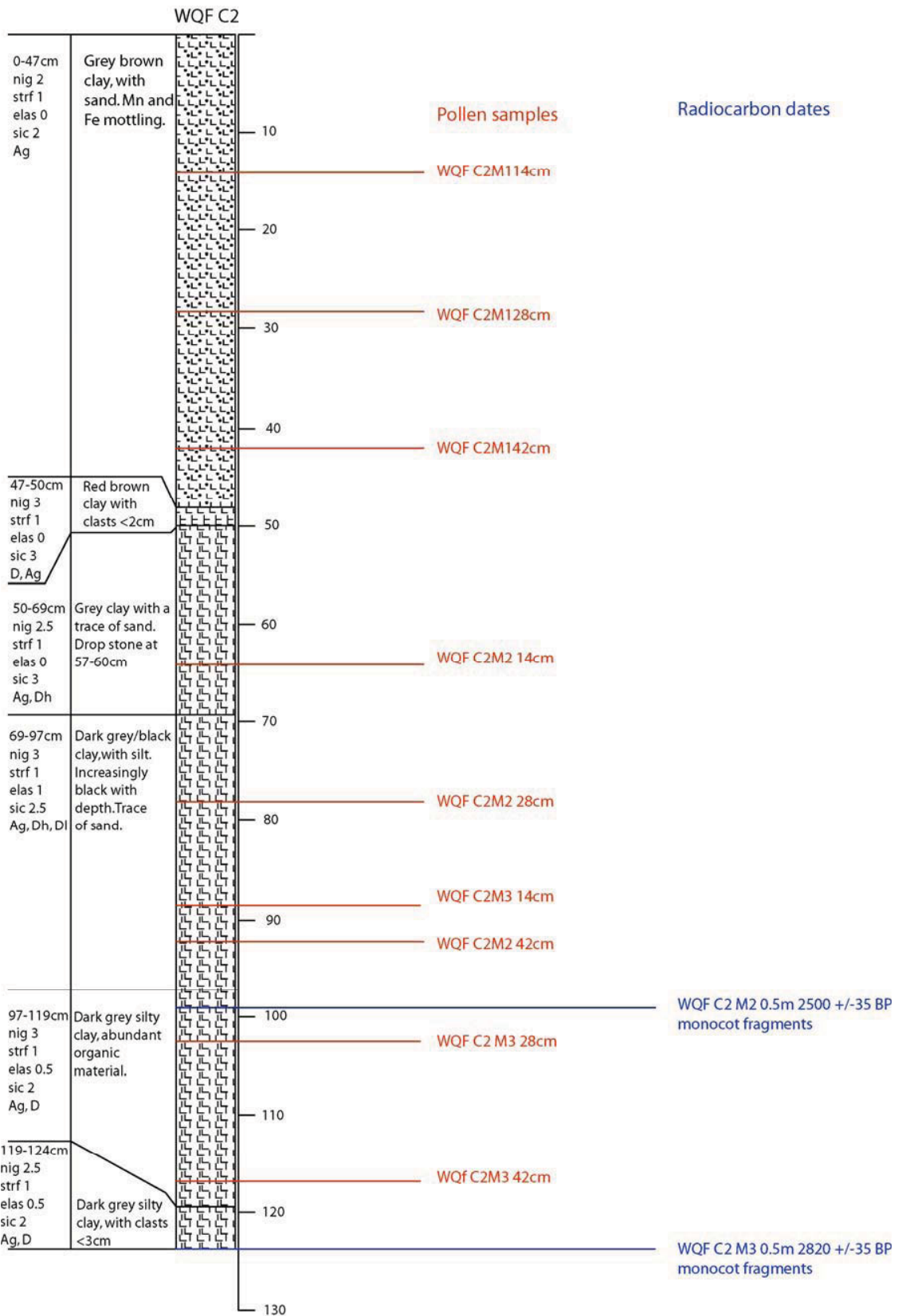


Fig 6.17: WQFC2 stratigraphy with pollen sample points and radiocarbon dates.

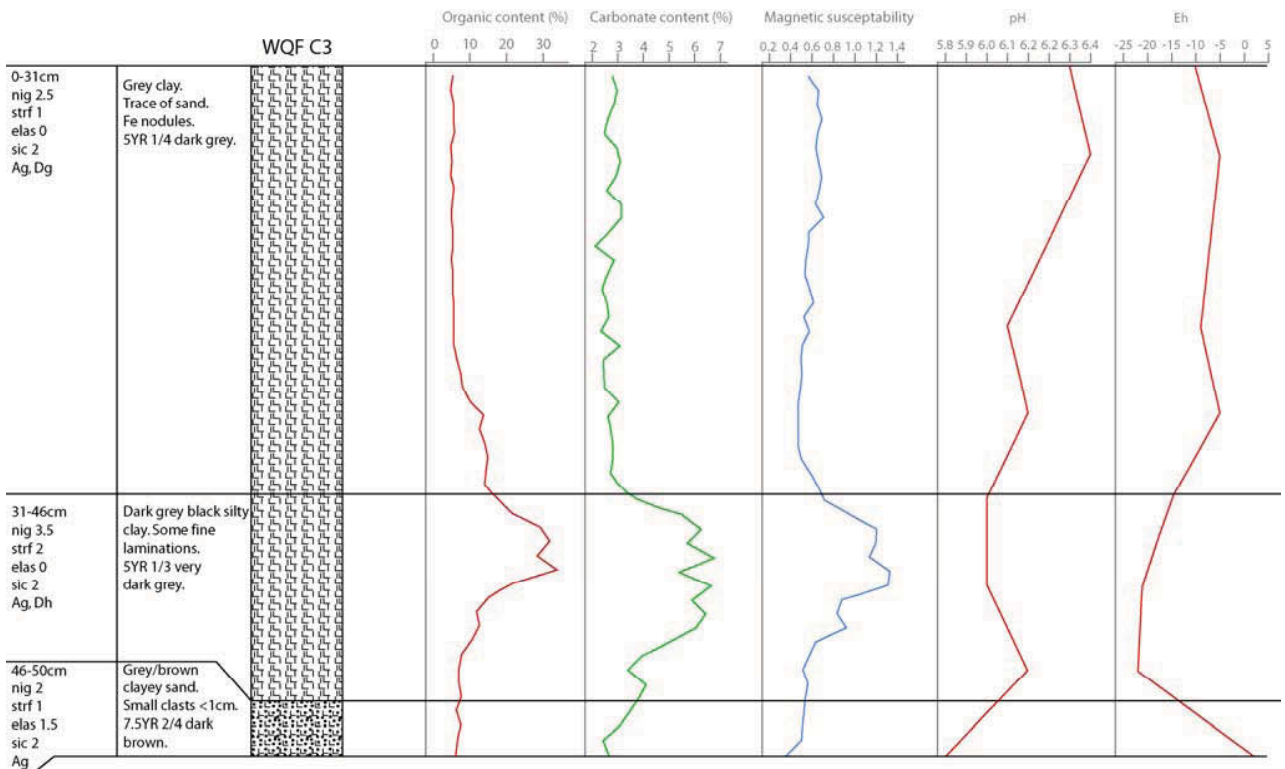


Fig 6.18: WQFC3 stratigraphy shown against organic content, carbonate content, magnetic susceptibility Eh and pH.

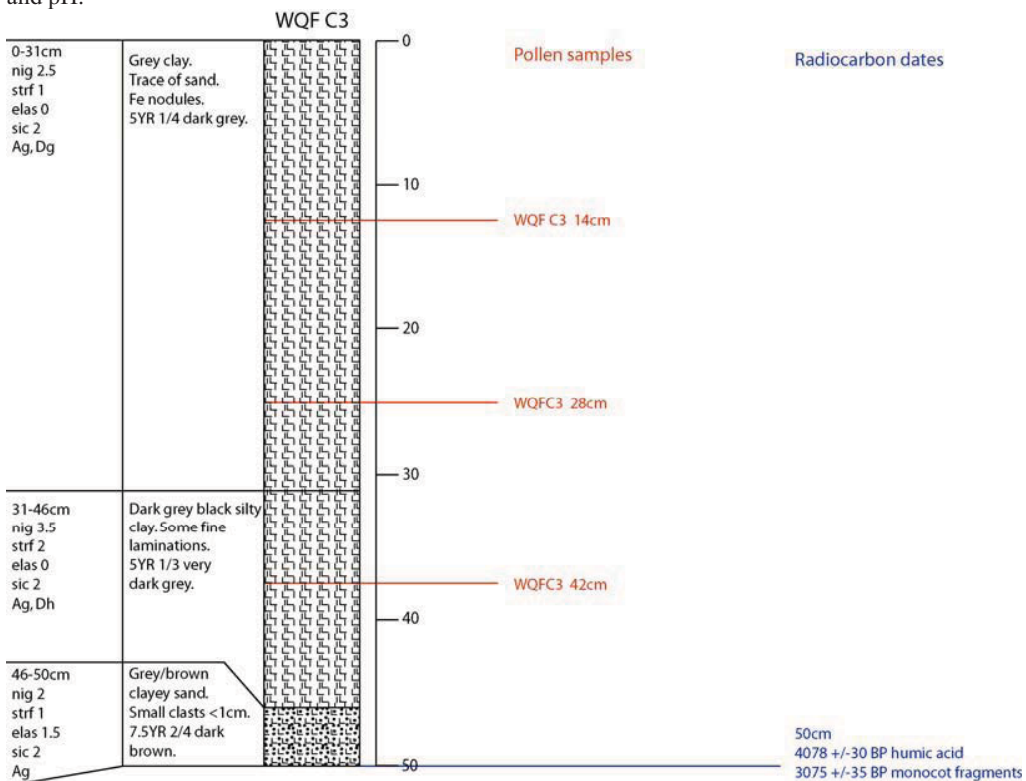


Fig 6.18: WQFC3 stratigraphy with pollen sample points and radiocarbon dates.

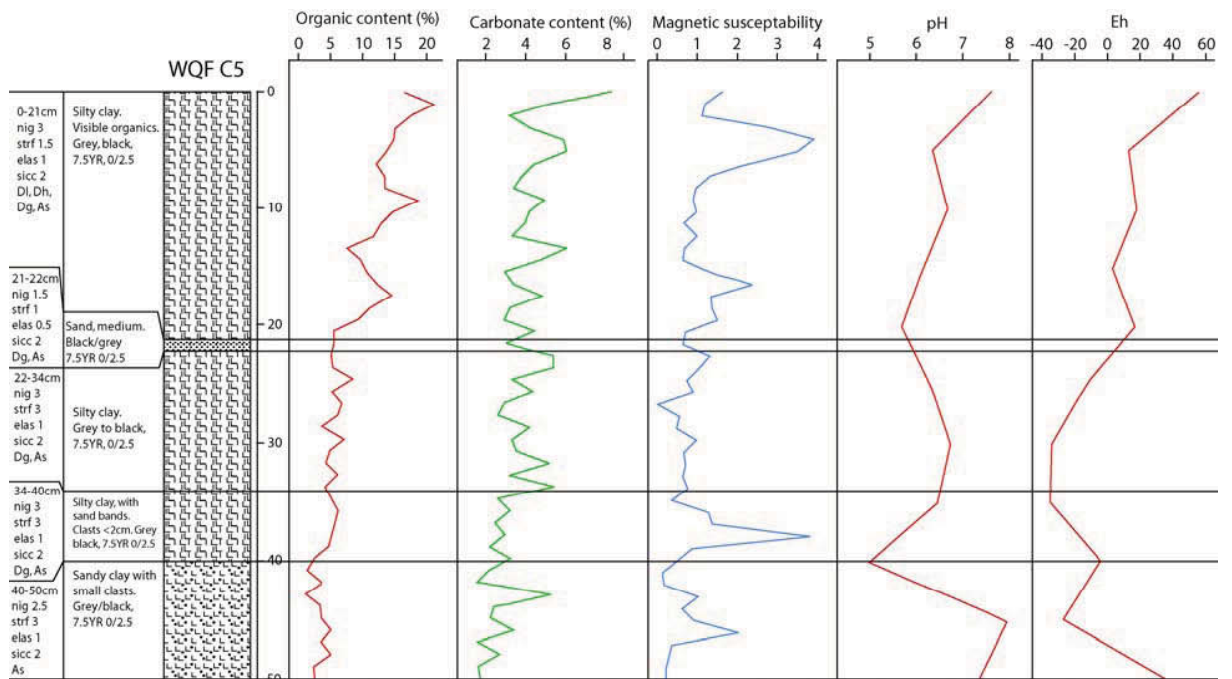


Fig 6.20: WQFC5 stratigraphy shown against organic content, carbonate content, magnetic susceptibility Eh and pH.

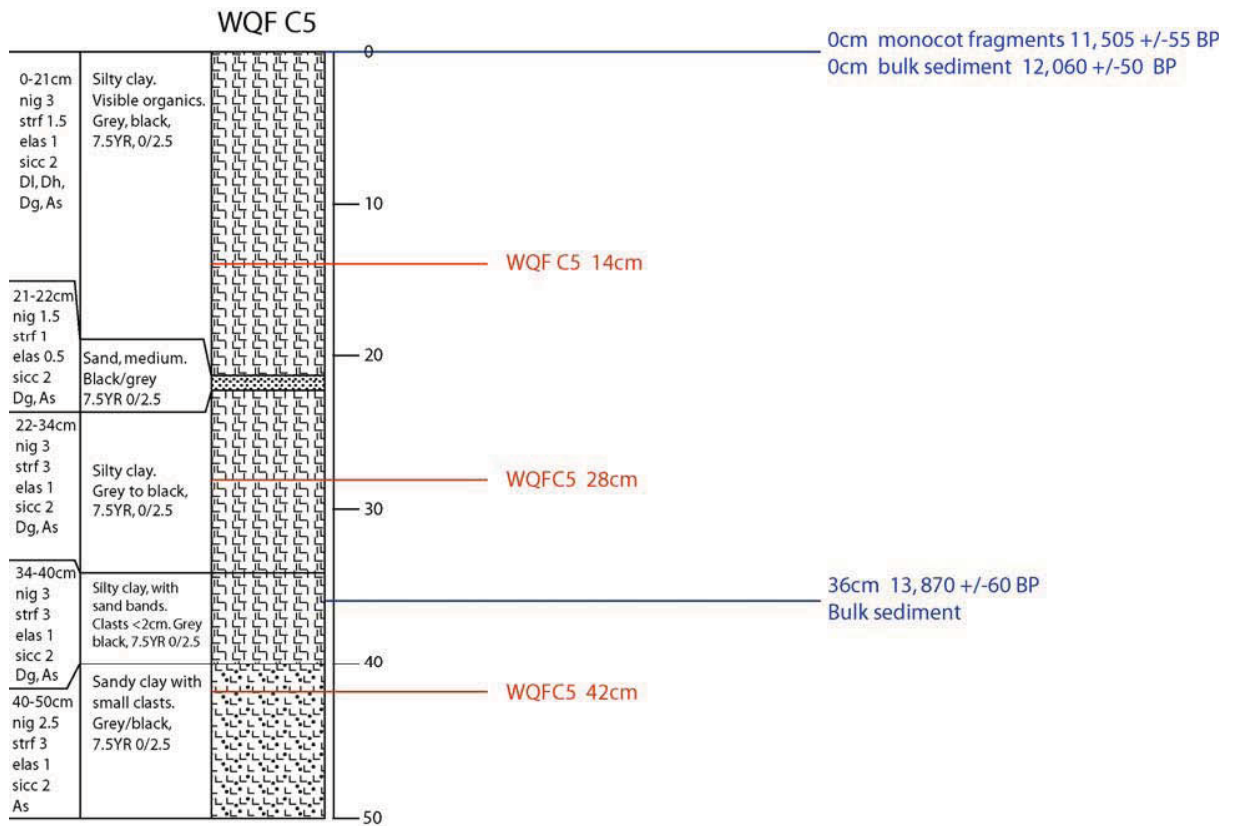
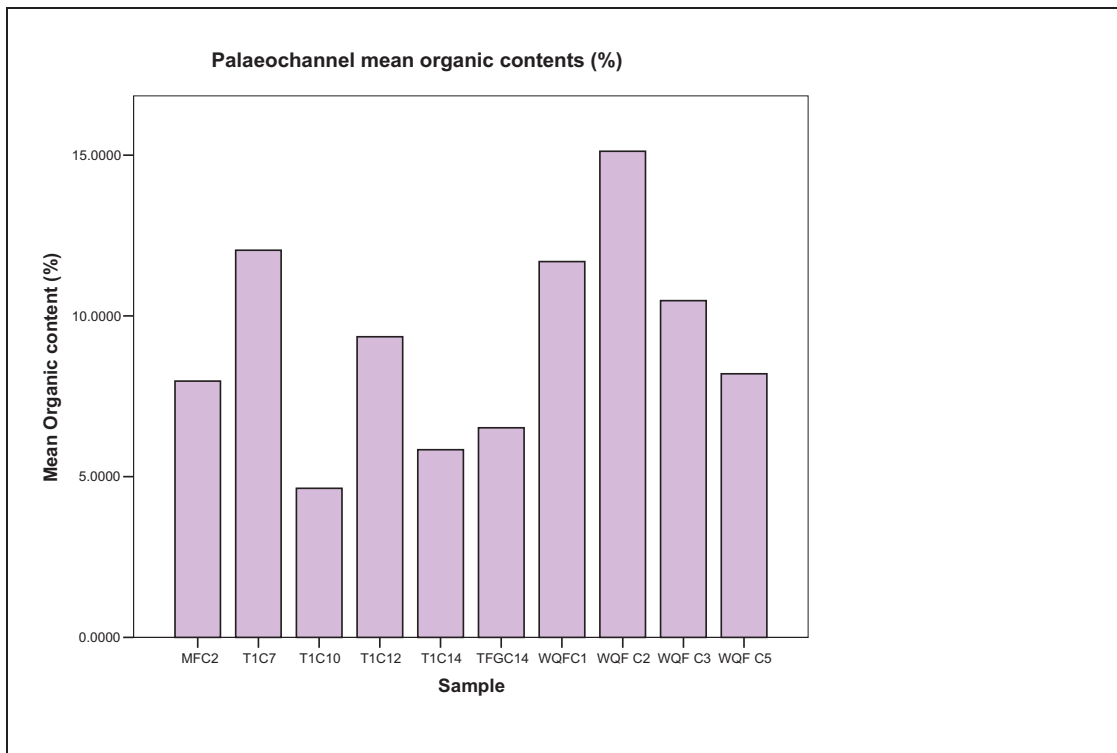
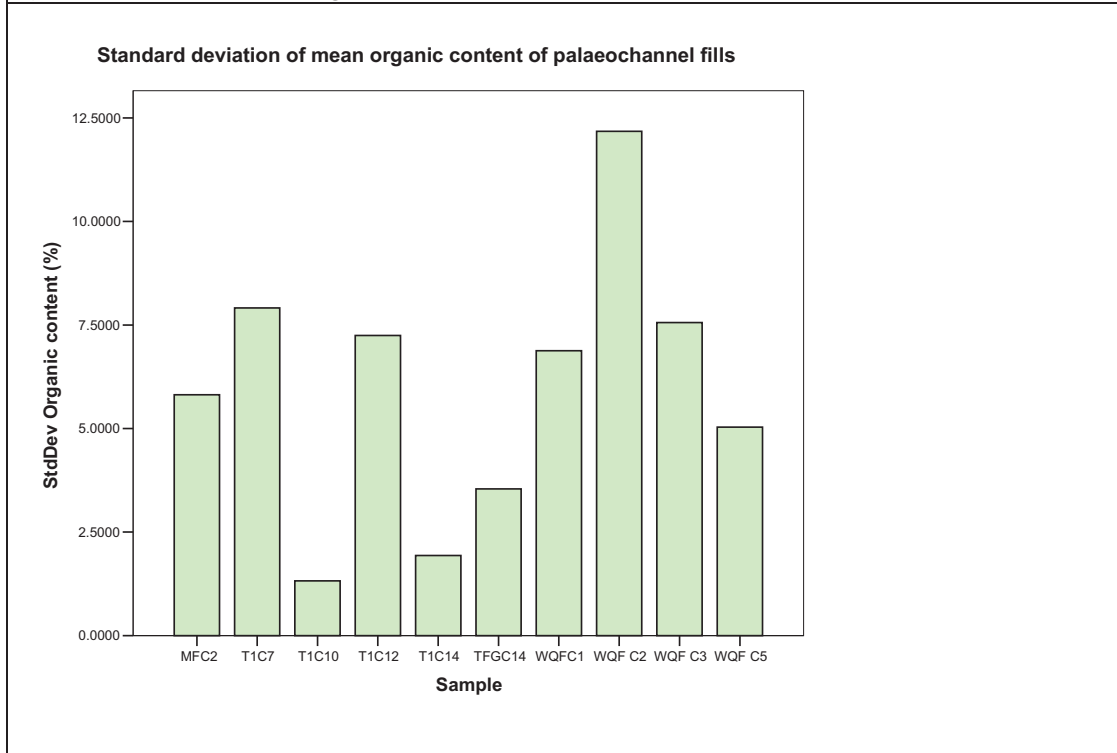


Fig 6.21: WQFC5 stratigraphy with pollen sample points and radiocarbon dates.



a) Palaeochannel mean organic contents.



b) Standard deviation of mean organic content of palaeochannel fills.

Fig 6.22: The palaeoenvironmental samples shown by mean organic content and standard deviation of organic content. The samples from Warren Farm quarry, T1C7 and T1C12 clearly stand out as having elevated organic contents.

6.2 Coleopteran analysis

6.2.1 Preservation

A series of samples recovered from cores and monolith tins were processed from across the site to establish, if any, variations in preservation of insect sclera and any possible relationship with factors such as pH, Eh, carbonate content etc.

This exercise enjoyed varying degrees of success; bulk samples recovered directly from the quarry face with a standard volume of 10 litres produced abundant, well-preserved and incredibly diverse assemblages. A notable exception is WFQ 5, preservation of insect sclera in both bulk and test samples was highly variable, this will be discussed in greater detail below.

Core Log

A sequence of eight samples were extracted to compare the preservation of insect remains, core-by-core. All samples were less than 250ml in size. The results of this study are discussed below (Tab. 6.1).

WFQ C1 (0-50cm):

With the exception of the basal sample (40-50cm), preservation of coleopteran sclera in the remaining four samples (0-40cm) was assessed as good to excellent. The organic nature of the matrix, combined with fine-grained alluvium, coupled with a low energy depositional regime, clearly provided optimal conditions for preservation. The nature of deposit formation would also have facilitated the accumulation of insect remains over a prolonged temporal scale, hence larger numbers of sclera recovered from these fine-grained deposits. The basal sample consisted of sands and gravel, no sclera were recovered from this sample. It seems likely that there are two reasons. Firstly, the free draining, coarser sands and gravels provide a less than favourable environment for preservation (Fig. 6.14). The second is that the initial, higher energy regime did not facilitate the accumulation of fragile insects remains that were simply swept away.

WFQ C1+ (0-10cm):

No insect remains were recovered from any of the five samples. All five samples from this suite were composed of sands and gravels, once again, it seems likely that this is a combined result of the nature of the minerogenic matrix and the initial depositional regime.

WFQ C1 (24-74cm):

The results from this sequence were similar to those of WFQ C1 (0-50cm), the upper samples, which were highly organic, combined with fine grained alluvium produced preservation deemed good to excellent. The basal sample, composed of sands and gravels, precluded preservation and deposit accumulation.

WFQ C2 M1:

The upper samples in this suite (0-40) all consisted of sands and gravels and no insect remains were recovered from any of the four upper samples. Preservation of sclera from the basal sample, (40-50cm), was excellent, once again, this was composed of organic rich alluvium.

Core	Depth cm	No. of samples	No preservation	Poor	Fair	Good	Excellent	Comments
WFQ C1	0-10	1				Y		
WFQ C1	10-20	1					Y	Abundant
WFQ C1	20-30	1					Y	Abundant
WFQ C1	30-40	1					Y	
WFQ C1	40-50	1	Y					Sand & gravel
WFQ C1 +	0-10	1	Y					Sand & gravel
WFQ C1 +	10-20	1	Y					Sand & gravel
WFQ C1 +	20-30	1	Y					Sand & gravel
WFQ C1 +	30-40	1	Y					
WFQ C1 +	40-50	1	Y					
WFQ C1	24-34	1					Y	
WFQ C1	34-44	1				Y		
WFQ C1	44-54	1					Y	
WFQ C1	54-64	1				Y		
WFQ C1	64-74	1	Y					
WFQ C2 M1	0-10	1	Y					Sand & gravel
WFQ C2 M1	10-20	1	Y					Sand & gravel
WFQ C2 M1	20-30	1	Y					Sand & gravel
WFQ C2 M1	30-40	1	Y					Sand & gravel
WFQ C2 M1	40-50	1					Y	
WFQ C2 M2	0-10	1				Y		
WFQ C2 M2	10-20	1			Y			
WFQ C2 M2	20-30	1					Y	
WFQ C2 M2	30-40	2				Y		
WFQ C2 M2	40-50	2			Y			
WFQ C2 M3	0-10	1		Y				
WFQ C2 M3	10-20	1					Y	
WFQ C2 M3	20-30	1					Y	
WFQ C3	0-10	1	Y					
WFQ C3	10-20	1	Y					
WFQ C3	20-30	1	Y					Sandy
WFQ C3	30-40	1				Y		
WFQ C3	40-50	1	Y					Sandy
WFQ C5	0-10	1				Y		
WFQ C5	10-20	1			Y			
WFQ C5	20-30	1	Y					
WFQ C5	30-40	1				Y		Sandy
WFQ C5	40-50	1	Y					Sandy

Tab 6.1: Preservation of insect sclera from the Warrens Farm Quarry cores.

WFQ C2 M2:

Preservation of insect remains in this suite varies considerably, from fair to excellent. None of the samples contained were of a particularly sandy nature, they did, however, contain a greater component of sandy, alluvial sediment than previously seen in the other four suites of samples. The sample, which contained significantly larger proportions of organic sediment (20-30cm), produced sclera deemed to be of excellent preservation.

WFQ C2 M3:

Once again, the sands and gravel base of the suite produced a poorly preserved and limited assemblage. In contrast, the assemblages from the organic rich alluvium enjoyed excellent preservation and sclera were abundant in the samples.

WFQ C3:

With the exception of a single sample, 30-40cm, primarily composed of alluvium with some organic component, insect remains were absent from the remaining four sand and gravel samples.

WFQ5:

Preservation in this core is similar to that seen in WFQ C2 M2 and preservation varies considerably between samples. Samples 40-50cm and 30-40cm were significantly sandier in comparison to the remaining three samples. Whilst sample 40-50cm produced no viable remains, the upper sandier sample, 30-40cm produced a reasonably large assemblage, the preservation of which was deemed as 'good'. Whilst organics were limited, the alluvial content of this sample was relatively high. The preservation in the upper two samples also varies, this does not, however appear to be associated with sedimentology as the composition of both was similar.

Discussion

In many cases, preservation and overall absence of insect remains in a single sample cannot simply be ascribed to taphonomic process, in many cases it also relates to the original depositional regime and sample size. WFQ C1+ for example which was largely composed of dark, highly organic alluvium, produced samples which produced good to excellent preservation, and only the basal sample, predominantly composed of yellow/brown sand and with a limited organic component, produced no viable sclera.

Similar preservation was observed in sand and gravel samples from WFQ C2 M1. Whilst the preservation of organic remains in these samples, such as wood and fragments of sedge and grass, was good, no insect remains were recovered. Only a single, organic rich sample at the base produced insect remains that, whilst limited due to sample size, were exceptionally well preserved. With a notable exception, the recovery of *any* insect remains from sand and gravel deposits was unusual.

Samples with mixed sedimentology, e.g. sand and alluvium did produced large, well-preserved assemblages. Bulk samples from channels WFQ 3b and WFQ 8 highlight the depositional issues from channels with higher energy flow regimes. Whilst preservation was good, the assemblages were more restricted than those were from channels that contained slow moving or standing water. It is also highly likely that these assemblages accumulated during slower periods of flow and that the sand in these deposits is a result of flood pulses.

Preservation of sclera from alluvial and organic rich deposits were generally good to excellent. Once again, this would appear to be directly related to the depositional regime. The slow moving or

standing waters that deposited these fine-grained sediments and permitted the development of backswamp vegetation would also have facilitated the accumulation of large assemblages of well-preserved insects. This is clearly illustrated by the bulk samples from Palaeochannels WFQ 1 and WFQ 2.

Conversely, preservation in the much older deposits of palaeochannel WFQ 5 is likely to be related to taphonomic process. Preservation of sclera from the organic rich, alluvial deposits varied greatly. Good to fair preservation is related to the stratigraphy of the tin WQFC5. The stratigraphy reflects changes in post depositional conditions of the varying sediment units, which themselves has affected the preservation of insect sclera. The physical impact of this preservation on insect sclera caused degradation and fragmentation; the sample from 20-30cm was most affected. However the remains from 10-20cm were considerably more degraded than the remaining two (0-10 and 30-40cm), this corresponds well with the geochemical data.

Sample size has been alluded to, and the importance of having large quantities (5l – 10l/3kg) of sediment to provide a representative assemblage cannot be underestimated (Coope and Osborne 1968, Kenward *et al.* 1980). Small quantities, such as those processed here, recovered from manual augers or monolith tins can only ever be used to gain an overview of site and preservation potential. Such small quantities should not be used to cast conclusive aspersions about a site.

6.2.2 *Coleopteran analysis: palaeoecology*

To aid interpretation, where applicable, the taxa have been assigned ecological groups following those of both Kenward (1978), Kenward and Hall (1995), Robinson (1981, 1983) and more particularly Smith, Osborne and Barrett (1997, 2000). The occurrence of each of the ecological groups is expressed visually (Fig 6.23). These totals have been calculated as percentages of the entire assemblage from each individual sample. The meaning of each ecological code is explained.

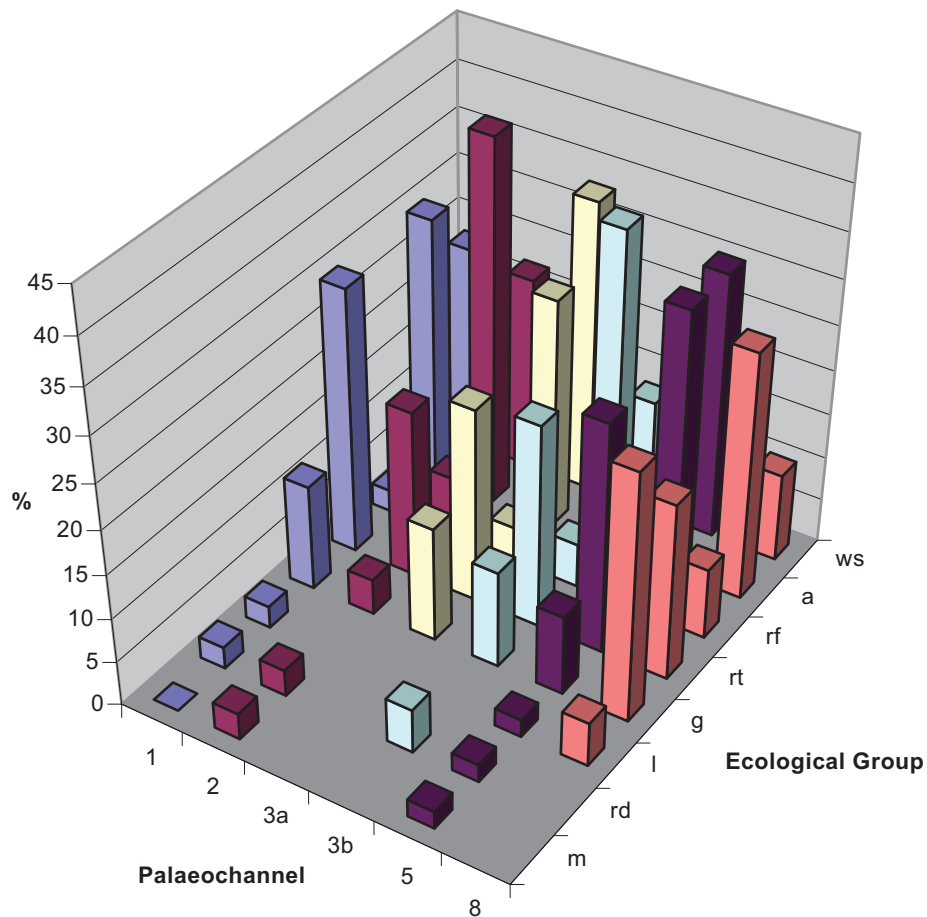


Fig 6.23: Warren Farm Quarry species ecological groups. Key: ws=waterside; a=aquatic species; rd=species primarily associated with drier organic matter; rt=species primarily associated with rotting organic matter; species primarily associated with foul organic, often dung; g=species associated with grassland; l=species associated with woodland.

WFQ 1

The assemblages from all seven samples of the palaeochannel 1 samples (Tab. 6.1) were exceptional, in both species abundance and diversity; they are exceeded only by the assemblages from palaeochannel 2. Evidence indicates the environment changes little throughout deposit formation, and suggests large grazing animal roamed the floodplain. Changes to the aquatic regime, whilst evident, are subtle.

The lowermost samples (70-50cm) are characterised by less specialised taxa, generally associated with damp, well vegetated country, such as the Carabidae, *Dyschirius globosus* and *Bembidion guttula* (Lindroth 1974, 1985) and muddy, ephemeral pools such as the Hydraenid family (Hansen 1987). The period directly after channel abandonment is clearly illustrated by the disappearance of the Elmidae or 'riffle beetles'. A small assemblage of this family, including *Limnius volkmari* and *Esolus parallelepipedus* were recovered from the basal sample, both are found in well oxygenated, flowing waters with sand and gravel armoured substrates (Holland 1972).

Above 50cm, the taxa include a number of phytophagous species, all commonly associated with sedges and other taller reeds, such as the Chrysomelidae, *Donacia obscura* and *Plateumaris*

discolor, and the Curculionidae, *Notaris* spp. and *Thryogenes* spp. (Koch 1992, Hyman 1992, Menzies and Cox 1996).

Other curculionids recovered from the upper samples, are associated with drier grassland such as the Apionidae and *Sitona* spp., both families are found upon vetches (*Vicia* spp, *Lathyrus* spp.), clovers (*Trifolium* spp.) and other leguminous vegetation (Koch 1992). A number of Carabidae or 'ground beetles' are found on sparsely vegetated, dry, sands and gravels such as *Agonum mulleri*, *Amara aenea* and *A. familiaris* (Lindroth 1974, 1986). These three species probably lived at the periphery of the palaeochannel, on the exposed sands and gravels of the former riverbank.

Throughout the formation of this deposit, the floodplain is increasingly utilised for grazing, a comprehensive suite of dung beetles or Scarabaeidae is recovered from all seven samples and are particularly abundant in the upper samples. Taxa associated with dung and other, foul rotting material are limited which does not suggest large accumulations of this type of material.

Species found on distinctly aquatic vegetation are scant, as are aquatic coleoptera associated with deep, permanent pools or slow moving water. The Elmidae, which are virtually absent after the small assemblage recovered from the basal sample are replaced by the Hydraenidae and the Hydrophilidae. Both families are largely composed of semi-aquatic and hydrophilous species associated with muddy, ephemeral pools and the muddy banks and shores of ponds and streams (Hansen 1987). A single, largely aquatic hydrophilid, *Hydrobius fuscipes*, is relatively abundant in the upper samples, these species is most commonly associated with the well-vegetated shallows of stagnant and slow moving water (Hansen 1987).

WFQ 2

Palaeochannel 2 produced the most diverse, abundant and well-preserved assemblages recovered from any of the Warrens Farm palaeochannels. Unlike palaeochannel 1, the depositional environment in the basal samples appears to have been waterlain. The basal samples (60-30cm) are particularly rich in taxa associated with aquatic plants and deep standing or slow moving waters.

The Chrysomelidae, *Donacia crassipes* and *Plateumaris sericea* are both found on white water lily (*Nymphaea alba*), the latter is also associated with yellow flag (*Iris pseudocorus*) and carices (Menzies and Cox 1996), a third chrysomelid, *Donacia versicolorea*, is found on broad leaved pondweed (*Potamogeton natans*) (Menzies and Cox 1996). The aquatic taxa are less indicative of this, the Dytiscidae or 'predacious diving beetles' from this sample are associated with shallower waters with lush, emergent vegetation.

Whilst there is little evidence from the lower samples that indicates the type of environments that surround the palaeochannel, the few that do are associated with marshy, sedge-dominated biomes, the upper samples (30cm+) clearly indicate increasingly dry conditions. Whilst phytophagous taxa associated sedge and taller reeds persist, such as the curculionid family *Thryogenes* spp. and to a lesser degree *Notaris* spp. persist; many taxa found in these samples are associated with drier grassland. A small component suggestive of mixed deciduous woodland was also recovered.

Many of the Curculionidae are phytophagous beetles associated with a variety of plants commonly found in both meadows and disturbed ground and include the Curculionidae or weevils of the *Apion* and *Sitona* families. *Apion urticarium* is found on nettles (*Urtica* spp.) as is the nitidulid *Brachypterous urticae* Other phytophagous beetles associated with a variety of plants commonly found in both meadows and disturbed ground include the Curculionidae or weevils of the *Apion* and *Sitona* families. *Apion aeneum* and *Apion radiolus* are found on mallows (Malvaceae), in disturbed

ground, waysides and hedgerows, *Apion ervi* is found in hedgerows with vetches (*Vicia* spp.) (Bullock 1993, Koch 1989b, 1992). *Sitona puncticolis* and *Sitona tibialis* are both found with vetches, clovers (*Trifolium* spp.) and trefoils (*Lotus* spp.) (Koch 1992). Finally, *Mecinus pyraster* is found on plantains, particularly ribwort plantains (*Plantago lanceolata*) (Bullock 1993). *Apion viciae* is found in hedgerows with tufted vetch (*Vicia cracca*), whilst both *Apion ervi* and *Apion subulatum* are found on meadow vetchling (*Lathyrus pratense*) (Bullock 1993, Koch 1992). *Sitona puncticolis* and *Sitona tibialis* are both found with vetches, clovers (*Trifolium* spp.) and trefoils (*Lotus* spp.) (Koch 1992). Finally, *Mecinus pyraster* is found on plantains, particularly ribwort plantains (*Plantago lanceolata*) (Bullock 1993). The Carabidae *Clivina fossor*, *Harpalus tenebrosus* and the nitidulid *Brachypterolus pulicarnis*, *C. fossor* was recovered in some abundance, all three species are commonly found in open country on sands and gravels (Lindroth 1974, 1985, 1986). Analogous to these drier conditions are the increasingly large numbers of dung beetles that are found throughout the profile but become particularly abundant in the upper samples (30+).

Lignacious taxa are found in all five samples. Whilst none are found in large numbers, their presence in the assemblages, particularly species associated with alder, is significant. The greatest concentration of woodland taxa is found in samples from the middle of the section (50-20cm). Three species are associated with alder carr. The chrysomelid, *Melasoma aeneae* and the curculionid, *Anoplus roboris*, are both phytophages which feed upon alder, a third species found in alder-dominated woodland is the carabid *Leistus rufascens*, as is the coccinellid *Chilocorus renipustulatus* which is also found with willows (*Salix* spp.) (Koch 1989b, 1992). The Scolytidae, *Scolytus multistriatus*, found on elm (*Ulmus* spp.) and *Kissophagus hederiae*, found on ivy (*Hedera helix*) were also recovered (Koch 1992).

WFQ 3

WFQ3 both samples from this palaeochannel produced relatively small assemblages, preservation was good and both assemblages are readily interpretable. The environment changes little throughout the formation of the deposit; hence both samples will be discussed together.

The Carabidae, *Bembidion guttula* and *B. unicolor* suggest a damp well vegetated floodplain, the Chrysomelidae, *Plateumaris discolor* and the Curculionidae, *Notaris acridulus* and *Thryogenes* spp. suggest is dominated by carices and other damp-grassland species such as *Glyceria* spp. (Koch 1992, Lindroth 1974, 1985). Drier ground is indicated by the carabidae *Harpalus* spp (Lindroth 1974, 1986). The presence of scarabaeids or 'dung beetles' clearly suggest grazing herbivores nearby.

Distinctly aquatic species are restricted to the Elmidae or 'riffle beetles', which are abundant in the basal sample, these are replaced in the upper sample by members of the Hydraenidae which are particularly abundant and are associated with muddy, ephemeral pools (Hansen 1987). Two species do indicate that the palaeochannel contained deeper pools of standing water, the chrysomelid *Donacia crassipes*, previously found in palaeochannel 2 and associated with white water lily was recovered. The curculionid, *Eubrychius velatus*, is found on water milfoils (*Myriophyllum* spp.), whilst this aquatic plant does not require particularly deep water, much of the biomass is submerged (Haslam *et al.* 1982), hence deeper, more permanent water is required.

WQF 4

The insect remains from palaeochannel 4 produced well preserved but relatively restricted assemblage, despite this, it produced the most comprehensive and informative series of assemblages associated with aquatic conditions and flow regime at the site. The assemblages change little throughout formation of the deposit.

The assemblage is dominated by the Elmidae or 'riffle beetles', which clearly suggest regular influxes of water from a fast flowing source. Many Elmidae, are associated with well oxygenated, swiftly flowing streams and rivers which flow over gravel and sand armoured substrates. The quartet of elmids, *Limnius volkmari*, *Esolus parallelepipidus*, *Oulimnius* spp. and *Machronychus quadrituberculatus* are no exception, the latter is particularly associated with submerged wood (Holland 1972).

The remainder of the assemblage provides little information on the environments surrounding the channel. Many species are cosmopolitan taxa associated with damp, wetland habitats from woodlands to marshy meadows, such as the Carabidae, *Trechus secalis* and *Trichocellus placidus* (Lindroth 1974, 1985, 1986). The nitidulid, *Brachypterus urticae*, which is found with nettles (*Urtica dioica*) and suggests areas of disturbed ground (Koch 1989b).

WFQ 5

The palaeochannel 5 deposits produced cold stage insects assemblages clearly associated with a stadial event and contain several stenothermic taxa and species tolerant of cooler climates. The assemblages were less well preserved than those of the other five samples, in many cases the sclera were fragmented and in a considerably more degraded condition. In many cases, the sclera were still identified to species level and have produced a diverse and readily interpretable assemblage.

Once more, the environment changes little during the formation of the deposit. The area surrounding the palaeochannel is vegetated by low growing mosses and sedges, with tall reeds fringing the periphery of the palaeochannel itself. Further away from the channel, several taxa hint at drier heathland type vegetation.

Phytophagous taxa, found in sedge-dominated communities, include the chrysomelid, *Plateumaris sericea*, which is particularly associated with cotton grasses (*Eriophorum* spp.), whilst more generalised wetland coleoptera include the Carabidae or 'ground beetles', *Loricera pilicornis*, and the *Bembidion* spp. (Lindroth 1974, 1985; Menzies and Cox 1996). The stenothermic staphylinidae, *Pycnoglypta lurida*, and the carabid, *Agonum thoreyi*, are both found amongst tall reeds, particularly the common reed (*Phragmites australis*) and club-rush (*Schoenoplectus lacustris*) (Koch 1989a, Lindroth 1974, 1985). Indicators of tall reeds continue throughout the profile, in the upper samples, *A. thoreyi* persists and is joined by *Donacia impressa* and *Donacia simplex* (Menzies and Cox 1996). This perhaps suggests tall reed swamp has begun to encroach upon much of the site and the area immediately surrounding the palaeochannel.

Species from drier localities, probably situated relatively close to the palaeochannel are heath and moorland taxa, two of these, *Haltica britteni*, and a second stenothermic staphylinidae, *Eucnecosum brachypterum*, are both phytophagous and found on heather (Koch 1989a, 1992). The curculionid, *Phyllobius pyri*, is found on birch (*Betula* spp.).

Probably the most significant component of this assemblage are the stenothermic species, two distinct stenophilous taxa were present in all four samples, the Staphylinidae, *Pycnoglypta lurida* and *Arpedium brachypterum*. *Arpedium brachypterum* persist in the British Isles in northern and montane habitats (Tottenham 1954) and is found in swamps and damp meadows, beneath reed and flood debris in Europe (Koch 1989b). Insects associated with cooler environments but not distinct stenotherms include the chrysomelid, *Chrysomela cerealis*, which feeds at the roots of wild thyme (*Thymus* spp.) and is found in upland and montane habitats (Shirt 1987). The current range of this species in modern Britain is restricted to Snowdonia (Hyman 1992,

Shirt 1987). The curculionid, *Otiorhynchus rugifrons*, most commonly found in montane and upland environments in north, central and eastern Europe and finally, the scarabaeid, *Aphodius lapponum*, a species found with dung in upland habitats (Jessop 1972).

WFQ 6

Palaeochannel 6 produced two, well preserved and diverse assemblages. Conditions surrounding this channel are subtly different to those seen around the other five channels. Conditions are significantly drier, the assemblages are composed of grassland and disturbed ground taxa, those of flowing water and a comprehensive bevy of Scarabaeidae.

Aquatic conditions are strikingly similar to those seen in palaeochannel 4. The large assemblage of Elmidae clearly indicates regular influxes of water from a rapidly flowing source. Indicators of reeds, sedges and other wetland flora are absent, which suggests that the channel was relatively free of aquatic and emergent plants throughout deposition.

A variety of Curculionidae indicate species rich grassland, a profusion of *Apion* and *Sitona* spp. occur in both samples and indicate a rich mix of vetches including tufted vetch (*Vicia cracca*) and meadow vetchling (*Lathyrus pratense*), clovers (*Trifolium* spp.) and medicks (*Medicago* spp.) (Koch 1992). There is also some limited evidence for areas of disturbance, suggested by a further two Apionidae, *Apion urticarium*, as the name suggests if found with nettles (*Urtica dioica*), whilst *Gymnetron pascuorum* is found with plantains (*Plantago* spp.) (Koch 1992). The large numbers of Scarabaeidae recovered from both samples, clearly suggest that this lush, verdant grassland provided nutritious grazing for herbivorous animals.

Finally, the Scolytidae, *Scolytus ratzbergi* and *Scolytus scolytus* both suggest nearby woodland. Both are species specific, *S. ratzbergi* to birch and *S. scolytus* to elm. The former is restricted to dead specimens, whilst the latter is associated with living trees (Bullock 1993).

6.2.3 Discussion

Vegetation and the surrounding environment:

Chronostratigraphically the oldest palaeochannel is WFQ5, which radiocarbon dating currently suggests developed c. 16ka BP, during GS-2a (Björk *et al.* 1998). This would place palaeochannel development at the height of the Devensian glaciation, comparison between the assemblages from the channel and other sites in the Trent Valley and other British sites, also suggest a slightly later date. Climatic implications of this fauna will be discussed in greater detail below.

The vegetation is characteristic of this type of a cooler climate ecotone and indicates a mosaic of wetland species composed of lower growing sedges and taller reeds which, probably fringed the palaeochannel and encroached upon the wetter areas of the riparian zone. Scrubby heathland species such as heather (*Calluna* spp.) and birch (*Betula* spp.) colonise the drier gravel terraces. Comparable 'cold stage' fauna's sites in the Trent Valley include Bellmoor (Howard *at al.* 1999, Tetlow 2005), Birstall (Ripper 2005), Croft, Hemington and Yoxall (Greenwood and Smith 2005, Smith and Howard 2004).

Similarities between the later palaeochannels vary. Several channels indicate damp, well-vegetated marshland with few indicators of specific herbaceous taxa. The basal samples of both palaeochannels 1 and 2 and all three samples from palaeochannel 3b are particularly ambiguous. As succession continues, similarities between palaeochannels 1 and 2 diverge. The environs of

palaeochannel 1 and 3a demonstrate a degree of similarity with sedge and reed-dominated vegetation becoming established.

In the upper samples of palaeochannels 1 and 2 and palaeochannel 6, conditions become increasingly dry. Many of the insect taxa indicate considerably drier conditions, with large numbers of Curculionidae or 'weevils' such as the Apionidae and *Sitona* spp. which suggest species rich grassland. It is also clear grazing animals increasingly used the floodplain, with the exception of palaeochannels 3a and 3b, it seems likely that the floodplain directly adjacent to the palaeochannels was subject to grazing.

Evidence of grazed pasture, directly fringing the channel was found in early Bronze Age contexts at Staythorpe, Nottinghamshire (Davies 2001) and later Bronze Age contexts at South Ings, Rampton (Howard and Knight 2001). At Kirby Muxloe, close to the headwaters of the Soar, insects from Iron Age contexts indicate clearance and grazing by this period (Cooper 1994, Greenwood and Smith 2005). At Waycar Pasture, near Girton, Nottinghamshire, clear evidence of pastoral farming is evident in the insect record from 2000 BC to the Romano-British period (Howard *et al.* 1999).

Direct and unequivocal evidence of pasture and grazing of the floodplain directly adjacent to channels at a number of locations in the Trent and Soar Valleys is limited. At Croft, Neolithic and Iron Age contexts produced limited assemblages of dung beetles and few indicators of open grassland (Smith and Howard 2004, Smith *et al.* 2005). Similarly, at Bole Ings, assemblages from very late Mesolithic to Iron Age contexts of produced little evidence of grassland or grazing (Dinnin 1997). At Langford, Howard *et al.* (1999) suggest the grassland and dung beetle assemblages are a result of grazing in clearances and glades amongst the dense woodland that covered the site during the Neolithic and the early Bronze Age.

The key at these other three sites would appear to be the dense areas of well developed woodland which covered the banks of both the Rivers Trent and Soar during later prehistory. At Croft, the Bronze Age contexts are more indicative of open grassland, however the assemblages are less than conclusive and a small woodland assemblage persists (Smith *et al.* 2005). Conversely, entomological evidence of dense woodland at the confluence zone of the Trent and Soar is limited. Whilst lignacious and saproxylic taxa are present, they are restricted to Scolytidae, which are ready fliers and which were recovered in very restricted numbers and several indicators of alder carr.

The definition of alder carr in the archaeological record using entomological methods is problematic and has previously been discussed at length (Girling 1985, Paddock 2001, Robinson 1993, Tetlow 2003, 2005, Smith *et al.* 2000, Smith and Whitehouse 2005). Two factors compound this issue, the first relates to the limited number of taxa (14) associated with alder in comparison with other tree e.g. Oak (93) (Bullock 1993). The second relates to the lack of modern entomological knowledge of this habitat. Several species recovered from the palaeochannel 2 samples are obligate phytophages of alder, several others, whilst not restricted to alder, the species is their tree of preference. Establishing the presence of alder carr at other notable wetland sites e.g. Goldcliff, Goldcliff East, the Somerset Levels and Mingies Ditch has been problematic (Girling 1985, Robinson 1993, Tetlow 2003, 2005, Smith *et al.* 2000). At sites such as Goldcliff, the presence of large tracts of alder carr has been established by wood identification, whilst any indicators in the entomological record have been entirely absent (Tetlow 2003, 2005). When considering the significant degree of entomological ambiguity at Goldcliff and these other sites, the presence of alder-dwelling creatures at Lockington can be taken as unequivocal indicators of alder carr, close to palaeochannel 2.

This, in itself is intriguing considering the paucity of lignacious or saproxylic taxa in virtually every other palaeochannel and the contemporaneous nature of deposit formation, channel by channel. The implications for deposit and channel relationship, will be discussed in greater detail in Chapter 7.

In the wider context of the Trent and Soar Valley, alder carr appears to persist much later into the Bronze Age at Lockington than has been recorded at other sites. At Birstall, in the middle reaches of the Soar, the potential for a wooded floodplain persists until the early Bronze Age (3530 ± 70 ^{14}C years BP, SRR-3507, Brown *et al.* 1994). By the later Bronze Age, this woodland had given way to open pasture (Smith and Tetlow 2004), with a suite of coleoptera strongly reminiscent of those from Warren's Farm. In the Trent Valley at Yoxall, Staffordshire, dense woodland is still recorded 2780 ± 60 ^{14}C years BP (Beta-73350, 1110-800 cal BC). Further afield, cleared floodplains are recorded at Staythorpe, woodland has been cleared from the site in the early Bronze Age (Davis 2001) and in the later Bronze Age at Shardlow and Aston, Derbyshire (Greenwood and Smith 2005, Howard *et al.* Forthcoming). In the middle and lower Trent, clearance of the floodplain at Bole Ings and Girton is evident by 2690 ± 100 ^{14}C years BP (Beta-75720, 1050-540 cal BC) and 2890 ± 60 ^{14}C years BP (AA-29321, 1290-900 cal BC) (Brayshay and Dinnin 1999, Dinnin 1997, Howard *et al.* 1999). At a second site in the Staffordshire Trent Valley at Fisherwick, a dramatic decline in arboreal pollen is recorded from the mid Bronze Age (Smith 1979). At Repton in the lower Trent, a mosaic of reedswamp, woodland and pasture is recorded between 1000-400 cal BC (Greenwood and Smith 2005).

It is possible that the alder carr at Lockington is a result of a brief episode of carr regeneration. Both woodland regeneration and wetland re-expansion are recorded in the Trent Valley during the first millennium BC (Knight and Howard 2004). The onset of cooler and wetter conditions is associated with later Bronze Age and would have produced increasingly unstable floodplain conditions. The impact would have been particularly intense when coupled with increased over-land run off associated with woodland clearance and primitive agricultural practices and rising groundwater tables. At sites such as Scaftworth, close to the confluence of the Trent and Idle Valley, overbank floods and paludification cause significant broadening and expansion of the floodplain (Dinnin and Weir 1997). It is not unfeasible that similar expansion was experienced at the Trent/Soar confluence. At South Ings, Rampton, alder carr clearly exploits and expanding wetland niche, perhaps encroaching upon an already established area of drier woodland as conditions become increasingly wet (Knight and Howard 2001).

Aquatic Regime:

The aquatic regime in each channel divides the palaeochannels at Warrens Farm Quarry into three, distinct groups. In palaeochannel 1 and 3a, the episode of abandonment is clearly illustrated, relatively large assemblages of Elmidae, or 'riffle beetles' are found at the base of both channels. In subsequent samples this family appear in considerably restricted numbers that suggest that regular influxes of water from rapidly flowing sources has ceased. This is replaced by species associated with leaf filled, muddy, detrital pools. Palaeochannel 3a is a much shallower feature, which appears to have infilled relatively rapidly. In contrast, alluviation in palaeochannel 1, particularly in the top most deposits, appears to have been relatively slow. There appears to have been no further catastrophic reactivation, which would have scoured the channel but a period of relatively slow alluviation. This is particularly pronounced in the upper two samples. Throughout this accumulation of these deposits, the palaeochannel acted as a natural 'pitfall trap', facilitating the accumulation of the large and diverse insect assemblages recovered, a trend reflected in the upper deposits of palaeochannel 2.

Conditions within palaeochannel 2 are subtly different; indicators of flowing waters are virtually absent in all six samples. During early stages of deposition, the channel appears to have been filled with relatively deep, standing or very slow moving water. This is suggested not only by a relatively diverse and abundant assemblage of insects associated with permanent, deeper pools of water which are considerably more limited in palaeochannels contemporary with WFQ (WFQ1, 3a, 3b, 6) but by a further group of species associated with specific aquatic and emergent vegetation.

Several of the Chrysomelidae found in this sample are found on specific species of aquatic plant, white water lily and broad-leaved pondweed. Both the lily and pondweed require water between 30 and 50 cm deep (Haslam *et al.* 1982), which suggests an expanse of relatively deep, open water, ultimately adding further depth to this argument. It is quite possible that such conditions prevailed in WFQ2 throughout the formation of the deposit.

In total contrast to the other three channels, diverse assemblages of Elmidae in both WFQ3b and WFQ8 suggest rapidly flowing water, in both channels throughout deposit development. This regime would also explain the relatively limited nature of the assemblages from both of these deposits. Rapidly flowing water would have scoured any significant deposits and precluded any further extensive deposition.

Comparison between the aquatic assemblages from this site and others in the Trent and Soar Valleys, particularly those studied by Smith and Howard (2004) has produced a significant dichotomy. This dichotomy has implications for both the depositional regime and the application of entomology in alluvial locations.

The aquatic assemblages from Warrens Farm Quarry, provides good corroborative evidence for defining flow regime using biometric data, in this case coleoptera. Both palaeochannel WFQ3b and WFQ8 strongly indicate deposition in a higher energy regime; two factors lead to this conclusion. The first is the abundance of coleopteran taxa associated with flowing water and higher energy conditions, juxtaposed with those of stagnant and standing waters in samples from both channels. The second relates to the abundance of coleoptera found on emergent and aquatic vegetation which, are virtually absent in both WFQ 3 and 8 and prevalent in palaeochannels WFQ1, 2, 3a, particularly palaeochannel 2. All of which produce coleopteran taxa characteristic of standing water. A further suite of coleoptera associated with aquatic vegetation such as white water lily (*Nymphaea alba*), water dropwort (*Oenanthe aquatica*) and taller reeds such as clubrush (*Schoenoplectus* spp.) and bulrush (*Typha* spp.) was also recovered from WFQ 1, 2 and 3a and are absent in WFQ 3b and 8. These herbaceous species are clear indicators of standing water; many are also associated with silty substrates (Haslam *et al.* 1982), sedimentological conditions anathema to the elmid family.

Hence this combined data conclusively suggests rapidly flowing water in WFQ 3b and 8 and a much more pedestrian regime in channels 1, 2 and 3a. Due to the much earlier deposition of WFQ 5, this palaeochannel has been omitted from the general discussion, it does fall into the same category as WFQ 1, 2 and 3a. Whilst a number of elmids were recovered, the aquatic insects are those of relatively shallow standing water, muddy detrital pools and aquatic vegetation unable to withstand a rapid flow regime.

The palaeochannels at Lockington contain a coleopteran assemblage completely in contrast to that Croft, Langford, Hemington, Yoxall and Castle Donnington (Brown *et al.* 2001, Cooper and Ripper 1994, Forthcoming, Howard *et al.* 1999, Smith and Howard 2004, Smith *et al.* 2001, Smith *et al.* 2005). These five sites were divided into two, sites where sedimentology and coleoptera indicated a

flowing aquatic regime (Croft, Langford and Hemington) and standing or slow moving water (Yoxall and Castle Donnington). The aquatic assemblages used to infer these conditions are comparable to those used to imply aquatic conditions at Warrens Farm Quarry, it is at this point the similarity ends. In complete contrast to the palaeochannels at Lockington, the channels from sites that suggested a flowing aquatic regime produced the largest and most diverse assemblages, whilst those from the slower channels produced considerably more restricted faunas (Smith and Howard 2004).

The disparity between these two data sets has produced a significant interpretative issue that can only be resolved by further assimilation of coleoptera from the Trent, its tributaries and other catchments in the British Isles.

6.1.4 Palaeochannel Relationships

Comparison between the aquatic and terrestrial coleoptera from WFQ 1, 2, 3a, 3b and 8 and their spatial and temporal relationship allow several tentative extrapolations to be drawn.

Coleoptera suggest that palaeochannel WFQ 3a may have developed contemporaneously with the upper samples (30+) from WFQ 1. Both aquatic and terrestrial components from both samples are strikingly similar. Radiocarbon dates from the base of the channels indicate a reasonable overlap, whilst OSL dates suggest greater degree of synchronicity, WFQ 3a formed after 1150 ± 300 and WFQ 1 after 1050 ± 300 .

Further similarities exist between WFQ 3b and WFQ 8, both suggest flowing water and similar bankside vegetation. Whilst the dates for WFQ 3b can be taken as the same as those of 3a (they were recovered from a single, potentially continuous channel), complex stratigraphy precludes any firm assertions. Stratigraphy is complex and the area from which sample 3b was recovered is possibly a re-cut, the result of scouring associated a flood-pulse and followed by a more prolonged period of flowing water. Similarities between the two samples are strong, hence the relationship between these two samples, particularly considering the stratigraphic evidence, possible scouring and re-cutting make this hypothesis plausible.

No distinct correspondence exist between the assemblages from WFQ 2 and those from the WFQ 1, 3a/b, 8 complex. Conditions in the upper deposits of WFQ 2 (30-10cm) display similarities to those from WFQ 1 (50cm+), it is the differences between WFQ 2 and the other suites of samples that are outstanding. These include the woodland fauna and greater numbers of Scarabaeidae and other species associated with dung and rotting material. Radiocarbon dates support this theory and suggest formation several hundred years later than that of the other palaeochannels, c. 1060-890 cal BC, no OSL dates are available for this channel.

The climatic implications of Palaeochannel WFQ 5:

two distinct stenophilous taxa were present in all four samples, the Staphylinidae, *Pycnoglypta lurida* and *Arpedium brachypterum* collectively, they may be assigned a mutual climatic range or 'MCR' of between $T_{\min} -35$ to $+3^{\circ}\text{C}$ (T_{\min} range 38) and $T_{\max} 7-16^{\circ}\text{C}$ (T_{\max} range 9) (Elias 2000). The second staphylinid, is *Pycnoglypta lurida*, a taxa absent from the modern British fauna, whilst this species cannot be described as an 'Arctic stenotherm', its current distribution is in montane and northern regions of Europe (Osborne 1973). Despite its absence from the modern British fauna, the climatic range of *Pycnoglypta lurida* is less extreme than that of *Arpedium brachypterum*. The

MCR of *Pycnoglypta lurida* is between T_{\min} -34.5 to $+4.75^{\circ}\text{C}$ (T_{\min} range 39.25) and T_{\max} $9.5-24^{\circ}\text{C}$ (T_{\max} range 14.5) (Elias 2000).

Both *Pycnoglypta lurida* and *Arpedium brachypterum* have been recovered from a number of sites throughout Britain particularly associated with climatic cooling at the end of the Lateglacial and the beginning of the Loch Lomond stadial *c.* 12,000-11,500 ^{14}C BP. In the main body of the Trent Valley, sites include Repton, Langford, Holme Pierrepont and Hemington (Greenwood and Smith 2005, Tetlow 2007). Comparable cold stage faunas have been recovered from several tributaries of the Trent, Birstall and Barrow on Soar in the Soar catchment (Smith and Tetlow 2004, Tetlow 2007) and at Bellmoor on the River Idle in North Nottinghamshire (Howard *et al.* 1999, Tetlow *et al.* 2005). A further site, north of Wroxeter on the east bank of the River Dove has also recently been identified (Challis *et al.* 2006). Other sites are in the English Midlands at Church Stretton, West Bromwich, Abingdon and Glanllynau, Gwynedd (Aalto *et al.* 1984, Coope and Brophy 1972, Osborne 1972, 1973).

At Glanllyau, Coope and Brophy suggest that *Pycnoglypta lurida*, *Arpedium brachypterum* and other insects also recovered from Holme Pierrepont, indicate that *c.* 11,300 \pm 300 ^{14}C BP (14,087-12,771 cal BP, 12,137- 10,821 cal BC*) the mean July temperature at Glanllynau was 14°C , several degrees lower than that of the present July mean (Coope and Brophy 1972, Lowe and Walker 1997). Of the other taxa associated with cooler conditions, no are as distinct as this pair of Staphylinidae. Several are of note, the Chrysomelid, *Chrysomela cerealis* or 'rainbow leaf beetle' is currently endangered in the British Isles and is found only in the area of Y Wyddfa in Snowdonia (Hyman 1992).

6.1.5 Conclusions

The assemblages from Warrens Farm Quarry have been informative on a number of levels. The exceptional preservation and abundance of insect remains from the majority of samples has the potential to produce a detailed picture of changing conditions within the palaeochannels and vegetative succession during deposit formation from the Lateglacial to the late Bronze Age. Contrary too much of the Trent and Soar Valley, the floodplain at Lockington was not heavily wooded. A significant impact on vegetative succession at the site is the highly dynamic nature of the Trent/Soar confluence during later prehistory. It is not difficult to conclude that this instability precluded succession further than damp, open grassland. This lush, verdant grassland would have provided an area of prime pasture, which was grazed during both major periods of organic deposition. Evidence also indicates alder carr encroachment or regeneration during the very late Bronze Age and the early Iron Age, a phenomenon recorded a several other sites during this period and likely to be associated with climatic deterioration and the onset of cooler and wetter conditions during this period.

6.2 Pollen and Spore Assessment

The results of the assessment are discussed in the same order as given (Tab. 6.3) and for ease of description the following terms are used to describe the concentration values (Tab. 6.2):

No. of pollen & spore grains per 100 exotics	Pollen & spore concentration Grains ml ⁻¹	Descriptive class
0-50	0-5000	very low
50-100	5000-10,000	low
100-300	10,000-30,000	moderate
300-500	30,000-50,000	high
>500	>50,000	very high

Tab. 6.2: Pollen and spore concentrations and descriptive classes.

MFC2

Pollen concentrations vary from very low to very high with the majority in the moderate class. The lowest values occur at adjacent levels mid core (98cm, 112cm) and at the base of the core (168cm, 184cm). These levels correspond with a relatively inorganic (c. 5% LOI) red-brown silty clay with a trace of fine sand. Conversely the highest concentration, which is very high at 70cm, corresponds with a band of dark grey-black silty clay with an average LOI of 20-25%. This is most likely an artefact of a variable accumulation rate as the percentage of damaged grains is high throughout the core suggesting poor conditions of preservation with alternating wet and dry soil moisture conditions.

TIC7

Pollen and spore concentrations vary from low to moderate. There is a distinctly lower concentration in the central part of the core from 154cm to 98cm depth. These levels also have generally higher percentages of unidentified grains and damaged grains, which reaches a peak at 126cm of 51.8%. These levels correspond with the lowest organic contents in the profile at the base of the blue-grey clay unit.

TIC12

Pollen and spore concentrations vary from very low to high with the lowest values from the upper part of the core (112cm-42cm) excluding the uppermost levels. The percentage unidentified are very erratic with adjacent values varying from 1.4% to 14.2% with similar pollen concentrations. The percentage damaged is less variable but consistently higher than the other cores, with the exception of the basal three levels. Again the lowest concentrations correspond with the lowest organic matter percentages and the upper part of the red-brown silty-clay unit. The highest concentrations and lowest percentage unidentified and damaged correspond with grey clay increasingly gleyed with depth and a transition to black-grey clay with organic macrofossils.

TIC10

Pollen and spore concentrations vary from very low to moderate but are heavily biased to the very low concentration class. The very low concentrations below 10 grains per 100 exotics encountered unfortunately made the % unidentified and % damaged figures rather erratic varying for example from 0% to 33% or 66% between two levels with 2 and 3 grains respectively on the basis of one or

two grains. However, it is noteworthy that the % damaged grains remained high when the pollen concentration had risen to moderate at the base of the core.

TFGC14

Pollen and spore concentrations vary from very low to moderate with a distinct pattern – higher concentrations in the upper part of the samples section of the core (266cm-294cm) in comparison with the lower sections (294-378cm). This variation is not surprising given the stratigraphy of the core although the pertinent variation is subtle. At 305cm the stratigraphy changes from olive brown peaty clay with a trace of sand and abundant organic fragments to olive brown sandy clay. The sand remains a significant component of the sediment to the base of the core (392cm). Despite its probably waterlogged accumulation the presence of significant sand probably indicates very rapid deposition thus reducing pollen concentrations. However, despite the generally low concentrations the percentage unidentified and the percentage damaged are all low with one exception (level 336cm) again suggesting the concentration curve is related to the sediment accumulation rate.

TIC14

Pollen and spore concentrations vary from very low to moderate with all but two being of low concentration. The percentage unidentified is variable and has some small number effects, however, the percentage damaged grains are all high. The core is entirely composed of silty clays and there is no discernable relationship between the stratigraphic units and pollen and spore values.

WFQC1

The pollen and spore concentrations from this channel in Warren Farm Quarry vary from moderate to high. The level-to-level variation is low and the percentage unidentified and damaged are also uniformly low. This is probably related to the protection of the relatively organic rich palaeochannel sediments by a silty clay and accords with the good preservation of plant macrofossils.

WFQC2M1, WFQC2M2 and WFQCH2M3

The pollen and spore concentrations from this channel in Warren Farm Quarry vary from moderate to high/very high. The level-to-level variation is very low and the percentage unidentified and damaged are also generally low but with the exception of WFQC2M1 where uniformly higher levels are revealed. This is probably related to the protection of the relatively organic rich palaeochannel sediments by a silty clay and accords with the good preservation of plant macrofossils.

WFQC3

All four samples from this palaeochannel in Warren Farm Quarry had moderate pollen and spore concentrations, with percentage unidentified being low but the two upper samples having a moderately high (c. 20%) percentage of damaged grains. Both of these levels occur in the upper unit of grey clay with a trace of sand and it is most likely that the cause of this high value is due to sand abrasion.

WFQC5

Pollen and spore concentrations in this intra-gravel palaeochannel fill at Warren Farm Quarry vary from low to moderate with the highest concentration being 165 grains per 100 exotics. However, despite these concentrations few grains were unidentified or damaged. By far the highest percentage damaged occurred in the uppermost level and this is probably due to the high Eh reading (60) and the sediments were all organic-rich silty clays.

Core and monolith comparisons can be made by reference to summary statistics (Tab. 6.3).

Core Number	Mean conc.	St dev of conc.	Mean % unid.	St. deviation of % unid.	Mean % damaged	St deviation of % damaged	Mean pH	Mean Eh
MFC2	213	177	20.1	12.5	69.0	17.0	5.4	2.8
T1C7	143	82	4.3	4.9	19.9	13.6	5.3	-6.4
T1C12	163	142	9.5	11.2	34.4	27.7	7.1	-12.4
T1C10	39	47	20.4	28.0	48.0	28.6	6.5	-4
TFGC14	83	72	3.7	4.1	10.2	11.8	5.2	12.0
T1C14	56	34	16.2	10.6	47.7	11.9	7.1	-46.3
WFQC1	338	92	1.1	0.75	10.2	7.3	4.8	-2
WFQC2	342	91	10.5	4.03	25.9	22.3	4.8	-24
WFQC3	279	167	2.8	1.8	13.2	8.5	5.5	5.5
WFQ5	121	41	3.1	2.3	6.3	3.7	6.3	5.3

Tab 6.3: Summary statistics for pollen and spore assessment.

As can be seen above the mean concentrations vary by over a factor of x8. There is also a tendency for the standard deviation to decrease relative to the concentration, however, caution must be exercised here as the number of observations also varies by a factor of x3 (4-16). Secondly, the sites with the lower number of observations (Warren Farm Quarry sites) did not include pollen assessment of the overburden. However, the tendency of the standard deviation to decrease as the values increase for % unidentifiable and % damaged (i.e. in opposite direction to concentration) suggests that this is a real phenomenon and is due to the greater variation associated with overall less well preserved sequences. As might be expected there are some reasonable internal relationships in the dataset with strong correlations between:

- mean % damaged & mean % unidentified (0.9)
- mean % unidentified & mean % damaged (0.8)
- st. dev. damaged & st. dev. unidentified (0.7)
- st dev. damaged & mean % concentration (0.7)

As expected both the means and variations of damaged and unidentified grains are related and they are both correlated less strongly with the mean concentration. This suggests that two measures would probably be used to capture the taphonomic variance; the concentration and a measure of damaged grains. Relationships with environmental and sedimentary variables are examined in section 6.3. Exploratory data analysis of was performed on the data set (Tab. 6.4).

<i>Depth</i>	<i>Organic</i>	<i>Carbonate</i>	<i>Mag sus</i>	<i>rel conc</i>	<i>% unid</i>	<i>%</i>	<i>pH</i>	<i>Eh</i>
--------------	----------------	------------------	----------------	-----------------	---------------	----------	-----------	-----------

	<i>content</i>					<i>degraded</i>				
Depth	1									
Organic content	-0.10711	1								
Carbonate	-0.08521	0.174054	1							
Mag sus	-0.06655	0.150102	0.081744	1						
rel conc	-0.26269	0.273563	0.176238	0.119556	1					
% unid	-0.10533	-0.22807	-0.33175	-0.07693	-0.31635	1				
% degraded	-0.20516	-0.12907	-0.36292	0.037632	-0.16484	0.752024	1			
pH	-0.11562	-0.19689	0.012868	-0.15603	-0.3517	0.184801	0.244623	1		
Eh	0.179676	0.100916	-0.12139	0.131256	0.038662	0.022806	0.049315	-0.28324	1	

Tab 6.4: Correlation matrix for sediment, pollen and environmental variables.

As can be seen above all the correlations are very low with the exception of internal relationships between the taphonomic variables. This probably because of the range of values contained in the different cores created overwhelming noise. However, there are certainly no clear correlations between depth and the pollen variables, although on a core-by-core basis this can be seen. A probable additional cause of the poor relationships in the total dataset is the difference in environmental conditions in the exposed faces in Warren's Farm Quarry (particularly affecting Eh but also possibly pH). The correlation was therefore repeated using only the core data (Tab. 6.5).

	<i>Depth</i>	<i>Organic content</i>	<i>Carbonate</i>	<i>Mag sus</i>	<i>rel conc</i>	<i>% unid</i>	<i>% degraded</i>	<i>pH</i>	<i>Eh</i>
Depth	1								
Organic content	-0.18569	1							
Carbonate	-0.04071	0.207769	1						
Mag sus	-0.20588	0.17273	0.078291	1					
rel conc	-0.09994	0.300442	0.343797	0.281331	1				
% unid	-0.20971	-0.1984	-0.35312	-0.06036	-0.29016	1			
% degraded	-0.41751	-0.02222	-0.34437	0.114564	0.02087	0.73623	1		
pH	-0.26526	-0.01767	-0.00098	-0.16234	-0.14183	0.078259	0.091004	1	
Eh	0.266523	-0.00994	-0.30763	0.04996	0.019346	0.13883	0.195161	-0.29158	1

Tab 6.5: Correlation matrix for sediment, pollen and environmental variables, core samples only.

As can be seen above the correlations are improved but not substantially. Particularly improved are the correlations with depth as illustrated by Figs. 6.24 and 6.25.

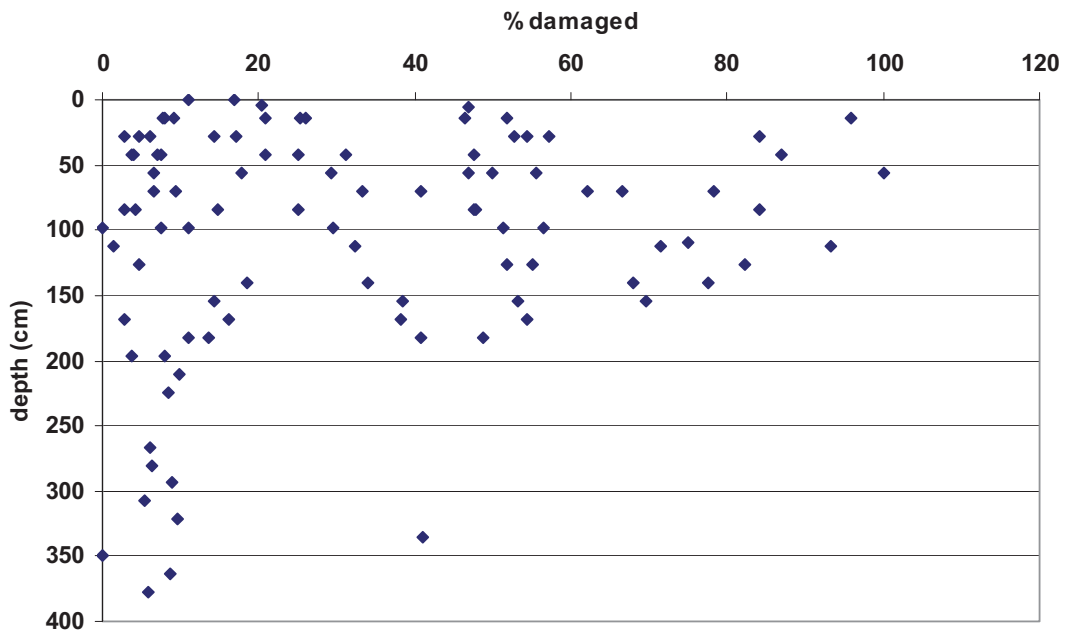


Fig 6.24: Variation of % damaged (grains) with depth all data.

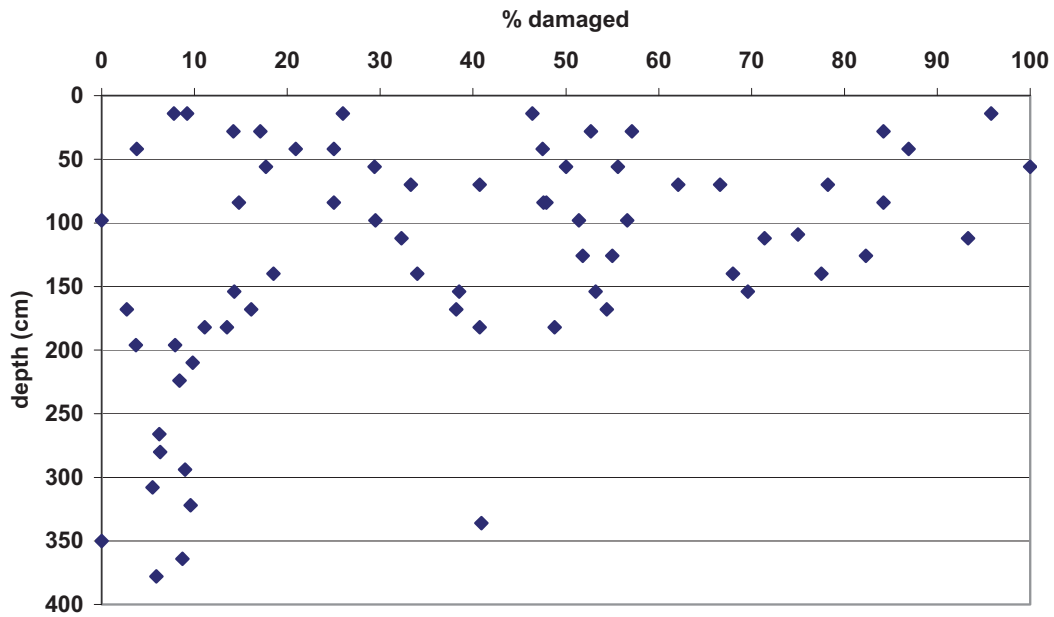


Fig 6.25: Variation of % damaged (grains) with depth cores only.

It was therefore decided to look at the relationships on a core by core basis using the descriptive data. EDA suggested that the only relationship between the environmental variables and the mean pollen data is between mean pH and the mean pollen and spore concentration (Fig. 6.26: Tab. 6.6).

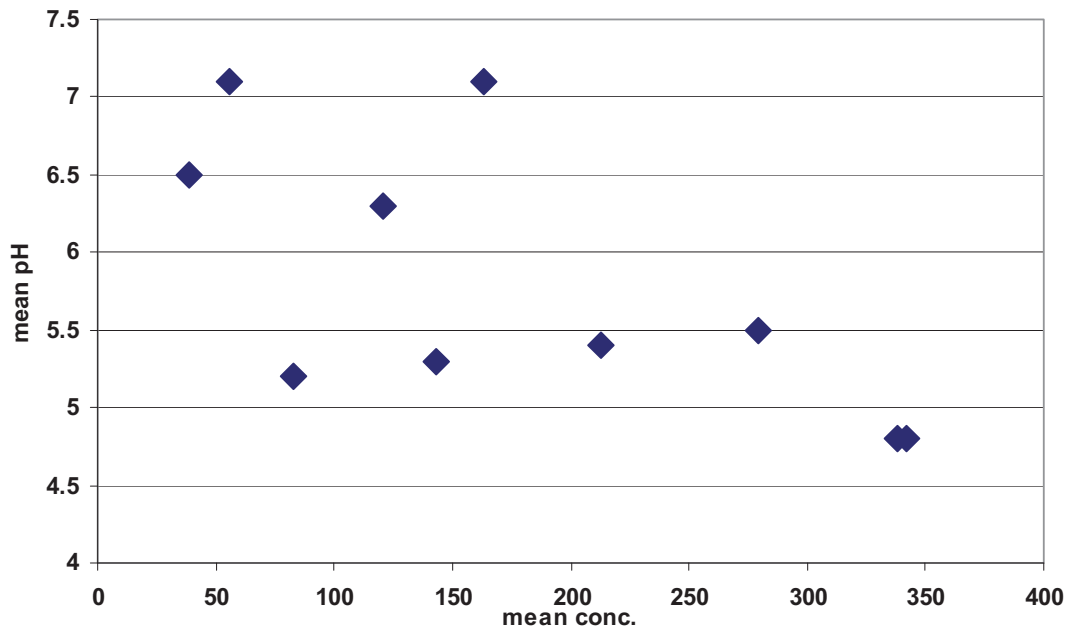


Fig 6.26: Mean concentration of pollen and spores against mean core pH.

	Mean conc.	St dev of conc.	Mean % unid.	St. deviation of % unid.	Mean % damaged	St deviation of % damaged	Mean pH	Mean Eh
Mean conc.	1							
St dev of conc.	0.545485	1						
Mean % unid.	-0.36646	0.006148	1					
St. deviation of % unid.	-0.56347	-0.15076	0.839052	1				
Mean % damaged	-0.25461	0.226981	0.949565	0.720448	1			
St deviation of % damaged	-0.15506	0.13346	0.639511	0.736572	0.56625	1		
Mean pH	-0.67645	-0.25994	0.415751	0.522644	0.362077	0.30371	1	
Mean Eh	0.089786	0.332775	-0.40273	-0.16418	-0.37099	-0.25084	-0.41988	1

Tab 6.6: Mean values for pollen taphonomic variables against mean core pH and Eh.

This relationship is probably an indirect one through the difference between the higher pollen concentration of the more organic-rich exposures and the lower mean concentrations of the clastic-rich cores. However, an unusual element in this area is that the groundwater is known to be sulphur-rich and through oxidation the oxidation of autogenic pyrite weak sulphuric acid can be formed (Ellis and Brown, 1999; Brown et al. in prep.) and this would almost certainly help preserve pollen and spore grains from microbial attack.

6.3 Map of palaeoenvironmental potential over the study area

The cores have been ordered in terms of their average palaeoenvironmental by using the mean concentration, as this factor is crucial in achieving statistically reliable counts. Some of the cores with the higher mean concentrations had high % damaged grains but these were often crumpled and the percentage unidentified is not significantly higher (Tab. 6.7).

Core	Rank	Period covered
MFC2	1	Bronze Age-
T1C12	2	Later Medieval-
T1C7	3	Later Medieval-
TGFC14	4	Neolithic-
T1C14	5	Bronze Age-
T1C10	6	Roman-British-

Tab 6.7: Ranks of the palaeoenvironmental (pollen and spore) potential of the cores.

6.4 Summary

Both the Coleopteran and pollen assessment show that there are strong taphonomic factors affected in the preservation of both beetles and pollen and spores. However, the beetles data also suggests an important role for depositional regime as recently demonstrated by *Davis et. al* (2007). . The pollen data is poorly explained by environmental factors with the possible exception of pH and it is likely that the taphonomic effect is partial through a combination of factors and the depositional regime and immediate post depositional history. More work is underway with this dataset to explore these factors thoroughly.

Chapter 7: Investigating backscattered intensity of Airborne LiDAR

There are four survey locations within the study area (Fig. 7.1). MF on the lowest floodplain closest to the modern channel junction, FF upstream and on the low floodplain adjacent to the River Trent, MTF in one of the large palaeochannel belts at the edge of the floodplain and VF on terrace 1, of which the results from MF, FF and MTF are discussed. Results for area VF are incomplete and are not considered herein (Fig. 7.1). This chapter investigates the relationships of NIR wavelengths to soil moisture and organic content of surface soils. Such data feeds into understanding the NIR reflectance patterns seen in LiDAR intensity data and can be partially used to assess its effectiveness at identifying organic rich water saturated deposits.

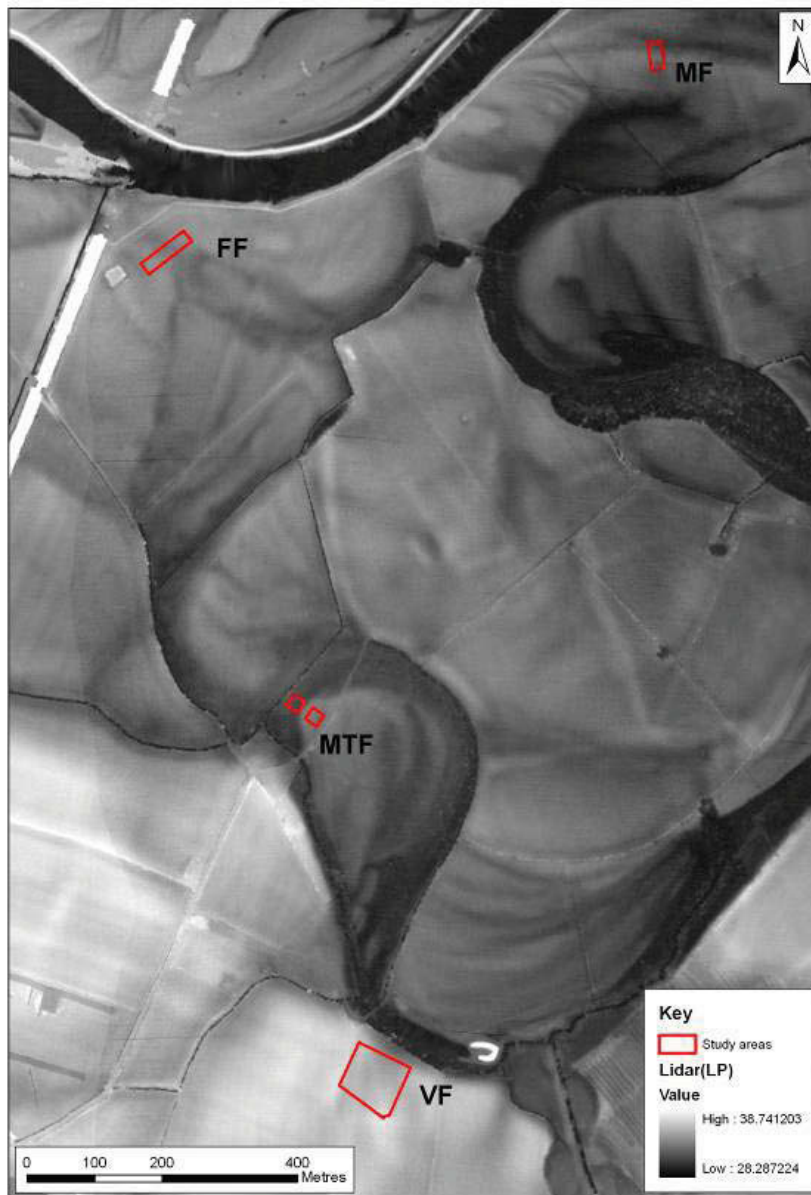


Fig 7.1: Lockington study area. LiDAR LP elevation data with detailed LiDAR intensity study areas highlighted in red.

7.1 Topsoil Moisture and Intensity: Broad Area Survey

Examination of the relationship between volumetric soil moisture and intensity for the entire study area shows a highly dispersed scatter (Fig. 7.2) with only a weak correlation ($R^2 = 0.08$) between soil moisture and LiDAR intensity. Clearly the diversity of sediment type and geomorphological feature across the study area is unlikely to be represented by examination of these data in aggregate.

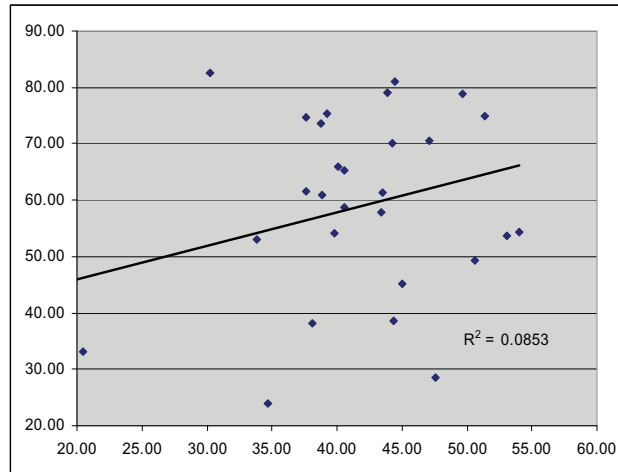


Fig 7.2: Scatter plot of LiDAR intensity (y) and volumetric soil moisture (x) for study area.

Examination of data for just the Hemington Terrace (Fig. 7.3) shows a similar weak correlation ($R^2 = 0.08$) between soil moisture and LiDAR intensity. However, examination of data for just the alluvium indicates a stronger negative correlation ($R^2 = 0.22$) between soil moisture and LiDAR intensity (Fig. 7.4).

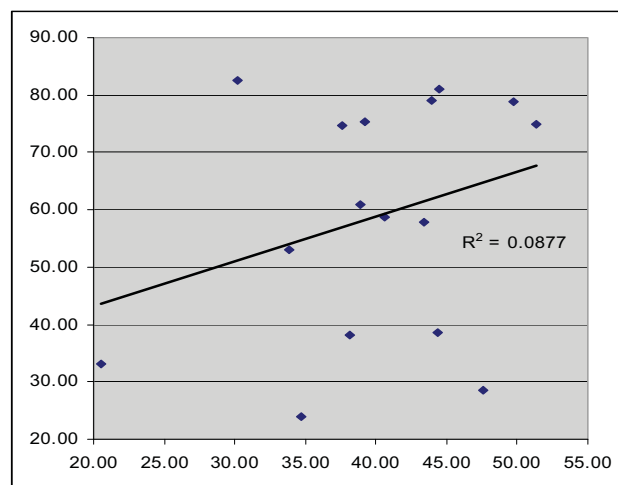


Fig 7.3: Scatter plot of LiDAR intensity (y) and volumetric soil moisture (x) for Hemington Terrace only.

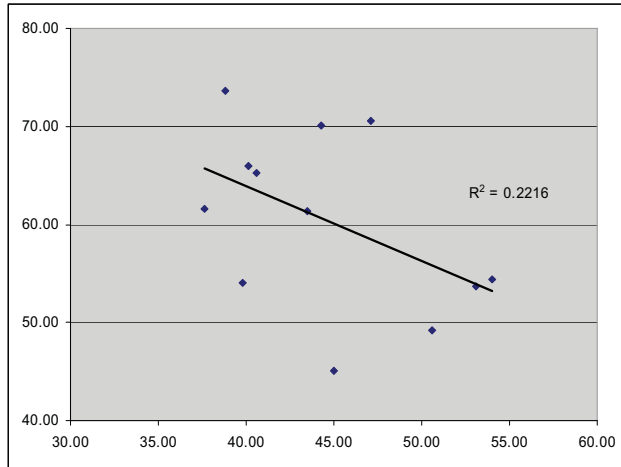


Fig 7.4: Scatter plot of LiDAR intensity (y) and volumetric soil moisture (x) for alluvium only.



Fig 7.5: Lockington, selected sample locations.

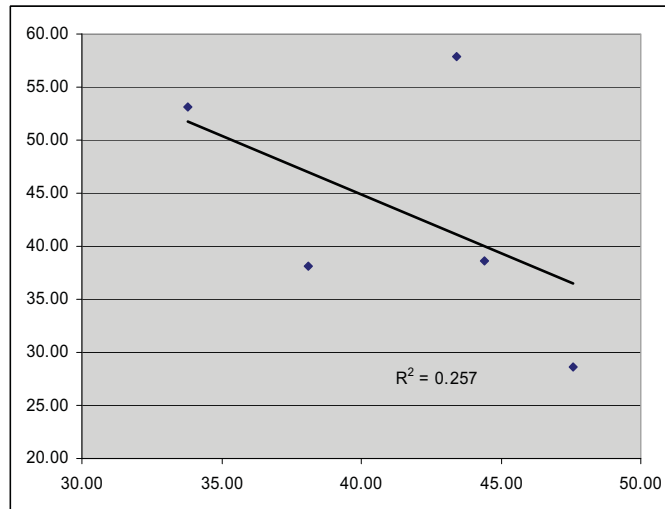


Fig 7.6: Scatter plot of LiDAR intensity (y) and volumetric soil moisture (x) for sample locations shown in figure 7.4.

Finally, selection of sample points relating only to a single discrete location with clear contrast in the LiDAR intensity data, in this case clearly defined ridge and swale and a channel feature (Fig. 7.5) demonstrates a similar negative correlation ($R^2 = -0.25$) between intensity and volumetric soil moisture (Fig. 7.6) although with too few data points to place great significance on this isolated result.

7.1.1 Discussion

Initial examination of these data suggest that factors other than soil moisture play a role in influencing LiDAR intensity and that it is in all probability these unknown factors that most significantly influence variations in LiDAR intensity.

A number of factors may be involved. Ground cover will undoubtedly significantly influence backscattered intensity. Ground cover varies significantly across the Hemington Terrace as the majority of this area is given over to arable agriculture – at the time of the LiDAR flight (February) fields will have been in varying states ranging from bare earth to light spring sown crop and dense brassica. Unfortunately no record of ground cover at the time of the survey flight exists and it is not possible to determine the influence of this factor. The alluvial areas at Hemington are given over to uniform permanent pasture; variations in intensity in the alluvial areas are therefore more likely to represent changes in vegetation due to underlying sediment character rather than differing vegetation *per se*.

Finally, examination of areas of highly contrasting intensity data, that is where it is clear that some characteristic of soil, sediment or ground cover is uniformly affecting intensity, suggest that there is a possibility of a robust relationship between intensity and soil moisture (and probably other factors although these are not considered here). As such it is suggested that in such circumstances at least it should be possible on the basis of careful examination of intensity data to predict areas of wetter sediments.

7.2 Topsoil Moisture, Organic Content and Intensity: Detailed Study

7.2.1 AREA FF

Area FF comprises a part of the Hemmington Terrace (Fig. 7.7) deposits where a minor palaeochannel bisects the terrace. The channel shows as a slight topographical feature, approximately 30m wide and 0.5m deep. The channel is readily apparent in LiDAR elevation and intensity data (Fig. 7.8). The study area is given over to permanent pasture (grassland) and was covered with low closely cropped grass at the time of survey, which took place in November 2006 in dry, clear weather conditions.

Samples for soil organic content and moisture were collected at c 4m intervals over a 40 x 20m area covering the channel and its immediate environment. Samples were processed using the method set out in chapter 3, section 3.10 and sample values used to generate continuous surfaces for visual examination as well as scatter plots.



Fig 7.7: Lockington study area FF, panoramic view showing ground conditions at the time of sample collection.

Topsoil Organic Content varies across the sample area (Figs. 7.9; 7.10; 7.11; 7.15) such that the outline of the channel feature is clearly evident as variations in topsoil organic content. Overall organic content is low (between 4.5 and 8.9%). Unexpectedly the soils within the channel feature have a lower organic content than those to either side. The scatter plots of LiDAR intensity values and topsoil organic content indicates a slight positive correlation between these two (Fig. 7.10; $R^2=0.28$) but the point scatter is dispersed and given the low topsoil organic of the channel fill it is hard to derive any definite relationship between intensity and organic content in this instance.

Volumetric Soil Moisture varies across the sample area (Fig. 7.9; 7.12; 7.13; 7.14) widely (from 24-50%) giving a highly heterogeneous continuous surface plot, although with areas of highest soil moisture contained within the channel feature such that its outline is just discernable in the moisture data. The scatter plot of intensity values and topsoil moisture content (Fig. 7.13) indicates a slight negative correlation between these two ($R^2=0.016$), but with a dispersed point scatter suggesting little confidence can be placed in this relationship.

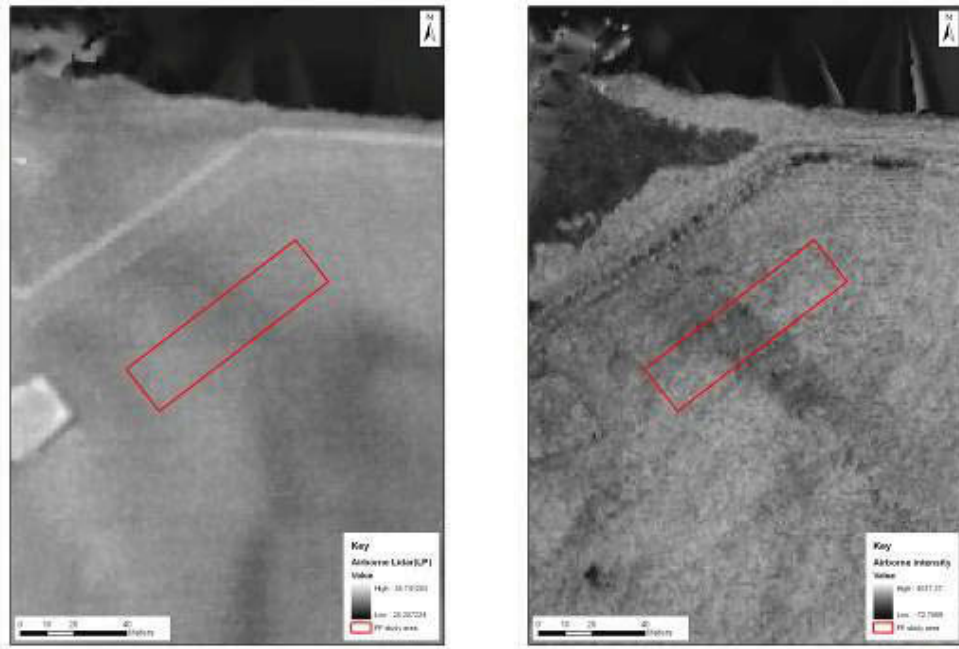


Fig. 7.8: Lockington area FF showing left airborne LiDAR DSM and right airborne LiDAR intensity. The outline of the sample collection area is shown in red.

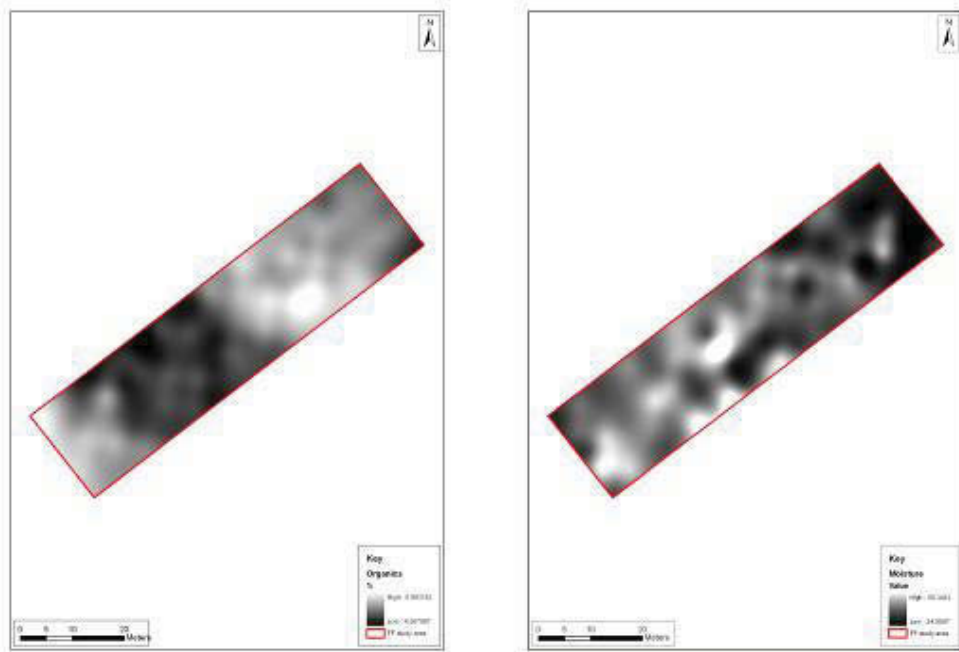


Fig 7.9: Lockington area FF greyscale images showing left topsoil organic content and right volumetric soil moisture of topsoil.

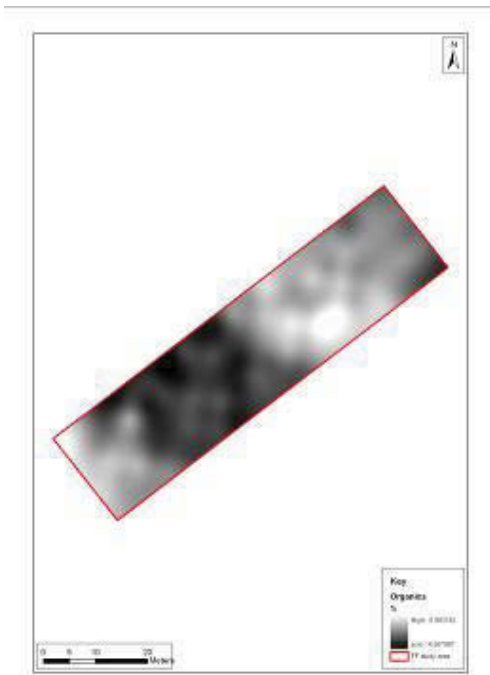


Fig 7.10: Lockington area FF greyscale image showing topsoil organic content.

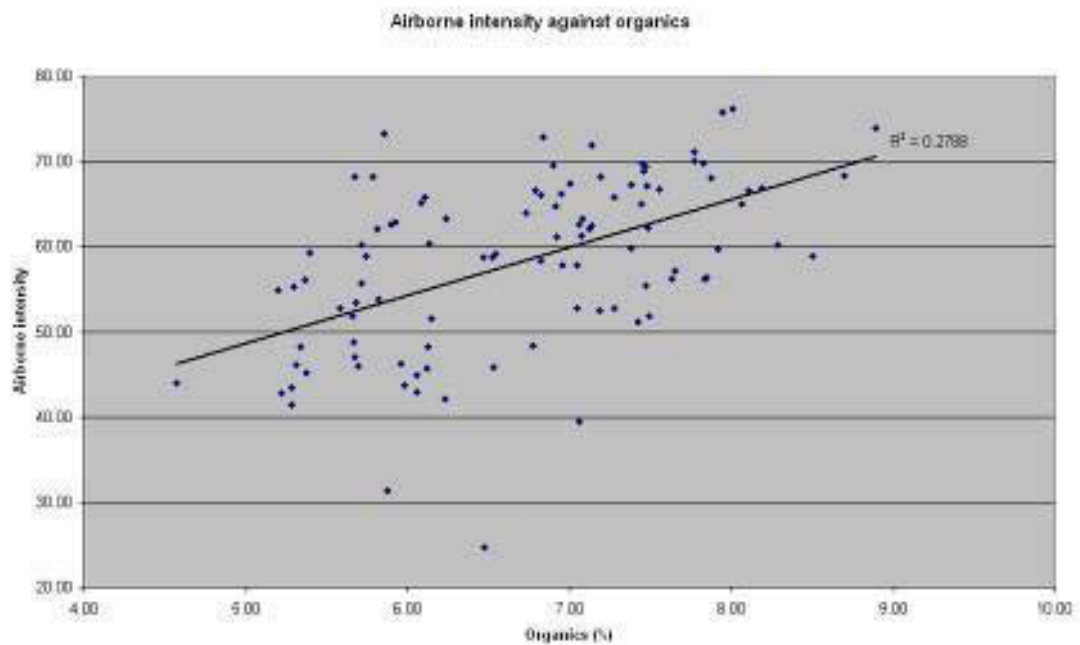


Fig 7.11: Lockington area FF scatter plot showing topsoil organic content (x) and LiDAR intensity (y).

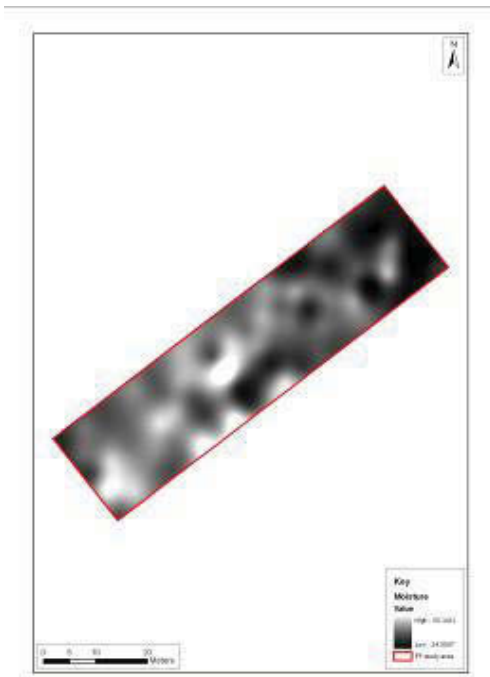


Fig 7.12: Lockington area FF greyscale showing topsoil volumetric soil moisture.

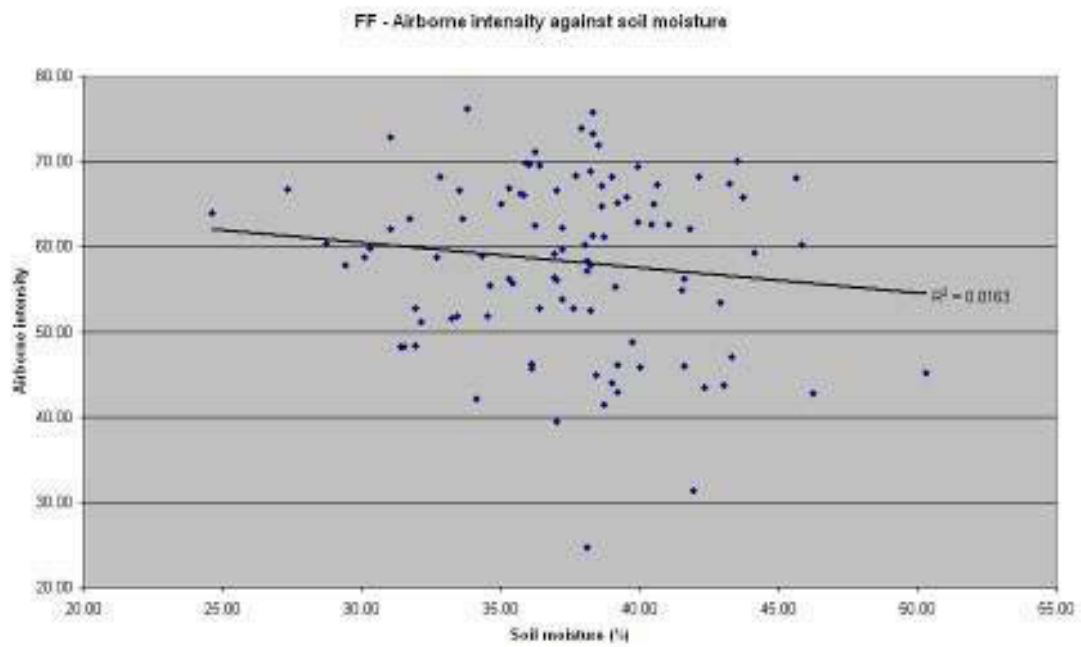
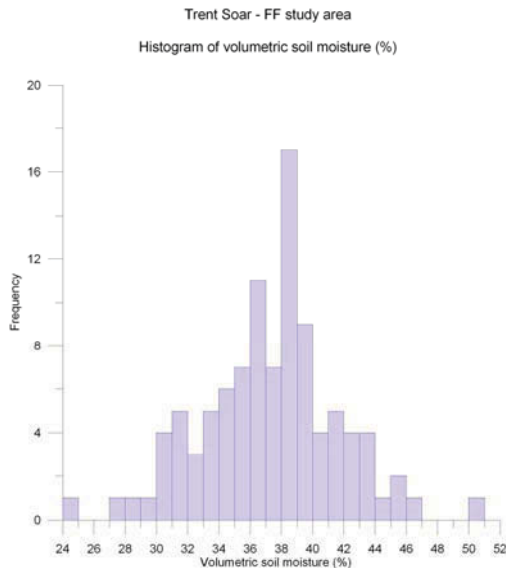
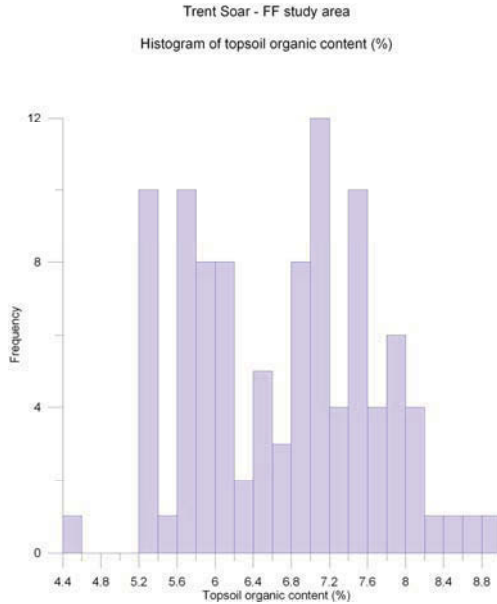


Fig 7.13: Lockington area FF scatter plot showing topsoil volumetric soil moisture (x) and LiDAR intensity (y).



Minimum	24.6
Maximum	50.3
Mean	37.33
Median	37.8
Standard deviation	4.3354889743217
Kurtosis	0.561

Fig 7. 14: L o ckington, FF study ar ea, hist ogram of volumetric soil measurements and summ ary statistics.



Minimum	4.5701
Maximum	8.8897
Mean	6.7051924
Median	6.8277
Standard deviation	0.9452497165429
Kurtosis	-0.859

Fig 7. 15: L o ckington, F F study ar ea, hist ogram of topsoil or ganic content values and s ummary statistics.

Discussion

Overall results from area FF are disappointing. While both topsoil organic content and moisture display a relationship to LiDAR intensity these relationships are weak and suggest insufficient confidence to allow use of LiDAR intensity as a predictor of these variables. The apparent anomalous nature of the organic content of topsoil in and around the channel requires explanation and undermines any confidence that could be placed in results for this area.

7.2.2 AREA MTF

Area MTF comprises a fragment of the Hemington Terrace deposits at the western edge of a major palaeochannel. Auger survey demonstrated up to 1.5m of channel fill of silty clay alluvium overlying sands above the gravel, while terrace deposits proved to be capped by up to 1.5m of silty clay, perhaps deposited by overbank flooding. The channel shows as a significant topographical feature, up to 75 m wide and 0.7 m deep. The channel is readily apparent in LiDAR elevation data (Fig. 7.16) but is significantly less marked in the intensity data, although the sloping side of the channel feature is clearly defined as a low intensity feature, perhaps due to the effect of topography on the intensity of the reflected laser pulse (pulses reflected from a sloping surface are dispersed over a wider ground footprint and so tend to be of lower intensity; Fig. 7.16). The study area is given over to permanent pasture (grassland) and was covered with low closely cropped grass at the time of survey, which took place in November 2006 in dry, clear weather conditions.

Samples for volumetric soil moisture were collected at c 4m intervals over two 20 x 20m area one (MTF1) focused on the channel and the other (MTF2) the terrace. Samples were processed using the method set out in section chapter 3, section 3.10 and sample values used to generate continuous surfaces for visual examination as well as scatter plots.

Volumetric Soil Moisture varies across the sample area (Figs.7.17 – 7.21) widely, giving a highly heterogeneous continuous surface plot, although again areas of high soil moisture are contained within the channel feature (MTF1 – from 34-45%). The scatter plot of intensity values and topsoil moisture content for MTF1 (Fig. 7.18) is highly dispersed and indicates no significant relationship between these two, however visual inspection suggest that the low intensity values of the sloping terrace edge are reflected in lower soil moisture. The scatter plot of intensity values and topsoil moisture for the terrace feature (MTF2; Fig. 7.19) is also highly dispersed, with no discernable relationship between these two. Interestingly overall soil moisture on the terrace shows little difference to the channel (range 31-50% with both areas showing a mean value of c.39%). It is probable that the clay capping of the terrace feature masks any significant contribution to drainage and sediment character caused by underlying coarse-grained terrace material.

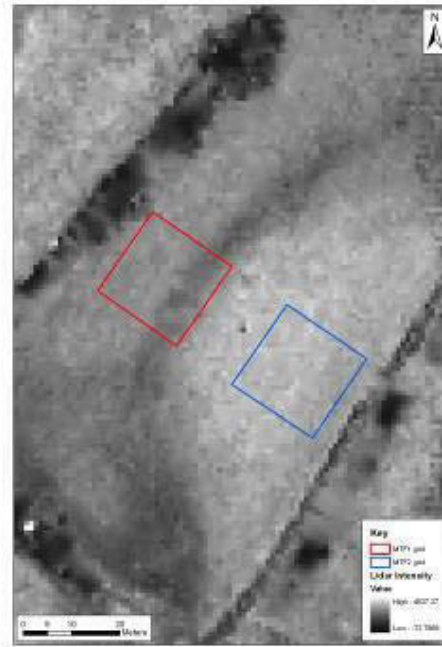
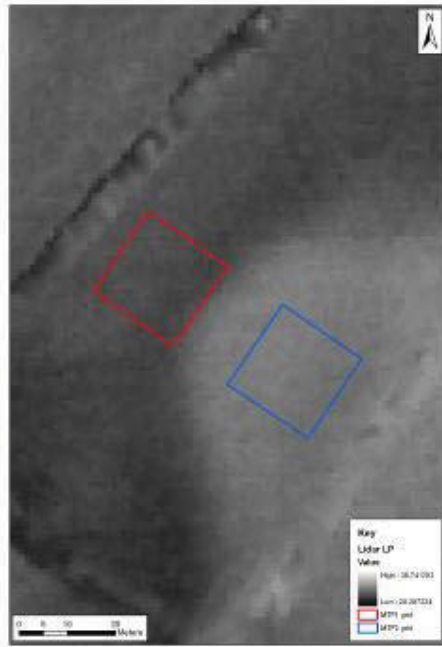


Fig 7.16: Lockington area MTF: Left, LiDAR elevation data and right LiDAR intensity values, red and blue outlines show sample collection areas.

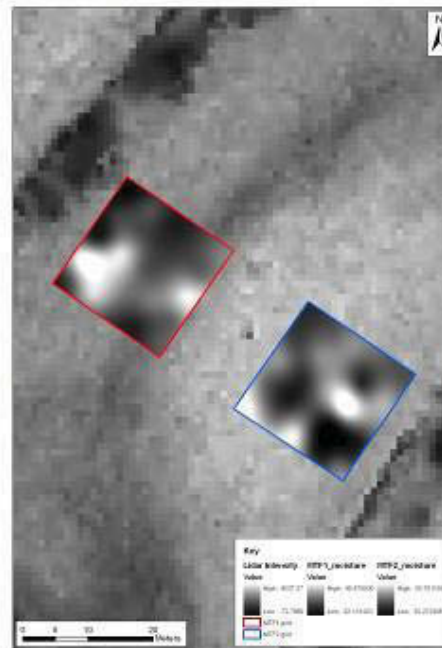
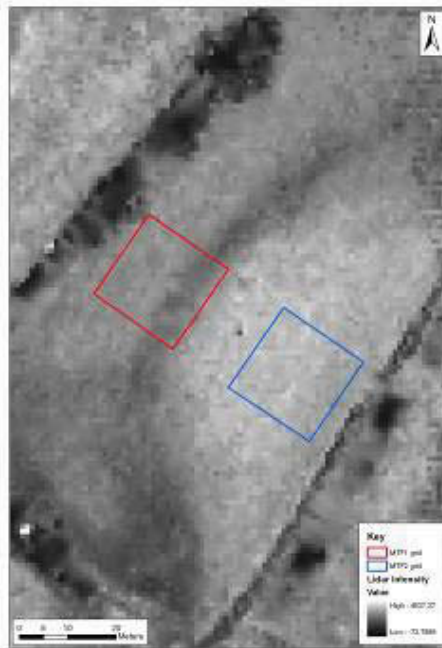


Fig 7.17: Lockington area MTF: Left, LiDAR intensity values and right intensity with greyscale of interpolated volumetric soil moisture for each study area superimposed.

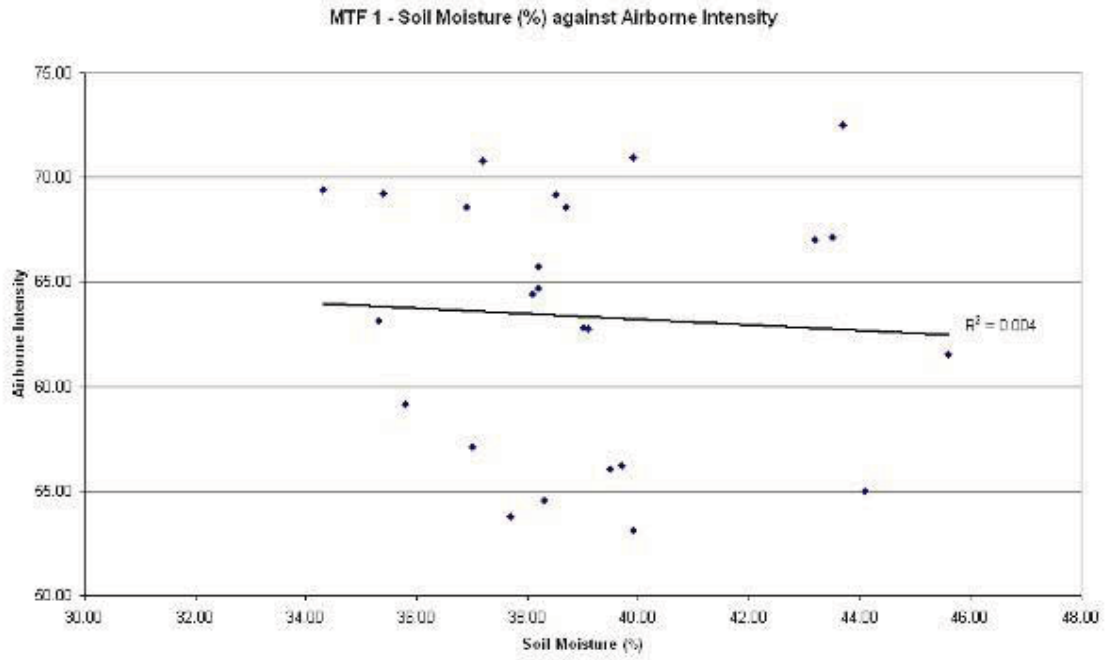


Fig 7.18: Lockington area MTF1: Scatter plot of LiDAR intensity (y) and volumetric soil moisture (x).

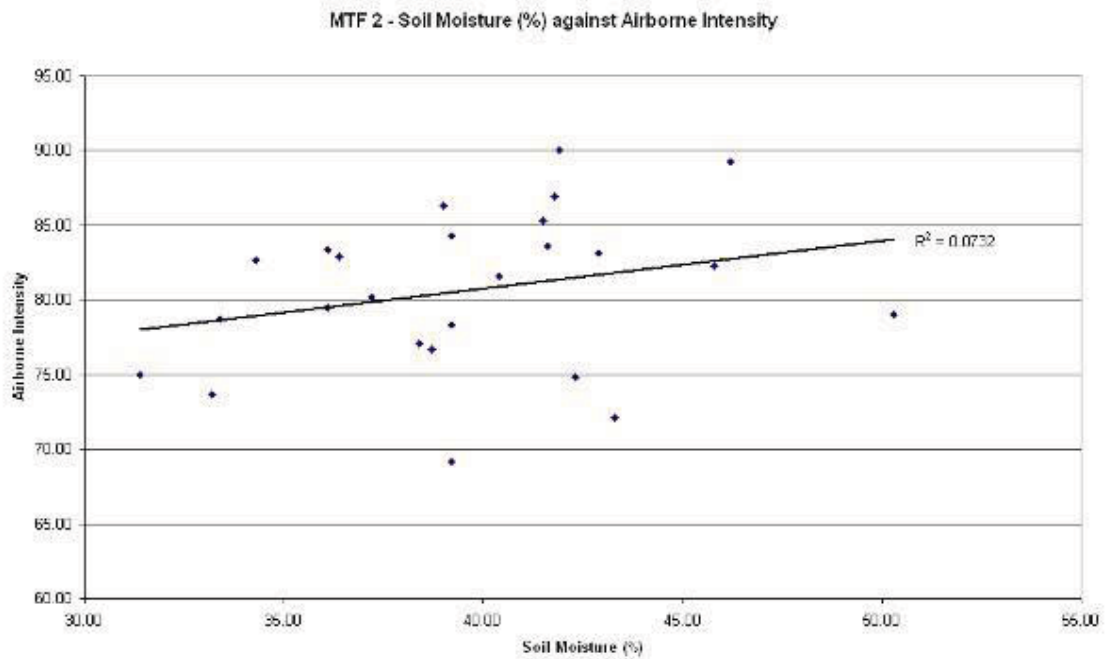
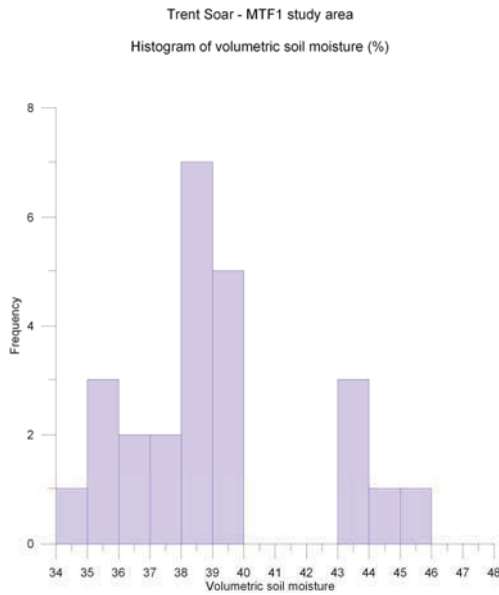
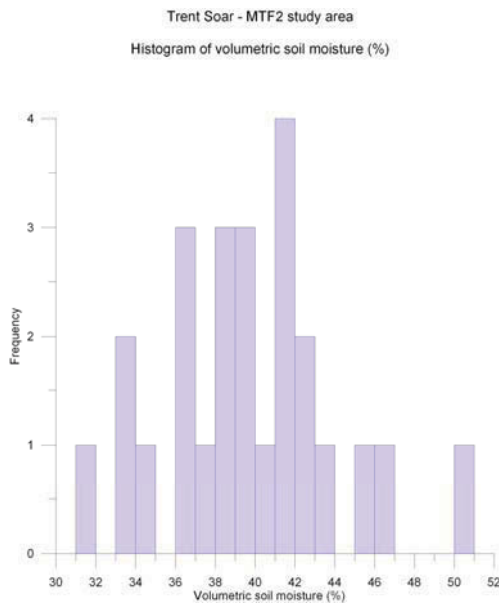


Fig 7.19: Lockington area MTF2: Scatter plot of LiDAR intensity (y) and volumetric soil moisture (x).



Minimum	34.3
Maximum	45.6
Mean	39.072
Median	38.5
Standard deviation	2.9371
Kurtosis	-0.059

Fig 7.20: Lockington MTF 1 study area, histogram of volumetric soil moisture values and summary statistics.



Minimum	31.4
Maximum	50.3
Mean	39.592
Median	39.2
Standard deviation	4.402
Kurtosis	0.27

Fig 7.21: Lockington, MTF2 study area, histogram of volumetric soil moisture values and summary statistics.

Discussion

Overall results from area MTF are again disappointing. Topsoil moisture is highly variable and shows no apparent relationship either to geomorphological feature type. This may in part be due to the fact that soil moisture is uniformly high, with little apparent contrast between average soil moisture for the channel feature and the terrace.

7.2.3 AREA MF

Area MF comprises a part of the modern floodplain of the River Trent where a linear channel like feature lies parallel to a raised linear ridge of sand and gravel, probably a channel bar (Fig. 7.22). The channel shows as a slight topographical feature, approximately 20m wide and 0.5m deep the bar as a broader c.40m wide c.0.4m high feature. Both channel and bar show clearly in LiDAR elevation data, while the channel is slightly apparent in the LiDAR intensity data (Fig. 7.23). The study area is given over to permanent pasture (grass land) and was covered with low closely cropped grass at the time of survey, which took place in July 2006 in exceptionally dry weather conditions. At the time of the survey the linear gravel bar was clearly apparent as a well-defined parchmark in the grass.



Fig 7.22: Lockington panoramic photograph of study area MF at time of sample collection showing channel (left) and bar feature (right).

Samples for soil organic content and moisture were collected at c 4m intervals over a 40 x 20m area covering the channel and adjacent bar. Samples were processed using the method set out in section 3.10 and sample values used to generate continuous surfaces for visual examination as well as scatter plots.

Topsoil Organic Content varies across the sample area from c 5 – c 10.5% (Figs. 7.24; 7.25; 7.26; 7.27) such that the outline of the channel feature and bar are clearly evident as variations in topsoil organic content. Soils within the channel feature have a markedly higher organic content than those associated with the bar feature. The scatter plots of LiDAR intensity values and topsoil organic content indicates a slight negative correlation between these two (Fig 7.26; $R^2 = -0.06$) but the point scatter is

dispersed and it is therefore difficult to deduce a definite relationship between intensity and organic content in this instance.

Volumetric Soil Moisture varies across the sample area (Figs. 7.25; 7.28; 7.29; 7.30) widely from 4 – 21%, giving a heterogeneous continuous surface plot within which it remains possible to identify the bar as an area of very dry soils and the channel feature as contrasting and progressively wetter soil. The scatter plot of intensity values and topsoil moisture content indicates no correlation between these two (Fig. 7.28; $R^2 = -0.005$).

Discussion

Overall results from area MF are mixed. Both topsoil organic content and moisture vary markedly in relation to the geomorphological features investigated and these variations are similarly reflected in the LiDAR elevation and intensity data. While there is a slight correlation between LiDAR intensity and soil organic content there is no correlation between LiDAR intensity soil moisture; this in spite of the apparent visual correlation between these two. It should be noted that while the original LiDAR survey was undertaken in February, when the floodplain will have been wet, with some areas showing signs of standing water, the field investigation took place at the height of summer when soils were extremely dry. This discrepancy will undoubtedly have influenced results and may explain the lack of correlation between LiDAR intensity and soil moisture.

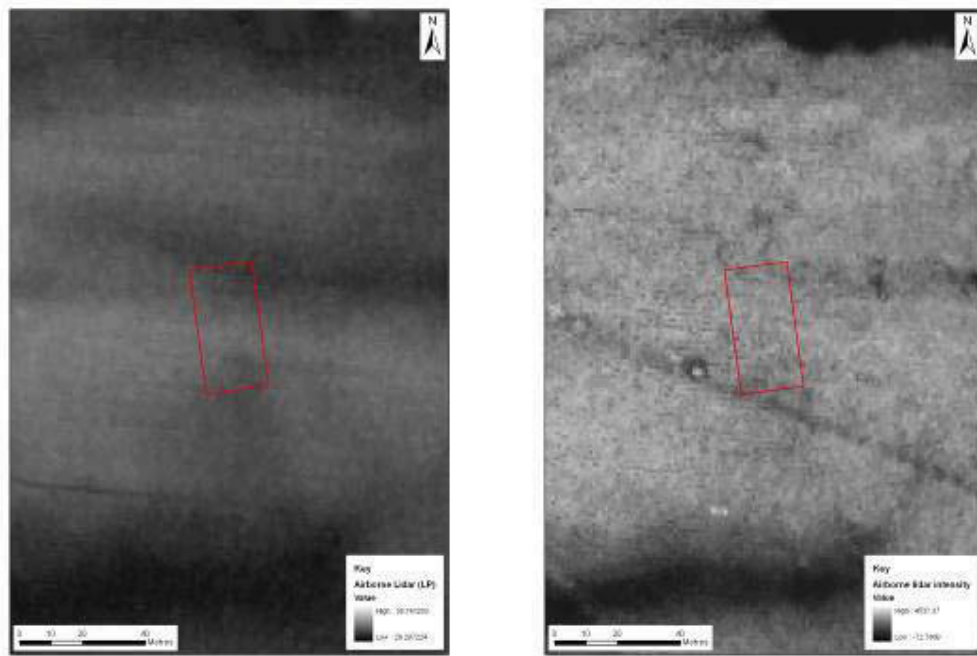


Fig 7.23: Lockington study area MF LiDAR elevation (left) and intensity (right), red outline shows sample collection area.

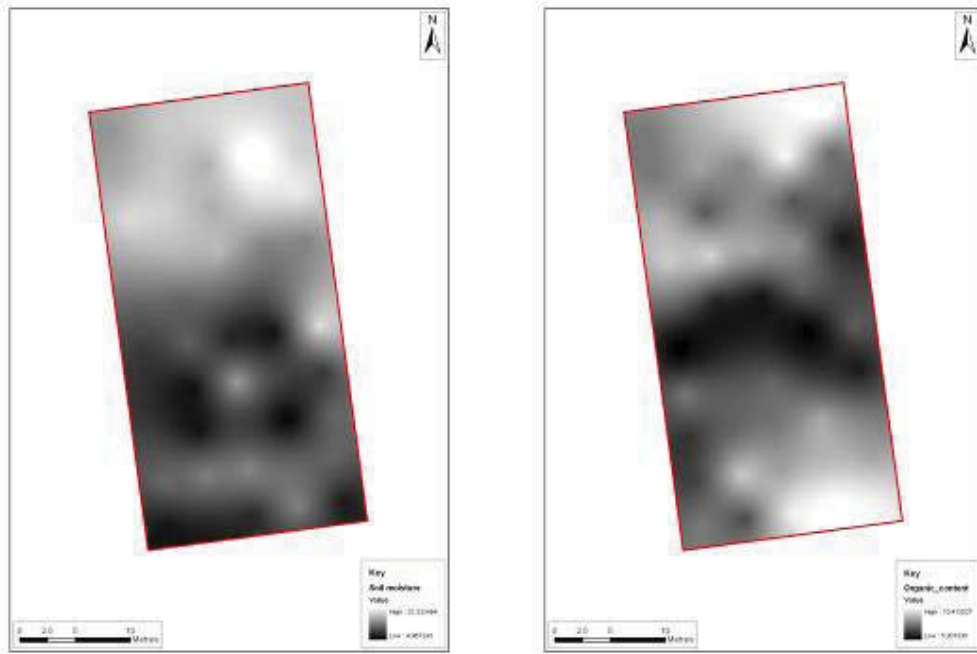


Fig 7.24: Lockington study area MF greyscale images of volumetric soil moisture (left) and topsoil organic content (right).

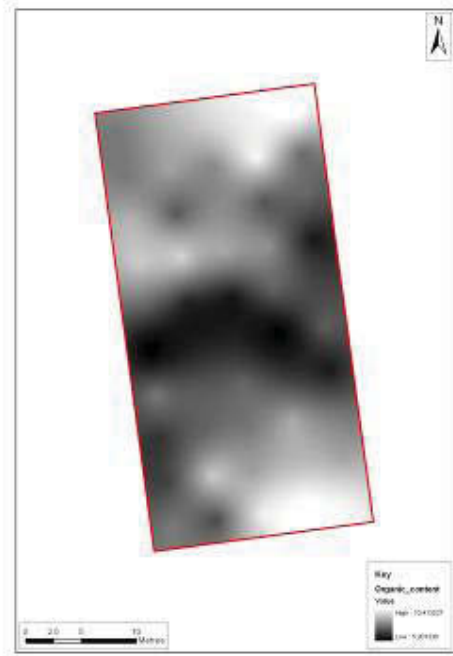


Fig 7.25: Lockington study area MF greyscale image of topsoil organic content.

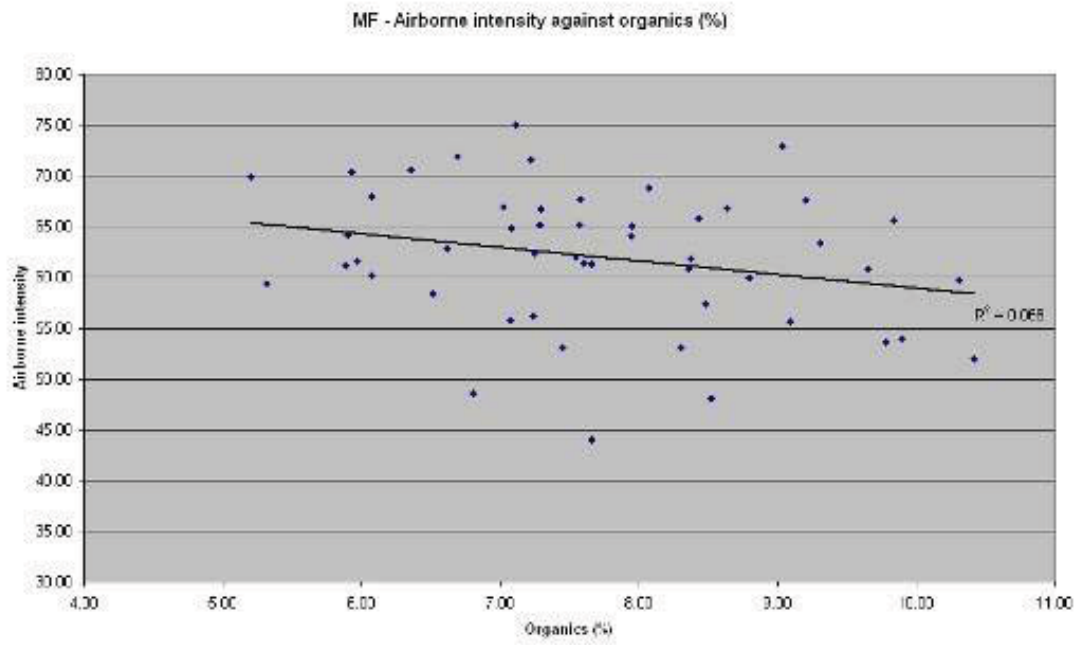


Fig 7.26: Lockington study area MF scatter plot of LiDAR intensity (y) and topsoil organic content (x).

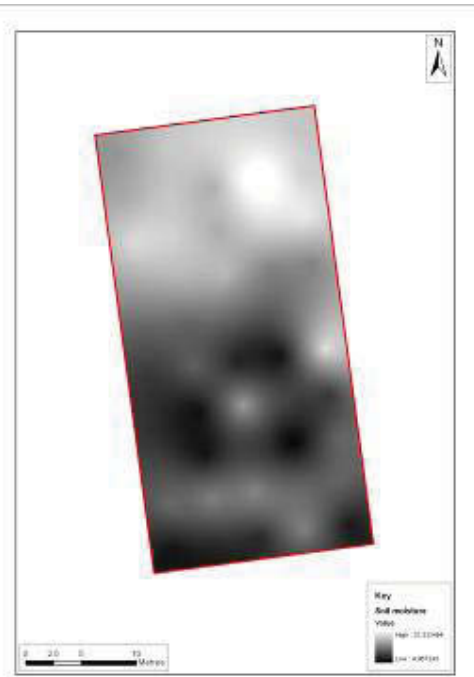


Fig 7.27: Lockington study area MF greyscale image of volumetric soil.

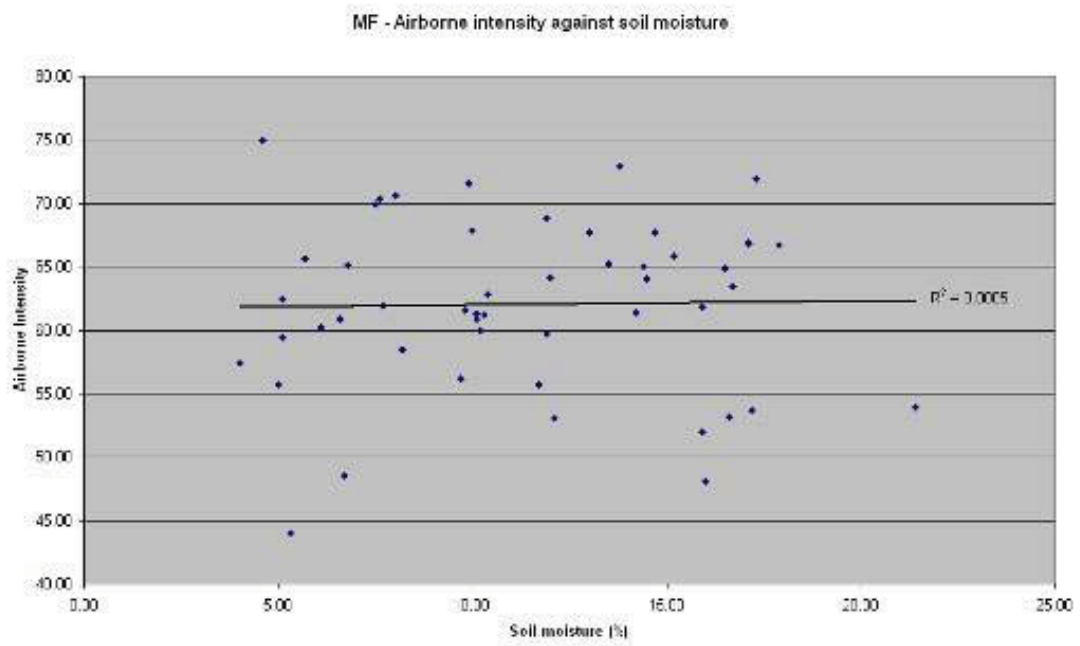
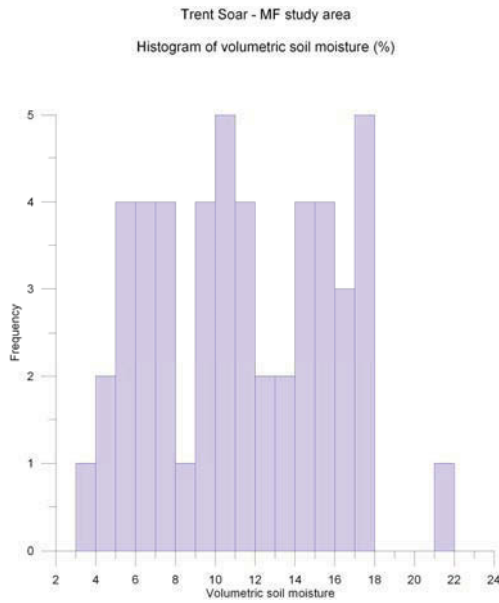
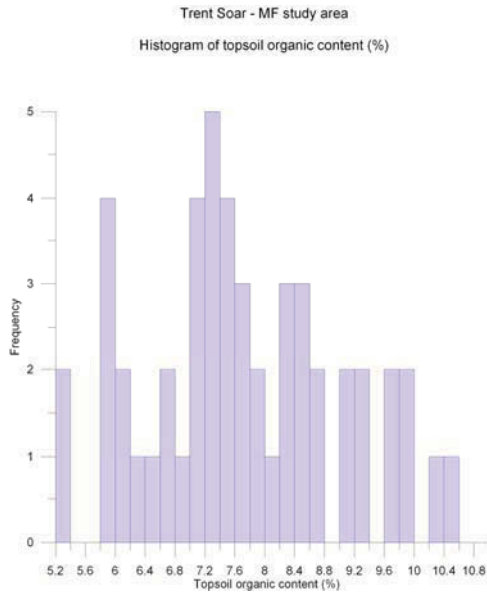


Fig 7.28: Lockington study area MF scatter plot of LiDAR intensity (y) and volumetric soil (x).



Minimum 4
 Maximum 21.4
 Mean 11.38
 Median 11.05
 Standard deviation 4.4069981453435
 Kurtosis -0.996

Fig 7.29: Lockinton, MF study area, histogram of volumetric soil moisture values and summary statistics



Minimum 5.20123004913
 Maximum 10.413526535
 Mean 7.7064081764208
 Median 7.57260394096
 Standard deviation 1.3129466914432
 Kurtosis -0.594

Fig 7.30: Loc kington, M F st udy ar ea, hist ogram of topsoil organic c ontent va lues a nd s ummary statistics

7.3 Conclusions

This study presents a number of problems, an awareness of which must serve to qualify the results achieved to date.

Chief amongst these is the fact that soil moisture and sediment samples for the study areas were not collected simultaneously with the LiDAR flight making the establishment of direct links between sediment character and intensity perilous. To some extent this was overcome by examining the site at several seasons (both summer and late autumn/winter) but ideally contemporary ground based survey is desirable

No ground-covered data exists for the study area for the time of the survey flight. While it is to some extent possible to comment on the influence of ground cover based on known patterns of land use and visual interpretation of the intensity data, precise knowledge of crop cover and extent of exposed soil would be beneficial

With these *caveats* in mind a number of conclusions may be drawn. Overall, analysis of LiDAR intensity data in relation to volumetric soil moisture and sediment organic content suggest that no single factor can be clearly associated with variations in intensity.

While there is an apparent (generally negative) correlation between soil moisture and intensity this is too weak to be regarded as significant. A slightly stronger correlation between organic content of soils and intensity is clouded by uncertainty over the meaning of some results (area FF) and the uncertain link between soil organic content and ground cover – since no areas studied were bare soil.

Analysis of small areas of high contrast intensity data suggest that the variations in intensity are reflected in the two sediment characters examined – but crucially the relationship is not fixed and predictable; other unknown factors are clearly at play including vegetation character (green vegetation reflect highly in the NIR and so differences between leaf colour and between vegetated and unvegetated areas will be strong) and sediment coarseness, likely to affect the degree to which the laser pulse is scattered on striking bare soil.

Further more detailed work is required to examine these diverse factors. While further examination of archive LiDAR data such as that for Lockington may prove profitable it is suggested that the greatest advances are to be made in examination of ground based samples collected simultaneously with LiDAR flight data.

Chapter 8: Electrical resistivity survey

The results for the ER surveys are broken down by geomorphological unit, with separate sections for terrace 2, terrace 1 and the modern floodplain. An assessment of the technique and methodological considerations will be given after the general description of results. The presentations of the results follows simple conventions. A location map shows the transect placed on the LiDAR LPDTM (last pulse digital terrain model) corrected to height above sea level. Gouge core stratigraphy is codified by numbers, whilst ER interpreted stratigraphy is codified by letters. The letters and numbers assigned to each sediment/geomorphological unit are unique in each transect, i.e. gouge core unit 20 is not the same in transects T1A and T1E, etc.

A term that will be used commonly throughout this chapter is biotaphonomic potential. This term is used to indicate areas within palaeochannel belts or along floodplain transects that are likely to have well preserved organic remains. The process of deposition and storage of organic remains is complicated, but can be broken down into two steps. Firstly, there is deposition of organic material within a sediment matrix. This is first affected by depositional factors, such as flow regime, rate of sediment accumulation and localised ecological habitats. ER cannot be used to produce data on these factors.

Secondly, there is the storage (or taphonomy) of organic remains within sediments. The conditions that affect the storage (or taphonomy) of organic remains are a product of sediment architecture. Factors such as Eh, pH and water logging are critical components of storage of the organic remains, and these are partly determined by the sediment architecture. ER can be used to provide data on the nature of the sediments fills of geomorphological units such as palaeochannels. Therefore, the term biotaphonomy is used to indicate areas of a palaeochannel where there is likely to be good preservation of organic materials. It cannot take into account deposition factors such as sedimentation rates. ER can be used to produce meaningful data on sediment architecture and below ground sediment conditions. It can therefore be used to partly elucidate preservation potentials and hence the use of term biotaphonomy.

8.3 Terrace 2 ER surveys

The primary aim of using ER within this study was to understand palaeochannel stratigraphy. From this perspective the application of ER survey on terrace 2 is limited, due to this terrace having no recorded palaeochannels of any significant depth recorded in this study through GPR survey (Phase I), gouge core survey (Phase I) or OSL sampling (Phase II). The general alluvial covering on top of the terrace gravels is known to be thin, c. <60cm over the terrace, as discerned by gouge core/GPR transect T2T1 (Phase I) and GPR grid plan survey T2G1.

8.3.1.1 Transect T2A

ER transect T2A is a good example of the application of ER on this type of geomorphological unit, of a thin alluvial covering on top of terrace gravels with no significant palaeochannels. The location of T2A is given (Fig. 8.1; it should be noted that it is the same field as survey T2G1 GPR survey from phase I) with the transect results (Fig. 8.2). The electrode spacing was 1m, giving a maximum depth penetration of c. 6m. The overall transect length was 80m.

The ER transect clearly shows the terrace gravels as an area of high resistance, which is the central band running across the centre of section (units B and C). The thin alluvial covering on top of the gravels is also evident (unit A). It should be noted that this very thin sediment unit is only just evident at this electrode spacing and a smaller electrode spacing, such as 0.5m, would have a given better data resolution and interpretative potential of this above gravel alluvial unit.

Within the gravel body areas of higher resistance are identifiable (unit C), interpretable as areas of either higher clast size or less matrix (sand) dominated. Conversely, areas of lower resistance are also identifiable (unit B) within the gravels, interpretable as areas that are matrix (sand) dominated or have lower gravel clast sizes. The interface between the gravel body and the Mercian Mudstone (unit D) can be interpreted from the sections, due to the gravel body having a relatively high resistance when compared to the immature Mercian Mudstone, with its relatively high clay and water contents.

The ability to identify units of lower resistance within gravel bodies has importance on terrace 2. As demonstrated by Greenwood *et al* (2003, 18) organic horizons dating from the Upper Palaeolithic have been identified within late Pleistocene gravels on the middle Trent such as at Hemington. At Hemington Trichoptera (the insect Order containing Caddis fly) larval assemblages were used to indicate a cut off channel system with slow flowing/standing water. This is a scarce palaeoecological resource that can allow late Pleistocene/early Holocene climates and habitats to be reconstructed.

Therefore, having the ability to identify areas of lower resistance within the terrace 2 gravels allows units to be located that have a higher potential of organic survival. The lower resistance of these sediment units is due to smaller clast sizes/matrix dominated architectures. These factors both promote water retention/saturation in negative redox conditions. Whilst it is not suggested that the lower resistance areas of gravel in this transect represent areas of high organic survival, it highlights the potential of using multiple ER transects across terrace 2 to find the areas of lowest resistance gravels within the terrace and thus the highest potential for organic survival.

Transect T2A summary:

- The main sediment units of above gravel alluvium and gravels were identifiable from the ER section.
- Identification of areas of lower resistance within the gravels was possible, allowing the possibility of areas of higher palaeoecological importance within the gravel body to be identified.

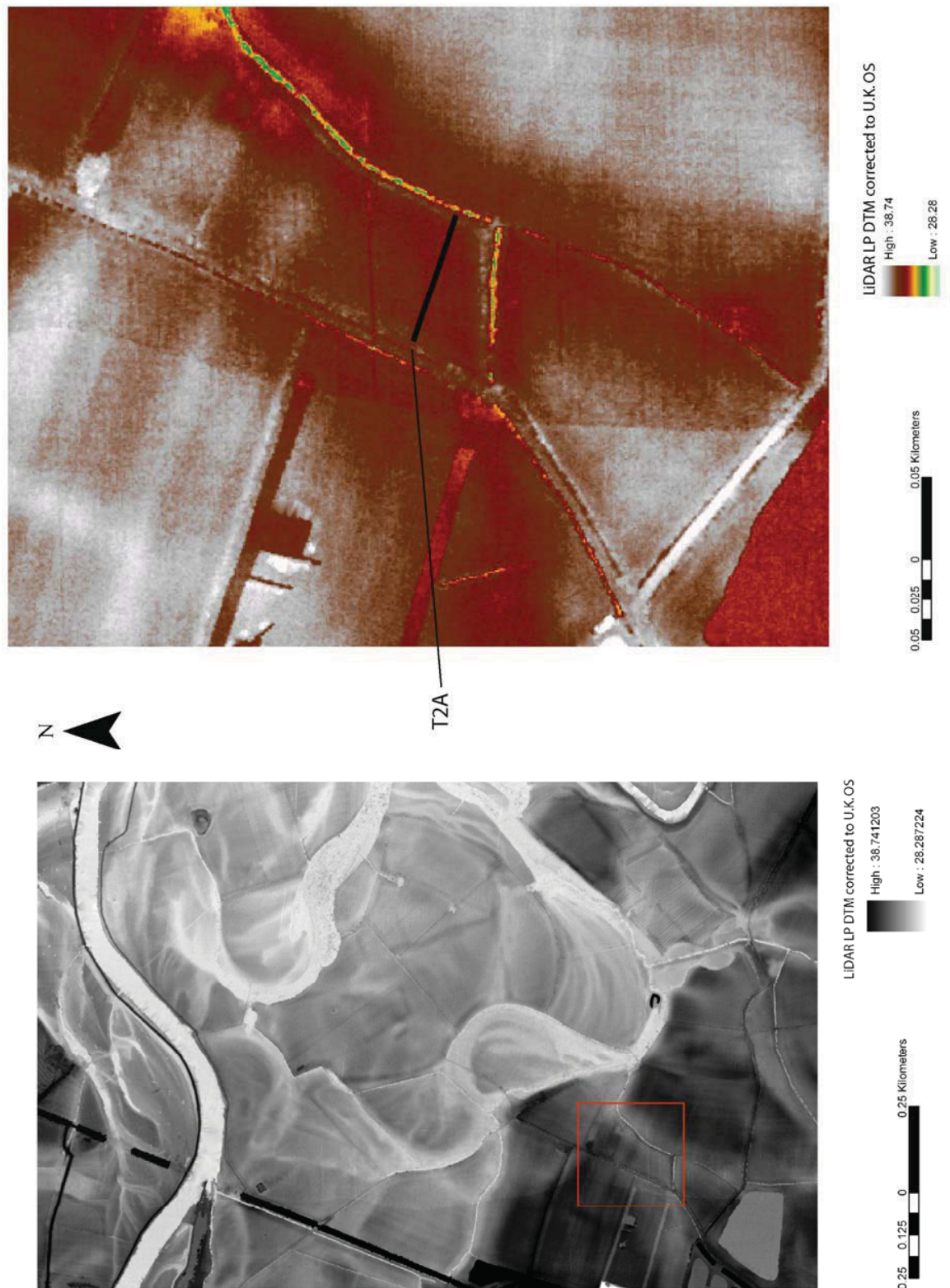


Fig 8.1: The location of T2A on the upper Devensian Holme Pierrepont terrace 2.

Transect T2A

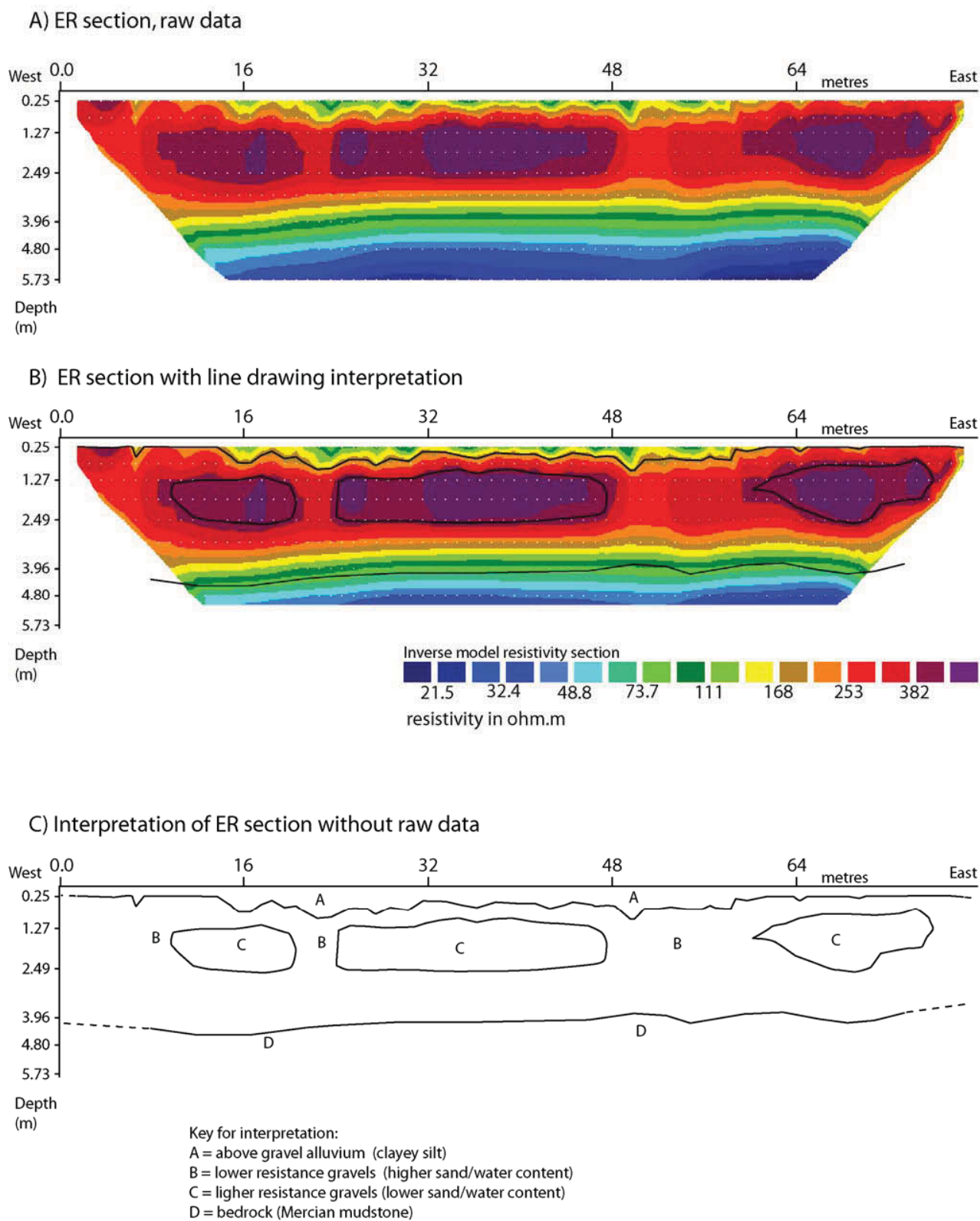


Fig 8.2: Transect T2A ER section. The junction between the gravels and the Mercian mudstone is clearly visible, as is the thin covering of alluvial soil on top of the gravel body.

8.4 Terrace 1 ER surveys

In contrast to terrace 2, it was already known that terrace 1 had a series of relatively deep palaeochannels (<3m), through the results of gouge coring in phase 1. Therefore a variety of targets were chosen for ER survey on terrace 1, in order to explore how effective ER can be for elucidating palaeochannel stratigraphy and palaeoecological and cultural archaeological potential.

8.4.1 *Transect T1A*

The ER transect T1A was located on what was originally interpreted as an area of terrace adjacent to a large palaeochannel, defining the junction between terrace 2 and terrace 1 (Fig. 8.3). However, during OSL sampling a relatively deep alluvial sequence above gravels was found (c. 4m) and therefore provided an ideal opportunity to test ER in alluvial environments. A gouge core transect of this area along the ER section revealed a palaeochannel with a relatively deep and complex stratigraphy (Fig. 8.4). This palaeochannel is somewhat anomalous within the study area, as it is deeper than any of the other palaeochannels encountered (see chapters 4 and 5). The within palaeochannel stratigraphy was complex, formed of several discrete sediment units. The LiDAR LP DTM reveals little in the way of topographic variation to identify the presence of a palaeochannel in this field. The ER section was 91m long, using a 1m electrode spacing, with a complimentary GPR transect and gouge core transect (cores at 10m intervals).

The T1A transect reveals the presence of a palaeochannel within the section, a palaeochannel not definable from ground surface topographic expression (Fig. 8.5). The GPR transect clearly demonstrates the limitation of using GPR in investigating water filled/clay filled palaeochannels (Fig. 8.5). The terrace gravels are definable at the start of the GPR transect, but as soon as the edge of the palaeochannel is encountered the GPR produces no interpretable data. The alluvium/terrace gravel interface and edge of palaeochannel/terrace gravel junction closely correlate between the gouge core and GPR survey. No within channel sediment stratigraphy is revealed through the GPR. Definition of the terrace stratigraphy is possible from the GPR section.

In contrast the ER section shows the two major units of the terrace (high resistance features, units A and B) and the palaeochannel (low resistance features C and D). The interface between the top of alluvium and the gravels is not precise from the ER section, when compared to the gouge core stratigraphy. The boundary between the palaeochannel and the terrace gravels as derived from the ER section agrees with the gouge core survey. The GPR section produces better data on the depth of the alluvium above gravels on the terrace and the general sediment architecture of the terrace.

However, in contrast to GPR, the ER section produces good quality data within the palaeochannel, although the data does not define stratigraphy directly. The comparison of the gouge core data against the ER sections reveals that ER data is relatively poor at defining the within palaeochannel sediment stratigraphy. The palaeochannel sediment units of 18 (blue/grey gleyed clay with Fe and Mn mottling), 19 (blue grey clay), 20 (olive brown dark grey clay) and 21 (olive brown/dark grey medium sand) are not identifiable as discrete entities within the ER section. Of these unit 20 (olive brown dark grey clay) and unit 19 (blue grey clay) are known to have high biotaphonomic potentials (see chapter 6). The boundaries and interfaces between the different sediment units defined through gouge coring within the palaeochannel are not interpretable on the ER section. The silt and sand clay units at the top of the palaeochannel are partly identified by the ER section (unit C). The area of the lowest resistance within the palaeochannel is identifiable (unit D). There is

good agreement between the depth of the palaeochannel , defined by the depth to gravels, between the gouge core stratigraphy and the ER section.

The interpretation of the ER section allows the area of highest biotaphonomic potential within the palaeochannel to be defined, based on the identification of the lowest resistance area within the palaeochannel. This area approximates with the deepest section of unit 20, as defined by the gouge core stratigraphy. This olive brown clay (unit 20) had a very high organic content and was shown to contain a good palaeoecological record. This lowest resistance area of the palaeochannel is a product of a small grain size coupled with high water content. The ER section does not define the stratigraphy of the palaeochannel fill as recorded by gouge core, but it does allow an assessment of biotaphonomic potential across the channel, based on resistivity. Therefore, if this ER section was the only information available before sampling for palaeoecological remains, then the first area to investigate within this palaeochannel would be the area of highest moisture content (unit E).

Transect T1A summary:

- The correlation of the identification of the main geomorphological units between the ER section and GPR section is good, i.e. both techniques identify an area of terrace, a palaeochannel and above gravel alluvium on the terrace.
- The GPR section produces good definition of the gravels and above gravel alluvium.
- The GPR section produces no real definition of the palaeochannel.
- The ER section provides definition of the depth and width of the channel and the boundary between the base of the palaeochannel and gravels.
- The ER section does not define the internal palaeochannel stratigraphy/sediment architecture, as witnessed by the gouge core transect.
- The ER section locates the area of lowest resistance within the palaeochannel fill. This is liable to be the area of highest biotaphonomic potential.

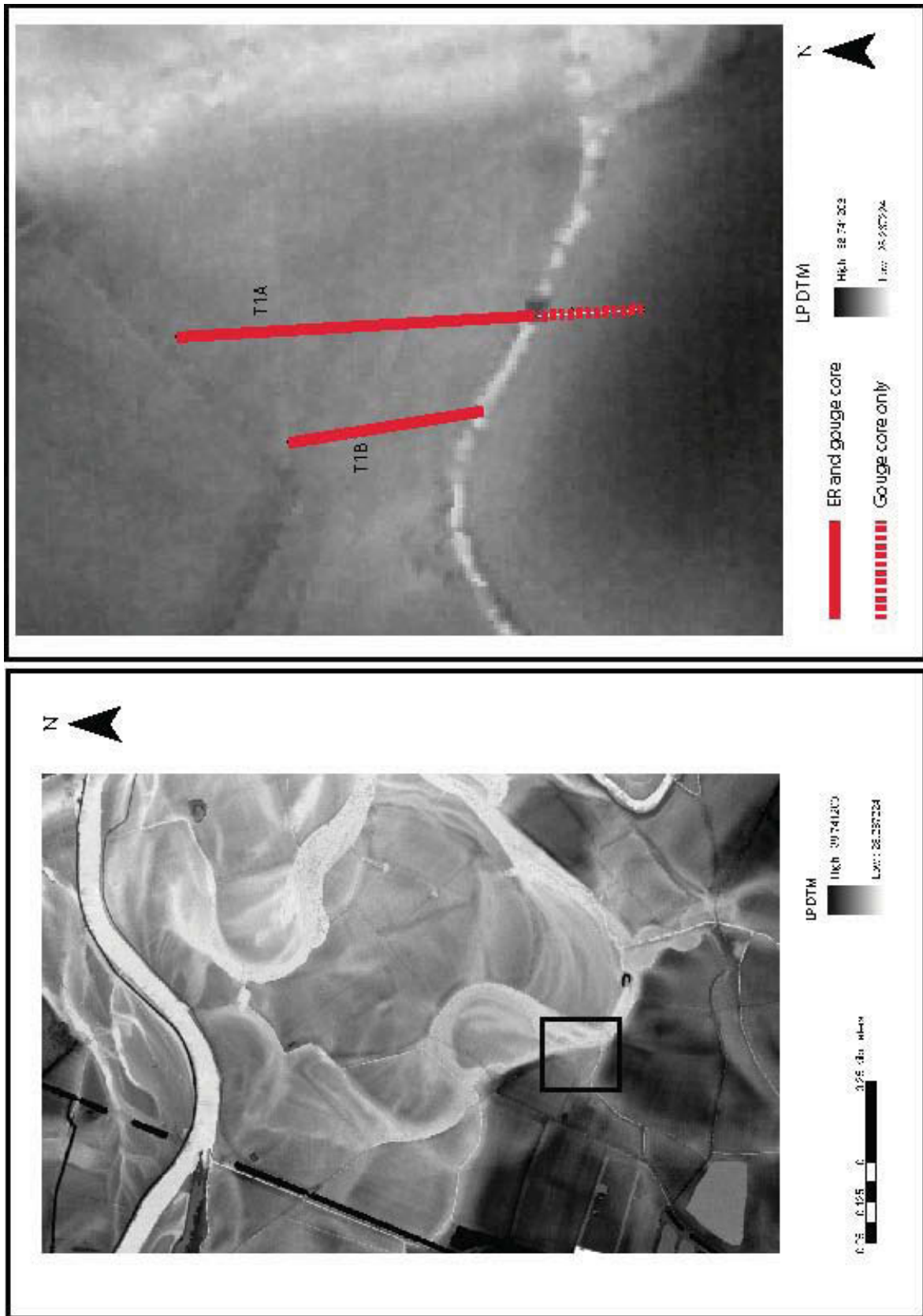


Fig 8.3: The location of transects T1A and T1B, at the junction between terrace 2 and terrace 1.

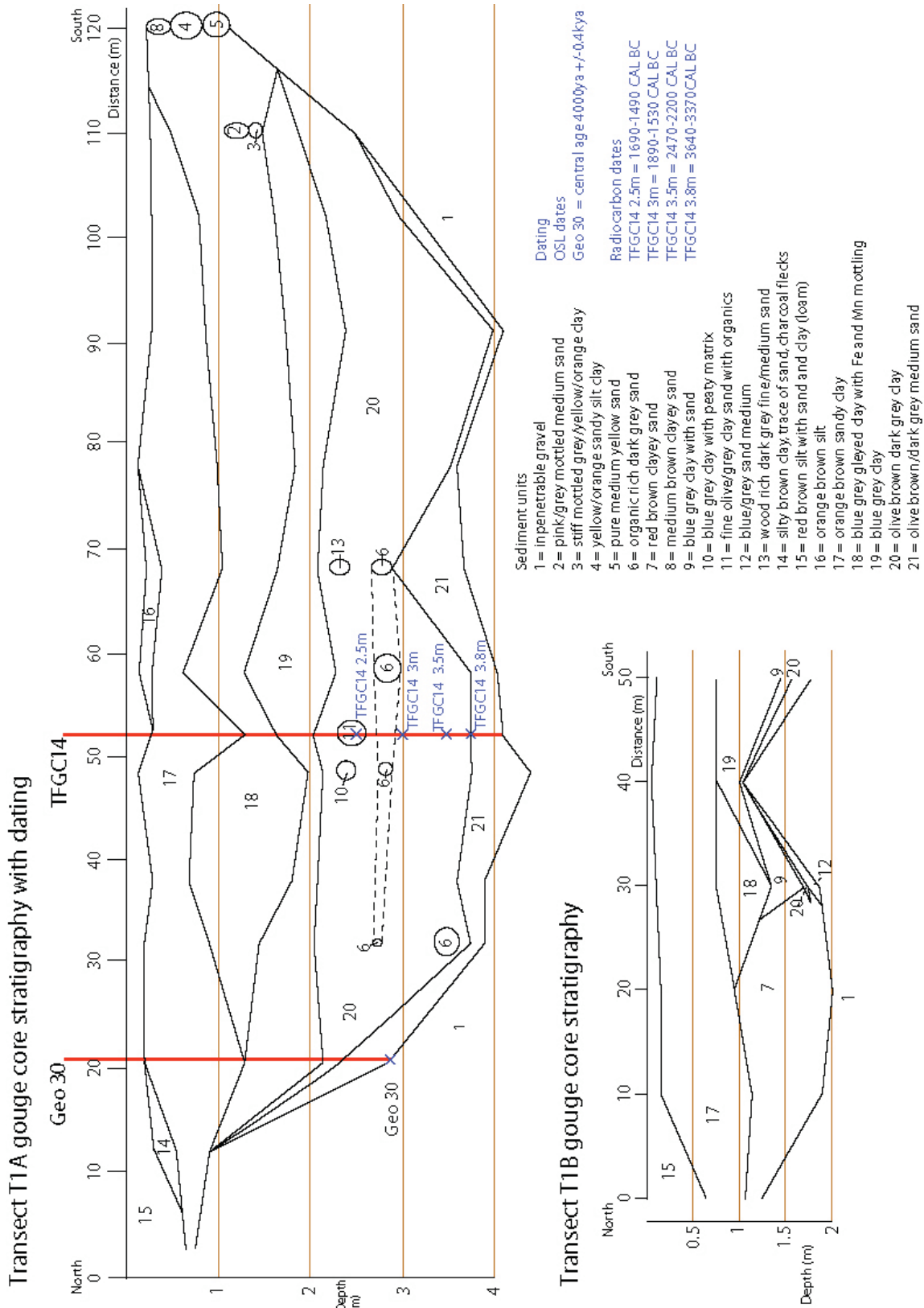
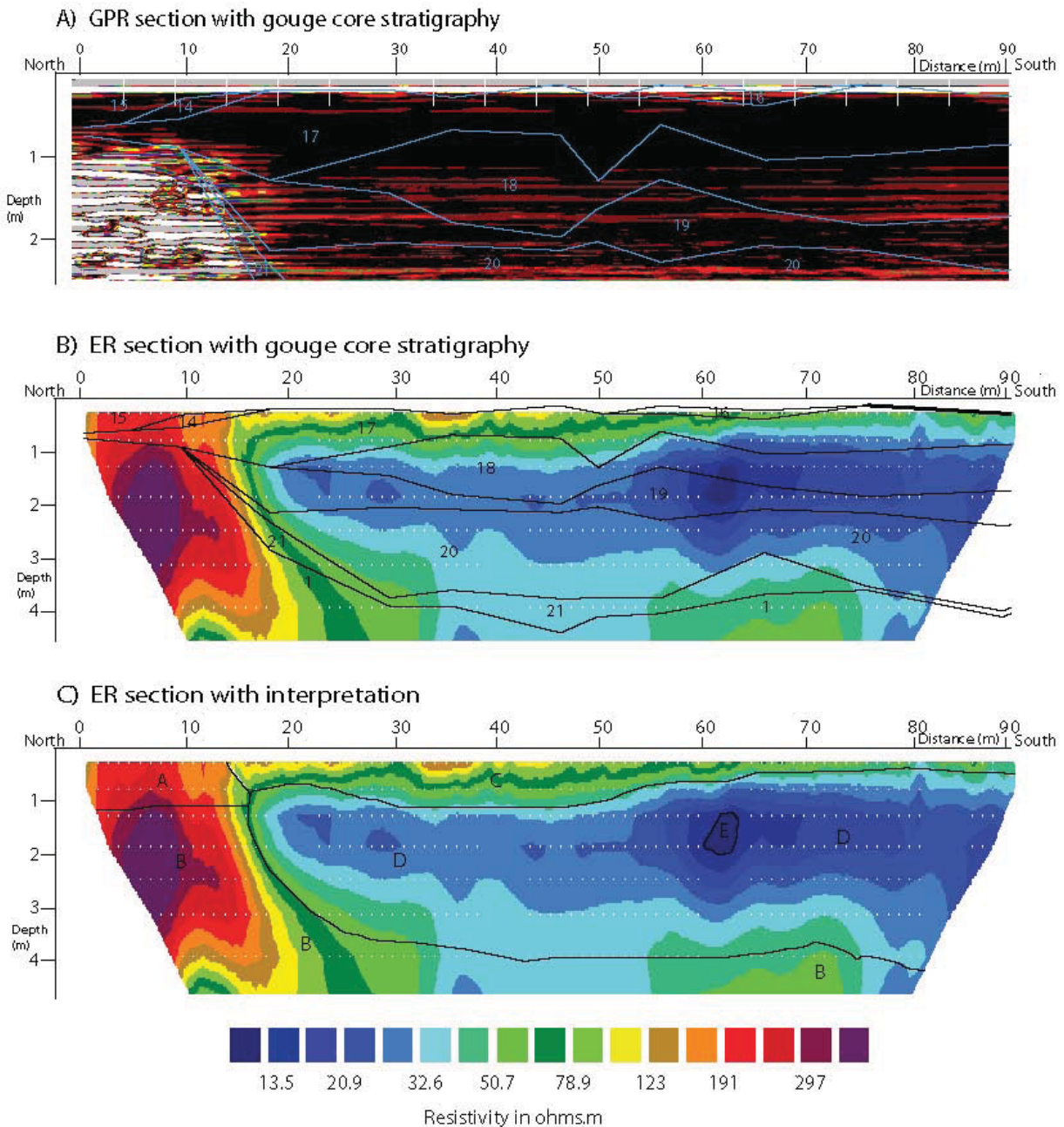


Fig 8.4: The stratigraphy of transects T1A and T1B. This palaeochannel was shown to have the deepest stratigraphy (c. 4m) of any of the palaeochannels sampled within the study area.

Transect T1A



Key for interpretation:

- A = alluvium above gravel (silty clay)
- B = gravels
- C = alluvium above palaeochannel fill
- D = palaeochannel
- E = area of lowest resistance within palaeochannel

Key gouge core stratigraphy:

- 1 = impenetrable gravel
- 2 = pink/grey mottled medium sand
- 3 = stiff mottled grey/yellow/orange clay
- 4 = yellow/orange sandy silt clay
- 5 = pure medium yellow sand
- 6 = organic rich dark grey sand
- 7 = red brown clayey sand
- 8 = medium brown clayey sand
- 9 = blue grey clay with sand
- 10 = blue grey clay with peaty matrix
- 11 = fine olive/grey clay sand with organics

- 12 = blue/grey sand medium
- 13 = wood rich dark grey fine/medium sand
- 14 = silty brown clay, trace of sand, charcoal flecks
- 15 = red brown silt with sand and clay (loam)
- 16 = orange brown silt
- 17 = orange brown sandy clay
- 18 = blue grey gleyed clay with Fe and Mn mottling
- 19 = blue grey clay
- 20 = olive brown dark grey clay
- 21 = olive brown/dark grey medium sand

Fig 8.5: ER transect T1A. A large palaeochannel is clearly evident within the section as a low resistance feature. There is a strong correlation of features between the ER section and the gouge core and GPR sections.

8.4.2 *Transect T1B*

After transect T1A had been conducted, it was clear that this palaeochannel had significance, due to its depth, its potential age and quality of the palaeoecological resource within it. In order to further understand this palaeochannel and its biotaphonomic potential, a second ER transect was undertaken (transect T1B, Fig. 8.3). T1B was 47.5m in length and utilised a 0.5m electrode spacing, in order to provide better data resolution in the depth range of 0-3m. Again a GPR transect and a gouge core transect (10m core spacing) were run alongside the ER transect for inter-technique comparison and also to aid in the interpretation of the ER data. Like with transect T1A there was no surface expression of the palaeochannel.

The ER section revealed (Fig. 8.6) a greater data resolution in the top 3m of the alluvial profile compared to the 1m electrode spacing used on transect T1A, although there is less depth penetration. Again the gouge core transect shows good agreement with the GPR data. The top of the terrace gravels defined by the GPR agrees with the gouge core data at the start of the transect. However, as soon as the transect encounters the palaeochannel fill nearly all data definition is lost in the GPR. The exception to this is the rise in gravels seen within the palaeochannel (within palaeochannel bar, unit F), which is visible within the GPR trace as a faint reflector. This shows excellent agreement with gouge core transect.

The GPR section does not reveal any definition of within palaeochannel stratigraphy. The GPR transect is appearing to define the difference between a red brown clayey sand (sediment unit 7) and an orange brown sandy clay (sediment unit 7) on the edge of the terrace, although both are relatively weakly reflecting units. The alluvium/gravel interface is not definable from the GPR transect and overall the GPR transect is over limited use for definition of subsurface sediment architecture on this particular section.

In contrast, the ER section clearly defines the major geomorphological units of the terrace and the palaeochannel. The terrace/palaeochannel boundary is more clearly defined in the ER section than the GPR, with a close correlation between gouge core palaeochannel stratigraphy and the ER section. The rise in height of gravels within the palaeochannel is clear within the ER section, interpreted as a within palaeochannel bar (unit F). It is interesting how the gouge core spacing distorts the relatively small feature of the within channel bar, making the depth of gravels artificially appear to rise either side of the bar, a product of the 10m gouge core spacing. The ER section gives a much better definition of this feature. The alluvium above the palaeochannel, consisting of an orange brown sandy clay (unit 17) is partially discernable in the ER section.

In this instance the ER section provides the depth of the palaeochannel more clearly than either the GPR or gouge core transects. The stratigraphy of the terrace sediments is unclear based on the ER data in isolation. Likewise, the within palaeochannel stratigraphy detailed in the gouge core sections is not interpretable based on the ER data. The palaeo stratigraphy can be defined as units 18 (blue grey clay with Fe and Mn mottling), 19 (blue grey clay), 9 (blue grey clay with sand), 20 (olive brown dark grey clay) and 12 (blue grey medium sand). None of these units are definable as discrete entities from the ER section. The units are labelled the same as transect T1A and the units with the highest biotaphonomic potential are units 20 and 19.

From the ER section the main geomorphological units of the terrace alluvium (unit A), palaeochannel (units D and E) and gravels (units B and F) are identifiable. The area of the lowest resistance is again clearly identifiable within the palaeochannel (unit E). This area will have the highest water content within the palaeochannel and as a result is likely to have the highest biotaphonomic potential. Again the areas identified as unit E correlate closely with the units of 19

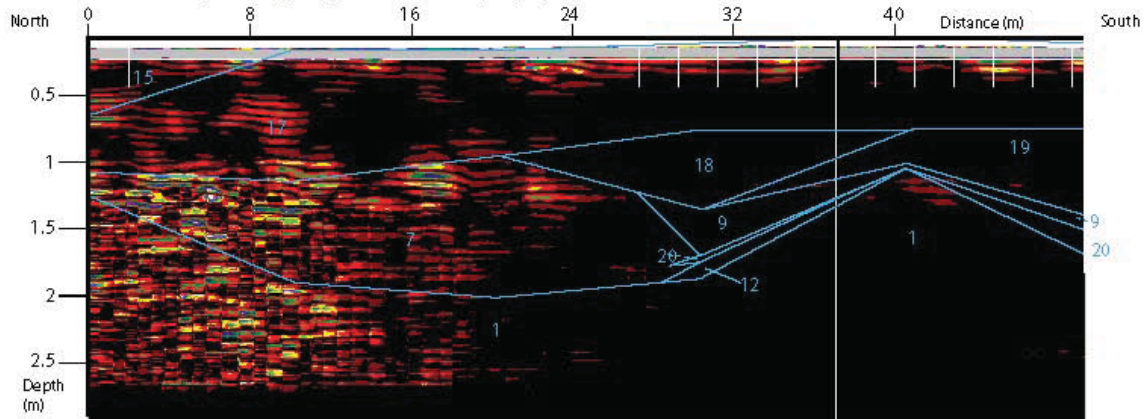
and 20, with the palaeochannel at its maximum depth at these points. From the ER section it is also apparent that the palaeochannel is smaller on transect T1B than it is on transect T1A, both in terms of width and depth.

T1B summary:

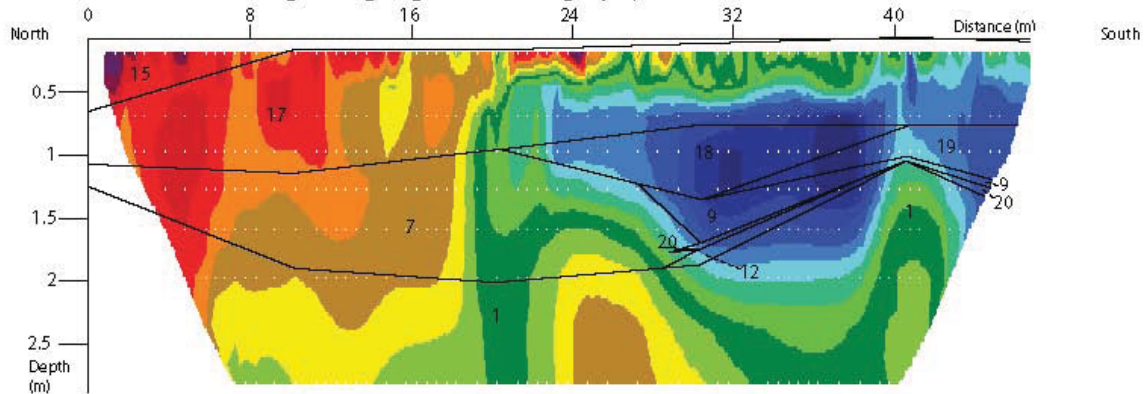
- The GPR section does not produce a clear correlation with the gouge core data and in isolation the GPR data would be difficult to interpret.
- The GPR section produces very poor definition of the within palaeochannel stratigraphy, although a within palaeochannel bar is evident as a weak reflector.
- The ER section provides definition of the depth and width of the channel and the boundary between the base of the palaeochannel and gravels, and the location of a within palaeochannel bar (unit F).
- The ER section does not define the internal palaeochannel stratigraphy/sediment architecture, as witnessed by the gouge core transect.
- The ER section locates the area of lowest resistance within the palaeochannel fill. This is liable to be the area of highest biotaphonomic potential.
- The ER section provides a more accurate representation of the palaeochannel morphology, particularly the depth to the gravels, when compared to either the gouge core or GPR transects.
- The ER section provided information on a palaeochannel that was not evident through topographic expression.

Transect T1B

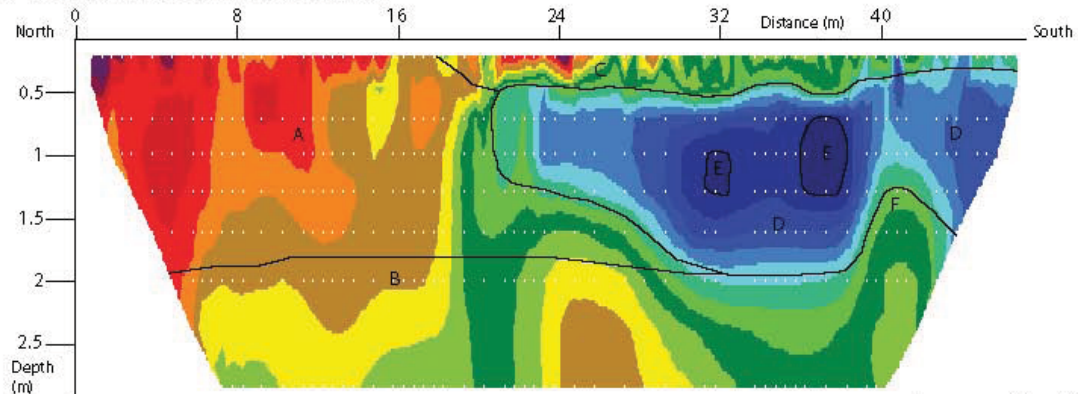
A) GPR shown against gouge core stratigraphy



B) ER transect shown against gouge core stratigraphy

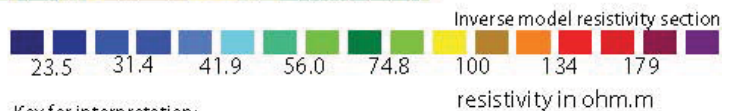


C) ER transect with interpretation



Key gouge core stratigraphy:

- 1 = impenetrable gravel
- 7 = red brown clayey sand
- 9 = blue grey clay with sand
- 12 = blue/grey sand medium
- 15 = red brown silt with clay and sand (loam)
- 17 = orange brown sandy clay
- 18 = blue grey gleyed clay with Fe/Mn mottling
- 19 = blue grey clay
- 20 = olive brown/dark grey clay



Key for interpretation:

- A = alluvium above gravels
- B = gravels
- C = alluvium above palaeochannel
- D = palaeochannel
- E = area of lowest resistance within palaeochannel
- F = within palaeochannel gravel bar

Fig 8.6: ER transect T1B. The palaeochannel in the section is an obvious feature.

8.4.3 *Transect T1C and T1D: comparison of electrode spacing*

A single transect was conducted on an area of terrace 1, that utilised two electrode spacings (1m and 0.5m). Both ER sections were compared to GPR and gouge core transects. This experimentation allows comparison between the types of data obtained by the two different electrode spacings. Each of the transects will be described, then a comparison of the electrode spacings will follow.

8.4.3.1 Transect T1C

Transect T1C was undertaken at the junction between a palaeochannel and an area of terrace 1. Both the terrace and palaeochannel are evident through topographic expression, as shown through the LiDAR LP DTM (Fig. 8.7). The ER transect ran for 47m, using a 1m electrode spacing. GPR and gouge core sections (10m core spacing) were run along the same transect. The terrace gravels are evident on the GPR section (Fig. 8.8). The depth to the impenetrable gravels correlates closely between the GPR and gouge core sections. The above terrace alluvial stratigraphy and the within palaeochannel stratigraphy cannot be seen from the GPR section.

The ER section has a good correlation with the stratigraphy revealed by the gouge core transect. The ER section identifies unit A above terrace gravels, which correlates with unit 2, a red brown silty clay. Below this is a higher resistance unit B, which approximates to unit 4 (red brown clayey sand), unit 7 (brown grey clay with sand) and unit 8 (blue grey sandy clay). These units all have higher sand content and are shown to have higher resistivity values.

The palaeochannel is dominated by units 6 (brown grey clay with Fe and Mn mottling), 8 (blue grey sandy clay), 9 (brown grey clayey sand) and 10 (red brown sand, small Fe nodules). The junction between the palaeochannel (unit 6 brown grey clay with Fe and Mn mottling) and the terrace alluvial deposit (unit 2 red brown silty clay) lies somewhere between 20m and 30m on the transect. However, due to the spacing of the gouge cores this is not clearly defined and an estimated break is placed at 25m on the gouge core stratigraphy.

In comparison the ER section defines the palaeochannel (units C, D and E) clearly, with the junction between the palaeochannel and the terrace silty clay (unit A) and sandy clays/clayey sands (unit B) clearly defined. Again the area of lowest resistance within the palaeochannel is located (unit D), correlating with the greatest depths of 6 and 8, both clay units. Thus unit D is suggested to have the highest potential for biotaphonomic potential preservation within the palaeochannel. The ER section also appears to define the basal sands within the palaeochannel (unit E).

As a 1m electrode spacing was used on this transect the entire depth of Holocene alluvial gravels is evident (units G and F). There is a clear boundary between the sand (units B and E) and the gravels (units F and G). Unit G has a higher resistivity and is located under the terrace deposit. Unit F is a lower resistance gravel and partially correlates with the area below the palaeochannel (units E, C and D). This lower resistivity value in unit F is probably a function of increased water retention, itself probably caused by the palaeochannel above it. The junction between the Mercian Mudstone (unit H) and the gravels (units G and F) can also be interpreted.

Transect T1C summary:

- The GPR provided no definition of the palaeochannel stratigraphy.
- The ER section allowed an interpretation of the palaeochannel, terrace alluvium, gravels, and gravel/bedrock junction.

- There was a good correlation between the general stratigraphy recorded by gouge core transect and the ER transect.

8.4.3.2 Transect T1D

The ER transect T1D was collected in the same location as T1C (Fig. 8.7), with the same orientation. T1D was 48m long and this time used a 0.5m electrode spacing. GPR and gouge core sections (10m core spacing) were run along the same transect. In order to avoid repetition the GPR transects and the gouge cores transects are the same as T1C (section 8.4.3.2). The GPR reveals no internal palaeochannel stratigraphy and only reveals the depth of basal gravels on the terrace section. This interpretation is confirmed by the gouge core transect (Fig. 8.9).

The ER section only penetrates to c. 3m and the depth to the gravel/bedrock junction is not evident, as seen in the 1m electrode spacing (transect T1C). The palaeochannel is well defined by this electrode spacing (unit C), which again relates to the sediment units 6 (brown grey clay with Fe nodules), 7 (blue grey sandy clay with Fe nodules), 8 (blue grey sandy clay), 9 (brown grey clayey sand) and 10 (red brown sand with Fe nodules). The palaeochannel has a fill consisting of clay dominated sediments in its upper fill and the clayey sands in the lower fill. Due to the sediment architecture of these fills containing clay, the palaeochannel is evident as a feature with low resistivity values.

The terrace deposits are evident as higher resistance features, with the terrace deposit mainly defined by unit 2 (red brown silty clay with a trace of sand), which approximates with unit A in the interpretation. The higher resistance units at the junction between the terrace alluvium and gravels are units 3 (gleyed grey clay with Fe and Mn mottling), 4 (red brown clayey sand), 5 (coarse red/brown/pink sand) and 7 (blue grey sandy clay with Fe nodules). These sediment units approximate with unit B on the interpretation, an area of intermediate resistance between the gravels and the terrace alluvium.

Overall the interpretation of the ER section is straightforward. The main units of the palaeochannel (unit C), gravels (unit F and D) and terrace alluvium (units A and B) are identifiable. The palaeochannel morphology is well defined. The areas of lowest resistivity within the palaeochannel are highlighted (unit G), and as discussed above, these are likely to be the areas of highest biotaphonomic potential within this section of palaeochannel. The variation of the resistivity values within the gravels is depicted more clearly using the 0.5m electrode spacing, with the lower resistivity unit D more tightly defined. As was seen through the identification and subsequent dating of oak trees in Warren Farm Quarry (section 5.4), the gravels may contain a significant geoarchaeological resource dating from the Neolithic onwards. Therefore, the identification of lower resistivity areas within the gravels can help to identify areas with higher geoarchaeological potentials.

The palaeochannel morphology is not visible through the GPR or gouge core transects. It is the ER section that provides information on the palaeochannel. However, the ER section does not provide a section where the individual sediment units are identifiable, as in the gouge core transect. Broader changes in resistivity values are evident that reflect geomorphological units.

Transect T1D summary:

- The GPR provided no definition of the palaeochannel.
- The ER section defined the morphology of the palaeochannel well and identified the areas of lowest resistivity within the palaeochannel.

- The floodplain units of the terrace alluvium, gravels and palaeochannel were interpretable from the ER section.
- There was a relationship between the sediments identified through the gouge core transect and ER section, although the ER section did not identify the individual sediment units.
- Variation in resistivity values were seen in the gravels, with areas of higher and lower resistance visible.

8.4.3.3 A comparison between ER transects T1C and T1D

The two transects T1C and T1D allowed a comparison between the two electrode spacings and the types of information that can be gained using each. By comparing Figs. 8.8 and 8.9, a series of differences are obvious between the two transects. These can be summarised as:

- Using a 1m electrode spacing allows a much greater depth penetration (c. 6m).
- This greater depth penetration allows loss of data resolution in the upper part of the profile.
- The 1m electrode spacing allows the gravel/bedrock interface and the extent of the gravels to be seen.
- The 0.5m electrode spacing gives greater data resolution in the upper c. 3m of the profile.
- The 0.5m electrode spacing produces better definition of the palaeochannel morphology, the terrace alluvium and the variation in upper gravel body.
- Both electrode spacings identify the main geomorphological units in the section.

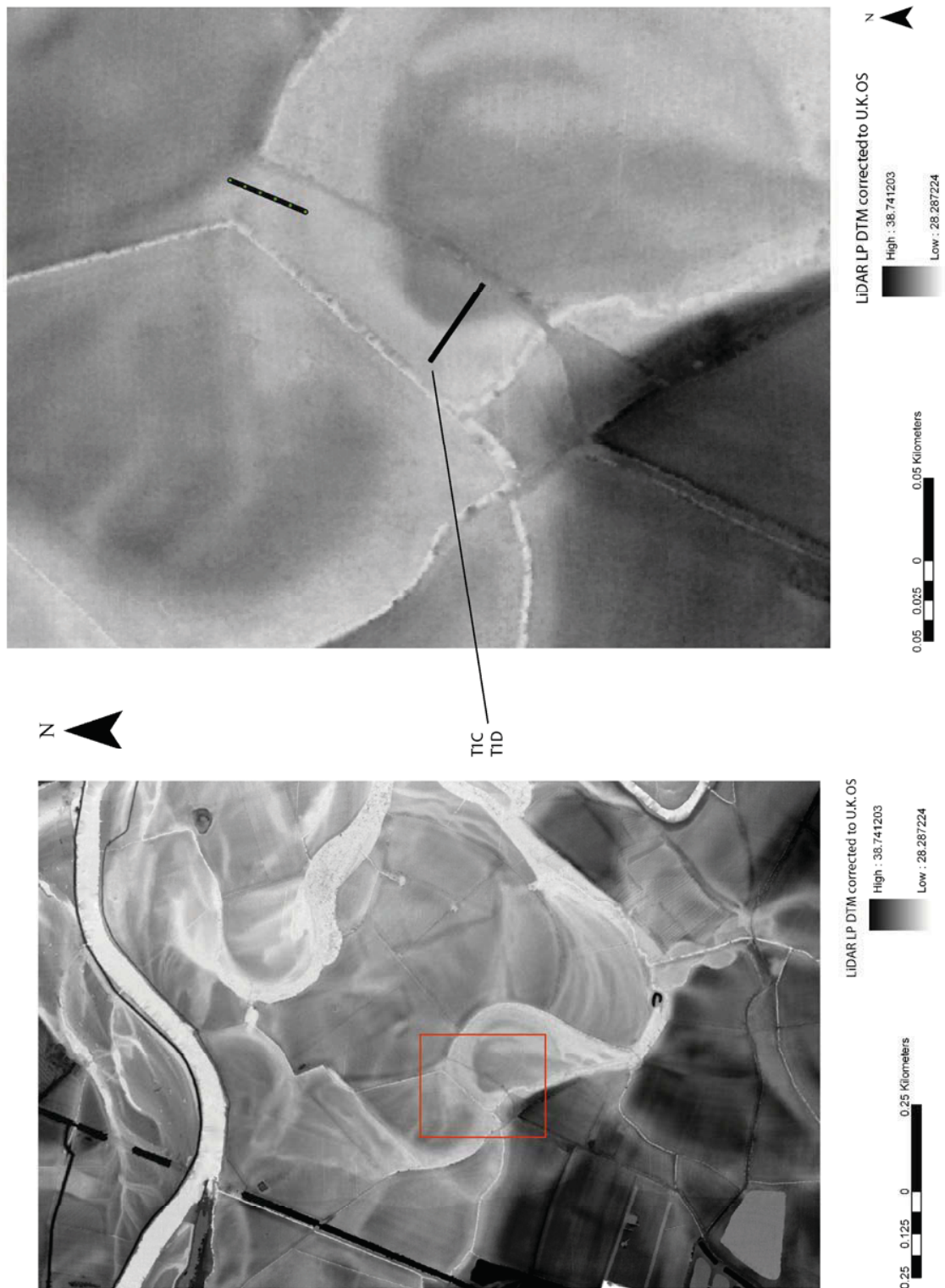
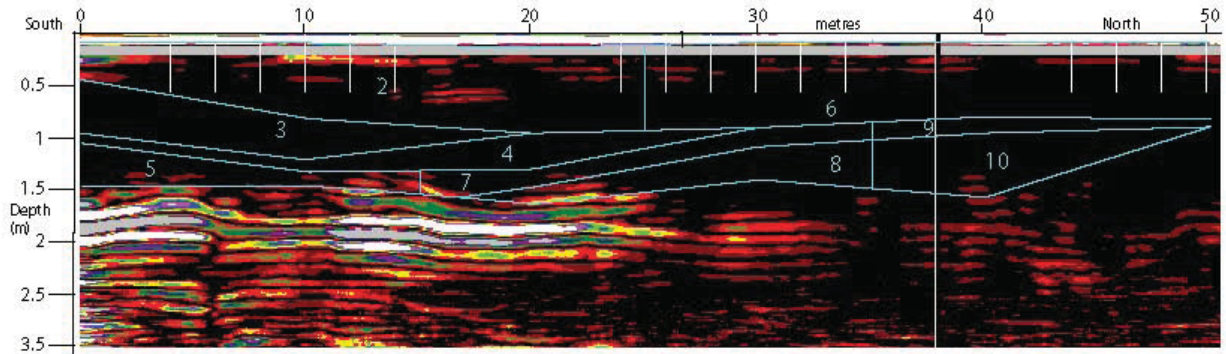


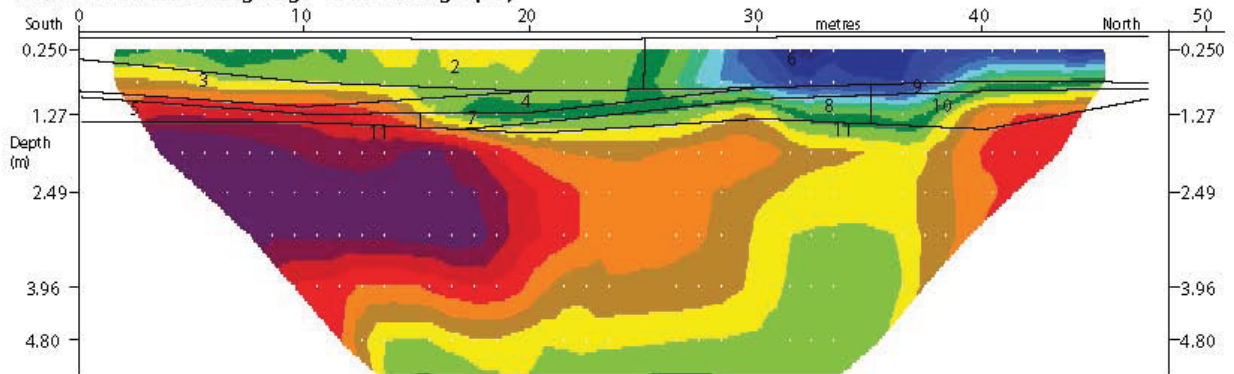
Fig 8.7: The location of ER transects T1C and T1D.

Transect T1C

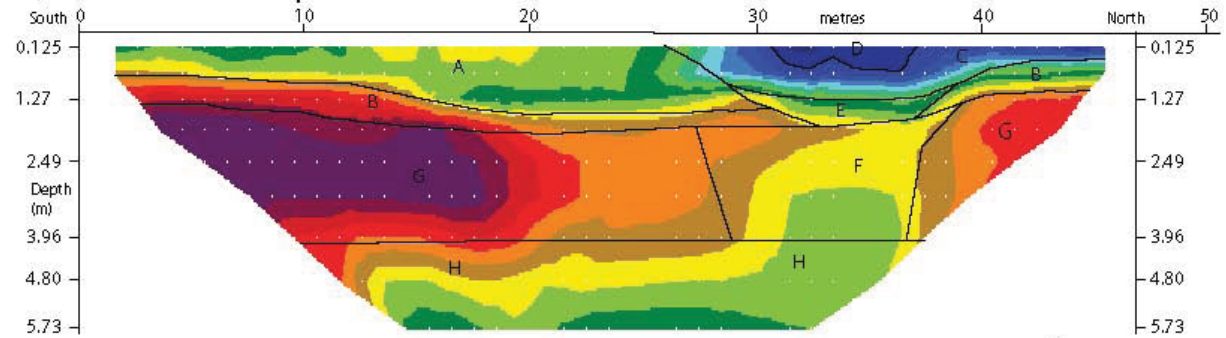
A) GPR section with gouge core stratigraphy



B) ER section with gouge core stratigraphy

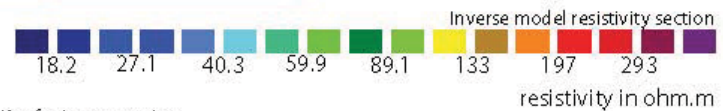


C) ER section with interpretation



Key gouge core stratigraphy:

- 1 = brown clayey silt, trace of sand
- 2 = red brown silty clay trace of sand
- 3 = gleyed grey clay, with Fe and Mn mottling
- 4 = red brown sand with clay
- 5 = coarse red/brown/pink sand
- 6 = brown grey clay with Fe nodules
- 7 = blue grey clay with sand and Fe nodules
- 8 = blue grey sandy clay
- 9 = brown grey clayey sand
- 10 = red brown sand, small Fe nodules



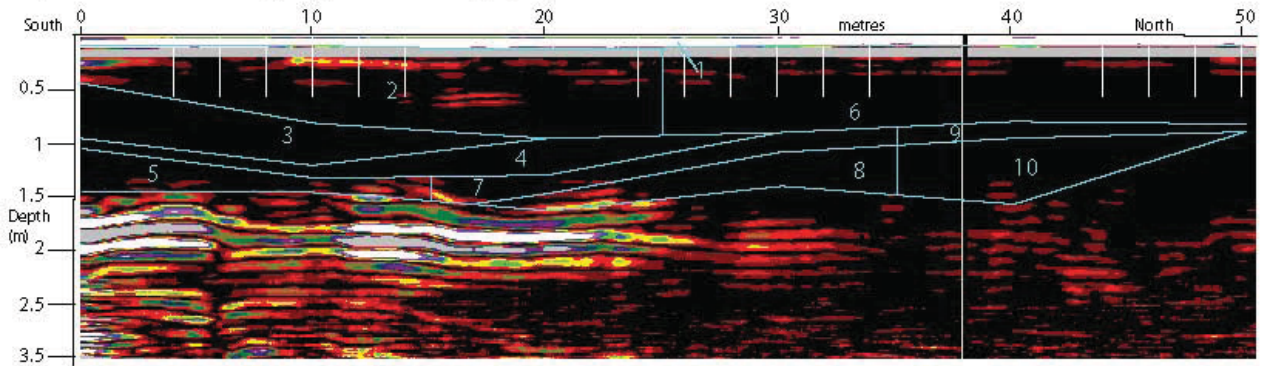
Key for Interpretation:

- A = terrace deposit silty clay
- B = terrace deposit clayey sand
- C = palaeochannel silty clay
- D = area of lowest resistance within palaeochannel
- E = palaeochannel basal sand
- F = gravel (low resistance matrix supported/high water content)
- G = gravel (high resistance clast supported/low water content)
- H = bedrock (Merican mustd one)

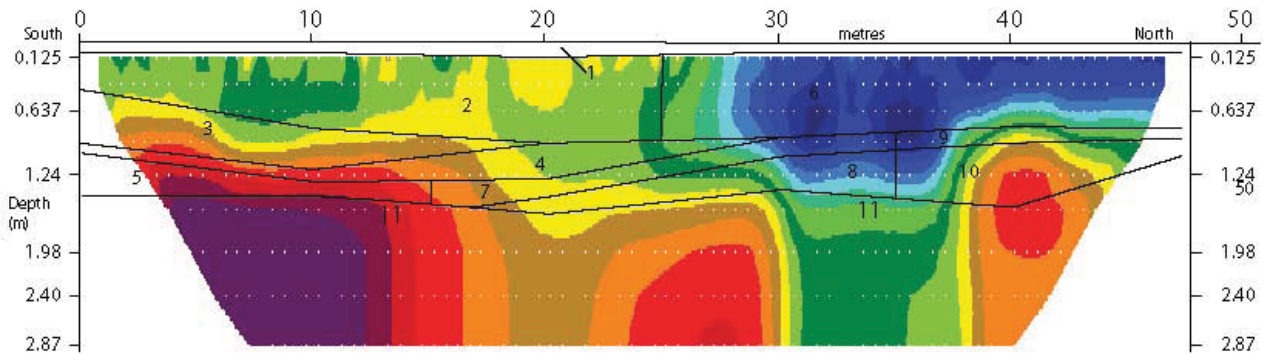
Fig 8.8: The ER transect T1C. The correlation in features between the GPR and gouge cores sections and the ER section is again high.

Transect T1D

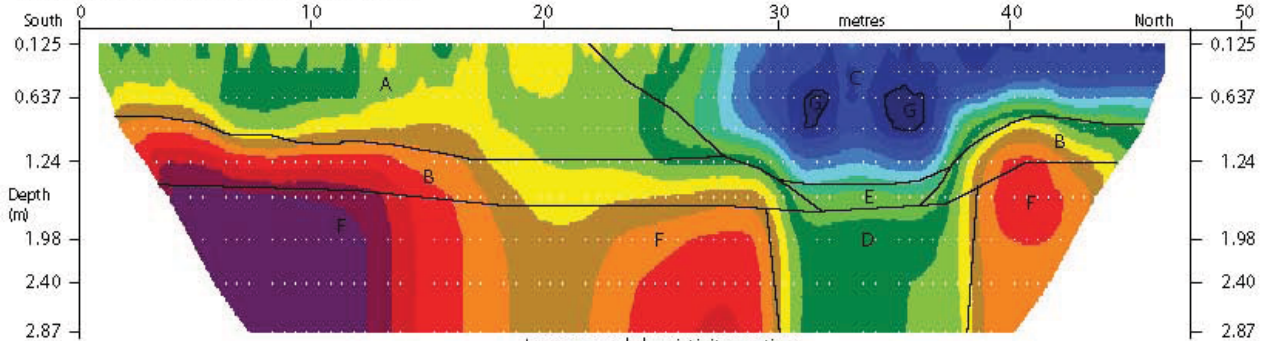
A) GPR section with gouge core stratigraphy



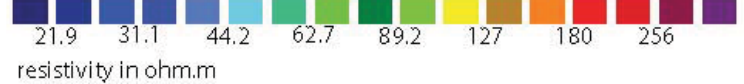
B) ER section with gouge core stratigraphy



C) ER section with interpretation



Inverse model resistivity section



Key gouge core stratigraphy:

- 1 = brown clayey silt, trace of sand
- 2 = red brown silty clay trace of sand
- 3 = greyed grey clay, with Fe and Mn mottling
- 4 = red brown sand with clay
- 5 = coarse red/brown/pink sand
- 6 = brown grey clay with Fe nodules
- 7 = blue grey clay with sand and Fe nodules
- 8 = blue grey sandy clay
- 9 = brown grey clayey sand
- 10 = red brown sand, small Fe nodules

Key for Interpretation:

- A = terrace deposit silty clay
- B = terrace deposit clayey sand
- C = palaeochannel silty clay
- D = gravel (low resistance matrix supported/higher water content)
- E = palaeochannel basal sand
- F = gravel (higher resistance clast supported/lower water content)
- G = areas of lowest resistivity values within the palaeochannel

Fig 8.9: The ER transect T1D.

8.4.4 *Transect TIE*

This transect was undertaken to provide complimentary data for terrestrial NIR (near infra red 950nm) scanning over a palaeochannel, which itself was comparative data for airborne LiDAR intensity (1047nm) survey. The location of this ER transect was an area of terrace 1 (Fig. 8.10). It has been proposed that LiDAR intensity can act as a proxy for subsurface sediment architectures and hence geoarchaeological potential (*Carey et. al 2007*). Therefore, it is important to be able to quantify surface and subsurface sediment relationships. The ER transect was 91m long and used a 1m electrode spacing, giving a depth coverage of c. 6m. As NIR scanning was being undertaken, time taken for the ER sections was limited, and only a limited gouge core transect was completed in the time available (10m core spacing).

From the LiDAR LP DTM a palaeochannel is evident as a topographic feature (Fig. 8.10), which is also evident through LiDAR intensity survey (Fig. 8.11) and ground based earth resistance survey (Fig. 8.12). The ER section clearly defines a palaeochannel (units D and E) between two areas of terrace (units A and B; Fig. 8.13). The ER data shows a close correlation with the limited gouge core transect. There is a good agreement in the depth to the gravels within the palaeochannel between the ER and gouge core data. The palaeochannel/terrace interface is also evident from the ER section and closely matches that depicted by the gouge core transect.

The relationship of the gouge core data to the ER section is revealing. The palaeochannel is at its deepest where the area of lowest resistivity defined by unit E is located. At this point the palaeochannel is dominated by unit 2 (stiff red brown silty clay, with Fe and Mn mottling), unit 4 (dark grey clay with a trace of sand) and unit 5 (dark grey clayey sand). A dark grey peaty clay (unit 7) is seen in the palaeochannel, but this does not coincide with unit E, the area of lowest resistivity. However, based on its field description unit 7 is likely to have the highest organic content of the palaeochannel sediment units. Again the ER section does not define the sediment units to match the gouge core transect, although broad changes in resistivity can be attributed to changes in the sediment stratigraphy recorded through the gouge core transect.

The interpretation of the ER section allows the identification of the alluvium on top of the terrace gravels (unit A). The general palaeochannel morphology is evident (units D and E), with the base of the palaeochannel/gravel interface (c. 2.5m deep) and the edge of the palaeochannel/terrace interface well defined. The area of lowest resistance within the palaeochannel is identified (unit E). The depth to gravels is evident both on the terrace and below the palaeochannel (units B and F). A higher resistivity unit on top of the palaeochannel is seen in the ER section (unit C), although no equivalent sediment unit was identified on the gouge core transect.

The profile of the gravel body is evident from the ER section. Again two units can be seen within the gravels. Unit B has a high resistivity value and represents either a clast supported gravel, a gravel with lower water content or a combination of the two factors. Unit F has a lower resistivity value and represents either a matrix supported gravel, a gravel with higher water content or a combination of the two factors. It is unlikely that the location of the palaeochannel above the gravel unit F is a coincidence and they are probably related factors, i.e. the palaeochannel above the gravel is restricting water loss, increasing the water content of the gravel below it. The lower resistivity value of the gravel unit F indicates an area of higher biotaphonomic potential within the gravel body. This again has importance for the preservation of organic material within the gravel. A suggested boundary between the gravels (units B and F) and the Mercian Mudstone is given (unit G). This is a good example of the integration of the airborne prospection with ground based

prospection, whereby a palaeochannel identified though airborne prospection can have its general morphology defined through ground based geopropection.

Transect T1E summary:

- There is close agreement between the gouge core transect and the ER section.
- The main geomorphological units of palaeochannel and terrace are defined by the ER transect.
- The alluvial covering on top of the terrace gravels is definable.
- The area of lowest resistance within the palaeochannel is identifiable, identifying the area of the palaeochannel with the highest biotaphonomic potential.
- The gravel bedrock interface is interpreted from the ER section.

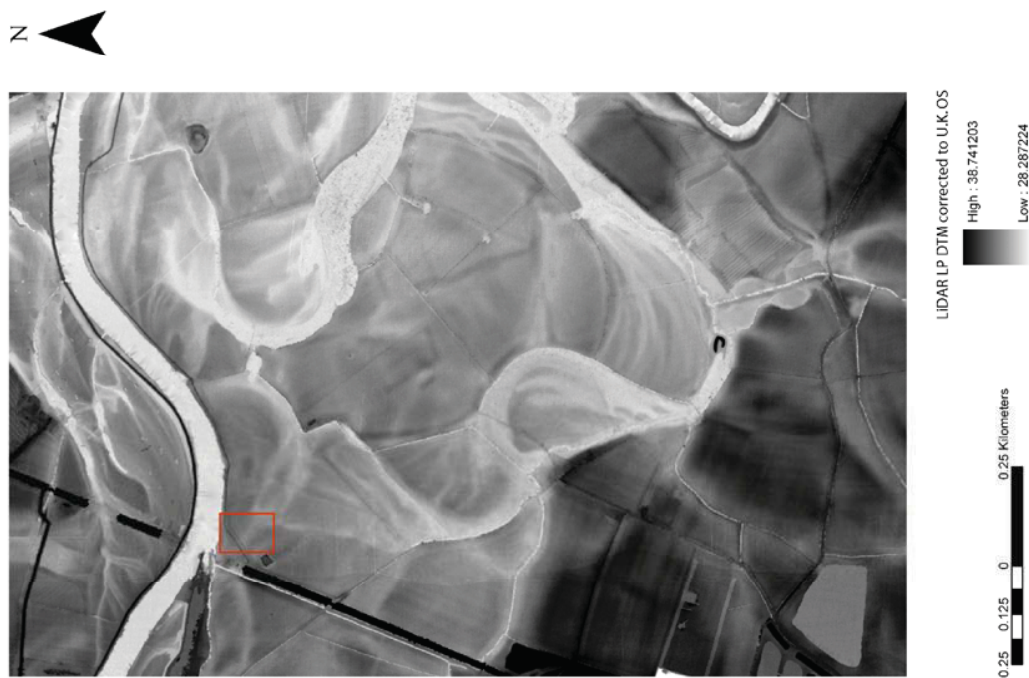
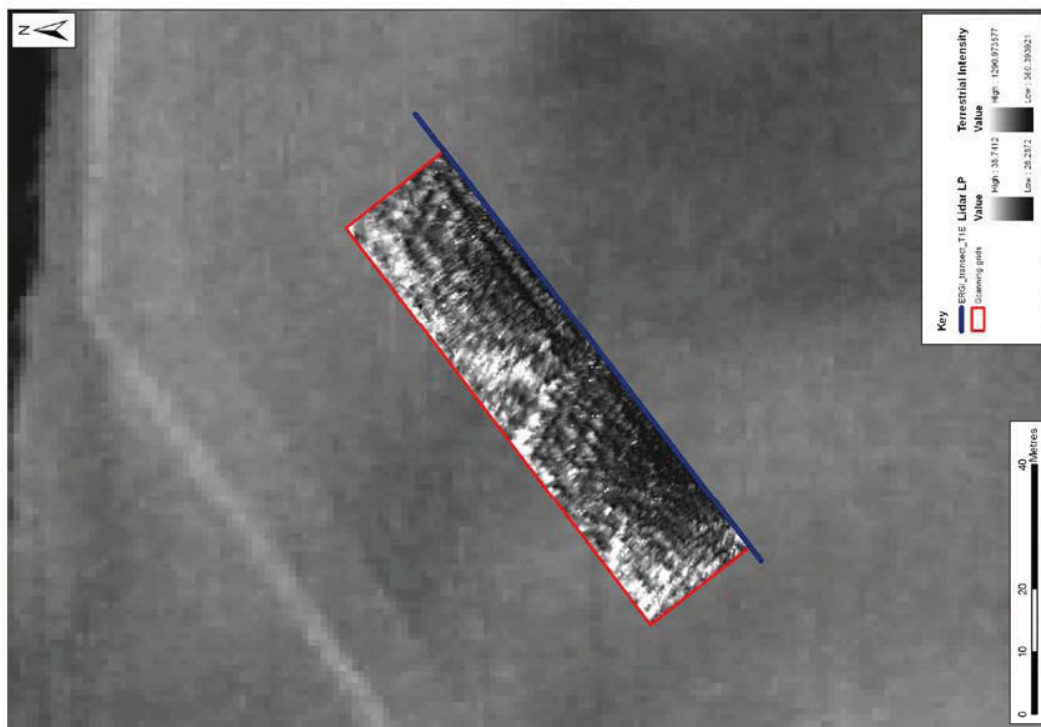


Fig 8.10: The location of ER transect T1E, placed on the LiDAR LP DTM. The palaeochannel is evident as a topographic feature.

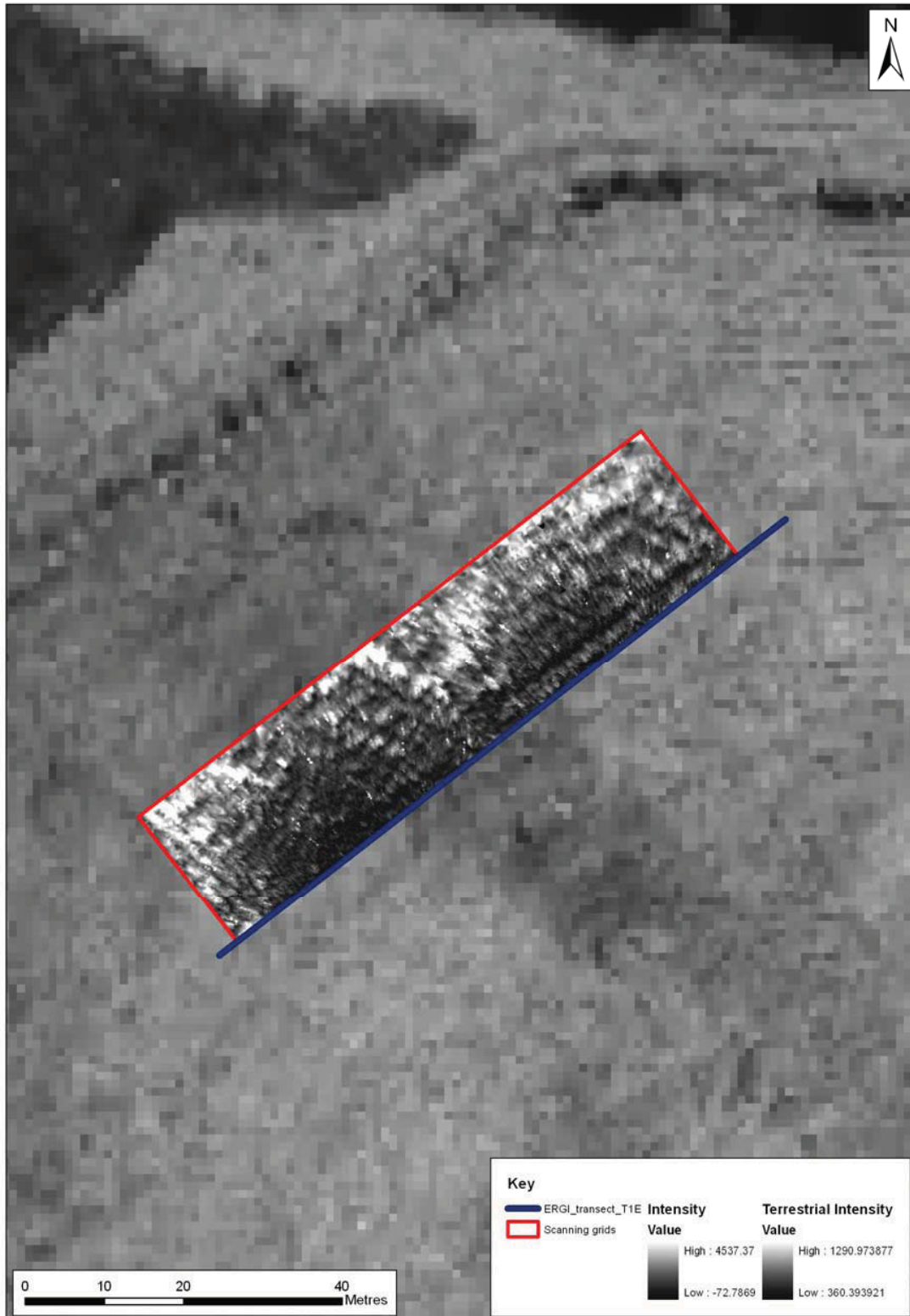


Fig 8.11: ER transect T1E placed on the LiDAR intensity survey.

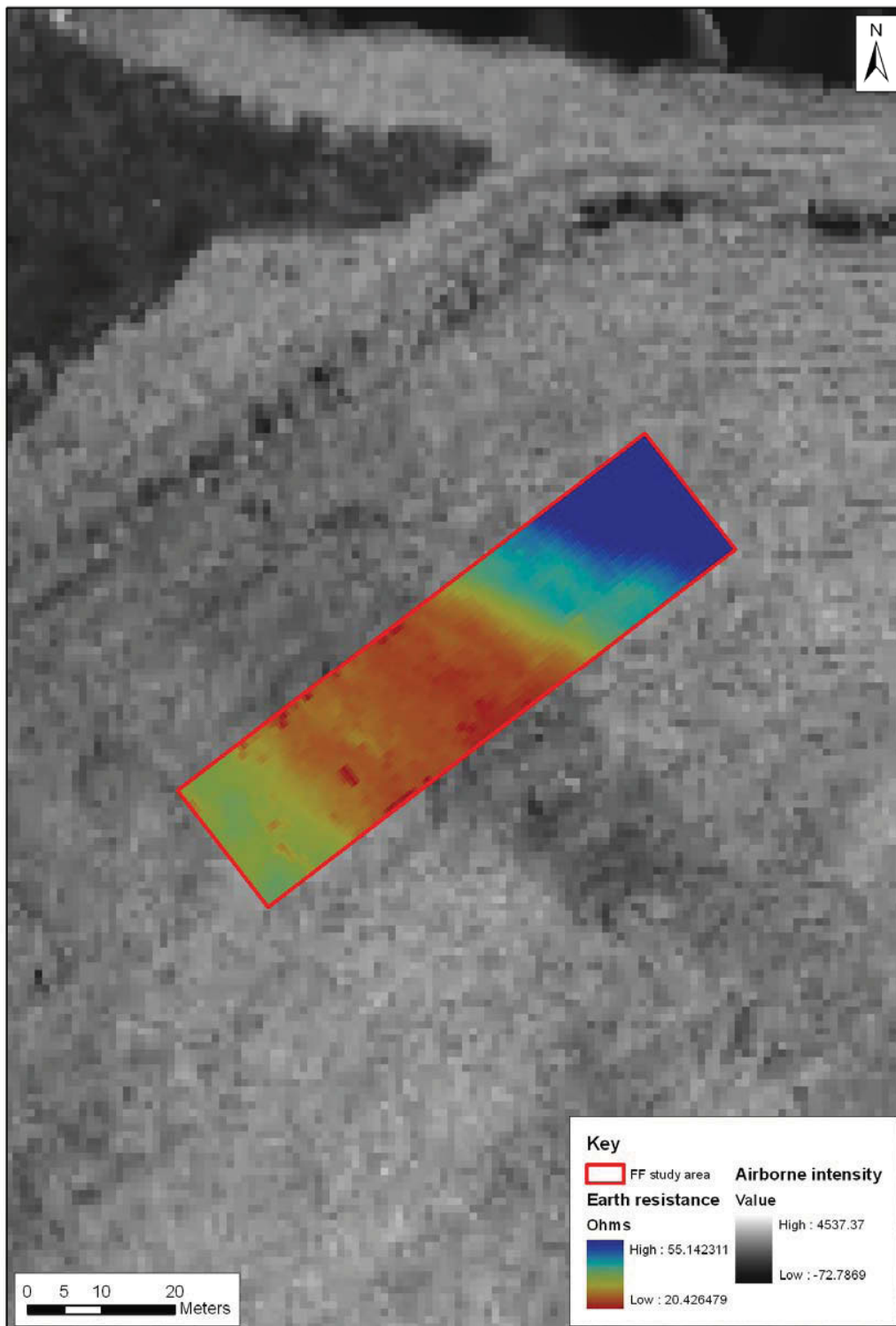
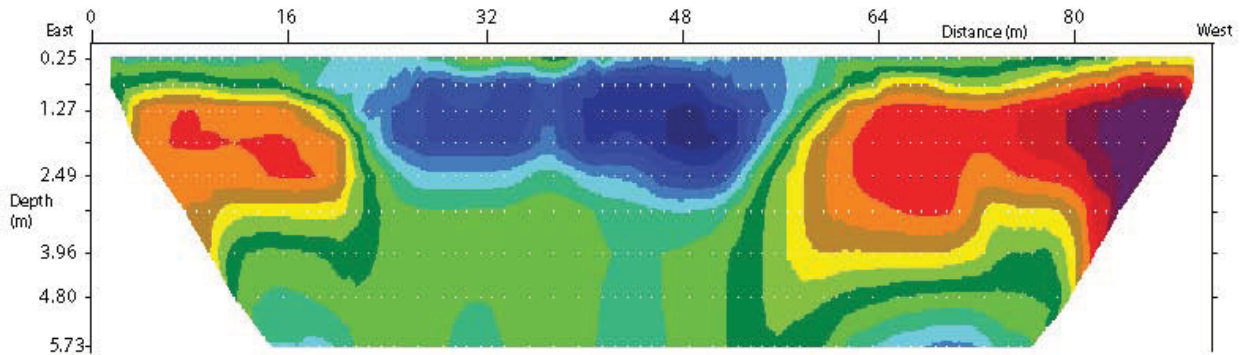


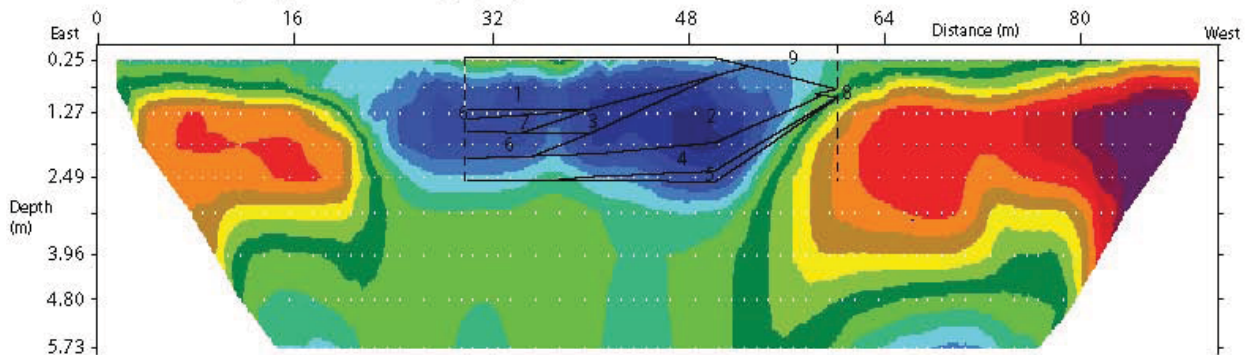
Fig 8.12: Earth resistance survey over the same area as T1E. The palaeochannel is evident as a low resistance feature.

Transect T1E

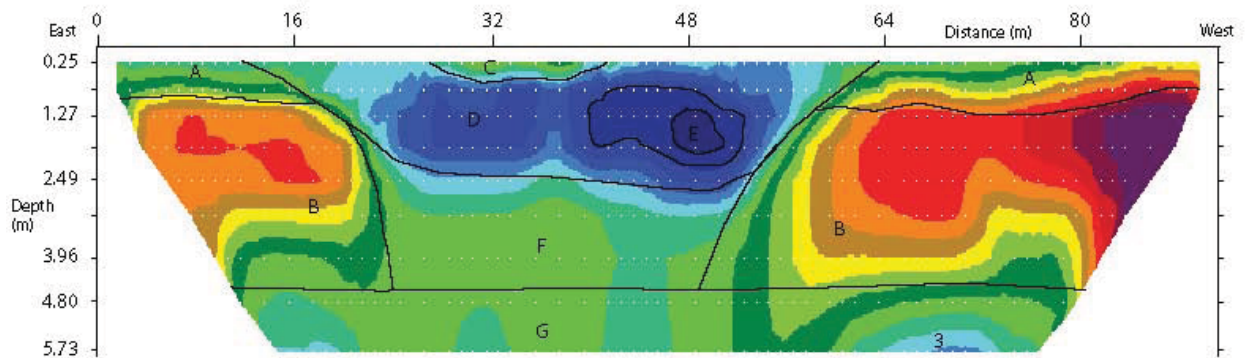
A) ER section raw data



B) ER section with gouge core stratigraphy



C) ER section with interpretation



Key gouge core stratigraphy

- 1= Very fine compact grey sand
- 2 = Stiff red brown silty clay, with Fe and Mn mottling
- 3 = Fine compact grey sand
- 4 = Dark grey clay, trace of sand
- 5 = Dark grey clayey sand
- 6 = Grey sandy clay with Mn and Fe mottling
- 7 = Dark grey peaty clay
- 8 = Brown silty clay
- 9 = Brown clayey silt

Key for interpretation:

- A = terrace alluvium (red brown silty clay)
- B = gravel higher resistance (clast supported/higher water content)
- C = area of drier alluvium above palaeochannel fill
- D = palaeochannel
- E = area of palaeochannel with highest water content
- F = gravel lower resistance (matrix supported/lower water content)
- G = bedrock (Merican mudstone)

Fig 8.13: ER transect T1E.

8.4.5 ER transect T1F

Transect T1F was undertaken on a palaeochannel thought to be a relatively recent palaeochannel of the river Soar (Fig. 8.14). Much of this palaeochannel holds water throughout the year and has an extensive reed bed, making survey into the palaeochannel difficult (Fig. 8.15). An ER transect ran from the terrace edge part way into the palaeochannel, in an attempt to ascertain some of the palaeochannel morphology. The transect ran for 58m, using a 1m electrode spacing.

The ER section defined the major geomorphological units within the transect (Fig. 8.16). The palaeochannel (unit 2) is clear, sloping away from the terrace alluvium (unit A) and incising into the gravels (unit B). The junction between the above gravel alluvium (unit A) and the gravel (units B and C) is interpreted. The junction between the gravel (units B and C) and bedrock (unit E) is also interpreted. Again variation is seen in the resistivity values of the gravels, with areas of lower resistivity values having higher potential to preserve organic remains.

From the interpretation of the ER section it is clear that the transect has only covered the edge of the palaeochannel. The palaeochannel is relatively shallow throughout the section and based on these ER results it would not be cored for palaeoenvironmental samples, due to its shallow morphology.

Transect T1F summary:

- The main geomorphological units are identified by ER.
- The edge of the palaeochannel is relatively shallow and has a low biotaphonomic potential.
- Variation in the resistivity values of the gravels are evident.
- The boundary between the Mercian Mudstone and the gravels is evident.



Fig 8.15: Photograph of ER transect T1F. The palaeochannel still holds water, as evidenced by the abundant reeds.

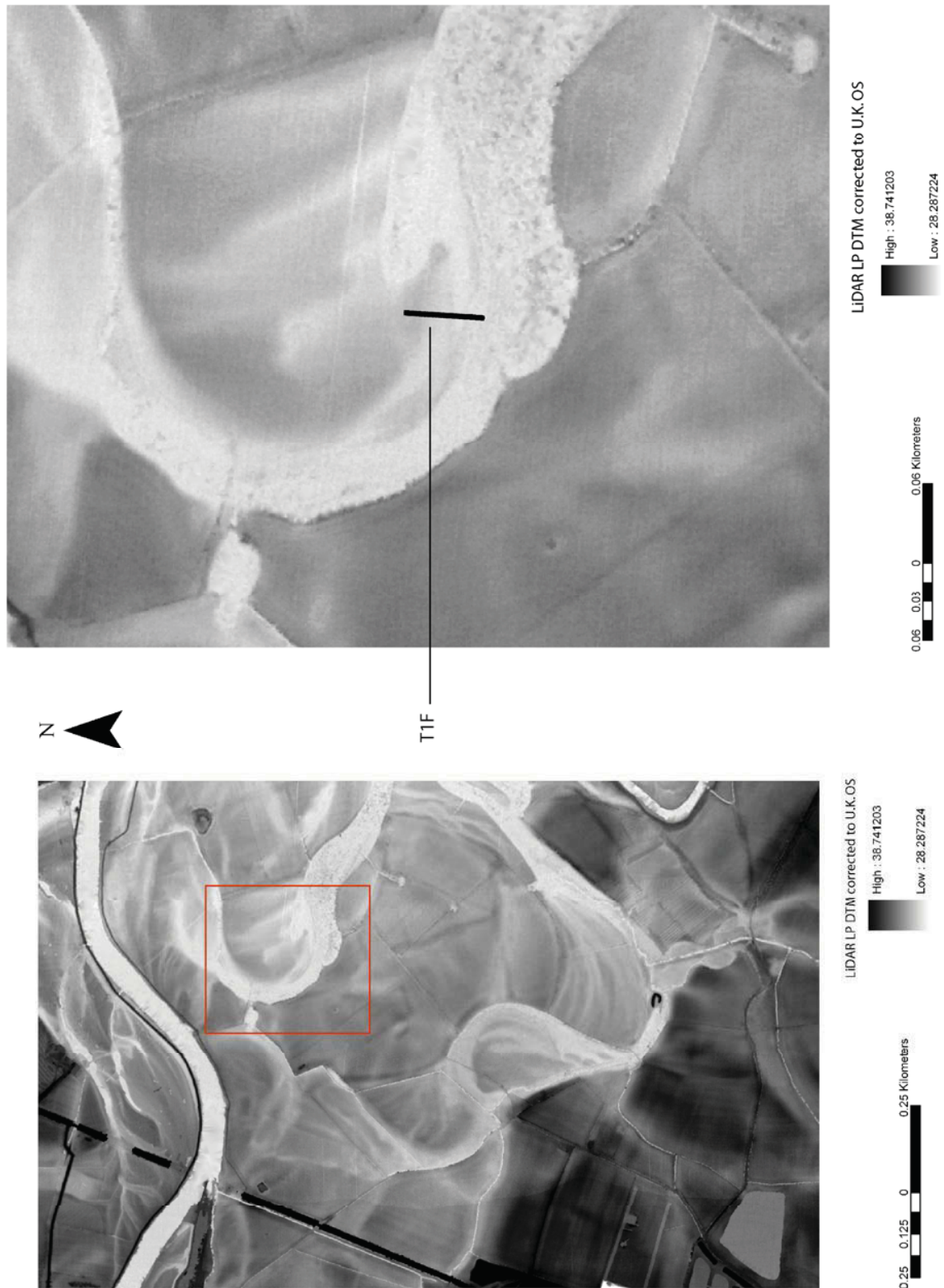
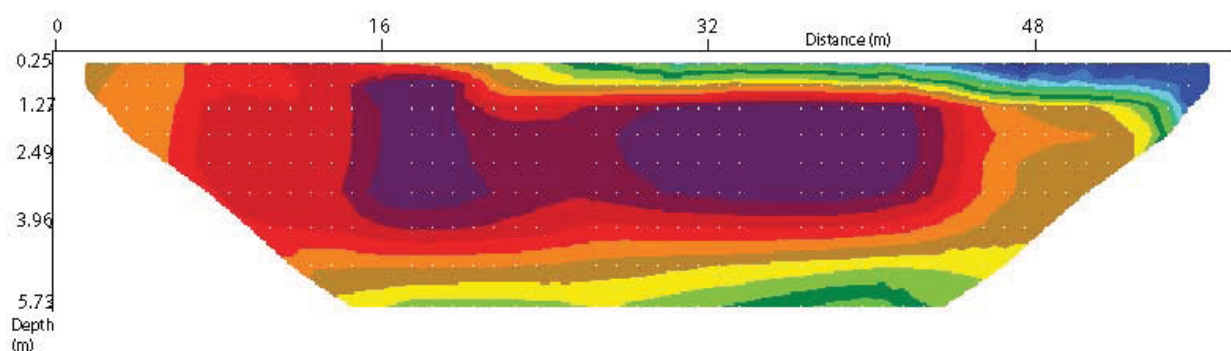


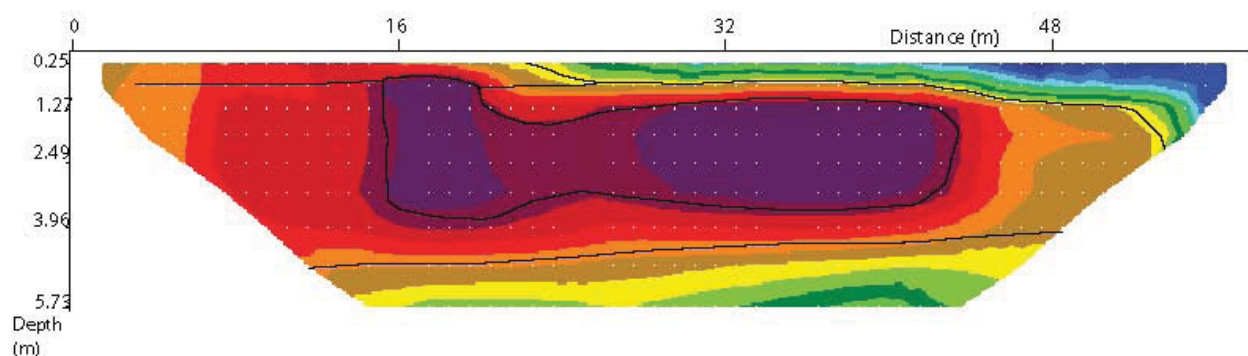
Fig 8.14: Location of the ER transect T1F.

Transect T1F

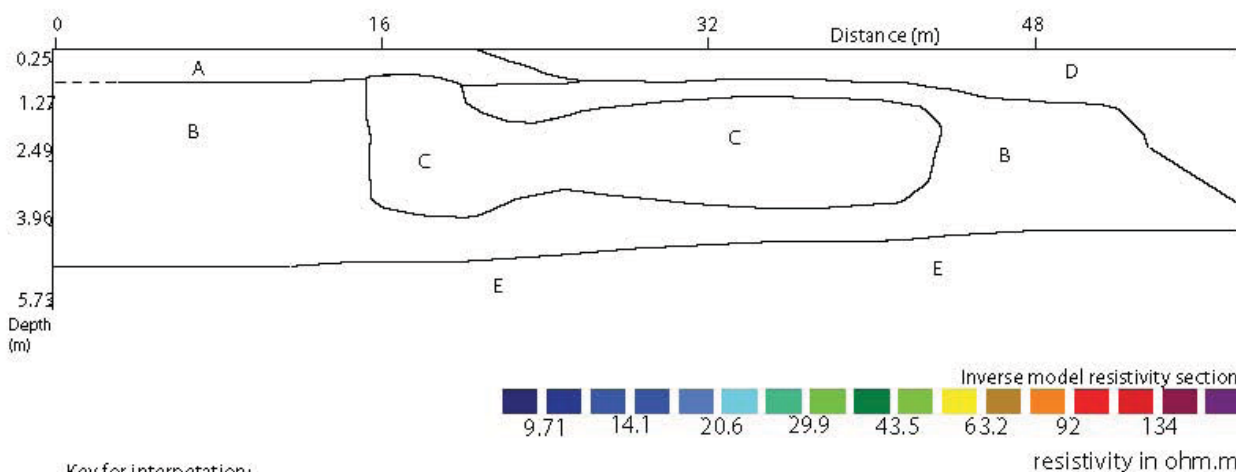
A) ER section raw data



B) ER section with interpretation



C) Interpretation of ER section without raw data



Key for interpretation:
 A = above gravel alluvium (silty clay)
 B = gravels higher resistance: lower water/sand content
 C = gravels lower resistance: higher water/sand content
 D = palaeochannel (edge of)
 E = bedrock Mercian mudstone

Fig 8.16: ER transect T1F.

8.4.6 ER transect T1G

This palaeochannel was located in the field adjacent to the transects T1A and T1B (Fig. 8.17). The ER transect ran across the widest section of this field in order to provide baseline information on the general morphology of this palaeochannel. This palaeochannel demarcates the boundary between the Holme Pierrepont terrace 2 and the later Holocene Hemington terrace 1, and has importance for understanding the general chronostratigraphy of the study area. However, due to the high ground water table of this area (the surface sediments were saturated), attempts to understand the stratigraphy of the palaeochannel using GPR were abandoned. The transect ran for 83m, using a 0.5m electrode interval. A gouge core transect recorded sediment stratigraphy at 10m intervals along the ER transect.

The ER transect revealed the upper section of the profile to have two palaeochannels (units A and C) separated by a feature (unit B). The gouge core stratigraphy shows sediment unit 6 (stiff red black silty clay with organics) and partly sediment unit 4 (red brown humic clay) to correlate with palaeochannel defined by unit A. The palaeochannel unit C, again correlates with unit 6 and also partly unit 5 (brown silty A horizon).

The feature that occurs between these two palaeochannels is unit B. This correlates closely with the two sediment units 6a (stiff red grey silty clay) and 6b (stiff brown silty clay). The two units 6a and 6b, represent a marginal difference in sediment composition from unit 6. However, unit 6 was recorded as having a much higher organic content and the ER section makes a clear distinction between units A, B and C. Unit B on first impressions may be thought to be a gravel bar in a shallow braided channel. However, the sediment composition of feature B shows it is not a gravel bar and was formed within a low energy depositional regime. Unit B has a relatively low resistivity value compared to the gravels lower in the section. It possibly represents a hiatus in occupation of a larger channel system.

Below the units A, B and C, unit D is interpreted as sands lying at the top of the gravel. This unit corresponds to units 3 (grey black coarse sand), 7 (grey brown organic peaty clay), 8 (grey medium clayey sand), 9 (dark grey black silty clay) and 10 (red clayey sand) on the north side of the section. Therefore, there is some correlation with sand dominated units above the gravels, although some of these units are clays, which should have lower resistivity values. On the south side of the section there is unit 12 (grey coarse sand) lying at the top of the gravel unit.

From the ER section the geomorphological features of the palaeochannels (units A and C), the between palaeochannel feature (unit B) and the gravels (and E and F) are interpretable. Again variation in the resistivity values of the gravels is seen, with unit F having a lower value, lying underneath the palaeochannel unit C.

Transect T1G summary:

- The ER section showed a good level of correlation with the gouge core stratigraphy.
- Two palaeochannels (units A and C) were evident either side of a feature (unit B).
- The junctions between the palaeochannel fill (units A and C) and the between channel feature (unit B), and the gravels is interpretable.
- Variation in the resistivity values of the gravels were seen, again correlating with the gravels below the palaeochannel having a lower resistance.

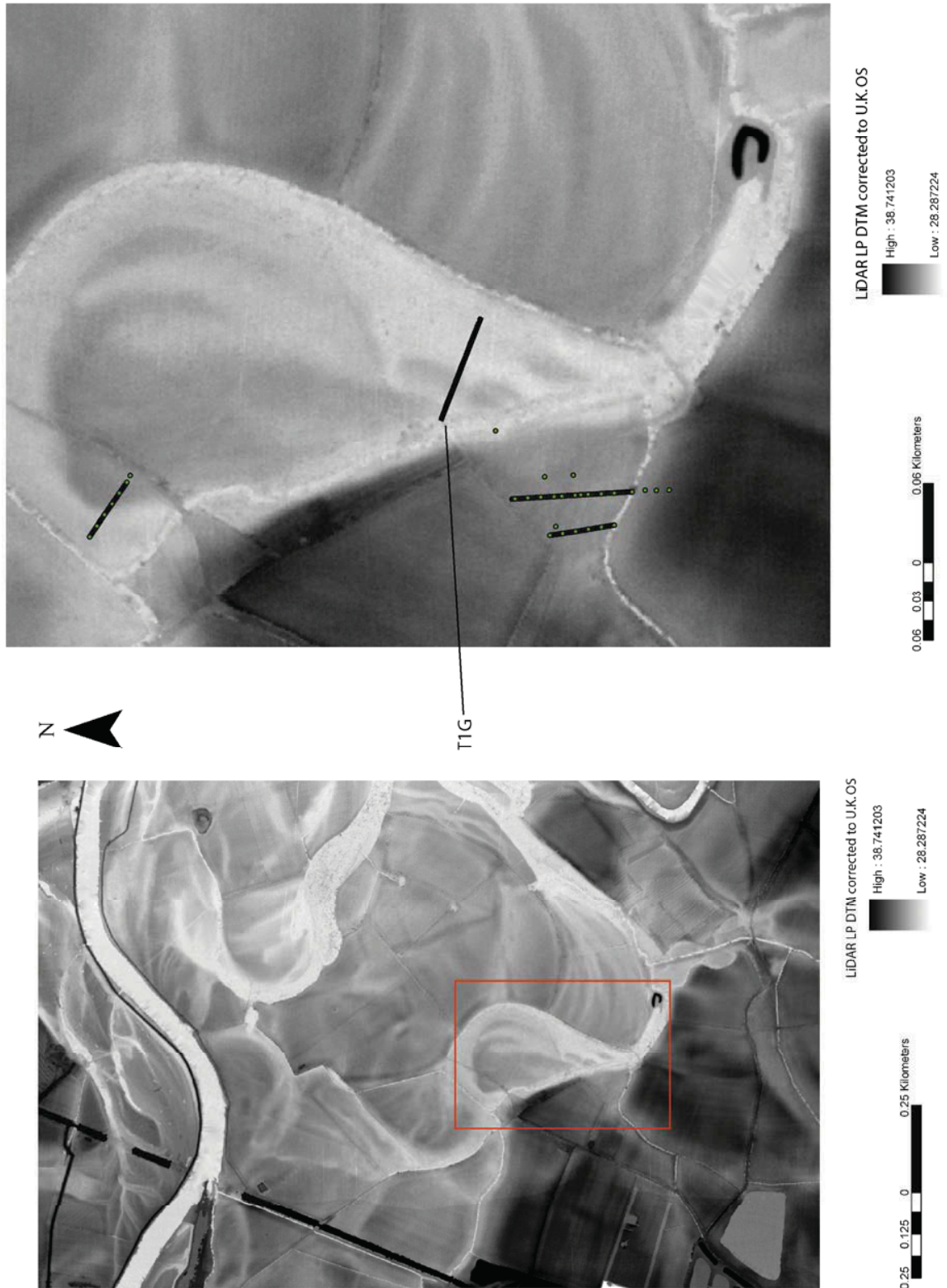
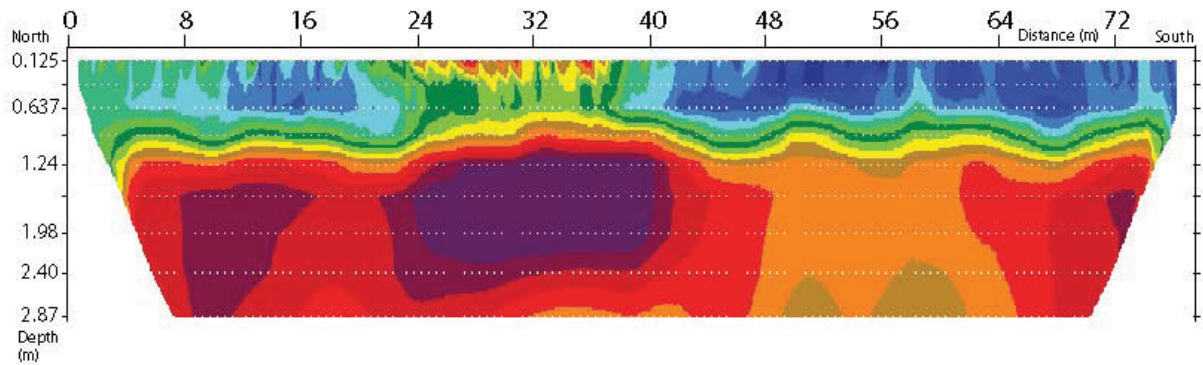


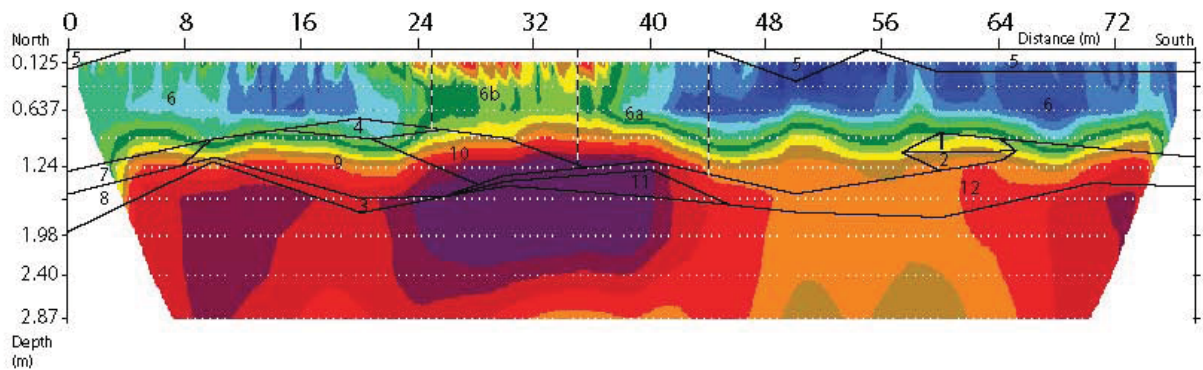
Fig 8.17: Location of ER transect T1G.

Transect T1G

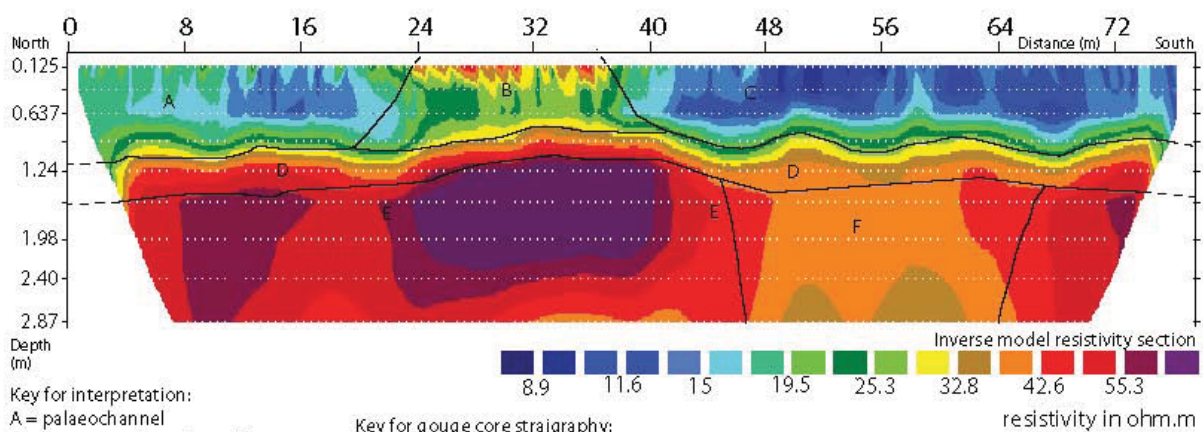
A) ER section raw data



B) ER section with gouge core stratigraphy



C) ER section with interpretation



Key for interpretation:

- A = palaeochannel
- B = between palaeochannel feature
- C = palaeochannel
- D = sand on top of gravels
- E = gravels (higher resistance clast supported/lower water content)
- F = gravels (lower resistance matrix supported/higher water content)

Key for gouge core stratigraphy:

- 1 = Grey gleyed organic silty clay
- 2 = Black grey silty clay
- 3 = Grey black coarse sand
- 4 = Red brown humic clay
- 5 = Brown silty A horizon
- 6 = stiff red black silty clay with organics
- 6a = Stiff red grey silty clay
- 6b = Stiff brown silty clay
- 7 = Grey brown organic peaty clay
- 8 = Grey medium clayey sand
- 9 = Dark black grey silty clay
- 10 = Red clayey sand
- 11 = Orange Fe stained coarse sand
- 12 = Grey coarse sand

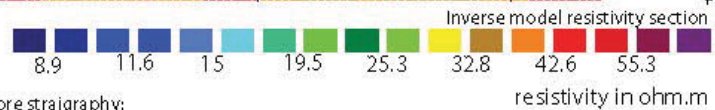


Fig 8.18: The ER transect T1G.

8.4.7 ER transect T1H

Transect T1H was undertaken at the junction between a palaeochannel and an area of terrace 1, in close proximity to transects T1C and T1D. Both the terrace and palaeochannel are evident through topographic expression, as shown through the LiDAR LP DTM (Fig. 8.19). The ER transect ran for 48m, using a 0.5m electrode spacing. The end of the ER data file corrupted, so the results are for the first 40m of the transect only. GPR and gouge core sections (10m core spacing) were run along the same transect. This palaeochannel was cored to retrieve the core T1C8 and the ER section aimed to provide further information on its morphology, stratigraphy and biotaphonomic potential.

The GPR transect provides an interesting contrast to the gouge core data. The depth to gravels is shown by the gouge core stratigraphy at c. 1.6m across the transect. However, the GPR trace reveals a strong reflecting unit at c. 2m and a weaker reflecting unit, varying between 1.4 and 1.7m. The depth to impenetrable gravel is not seen as a reflective discontinuity on the GPR trace. However, the angle of dip of the gravels on the west side of the transect is mimicked by the GPR trace, suggesting that the plane of deposition has been detected by the GPR.

The centre of the GPR trace is seen as a blank area of no reflectance and the gouge core data reveals the units of 2 (brown grey clay, with a trace of sand and Fe and Mn mottling), unit 3 (blue grey clay, with a trace of sand and Fe and Mn mottling), unit 4 (dark blue grey organic rich clay), unit 7 (brown grey sand clay) and unit 8 (grey pink sand) in this blank GPR area. There is a weak relationship between the GPR data and the stratigraphy revealed through the gouge core.

The relationship of the ER section to the gouge core stratigraphy is easier to interpret compared to the GPR data, but the relationship between the two data sets is still not precise. The palaeochannel A1 partially correlates with the two sediment units 3 and 4, both clay dominated units. Unit 4 is recorded as being organic rich and matches in a horizontal location with unit B, identified as the area of the lowest resistivity value within the palaeochannel. This stated, unit 4 is lower than unit B (c. 40cm difference). Palaeochannel A2 correlates with unit 2 (brown grey clay, with a trace of sand and Fe and Mn mottling), but unit 2 extends away from the palaeochannel. Underneath palaeochannel A2 a relatively deep pink grey sand (unit 8) is recorded, which correlates with the interpreted unit C, a sand layer above the gravels. The depth to gravels is not clear from the ER trace, but with the gouge core stratigraphy it is possible to interpret this junction.

In isolation the ER section allows the identification of the palaeochannel A1, with its morphology well defined. Palaeochannel A2 has a higher resistance feature roughly at its centre, but this is not witnessed in the gouge core stratigraphy, although it is located between the 20m and 30m coring stations. A relatively large unit of intermediate resistivity value (unit C) is seen between the gravels (units E and D) and the palaeochannels (units A1, A2 and B), and is interpreted as sands above the gravels. Again variation in the resistivity values of the gravels is seen.

T1H summary:

- There is little correlation between the GPR trace and the gouge core stratigraphy.
- There is a stronger correlation between gouge core stratigraphy and the ER section.
- The depth to impenetrable gravel on the ER section alone would be difficult to interpret.
- The interpretation of the ER section reveals two palaeochannels and sands lying above the gravels, an interpretation largely supported by the gouge core stratigraphy.
- More gouge cores at a closer spacing may have provided a closer correlation with the ER section.

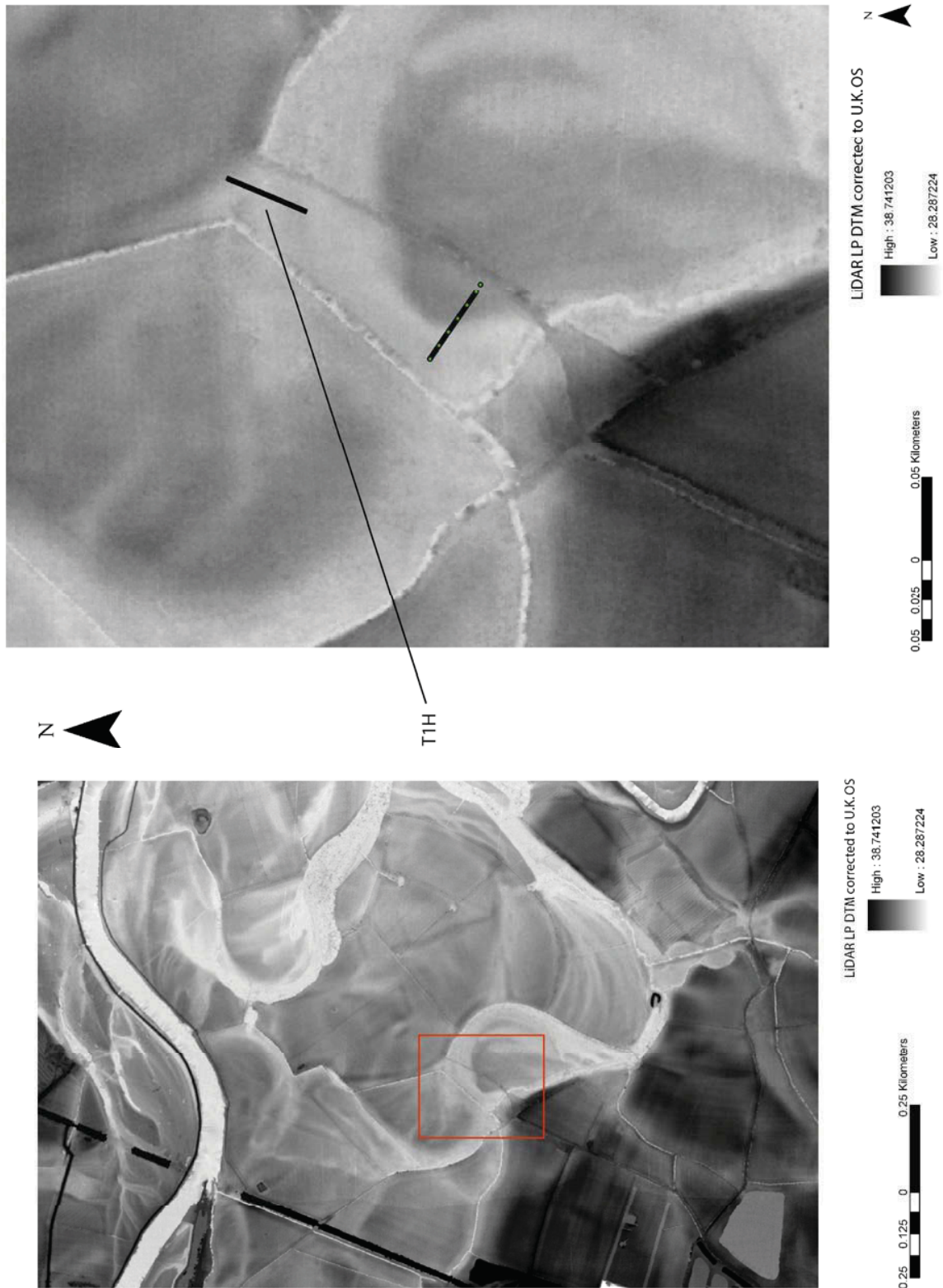
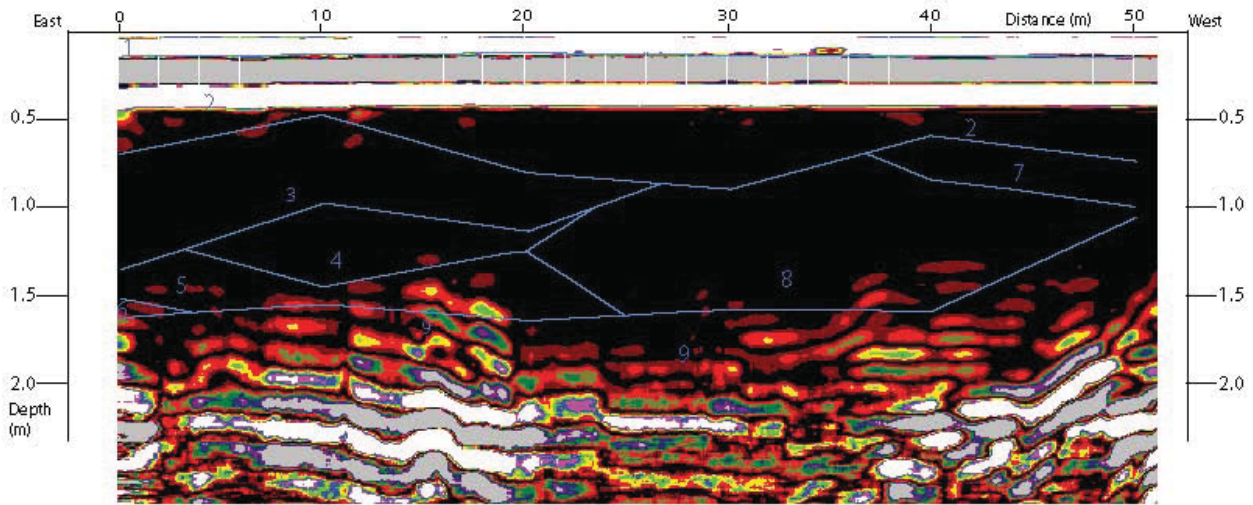


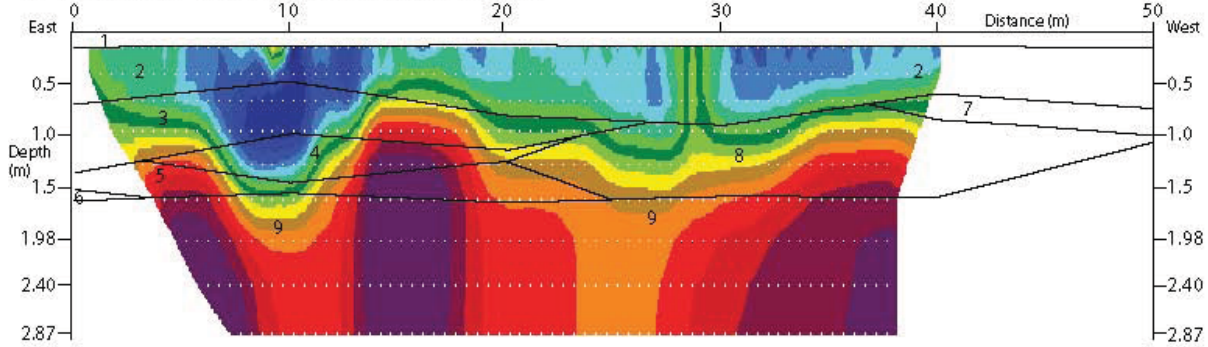
Fig 8.19: Location of transect T1H on terrace 1.

Transect T1H

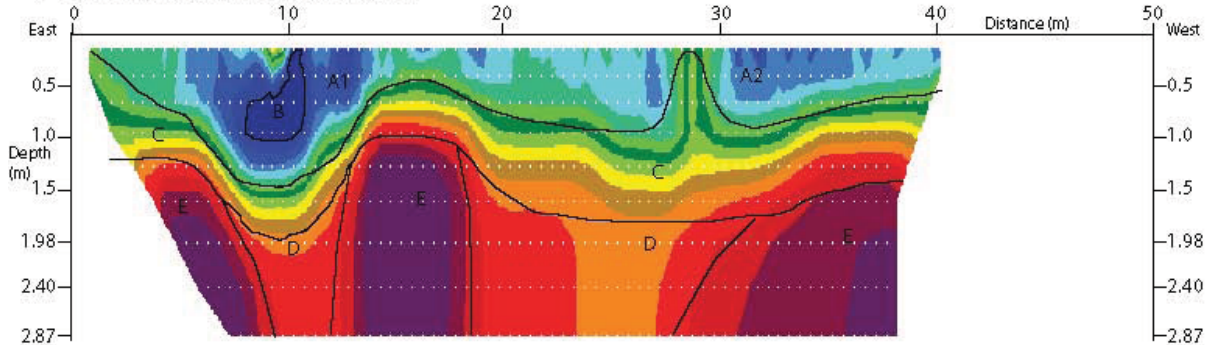
A) GPR section with gouge core stratigraphy



B) ER section with gouge core stratigraphy

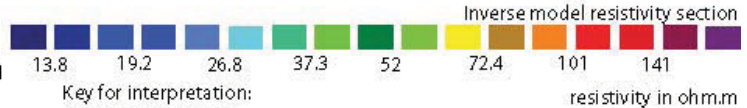


C) ER section with interpretation



Key gouge core stratigraphy:

- 1 = brown clayey silt A horizon
- 2 = brown grey clay, trace of sand, Fe and Mn mottling
- 3 = blue grey clay, trace of sand, Fe and Mn mottling
- 4 = dark blue/grey organic rich clay
- 5 = dark blue grey clayey sand, organic rich
- 6 = pink orange medium sand
- 7 = brown grey sandy clay
- 8 = grey pink sand
- 9 = impenetrable gravel



Key for interpretation:

- A1 = palaeochannel
- A2 = palaeochannel
- B = area of lowest resistance within palaeochannel A1
- C = sands above gravels
- D = gravels low resistance (matrix supported/high water content)
- E = gravels high resistance (clast supported/low water content)

Fig 8.20: ER transect T1H.

8.4.8 ER transect T1J

The ER transect T1J was conducted on an area of terrace 1, targeting a palaeochannel that separates the Holocene Hemington terrace 1 deposits from the more recent floodplain deposits (Fig. 8.21). The palaeochannel can be seen as a topographic feature from the LiDAR LP DTM and is visible in 'the field'. The transect ran for 135m and used a 1m electrode interval. A gouge core transect (10m core spacing) and a GPR transect were also conducted to provide complementary data. The gouge core transect revealed a complicated stratigraphy (Fig. 8.22). The GPR section produces a depth to gravel that agrees with the gouge core data. The level of alluvium above the gravels gets noticeably shallower at c. 45m, with the GPR sections showing a strongly reflecting unit at this point, interpreted as gravel bar.

For the most part of the GPR trace there is a blank 'middle area of the section', which corresponds to the above gravel alluvium and palaeochannel fills. The sediment stratigraphy of these units is complex and consists of a series of sandy clays, clays and clayey sands, sands and a very dense fine grey sand (unit 19). From the GPR section the terrace and the palaeochannel are not identifiable. The only identifiable features are the areas of denser gravel at the junction between the top of the gravels and the alluvium.

The ER section provides a much clearer picture of the subsurface features (Figs. 8.22 and 8.23). From the ER section it is clear that there is either a bifurcated channel or two separate palaeochannels (units E1 and E2). Palaeochannel E2 is the larger of two channels and correlates with a series of sediment units representing a palaeochannel fill such as unit 19 (a very dense fine grey sand), unit 20 (light brown clay with bone, shell fragments and fired clay), unit 21 (blue grey clay with organic staining and pieces of flint), unit 22 (blue grey green clay, with pieces of flint) unit 23 (dark brown grey clay with organic staining), unit 14 (brown grey clay trace of sand), unit 15 (brown grey clay, Fe and Mn mottling), unit 16 (orange grey clay, Fe and Mn mottling), unit 17 (blue grey clay, Fe and Mn mottling) and unit 18 (dark grey clay organic rich). All of these units are clay dominated, with units 20 and 21 being strong candidates for containing cultural material.

Palaeochannel E1 is much smaller than E2, both in width and depth. It contains unit 3 (orange brown clay, trace of silt and sand), unit 5 (gleyed orange brown clay) and unit 6 (orange brown clayey sand). Again these are all clay dominated sediment units and would be expected to have these low resistivity values. The ER section also has a close correlation between areas of higher resistivity values and areas of terrace/gravel. For example, at c. 50m an interpreted gravel bar is visible, with the units above the gravel being recorded as unit 10 (orange brown sand clay), unit 11 (grey brown clay with organics) and unit 12 (pink grey sandy clay, Fe and Mn mottling). These units have higher sand contents and therefore produce higher resistivity values.

The interpretation of the ER section shows the two palaeochannels E1 and E2, with basal sands in the palaeochannels identified as unit D. From the ER section it is clear that palaeochannel E1 has a lower biotaphonomic potential than palaeochannel E2. Palaeochannel E2 is wider, deeper and has its lowest resistivity value highlighted as unit F. Unit F is where biotaphonomic potential is likely to be highest due to higher water/clay contents.

The alluvium on top of the gravels is interpreted as a lower resistivity unit A (clay silt dominated), with a higher resistivity unit B (sand dominated) located beneath it. The gravels again show variation in resistivity values with the higher resistivity units C and the lower resistivity units G.

The higher resistivity units C clearly correlate with the gouge core data and also the GPR trace. The large high resistance unit C at c. 45m is interpreted as a clast supported gravel bar. It is visible on the GPR section as a strongly reflecting unit and the gouge core stratigraphy shows a rise in gravel at this point. Again the lower resistivity gravels unit (G) correlates with the gravels underneath the palaeochannels and could either be the product of matrix-supported gravels, higher water content or a combination of the two factors. The junction between the Mercian Mudstone bedrock (unit H) and the gravels is evident (unit C and H). The Mercian Mudstone is seen as a lower resistance unit compared to the gravels, due to its higher clay and water contents.

Over transect T1J is an excellent example of ER survey in alluvial environments and the correlation of ER with other techniques. A summary of the main features is:

- ER penetrates deeper than either GPR or gouge core data (using a 1m electrode spacing).
- There is a strong correlation of features between the GPR and ER sections, such as the hard reflecting/higher resistance gravel units.
- The relationship of the depth to impenetrable gravels between the GPR and gouge core survey is almost exact.
- The GPR section revealed no detail of the above gravel stratigraphy.
- The ER section shows a good degree of correlation with the gouge core survey, especially the depth to gravel across the survey.
- The ER section revealed the geomorphological units of two palaeochannels, silt clay dominated alluvium over the terrace, sand dominated unit above the gravels, low resistivity gravels, high resistivity gravels and the gravel/bedrock junction.
- The protrusion of the high resistivity gravel unit G at c. 45m is interpreted as a clast supported gravel bar.
- Palaeochannel E2 is interpreted as having a higher level of biotaphonomic potential than palaeochannel E1.

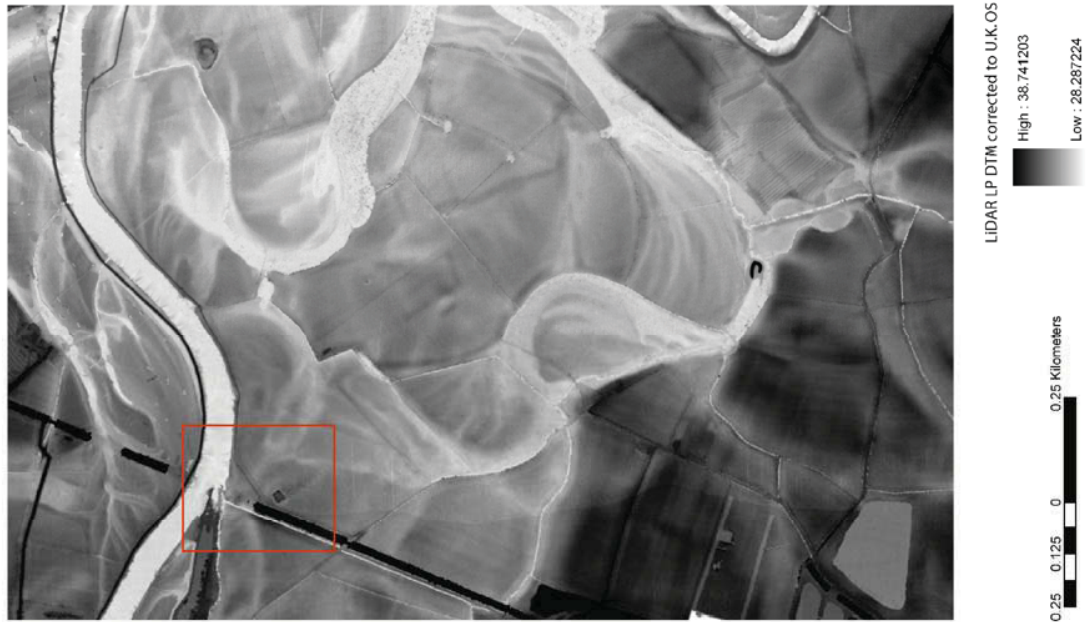
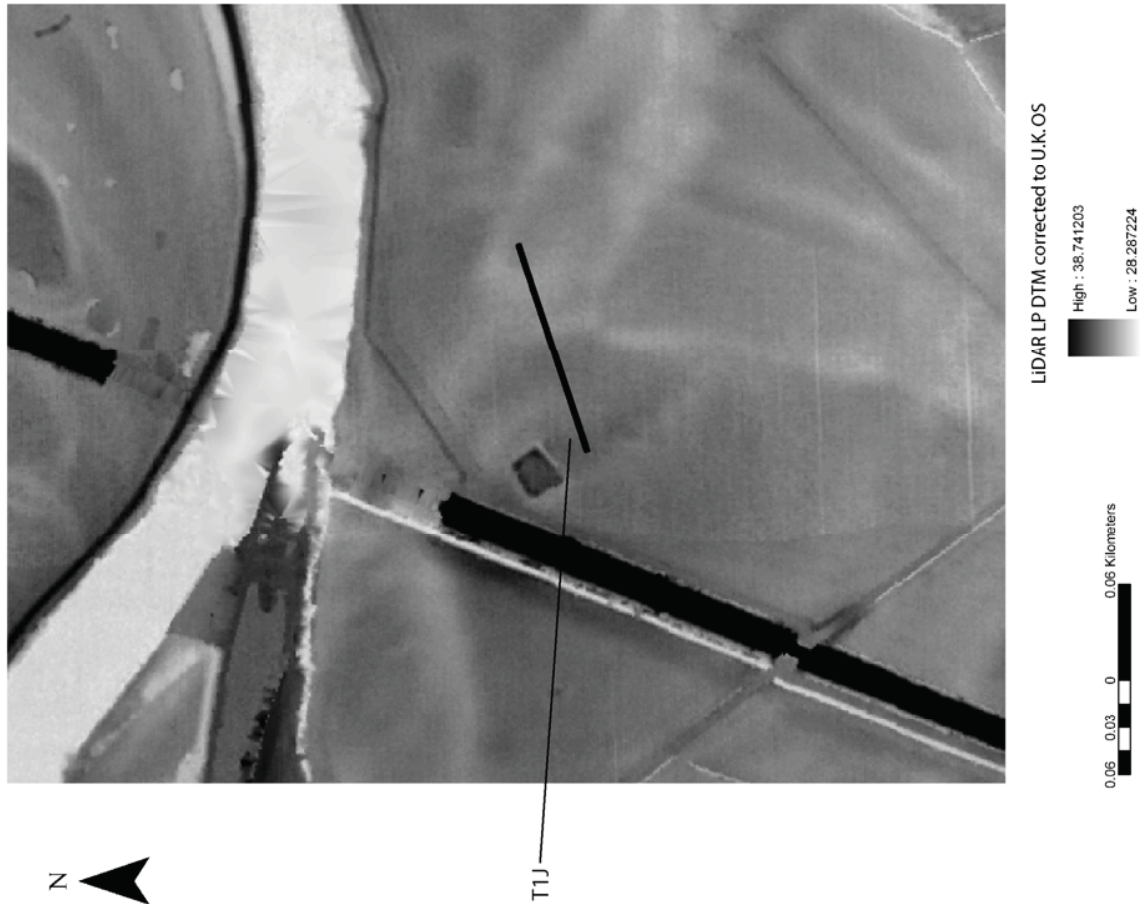


Fig 8.21: The location of transect T1J.

Transect T1J

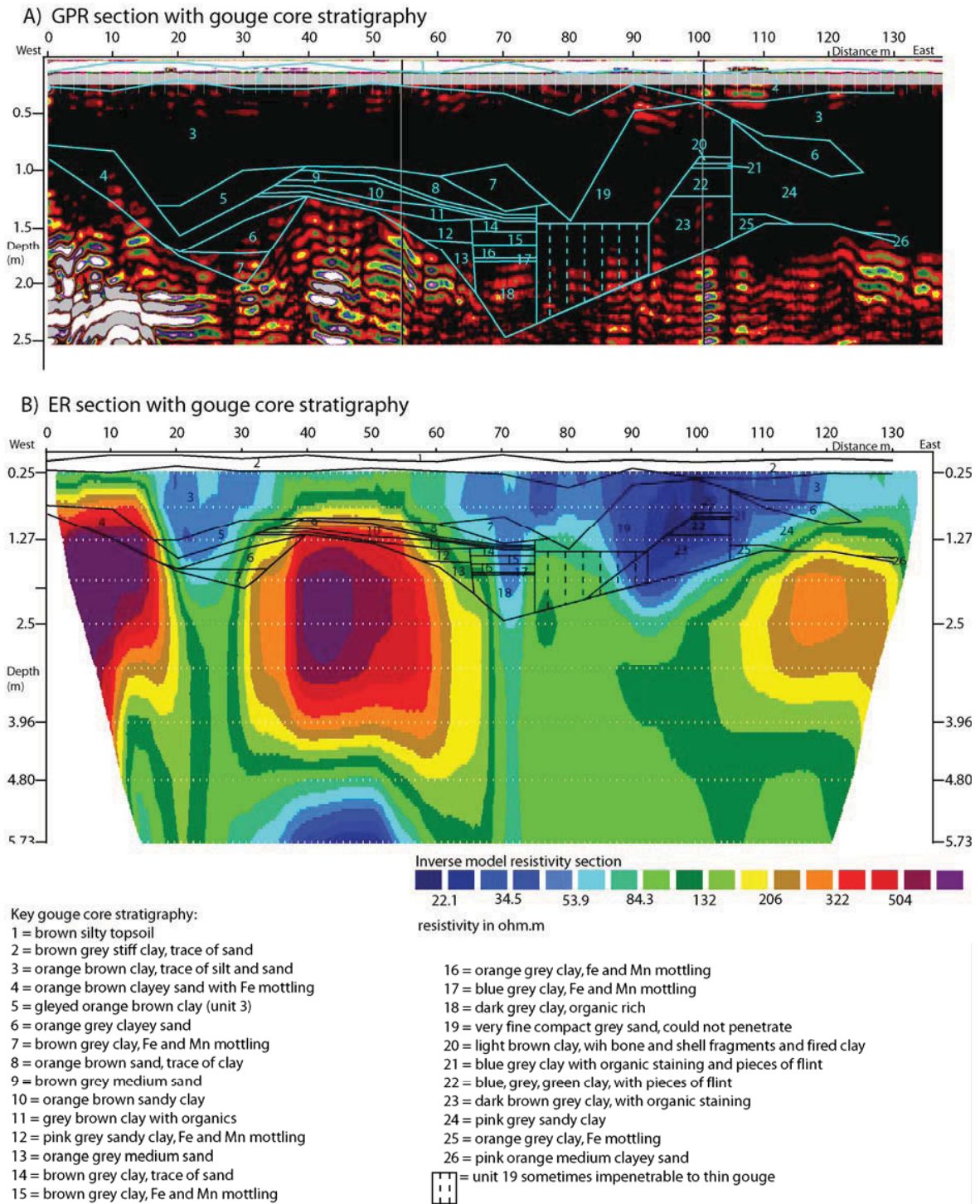


Fig 8.22: The ER transect T1J, gouge core stratigraphy combined with GPR and ER sections.

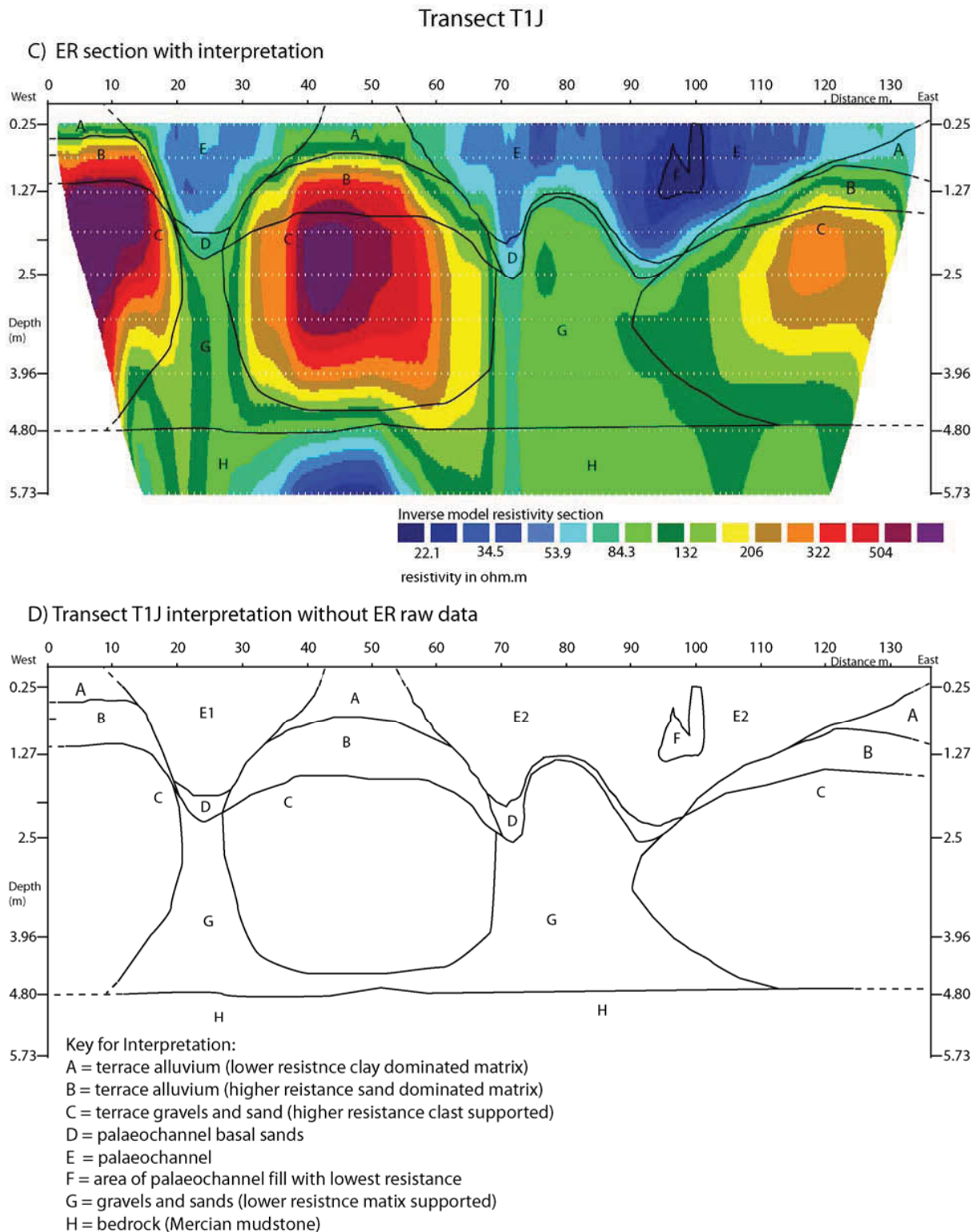


Fig 8.23: The ER transect T1J with interpretation.

8.4.9 ER transect T1K

Transect T1K was also undertaken on terrace 1 (Fig. 8.24) and was located in the same place as transect T1A (section 8.4.1). Unlike T1A, ER transect T1K used a 2m electrode spacing, running for 95m. The aim was to compare the data obtained from the 2m electrode spacing with that obtained by the 1m electrode spacing. A GPR section and gouge core transect (10m core interval) were also undertaken. The ER transect T1K has a much greater depth of penetration to c. 15.5m (Figs. 8.25 and 8.26), than using either the 0.5m or 1m electrode spacings. For this reason there is little point in comparing the GPR data with the ER section, due to the relatively shallow depth of GPR penetration compared to the deep penetration of the ER survey.

The ER section still clearly shows an area of terrace with a palaeochannel (Fig. 8.25). The relationship with the gouge core stratigraphy is strong, with the lower resistivity palaeochannel values dipping away from the higher resistance terrace feature in approximate agreement with the gouge core stratigraphy. The palaeochannel is dominated by unit 18 (blue grey gleyed clay with Fe and Mn mottling), unit 19 (blue grey clay), unit 20 (olive brown/dark grey clay) and unit 21 (olive brown/dark grey medium sand) and these correlate well with the palaeochannel identified on the ER section through low resistivity values (Fig. 8.26).

The ER section provides limited data to interpret the stratigraphy of the above gravel deposits. A higher resistivity unit is seen above the palaeochannel (unit E), with the above terrace alluvium just interpretable (unit A). The palaeochannel is well defined (unit D), with the gravel body evident (unit B). The Mercian Mudstone is visible as unit C. From the interpretation it is clear that almost half of the section depth is surveying Mercian Mudstone geology, not the gravels and alluvium, which are the strata of archaeological interest. Using the 2m electrode spacing there is a loss of data resolution in the upper profile, which contain the archaeologically important deposits. This loss of data resolution in the upper profile is highlighted by comparison with the 1m electrode interval transect T1A (Fig. 8.27).

The most striking comparison between the interpretations of T1K and T1A is the ability to define the palaeochannel morphology. T1A gives an excellent definition to the palaeochannel morphology, with a sharp boundary being seen with the gravel junction at the terrace edge and below the palaeochannel. In contrast T1K only produces a generic picture of the main geomorphological units. Although the palaeochannel is visible the detail of its precise morphology and within channel variation is lacking compared to T1A.

T1K summary:

- T1K used a 2m electrode spacing that gave a much deeper depth penetration (c. 15.5m).
- Most of the ER section surveyed Mercian Mudstone bedrock, which is archaeologically sterile.
- The archaeologically important units were at the top of the ER section, with relatively poor data resolution.
- There was still a good correlation between the gouge core stratigraphy and the ER section.
- The main geomorphological units along the transect were identifiable, but the definition of their morphology is poor compared to the 1m electrode spacing T1A survey.

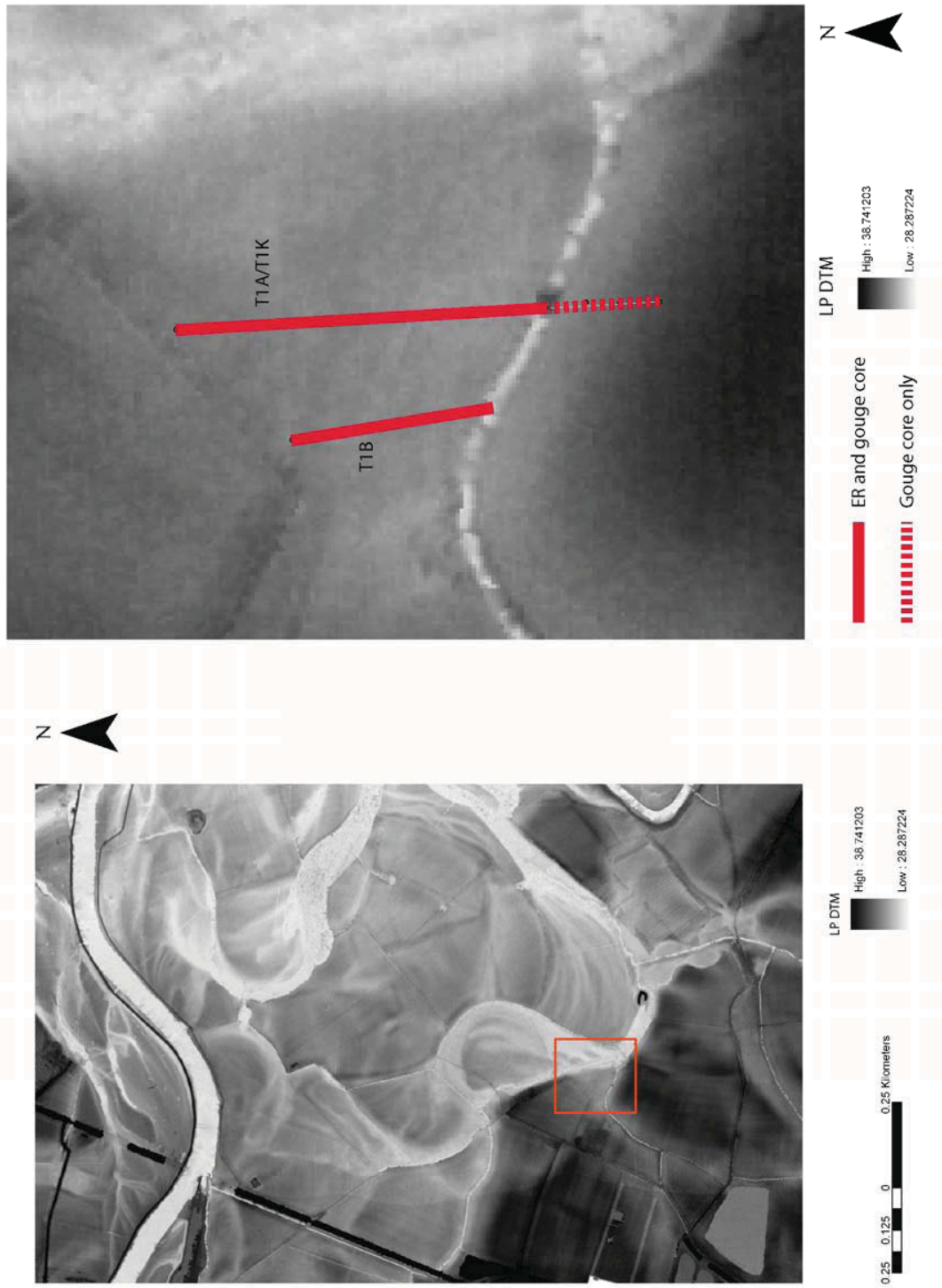


Fig 8.24: Location of ER transect T1K, on the same transect line as T1A.

Transect T1K

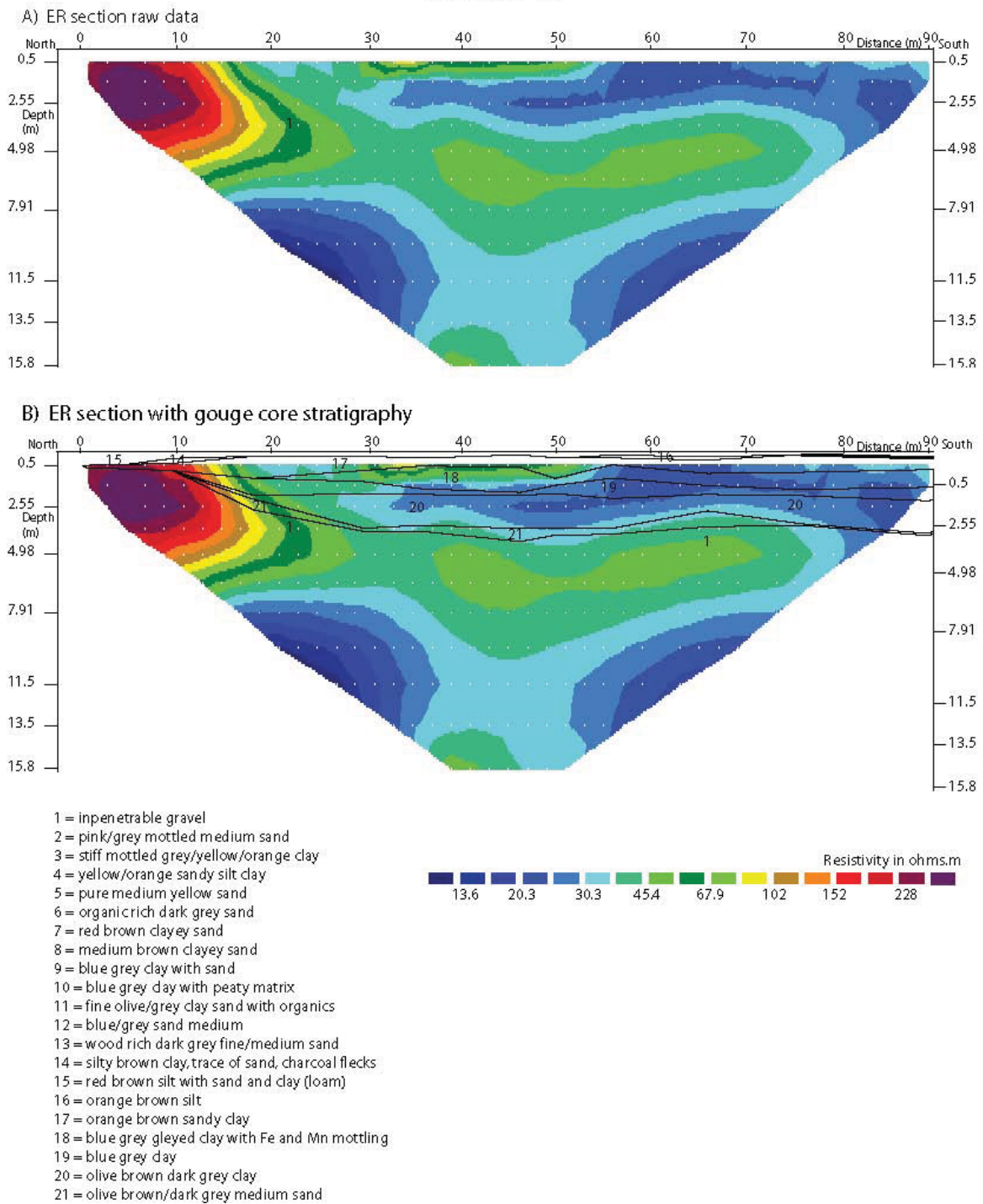


Fig 8.25: ER transect T1K, raw data (top) and with gouge core stratigraphy (bottom).

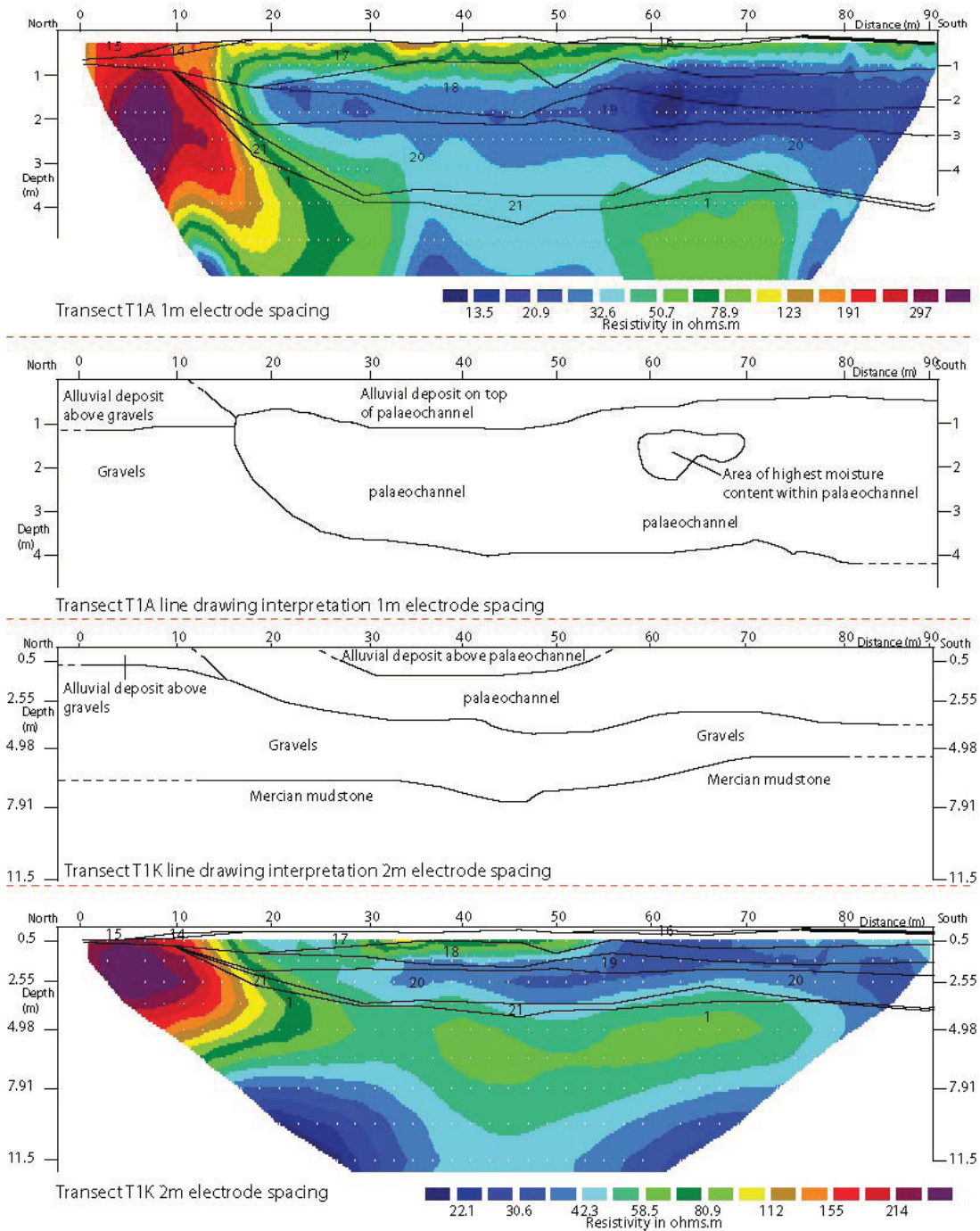


Fig 8.27: Comparison of the ER sections T1K and T1A, comparing the 2m and 1m electrode spacings. The 2m spacing has caused loss in data resolution in the upper section, with poorer definition of the main geomorphological units compared to T1A.

8.5 Modern Floodplain ER surveys

Two ER surveys were undertaken on a section of the modern floodplain. Both these sections followed the same transect but one was sampled with a 1m electrode spacing and the other with a 0.5m electrode spacing (Fig. 8.28).

8.5.1 ER Transect MFA 1m electrode spacing

The ER transect MFA was a long transect investigating two palaeochannels on the lower floodplain. The ER section clearly reveals the general morphology of the two palaeochannels (units A1 and A2), the general gravel body (units B and C), above gravel alluvium (unit D) and the boundary with the Mercian Mudstone (unit E) (Fig. 8.29).

The interpretation of the ER sections is relatively simple. The two palaeochannels are obvious as A1 and A2, separated by a bar at c. 50m, indicated as an area of deeper gravels, with shallow over gravel alluvium. This interpreted gravel bar occurs where unit C occurs, a higher resistivity value gravel unit, indicating either a clast supported gravel/lower water content gravel. Palaeochannel A1 is interpreted as being deeper than palaeochannel A2. Palaeochannel A1 has a relatively regular cross section, with the area of lowest resistance in the middle of the palaeochannel.

Palaeochannel A2 has a different morphology, with a steep bank on its southside indicating either an old river bank line or the edge of a chute channel. This morphology can be of use in deciding where to sample for palaeoecological remains. However, most of palaeochannel A2 is relatively high resistance and has a relatively low water content, indicating a lower biotaphonomic potential.

The two palaeochannels have little within channel variation evident at the 1m electrode spacing, acting as a guide to within palaeochannel sediment stratigraphy. However, based on the interpretation of this ER section palaeochannel A1 is deeper with lower resistivity values, indicating a higher biotaphonomic potential than palaeochannel A2. The over gravel alluvium is well defined (unit D) and is known to consist of an upper sediment unit of clayey silt, with a lower silty clay unit. The gravels are again clear, with the boundary with the alluvium, and the lower boundary with the Mercian Mudstone bedrock interpreted. Overall this ER transect reflects the general stratigraphy of this lower unit well, as ascertained in phase 1, with a generally low level of alluvium overlying terrace gravels

Transect MFA summary:

- Two palaeochannels (A1 and A2), the alluvium, gravels and junction between the bedrock and gravels are identifiable.
- The morphology of palaeochannel A1 shows a symmetrical channel form.
- The morphology of palaeochannel A2 shows a non symmetrical form, with a higher energy/erosive south bank and a lower energy/depositional north bank.
- Due to the deeper depth penetration the junction between the gravels and the bedrock is visible.

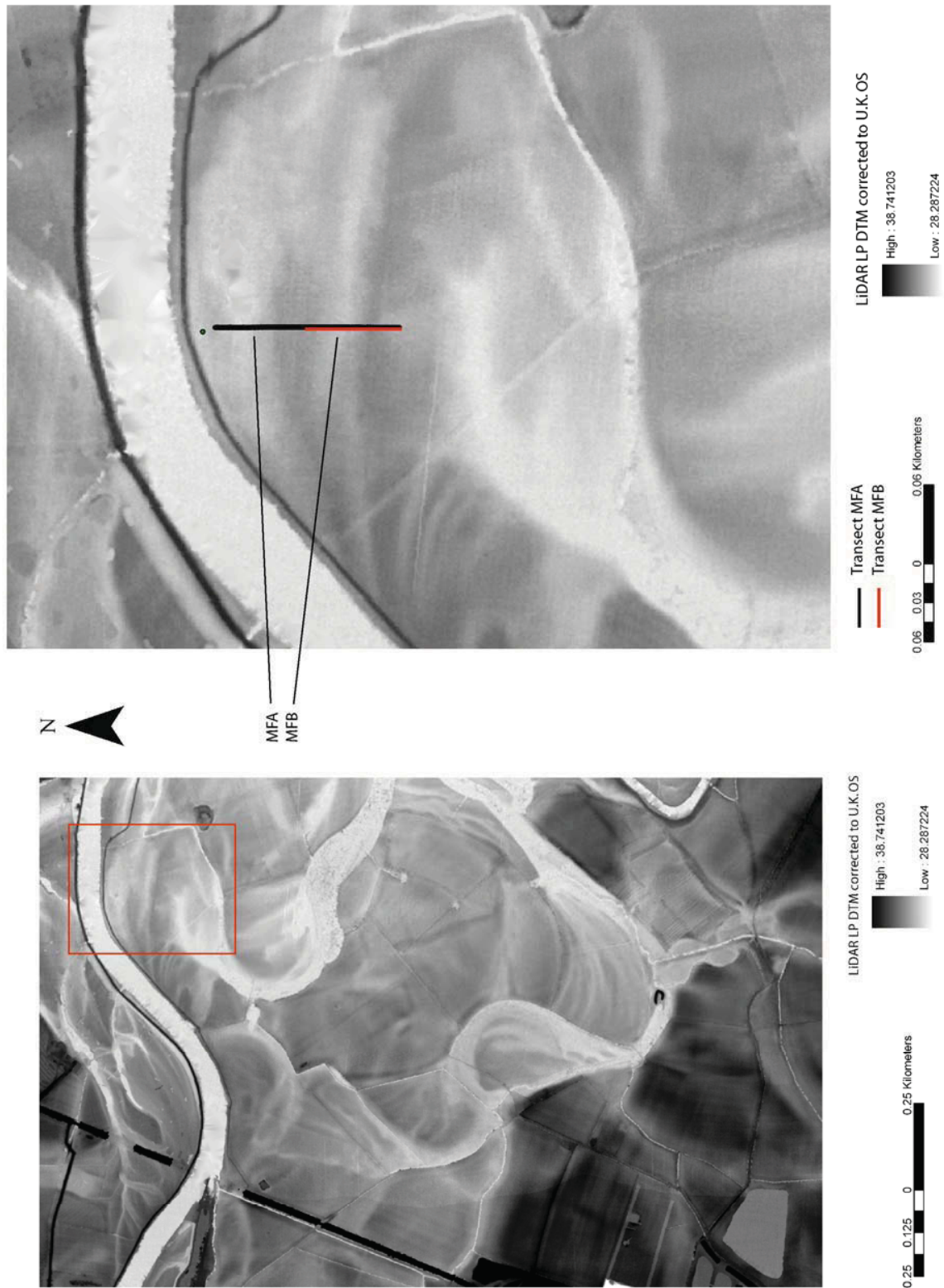


Fig 8.28: The location of transects MFA and MFB.

8.5.2 *ER transect MFB 0.5m electrode spacing*

The 0.5m electrode spacing MFB transect offers a useful comparison to the MFA 1m electrode spacing transect. The transect location relative to MFA is given (Fig. 8.28). Transect MFB started at 70m on the MFA transect and ran for 54m to 124m on the MFA transect, effectively covering palaeochannel A2. The aim of undertaking the 0.5m electrode spacing along the same transect line was so that a useful comparison could be made between the two. A general transect description will be given of transect MFB before a contrast with MFA.

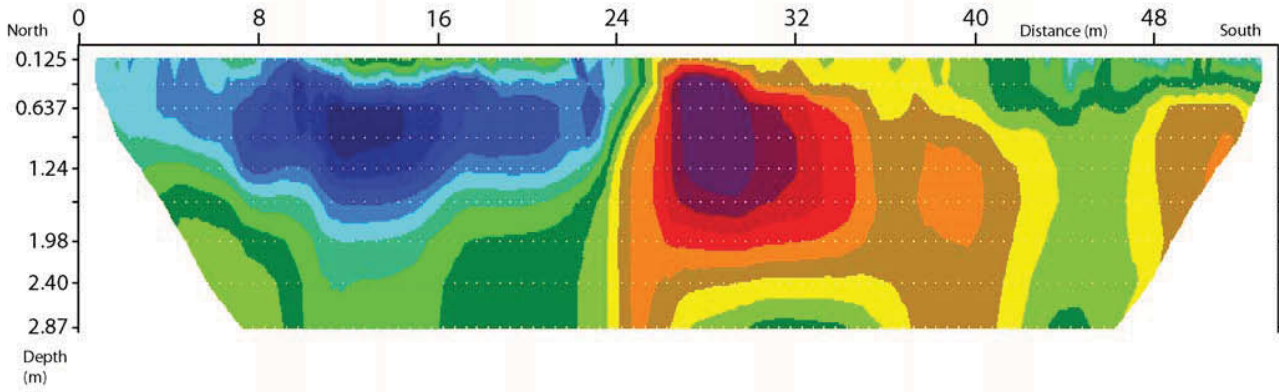
The results from the 0.5m electrode spacing revealed a depth penetration to c. 3m (Fig. 8.30). The interpretation of the ER section is similar to transect MFA. Palaeochannel A2 has a much greater definition, with the palaeochannel morphology well defined and within channel variation evident. The junction at the base of palaeochannel with the gravels is clearly evident and the area of lowest resistivity value within the palaeochannel is highlighted (unit F). Again variation in the resistivity values of the gravels are evident, with another high resistivity value gravel bar (unit C) located just to the south of palaeochannel A2 and lower resistivity gravels located beneath the palaeochannels. Another shallow palaeochannel is also visible as unit A3.

Summary transect MFB:

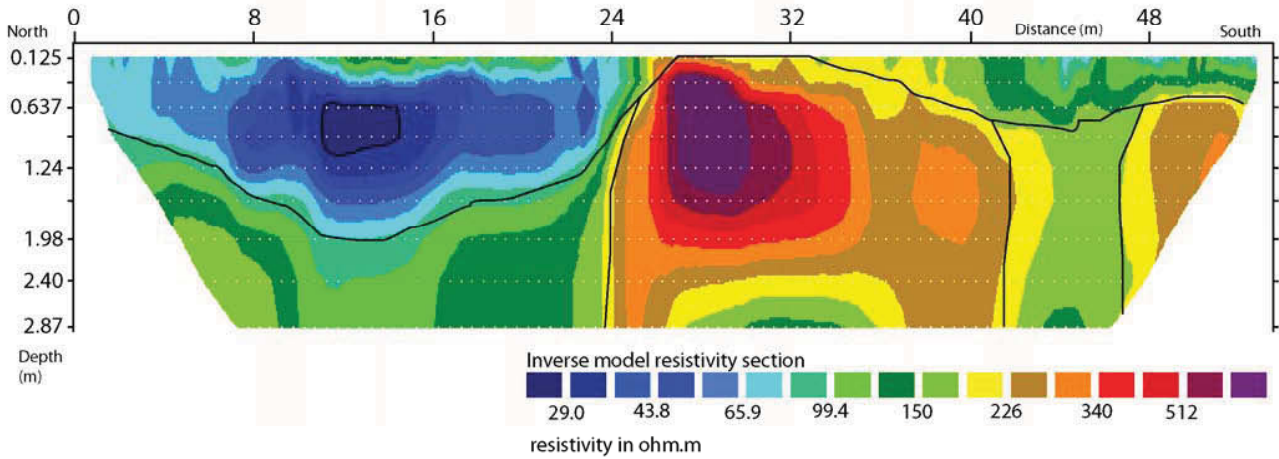
- The morphology of palaeochannel A2 is more clearly defined than in transect MFA.
- The area of lowest resistance is seen within palaeochannel A2, indicating the area of highest biotaphonomic potential.
- Due to the shallower depth penetration the junction between the gravels and the bedrock is not visible.

Transect MFB

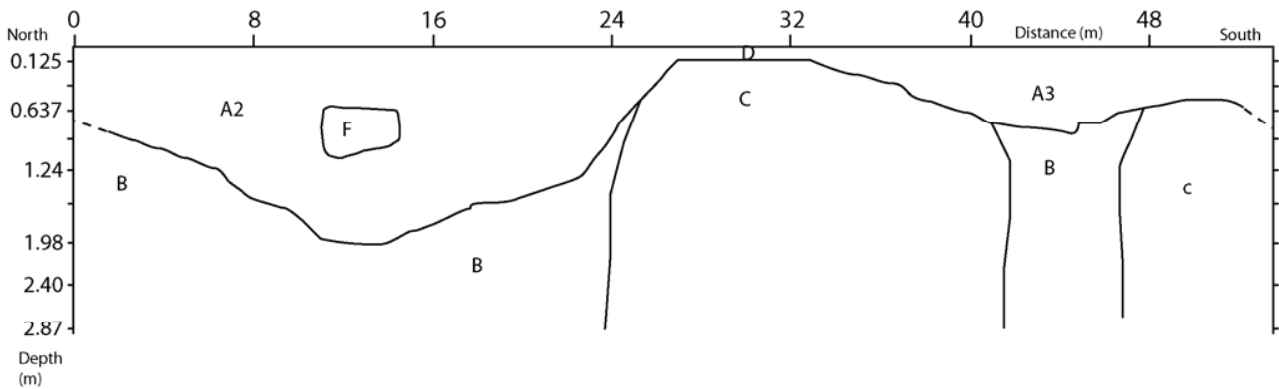
A) ER section, raw data



B) ER section with interpretation



C) Interpretation without raw data



- A = palaeochannel
- B = gravel lower resistivity (matrix supported/higher water content)
- C = gravel higher resistivity (clast supported/higher water content)
- D = above gravel alluvium
- F = area of lowest resistivity within palaeochannel

Fig 8.30: ER transect MFB.

8.5.3 Comparing 1m and 0.5m electrode spacing on the Modern Floodplain

The two ER transects on the modern floodplain provided a useful test for comparison of 1m and 0.5m electrode spacings. When Figs. 8.29 and 8.30 are compared there are several distinct differences between the two transects. These are summarised as:

- Both electrode spacings identified the main units of the palaeochannels (unit A), the above gravel alluvium (unit D) and the gravels (units B and C).
- Using both electrode spacings the gravel bar between the palaeochannels is evident.
- The 1m electrode spacing allows the junction between the gravel and the Mercian Mudstone to be interpreted. The 0.5m electrode spacing does not allow the depth of the bedrock/gravel interface to be seen, due to a shallower depth penetration.
- The 0.5m electrode spacing gives much greater clarity in palaeochannel morphology.
- The 0.5m electrode spacing brings out a much greater clarity of within palaeochannel variation when compared to the 1m, due to a greater data resolution at shallower depths.
- Although both diagrams are comparable there are differences in the general morphology between diagrams. For example the interface between the alluvium and gravel has much greater clarity from the 0.5m electrode spacing.

8.6 Methodological considerations of using ER

It is clear that ER survey has the potential to produce information for geoarchaeological assessments within alluvial environments. There are several methodological considerations when using ER in alluvial environments, which will optimise data capture and hence data usefulness. The following summary of ER methodology is derived only from the surveys undertaken on this project. Therefore, it is an assessment of ER applied to river confluences such as the river Trent, where alluvial sequences to the top of gravel is c. <4m. These can be summarised as:

1. Relationship of ER data to electrode spacings.
2. Relationship of ER data to stratigraphy.
3. Relationship of ER data to GPR data.

8.6.1 Relationship of ER data to electrode spacing

From the preceding discussions in chapter 8, it can be seen that three electrode spacings were experimented with for data capture, being 0.5m, 1m and 2m electrode spacings. Each of these three different electrode spacings provides different data capture characteristics. These are summarised (Tab. 8.1). To give an indication of cost/data capture ratios, each transect takes 50 minutes, regardless of electrode spacings at these intervals. Therefore, distance covered after 3 transects could also equate to distance covered after 2hrs 30mins

Electrode spacing	Maximum depth of penetration	Distance of first transect	Distance covered after 3 transects (2hrs 30mins)
2m	15.5m	94m	142m
1m	6m	47m	69m
0.5m	3m	23.5m	35.5m

Tab 8.1: Summary of field considerations of using different electrode spacings.

From this summary it can be seen that as electrode spacing increases, depth penetration increases, but there is an associated loss in data resolution. From the comparison it can be seen that the 2m electrode spacing allows rapid distance coverage and deep penetration. However, data resolution is generally poor in the gravels and alluvium, with most of the section detailing variation in bedrock, although features such as large palaeochannels are visible. Therefore, a 2m electrode spacing has very limited application in surveys within this type of alluvial environment, due to poor data resolution in the sediment units that are liable to contain archaeological materials dating from the Holocene.

The 1m electrode spacing provides good all round data capture, allowing features such as the bedrock/gravel junction and alluvium/gravel interface to be mapped. The detail in the above gravel alluvium is good, allowing identification of features such as palaeochannels and gravel/palaeochannel bounding surfaces to be identified. The whole gravel section is evident with using the 1m electrode spacing and variation in gravel structure is evident. Areas of higher and lower resistivity values can be identified, which has importance for identifying rare Pleistocene deposits that may contain organic material. The 1m electrode spacing allows a depth of penetration to 6m, which is sufficient within this environment and allows relatively rapid coverage. A 1m electrode spacing should be used for initial assessment of deposits.

The 0.5m electrode spacing allows a high level of data resolution within the upper gravels and the above gravel alluvium. The depth of gravels and the interface with bedrock is not evident, due to penetration being too shallow. However, the high level of data resolution in the upper deposits allows variations in resistivity values to become readily apparent, allowing areas of high biotaphonomic potential within palaeochannels to be identified. The rate of ground coverage is much lower than the 1m electrode spacing and therefore it is not suggested that the 0.5m electrode spacing is used for initial sediment assessment, but instead used selectively to target areas already identified through other techniques, e.g. gouge core survey or remote sensed data etc. A summary of the assessment of the different type of electrode spacings is given (Tab. 8.2).

Electrode spacing	Ability to identify above gravel alluvial variation (0 – 4m range), e.g. palaeochannel top of terrace	Ability to identify alluvial gravel interface	Ability to identify depth of gravels and variation within the gravel	Ability to identify gravel bedrock interface
2m	Low	Moderate	Moderate	Moderate
1m	Moderate	Moderate	High	Moderate
0.5m	High	High	Low/not possible	Low/not possible

Tab 8.2: Summary of the data capture properties of different electrode intervals.

8.6.2 Relationship of ER data to stratigraphy

The relationship of ER data to gouge core stratigraphy has shown that ER is successful in identifying large changes in subsurface sediment architecture, such as the difference between an area of terrace and a palaeochannel. ER sections do not have the ability to identify much smaller more discrete changes in stratigraphy, such as thin sand lenses interspersed by clay units in palaeochannel fills. The relationship of ER to sediment architecture, as revealed through gouge core survey, can be summarised under its ability to map ‘macro-stratigraphy’ and ‘micro-stratigraphy’.

Macro-stratigraphy in this sense can be defined as the identification of major geomorphological units such as palaeochannels, gravels units, above gravel alluvium, etc. In this sense ER data can be used to identify these features and define their dimensions and morphologies. Numerous examples have been given of ER defining features such as palaeochannels, with these palaeochannels also revealed through gouge core survey. The relationship of the depth to gravels between the ER sections and the gouge core survey has also been very strong, with little disagreement between the two.

Microstratigraphy can be defined as the variation of sediments within macro-stratigraphic units, e.g. variation in the sediment architecture of a palaeochannel fill. In this sense ER is less useful, as slight changes between sediments e.g. a clay changing to a sandy clay, and also very thin sediment units, e.g. thin sand lenses in between clay units, were simply not evident in the ER data, even when using the 0.5m electrode spacing. However, some form of micro-stratigraphy was detected when changes in sediment composition between adjacent units were large, such as the change between a fine clay and a coarse basal sand in a palaeochannel.

Further to this changes in the composition of macro-stratigraphic features could be inferred based on resistivity values, although this would not directly relate to changes in sediment units as revealed through the gouge core survey. For example, palaeochannels had the areas of lowest resistivity values identified, and these were considered to be the areas of highest biotaphonomic potential. Such areas often corresponded to where the palaeochannel was deepest and therefore had a greater capacity to retain water. Such areas of low resistivity values did often correspond to recorded sediment units that had a high biotaphonomic potential, based on field observations.

In summary ER survey cannot be used to map individual sediment units. Macro-stratigraphic features such as palaeochannels are easily identifiable, as are large-scale variations within their composition. The depth to the gravels was consistent with that recorded by gouge core. However, if mapping individual sediment units is the goal of the survey it is essential to use gouge core stratigraphy combined with ER.

8.6.3 Relationship of ER data to GPR data

GPR had already been extensively tested within the Trent/Soar project, to assess its usefulness within alluvial environments. Its major shortcoming was its inability to penetrate and map the sediment within palaeochannels. Therefore, ER survey was used to investigate sediment stratigraphies of palaeochannel fills. As shown above (chapter 8), numerous transects were conducted using the dual approach of GPR and ER. This has allowed a comprehensive assessment of the two techniques working in tandem and the differences and similarities between them. Generally, the ER sections shown in this chapter were undertaken on palaeochannels or areas

immediately adjacent to palaeochannels. From Phase I of this project it can be seen that these are the areas where GPR performed worse.

The comparison of the GPR data with the ER data is purely based on visualisation, not on numerical data values in this instance. It is acknowledged that mathematical modelling could be carried out between the two data sets, to investigate correlations between geomorphological features and numerical values. However, this is outside of the scope of the current discussion. Furthermore, as the identification of features was based on visual assessment of data, it is acceptable to compare data sets based on visualisation at this stage of the analysis.

Transect T1J is shown at a series of transparencies to illustrate the general comparisons between ER and GPR. From the four diagrams (Figs. 8.31 – 8.34) it is clear that both the GPR and ER reveal the depth to gravel, and both techniques correlate on this depth. The correlation between the ER and GPR data in the gravels is excellent, with both techniques identifying a series of higher reflecting/resistivity units in the gravels. The GPR reveals more of the internal structure of the gravel bodies, with the harder reflecting areas relating to the structure of gravel, i.e. a harder reflecting gravel equates to a larger clast size/drier gravel body. Likewise, the ER data displays areas of higher resistivity values where the GPR reveals units of higher reflectance in the gravels. Above the gravels the GPR reveals no real information on the stratigraphy of the alluvium. In contrast the ER section shows areas of lower resistivity values that define the morphologies of two palaeochannels.

This pattern has repeated itself throughout the combined ER and GPR transects. In all of the transects shown in this chapter GPR failed to map the sediments within the palaeochannels. On the sides of the palaeochannels GPR has mapped the gravel bedrock interface, but generally not the alluvium above gravel. However, on areas of terrace GPR does have the ability to map individual sediment units, and as shown in Phase 1, this can be related to gouge core stratigraphies very closely. This is due to sharp boundaries between different units producing different RDP's and resulting in discontinuities. In contrast ER survey does produce data within palaeochannels. As discussed above (chapter 8) this does not necessarily relate to discrete sediment units identified through gouge core survey, but more generally changes in subsurface stratigraphy that reflect 'macro stratigraphy' not 'micro stratigraphy', i.e. a palaeochannel is identified, with areas of lowest resistivity values interpreted (macro-stratigraphy), but discrete changes in different sediment units in the palaeochannel fill as revealed through the gouge core are not revealed (micro-stratigraphy).

Thus the relationship between the two techniques and the data they can reveal is clear. ER sections can produce information on the morphology of palaeochannels and variation in resistivity values related to stratigraphy within palaeochannels. ER can also identify the depth to the alluvial gravel interface. In contrast GPR cannot be used to determine palaeochannel stratigraphy. It is of most use to map the depth to gravels and variations within the gravels composition. It can also be used to map areas of drier terrace to show changes in the above gravel stratigraphy.

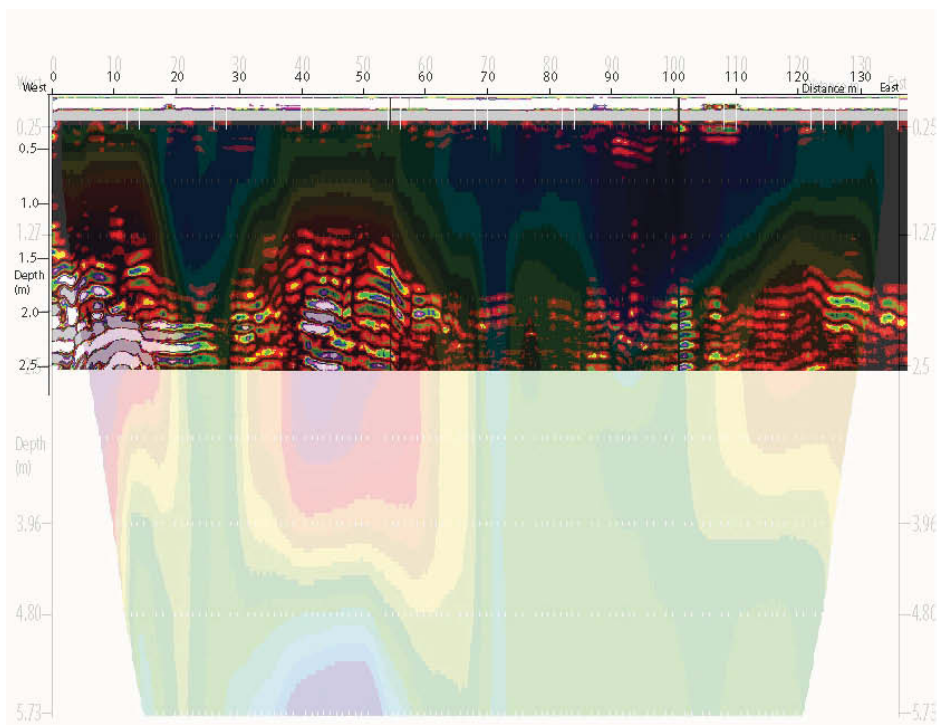


Fig 8.31: Combined visualisation of GPR and ER data, with the ER section at 80% transparency.

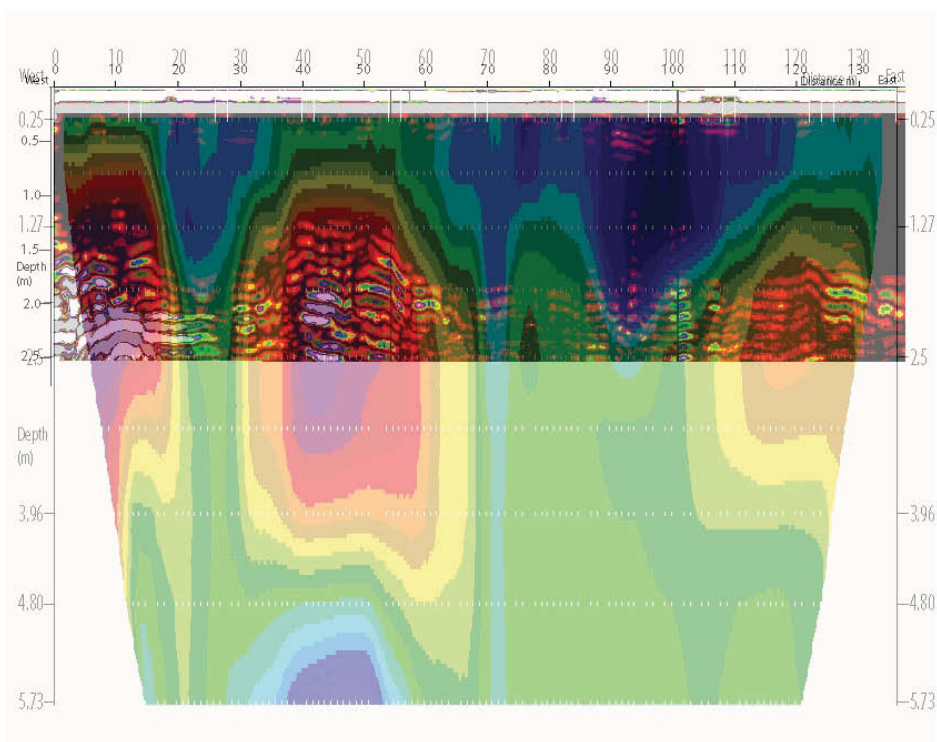


Fig 8.32: Combined visualisation of GPR and ER data, with the ER section at 60% transparency.

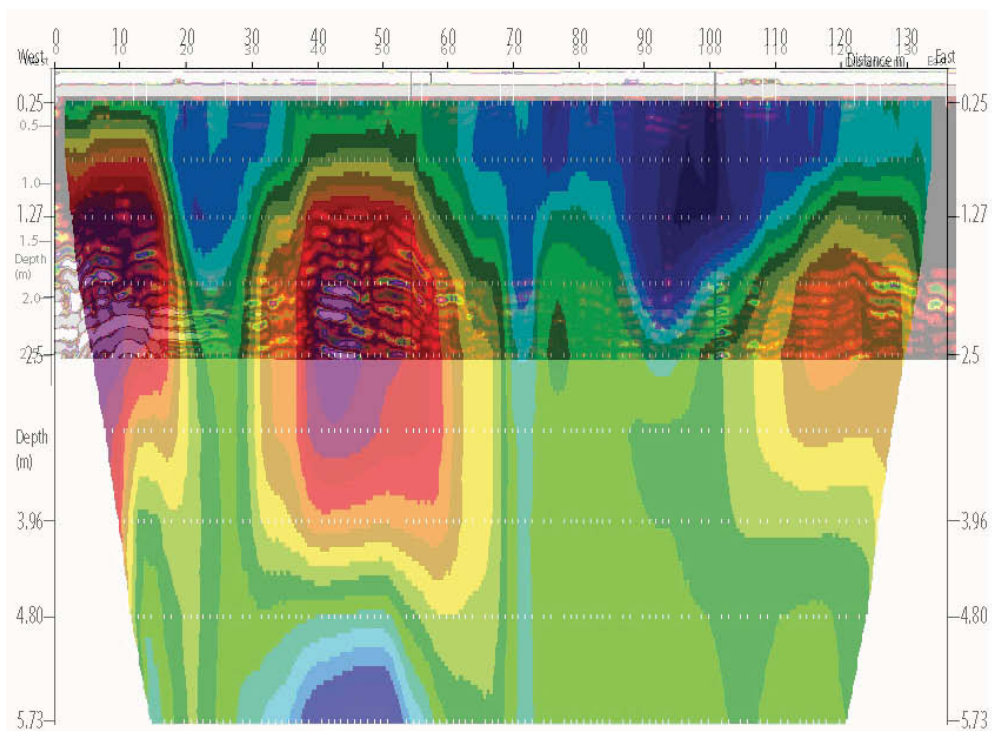


Fig 8.33: Combined visualisation of GPR and ER data, with the ER section at 40% transparency.

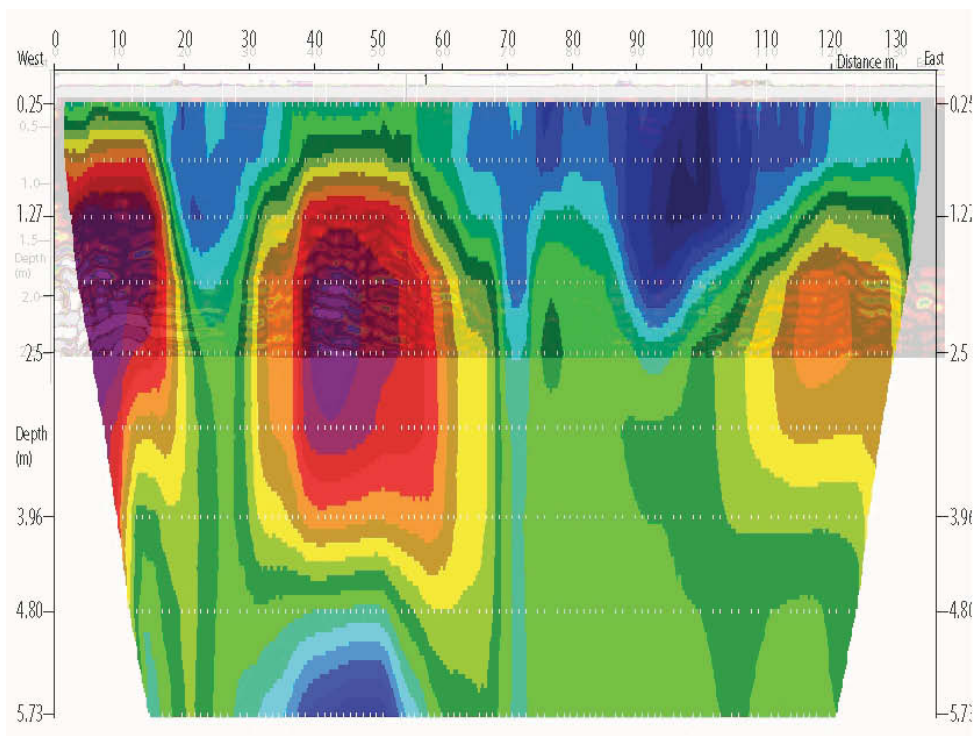


Fig 8.34: Combined visualisation of GPR and ER data, with the ER section at 20% transparency.


8.7 Ranking palaeochannels by biotaphonomic potential based on ER resistivity values

With the application of ER in this study, its ability to map palaeochannel and highlight variation in their composition has been discussed. However, is it possible to take this data further and rank the biotaphonomic potential of the different palaeochannels, based on their resistivity values? The resistivity values of the palaeochannels is partly a function of sediment architecture, although as discussed above, ER does not define discrete sediment units as mapped by gouge core survey. It is also a function of the depth and morphology of the palaeochannel and both of these have important taphonomic consequences for the preservation of organic remains.

Based on this logic it should be possible to rank the palaeochannels based on their lowest resistivity values and this ranking should relate to biotaphonomic potential. Although different electrode spacings were used, the resistivity values are given in ohm.m, and so it should be possible to compare between electrode spacings. This stated, a smaller electrode spacing gives better data resolution in the top 3m of the soil profile, which in this study is where the palaeochannels are located. Therefore, smaller electrode spacings are likely to produce lower resistivity values overall, due to their ability to map more variation in palaeochannel fills.

The ranking criteria is simple. The palaeochannel with the lowest resistivity value is considered to have the highest biotaphonomic potential. Whilst this is clearly a gross over simplification, it is known that palaeochannels display the lowest resistivity values where they are deepest. Thus factors such as depth and general channel morphology are already partly related to the resistivity value. However, it is obvious that it would be easier to provide a more complex model, factoring characteristics such as palaeochannel depth, palaeochannel width, etc.

From this simple criteria the palaeochannels are ranked (Tab. 8.3), with the palaeochannels at the top having the lowest value.

ER section	Lowest within palaeochannel resistivity value	Electrode spacing	Biotaphonomic potential (based on resistivity values)
T1E	5.1	1m	Highest  Lowest
T1F	5.3	1m	
MFA	5.9	1m	
T1A	6.1	1m	
T1G	6.2	0.5m	
T1K	6.9	2m	
T1H	8.4	0.5m	
T1C	9.3	1m	
T1J	9.7	1m	
T2A	10.6 (gravel value)	1m	
T1D	12.7	0.5m	
MFB	14.2	0.5m	
T1B	15.6	0.5m	

Tab 8.3: Ranking of biotaphonomic potential of palaeochannels based on resistivity values.

From the table it can be seen that the resistivity values do show a broad trend in biotaphonomic potential. Palaeoenvironmental samples were taken from close to transects T1A/T1K, which were

considered to have a high biotaphonomic potential. The palaeochannel in MFA A1 clearly has a higher potential than palaeochannel A2 in MFB.

From the ER transects within this study it can be seen there are a lot of palaeochannels with the range of between 6 – 10 ohms.m. This can be considered to be a median value, and any palaeochannels in this range should be cored for palaeoenvironmental samples. Palaeochannels with minimum values over this range of 10 ohm.m can be considered to have a low biotaphonomic potential. However, there are clearly factors that are also skewing this ranking order. Of prime importance is the degree of standing water within the palaeochannel. The palaeochannel investigated through ER transect F was interpreted ‘in the field’ as having a low potential, but it is very high in this ranking, primarily due to it holding standing water. In addition, the potential of a palaeochannel for palaeoenvironmental deposits is also a function of depth, which this particular model does not directly take account of. Thus although palaeochannel T1F is extremely shallow and has a low biotaphonomic potential in reality, based on this simple model it is given a high potential.

8.8 Overview and summary

Overall ER has been effective within this study. The main points of using ER within alluvial geoarchaeological assessments can be summarised as:

- Different electrode spacings produce different data outputs.
- A 1m electrode spacing should be used for initial assessment of subsurface floodplain features.
- A 0.5m electrode spacing should be used for more detailed investigations of specific features, e.g., detailed mapping resistivity variation of a palaeochannel.
- A 1m electrode spacing allows the alluvium/gravel junction, the depth of the gravel body and the gravel/bedrock interface to be seen.
- A 0.5m electrode spacing only allows the alluvium/gravel junction to be imaged, although greater data resolution is provided in the upper part of the profile.
- A 2m electrode spacing does not produce data of a sufficient quality to accurately map geomorphological features in this depth range (0 – 6m).
- ER can be used to map macro-stratigraphic features, e.g. palaeochannels, gravel bodies, etc.
- ER can be used to assess sediment variation within large geomorphological units, such as resistivity differences in palaeochannels and gravel units.
- ER is not effective at defining microstratigraphy, such as slight changes between thin layers of sediments within a palaeochannel.
- ER and GPR work well when combined together to model sub-surface stratigraphy.
- ER and GPR show good agreement on the depth to gravels on areas of terrace.
- ER works effectively with gouge core survey to define sub surface sediments.
- ER and gouge core stratigraphy show good agreement on the depth to top of gravels.
- ER is most effective at providing data on the morphology of palaeochannels and changes in their fill resistivities.
- GPR is most effective at defining sub surface stratigraphies on areas of terrace.
- ER cannot be used in absolute terms to define sub surface sediments, e.g. a reflective unit of 93.6ohms.m equates to a blue grey sandy clay unit. Rather, changes in subsurface sediments have to be interpreted from the contouring of ER section. This is a subjective process, rather than an exact science. Differences in interpretation between different human operators can occur!

Chapter 9. A geoarchaeological model of the Trent-Soar Confluence Zone

9.1 Generalising and modelling the chronostratigraphy

On the basis of the radiocarbon dates and the OSL dates it has been possible to date the floodplain according to basal age of the floodplain and fine sediments above the gravels (overburden). This can be compared with the chronostratigraphic model proposed in Phase I and re-introduced in Section 5.1 of this report (Figs. 9.1, 9.2 and 9.3).

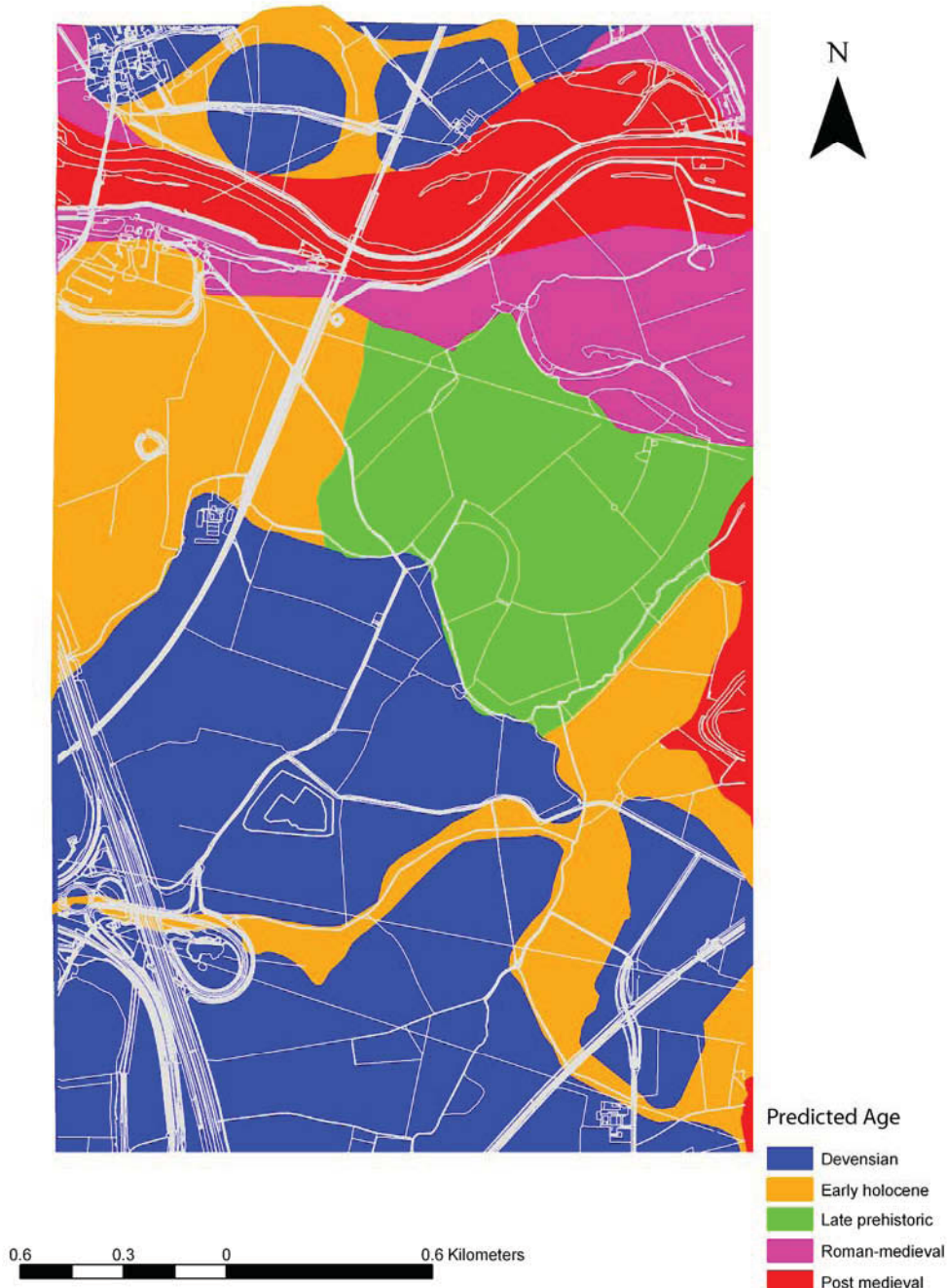


Fig 9.1: The original chronostratigraphic model produced in phase I.

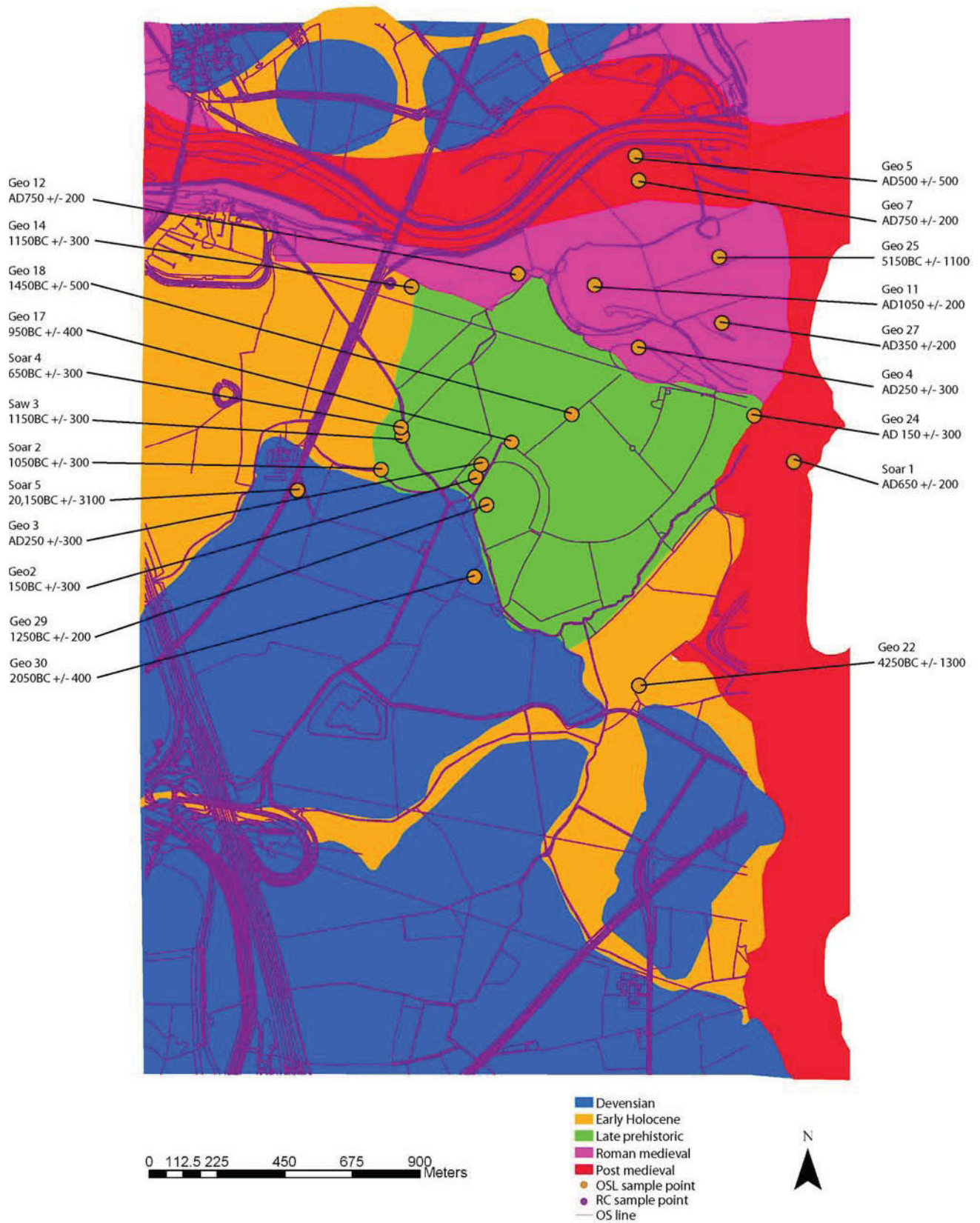


Fig 9.2: A map of the confluence area zoned into landscape blocks of a predominant age with OSL dates superimposed.

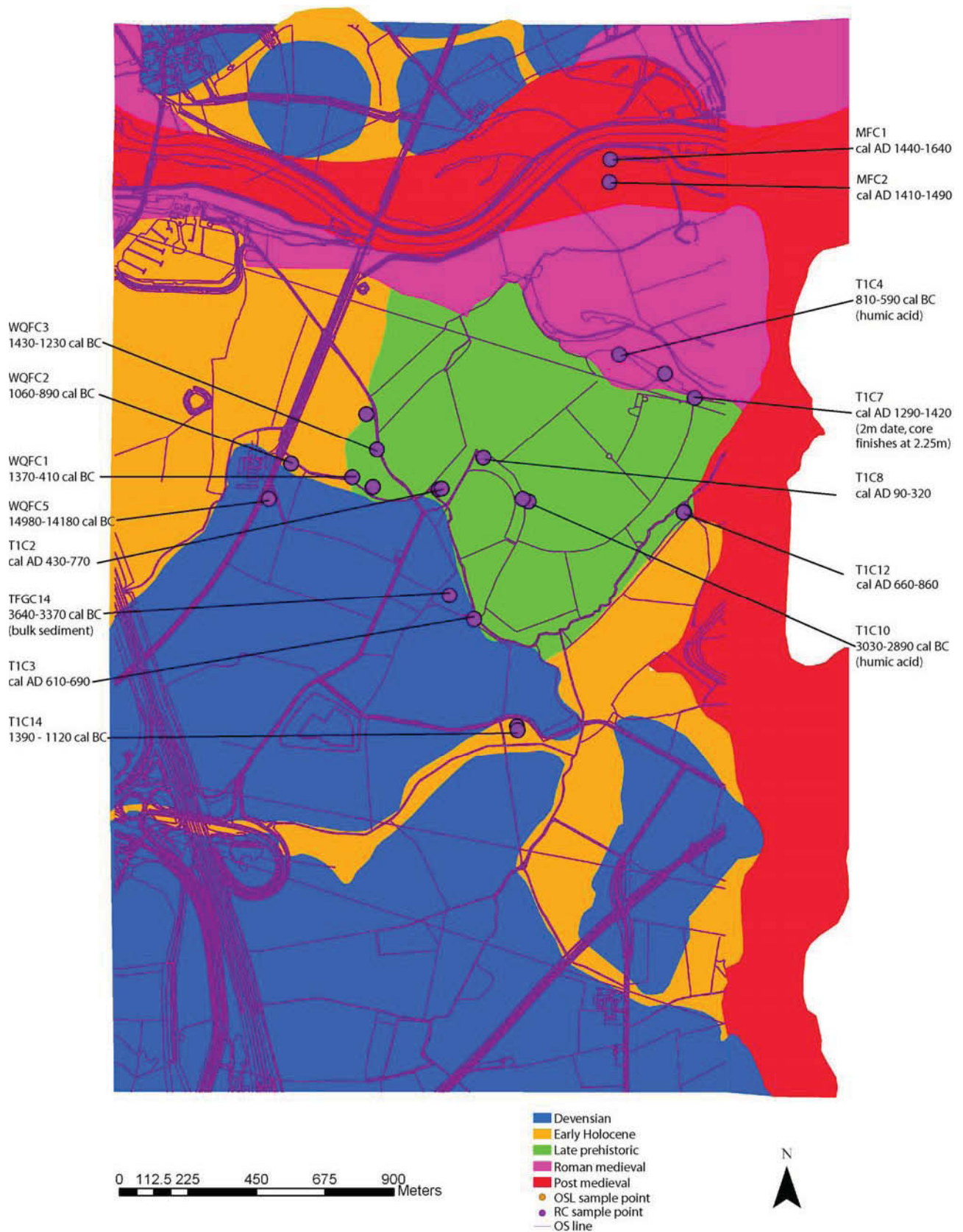


Fig 9.3: A map of the confluence area zoned into landscape blocks of a predominant age with 14C dates superimposed.

		Chronostratigraphic model				
		<i>Devensian</i>	<i>Early Holocene</i>	<i>Late Prehistoric</i>	<i>Roman-Medieval</i>	<i>Post Medieval</i>
Observed	<i>Devensian</i>	-				
	<i>Neolithic</i>		1			
	<i>Bronze Age</i>		6	3	1	
	<i>Roman-British</i>			3		
	<i>Late Medieval</i>				3	1

Tab. 9.1: Correspondance (confusion) of matrix of chronostratigraphic model with observed dates.

As can be seen from a comparison of the chronostratigraphic model with the observed model there are strong similarities and differences (Tab. 9.1).

9.2 Development of a valley floor evolution model

The dating and the stratigraphy have been combined to produce a model of the evolution of the confluence area in the Late Devensian-Holocene using archaeological time periods (Figs. 9.4 – 9.9). The phasing is not absolute and we get glimpses of earlier phases preserved in predominantly later phases of depositional activity, the best example being the Neolithic palaeochannel which crosses the meander core of the major central meander loop which is occupied (probably reoccupied) in the Romano-British period. Further work is currently underway to refine this model.

However, from the extensive dating programme some pertinent observations can be made regarding the evolution of the floodplain and its geoarchaeological potential. Of primary importance is the antiquity of the gravels of terrace 1. These clearly predate the majority of the palaeochannels on terrace 1, and as the OSL dates and dendrochronological dates clearly show, date from the Neolithic onwards. In addition WQFC5, located just above the Devensian gravels, shows some areas of terrace 1 have even earlier dates of formation, with potential preservation of human material culture and palaeoecological remains from the early Mesolithic. Clearly the paucity of archaeological remains on terrace 1 is a function of floodplain development, with a relatively deep alluvial blanket on top of gravels hiding archaeological remains to conventional methods of archaeological prospection.

The second important observation is that most of the palaeochannels have incised into older gravels deposits and largely post date the gravels. This model of floodplain evolution places heavy emphasis on avulsion, the re-occupation of channels and levee and overbank sedimentation as the key processes that pattern the geoarchaeological record and not meander migration, lateral erosion and aggradation that are normally seen as the patterning processes. This has important implications for similar high-energy floodplains as well as the lower sedimentary fills of lowland floodplains. Thus large portions of terrace 1 have the potential for preservation of archaeological and palaeoecological remains, with erosion being generally related to avulsion events and reoccupation of existing palaeochannels. Meander migration has been limited and thus the high level of overbank sedimentation has created a generally ‘preserving’ environment on terrace 1 through accumulation of overbank sedimentation. In addition to the known archaeological record located on terrace 2, terrace 1 has a high geoarchaeological potential from the Neolithic onwards.

The main caveat of this model is that the landscape units defined here are themselves diachronous to a variable degree. However, this variation is almost certainly systematic with the palaeochannel belts being of limited diachrony (decades to a century or two) whilst the intervening floodplain units can be diachronous over millennia, the extreme example being the composite terrace to the southern end of Warren Farm Quarry. Whilst this does not render the floodplain chronostratigraphic zonation methodology invalid it does place some limits on predictive resolution.

There are many ways in which the archaeological resource as revealed by Chapter 2 relates to the sedimentological and chronostratigraphic model devised here. These include the spatial patterning of the archaeological resource in the target area. For example the very uneven distribution of find locations is well explained by the chronostratigraphic and dated confluence evolution model with high density in the SW of the area on terrace 2 and only occasional finds on terrace 1 and the lower floodplain. However, as the model demonstrates, finds do and will occur on the terrace 1 and lower floodplain (almost certainly under the veneer of overbank sediments), due to the avulsive nature of channel change hypothesised in the model and proven by the dating. The reason is that this particular type of confluence evolution in effect preserves segments of older floodplain between younger channel belts. The result is two contexts of preservation, one on and in old floodplains preserved under a blanket of later overbank deposition and secondly archaeology related to channels and riverbanks located in the palaeochannel zones. By this mechanism artefacts of almost any period could be preserved, but they will be strongly patterned by this history of channel and confluence evolution.

The model also helps to explain cultural and technological aspects of the archaeology. The Romano-British settlement on the low terrace in the SW of the study area was almost certainly deliberately located along the edge of the then River Soar, which would have been used for water supply and waste disposal. Chapter 2 also alludes to possible crossing points in the Anglo-Saxon, Medieval and Post-medieval periods. The lack of a definite location and the fact that the first bridge appears to be built (in the detailed study area) across the Soar, at Ratcliffe-on-Soar, only in the Post Medieval period suggests that no permanent crossing points existed, but instead there were fords at suitably shallow locations. This is supported as being likely by the model as the crossing point of the Soar would have had to move eastwards as the confluence migrated in avulsive episodes. Chapter 2 also mentions the documentary evidence of channel change that includes reference to a major avulsion in 1402 which may have created the Sawley Loop palaeochannel. The dating in the study area suggests that it may also have been responsible for the abandonment of the southerly palaeochannel and occupation by the main channel flow of the northerly Soar palaeochannel.

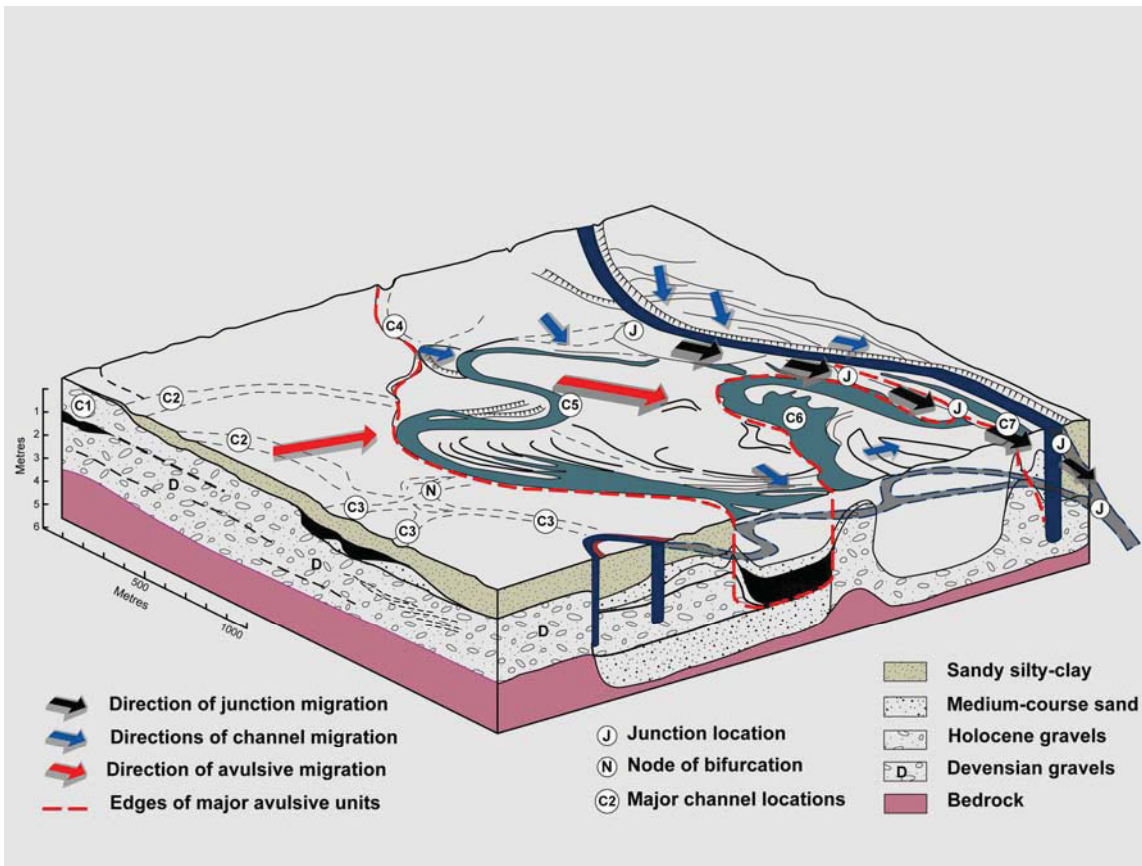


Fig 9.4: Neolithic channels flowing approximately S-N and depositing terrace 1.

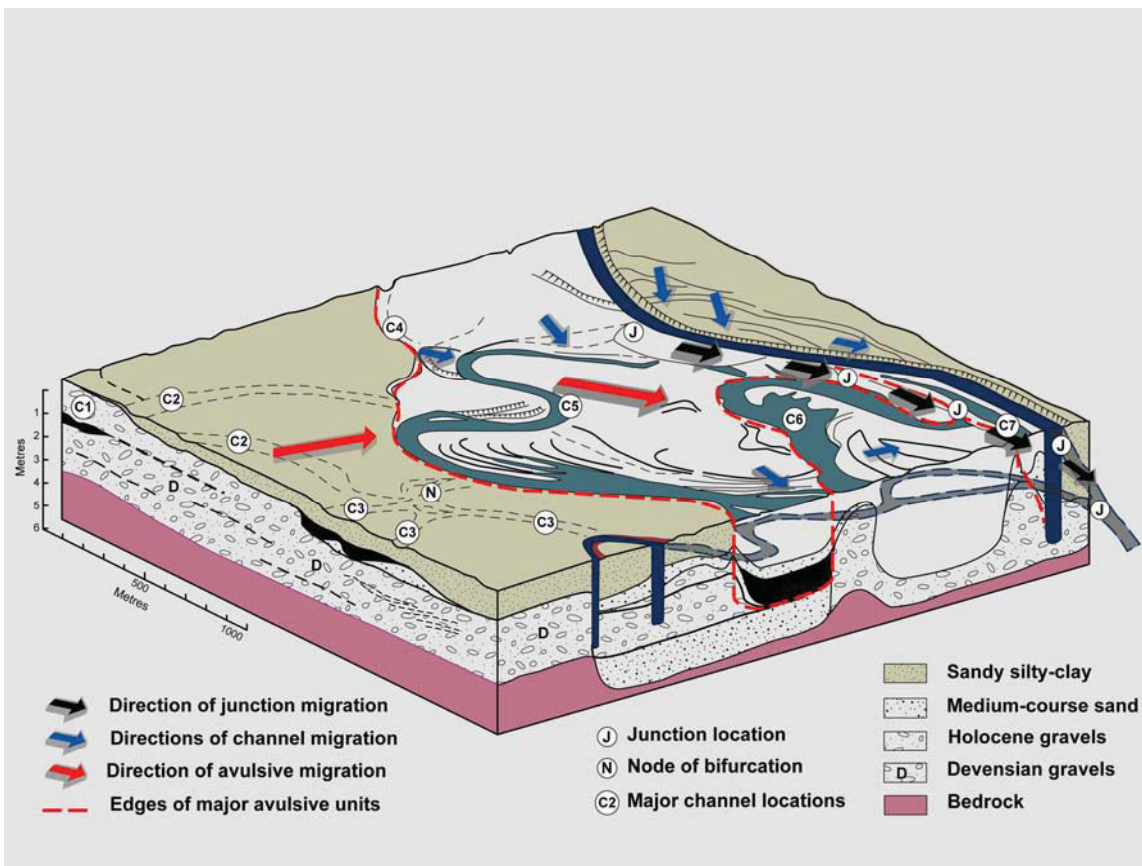


Fig 9.5: Bronze Age channels trending SE-NW abandoned on terrace 1.

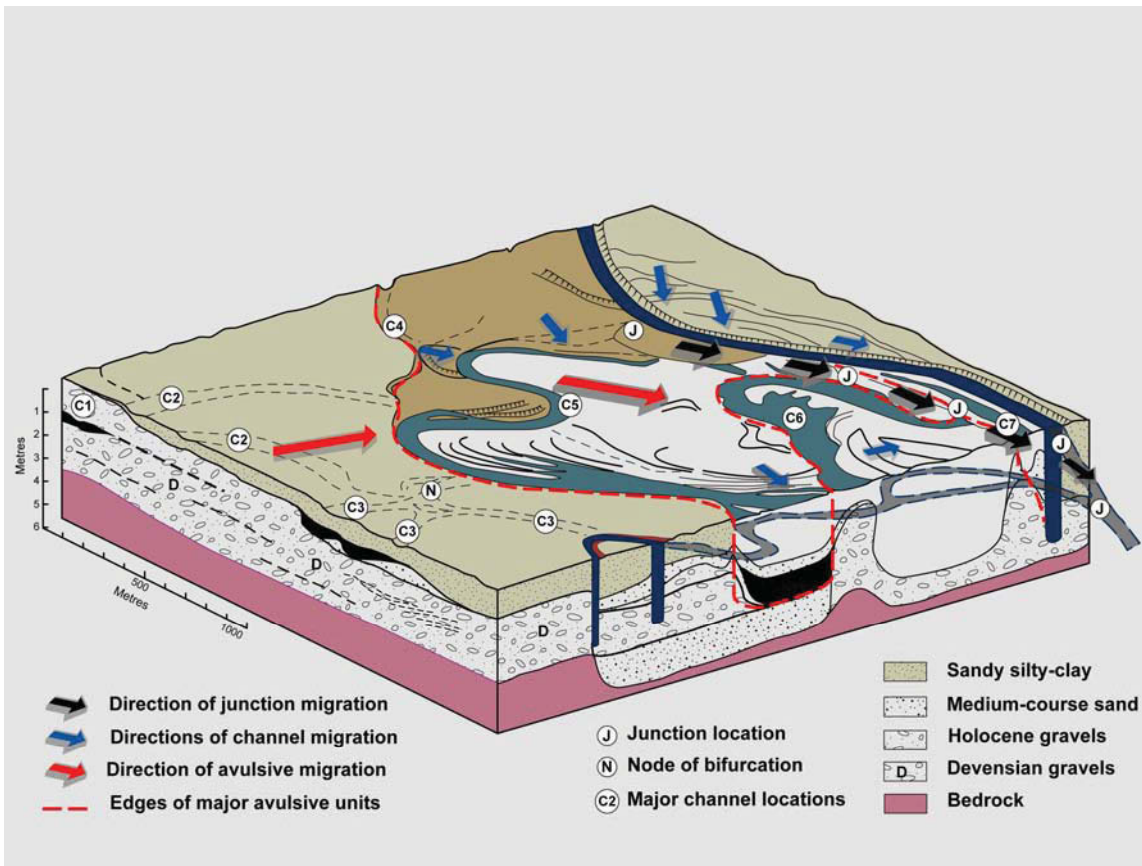


Fig 9.6: Iron-Age-early Post Roman. Note older Neolithic – Bronze Age core within meander loop.

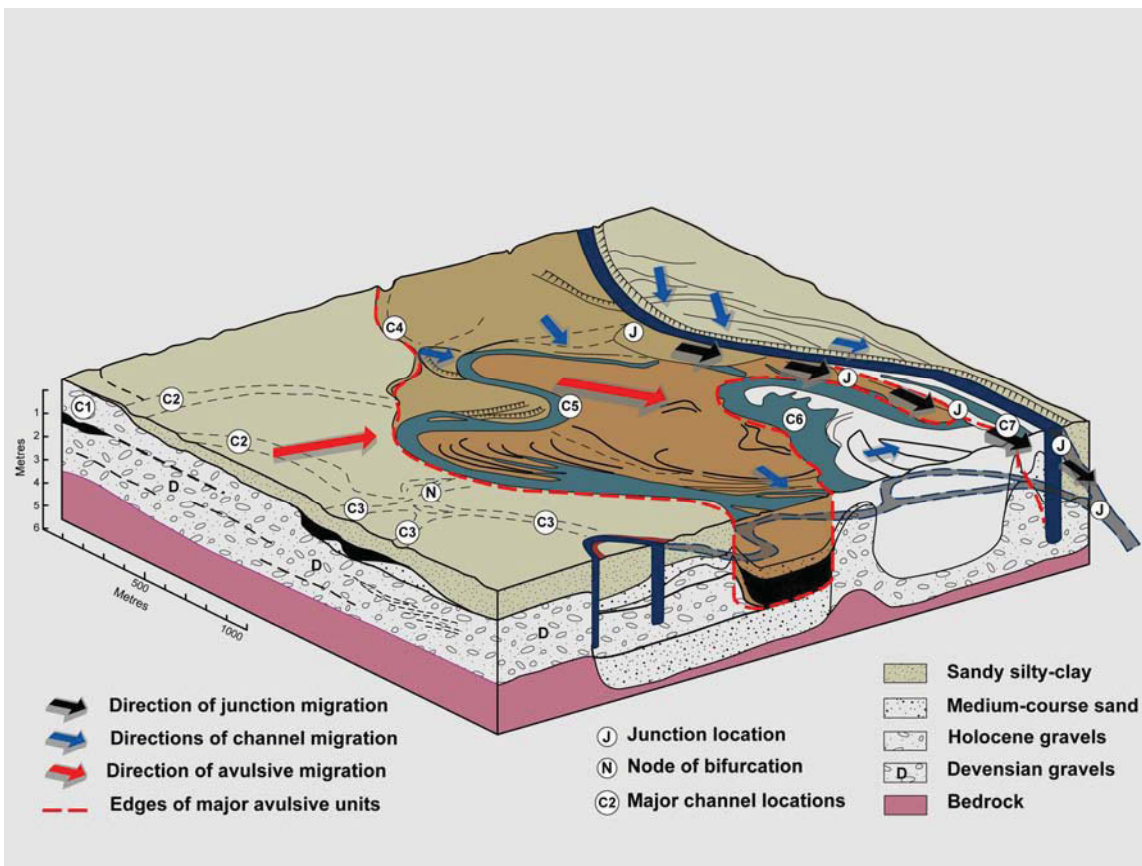


Fig 9.7: New Soar channel location Romano-British – Medieval.

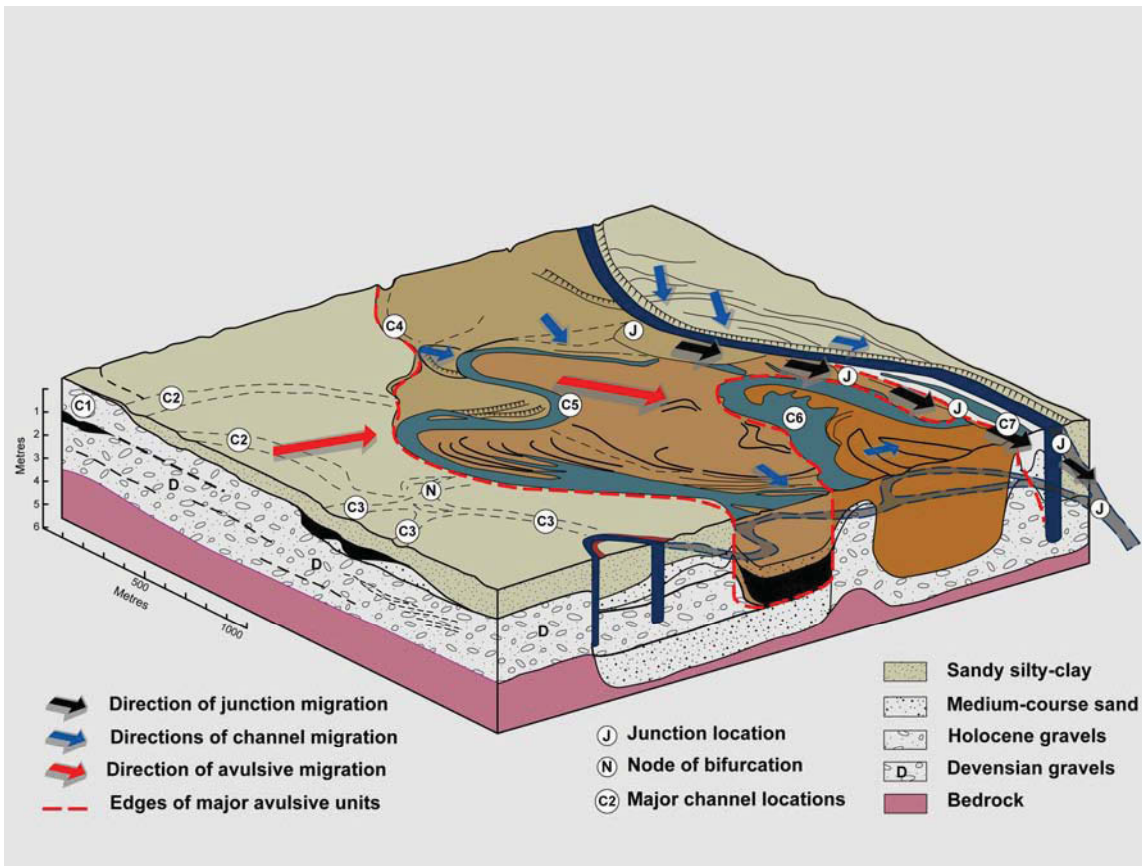


Fig 9.8: Medieval-early Historic abandonment of loop and channel shift to the NE.

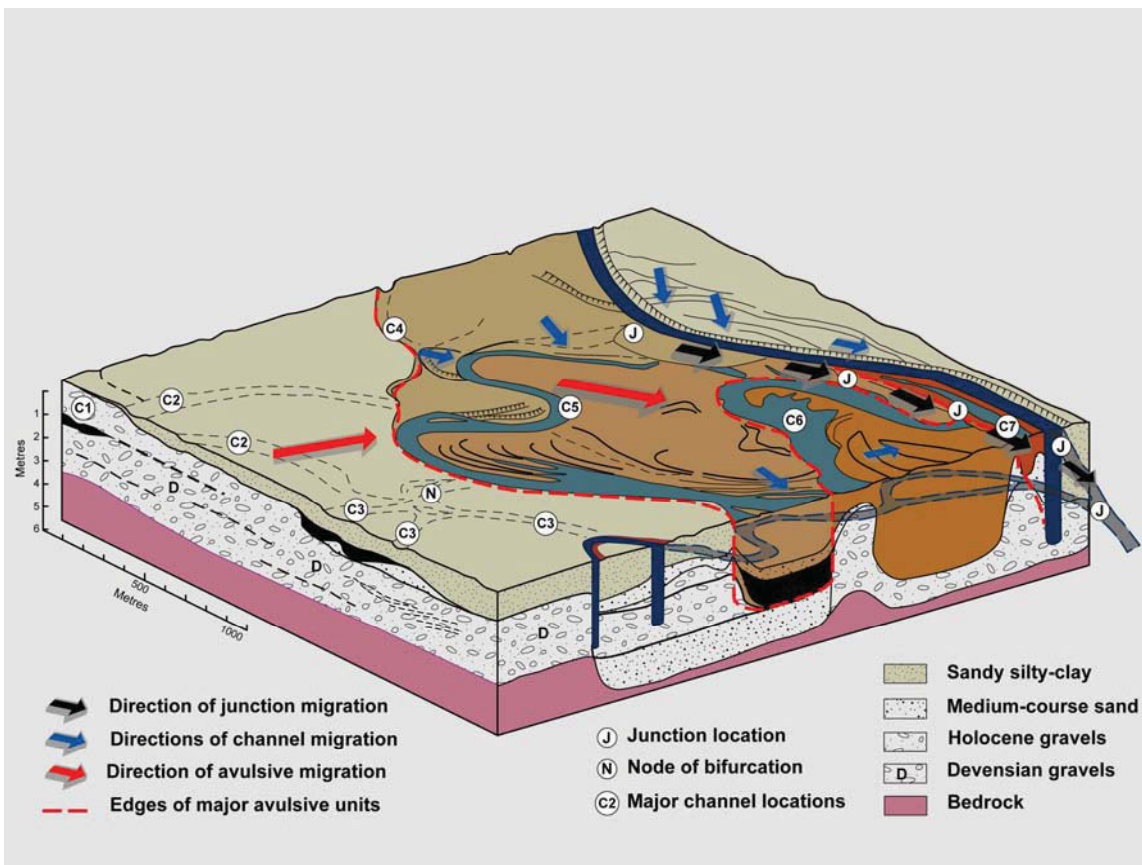


Fig 9.9: Post Medieval northward migration of Trent channel and establishment of the present junction.

Chapter 10. Conclusions and methodological Implications

10.1 Conclusions

- Stratigraphic modelling has showed the limitations of borehole modelling at the scale of an individual floodplain and how it could be improved with increased core density. The integration of exposure/section data with such models is possible but still presents technical problems.
- Radiocarbon dating of the cores and exposures has shown that there is a relationship between channel ages and ground surface height (OD) and a consistent spatial pattern produced by the history of channel change. Generally, older palaeochannels have a higher topography, whilst younger palaeochannels have a lower topography. From this the archaeological potential of palaeochannels can be estimated.
- OSL dating, which was largely successful, showed a greater Holocene age range than the radiocarbon dating indicating both earlier occupation of palaeochannels (i.e. indicating later re-occupation) and overbank deposition at times when no channel fills were being deposited or were deposited but since have been eroded (e.g. the Mesolithic).
- Dendrochronological dating of the tree trunks of Warrens Farm Quarry suggests that all the channels are of late Neolithic – early Bronze Age date (c. 2700-2500 BC) and several may have been felled at the same time. Apart from providing excellent dating of the channel activity it may also be archaeologically significant as it clearly represents floodplain deforestation, whether natural or human induced.
- The use of standard sedimentological analyses (e.g. LOI, CaCo₃, magnetic susceptibility) illustrated well the complex nature of some of the channel fills and hiatuses caused by channel abandonment and re-occupation.
- The beetle assessment showed considerable variation in the preservation of sclera but a clear relationship with pH, preservation being better at the lower pH's in the dataset. Also important is depositional environment and sample size, as it appears that the combination of these factors are the most important in producing high quality data.
- The beetles data also indicated a predominantly species-rich grassland with grazing animals surrounded the channels during the Bronze Age at Warrens Farm Quarry with alder carr adjacent to one of the palaeochannels. A reconstruction of the thermal regime is made from the Devensian palaeochannel.
- Pollen and spore preservation and concentration is highly variable, with % damaged varying from 0 to nearly 100% and concentration varying from <743 grains ml⁻¹ to 199,581 grains ml⁻¹. The only correlation with an environmental variable is with mean core pH and this is probably indirect. There is clearly a complex relationship between damaged grain concentration and depth although this is difficult to explore further given the variation in the depths of the sequences.
- Studies using NIR scanning of parts of the floodplain with the idea of detecting buried archaeological features through variations in soil moisture were not successful due primarily to technical limitations.

- The transect surveys showed that ER is a valuable tool for investigating the depth and internal stratigraphy of palaeochannel fills and is complimentary to the GPR survey used in Phase I.
- Comparison of the chronostratigraphic model with the observed dates from the palaeochannel fills revealed a good correspondence but with a slight tendency to misclassify Neolithic and Bronze Age channels as early Holocene. This would have been rectified easily if only the dendrochronological, or exposed face radiocarbon dates had been used in the initial chronostratigraphic model.
- Using all the data presented in Phases I and II a developmental/diachronic model of channel change is presented and it is suggested that it is driven by avulsion and palaeochannel re-occupation rather than channel migration.
- Lastly a methodological statement is presented which suggests a coherent and ordered set of tasks that can be used in an assessment and evaluation of a large floodplain area prior to intrusive studies and excavation which will maximise pre-intervention knowledge and set any intervention into its full environmental and geoarchaeological context.
- There is a strong predictable element in the results as in effect the chronostratigraphic model and associated environmental potential hypotheses in Phase I from LiDAR is largely proven by the analytical results in Phase II. Indeed with only the LiDAR and some subsurface information from boreholes, cores or combined GPR/ER a model of the archaeological potential could be proposed which would have been substantially correct. In this case the archaeological potential is defined by a combination of the age and type of deposit.

10.2 New research directions

This phase of the project has suggested a number of future directions for both research and management. The research directions are largely technical but not exclusively so. The research directions are:

- More work is definitely needed on the core density required to be able to produce subsurface models of an appropriate resolution for geoarchaeological purposes in conjunction with modelling packages such as ROCKWORKS.
- An illustrative application of both radiocarbon (including AMS fraction dating) and OSL of a single complex palaeochannel as exposed in a gravel quarry would be very useful as it could identify the optimum locations for future sampling.
- Core scanning (using Xray dispersive energy – e.g. ITRAX) needs to be investigated as a much faster and possibly cost effective method of characterising palaeochannel fill cores.
- Ground scanning has to be undertaken either from a height of 10+m and nearly vertical or new scanners need to be used which have technical fixes to the problem of range induced intensity variations.

- More research is required on improving the sensitivity of ER and coupling it with dGPS.

The management and implementation future directions are:

- The routine use of LiDAR for areas of floodplain assessment and evaluation and its use as the DEM basemap.
- Coupled use of GPR and ERGI to characterise palaeochannel and terrace deposits observed in the LiDAR data.
- The use of powered coring with automatic geolocation should be encouraged.
- Routine analyses (LOI and magnetic susceptibility) should be required of a selection of palaeochannel fills prior to other environmental analyses.

10.3 Methodological Statement for Archaeological Prospection in Confluence Zones

This report has demonstrated that river confluences are significant zones of archaeological activity. However, the evolution of confluences is complex (Best, 1988) and understanding their development is essential to identifying and managing the archaeological record. As with all alluvial environments, the key to elucidating their development and hence the character of the archaeological record is to understand the nature and timing of physical processes.

A number of research papers and other documents already exist, which provide generic methodologies for investigating alluvial valley floors (Howard and Macklin, 1999; Passmore et al., 2002; Passmore et al., 2006; Waddington and Passmore, 2006) as well as other best practice sampling strategies (e.g. Hey and Lacey 2001). Therefore, this document does not seek to repeat this corpus of information, but rather focuses on two key aspects of this work:

- Providing a methodological statement for confluence zones, which merit discussion in their own right.
- Demonstrating the value of taking an integrated approach to geoprospection using a combination of non-invasive remote sensing and geophysical techniques, calibrated through invasive coring and other field investigations.

1. Step 1. Desk-Based Assessment (DBA) of the Study Area

DBA should involve the collation of all relevant data and information in existence relating to the physical, cultural and environmental landscape. Preferably, this information should be collated and stored within a project GIS; for this study, we used ARC GIS, but it should be recognized that other systems are available. A key consideration when choosing a GIS should be compatibility of systems between project partners and end users, especially local government.

Key datasets to collect:

1a. Geological Data

Information relating to the solid and superficial geology of all of the British Isles has been collected by British Geological Survey (BGS) field geologists since the earlier 20th century. Originally produced as paper maps at varying scales, it is now also available as digital (Raster and Vector) datasets for capture within a GIS framework. In some cases, it may be that the solid geology is of relevance to the study, but in most cases, it will be the superficial (i.e. soft) sediments that are of interest. These will include the distinction of river terraces, alluvium, peats and other deposits such as colluvium and may allow major landforms such as palaeochannels to be identified and delimited; mapped data at a scale of 1:50,000 are of greatest use for reach scale geoarchaeological studies.

Assessment of stratigraphy and three-dimensional architecture of sediments can be obtained through the analysis of site-investigation boreholes and test pits where no surface exposures are available. The National Geosciences Data Centre collects site investigation information generated by the BGS and its precursors, as part of its national strategic mapping programme, in addition to data provided by external organizations (e.g. mineral companies, public utilities). In some cases, not all the information will be publically available and even if accessible, the quality of these records does vary; nevertheless this data provides a valuable source of information.

Contact: British Geological Survey (www.bgs.ac.uk)

1b. Soils Data

Information relating to the soils developed on both solid and superficial geologies in England and Wales is now held by National Soils Resources Institute (previously collected by the Soil Survey of England and Wales). Traditionally published as paper maps of varying scale, this information is now available in a digital format.

Contact: National Soils Resources Institute (www.silsoe.cranfield.ac.uk/nsri)

1c. Hydrological Data

The NERC-funded Centre for Ecology and Hydrology at Wallingford (UK) holds a 'National Water Archive' comprising the 'National River Flow Archive' and the 'National Groundwater Level Archive'. This information may be used to model groundwater flows and in the case of extraction areas, can often be supplemented by groundwater data collected by individual mineral companies as part of their programmes of environmental monitoring.

Contact: Centre for Ecology and Hydrology (www.ceh.ac.uk)

1d. Historic Map Data

Since rivers are often laterally mobile, collation of the available historic map data will provide an indication of the position and character of former channels. 1st edition Ordnance Survey (OS) maps are available for the British Isles from approximately 1850 and can be purchased in digital format for collation within a project GIS. The position of former administrative boundaries may indicate the position of palaeochannels.

In addition, to OS sheets, Tithe maps and other cartographic sources provide additional information and full lists of such resources are usually available through county HERs.

Contact: Local government Records Office/HER

1e. Aerial Photographs (APs)

For identifying the natural landscape features of any study area including river terraces and palaeochannels, both oblique and vertical aerial photographs form an invaluable resource. The majority of county HERs holds multiple runs of both black and white and colour APs taken over several decades; the earliest are often attributable to the RAF in the immediate post WWII years. Given local meteorological conditions, especially the presence of cloud, it may be necessary to use multiple sets of APs; as with cropmarks (see below), the identification of landforms, especially wetter palaeochannels may vary from year to year depending on climatic conditions. As with other data sources, APs should be geo-rectified and incorporated within the GIS framework to allow the delimitation and plotting of landforms as discrete GIS layers.

If working in some more remote parts of the world, declassified (CORONA) aerial photography collected by US military satellites between 1960-1972 may prove particularly valuable (see Challis et al., 2004).

Contact: Local government HER

1f. Archaeological Data

All data relating to the 'known' archaeological resource of any area will be held within the local government HER (formerly the SMR). English Heritage has a supplementary database (MONARCH), which often includes additional records.

Traditionally, this information has taken the form of paper records and maps, but it is increasingly available in digital format. Whilst a valuable starting point, the robustness of these datasets are often lacking in several key respects:

- The distribution of data often shows spatial biases usually associated with interested amateurs/groups.
- The distribution of data does not take account of our present understanding of landscape evolution and geological filtering.
- The data usually is illustrated as single points, yet archaeological sites can cover several hectares.
- The location of and information relating to data points is often inaccurate and/or duplicated. HER data often requires significant cleaning within a GIS framework before meaningful assessments and interpretations can be made. This is especially true when attempting to dovetail HER-MONARCH databases.

In addition to the point data, the HER will also collate grey literature relating to archaeological interventions within the area of interest. If desired, this information can be collated and linked via a database (ACCESS) to a project GIS.

As part of English Heritage's National Mapping Programme (NMP), cropmarks have been systematically recorded across extensive tracts of English landscape. Traditionally produced in paper form, it is now available digitally for inclusion within GIS frameworks. The addition of this information to point data can considerably improve our understanding of the spatial extent of archaeological sites. It is unfortunate that in the majority of cases, aerial archaeologists have not

mapped features relating to the natural landscape (e.g. landforms) since this would add considerably to these rich archaeological datasets.

Contacts: Local government HERs & English Heritage (www.english-heritage.org.uk).

1g. LiDAR Data

LiDAR provides a tool for the rapid and accurate mapping of topography and geomorphology over large areas of valley floor (Challis, 2006). The technique uses the properties of coherent laser light, coupled with precise kinematic positioning provided by a differential global positioning system (dGPS) and inertial altitude determination provided by an inertial measurement unit (IMU), to produce horizontally and vertically accurate elevation measurements. An aircraft mounted laser projects a coherent beam of light at the ground surface with the reflections recorded by a receiver. Travel times for the pulse/reflection are used to calculate the distance from the laser to the reflecting object. The vertical resolution of LiDAR is estimated to be 10cm-15cm.

Post-survey processing of the simultaneously recorded laser, location and altitude data allows reconstruction of elevation values for the ground surface. Raw survey data in the form of a three dimensional point-cloud are projected to a local map datum, sorted, filtered and used to generate a regular grid of elevation values. The laser receiver is able to record multiple returns for a single pulse, recording a partial return from the top of a semi-opaque object such as a woodland canopy (FP) and from the opaque ground beneath the canopy (LP). Other information, such as the intensity (amplitude) is also recorded. Intensity data provides a record of the backscattered intensity of reflection of each laser pulse. Backscattered intensity values vary according to changes in the reflectance of differing earth surface materials at NIR wavelengths (Wehr and Lohr, 1999).

As part of flood risk management studies, the Environment Agency (EA) has owned a LiDAR sensor for a number of years and flown the majority of river valley corridors in the England. This data can be bought in a standard processed format from the EA. In the past couple of years NERC has also acquired its own sensor and its services can be sought in the usual NERC equipment bidding rounds. In addition, private companies such as Infoterra have their own instrumentation and can provide a bespoke data collection service.

Contacts: Environment Agency (www.environment-agency.gov.uk); NERC (www.nerc.ac.uk); Infoterra (www.infoterra-global.com).

1h. Multi-Spectral Imagery Data

For a number of years, NERC has generated multi-spectral imagery using two airborne scanners: the Daedalus 1268 Airborne Thematic Mapper (ATM) and the Compact Airborne Spectrographic Imager (CASI).

The Daedalus 1268 ATM records spectral reflectance and infrared radiation in 11 discrete bands; these range in wavelength from visible blue to thermal infrared. In contrast, the CASI-2 is a configurable hyper-spectral scanner capable of recording spectral reflectance in up to 288 spectral channels at varying spatial resolution.

Both instruments have produced data stored as digital archives by NERC. Such datasets offer potential to identify contrasts in vegetation, which may be related to discrete landforms such as

palaeochannels, however, the potential of neither has been rigorously investigated by the archaeological community.

Contacts: NERC (www.nerc.ac.uk).

1.1. End Product of DBA Stage 1 of Project

At the end of the desk-based assessment, any project should have a robust GIS containing information that allows a preliminary understanding of the following issues:

- The geological evolution of the study area including the character of the sediments, landforms and the major geomorphological processes operating through time.
- A LiDAR generated Digital Terrain Model of the project area allowing the identification of major landforms with respect to the archaeological record. This will produce a 'Landform Assemblage Map' (see Passmore et al., 2002).
- Preliminary assessment and mapping of the spatial distribution of archaeology by period and type with respect to both landforms and geologies.
- A relative chronology of recent landscape development based on successive maps and other resources (e.g. APs).
- An assessment of the three dimensional geological record and its implications for archaeological prospection and preservation.

2. Step 2. Collection of Field Data of the Study Area

2a. Ground Truthing of Landform Assemblage Map

Whilst the identification and mapping of landforms can be undertaken within a GIS framework from the datasets collated in Stage 1, it is essential that ground truthing and additional geomorphological and geological field mapping is undertaken in order to determine the precise stratigraphic relationships between landforms and key sedimentological units. If necessary additional information about landforms and other units such as their further extent can be delimited and spatially referenced using a GPS to augment other data already held within the project GIS.

2b. Non-Invasive Stratigraphic Investigations

The application of GPR and ER prospection have a pivotal role to place in future geoarchaeological investigations. Both ER and GPR can be used to provide 2D sections, to look at the cross sections and stratigraphic relationships of different floodplain components, and also 3D surveys to produce volumetric diagrams of different features, such as palaeochannels or areas of terrace. GPR has proved itself to be reliable in identifying sediment sequences within gravel bodies and of overlying alluvial deposits, where the alluvium has low clay and water contents. In such instances basic stratigraphy can be modelled and inferences made on sediment composition based on the intensity of reflection. GPR is ineffective at revealing the stratigraphy of palaeochannel fills, when sediments are clay rich or have high water contents. Typically a 200MHz antenna can give good data resolution to c. 3m depth.

ER can be effectively coupled with GPR survey, to provide information on palaeochannel fills. ER does not define stratigraphy as well as GPR on areas of terrace, but major floodplain components can be defined, such as palaeochannels. In addition information can be gained on the nature of palaeochannel fill, such as the where areas of highest biotaphonomic potential are. In addition ER

has a greater depth penetration potential than GPR using a 200MHz antenna and can be used to investigate the nature of gravel deposits, to locate/investigate deposits within the gravel body of higher biotaphonomic potential. The use of ER and GPR is strongest when the two techniques are used in conjunction. In addition, the use of gouge core survey (see below) can provide additional complimentary data that is useful for interpretation of the ER and GPR sections.

1c. Invasive Stratigraphic Investigations - Augering

Where sedimentary exposures are unavailable, augering can be used to record stratigraphy, calibrate instrumentation and provide samples for environmental analysis and landscape reconstruction. If collected on (relatively) regularly spaced grid intervals, such subsurface information can be used for 3d modelling of valley floor architecture using a range of software linked to a GIS framework (see Bates, 2003; Challis & Howard, 2003).

1d. Geochronology

As with all alluvial environments, the key to elucidating their development and hence the character of the archaeological record is to understand the nature and timing of physical processes. It is essential that the investigation of any site is accompanied by a well-designed and robust dating programme. Depending on the timescale and nature of datable materials, this may include the use of Radiocarbon techniques or other developing methods such as Optically Stimulated Luminescence (OSL) or Amino Acid Racemization. The possibilities for dating of sediments etc should be discussed early in any programme of work with suitable qualified dating specialists.

2.1. End Product of Fieldwork at Stage 2 of Project

At the end of fieldwork, any project should have a robust dataset that allows an understanding of the following issues:

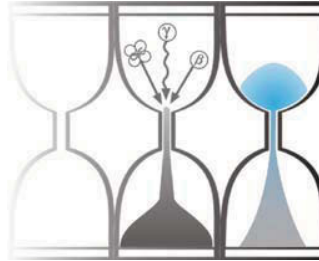
- The geological evolution of the study area including the character of the sediments, landforms and the major geomorphological processes operating through time.
- A thorough understanding of the three dimensional geological record and its implications for archaeological prospection and preservation.
- A ground truthed Landform Assemblage Map that provides a thorough understanding of major landforms with respect to the archaeological record.
- A thorough understanding of the spatial distribution of archaeology by period and type with respect to both landforms and geologies.
- An absolute chronology of landscape development and the timing of key geomorphological events (e.g. erosion and sedimentation) and an assessment of the impacts of landscape evolution on the archaeological record.

12 Appendices



University of Gloucestershire

Geochronology Laboratories



**Optical dating report for the ALSF project
'Predictive Modelling of Multi-Period Geoarchaeological resources
at a River confluence'**

to

Prof. A.G. Brown, University of Exeter

Prepared by Dr P.S. Toms, 19th February 2007

Copyright Notice

Permission must be sought from the University of Gloucestershire in using the content of this report, in part or whole, for the purpose of publication.

English Heritage Centre for Archaeology Optical dating report for the ALSF project 'Predictive Modelling of Multi-Period Geoarchaeological resources at a River confluence'

Dr P.S. Toms¹, Prof. A.G. Brown², Dr C.J. Carey², Dr A.J. Howard³ and Dr K. Challis³

Summary

This study contributes to Phase 2 of the 'Predictive Modelling of Multi-Period Geoarchaeological resources at a River confluence' ALSF project. The aim of this dating study is to generate chronological controls based on Optical dating to assist in the construction of a secure, high resolution stratigraphic framework to refine landscape evolution models of the Rivers Trent & Soar study area developed during Phase 1. Given the bulk of sediments of interest were likely deposited in the Holocene by fluvial processes, partial resetting of the time dependent signal prior to burial may force a significant age overestimation if adopting conventional multi-grain single aliquot methods of Optical dating. In an attempt to circumvent this issue, aliquots composed of single grains of quartz sand have been dated in order to gain a measure of inter-grain age variability and to isolate that minimum age region representing those grains whose time dependent signal was near or fully reset prior to burial. Age estimates span from as little as 0.38 ka to as much as 8.16 ka and, exceptionally, 25.3 ka. Five samples have proven analytically acceptable. Limits upon the mass of datable material create some minor uncertainty in the reliability of age estimates from four samples, whilst intrinsic tests and measures of U disequilibrium highlight some minor uncertainties in the remaining data set. However, only one sample is rejected outright.

Keywords

Optical dating, Single Grains, Holocene, Fluvial

Authors' addresses

¹Geochronology Laboratories, Department of Natural and Social Sciences, University of Gloucestershire, Swindon Road, Cheltenham. GL50 4AZ. Tel: 01242 544091. Email: ptoms@glos.ac.uk

²Department of Geography, University of Exeter, Amory Building, Rennes Drive, Exeter. EX4 4RJ.

³Institute for Archaeology and Antiquity, University of Birmingham, Edgbaston, Birmingham. B15 2TT.

1.0 Introduction

This study contributes to Phase 2 of the 'Predictive Modelling of Multi-Period Geoarchaeological resources at a River confluence' project, funded through the Aggregates Levy sustainability Fund administered by English Heritage (EH project number: 3357MAIN). The aim of this ALSF project is to predictively model the landscape of a major river confluence over a time-scale of millennia and at a spatial scale appropriate for archaeological management. The study area is 2 by 4 km in extent located across the confluence of the Rivers Trent and Soar. The aim of this dating study is to generate chronological controls based on Optical dating to assist in the construction of a secure, high resolution stratigraphic framework, thereby refining the detailed surface and subsurface landscape evolution models of the study area developed during Phase 1. The rationale for this is to show how much archaeological data can be generated for alluviated aggregate sites prior to excavation.

2.0 Optical dating: Mechanisms and principles

Upon exposure to ionising radiation, electrons within the crystal lattice of insulating minerals are displaced from their atomic orbits. Whilst this dislocation is momentary for most electrons, a portion of charge is redistributed to meta-stable sites (traps) within the crystal lattice. In the absence of significant optical and thermal stimuli, this charge can be stored for extensive periods. The quantity of charge relocation and storage relates to the magnitude and period of irradiation. When the lattice is optically or thermally stimulated, charge is evicted from traps and may return to a vacant orbit position (hole). Upon recombination with a hole, an electron's energy can be dissipated in the form of light generating crystal luminescence providing a measure of dose absorption.

Herein, quartz is segregated for dating. The utility of this minerogenic dosimeter lies in the stability of its datable signal over the mid to late Quaternary period, predicted through isothermal decay studies (e.g. Smith *et al.*, 1990; retention lifetime 630 Ma at 20°C) and evidenced by optical age estimates concordant with independent chronological controls (e.g. Murray and Olley, 2002) This stability is in contrast to the anomalous fading of comparable signals commonly observed for other ubiquitous sedimentary minerals such as feldspar and zircon (Wintle, 1973; Templer, 1985; Spooner, 1993).

Optical age estimates of sedimentation (Huntley *et al.*, 1985) are premised upon reduction of the minerogenic time dependent signal (Optically Stimulated Luminescence, OSL) to zero through exposure to sunlight and, once buried, signal reformulation by absorption of litho- and cosmogenic radiation. The signal accumulated post burial acts as a dosimeter recording total dose absorption, converting to a chronometer by estimating the rate of dose absorption quantified through the assay of radioactivity in the surrounding lithology and streaming from the cosmos.

$$\text{Age} = \frac{\text{Mean Equivalent Dose (D}_e\text{, Gy)}}{\text{Mean Dose Rate (D}_r\text{, Gy.ka}^{-1}\text{)}}$$

Aitken (1998) and Bøtter-Jensen *et al.* (2003) offer a detailed review of optical dating.

3.0 Sample Collection and Preparation

Twenty one conventional sediment samples – those located within matrix-supported units composed predominantly of sand and silt - were collected within opaque plastic tubing from either sections by means of tubing (150x45 mm) forced into each face (samples GL06005 to GL06009) or from boreholes excavated by a Geoprobe (in tubing 1000x45 mm). Each sample location marked the deepest points of palaeochannels within the study area. Each tube was wrapped in cellophane and parcel tape in order to preserve moisture content and integrity until ready for laboratory preparation. To

preclude optical erosion of the datable signal prior to measurement, all samples were prepared under controlled laboratory illumination provided by Encapsulite RB-10 (red) filters. To isolate that material potentially exposed to daylight during sampling or that which had been relocated by the process of coring, sediment located within the outer 5 mm of each sample was removed.

The remaining sample was dried and then sieved. Quartz within the fine sand (125-180 μm or 180-250 μm) fraction was then segregated (Table 1). Samples were subjected to acid and alkali digestion (10% HCl, 15% H₂O₂) to attain removal of carbonate and organic components respectively.

A further acid digestion in HF (40%, 60 mins) was used to etch the outer 10-15 μm layer affected by α radiation and degrade each samples' feldspar content. During HF treatment, continuous magnetic stirring was used to effect isotropic etching of grains. 10% HCl was then added to remove acid soluble fluorides. Each sample was dried, resieved and quartz isolated from the remaining heavy mineral fraction using a sodium polytungstate density separation at 2.68g.cm⁻³. Where sufficient datable mass existed, 24 multi-grain aliquots (c. 3-6 mg) of quartz from each sample were then mounted on aluminium discs to establish optimum, average measurement conditions for single grain aliquots. Around 2400 sand grains from each sample were located individually in 200 mm (diameter and depth) holes drilled as a 10x10 grid into anodised aluminium discs (Duller *et al.*, 1999) to gain a measure of inter-grain D_e distribution.

All drying was conducted at 40°C to prevent thermal erosion of the signal. All acids and alkalis were Analar grade. All dilutions (removing toxic-corrosive and non-minerogenic, luminescence-bearing substances) were conducted with distilled water to prevent signal contamination by extraneous particles.

4.0 Acquisition and accuracy of D_e value

All minerals naturally exhibit marked inter-sample variability in luminescence per unit dose (sensitivity). Therefore, the estimation of D_e acquired since burial requires calibration of the natural signal using known amounts of laboratory dose. D_e values were quantified using a single-aliquot regenerative-dose (SAR) protocol (Murray and Wintle 2000; 2003) facilitated by a Risø TL-DA-15 irradiation-stimulation-detection system (Markey *et al.*, 1997; Bøtter-Jensen *et al.*, 1999; Duller *et al.*, 1999). Within this apparatus, optical signal stimulation of multi-grain aliquots was provided by an assembly of blue diodes (5 packs of 6 Nichia NSPB500S), filtered to 470±80 nm conveying 15 mW.cm⁻² using a 3 mm Schott GG420 positioned in front of each diode pack. Optical stimulation of single grain aliquots emanated from a focussed solid state 532 nm (green), 10 mW stabilised laser (Laser 2000 LCL-LCM-T-11ccs) scanned across grains by means of mirrors mounted on and moved by motorised linear stages. Infrared (IR) stimulation, provided by 6 IR diodes (Telefunken TSHA 6203) stimulating at 875±80nm delivering ~5 mW.cm⁻², was used to indicate the presence of contaminant feldspars (Duller, 2003). Stimulated photon emissions from quartz aliquots are in the ultraviolet (UV) range and were filtered from stimulating photons by 7.5 mm HOYA U-340 glass and detected by an EMI 9235QA photomultiplier fitted with a blue-green sensitive alkali photocathode. Aliquot irradiation was conducted using a 1.48 GBq ⁹⁰Sr/⁹⁰Y β source calibrated for single and multi-grain aliquots of each isolated quartz fraction against the 'Hotspot 800' ⁶⁰Co γ source located at the National Physical Laboratory (NPL), UK. In calibrating single sand grain aliquots, no significant spatial variation in dose rate from the β source was found.

SAR by definition evaluates D_e through measuring the natural signal (Fig. 1) of a single aliquot and then regenerating that aliquot's signal by using known laboratory doses to enable calibration. For each aliquot, at least 4 different regenerative-doses were administered so as to image dose response. D_e values for each aliquot were then interpolated, and associated counting and fitting errors calculated, by way of exponential or exponential plus linear regression (Fig. 1). The accuracy with which D_e equates to total absorbed dose and that dose absorbed since burial is assessed. The former

can be considered a function of laboratory factors, the latter, one of environmental issues. Diagnostics were deployed to estimate the influence of these factors and criteria instituted to optimise the accuracy of D_e values.

4.1 Laboratory Factors

4.1.1 Feldspar contamination

The propensity of feldspar signals to fade and underestimate age, coupled with their higher sensitivity relative to quartz makes it imperative to quantify feldspar contamination. At room temperature, feldspars generate a signal (IRSL) upon exposure to IR whereas quartz does not. The signal from feldspars contributing to OSL can be depleted by prior exposure to IR. For all aliquots the contribution of any remaining feldspars was estimated from the OSL IR depletion ratio (Duller, 2003). If the addition to OSL by feldspars is insignificant, then the repeat dose ratio of OSL to post-IR OSL should be statistically consistent with unity. Any aliquots that did not fulfil this criterion were rejected.

4.1.2 Preheating

Preheating aliquots between irradiation and optical stimulation is necessary to ensure comparability between natural and laboratory-induced signals. However, the multiple irradiation and preheating steps that are required to define single-aliquot regenerative-dose response leads to signal sensitisation, rendering calibration of the natural signal inaccurate. The SAR protocol (Murray and Wintle, 2000; 2003) enables this sensitisation to be monitored and corrected using a test dose, here set at c 5 Gy preheated to 220°C for 10s, to track signal sensitivity between irradiation-preheat steps. However, the accuracy of sensitisation correction for both natural and laboratory signals can be preheat dependent. Three diagnostics were used to assess the optimal preheat temperature for accurate correction and calibration.

Irradiation-preheat cycling (Fig. 2) quantifies the preheat dependence of sensitisation correction for laboratory-induced signals. If sensitisation is accurately corrected, then the same regenerative-dose should yield an equivalent sensitivity corrected value irrespective of the number of times it is applied and its associated signal measured. The ratio of subsequent to initial corrected regenerative-dose signals should be statistically concordant with unity. Alternatively, this ratio may differ from unity yet attain consistency after one or more cycles evidencing accurate sensitivity correction exists if the sample is primed by irradiation-preheat cycles. For this diagnostic, and where sufficient material was available, 18 multi-grain aliquots were divided into sets of 3 and assigned a 10 s preheat between 180°C and 280°C.

D_e preheat dependence (Fig. 3) quantifies the combined effects of thermal transfer and sensitisation on the natural signal. Insignificant adjustment in D_e values in response to differing preheats may reflect limited influence of these effects. Samples generating D_e values <10Gy and exhibiting a systematic, statistically significant adjustment in D_e value with increasing preheat temperature may indicate the presence of significant thermal transfer; in such instances low temperature (<220°C) preheats may provide the apposite measure of D_e . For this diagnostic, the D_e value of each of the same 18 multi-grain aliquots and their assigned preheat was assessed.

Dose Recovery (Fig. 4) attempts to replicate the above diagnostic, yet provide improved resolution of thermal effects through removal of variability induced by heterogeneous dose absorption in the environment, using a precise laboratory dose to simulate natural dose. The ratio between the applied dose and recovered D_e value should be statistically concordant with unity. For this diagnostic, a further 6 multi-grain aliquots were each assigned a 10 s preheat between 180°C and 280°C.

That preheat treatment fulfilling the criterion of accuracy for all three diagnostics was selected to refine the final D_e value for 2400 single grain aliquots. Further thermal treatments, prescribed by Murray and Wintle (2000; 2003), were applied to optimise accuracy and precision. Optical stimulation occurred at 125°C in order to minimise effects associated with

photo-transferred thermoluminescence and maximise signal to noise ratios. Inter-cycle optical stimulation was conducted at 280°C to minimise recuperation.

4.1.3 Irradiation

Laboratory irradiation effects may evolve from the contrasting rates of natural dose exposure and the calibrating laboratory dose, the latter delivered to each aliquot at 9 orders of magnitude faster than the former. Bailey (2004) has suggested that for doses in excess of ~40 Gy an overestimation of age may arise due to competing mechanisms of signal accumulation within the crystal lattice of quartz. Only one sample (GL06009) generated single grain D_e values >40 Gy. These accounted for the minority of D_e values obtained for GL06009 and therefore laboratory irradiation effects were not considered significant in this study.

4.1.4 Internal consistency

Radial plots (Fig. 5; cf Galbraith, 1990) are used to illustrate inter-aliquot D_e variability for natural and regenerated signals. D_e values are standardised relative to the central D_e value (Galbraith *et al.*, 1999) for natural signals and applied dose for regenerated signals. D_e values are described as overdispersed when >5% lie beyond $\pm 2\sigma$ of the standardising value; resulting from a heterogeneous absorption of burial dose and/or response to the SAR protocol. Overdispersion for natural signals does not necessarily imply inaccuracy. However where overdispersion is observed for regenerated signals, the age estimate from that sample should be accepted tentatively.

4.2 Environmental factors

4.2.1 Incomplete zeroing

Post-burial OSL signals residual of pre-burial dose absorption can result where pre-burial sunlight exposure is limited in spectrum, intensity and/or period, leading to age overestimation. This effect is particularly acute for material eroded and redeposited sub-aqueously (Olley *et al.*, 1998, 1999; Wallinga, 2002) and exposed to a burial dose of <20 Gy (e.g. Olley *et al.*, 2004). It can have some influence in sub-aerial contexts but is rarely of consequence where aerial transport has occurred. Optical dating of dominantly Holocene fluvial sands within this study warrants that this environmental effect be addressed.

Within single-aliquot regenerative-dose optical dating there are two diagnostics of partial resetting (or bleaching); signal analysis (Agersnap-Larsen *et al.*, 2000; Bailey *et al.*, 2003) and inter-aliquot D_e distribution studies (Murray *et al.*, 1995).

Within this study the latter has been used, taking aliquots of single sand grains to quantify inter-grain D_e distribution. At present, it is contended that asymmetric inter-grain D_e distributions are symptomatic of partial bleaching and/or pedoturbation (Murray *et al.*, 1995; Olley *et al.*, 1999; Olley *et al.*, 2004; Bateman *et al.*, 2003). For partial bleaching at least, it is further contended that the D_e acquired during burial is located in the minimum region of such ranges. The Minimum Age Model (Galbraith and Laslett, 1993) is the most regularly applied statistical approach in quantifying the breadth of minimum dose regions. Olley *et al.* (2004) recommend this model for Holocene fluvial samples based upon its agreement with independent age controls for a number of samples. Yet such models have been found to underestimate post-burial D_e values owing to post depositional turbation (Roberts *et al.*, 1998) or as a product of a minority of outlying low D_e values (Rodnight, 2006). The Finite Mixture Model (Galbraith and Green, 1990) offers an alternative statistical method by which to compute the minimum dose region reflecting post-burial D_e . It identifies the number of dose components within an inter-grain D_e distribution along with the mean D_e and proportion of grains in each component. In the Finite Mixture Model each component is assumed to have an equivalent level of overdispersion (σ , herein set at 0.10; Jacobs *et al.*, 2006; Rodnight *et al.*, 2006). Rodnight *et al.* (2006) advocate use of the youngest component unless it comprises less than 10% of aliquots, whereupon the next youngest component is taken to reflect post-burial D_e . However, the mean and breadth of this minimum region in all models is the subject of current debate, as it is additionally

influenced by heterogeneity in microdosimetry, variable inter-grain response to SAR and residual to post-burial signal ratios. The Central Age Model (Galbraith et al., 1999) assumes all inter-grain D_e variation is forced by spatial variations in dose rate and natural irradiation effects that can be accurately replicated by laboratory irradiation, and thus the mean D_e value coupled with the mean D_r value will generate an accurate age estimate of burial. At present, it is clear that age defined by the D_e interval delimited by the Minimum and Central Age Models will be accurate but have limited precision (Table 1). In this study, the Finite Mixture Model has been adopted to produce a more refined estimate of age (Table 1) based on the success of its implementation by Rodnight *et al.* (2006) in sediments equivalent in age and genus to those in this study.

4.2.2 Turbation

The accuracy of sedimentation ages can further be controlled by post-burial trans-strata grain movements forced by pedo- or cryoturbation. Berger (2003) contends pedogenesis prompts a reduction in the apparent sedimentation age of parent material through bioturbation and illuviation of younger material from above and/or by biological recycling and resetting of the datable signal of surface material. Berger (2003) proposes that the chronological products of this remobilisation are A-horizon age estimates reflecting the cessation of pedogenic activity, Bc/C-horizon ages delimiting the maximum age for the initiation of pedogenesis with estimates obtained from Bt-horizons providing an intermediate age 'close to the age of cessation of soil development'. Singhvi *et al.* (2001), in contrast, suggest that B and C-horizons closely approximate the age of the parent material, the A-horizon, that of the 'soil forming episode'. At present there is no post-sampling mechanism for the direct detection of and correction for post-burial sediment remobilisation. However, intervals of palaeosol evolution can be delimited by a maximum age derived from parent material and a minimum age obtained from a unit overlying the palaeosol. Pedogenic effects are not considered significant within this study owing to the lack of visible soil development. Inaccuracy forced by cryoturbation may be bidirectional, heaving older material upwards or drawing younger material downwards into the level to be dated. However, only one sample (GL06009) was retrieved from a section of sediments likely dating to the last Glacial stage; no evidence was observed of cryogenic deformation.

5.0 Acquisition and accuracy of D_r value

Lithogenic D_r values were defined through measurement of U, Th and K radionuclide concentration and conversion of these quantities into β and γ D_r values (Table 1). β contributions were estimated from sub-samples by Neutron Activation Analysis (NAA) delivered by Becquerel Canada. γ dose rates were estimated for samples GL06005 to GL06009 from *in situ* NaI γ spectrometry. Where direct measurements of γ dose rate were not possible, laboratory-based Ge γ spectrometry was conducted on sub-samples composed of material at intervals within 300 mm above and below the centre of each sample within each core (weighted by relative γ contributions; Aitken, 1985). *In situ* measurements were conducted using an EG&G μ Nomad portable NaI γ spectrometer (calibrated using the block standards at RLAHA, University of Oxford); these reduce uncertainty relating to potential heterogeneity in the γ dose field surrounding each sample. Laboratory-based γ spectrometry was conducted using an Ortec GEM-S high purity Ge coaxial detector system, calibrated using certified reference materials supplied by CANMET. Estimates of radionuclide concentration were converted into D_r values (Adamiec and Aitken, 1998), accounting for D_r modulation forced by grain size (Mejdahl, 1979) and present moisture content (Zimmerman, 1971). Cosmogenic D_r values are calculated on the basis of sample depth, geographical position and matrix density (Prescott and Hutton, 1994).

The spatiotemporal validity of D_r values can be considered as a function of five variables. Firstly, age estimates devoid of *in situ* γ spectrometry data should be accepted tentatively if the sampled unit is heterogeneous in texture or if the sample is located within 300 mm of strata consisting of differing texture and/or mineralogy. However, where samples are obtained throughout a vertical profile, consistent values of γ D_r based solely on, for example, NAA may evidence the

homogeneity of the γ field and hence accuracy of γ D_r values. Secondly, disequilibrium can force temporal instability in U and Th emissions. In this study, the potential for long-term instability in D_r values forced by U disequilibrium has been considered. The impact of this infrequent phenomenon (Oley *et al.*, 1996) upon age estimates is usually insignificant given their associated margins of error, however this effect is pronounced for at least two samples in this study (>50% disequilibrium between ^{238}U and ^{226}Ra , samples GL06014 & GL06025; Fig. 6). Thirdly, pedogenically-induced variations in matrix composition of B and C-horizons, such as radionuclide and/or mineral remobilisation, may alter the rate of energy emission and/or absorption. If D_r is invariant through a dated profile and samples encompass primary parent material, then element mobility is likely limited in effect. In this study, there is limited evidence of pedogenesis in any unit sampled. Fourthly, spatiotemporal deviations from present moisture content are difficult to assess directly, requiring knowledge of the magnitude and timing of differing contents. However, the maximum influence of moisture content variations can be delimited by recalculating D_r for minimum (zero) and maximum (saturation) content. Finally, temporal alteration in the thickness of overburden alters cosmic D_r values. Cosmic D_r often forms a negligible portion of total D_r . It is possible to quantify the maximum influence of overburden flux by recalculating D_r for minimum (zero) and maximum (surface sample) cosmic D_r .

6.0 Estimation of Age

Age estimates reported in Table 1 provide an estimate of sediment burial period based on mean D_r values and D_e values derived from Minimum, Finite Mixture and Central Age Models, along with associated analytical uncertainties. Uncertainty in Finite Mixture age estimates is reported as a product of systematic and experimental errors, with the magnitude of experimental errors alone shown in parenthesis (Table 1). Probability distributions indicate the inter-aliquot variability in age (Fig. 7). The maximum influence of temporal variations in D_r forced by minima-maxima variation in moisture content and overburden thickness, coupled with Finite Mixture D_e values, is illustrated in Fig. 7. Where uncertainty in these parameters exists this age range may prove instructive, however the combined extremes represented should not be construed as preferred age estimates.

7.0 Analytical uncertainty

All errors are based upon analytical uncertainty and quoted at 1σ confidence. Error calculations account for the propagation of systematic and/or experimental (random) errors associated with D_e and D_r values.

For D_e values, systematic errors are confined to laboratory β source calibration. Uncertainty in this respect is that combined from the delivery of the calibrating γ dose (1.2%; NPL, pers. comm.), the conversion of this dose for SiO_2 using the respective mass energy-absorption coefficient (2%; Hubbell, 1982), reproducibility in laser positioning (3.5%; Truscott *et al.*, 2000) and experimental error, totalling 4.3%. Mass attenuation and bremsstrahlung losses during γ dose delivery are considered negligible. Experimental errors relate to D_e interpolation using sensitisation corrected dose responses. Natural and regenerated sensitisation corrected dose points (S_i) are quantified by,

$$S_i = (D_i - x.L_i) / (d_i - x.L_i) \quad \text{Eq.1}$$

where D_i = Natural or regenerated OSL, initial 0.2 s
 L_i = Background natural or regenerated OSL, final 5 s
 d_i = Test dose OSL, initial 0.2 s
 x = Scaling factor, 0.08

The error on each signal parameter is based on counting statistics, reflected by the square-root of measured values. The propagation of these errors within Eq. 1 generating σS_i follows the general formula given in Eq. 2. σS_i are then used to define fitting and interpolation errors within linear or exponential regressions (Green and Margerison, 1978; Ixaru *et al.*, 2004).

For D_i values, systematic errors accommodate uncertainty in radionuclide conversion factors (5%), β attenuation coefficients (5%), matrix density (0.20 g.cm^{-3}), vertical thickness of sampled section (specific to sample collection device), saturation moisture content (3%), moisture content attenuation (2%), burial moisture content (25% relative, unless direct evidence exists of the magnitude and period of differing content), NaI gamma spectrometer calibration (3%) and/or NAA (2%). Experimental errors are associated with radionuclide quantification for each sample by γ spectrometry and/or NAA.

The propagation of these errors through to age calculation is quantified using the expression,

$$\sigma y (\delta y / \delta x) = (\sum ((\delta y / \delta x_n) \cdot \sigma x_n)^2)^{1/2} \quad \text{Eq. 2}$$

where y is a value equivalent to that function comprising terms x_n and where σy and σx_n are associated uncertainties.

Errors on age estimates based on the Finite Mixture Model are presented as combined systematic and experimental errors and experimental errors alone. The former (combined) error should be considered when comparing luminescence ages herein with independent chronometric controls. The latter assumes systematic errors are common to luminescence age estimates generated by means equal to those detailed herein and enable direct comparison with those estimates.

8.0 Intrinsic Assessment of Reliability

In this study, intrinsic assessment of reliability is restricted to analytical acceptability. Table 2 details the analytical acceptability of age estimates evolved in this study, drawn principally from diagnostics illustrated in Figs. 1 to 6 and detailed in sections 4.0 to 5.0. Other indexes of reliability in Optical dating can be drawn by inference. Intra-site stratigraphic consistency of ages, quantified by Bayesian modelling, and the convergence of age estimates from stratigraphically equivalent units of divergent dosimetry are key intrinsic measures of reliability (Toms *et al.*, 2005). However, the low sampling density per dated level and ambiguity in inter-core relative stratigraphic position of samples precluded the use of these inferential methods.

9.0 Summary

This study has generated optical age estimates which commonly span from as little as 0.38 ka to as much as 8.16 ka, with one sample potentially as old as 25.3 ka. Five samples (GL06 006, 008, 020, 024, 026) have proven analytically acceptable. The quality of the data from four samples (GL06 016, 018, 022, 028) is potentially limited by a dearth of datable material whilst overdispersion in regenerative-dose data and minor U disequilibrium may have some bearing on the accuracy of the remaining age estimates. However, the age estimate from only one sample (GL06017) is rejected.

Field Code	Lab Code	Location	Overburden (m)	Grain size (µm)	Moisture content	Ge-y-spectrometry (lab based) (²³⁵ U or Na/y-spectrometry (in situ))		γ D _e (Gy/ka ²)	Neutron Activation Analysis			Total D _e (Gy/ka ²)	Preheat (°C for 10s)	MAM D _e (Gy)	CAM D _e (Gy)	FMM D _e (Gy)	FMM Age (ka)	MAM to CAM Age (ka)	
						K (%)	Th (ppm)		U (ppm)	K (%)	Th (ppm)								U (ppm)
SOAR01†	GL06005	53°N, 1°W, 20 m	0.9	125-180	0.21 ± 0.05	0.38 ± 0.01	1.53 ± 0.11	0.86 ± 0.11	0.26 ± 0.01	2.06 ± 0.09	7.60 ± 0.32	1.76 ± 0.09	1.45 ± 0.16	0.18 ± 0.02	1.89 ± 0.16	1.6 ± 0.1	2.4 ± 0.3	1.8 ± 0.1	0.94 ± 0.09 (0.08)
SOAR02†	GL06006	53°N, 1°W, 20 m	2.0	125-180	0.22 ± 0.06	0.62 ± 0.02	3.26 ± 0.16	2.57 ± 0.12	0.60 ± 0.02	1.43 ± 0.07	6.86 ± 0.31	2.55 ± 0.13	1.14 ± 0.13	0.15 ± 0.01	1.88 ± 0.13	3.2 ± 0.7	5.6 ± 0.5	4.9 ± 0.3	2.62 ± 0.24 (0.22)
SOAR03†	GL06007	53°N, 1°W, 20 m	1.5	125-180	0.12 ± 0.03	0.54 ± 0.02	2.48 ± 0.15	1.73 ± 0.11	0.45 ± 0.02	0.62 ± 0.03	2.87 ± 0.14	1.33 ± 0.07	0.59 ± 0.05	0.16 ± 0.02	1.20 ± 0.05	2.2 ± 0.4	3.7 ± 0.4	4.2 ± 0.3	3.49 ± 0.31 (0.30)
SOAR04†	GL06008	53°N, 1°W, 20 m	1.6	125-180	0.14 ± 0.04	0.60 ± 0.02	3.42 ± 0.17	2.56 ± 0.13	0.60 ± 0.02	0.96 ± 0.05	4.41 ± 0.20	1.87 ± 0.09	0.87 ± 0.07	0.16 ± 0.02	1.63 ± 0.08	3.9 ± 0.4	4.3 ± 0.5	4.1 ± 0.3	2.52 ± 0.22 (0.21)
SOAR05	GL06009	53°N, 1°W, 20 m	3.7	125-180	0.15 ± 0.04	0.85 ± 0.04	4.05 ± 0.35	0.87 ± 0.07	0.41 ± 0.05	1.47 ± 0.06	2.54 ± 0.12	0.81 ± 0.05	1.02 ± 0.10	0.11 ± 0.01	1.55 ± 0.11	24.0 ± 8.0	34.1 ± 4.3	34.1 ± 4.3	22.1 ± 3.2 (3.0)
GEO 2	GL06014	53°N, 1°W, 20 m	1.3	125-180	0.17 ± 0.04	0.84 ± 0.05	4.32 ± 0.47	1.71 ± 0.11	0.49 ± 0.06	1.04 ± 0.05	5.57 ± 0.26	2.22 ± 0.12	0.93 ± 0.09	0.17 ± 0.02	1.59 ± 0.11	2.1 ± 0.5	3.4 ± 0.5	2.2 ± 0.4	1.38 ± 0.25 (0.24)
GEO 3	GL06015	53°N, 1°W, 20 m	1.4	125-180	0.15 ± 0.04	0.77 ± 0.04	4.35 ± 0.37	1.49 ± 0.09	0.47 ± 0.05	0.73 ± 0.03	3.55 ± 0.15	1.81 ± 0.08	0.68 ± 0.06	0.17 ± 0.02	1.31 ± 0.08	1.7 ± 0.1	2.2 ± 0.4	2.0 ± 0.1	1.50 ± 0.14 (0.12)
GEO 4	GL06016	53°N, 1°W, 20 m	1.0	125-180	0.13 ± 0.03	0.79 ± 0.05	4.62 ± 0.51	1.55 ± 0.11	0.59 ± 0.06	0.80 ± 0.03	3.93 ± 0.16	1.94 ± 0.08	0.78 ± 0.06	0.18 ± 0.02	1.46 ± 0.09	3.7 ± 0.8	4.5 ± 0.5	4.1 ± 0.3	2.80 ± 0.27 (0.23)
GEO 5	GL06017	53°N, 1°W, 20 m	0.7	125-180	0.07 ± 0.02	0.81 ± 0.04	4.88 ± 0.39	1.35 ± 0.08	0.54 ± 0.05	0.79 ± 0.03	4.20 ± 0.17	1.65 ± 0.07	0.82 ± 0.05	0.18 ± 0.02	1.55 ± 0.08	2.1 ± 0.9	2.1 ± 0.7	-	1.36 ± 0.46 (0.44)
GEO 7	GL06018	53°N, 1°W, 20 m	2.1	125-180	0.21 ± 0.05	0.91 ± 0.05	5.73 ± 0.43	1.74 ± 0.10	0.53 ± 0.06	1.14 ± 0.05	5.76 ± 0.23	2.27 ± 0.09	0.95 ± 0.10	0.15 ± 0.01	1.62 ± 0.12	1.6 ± 0.5	2.0 ± 0.2	2.0 ± 0.2	1.21 ± 0.16 (0.15)
GEO 11	GL06019	53°N, 1°W, 20 m	1.0	125-180	0.17 ± 0.04	0.80 ± 0.05	4.20 ± 1.51	1.51 ± 0.10	0.46 ± 0.06	1.01 ± 0.04	3.66 ± 0.15	1.55 ± 0.06	0.81 ± 0.08	0.18 ± 0.02	1.45 ± 0.10	0.7 ± 0.2	1.2 ± 0.2	0.7 ± 0.2	0.51 ± 0.11 (0.11)
GEO 12	GL06020	53°N, 1°W, 20 m	1.2	125-180	0.20 ± 0.05	1.00 ± 0.06	5.21 ± 0.47	1.63 ± 0.11	0.53 ± 0.07	1.26 ± 0.06	5.70 ± 0.26	2.10 ± 0.11	1.02 ± 0.11	0.17 ± 0.02	1.72 ± 0.13	1.8 ± 0.1	2.0 ± 0.3	1.8 ± 0.1	1.06 ± 0.11 (0.10)
GEO 14	GL06021	53°N, 1°W, 20 m	1.5	125-180	0.16 ± 0.04	0.90 ± 0.05	6.33 ± 0.46	1.85 ± 0.10	0.60 ± 0.07	1.22 ± 0.05	6.27 ± 0.26	2.47 ± 0.10	1.10 ± 0.10	0.16 ± 0.02	1.86 ± 0.12	4.1 ± 0.7	5.8 ± 0.5	5.8 ± 0.5	3.12 ± 0.34 (0.31)
GEO 17	GL06022	53°N, 1°W, 20 m	1.5	125-180	0.16 ± 0.04	0.71 ± 0.05	2.77 ± 0.41	0.87 ± 0.09	0.33 ± 0.05	0.83 ± 0.03	3.09 ± 0.13	1.63 ± 0.07	0.72 ± 0.06	0.16 ± 0.02	1.21 ± 0.09	2.6 ± 0.7	3.5 ± 0.4	3.5 ± 0.4	2.86 ± 0.38 (0.35)
GEO 18	GL06023	53°N, 1°W, 20 m	1.2	125-180	0.19 ± 0.05	1.04 ± 0.07	7.41 ± 0.73	2.32 ± 0.16	0.68 ± 0.09	1.17 ± 0.05	5.42 ± 0.22	2.50 ± 0.10	1.01 ± 0.10	0.17 ± 0.02	1.86 ± 0.14	3.0 ± 0.6	6.2 ± 0.8	4.8 ± 0.8	2.59 ± 0.47 (0.45)
GEO 22	GL06024	53°N, 1°W, 20 m	0.7	125-180	0.19 ± 0.05	1.54 ± 0.07	6.95 ± 0.46	1.37 ± 0.09	0.68 ± 0.08	2.23 ± 0.09	7.26 ± 0.29	1.73 ± 0.07	1.59 ± 0.16	0.19 ± 0.02	2.45 ± 0.18	2.1 ± 0.3	15.1 ± 2.9	2.1 ± 0.3	0.87 ± 0.14 (0.13)
GEO 24	GL06025	53°N, 1°W, 20 m	1.4	125-180	0.21 ± 0.05	0.92 ± 0.06	7.00 ± 0.56	2.25 ± 0.13	0.62 ± 0.08	1.17 ± 0.05	7.27 ± 0.29	2.81 ± 0.12	1.04 ± 0.11	0.17 ± 0.02	1.83 ± 0.14	1.2 ± 0.3	3.3 ± 0.6	1.3 ± 0.3	0.73 ± 0.17 (0.17)
GEO 25	GL06026	53°N, 1°W, 20 m	2.3	180-250	0.14 ± 0.04	0.70 ± 0.05	3.39 ± 0.53	1.04 ± 0.09	0.38 ± 0.06	0.84 ± 0.04	2.34 ± 0.10	0.86 ± 0.04	0.63 ± 0.06	0.14 ± 0.01	1.15 ± 0.08	5.6 ± 1.2	8.2 ± 1.1	6.4 ± 0.8	5.52 ± 0.78 (0.72)
GEO 27	GL06028	53°N, 1°W, 20 m	0.7	125-180	0.19 ± 0.05	1.04 ± 0.06	6.70 ± 0.56	2.03 ± 0.13	0.63 ± 0.08	1.24 ± 0.05	6.23 ± 0.26	2.47 ± 0.10	1.06 ± 0.11	0.18 ± 0.02	1.88 ± 0.13	2.3 ± 0.2	3.1 ± 0.4	2.4 ± 0.2	1.25 ± 0.13 (0.12)
GEO 29	GL06030	53°N, 1°W, 20 m	1.1	125-180	0.19 ± 0.05	0.78 ± 0.05	5.56 ± 0.55	1.91 ± 0.13	0.53 ± 0.07	0.91 ± 0.05	4.94 ± 0.23	2.06 ± 0.11	0.82 ± 0.08	0.18 ± 0.02	1.52 ± 0.11	3.3 ± 0.6	4.9 ± 0.7	3.4 ± 0.5	2.23 ± 0.35 (0.33)
GEO 30	GL06031	53°N, 1°W, 20 m	2.5	125-180	0.23 ± 0.06	1.15 ± 0.06	4.71 ± 0.40	1.09 ± 0.08	0.46 ± 0.06	1.44 ± 0.06	4.72 ± 0.19	1.89 ± 0.08	1.02 ± 0.12	0.14 ± 0.01	1.63 ± 0.14	5.4 ± 0.8	6.6 ± 0.4	5.3 ± 1.7	3.24 ± 0.09 (1.08)

Table 1 D_e, D_e and Age data of submitted samples. Uncertainties in age are quoted at 1σ confidence, are based on analytical errors and experimental variability and (in parenthesis) experimental variability alone (see 6.0). Blue indicates samples with accepted age estimates, red, age estimates with caveats (see Table 2), MAM, Minimum Age Model; FMM, Finite Mixture Model; CAM, Central Age Model (see 4.2.1)

Generic considerations	Field	Lab	Sample specific considerations
	Code	Code	
None	SOAR01	GL06005	Overdispersion of regenerative-dose data (see 4.1.4). Minor disequilibrium (see 5.0). Accept tentatively
	SOAR02	GL06006	Accept
	SOAR03	GL06007	Overdispersion of regenerative-dose data (see 4.1.4). Accept tentatively
	SOAR04	GL06008	Accept
	SOAR05	GL06009	Minor disequilibrium (see 5.0). Accept tentatively
	GEO 2	GL06014	Major disequilibrium (see 5.0). Accept tentatively
	GEO 3	GL06015	Minor disequilibrium (see 5.0). Accept tentatively
	GEO 4	GL06016	Insufficient mass to verify optimum D _e measurement conditions (see 4.1.2). Accept tentatively
	GEO 5	GL06017	Insufficient mass to verify optimum D _e measurement conditions (see 4.1.2). Insufficient number of aliquots to accurately quantify D _e value. Reject
	GEO 7	GL06018	Insufficient mass to verify optimum D _e measurement conditions (see 4.1.2). Accept tentatively
	GEO 11	GL06019	Insufficient mass to verify optimum D _e measurement conditions (see 4.1.2). Accept tentatively
	GEO 12	GL06020	Accept
	GEO 14	GL06021	Overdispersion of regenerative-dose data (see 4.1.4). Minor disequilibrium (see 5.0). Accept tentatively
	GEO 17	GL06022	Insufficient mass to verify optimum D _e measurement conditions (see 4.1.2). Accept tentatively
	GEO 18	GL06023	Minor disequilibrium (see 5.0). Accept tentatively
	GEO 22	GL06024	Accept
	GEO 24	GL06025	Insufficient mass to verify optimum D _e measurement conditions (see 4.1.2). Major disequilibrium (see 5.0). Accept tentatively
	GEO 25	GL06026	Accept
	GEO 27	GL06028	Insufficient mass to verify optimum D _e measurement conditions (see 4.1.2). Accept tentatively
	GEO 29	GL06030	Overdispersion of regenerative-dose data (see 4.1.4). Accept tentatively
	GEO 30	GL06031	Overdispersion of regenerative-dose data (see 4.1.4). Accept tentatively

Table 2 Analytical acceptability of sample suite age estimates and caveats for consideration

Fig. 1 Signal Calibration

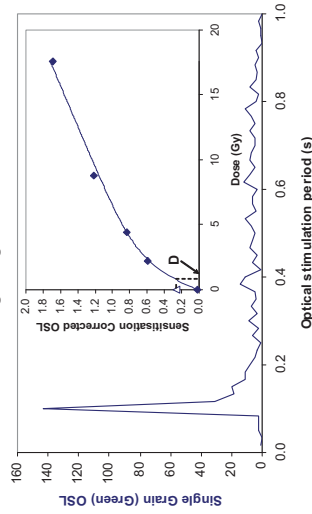


Fig. 1 Signal Calibration Single quartz sand grain natural (green) OSL signal. Inset, the natural green OSL signal (open triangle) of each aliquot is calibrated against known laboratory doses to yield equivalent dose (D_e) values.

Fig. 2 Irradiation-Preheat Cycling The acquisition of D_e values is necessarily predicated upon thermal treatment of aliquots succeeding environmental and laboratory irradiation. Repeated irradiation and thermal treatment results in aliquot sensitisation, rendering calibration of the natural signal inaccurate. This sensitisation can be monitored and corrected for. The accuracy of correction can be preheat dependent; irradiation-preheat cycling quantifies this dependence for laboratory-induced signals, examining the reproducibility of corrected OSL resultant of repeat laboratory doses. This element was based on multi-grain aliquots.

Fig. 3 D_e Preheat Dependence Quantifies the combined effects of thermal transfer and sensitisation on the natural signal. Insignificant adjustment in D_e may reflect limited influence of these effects. This element was based on multi-grain aliquots.

Fig. 4 Dose Recovery Attempts to replicate the above diagnostic, yet provide improved resolution of thermal effects through removal of variability induced by heterogeneous dose absorption in the environment and using a precise lab dose to the natural dose. This element was performed on multi-grain aliquots. Based on this method, preheat data an appropriate thermal treatment is selected to refine the final D_e value.

Fig. 5 Inter-grain D_e distribution Provides a measure of inter-grain dispersion in D_e values derived from natural and laboratory irradiation. Discordant data (those points lying beyond ±2 standardised in D_e) reflects heterogeneous dose absorption and/or inaccuracies in calibration. These estimates of post-burial D_e values are illustrated based on the Minimum Age Model and Central Age Models. n is the number of individual aliquots checked and Central Age Models. The D_e values are plotted about the Central D_e value; n is the fractional predispersion of D_e values about a known regenerative-dose value; k indicates the component number and P the proportion of grains within that component generated by the Finite Mixture Model.

Fig. 7 U Activity Statistical concordance (equilibrium) in the activities of the daughter radionuclides ²²⁶Ra with its parent ²³⁸U may signify the temporal stability of D_e emissions from these grains. Significant differences (dis-equilibrium; >50%) in activity ratios may indicate grain age differences, grain age heterogeneity, or disequilibrium and increased uncertainty in the accuracy of age estimates. 20% disequilibrium marker also shown.

Fig. 8 Age Range An estimate of sediment burial period based on mean D_e values and D_e values derived from Minimum, Finite Mixture and Central Age Models, along with associated analytical uncertainties. The probability distribution indicates the inter-grain variability in age. The maximum influence of temporal variations in D_e values is also shown. The probability distribution indicates the maximum influence of inter-grain variability in D_e values, here coupled with Finite Mixture D_e values, may provide instructive where there is uncertainty in these parameters, however the combined extremes presented should not be construed as preferred age estimates.

Fig. 2 Irradiation-Preheat Cycling

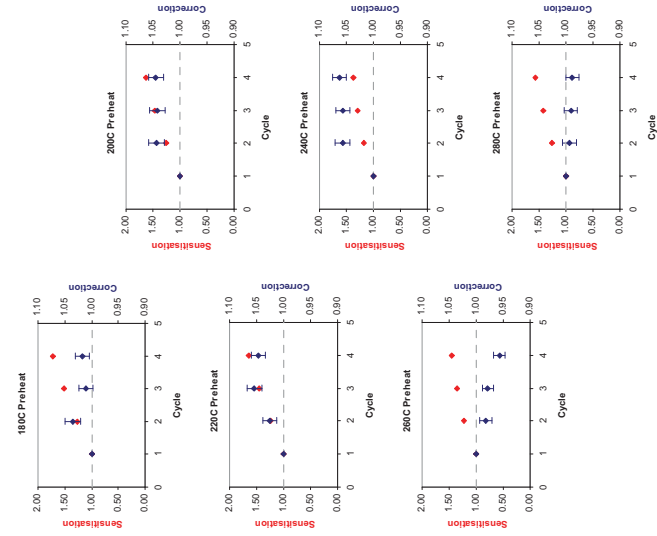


Fig. 3 D_e Preheat Dependence

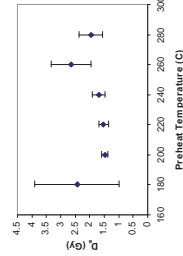


Fig. 4 Dose Recovery

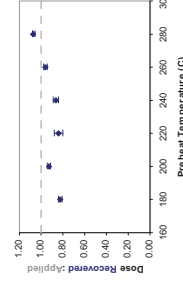


Fig. 5 Inter-grain D_e distribution

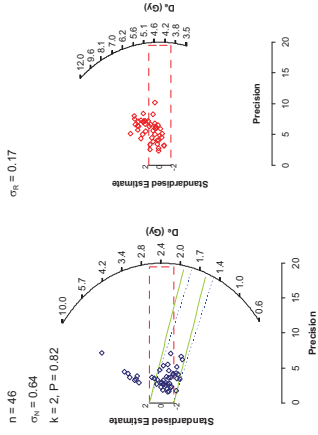


Fig. 6 U Activity

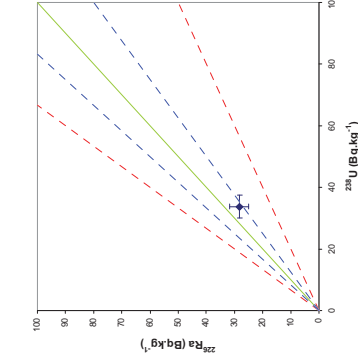
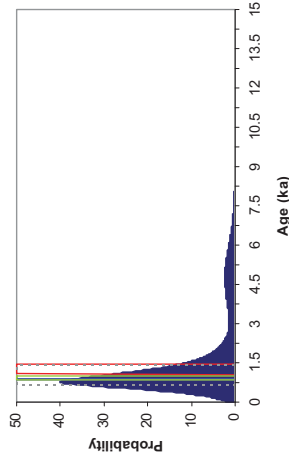


Fig. 7 Age Range



Sample: GL06005

Fig. 1 Signal Calibration

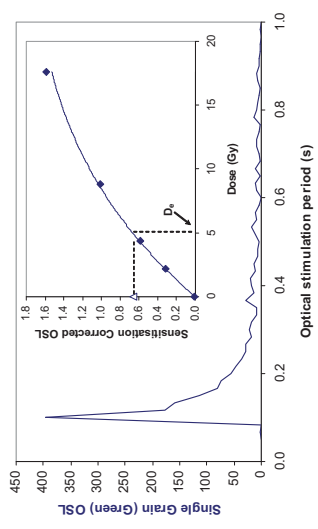


Fig. 1 Signal Calibration Single quartz sand grain natural (green) OSL signal. Inset, the natural green OSL signal (open triangle) of each aliquot is calibrated against known laboratory doses to yield equivalent dose (D_e) values.

Fig. 2 Irradiation-Preheat Cycling

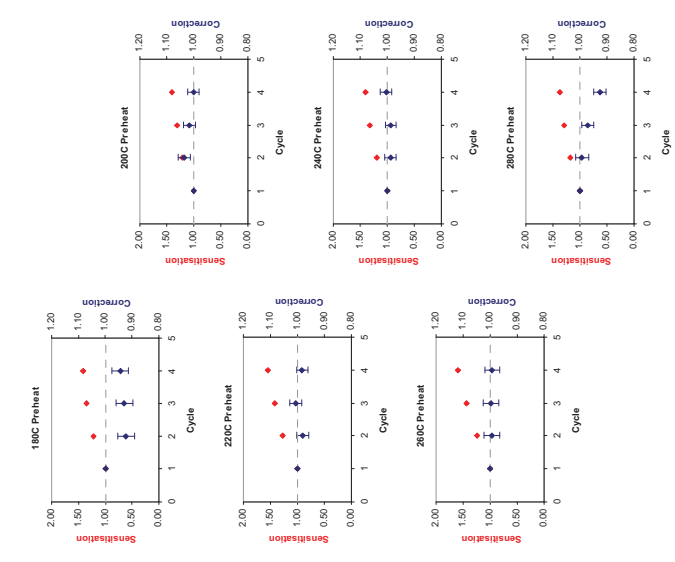


Fig. 3 D_e Preheat Dependence

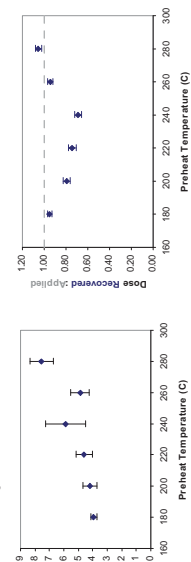


Fig. 4 Dose Recovery

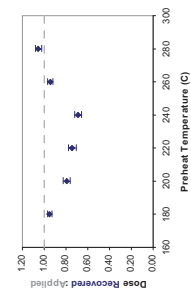


Fig. 5 Inter-grain D_e distribution

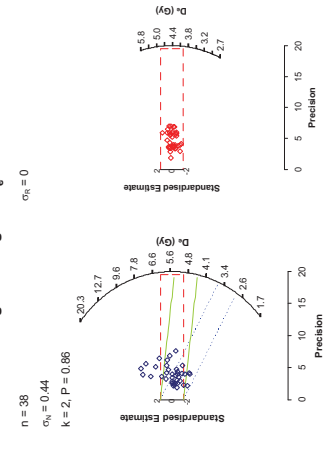


Fig. 6 U Activity

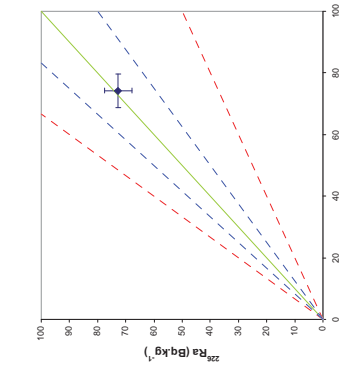
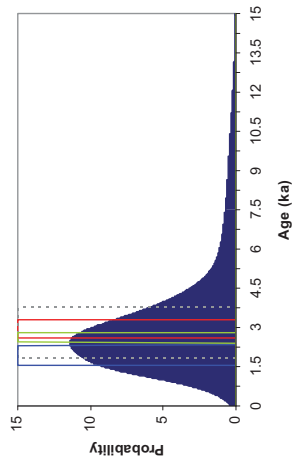


Fig. 7 Age Range



Sample: GL06006

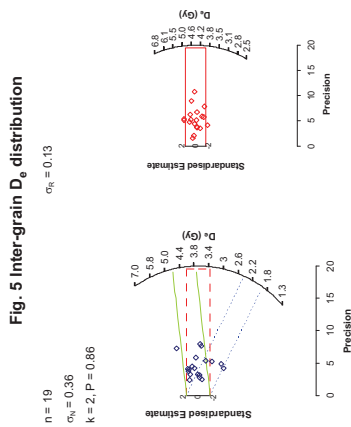


Fig. 1 Signal Calibration

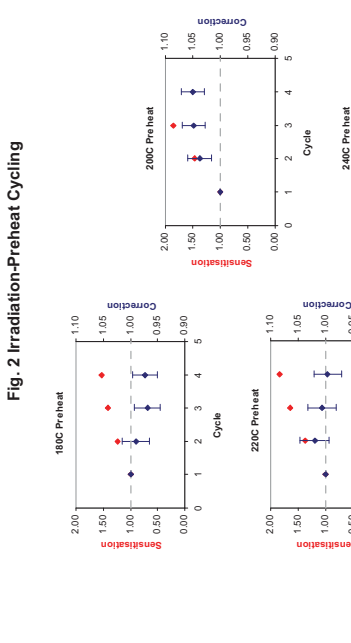


Fig. 2 Irradiation-Preheat Cycling

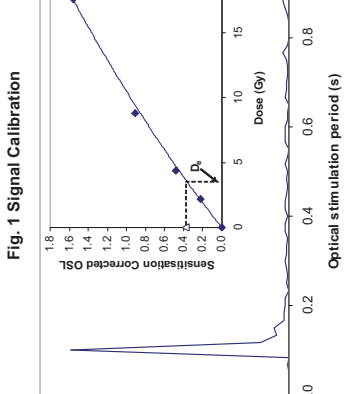


Fig. 3 D_e Preheat Dependence



Fig. 4 Dose Recovery

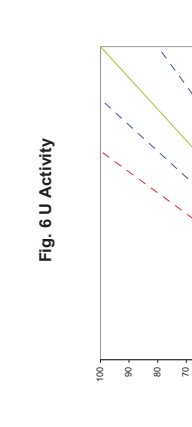


Fig. 5 Inter-grain D_e distribution

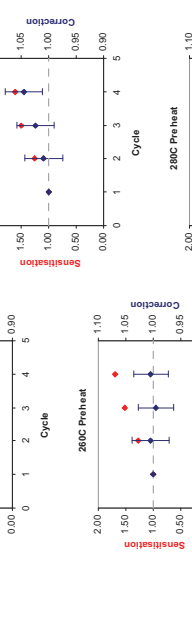


Fig. 6 U Activity

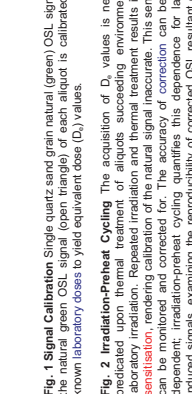


Fig. 7 Age Range



Fig. 8 Age Range

Fig. 1 Signal Calibration

Fig. 2 Irradiation-Preheat Cycling

Fig. 3 D_e Preheat Dependence

Fig. 4 Dose Recovery

Fig. 5 Inter-grain D_e distribution

Fig. 6 U Activity

Fig. 7 Age Range

Fig. 8 Age Range

Sample: GL06007

Sample: GL06007

Sample: GL06007

Sample: GL06007

Sample: GL06007

Sample: GL06007

Sample: GL06007

Sample: GL06007

Sample: GL06007

Sample: GL06007

Sample: GL06007

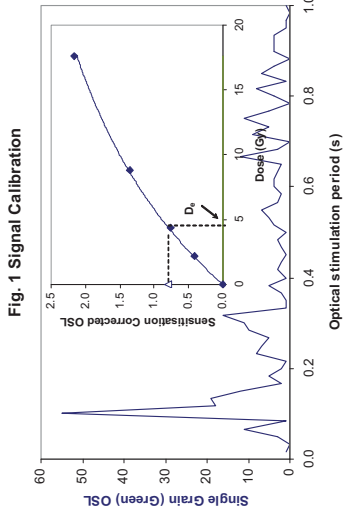


Fig. 1 Signal Calibration

Fig. 1 Signal Calibration Single quartz sand grain natural (green) OSL signal. Inset, the natural green OSL signal (open triangle) of each aliquot is calibrated against known laboratory doses to yield equivalent dose (D_e) values.

Fig. 2 Irradiation-Preheat Cycling The acquisition of D_e values is necessarily preceded by the thermal treatment of the sample. Repeated irradiation and thermal treatment results in altered sensitisation, rendering calibration of the natural signal inaccurate. This sensitisation can be monitored and corrected for. The accuracy of correction can be preheat dependent. Irradiation-preheat cycling quantifies this dependence for laboratory-induced signals, examining the reproducibility of corrected OSL resultant of repeat laboratory doses. This element was based on multi-grain aliquots.

Fig. 3 D_e Preheat Dependence Quantifies the combined effects of thermal transfer and sensitisation on the natural signal. Insignificant adjustment in D_e may reflect limited influence of these effects. This element was based on multi-grain aliquots.

Fig. 4 Dose Recovery Attempts to replicate the above diagnostic, yet provide improved resolution of thermal effects through removal of variability induced by heterogeneous dose absorption in the environment and using a precise lab dose to simulate natural dose. This element was performed on multi-grain aliquots. Based on this and preceding data an appropriate thermal treatment is selected to refine the final D_e value.

Fig. 5 Inter-grain D_e distribution Provides a measure of inter-grain dispersion in D_e values derived from natural and laboratory irradiation. Discordant data (those points lying beyond 2σ standardised in D_e) reflects heterogeneous dose absorption and/or inaccuracies in calibration. Three estimates of post-burial D_e values are illustrated based on the Minimum, Finite Mixture and Central Age Models. n is the number of grains fulfilling acceptability criteria. σ_n is the fractional overdispersion of D_e values about the Central D_e value; σ_n is the fractional overdispersion of D_e values about a known 'regenerative-dose' value; k indicates the component number and P the proportion of grains within that component generated by the Finite Mixture Model.

Fig. 7 U Activity Statistical concordance (equilibrium) in the activities of the daughter radionuclide ^{226}Ra with its parent, ^{238}U , may signify the temporal stability of D_e emissions from these chains. Significant differences (disequilibrium: $>50\%$) in activity indicate addition or removal of isotopes creating a time-dependent shift in D_e values and increased uncertainty in the accuracy of age estimates. 20% disequilibrium marker also shown.

Fig. 8 Age Range An estimate of sediment burial period based on mean D_e values and associated analytical uncertainties. The maximum age indicated by the inter-grain variability in age. The maximum influence of temporal variations in D_e forced by minima-maxima variation in moisture content and overburden thickness, here coupled with Finite Mixture D_e values, may prove instructive where there is uncertainty in these parameters, however the combined extremes represented should not be construed as preferred age estimates.

Fig. 2 Irradiation-Preheat Cycling

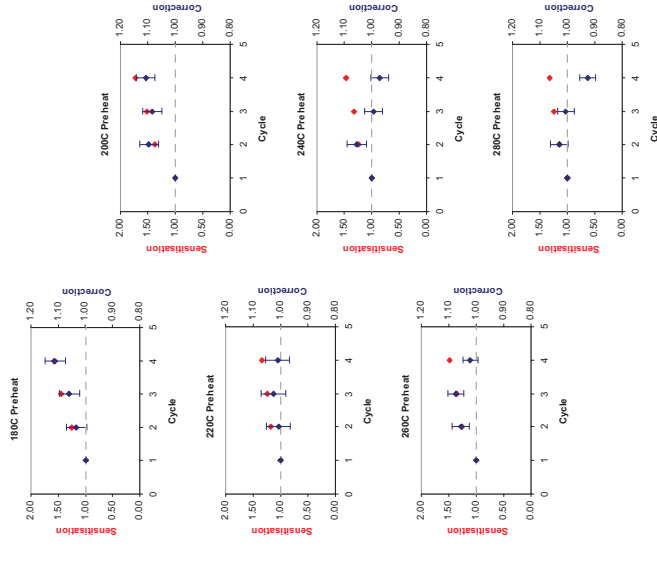


Fig. 3 D_e Preheat Dependence

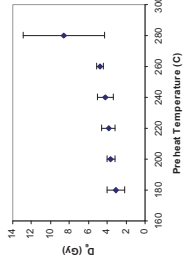


Fig. 4 Dose Recovery

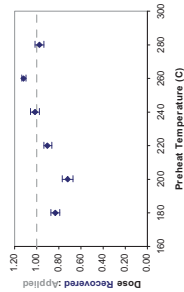


Fig. 5 Inter-grain D_e distribution

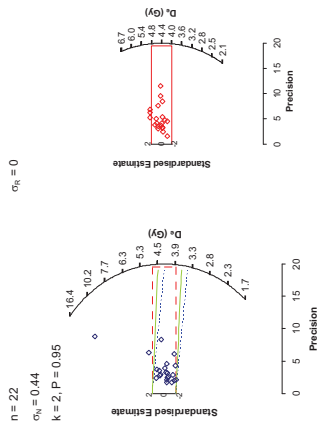


Fig. 6 U Activity

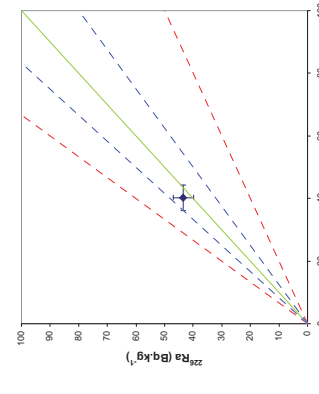
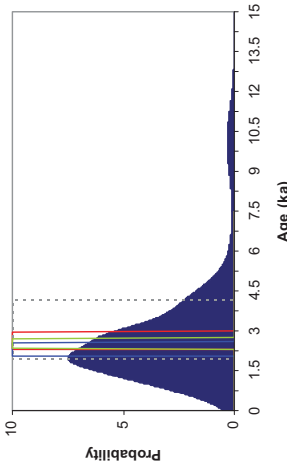


Fig. 7 Age Range



Sample: GL06008

Fig. 1 Signal Calibration

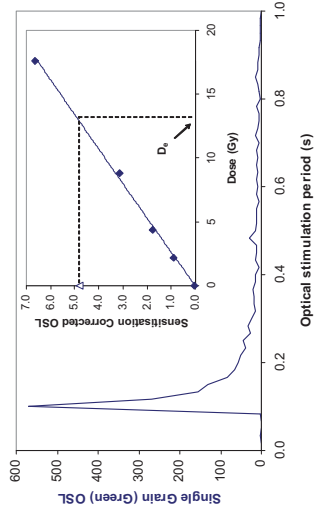


Fig. 1 Signal Calibration Single quartz sand grain natural (green) OSL signal. Inset, the green OSL signal dependence on optical stimulation period is calibrated against known laboratory doses to yield equivalent dose (D₀) values.

Fig. 2 Irradiation-Preheat Cycling The acquisition of D₀ values is necessarily predicated upon thermal treatment of aliquots succeeding environmental and laboratory irradiation. Repeated irradiation and thermal treatment results in aliquot sensitisation, rendering calibration of the natural signal inaccurate. This sensitisation can be monitored and corrected for. The accuracy of correction can be preheat dependent. Irradiation-preheat cycling quantifies this dependence for laboratory-derived signals using the Frittle Mixture Model. The result is a series of repeat laboratory doses. This element was based on multi-grain aliquots.

Fig. 3 D₀ Preheat Dependence Quantifies the combined effects of thermal transfer and sensitisation on the natural signal. Insignificant adjustment in D₀ may reflect limited influence of these effects. This element was based on multi-grain aliquots.

Fig. 4 Dose Recovery Attempts to replicate the above diagnostic, yet provide more realistic thermal effects through the use of a precisely defined, but heterogeneous dose absorption in the environment and using a precise lab dose to simulate natural dose. This element was performed on multi-grain aliquots. Based on this and preceding data an appropriate thermal treatment is selected to refine the final D₀ value.

Fig. 5 Inter-grain D₀ distribution Provides a measure of inter-grain dispersion in D₀ values derived from natural and laboratory irradiation. Discrepant data (those points that do not fall on the line) are assumed to be outliers and are excluded from the analyses in calibration. These estimates of post-burial D₀ values are illustrated based on the Minimum, Finite Mixture and Central Age Models. n is the number of grains fulfilling acceptability criteria; σ_n is the fractional overdispersion of D₀ values about the Central D₀ value; σ_n is the fractional overdispersion of D₀ values about a known regenerative-dose value; k indicates the component number and P the proportion of grains within that component generated by the Finite Mixture Model.

Fig. 6 U Activity Statistical concordance (agreement) in the activities of the daughter radionuclides, ²²⁶Ra with its parent ²³⁸U may signify the temporal stability of D₀ emissions from these chains. Significant differences (dis-equilibrium; >50%) in activity indicate addition or removal of isotopes creating a time-dependent shift in D₀ values and increased uncertainty in the accuracy of age estimates. 20% disequilibrium marker also shown.

Fig. 7 Age Range An estimate of sediment burial period based on mean D₀ values from the Frittle Mixture Model. Central Age Model. The probability of temporal variations in D₀ inter-grain variability in age. The maximum influence of temporal variations in D₀ forced by minima-maxima variation in moisture content and overburden thickness, here coupled with Frittle Mixture D₀ values, may prove instructive where there is uncertainty in these parameters, however the combined extremes represented should not be construed as preferred age estimates.

Fig. 2 Irradiation-Preheat Cycling

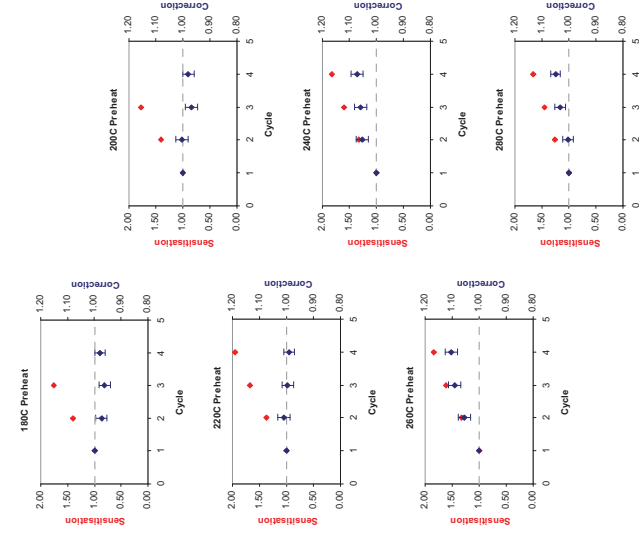


Fig. 3 D₀ Preheat Dependence

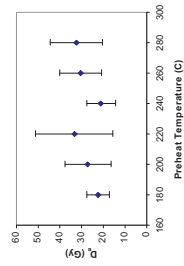


Fig. 4 Dose Recovery

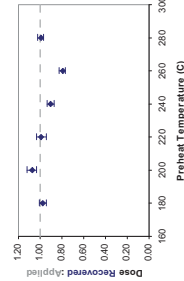


Fig. 5 Inter-grain D₀ distribution

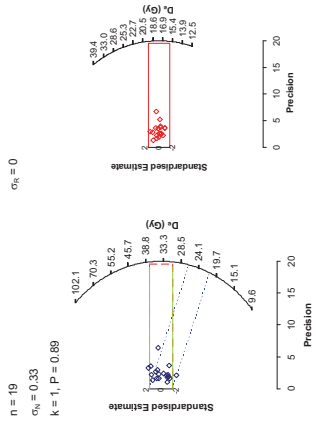


Fig. 6 U Activity

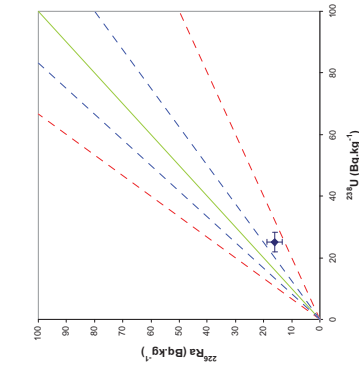
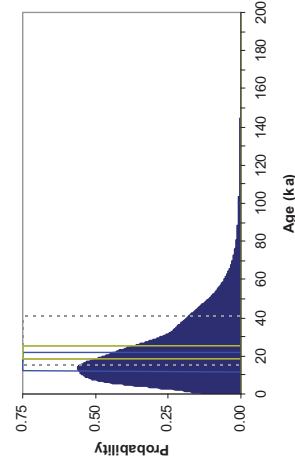


Fig. 7 Age Range



Sample: GL06009

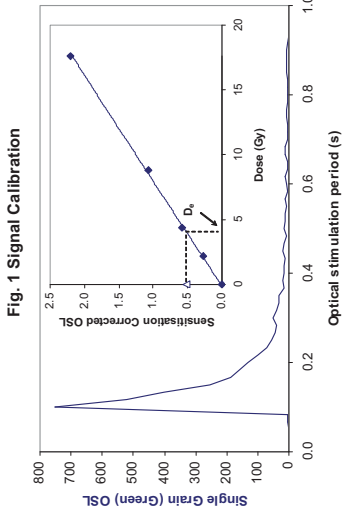


Fig. 1 Signal Calibration

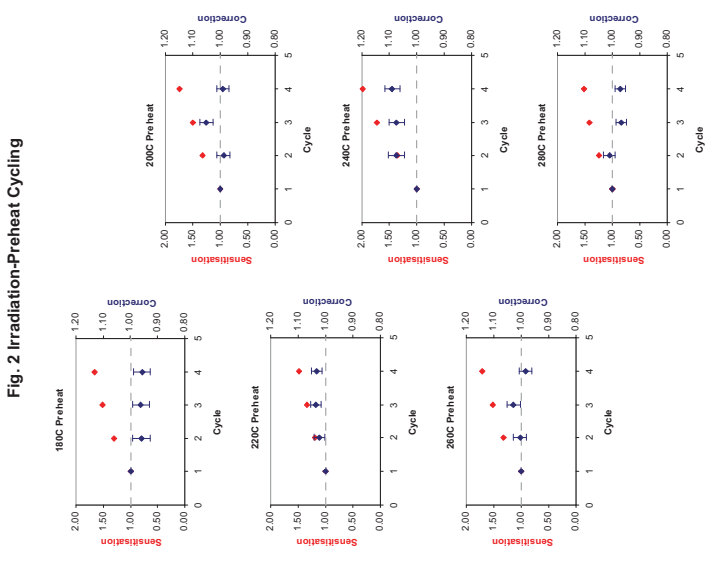


Fig. 2 Irradiation-Preheat Cycling

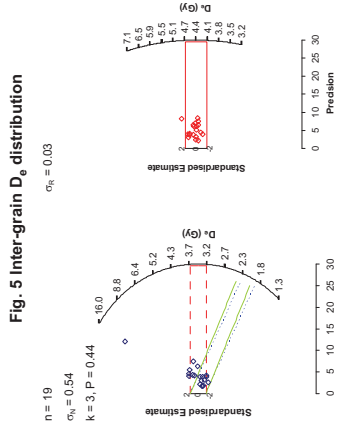


Fig. 3 D₀ Preheat Dependence

Fig. 1 Signal Calibration Single quartz sand grain natural (green) OSL signal. Inset, the natural green OSL signal (open triangle) of each aliquot is calibrated against known laboratory doses to yield equivalent dose (D₀) values.

Fig. 2 Irradiation-Preheat Cycling The acquisition of D₀ values is necessarily through repeated irradiation and thermal treatment. This sensitisation, resulting from repeated irradiation and thermal treatment, results in altered sensitisation, rendering calibration of the natural signal inaccurate. This sensitisation can be monitored and corrected for. The accuracy of correction can be preheat dependent. Irradiation-preheat cycling quantifies this dependence for laboratory-induced signals, examining the reproducibility of corrected OSL resultant of repeat laboratory doses. This element was based on multi-grain aliquots.

Fig. 3 D₀ Preheat Dependence Quantifies the combined effects of thermal transfer and sensitisation on the natural signal. Insignificant adjustment in D₀ may reflect limited influence of these effects. This element was based on multi-grain aliquots.

Fig. 4 Dose Recovery Attempts to replicate the above diagnostic, yet provide improved resolution of thermal effects through removal of variability induced by heterogeneous dose absorption in the environment and using a precise lab dose to simulate natural dose. This element was performed on multi-grain aliquots. Based on this and preceding data an appropriate thermal treatment is selected to refine the final D₀ value.

Fig. 5 Inter-grain D₀ distribution Provides a measure of inter-grain dispersion in D₀ values derived from natural and laboratory irradiation. Discordant data (those points lying beyond ±2 standardised in D₀) reflects heterogeneous dose absorption and/or inaccuracies in calibration. Three estimates of post-burial D₀ values are illustrated based on the Minimum, Finite Mixture and Central Age Models. n is the number of grains fulfilling acceptability criteria. σ_n is the fractional overdispersion of D₀ values about the Central D₀ value; σ_n is the fractional overdispersion of D₀ values about a known 'regenerative-dose' value; k indicates the component number and P the proportion of grains within that component generated by the Finite Mixture Model.

Fig. 7 U Activity: Statistical concordance (equilibrium) in the activities of the daughter radionuclide ²²⁶Ra with its parent, ²³⁸U may signify the temporal stability of D₀ emissions from these chains. Significant differences (disequilibrium: >50%) in activity indicate addition or removal of isotopes creating a time-dependent shift in D₀ values and increased uncertainty in the accuracy of age estimates. 20% disequilibrium marker also shown.

Fig. 8 Age Range An estimate of sediment burial period based on mean D₀ values from the Minimum and Central Age Models. The probability distribution indicates inter-grain variability in age. The maximum influence of temporal variations in D₀ forced by minima-maxima variation in moisture content and overburden thickness, here coupled with Finite Mixture D₀ values, may prove instructive where there is uncertainty in these parameters, however the combined extremes represented should not be construed as preferred age estimates.

Fig. 5 Inter-grain D₀ distribution

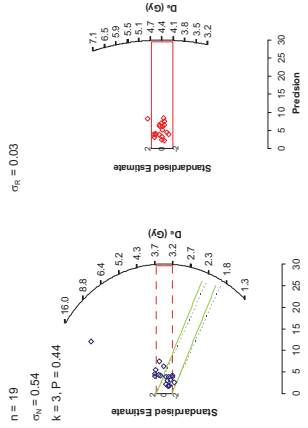


Fig. 6 U Activity

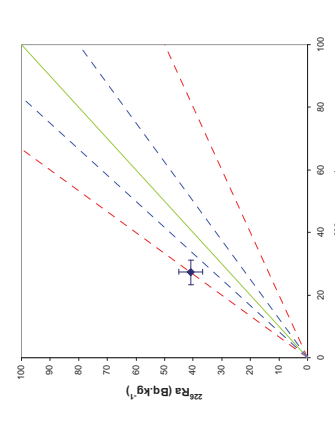
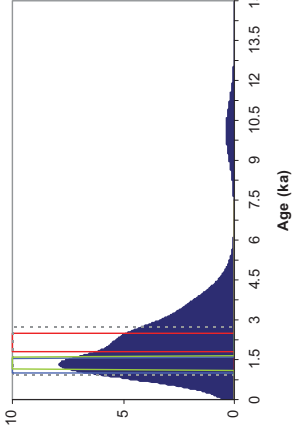


Fig. 7 Age Range



Sample: GL06014

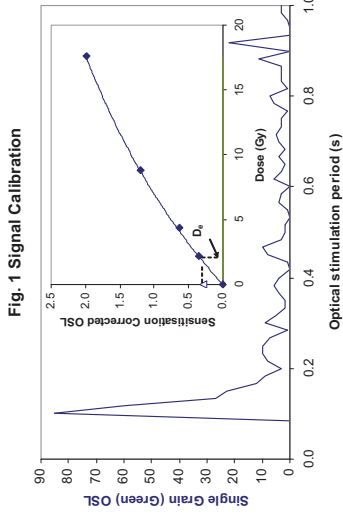


Fig. 1 Signal Calibration

Fig. 1 Signal Calibration Single quartz sand grain natural (green) OSL signal, inset, the natural green OSL signal (open triangle) of each aliquot is calibrated against known laboratory doses to yield equivalent dose (D_e) values.

Fig. 2 Irradiation-Preheat Cycling The acquisition of D_e values is necessarily through repeated irradiation and preheating. Repeated irradiation and preheating results in altered sensitisation, rendering calibration of the natural signal inaccurate. This sensitisation can be monitored and corrected for. The accuracy of correction can be preheat dependent; irradiation-preheat cycling quantifies this dependence for laboratory-induced signals, examining the reproducibility of corrected OSL resultant of repeat laboratory doses. This element was based on multi-grain aliquots.

Fig. 3 D_e Preheat Dependence Quantifies the combined effects of thermal transfer and sensitisation on the natural signal. Insignificant adjustment in D_e may reflect limited influence of these effects. This element was based on multi-grain aliquots.

Fig. 4 Dose Recovery Attempts to replicate the above diagnostic, yet provide improved resolution of thermal effects through removal of variability induced by heterogeneous dose absorption in the environment and using a precise lab dose to simulate natural dose. This element was performed on multi-grain aliquots. Based on this and preceding data an appropriate thermal treatment is selected to refine the final D_e value.

Fig. 5 Inter-grain D_e distribution Provides a measure of inter-grain dispersion in D_e values derived from natural and laboratory irradiation. Discordant data (those points lying beyond 2σ standardised in D_e) reflects heterogeneous dose absorption and/or inaccuracies in calibration. Three estimates of post-burial D_e values are illustrated based on the Minimum, Finite Mixture and Central Age Models. n is the number of grains fulfilling acceptability criteria, σ_n is the fractional overdispersion of D_e values about the Central Dose value, σ_n is the fractional overdispersion of D_e values about a known regenerative-dose value, k indicates the component number, and P the proportion of grains within that component generated by the Finite Mixture Model.

Fig. 7 U Activity Statistical concordance (equilibrium) in the activities of the daughter radionuclide ^{226}Ra with its parent, ^{238}U , may signify the temporal stability of D_e emissions from these chains. Significant differences (disequilibrium: $>50\%$) in activity indicate addition or removal of isotopes creating a time-dependent shift in D_e values and increased uncertainty in the accuracy of age estimates. 20% disequilibrium marker also shown.

Fig. 8 Age Range An estimate of sediment burial period based on mean D_e values and associated analytical uncertainties. The probability distribution indicates the inter-grain variability in age. The maximum influence of temporal variations in D_e forced by minima-maxima variation in moisture content and overburden thickness, here coupled with Finite Mixture D_e values, may prove instructive where there is uncertainty in these parameters, however the combined extremes represented should not be construed as preferred age estimates.

Fig. 2 Irradiation-Preheat Cycling

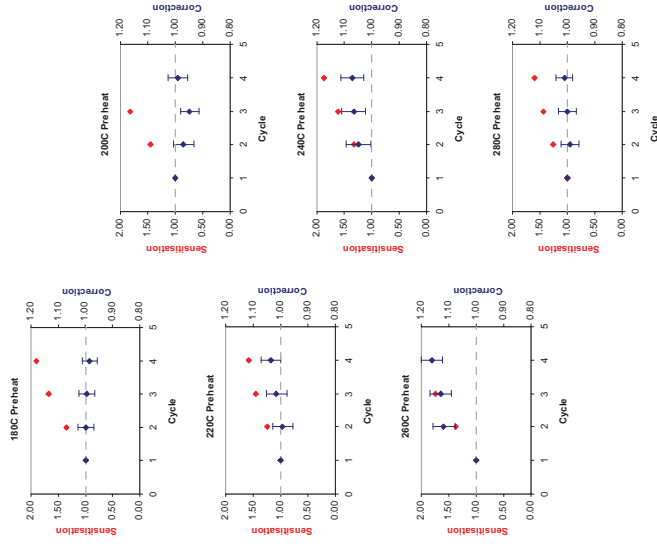


Fig. 3 D_e Preheat Dependence

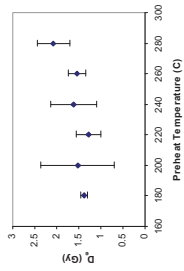


Fig. 4 Dose Recovery

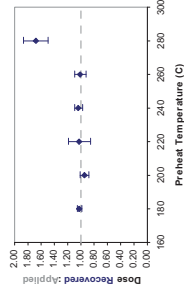


Fig. 5 Inter-grain D_e distribution

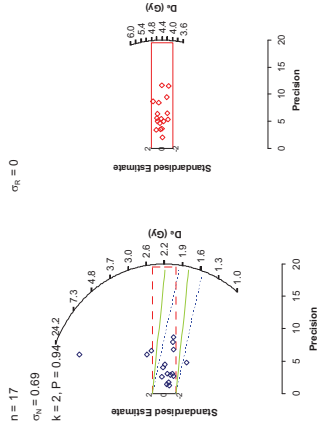


Fig. 6 U Activity

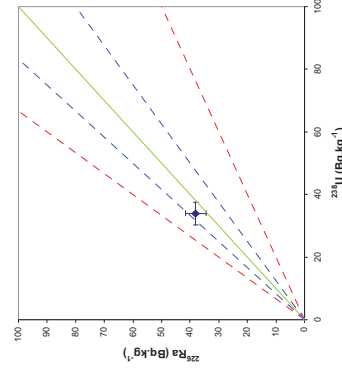
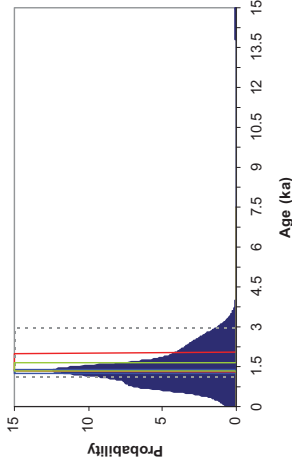


Fig. 7 Age Range



Sample: GL06015

Fig. 2 Irradiation-Preheat Cycling

Insufficient Sample Mass

Fig. 5 Inter-grain D_e distribution

$n = 20$
 $\sigma_n = 0.33$
 $k = 2, P = 0.92$
 $\sigma_n = 0$

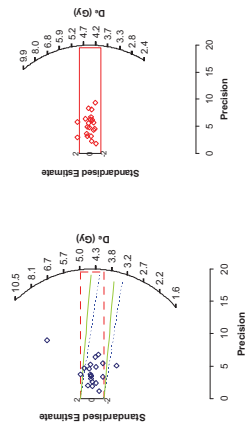


Fig. 6 U Activity

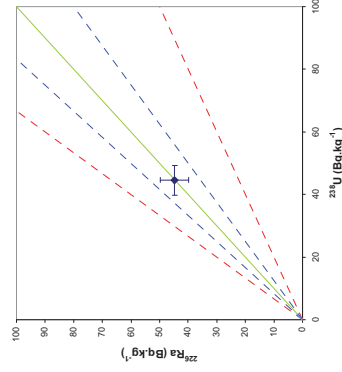
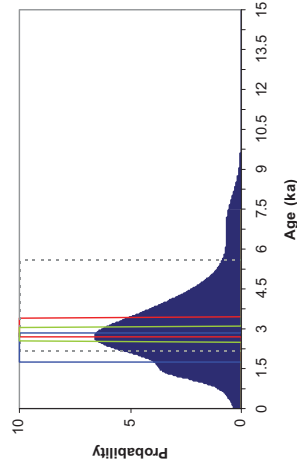


Fig. 7 Age Range



Sample: GL06016

Fig. 1 Signal Calibration

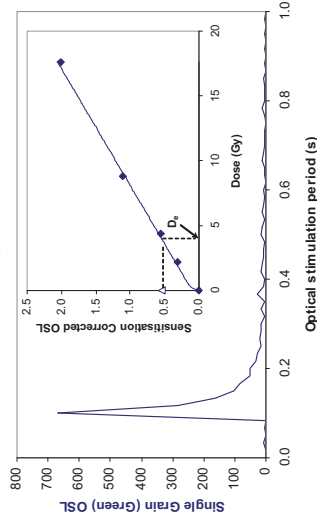


Fig. 1 Signal Calibration Single quartz sand grain natural (green) OSL signal. Inset, the natural green OSL signal (open triangle) of each aliquot is calibrated against known laboratory doses to yield equivalent dose (D_e) values.

Fig. 2 Irradiation-Preheat Cycling The acquisition of D_e values is necessarily dependent on the thermal history of the sample. Repeated irradiation and thermal treatment results in altered sensitivity, rendering calibration of the natural signal inaccurate. This sensitisation can be monitored and corrected for. The accuracy of correction can be preheat dependent. Irradiation-preheat cycling quantifies this dependence for laboratory-induced signals, examining the reproducibility of corrected OSL resultant of repeat laboratory doses. This element was based on multi-grain aliquots.

Fig. 3 D_e Preheat Dependence Quantifies the combined effects of thermal transfer and sensitisation on the natural signal. Insignificant adjustment in D_e may reflect limited influence of these effects. This element was based on multi-grain aliquots.

Fig. 4 Dose Recovery Attempts to replicate the above diagnostic, yet provide improved resolution of thermal effects through removal of variability induced by heterogeneous dose absorption in the environment and using a precise lab dose to simulate natural dose. This element was performed on multi-grain aliquots. Based on this and preceding data an appropriate thermal treatment is selected to refine the final D_e value.

Fig. 3 D_e Preheat Dependence

Insufficient Sample Mass

Fig. 4 Dose Recovery

Insufficient Sample Mass

Fig. 5 Inter-grain D_e distribution

Insufficient Sample Mass

Fig. 6 U Activity Provides a measure of inter-grain dispersion in D_e values derived from natural and laboratory irradiation. Discordant data (these points lying beyond ± 2 standardised in D_e) reflects heterogeneous dose absorption and/or inaccuracies in calibration. Three estimates of post-burial D_e values are illustrated based on the Minimum, Finite Mixture and Central Age Models. n is the number of grains fulfilling acceptability criteria. σ_n is the fractional overdispersion of D_e values about the Central D_e value; σ_n is the fractional overdispersion of D_e values about a known 'regenerative-dose' value; k indicates the component number and P the proportion of grains within that component generated by the Finite Mixture Model.

Fig. 7 U Activity Statistical concordance (equilibrium) in the activities of the daughter radionuclide ^{226}Ra with its parent ^{235}U may signify the temporal stability of D_e emissions from these chains. Significant differences (disequilibrium: $>50\%$) in activity indicate addition or removal of isotopes creating a time-dependent shift in D_e values and increased uncertainty in the accuracy of age estimates. 20% disequilibrium marker also shown.

Fig. 8 Age Range An estimate of sediment burial period based on mean D_e values from multiple aliquots and associated uncertainties. The probability distribution indicates the inter-grain variability in age. The maximum influence of temporal variations in D_e forced by minima-maxima variation in moisture content and overburden thickness, here coupled with Finite Mixture D_e values, may prove instructive where there is uncertainty in these parameters, however the combined extremes represented should not be construed as preferred age estimates.

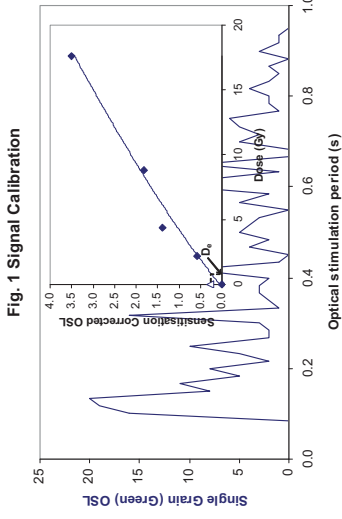


Fig. 1 Signal Calibration

Fig. 2 Irradiation-Preheat Cycling

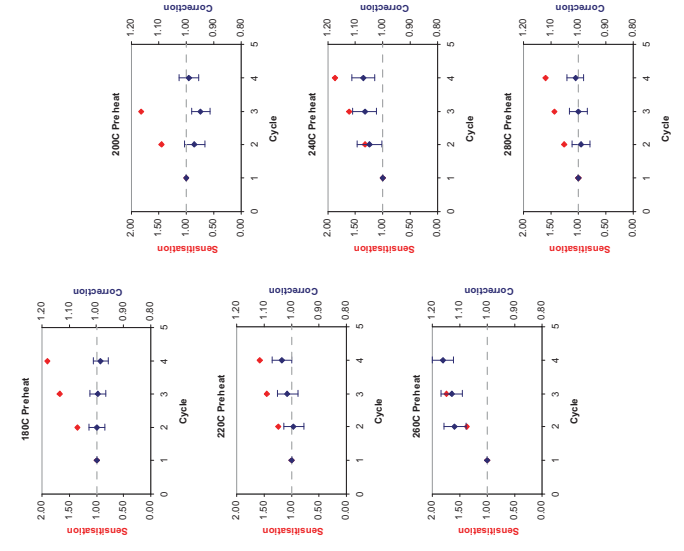


Fig. 5 Inter-grain D_e distribution

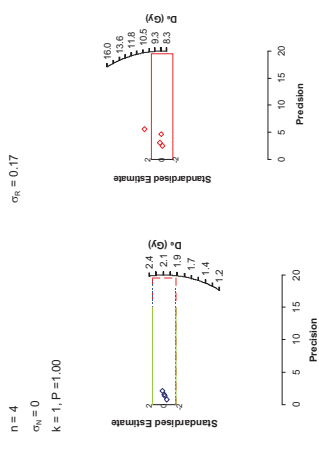


Fig. 1 Signal Calibration Single quartz sand grain natural (green) OSL signal. Inset, the natural green OSL signal (open triangle) of each aliquot is calibrated against known laboratory doses to yield equivalent dose (D_e) values.

Fig. 2 Irradiation-Preheat Cycling The acquisition of D_e values is necessarily through the repeated irradiation and thermal treatment of aliquots. This sensitisation, resulting from repeated irradiation and thermal treatment results in aliquot sensitisation, rendering calibration of the natural signal inaccurate. This sensitisation can be monitored and corrected for. The accuracy of correction can be preheat dependent. Irradiation-preheat cycling quantifies this dependence for laboratory-induced signals, examining the reproducibility of corrected OSL resultant of repeat laboratory doses. This element was based on multi-grain aliquots.

Fig. 3 D_e Preheat Dependence Quantifies the combined effects of thermal transfer and sensitisation on the natural signal. Insignificant adjustment in D_e may reflect limited influence of these effects. This element was based on multi-grain aliquots.

Fig. 4 Dose Recovery Attempts to replicate the above diagnostic, yet provide improved resolution of thermal effects through removal of variability induced by heterogeneous dose absorption in the environment and using a precise lab dose to simulate natural dose. This element was performed on multi-grain aliquots. Based on this and preceding data an appropriate thermal treatment is selected to refine the final D_e value.

Fig. 5 Inter-grain D_e distribution Provides a measure of inter-grain dispersion in D_e values derived from natural and laboratory irradiation. Discordant data (those points lying beyond 2 standardised in D_e) reflects heterogeneous dose absorption and/or inaccuracies in calibration. Three estimates of post-burial D_e values are illustrated based on the Minimum, Finite Mixture and Central Age Models. n is the number of grains fulfilling acceptability criteria. σ_n is the fractional overdispersion of D_e values about the Central D_e value; σ_n is the fractional overdispersion of D_e values about a known regenerative-dose value; k indicates the component number and P the proportion of grains within that component generated by the Finite Mixture Model.

Fig. 7 U Activity: Statistical concordance (equilibrium) in the activities of the daughter radionuclide ²²⁶Ra with its parent ²³⁸U may signify the temporal stability of D_e emissions from these chains. Significant differences (disequilibrium: >50% in activity indicate addition or removal of isotopes creating a time-dependent shift in D_e values and increased uncertainty in the accuracy of age estimates. 20% disequilibrium marker also shown.

Fig. 8 Age Range An estimate of sediment burial period based on mean D_e values and the maximum age indicated by the Central Age Model. The probability distribution indicates the inter-grain variability in age. The maximum influence of temporal variations in D_e forced by minima-maxima variation in moisture content and overburden thickness, here coupled with Finite Mixture D_e values, may prove instructive where there is uncertainty in these parameters, however the combined extremes represented should not be construed as preferred age estimates.

Fig. 6 U Activity

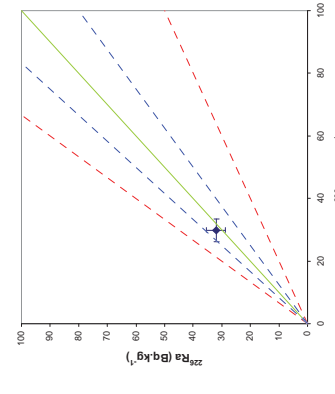


Fig. 7 Age Range

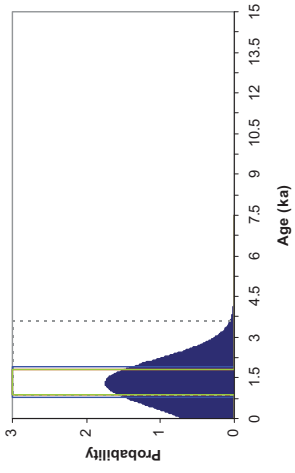


Fig. 3 D_e Preheat Dependence

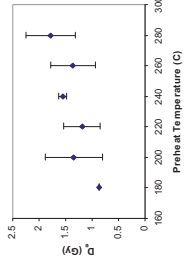
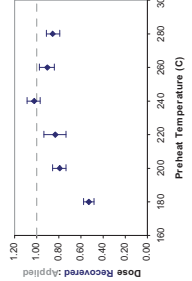


Fig. 4 Dose Recovery



Sample: GL06017

Fig. 2 Irradiation-Preheat Cycling

Insufficient Sample Mass

Fig. 5 Inter-grain D_0 distribution

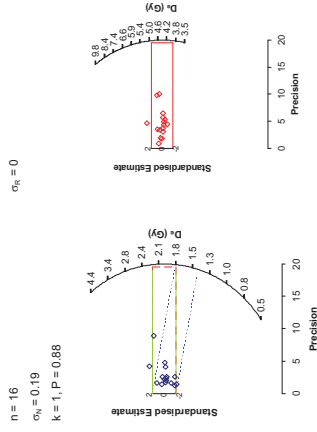


Fig. 1 Signal Calibration

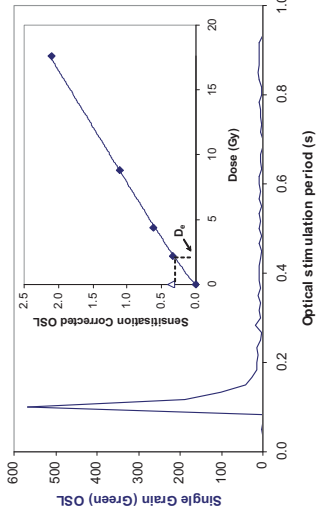


Fig. 1 Signal Calibration Single quartz sand grain natural (green) OSL signal. Inset, the natural green OSL signal (open triangle) of each aliquot is calibrated against known laboratory doses to yield equivalent dose (D_0) values.

Fig. 2 Irradiation-Preheat Cycling The acquisition of D_0 values is necessarily dependent on the thermal signal. Repeated irradiation and thermal treatment results in altered sensitivity, rendering calibration of the natural signal inaccurate. This sensitisation can be monitored and corrected for. The accuracy of correction can be preheat dependent. Irradiation-preheat cycling quantifies this dependence for laboratory-induced signals, examining the reproducibility of corrected OSL resultant of repeat laboratory doses. This element was based on multi-grain aliquots.

Fig. 3 D_0 Preheat Dependence Quantifies the combined effects of thermal transfer and sensitisation on the natural signal. Insignificant adjustment in D_0 may reflect limited influence of these effects. This element was based on multi-grain aliquots.

Fig. 4 Dose Recovery Attempts to replicate the above diagnostic, yet provide improved resolution of thermal effects through removal of variability induced by heterogeneous dose absorption in the environment and using a precise lab dose to simulate natural dose. This element was performed on multi-grain aliquots. Based on this and preceding data an appropriate thermal treatment is selected to refine the final D_0 value.

Fig. 5 Inter-grain D_0 distribution Provides a measure of inter-grain dispersion in D_0 values derived from natural and laboratory irradiation. Discordant data (these points lying beyond ± 2 standardised in D_0) reflects heterogeneous dose absorption and/or inaccuracies in calibration. Three estimates of post-burial D_0 values are illustrated based on the Minimum, Finite Mixture and Central Age Models. n is the number of grains fulfilling acceptability criteria. σ_0 is the fractional overdispersion of D_0 values about the Central Dose value; σ_0 is the fractional overdispersion of D_0 values about a known 'regenerative-dose' value; k indicates the component number and P the proportion of grains within that component generated by the Finite Mixture Model.

Fig. 7 U Activity. Statistical concordance (equilibrium) in the activities of the daughter radionuclide ^{226}Ra with its parent, ^{238}U may signify the temporal stability of D_0 emissions from these chains. Significant differences (disequilibrium: $>50\%$) in activity indicate addition or removal of isotopes creating a time-dependent shift in D_0 values and increased uncertainty in the accuracy of age estimates. 20% disequilibrium marker also shown.

Fig. 8 Age Range An estimate of sediment burial period based on mean D_0 values from multiple aliquots and associated uncertainties. The probability distribution indicates the inter-grain variability in age. The maximum influence of temporal variations in D_0 forced by minima-maxima variation in moisture content and overburden thickness, here coupled with Finite Mixture D_0 values, may prove instructive where there is uncertainty in these parameters, however the combined extremes represented should not be construed as preferred age estimates.

Fig. 6 U Activity

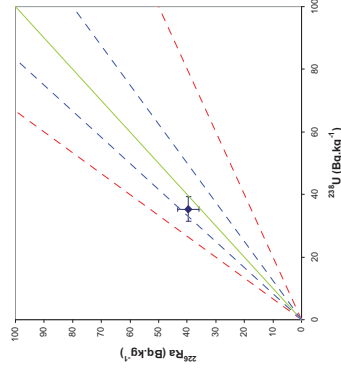
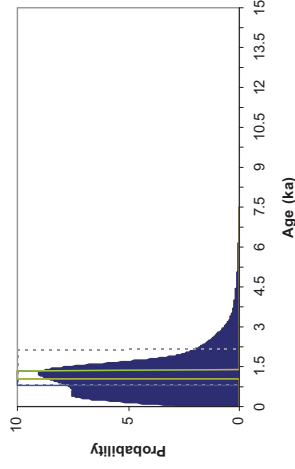


Fig. 7 Age Range



Sample: GL06018

Fig. 1 Signal Calibration

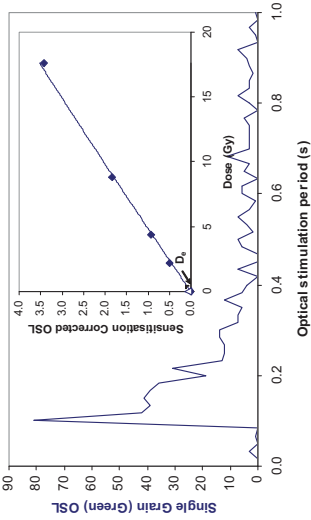


Fig. 2 Irradiation-Preheat Cycling

Insufficient Sample Mass

Fig. 5 Inter-grain D_0 distribution

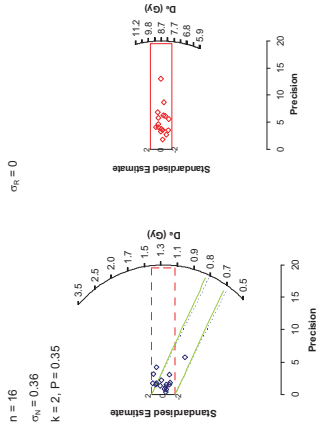


Fig. 1 Signal Calibration Single quartz sand grain natural (green) OSL signal. Inset, the natural green OSL signal (open triangle) of each aliquot is calibrated against known laboratory doses to yield equivalent dose (D_0) values.

Fig. 2 Irradiation-Preheat Cycling The acquisition of D_0 values is necessarily dependent on the pre-heat signal. Repeated irradiation and thermal treatment results in aliquot sensitisation, rendering calibration of the natural signal inaccurate. This sensitisation can be monitored and corrected for. The accuracy of correction can be pre-heat dependent. Irradiation-preheat cycling quantifies this dependence for laboratory-induced signals, examining the reproducibility of corrected OSL resultant of repeat laboratory doses. This element was based on multi-grain aliquots.

Fig. 3 D_0 Preheat Dependence Quantifies the combined effects of thermal transfer and sensitisation on the pre-heat signal. Insignificant adjustment in D_0 may reflect limited influence of these effects. This element was based on multi-grain aliquots.

Fig. 4 Dose Recovery Attempts to replicate the above diagnostic, yet provide improved resolution of thermal effects through removal of variability induced by heterogeneous dose absorption in the environment and using a precise lab dose to simulate natural dose. This element was performed on multi-grain aliquots. Based on this and preceding data an appropriate thermal treatment is selected to refine the final D_0 value.

Fig. 3 D_0 Preheat Dependence

Insufficient Sample Mass

Fig. 4 Dose Recovery

Insufficient Sample Mass

Fig. 6 U Activity

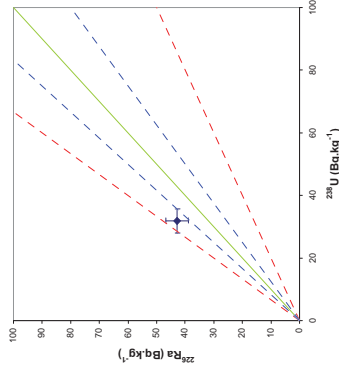
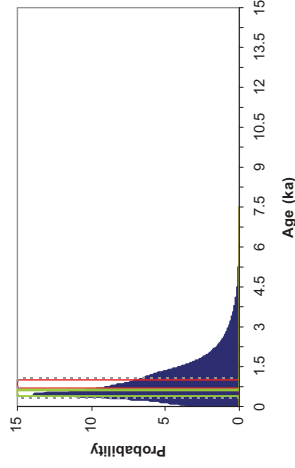


Fig. 7 Age Range



Sample: GL06019

Fig. 5 Inter-grain D_0 distribution Provides a measure of inter-grain dispersion in D_0 values derived from natural and laboratory irradiation. Discordant data (these points lying beyond 2σ standardised in D_0) reflects heterogeneous dose absorption and/or inaccuracies in calibration. Three estimates of post-burial D_0 values are illustrated based on the Minimum, Finite Mixture and Central Age Models. n is the number of grains fulfilling acceptability criteria. σ_n is the fractional overdispersion of D_0 values about the Central D_0 value; σ_n is the fractional overdispersion of D_0 values about a known 'regenerative-dose' value; k indicates the component, number, and P the proportion of grains within that component generated by the Finite Mixture Model.

Fig. 6 U Activity Statistical concordance (equilibrium) in the activities of the daughter radionuclide ^{226}Ra with its parent ^{238}U may signify the temporal stability of D_0 emissions from these chains. Significant differences (disequilibrium: $>50\%$) in activity indicate addition or removal of isotopes creating a time-dependent shift in D_0 values and increased uncertainty in the accuracy of age estimates. 20% disequilibrium marker also shown.

Fig. 7 Age Range An estimate of sediment burial period based on mean D_0 values and the maximum age indicated by the ^{226}Ra activity. The probability distribution indicates the inter-grain variability in age. The maximum influence of temporal variations in D_0 forced by minima-maxima variation in moisture content and overburden thickness, here coupled with Finite Mixture D_0 values, may prove instructive where there is uncertainty in these parameters, however the combined extremes represented should not be construed as preferred age estimates.

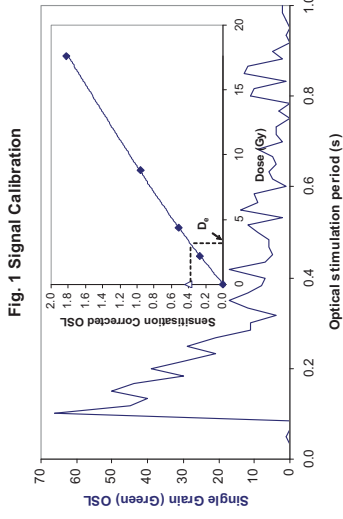


Fig. 1 Signal Calibration

Fig. 1 Signal Calibration Single quartz sand grain natural (green) OSL signal, inset, the natural green OSL signal (open triangle) of each aliquot is calibrated against known laboratory doses to yield equivalent dose (D_e) values.

Fig. 2 Irradiation-Preheat Cycling The acquisition of D_e values is necessarily through repeated irradiation and preheat cycles. The natural signal (these points) is compared to the laboratory irradiation and preheat results. This sensitisation, resulting in a D_e value, can be monitored and corrected for. The accuracy of correction can be preheat dependent. Irradiation-preheat cycling quantifies this dependence for laboratory-induced signals, examining the reproducibility of corrected OSL resultant of repeat laboratory doses. This element was based on multi-grain aliquots.

Fig. 3 D_e Preheat Dependence Quantifies the combined effects of thermal transfer and sensitisation on the natural signal. Insignificant adjustment in D_e may reflect limited influence of these effects. This element was based on multi-grain aliquots.

Fig. 4 Dose Recovery Attempts to replicate the above diagnostic, yet provide improved resolution of thermal effects through removal of variability induced by heterogeneous dose absorption in the environment and using a precise lab dose to simulate natural dose. This element was performed on multi-grain aliquots. Based on this and preceding data an appropriate thermal treatment is selected to refine the final D_e value.

Fig. 5 Inter-grain D_e distribution Provides a measure of inter-grain dispersion in D_e values derived from natural and laboratory irradiation. Discordant data (these points lying beyond ± 2 standardised in D_e) reflects heterogeneous dose absorption and/or inaccuracies in calibration. Three estimates of post-burial D_e values are illustrated based on the Minimum, Finite Mixture and Central Age Models. n is the number of grains fulfilling acceptability criteria. σ_n is the fractional overdispersion of D_e values about the Central Dose value; σ_n is the fractional overdispersion of D_e values about a known regenerative-dose value; k indicates the component number and P the proportion of grains within that component generated by the Finite Mixture Model.

Fig. 7 U Activity Statistical concordance (equilibrium) in the activities of the daughter radionuclide ^{226}Ra with its parent, ^{238}U , may signify the temporal stability of D_e emissions from these chains. Significant differences (disequilibrium: $>50\%$) in activity indicate addition or removal of isotopes creating a time-dependent shift in D_e values and increased uncertainty in the accuracy of age estimates. 20% disequilibrium marker also shown.

Fig. 8 Age Range An estimate of sediment burial period based on mean D_e values and associated uncertainties. The probability distribution indicates the inter-grain variability in age. The maximum influence of temporal variations in D_e forced by minima-maxima variation in moisture content and overburden thickness, here coupled with Finite Mixture D_e values, may prove instructive where there is uncertainty in these parameters, however the combined extremes represented should not be construed as preferred age estimates.

Fig. 2 Irradiation-Preheat Cycling

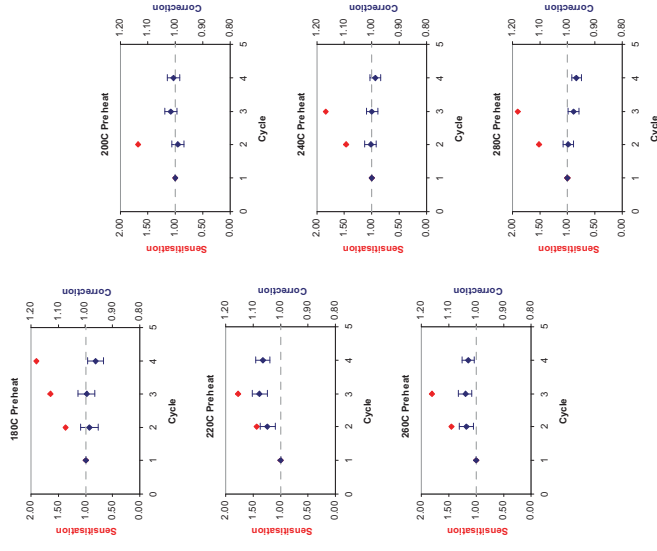


Fig. 3 D_e Preheat Dependence

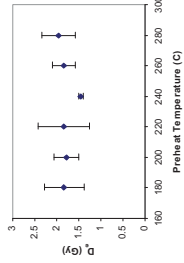


Fig. 4 Dose Recovery

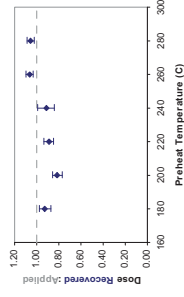


Fig. 5 Inter-grain D_e distribution

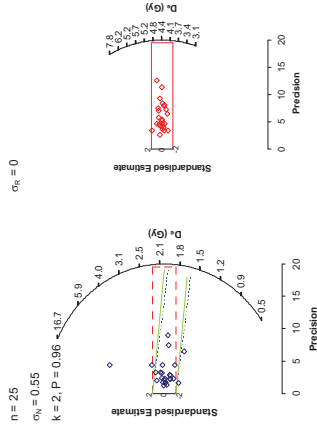


Fig. 6 U Activity

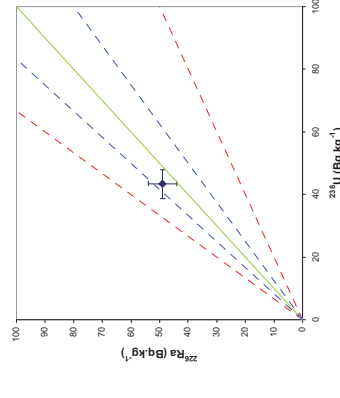
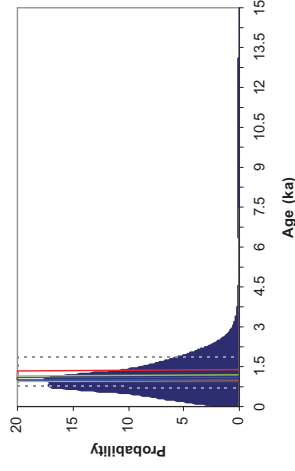


Fig. 7 Age Range



Sample: GL06020

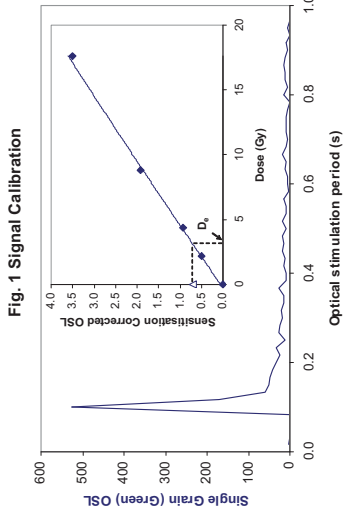


Fig. 1 Signal Calibration

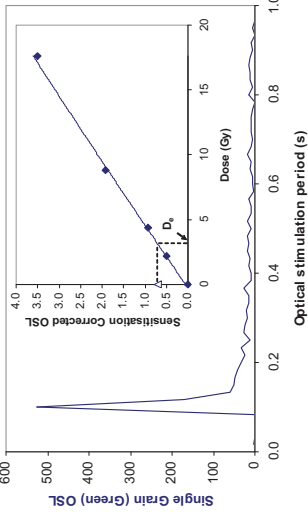


Fig. 2 Irradiation-Preheat Cycling

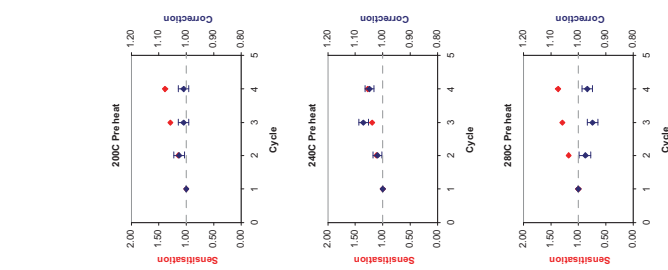


Fig. 3 D₀ Preheat Dependence

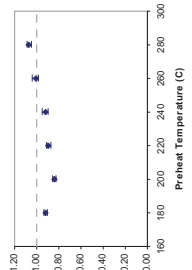


Fig. 4 Dose Recovery

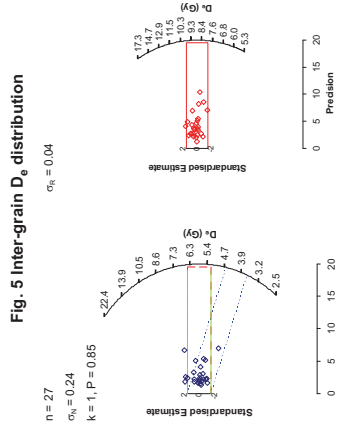


Fig. 5 Inter-grain D₀ distribution

Fig. 1 Signal Calibration Single quartz sand grain natural (green) OSL signal. Inset, the natural green OSL signal (open triangle) of each aliquot is calibrated against known laboratory doses to yield equivalent dose (D₀) values.

Fig. 2 Irradiation-Preheat Cycling The acquisition of D₀ values is necessarily preceded by a period of irradiation. Repeated irradiation and thermal treatment results in altered sensitisation, rendering calibration of the natural signal inaccurate. This sensitisation can be monitored and corrected for. The accuracy of correction can be preheat dependent. Irradiation-preheat cycling quantifies this dependence for laboratory-induced signals, examining the reproducibility of corrected OSL resultant of repeat laboratory doses. This element was based on multi-grain aliquots.

Fig. 3 D₀ Preheat Dependence Quantifies the combined effects of thermal transfer and sensitisation on the natural signal. Insignificant adjustment in D₀ may reflect limited influence of these effects. This element was based on multi-grain aliquots.

Fig. 4 Dose Recovery Attempts to replicate the above diagnostic, yet provide improved resolution of thermal effects through removal of variability induced by heterogeneous dose absorption in the environment and using a precise lab dose to simulate natural dose. This element was performed on multi-grain aliquots. Based on this and preceding data an appropriate thermal treatment is selected to refine the final D₀ value.

Fig. 5 Inter-grain D₀ distribution Provides a measure of inter-grain dispersion in D₀ values derived from natural and laboratory irradiation. Discordant data (those points lying beyond 2 standardised in D₀) reflects heterogeneous dose absorption and/or inaccuracies in calibration. Three estimates of post-burial D₀ values are illustrated based on the Minimum, Finite Mixture and Central Age Models. n is the number of grains fulfilling acceptability criteria. σ_n is the fractional overdispersion of D₀ values about the Central D₀ value; σ_n is the fractional overdispersion of D₀ values about a known 'regenerative-dose' value; k indicates the component number and P the proportion of grains within that component generated by the Finite Mixture Model.

Fig. 7 U Activity: Statistical concordance (equilibrium) in the activities of the daughter radionuclide ²²⁶Ra with its parent ²³⁸U may signify the temporal stability of D₀ emissions from these chains. Significant differences (disequilibrium: >50% in activity indicate addition or removal of isotopes creating a time-dependent shift in D₀ values and increased uncertainty in the accuracy of age estimates. 20% disequilibrium marker also shown.

Fig. 8 Age Range An estimate of sediment burial period based on mean D₀ values from natural and laboratory irradiation. The probability distribution indicates the inter-grain variability in age. The maximum influence of temporal variations in D₀ forced by minima-maxima variation in moisture content and overburden thickness, here coupled with Finite Mixture D₀ values, may prove instructive where there is uncertainty in these parameters, however the combined extremes represented should not be construed as preferred age estimates.

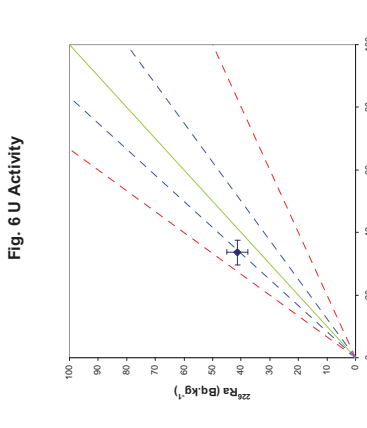


Fig. 6 U Activity

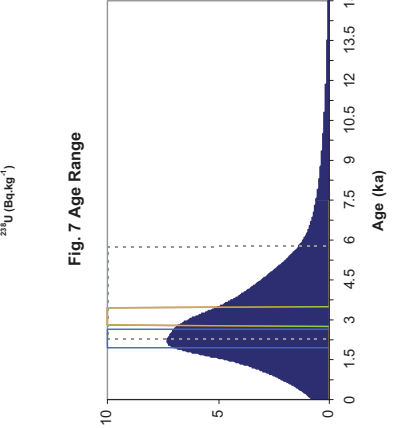


Fig. 7 Age Range

Sample: GL06021

Fig. 2 Irradiation-Preheat Cycling

Insufficient Sample Mass

Fig. 5 Inter-grain D_0 distribution

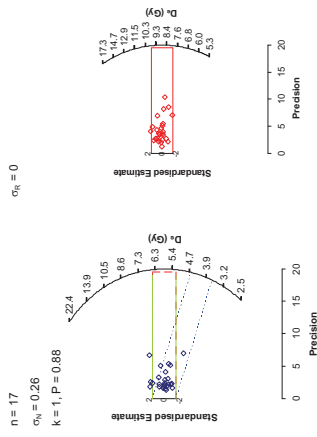


Fig. 6 U Activity

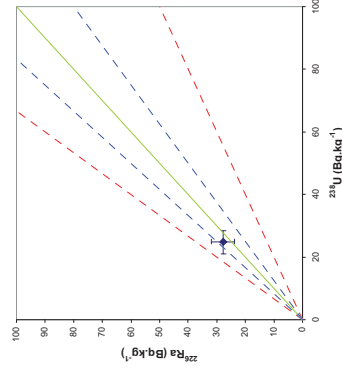
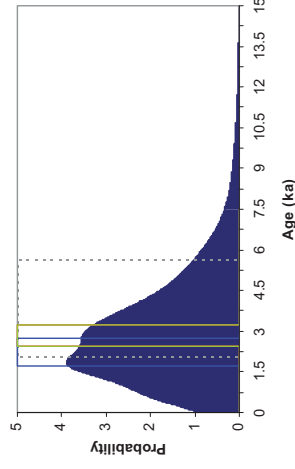


Fig. 7 Age Range



Sample: GL06022

Fig. 1 Signal Calibration

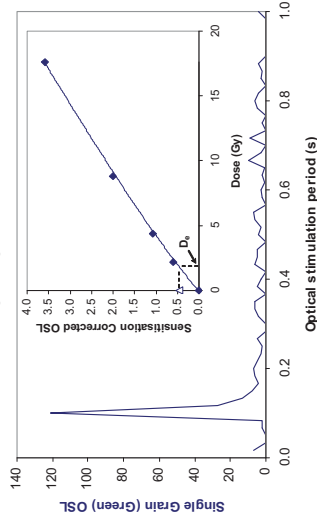


Fig. 1 Signal Calibration Single quartz sand grain natural (green) OSL signal. Inset, the natural green OSL signal (open triangle) of each aliquot is calibrated against known laboratory doses to yield equivalent dose (D_0) values.

Fig. 2 Irradiation-Preheat Cycling The acquisition of D_0 values is necessarily dependent on the thermal history of the sample. Repeated irradiation and thermal treatment results in altered **sensitisation**, rendering calibration of the natural signal inaccurate. This sensitisation can be monitored and corrected for. The accuracy of correction can be preheat dependent. Irradiation-preheat cycling quantifies this dependence for laboratory-induced signals, examining the reproducibility of corrected OSL resultant of repeat laboratory doses. This element was based on multi-grain aliquots.

Fig. 3 D_0 Preheat Dependence Quantifies the combined effects of thermal transfer and sensitisation on the natural signal. Insignificant adjustment in D_0 may reflect limited influence of these effects. This element was based on multi-grain aliquots.

Fig. 4 Dose Recovery Attempts to replicate the above diagnostic, yet provide improved resolution of thermal effects through removal of variability induced by heterogeneous dose absorption in the environment and using a precise lab dose to simulate natural dose. This element was performed on multi-grain aliquots. Based on this and preceding data an appropriate thermal treatment is selected to refine the final D_0 value.

Fig. 3 D_0 Preheat Dependence

Insufficient Sample Mass

Fig. 4 Dose Recovery

Insufficient Sample Mass

Fig. 5 Inter-grain D_0 distribution

Insufficient Sample Mass

Fig. 6 U Activity Provides a measure of inter-grain dispersion in D_0 values derived from natural and laboratory irradiation. Discordant data (these points lying beyond ± 2 standardised in D_0) reflects heterogeneous dose absorption and/or inaccuracies in calibration. Three estimates of post-burial D_0 values are illustrated based on the Minimum, Finite Mixture and Central Age Models. n is the number of grains fulfilling acceptability criteria. σ_n is the fractional overdispersion of D_0 values about the Central Dose value; σ_n is the fractional overdispersion of D_0 values about a known 'regenerative-dose' value; k indicates the component, number and P the proportion of grains within that component generated by the Finite Mixture Model.

Fig. 7 U Activity: Statistical concordance (equilibrium) in the activities of the daughter radionuclide ^{226}Ra with its parent, ^{235}U may signify the temporal stability of D_0 emissions from these chains. Significant differences (disequilibrium: $>50\%$) in activity indicate addition or removal of isotopes creating a time-dependent shift in D_0 values and increased uncertainty in the accuracy of age estimates. 20% disequilibrium marker also shown.

Fig. 8 Age Range An estimate of sediment burial period based on mean D_0 values from the sample and associated uncertainties. The probability distribution indicates the inter-grain variability in age. The maximum influence of temporal variations in D_0 forced by minima-maxima variation in moisture content and overburden thickness, here coupled with Finite Mixture D_0 values, may prove instructive where there is uncertainty in these parameters, however the combined extremes represented should not be construed as preferred age estimates.

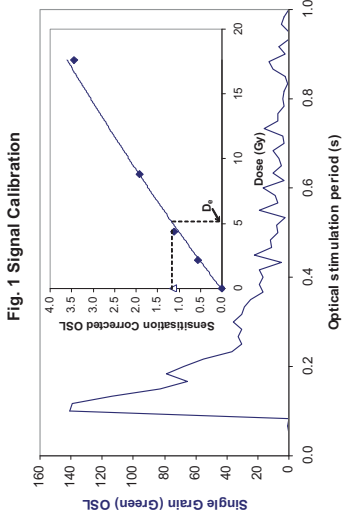


Fig. 1 Signal Calibration

Fig. 1 Signal Calibration Single quartz sand grain natural (green) OSL signal. Inset, the natural green OSL signal (open triangle) of each aliquot is calibrated against known laboratory doses to yield equivalent dose (D_e) values.

Fig. 2 Irradiation-Preheat Cycling The acquisition of D_e values is necessarily preceded by the irradiation of the sample. Repeated irradiation and thermal treatment results in altered sensitisation, rendering calibration of the natural signal inaccurate. This sensitisation can be monitored and corrected for. The accuracy of correction can be preheat dependent; irradiation-preheat cycling quantifies this dependence for laboratory-induced signals, examining the reproducibility of corrected OSL resultant of repeat laboratory doses. This element was based on multi-grain aliquots.

Fig. 3 D_e Preheat Dependence Quantifies the combined effects of thermal transfer and sensitisation on the natural signal. Insignificant adjustment in D_e may reflect limited influence of these effects. This element was based on multi-grain aliquots.

Fig. 4 Dose Recovery Attempts to replicate the above diagnostic, yet provide improved resolution of thermal effects through removal of variability induced by heterogeneous dose absorption in the environment and using a precise lab dose to simulate natural dose. This element was performed on multi-grain aliquots. Based on this and preceding data an appropriate thermal treatment is selected to refine the final D_e value.

Fig. 5 Inter-grain D_e distribution Provides a measure of inter-grain dispersion in D_e values derived from natural and laboratory irradiation. Discordant data (those points lying beyond ± 2 standardised in D_e) reflects heterogeneous dose absorption and/or inaccuracies in calibration. Three estimates of post-burial D_e values are illustrated based on the Minimum, Finite Mixture and Central Age Models. n is the number of grains fulfilling acceptability criteria. α_n is the fractional overdispersion of D_e values about the Central Dose value; σ_n is the fractional overdispersion of D_e values about a known 'regenerative-dose' value; k indicates the component number and P the proportion of grains within that component generated by the Finite Mixture Model.

Fig. 7 U Activity Statistical concordance (equilibrium) in the activities of the daughter radionuclide ^{226}Ra with its parent, ^{238}U may signify the temporal stability of D_e emissions from these chains. Significant differences (disequilibrium: $>50\%$) in activity indicate addition or removal of isotopes creating a time-dependent shift in D_e values and increased uncertainty in the accuracy of age estimates. 20% disequilibrium marker also shown.

Fig. 8 Age Range An estimate of sediment burial period based on mean D_e values and associated analytical uncertainties. The maximum influence of temporal variations in D_e inter-grain variability in age. The maximum influence of temporal variations in D_e forced by minima-maxima variation in moisture content and overburden thickness, here coupled with Finite Mixture D_e values, may prove instructive where there is uncertainty in these parameters, however the combined extremes represented should not be construed as preferred age estimates.

Fig. 2 Irradiation-Preheat Cycling

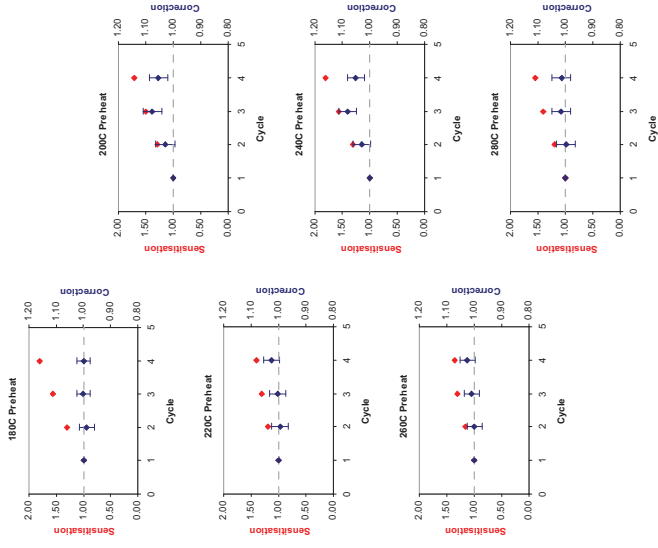


Fig. 3 D_e Preheat Dependence

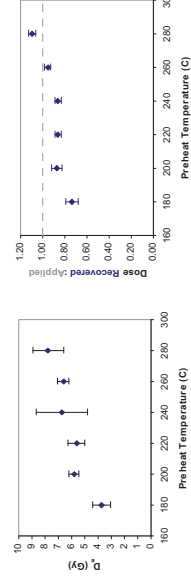


Fig. 4 Dose Recovery

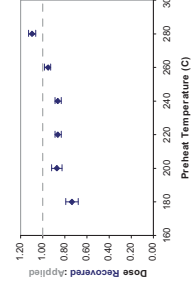


Fig. 5 Inter-grain D_e distribution

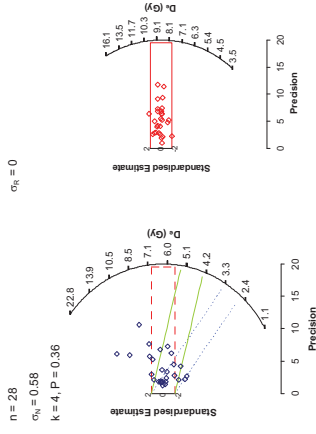


Fig. 6 U Activity

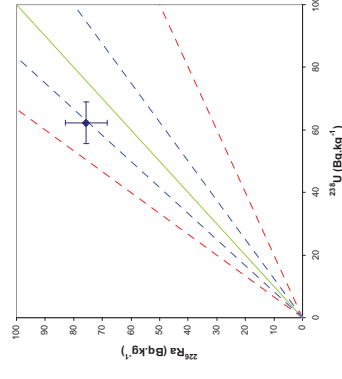
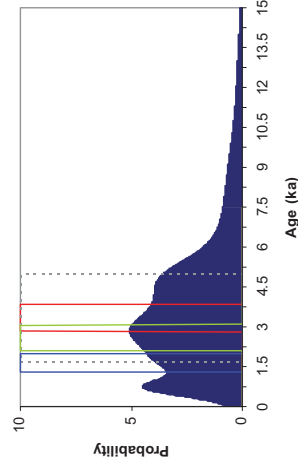


Fig. 7 Age Range



Sample: GL06023

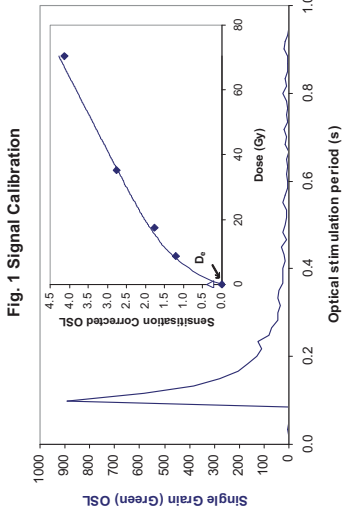


Fig. 1 Signal Calibration

Fig. 1 Signal Calibration Single quartz sand grain natural (green) OSL signal, inset, the natural green OSL signal (open triangle) of each aliquot is calibrated against known laboratory doses to yield equivalent dose (D_e) values.

Fig. 2 Irradiation-Preheat Cycling The acquisition of D_e values is necessarily preceded by the removal of any pre-existing signal. This is achieved by repeated laboratory irradiation. Repeated irradiation and thermal treatment results in aliquot sensitisation, rendering calibration of the natural signal inaccurate. This sensitisation can be monitored and corrected for. The accuracy of correction can be preheat dependent. Irradiation-preheat cycling quantifies this dependence for laboratory-induced signals, examining the reproducibility of corrected OSL resultant of repeat laboratory doses. This element was based on multi-grain aliquots.

Fig. 3 D_e Preheat Dependence Quantifies the combined effects of thermal transfer and sensitisation on the natural signal. Insignificant adjustment in D_e may reflect limited influence of these effects. This element was based on multi-grain aliquots.

Fig. 4 Dose Recovery Attempts to replicate the above diagnostic, yet provide improved resolution of thermal effects through removal of variability induced by heterogeneous dose absorption in the environment and using a precise lab dose to simulate natural dose. This element was performed on multi-grain aliquots. Based on this and preceding data an appropriate thermal treatment is selected to refine the final D_e value.

Fig. 5 Inter-grain D_e distribution Provides a measure of inter-grain dispersion in D_e values derived from natural and laboratory irradiation. Discordant data (those points lying beyond ± 2 standardised in D_e) reflects heterogeneous dose absorption and/or inaccuracies in calibration. Three estimates of post-burial D_e values are illustrated based on the Minimum, Finite Mixture and Central Age Models. n is the number of grains fulfilling acceptability criteria. σ_n is the fractional overdispersion of D_e values about the Central De value; σ_n is the fractional overdispersion of D_e values about a known 'regenerative-dose' value; k indicates the component number and P the proportion of grains within that component generated by the Finite Mixture Model.

Fig. 7 U Activity Statistical concordance (equilibrium) in the activities of the daughter radionuclide ^{226}Ra with its parent, ^{238}U , may signify the temporal stability of D_e emissions from these chains. Significant differences (disequilibrium: $>50\%$) in activity indicate addition or removal of isotopes creating a time-dependent shift in D_e values and increased uncertainty in the accuracy of age estimates. 20% disequilibrium marker also shown.

Fig. 8 Age Range An estimate of sediment burial period based on mean D_e values from the age range indicated. The probability distribution indicates the maximum inter-grain variability in age. The maximum influence of temporal variations in D_e forced by minima-maxima variation in moisture content and overburden thickness, here coupled with Finite Mixture D_e values, may prove instructive where there is uncertainty in these parameters, however the combined extremes represented should not be construed as preferred age estimates.

Fig. 2 Irradiation-Preheat Cycling

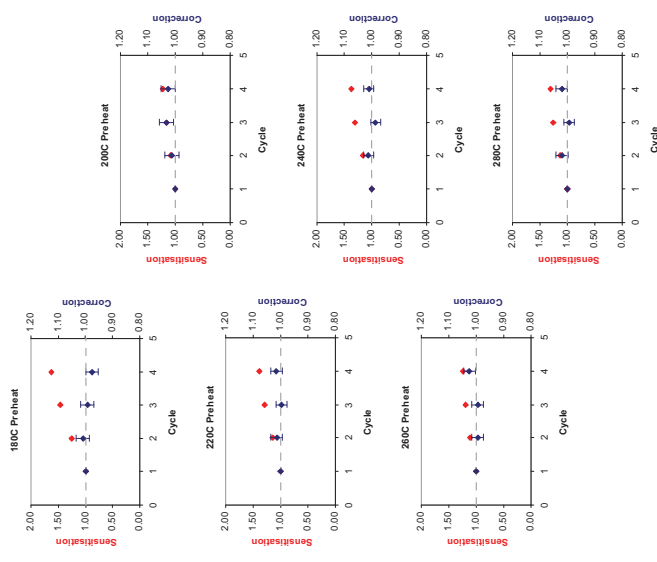


Fig. 3 D_e Preheat Dependence

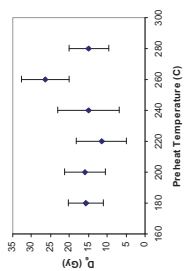


Fig. 4 Dose Recovery

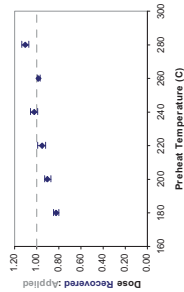


Fig. 5 Inter-grain D_e distribution

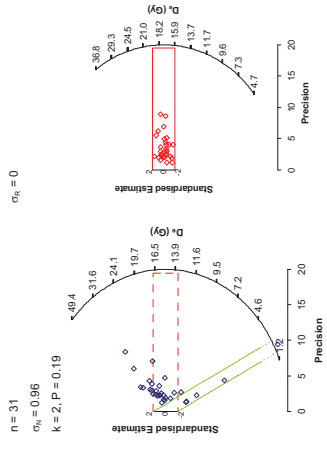


Fig. 6 U Activity

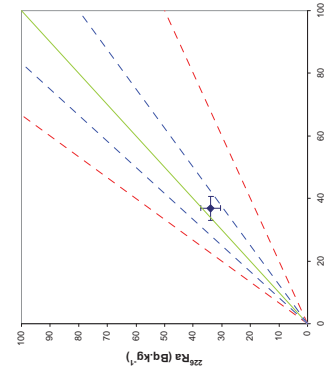
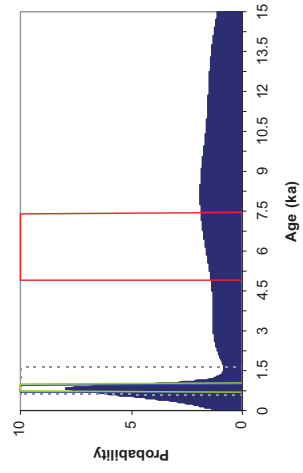


Fig. 7 Age Range



Sample: GL06024

Fig. 2 Irradiation-Preheat Cycling

Insufficient Sample Mass

Fig. 5 Inter-grain D_0 distribution

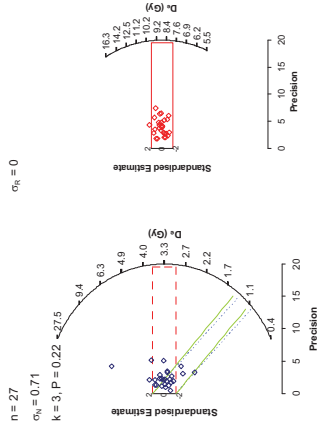


Fig. 1 Signal Calibration

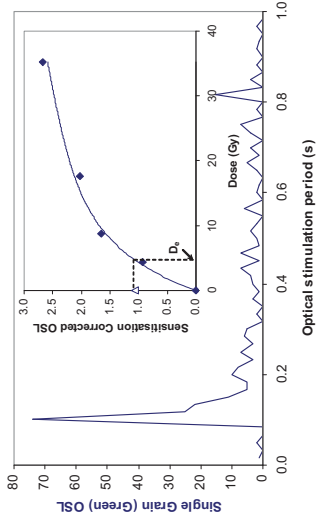


Fig. 1 Signal Calibration Single quartz sand grain natural (green) OSL signal. Inset, the natural green OSL signal (open triangle) of each aliquot is calibrated against known laboratory doses to yield equivalent dose (D_0) values.

Fig. 2 Irradiation-Preheat Cycling The acquisition of D_0 values is necessarily dependent on the thermal history of the sample. Repeated irradiation and thermal treatment results in altered **sensitisation**, rendering calibration of the natural signal inaccurate. This sensitisation can be monitored and corrected for. The accuracy of correction can be preheat dependent. Irradiation-preheat cycling quantifies this dependence for laboratory-induced signals, examining the reproducibility of corrected OSL resultant of repeat laboratory doses. This element was based on multi-grain aliquots.

Fig. 3 D_0 Preheat Dependence Quantifies the combined effects of thermal transfer and sensitisation on the natural signal. Insignificant adjustment in D_0 may reflect limited influence of these effects. This element was based on multi-grain aliquots.

Fig. 4 Dose Recovery Attempts to replicate the above diagnostic, yet provide improved resolution of thermal effects through removal of variability induced by heterogeneous dose absorption in the environment and using a precise lab dose to simulate natural dose. This element was performed on multi-grain aliquots. Based on this and preceding data an appropriate thermal treatment is selected to refine the final D_0 value.

Fig. 3 D_0 Preheat Dependence

Insufficient Sample Mass

Fig. 4 Dose Recovery

Insufficient Sample Mass

Fig. 6 U Activity

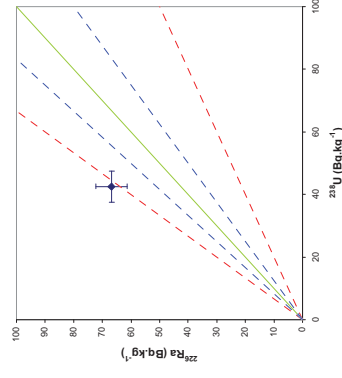


Fig. 7 Age Range

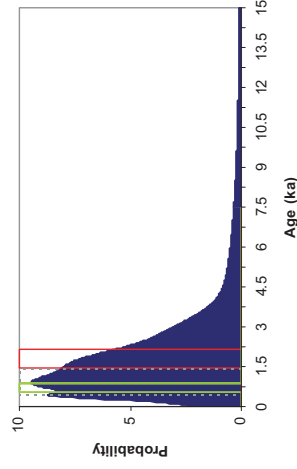


Fig. 5 Inter-grain D_0 distribution

Insufficient Sample Mass

Sample: GL06025

Fig. 6 U Activity

Fig. 7 U Activity Statistical concordance (equilibrium) in the activities of the daughter radionuclide ^{226}Ra with its parent ^{235}U may signify the temporal stability of D_0 emissions from these chains. Significant differences (disequilibrium: >50% in activity indicate addition or removal of isotopes creating a time-dependent shift in D_0 values and increased uncertainty in the accuracy of age estimates. 20% disequilibrium marker also shown.

Fig. 8 Age Range An estimate of sediment burial period based on mean D_0 values and associated uncertainties. The probability distribution indicates the inter-grain variability in age. The maximum influence of temporal variations in D_0 forced by minima-maxima variation in moisture content and overburden thickness, here coupled with Finite Mixture D_0 values, may prove instructive where there is uncertainty in these parameters, however the combined extremes represented should not be construed as preferred age estimates.

Fig. 1 Signal Calibration

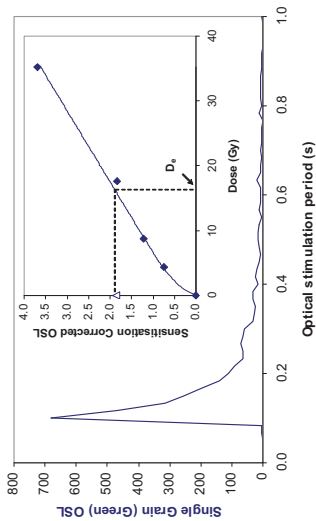


Fig. 1 Signal Calibration Single quartz sand grain natural (green) OSL signal. Inset, the natural green OSL signal (open triangle) of each aliquot is calibrated against known laboratory doses to yield equivalent dose (D_e) values.

Fig. 2 Irradiation-Preheat Cycling The acquisition of D_e values is necessarily preceded by the removal of any pre-existing signal. This is achieved by repeated laboratory irradiation. Repeated irradiation and thermal treatment results in aliquot sensitisation, rendering calibration of the natural signal inaccurate. This sensitisation can be monitored and corrected for. The accuracy of correction can be preheat dependent; irradiation-preheat cycling quantifies this dependence for laboratory-induced signals, examining the reproducibility of corrected OSL resultant of repeat laboratory doses. This element was based on multi-grain aliquots.

Fig. 3 D_e Preheat Dependence Quantifies the combined effects of thermal transfer and sensitisation on the natural signal. Insignificant adjustment in D_e may reflect limited influence of these effects. This element was based on multi-grain aliquots.

Fig. 4 Dose Recovery Attempts to replicate the above diagnostic, yet provide improved resolution of thermal effects through removal of variability induced by heterogeneous dose absorption in the environment and using a precise lab dose to simulate natural dose. This element was performed on multi-grain aliquots. Based on this and preceding data an appropriate thermal treatment is selected to refine the final D_e value.

Fig. 5 Inter-grain D_e distribution Provides a measure of inter-grain dispersion in D_e values derived from natural and laboratory irradiation. Discordant data (those points lying beyond ± 2 standardised in D_e) reflects heterogeneous dose absorption and/or inaccuracies in calibration. Three estimates of post-burial D_e values are illustrated based on the Minimum, Finite Mixture and Central Age Models. n is the number of grains fulfilling acceptability criteria. σ_n is the fractional overdispersion of D_e values about the Central D_e value; σ_n is the fractional overdispersion of D_e values about a known 'regenerative-dose' value; k indicates the component number and P the proportion of grains within that component generated by the Finite Mixture Model.

Fig. 7 U Activity Statistical concordance (equilibrium) in the activities of the daughter radionuclide ^{226}Ra with its parent, ^{238}U , may signify the temporal stability of D_e emissions from these chains. Significant differences (disequilibrium: >50% in activity indicate addition or removal of isotopes creating a time-dependent shift in D_e values and increased uncertainty in the accuracy of age estimates. 20% disequilibrium marker also shown.

Fig. 8 Age Range An estimate of sediment burial period based on mean D_e values (mean $\pm 2\sigma$) and 1σ standard deviation. The probability distribution indicates the inter-grain variability in age. The maximum influence of temporal variations in D_e forced by minima-maxima variation in moisture content and overburden thickness, here coupled with Finite Mixture D_e values, may prove instructive where there is uncertainty in these parameters, however the combined extremes represented should not be construed as preferred age estimates.

Fig. 2 Irradiation-Preheat Cycling

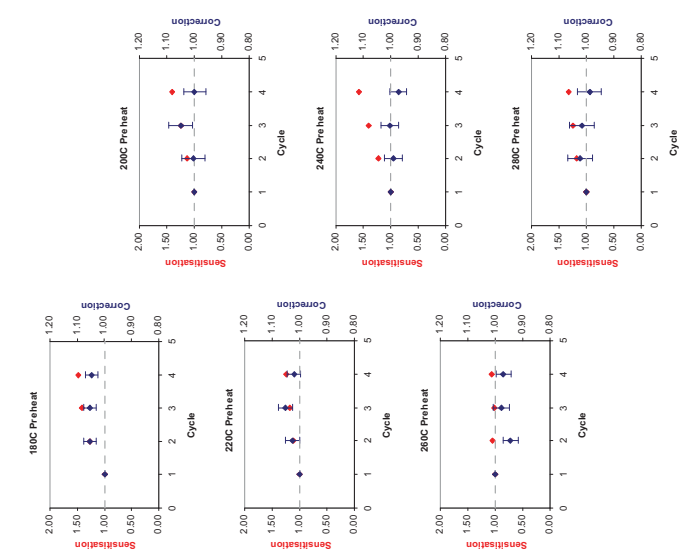


Fig. 3 D_e Preheat Dependence

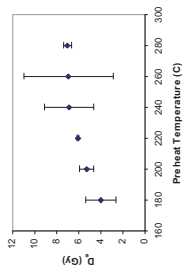


Fig. 4 Dose Recovery

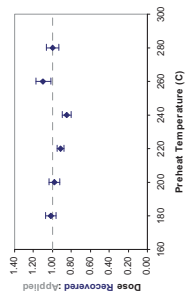


Fig. 5 Inter-grain D_e distribution

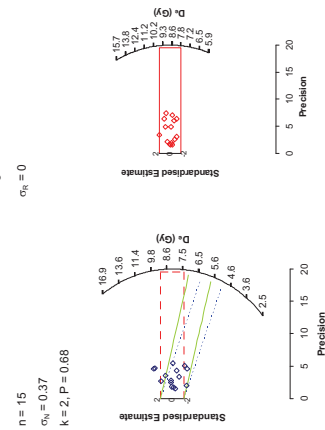


Fig. 6 U Activity

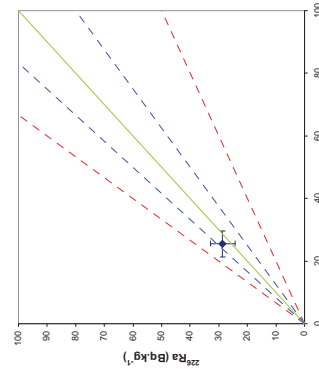
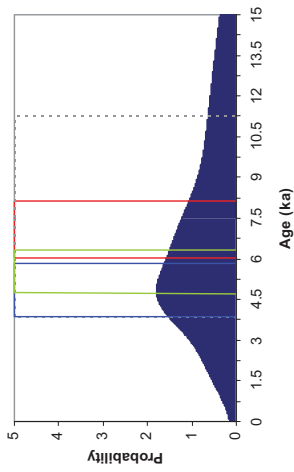


Fig. 7 Age Range



Sample: GL06026

Fig. 1 Signal Calibration

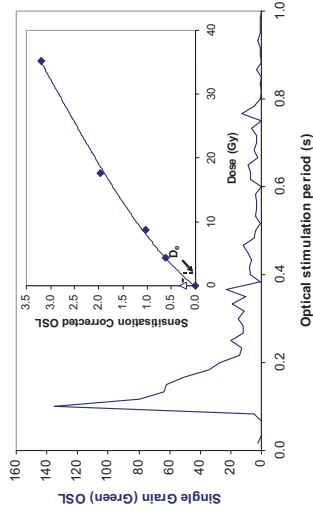


Fig. 2 Irradiation-Preheat Cycling

Insufficient Sample Mass

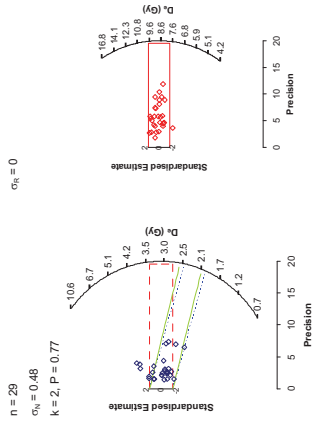


Fig. 5 Inter-grain D_0 distribution

Fig. 1 Signal Calibration Single quartz sand grain natural (green) OSL signal. Inset, green OSL signal dependence on stimulation period is calibrated against known laboratory doses to yield equivalent dose (D_0) values.

Fig. 2 Irradiation-Preheat Cycling The acquisition of D_0 values is necessarily predicated upon thermal treatment of aliquots succeeding environmental and laboratory irradiation. Repeated irradiation and thermal treatment results in aliquot sensitisation, rendering calibration of the natural signal inaccurate. This sensitisation can be monitored and corrected for. The accuracy of correction can be preheat irradiation-preheat cycling to determine the dependence for laboratory-induced signal on preheat temperature. The resulting OSL, resultant of repeat laboratory doses. This element was based on multi-grain aliquots.

Fig. 3 D_0 Preheat Dependence Quantifies the combined effects of thermal transfer and sensitisation on the natural signal. Insignificant adjustment in D_0 may reflect limited influence of these effects. This element was based on multi-grain aliquots.

Fig. 4 Dose Recovery Attempts to replicate the above diagnostic, yet provide more realistic thermal effects through a series of preheat treatments. A homogeneous dose absorption in the environment and using a precise lab dose to simulate natural dose. This element was performed on multi-grain aliquots. Based on this and preceding data an appropriate thermal treatment is selected to refine the final D_0 value.

Fig. 5 Inter-grain D_0 distribution Provides a measure of inter-grain dispersion in D_0 values derived from natural and laboratory irradiation. Discordant data (those points that do not fall on the calibration line) are highlighted. These estimates of post-burial D_0 values are illustrated based on the Minimum, Finite Mixture and Central Age Models. n is the number of grains fulfilling acceptability criteria; σ_{D_0} is the fractional overdispersion of D_0 values about the Central Age value; σ_n is the fractional overdispersion of D_0 values about a known regenerative-dose value; k indicates the component number and P the proportion of grains within that component generated by the Finite Mixture Model.

Fig. 6 U Activity Statistical concordance (equilibrium) in the activities of the daughter radionuclides, ^{226}Ra with its parent ^{238}U may signify the temporal stability of D_0 emissions from these chains. Significant differences (disequilibrium; $>50\%$) in activity indicate addition or removal of isotopes creating a time-dependent shift in D_0 values and increased uncertainty in the accuracy of age estimates. 20% disequilibrium marker also shown.

Fig. 7 Age Range An estimate of sediment burial period based on mean D_0 values from the Minimum, Finite Mixture and Central Age Models. The probability of age range with associated analytical uncertainties. The maximum influence indicates the inter-grain variability in age. The maximum influence of temporal variations in D_0 forced by minima-maxima variation in moisture content and overburden thickness, here coupled with Finite Mixture D_0 values, may prove instructive where there is uncertainty in these parameters, however the combined extremes represented should not be construed as preferred age estimates.

Fig. 6 U Activity

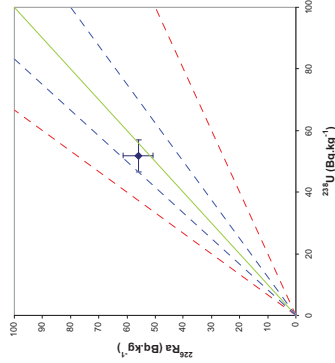


Fig. 4 Dose Recovery

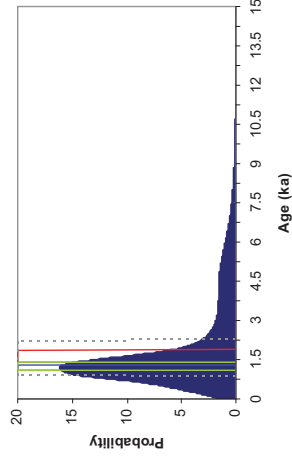
Fig. 3 D_0 Preheat Dependence

Fig. 5 Inter-grain D_0 distribution

Insufficient Sample Mass

Insufficient Sample Mass

Fig. 7 Age Range



Sample: GL06028

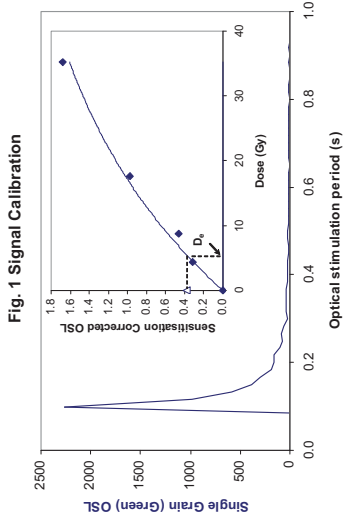


Fig. 1 Signal Calibration

Fig. 1 Signal Calibration Single quartz sand grain natural (green) OSL signal, inset, the natural green OSL signal (open triangle) of each aliquot is calibrated against known laboratory doses to yield equivalent dose (D_e) values.

Fig. 2 Irradiation-Preheat Cycling The acquisition of D_e values is necessarily through the repeated irradiation and preheat cycles. The results of repeated laboratory irradiation, repeated irradiation and thermal treatment results in altered sensitisation, rendering calibration of the natural signal inaccurate. This sensitisation can be monitored and corrected for. The accuracy of correction can be preheat dependent, irradiation-preheat cycling quantifies this dependence for laboratory-induced signals, examining the reproducibility of corrected OSL resultant of repeat laboratory doses. This element was based on multi-grain aliquots.

Fig. 3 D_e Preheat Dependence Quantifies the combined effects of thermal transfer and sensitisation on the natural signal. Insignificant adjustment in D_e may reflect limited influence of these effects. This element was based on multi-grain aliquots.

Fig. 4 Dose Recovery Attempts to replicate the above diagnostic, yet provide improved resolution of thermal effects through removal of variability induced by heterogeneous dose absorption in the environment and using a precise lab dose to simulate natural dose. This element was performed on multi-grain aliquots. Based on this and preceding data an appropriate thermal treatment is selected to refine the final D_e value.

Fig. 5 Inter-grain D_e distribution Provides a measure of inter-grain dispersion in D_e values derived from natural and laboratory irradiation. Discordant data (these points lying beyond 2σ standardised in D_e) reflects heterogeneous dose absorption and/or inaccuracies in calibration. Three estimates of post-burial D_e values are illustrated based on the Minimum, Finite Mixture and Central Age Models. n is the number of grains fulfilling acceptability criteria. σ_n is the fractional overdispersion of D_e values about the Central Dose value; σ_n is the fractional overdispersion of D_e values about a known 'regenerative-dose' value; k indicates the component number and P the proportion of grains within that component generated by the Finite Mixture Model.

Fig. 7 U Activity Statistical concordance (equilibrium) in the activities of the daughter radionuclide ^{226}Ra with its parent, ^{238}U may signify the temporal stability of D_e emissions from these chains. Significant differences (disequilibrium: $>50\%$) in activity indicate addition or removal of isotopes creating a time-dependent shift in D_e values and increased uncertainty in the accuracy of age estimates. 20% disequilibrium marker also shown.

Fig. 8 Age Range An estimate of sediment burial period based on mean D_e values from multiple aliquots and the associated uncertainties. The probability distribution indicates the inter-grain variability in age. The maximum influence of temporal variations in D_e forced by minima-maxima variation in moisture content and overburden thickness, here coupled with Finite Mixture D_e values, may prove instructive where there is uncertainty in these parameters, however the combined extremes represented should not be construed as preferred age estimates.

Fig. 2 Irradiation-Preheat Cycling

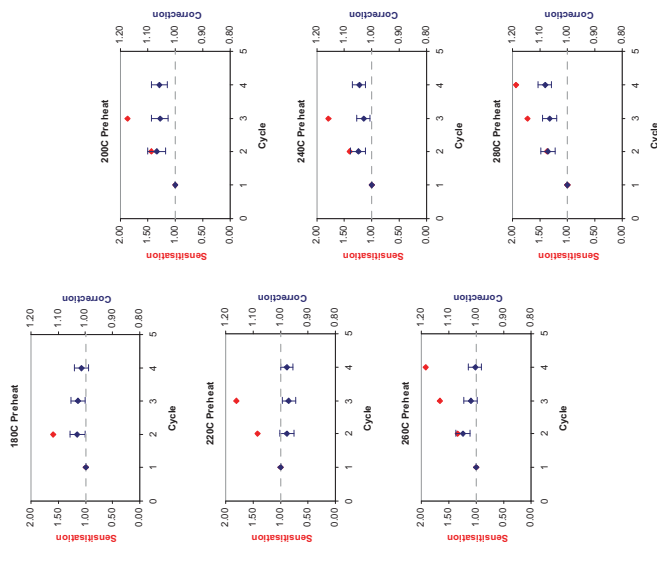


Fig. 3 D_e Preheat Dependence

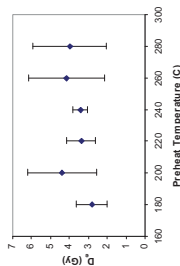


Fig. 4 Dose Recovery

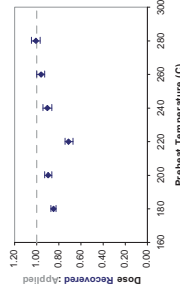


Fig. 5 Inter-grain D_e distribution

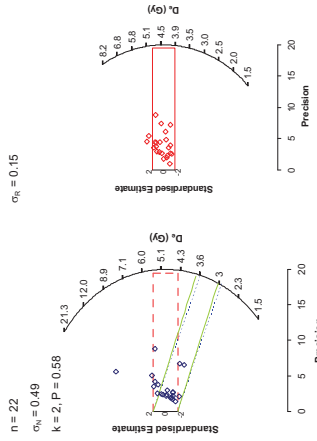


Fig. 6 U Activity

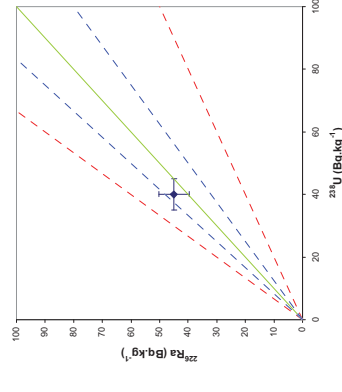
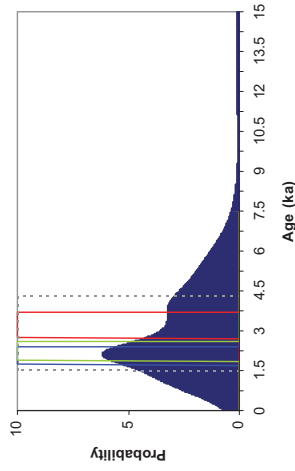


Fig. 7 Age Range



Sample: GL06030

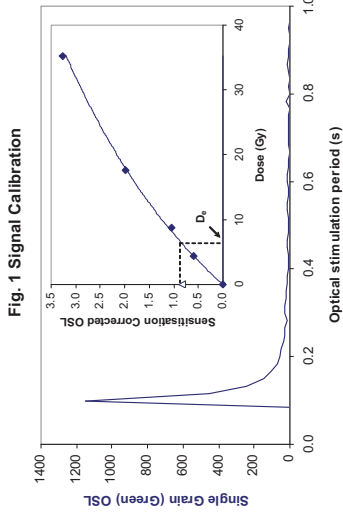


Fig. 1 Signal Calibration

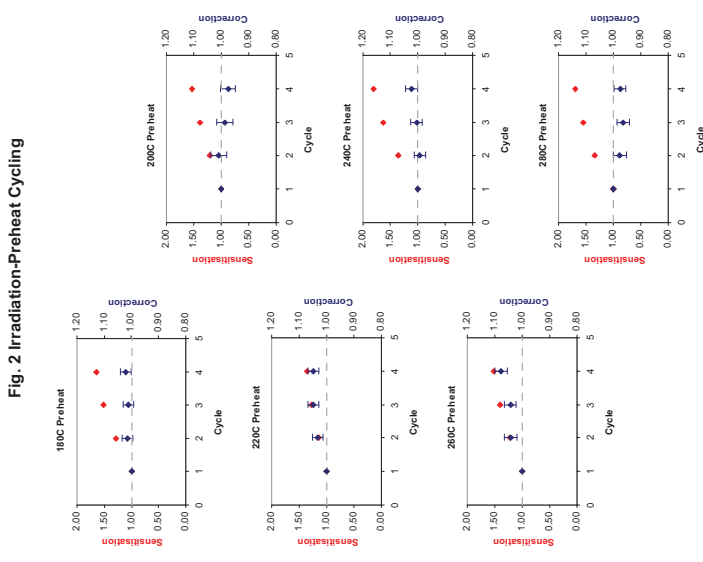


Fig. 2 Irradiation-Preheat Cycling

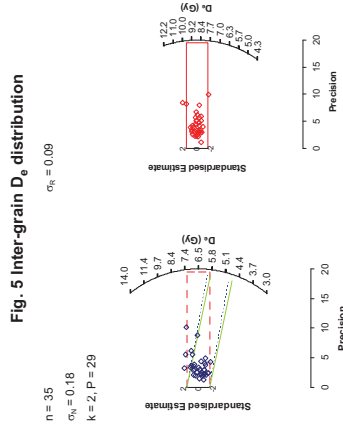


Fig. 5 Inter-grain D_0 distribution

Fig. 1 Signal Calibration Single quartz sand grain natural (green) OSL signal. Inset, the natural green OSL signal (open triangle) of each aliquot is calibrated against known laboratory doses to yield equivalent dose (D_0) values.

Fig. 2 Irradiation-Preheat Cycling The acquisition of D_0 values is necessarily through repeated irradiation and preheat cycles. The resulting D_0 values are subject to laboratory irradiation. Repeated irradiation and thermal treatment results in aliquot sensitisation, rendering calibration of the natural signal inaccurate. This sensitisation can be monitored and corrected for. The accuracy of correction can be preheat dependent. Irradiation-preheat cycling quantifies this dependence for laboratory-induced signals, examining the reproducibility of corrected OSL resultant of repeat laboratory doses. This element was based on multi-grain aliquots.

Fig. 3 D_0 Preheat Dependence Quantifies the combined effects of thermal transfer and sensitisation on the natural signal. Insignificant adjustment in D_0 may reflect limited influence of these effects. This element was based on multi-grain aliquots.

Fig. 4 Dose Recovery Attempts to replicate the above diagnostic, yet provide improved resolution of thermal effects through removal of variability induced by heterogeneous dose absorption in the environment and using a precise lab dose to simulate natural dose. This element was performed on multi-grain aliquots. Based on this and preceding data an appropriate thermal treatment is selected to refine the final D_0 value.

Fig. 5 Inter-grain D_0 distribution Provides a measure of inter-grain dispersion in D_0 values derived from natural and laboratory irradiation. Discordant data (those points lying beyond ± 2 standardised in D_0) reflects heterogeneous dose absorption and/or inaccuracies in calibration. Three estimates of post-burial D_0 values are illustrated based on the Minimum, Finite Mixture and Central Age Models. n is the number of grains fulfilling acceptability criteria. σ_n is the fractional overdispersion of D_0 values about the Central Dose value; σ_n is the fractional overdispersion of D_0 values about a known regenerative-dose value; k indicates the component number and P the proportion of grains within that component generated by the Finite Mixture Model.

Fig. 7 U Activity: Statistical concordance (equilibrium) in the activities of the daughter radionuclide ^{234}Th with its parent ^{238}U may signify the temporal stability of D_0 emissions from these chains. Significant differences (disequilibrium: $>50\%$) in activity indicate addition or removal of isotopes creating a time-dependent shift in D_0 values and increased uncertainty in the accuracy of age estimates. 20% disequilibrium marker also shown.

Fig. 8 Age Range An estimate of sediment burial period based on mean D_0 values and associated analytical uncertainties. The probability distribution indicates the inter-grain variability in age. The maximum influence of temporal variations in D_0 forced by minima-maxima variation in moisture content and overburden thickness, here coupled with Finite Mixture D_0 values, may prove instructive where there is uncertainty in these parameters, however the combined extremes represented should not be construed as preferred age estimates.

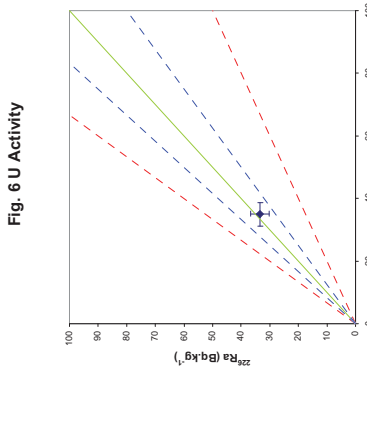


Fig. 6 U Activity

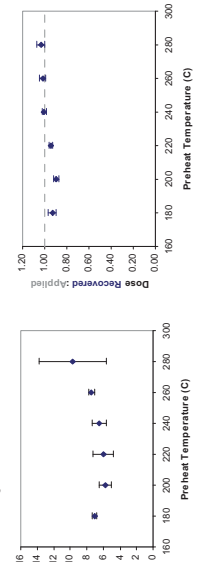


Fig. 3 D_0 Preheat Dependence

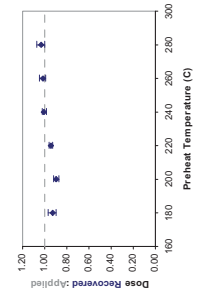


Fig. 4 Dose Recovery

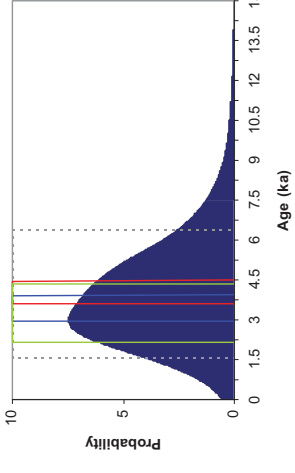


Fig. 7 Age Range

Sample: GL06031

References

- Adamic, G. and Aitken, M.J. (1998) Dose-rate conversion factors: new data. *Ancient TL*, 16, 37-50.
- Agersnap-Larsen, N., Bulur, E., Bøtter-Jensen, L. and McKeever, S.W.S. (2000) Use of the LM-OSL technique for the detection of partial bleaching in quartz. *Radiation Measurements*, 32, 419-425.
- Aitken, M.J. (1985) Thermoluminescence dating. Academic Press, London.
- Aitken, M. J. (1998) An introduction to optical dating: the dating of Quaternary sediments by the use of photon-stimulated luminescence. Oxford University Press.
- Bailey, R.M. (2004) Paper I—simulation of dose absorption in quartz over geological timescales and its implications for the precision and accuracy of optical dating. *Radiation Measurements*, 38, 299-310.
- Bailey, R.M., Singarayer, J.S. , Ward, S. and Stokes, S. (2003) Identification of partial resetting using D_e as a function of illumination time. *Radiation Measurements*, 37, 511-518.
- Banerjee, D., Murray, A.S., Bøtter-Jensen, L. and Lang, A. (2001) Equivalent dose estimation using a single aliquot of polymineral fine grains. *Radiation Measurements*, 33, 73-94.
- Bateman, M.D., Frederick, C.D., Jaiswal, M.K., Singhvi, A.K. (2003) Investigations into the potential effects of pedoturbation on luminescence dating. *Quaternary Science Reviews*, 22, 1169-1176.
- Berger, G.W. (2003). Luminescence chronology of late Pleistocene loess-paleosol and tephra sequences near Fairbanks, Alaska. *Quaternary Research*, 60, 70-83.
- Bøtter-Jensen, L., Mejdahl, V. and Murray, A.S. (1999) New light on OSL. *Quaternary Science Reviews*, 18, 303-310.
- Bøtter-Jensen, L., McKeever, S.W.S. and Wintle, A.G. (2003) Optically Stimulated Luminescence Dosimetry. Elsevier, Amsterdam.
- Duller, G.A.T. (2003) Distinguishing quartz and feldspar in single grain luminescence measurements. *Radiation Measurements*, 37, 161-165.
- Duller, G.A.T., Bøtter-Jensen, L., Kohsiek, P. and Murray, A.S. (1999) A high sensitivity optically stimulated luminescence scanning system for measurement of single sand-sized grains. *Radiation Protection Dosimetry*, 84, 325-330.
- Galbraith, R, F. (1990) The radial plot: graphical assessment of spread in ages. *Nuclear Tracks and Radiation Measurements*, 17, 207-214.
- Galbraith, R.F. and Green, P.F. (1990) Estimating the component ages in a finite mixture. *Nuclear Tracks and Radiation Measurements*, 17, 197-206.

Galbraith, R.F. and Laslett, G. (1993) Statistical models for mixed fission track ages. *Radiation Measurements*, 21, 459-470.

Galbraith, R. F., Roberts, R. G., Laslett, G. M., Yoshida, H. and Olley, J. M. (1999) Optical dating of single and multiple grains of quartz from Jinmium rock shelter (northern Australia): Part I, Experimental design and statistical models. *Archaeometry*, 41, 339-364.

Green, J. R. and Margerison, D. (1978) Statistical treatment of experimental data. Elsevier Scientific Publications. New York.

Hubble, J. H. (1982) Photon mass attenuation and energy-absorption coefficients from 1keV to 20MeV. *International Journal of Applied Radioisotopes*, 33, 1269-1290.

Huntley, D.J., Godfrey-Smith, D.I. and Thewalt, M.L.W. (1985) Optical dating of sediments. *Nature*, 313, 105-107.

Ixaru, L., Vandenberghe, G. and Hazewinkel, M. (2004) Exponential Fitting. Kluwer.

Jacobs, Z., Duller, G.A.T. and Wintle A.G. (2006) Interpretation of single grain D_e distributions and calculation of D_e . *Radiation Measurements*, 41, 264-277.

Markey, B.G., Bøtter-Jensen, L., and Duller, G.A.T. (1997) A new flexible system for measuring thermally and optically stimulated luminescence. *Radiation Measurements*, 27, 83-89.

Mejdahl, V. (1979) Thermoluminescence dating: beta-dose attenuation in quartz grains. *Archaeometry*, 21, 61-72.

Murray, A.S. and Olley, J.M. (2002) Precision and accuracy in the Optically Stimulated Luminescence dating of sedimentary quartz: a status review. *Geochronometria*, 21, 1-16.

Murray, A.S. and Wintle, A.G. (2000) Luminescence dating of quartz using an improved single-aliquot regenerative-dose protocol. *Radiation Measurements*, 32, 57-73.

Murray, A.S. and Wintle, A.G. (2003) The single aliquot regenerative dose protocol: potential for improvements in reliability. *Radiation Measurements*, 37, 377-381.

Murray, A.S., Olley, J.M. and Caitcheon, G.G. (1995) Measurement of equivalent doses in quartz from contemporary water-lain sediments using optically stimulated luminescence. *Quaternary Science Reviews*, 14, 365-371.

Olley, J.M., Murray, A.S. and Roberts, R.G. (1996) The effects of disequilibria in the Uranium and Thorium decay chains on burial dose rates in fluvial sediments. *Quaternary Science Reviews*, 15, 751-760.

Olley, J.M., Caitcheon, G.G. and Murray, A.S. (1998) The distribution of apparent dose as determined by optically stimulated luminescence in small aliquots of fluvial quartz: implications for dating young sediments. *Quaternary Science Reviews*, 17, 1033-1040.

Olley, J.M., Caitcheon, G.G. and Roberts R.G. (1999) The origin of dose distributions in fluvial sediments, and the prospect of dating single grains from fluvial deposits using -optically stimulated luminescence. *Radiation Measurements*, 30, 207-217.

Olley, J.M., Pietsch, T. and Roberts, R.G. (2004) Optical dating of Holocene sediments from a variety of geomorphic settings using single grains of quartz. *Geomorphology*, 60, 337-358.

Prescott, J.R. and Hutton, J.T. (1994) Cosmic ray contributions to dose rates for luminescence and ESR dating: large depths and long-term time variations. *Radiation Measurements*, 23, 497-500.

Roberts, R.G., Galbraith, R.F., Yoshida, H., Laslett, G.M., Olley, J.M. (2000) Distinguishing dose populations in sediment mixtures: a test of single-grain optical dating procedures using mixtures of laboratory dosed quartz. *Radiation Measurements*, 32, 459-465.

Rodnight, H., Duller, G.A.T, Wintle, A.G. and Tooth, S. (2006) Assessing the reproducibility and accuracy of optical dating of fluvial deposits. *Quaternary Geochronology*, 1, 109-120.

Singhvi, A.K., Bluszcz, A., Bateman, M.D., Someshwar Rao, M. (2001). Luminescence dating of loess-palaeosol sequences and coversands: methodological aspects and palaeoclimatic implications. *Earth Science Reviews*, 54, 193-211.

Smith, B.W., Rhodes, E.J., Stokes, S., Spooner, N.A. (1990) The optical dating of sediments using quartz. *Radiation Protection Dosimetry*, 34, 75-78.

Spooner, N.A. (1993) The validity of optical dating based on feldspar. Unpublished D.Phil. thesis, Oxford University.

Templer, R.H. (1985) The removal of anomalous fading in zircons. *Nuclear Tracks and Radiation Measurements*, 10, 531-537.

Toms, P.S., Hosfield, R.T., Chambers, J.C., Green, C.P. and Marshall, P. (2005) Optical dating of the Broom Palaeolithic sites, Devon and Dorset. English Heritage Centre for Archaeology dating report 16/2005.

Truscott, A.J., Duller, G.A.T, Botter-Jensen, L., Murray A.S. and Wintle, A.G. (2000) Reproducibility of optically stimulated luminescence measurements from single grains of Al₂O₃:C and annealed quartz. *Radiation Measurements*, 32, 447-451.

Wallinga, J. (2002) Optically stimulated luminescence dating of fluvial deposits: a review. *Boreas*, 31, 303-322.

Wintle, A.G. (1973) Anomalous fading of thermoluminescence in mineral samples. *Nature*, 245, 143-144.

Zimmerman, D. W. (1971) Thermoluminescent dating using fine grains from pottery. *Archaeometry*, 13, 29-52.

Predictive Modelling at a River Confluence: Radiocarbon dating

By W D Hamilton, P D Marshall, T Brown, C Carey, C Bronk Ramsey, and J van der Plicht

A total of 37 samples were submitted for radiocarbon dating by Accelerator Mass Spectrometry (AMS), producing a total of 39 results, to the Oxford Radiocarbon Accelerator Unit (ORAU) and the Centre for Isotope Study, the University of Groningen, The Netherlands. These consisted of two waterlogged twigs, 19 Monocotyledon samples, and 15 sediment samples.

The samples submitted to ORAU were prepared according to methods given in Hedges *et al* (1989) and measured as described in Bronk Ramsey *et al* (2004). Those submitted to Groningen were processed and measured as described by Aerts-Bijma *et al* (1997; 2001) and van der Plicht *et al* (2000).

Both laboratories maintain continual programmes of quality assurance procedures, in addition to participation in international inter-comparisons (Scott 2003). These tests indicate no laboratory offsets and demonstrate the validity of the measurements quoted.

The results, given in Table 1, are conventional radiocarbon ages (Stuiver and Polach 1977), and are quoted in accordance with the international standard known as the Trondheim convention (Stuiver and Kra 1986).

The calibrations of these results, relating the radiocarbon measurements directly to calendar dates, have been calculated using the calibration curve of Reimer *et al* (2004) and the computer program OxCal (v3.10) (Bronk Ramsey 1995; 1998; 2001). The calibrated date ranges for these samples are given in Table 1 and have been calculated using the maximum intercept method (Stuiver and Reimer 1986). They are quoted in the form recommended by Mook (1986), with the end points rounded outwards to 10 years. The graphical distributions of the calibrated dates, given in outline in Figures 1–4, are derived from the probability method (Stuiver and Reimer 1993).

Objectives

The overall aim of the scientific dating programme was to provide a chronological framework with which to interpret the palaeoenvironmental analyses and relate this to the known archaeological record for the area

Sampling

The dating of environmental cores and monoliths can present various problems, most of which can be investigated through a rigorous programme of radiocarbon dating and sample selection.

Macrofossils

Although macrofossils are now often preferred as samples from environmental cores, as they can be identified as short-lived material, care must be taken when they come from aqueous environments (*eg* fluvial, alluvial, estuarine, etc). In these instances there is some possibility that the macrofossils were in-washed. While in-washing is more likely to bring in material that is of an older, rather than younger, date, wet-dry cycles and invasive reeds, such as *Phragmites*, present the possibility of younger material being brought down through the

sediment column. Because of these potential problems, the radiocarbon programme employed is one with consistency as its foremost aim.

Consistency can be demonstrated in two ways. The first is through good overall agreement between the radiocarbon measurements and the core sequence. The second is through the replication of results from a specific level in the core. The replication of results is why it is preferred to have two macrofossils submitted from any given level, it is also part of the reasoning behind dating multiple fractions of peats, soils, and sediment, which are dealt with in the next section. If the resultant measurements are statistically consistent (*ie* $T' < 3.8$, $v=1$) then it is probable that the two dates correctly date that level. When the two dates are not statistically consistent, the data need to be re-evaluated.

Sediment

The second type of material submitted for radiocarbon dating consisted of sediment. The dating of sediment and the reliability of the resultant dates from various fractions (eg humins, humic acids, etc) has been a topic of contention in the literature (see Blaauw *et al* 2004; Kilian *et al* 1995; 2000; and Shore *et al* 1995). The two most commonly dated fractions from these samples are the humins (ie alkali and acid insoluble organic detritus) and the humic acids (ie alkali soluble and acid insoluble matter). A third fraction that is sometime dated consists of the fulvic acids (ie the acid soluble fraction). Finally, if there is not enough available material to date the separate fractions then the bulk sediment can be dated (ie humin and humic fractions combined).

As the humin fraction is composed of the actual organic detritus, the resultant date from measuring this fraction is subject to many of the same processes that affect the dating of macrofossils in the same type of environment. Firstly, organic material that forms all or part of the humin fraction could be in-washed, which would result in a date that is too old. Contamination of this material by geological age carbon (eg coal, hard-water error) would have the same effect. The humin fraction can also be too young, if for example the environment is prone to wet-dry episodes or bioturbation, allowing intrusive material to work its way down the sediment column. Therefore, the humin fraction is not necessarily homogenous, and so it might be best to avoid dating this fraction by AMS as the smallest contamination would greatly affect the resultant measurement. Humins may better be dated through conventional radiocarbon dating techniques, as it is unlikely that a sufficient volume of such contamination would be present to bias such results significantly.

The second fraction that is often dated is the humic acids, which are the *in situ* products of plant decay. Although they are produced *in situ* and imply a stability to the ground surface, it has been shown that they can be mobile in groundwater, both vertically and horizontally (Shore *et al* 1995), but that their mobility is probably limited. Therefore, humic acids cannot be relied upon to always correctly date the level from which they were collected either. However, unlike the humin fraction, humic acids are homogenous, as they are alkali soluble, and therefore can be more reliably dated through AMS.

Fulvic acids are acid soluble and therefore can be suspended in a homogenous solution. Shore *et al* (1995) have shown that fulvic acids are nearly always the youngest fraction within a sediment profile. However, they also show that in a few cases they are by far the oldest of the three dated fractions at a level. They go on to suggest that this is likely due to the fact that fulvic acids are soluble in water and therefore are highly mobile, moving up and down with the water table and laterally within the subterranean drainage patterns.

In some cases, when there is not enough material for dating of separate fractions, the humic acid and humin fractions can be bulked together to provide an average date for all the organic material in that level. As stated earlier however, it is preferable to have the dates on the two fractions as this provides the data necessary for using replication as a measure of consistency.

When the dates on two fractions are obtained, if they are statistically consistent, a weighted average can be taken before calibration as described in Ward and Wilson (1978). In most cases this creates a date that is more reliable. However, if the two results are not in agreement then the data need to be re-evaluated, in an attempt to determine which sample more reliably relates to the date of the level under consideration.

Results and Discussion

Three of the four series of dates have produced one or more results that calibrate to the modern period (post AD 1950). In total, five measurements have all of their calibrated date range in this period and one overlaps into this period upon calibration, but this is most likely due to the rounding of the resulting date. All of the five 'modern' samples are waterlogged macrofossils or wood, and while in some cases these samples may accurately date the level from which they were retrieved, in some cases they are likely to be the result of sampling contamination from the gouge corer. These dates are discussed in further detail in the relevant series sections below.

TFG

Four samples were submitted from locations along core TFG. The four radiocarbon measurements are consistent with their relative order in the sequence (Fig 1).

T1

Eighteen samples were submitted across nine cores from palaeochannels that form series T1. The results are presented in the proposed ordering of the palaeochannels, from earliest to most recent, based upon early chrono-stratigraphic work (Fig 2).

Two samples were dated from core C14, a proposed late Devensian/early Holocene sequence. The two results are consistent with their relative stratigraphic order, however, they suggest that the sequence spans the Bronze Age to Anglo-Saxon periods.

Six samples were submitted from five levels along core C7, a proposed early Holocene sequence with excellent preservation for palaeoenvironmental analysis. The result on monocotyledon fragments from the base of the sequence (OxA-15889) calibrates to the modern period and is likely to be the result of contamination through the use of the gouge corer. The two results from C7 1.51m (OxA-16159/60) on the humin fraction and humic acid, respectively, of sediment are not statistically consistent ($T' = 811.7$; $v = 1$; $T'(5\%) = 3.8$; Ward and Wilson 1978). Furthermore, both of these dates are significantly older than the resulting date on Monocotyledon fragments from almost a half metre below (GrA-31951). Also, it should be pointed out that the bulk sediment date from C7 0.95m is also older than GrA-31951. The lack of consistency within and between the two sample types (sediment and macrofossil) means this core must remain 'undated' with the radiocarbon measurements providing no means to tie the changes in land-use evident in the pollen record to the existing archaeological record from the area.

Three samples of Monocotyledon were dated from a sequence in core C12. The results are not in agreement with their relative stratigraphic order. This is again likely the result of sampling contamination given the result from C12 0.5m (GrA-31987) is modern in date.

Three results were produced on sediment from three levels in core C10. While the lower two results (GrA-31998 and OxA-15931) are consistent with their relative stratigraphic order, the uppermost result is over 3500 years older (OxA-15972). This discrepancy is likely the result of reworked organic material being inwashed and breaking down *in situ*.

A single sample was submitted from core C2 1.24m, and the result (OxA-15887) dates the infilling of this palaeochannel to the late-5th–8th centuries cal AD.

A single sample was submitted from core C6 1.61m, and the result (GrA-31949) is a modern date, suggesting that this level has been contaminated.

A single sample was submitted from core C3 1.6m, and the result (GrA-31774) dates the infilling of this palaeochannel to the 7th century cal AD.

A single sample was submitted from core C4 0.98m, and the result (OxA-15971) dates the infilling of this palaeochannel to the late-9th–early-6th centuries cal BC.

A single sample was submitted from core C8 1.3m, and the result (GrA-31986) dates the infilling of this palaeochannel to the late-1st–early-4th centuries cal AD.

WQF

A total of 12 radiocarbon results were obtained from four monoliths from exposed sections of the quarry at Sawley. While CH5 was clearly the earliest monolith, monoliths CH1–3 were unrelatable to one another based on stratigraphy (Fig 3).

Three samples were submitted from two levels of monolith CH5. The two measurements on samples from 0.0m depth in the monolith are not statistically consistent ($T'=55.3$; $v=1$; $T'(5\%)=3.8$; Ward and Wilson 1978). The earliest result (GrA-32001) came from bulk sediment while the later result (OxA-15893) was from Monocotyledon fragments. The later result provides a better estimate for this depth.

Two samples were submitted from CH3 0.5m and the two measurements are not statistically consistent ($T'=461.6$; $v=1$; $T'(5\%)=3.8$; Ward and Wilson). The earlier result (OxA-15932) is on the humic acid fraction of sediment, while the later result (GrA-31941) is on Monocotyledon fragments. The later result provides a better estimate for this depth.

Three samples of Monocotyledon fragments were submitted from CH2. Although one sample (OxA-15892) has produced a modern result, all three measurements are in agreement with their stratigraphic order and so based upon the radiocarbon measurements and the relative order there is no reason to question this result.

Finally, four measurements were made on material from three levels in monolith CH1. The lower two results, from Monocotyledon fragments (OxA-15891 and GrA-31953) are in agreement with their relative stratigraphy. However, the two results from CH1 0.24m are either earlier or apparently coeval with the results from the lowest level (OxA-15891). These two results from 0.24m (OxA-16128/9) were made on the humin fraction and humic acid, respectively, of a sediment sample. These results are not statistically consistent ($T'=166.0$; $v=1$; $T'(5\%)=3.8$; Ward and Wilson 1978).

Because of the many discrepancies within these results, it is imperative that all results are used with the utmost caution, and that these sediment dates from series WQF provide at best a *terminus post quem* (*tpq*) for deposition and the macros at worst a *terminus ante quem* (*taq*) for any given level.

MF

A total of four radiocarbon measurements were made on material from the two MF-series cores, with their calibrated probability distributions shown in Figure 4.

There was only one measurement from MFC1 (OxA-15894, 368 ± 28 BP), which provides a date of cal AD 1440–1640 (95% confidence) for 1.53m down the core.

The three measurements from MFC2 are not in the expected chronological order based upon their stratigraphy. These three measurements come from two sample locations (1.0 and 1.69m), with the two measurements from 1.0m differing by over 4500 years. If we accept that the modern result of Monocotyledon fragments (GrA-31989) is intrusive we are left with two results on the humic acid fraction of sediment samples that are not in agreement with their stratigraphic order. Based upon the information at hand, it is impossible to determine which, if either, of the two results accurately dates its level.

Conclusion

The discrepancy between the humic acid and humin fraction results in the results from this project can be attributed to reworking of sediment that contains old carbon in many cases. Additionally with cores WQF CH3 and CH5 we have also dated horizons by sediment and macrofossil where the macrofossil results were more recent than the sediment. Similar outcomes have been noticed before, which have produced the following possible and non-exclusive explanations/hypotheses (Hamilton *et al* forthcoming):

- 1) the humin fractions are contaminated/contain reworked mineral carbon
- 2) the humic acids reflect a small, but significant, component from older mineral older carbon, or contain humic acid from the breakdown of older plant material
- 3) the macrofossil material is intrusive

Because of the overall lack of consistency amongst these results it is difficult to say with any confidence that a level of a core/monolith has an accurate date. While the discrepancy amongst the sediment dates might lead us to the conclusion that the dates on macrofossil material is a more accurate representation of the true age at any given level, the fact that five out of the 21 macrofossil results (24%) are modern means we cannot place much faith in those results as 'reliable' either.

The sediment dates from the Trent/Soar project provide at best a *terminus post quem* (*tpq*) for deposition and the macros at worst a *terminus ante quem* (*taq*).

Table 1: Radiocarbon results from the Trent/Soar project

Laboratory ID	Sample ID and depth	Material	$\delta^{13}\text{C}$ (‰)	Radiocarbon Age (BP)	Calibrated Date (95% confidence)
<i>TFG</i>					
GrA-31771	C14 2.5m	unidentified twig	-29.9	3300 ±40	1690–1490 cal BC
OxA-15886	C14 3m	Monocotyledon fragments	-27.9	3410 ±60	1890–1530 cal BC
GrA-31456	C14 3.5m	Monocotyledon fragments	-29.9	3880 ±35	2470–2200 cal BC
GrA-31948	C14 3.8m	bulk sediment	-29.1	4725 ±40	3640–3370 cal BC
<i>TI</i>					
GrA-31986	C8 1.3m	Monocotyledon fragments	-28.6	1820 ±30	cal AD 90–320
OxA-15971	C4 0.98m	sediment, humic acid	-26.9	2561 ±30	810–590 cal BC
GrA-31774	C3 1.6m	Monocotyledon fragments	-28.7	1370 ±35	cal AD 610–690
GrA-31949	C6 1.61m	unidentified twig	-28.7	110.11 ±0.44%mod	cal AD 1996–1999
OxA-15887	C2 1.24m	Monocotyledon fragments	-25.9	1430 ±80	cal AD 430–770
OxA-15972	C10 1m	sediment, humic acid	-27.6	7300 ±40	6240–6060 cal BC
GrA-31998	C10 1.45m	bulk sediment	-26.6	3920 ±35	2550–2290 cal BC
OxA-15931	C10 1.8m	sediment, humic acid	-28.2	4334 ±30	3030–2890 cal BC
GrA-31987	C12 0.5m	Monocotyledon fragments	-29.4	109.31 ±0.39%mod	cal AD 1997–2001
OxA-15890	C12 1.93m	Monocotyledon fragments	-27.5	1174 ±35	cal AD 730–970
GrA-31988	C12 2.14m	Monocotyledon fragments	-29.5	1030 ±40	cal AD 890–1120
OxA-15888	C7 0.5m	Monocotyledon fragments	-27.4	129 ±31	cal AD 1660–1960
GrA-31950	C7 0.95m	bulk sediment	-29.5	1020 ±35	cal AD 970–1120
OxA-16159	C7 1.51m	sediment, humin fraction	-30.4	2638 ±31	840–780 cal BC
OxA-16160	C7 1.51m	sediment, humic acid	-28.6	1406 ±30	cal AD 590–670
GrA-31951	C7 2m	Monocotyledon fragments	-28.4	590 ±35	cal AD 1290–1420
OxA-15889	C7 2.25m	Monocotyledon fragments	-28.2	121.8 ±0.9%mod	cal AD 1958–1986
OxA-15973	C14 0.45m	sediment, humic acid	-28.6	1309 ±28	cal AD 650–780
GrA-31492	C14 0.9m	bulk sediment	-27.6	3005 ±35	1390–1120 cal BC
<i>WQF</i>					
OxA-16128	CH1 0.24m	sediment, humin fraction	-29.1	3517 ±30	1940–1740 cal BC
OxA-16129	CH1 0.24m	sediment, humic acid	-29.3	2989 ±28	1380–1120 cal BC
GrA-31953	CH1 0.5m	Monocotyledon fragments	-28.1	2580 ±35	810–600 cal BC
OxA-15891	CH1 0.68m	Monocotyledon fragments	-28.8	2730 ±160	1370–410 cal BC
OxA-15892	CH2 M1 0.5m	Monocotyledon fragments	-26.1	104.0 ±0.3%mod	modern
GrA-31940	CH2 M2 0.5m	Monocotyledon fragments	-27.2	2500 ±35	790–410 cal BC
GrA-31999	CH2 M3 0.5m	Monocotyledon fragments	-30.8	2820 ±35	1060–890 cal BC

OxA-15932	CH3 0.5m (a)	sediment, humic acid	-28.2	4078 ±30	2860–2490 cal BC
GrA-31941	CH3 0.5m (b)	Monocotyledon fragments	-29.1	3075 ±35	1430–1260 cal BC
OxA-15893	CH5 0m (a)	Monocotyledon fragments	-27.5	11505 ±55	11510–11290 cal BC
GrA-32001	CH5 0m (b)	bulk sediment	-29.4	12060 ±50	12100–11830 cal BC
GrA-31943	CH5 0.36m	bulk sediment	-28.2	13870 ±60	14980–14180 cal BC
<i>MFC</i>					
OxA-15894	1 1.53m	not identified on form?!?!	-28.2	368 ±28	cal AD 1440–1640
OxA-15974	2 1m (a)	sediment, humic acid	-26.6	4168 ±31	2890–2620 cal BC
GrA-31989	2 1m (b)	Monocotyledon fragments	-29.6	109.0 ±0.78%mod	1996–present
OxA-16161	2 1.69m	sediment, humic acid	-27.7	2609 ±32	800–510 cal BC

Figure 1: Calibrated radiocarbon dates from core TFG. The probability distributions have been calculated following Stuiver and Reimer (1993)

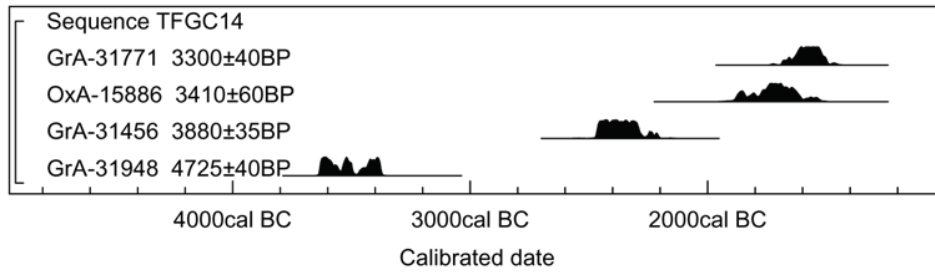


Figure 2: Calibrated radiocarbon dates from cores in the T1 series. The dates have been ordered by the proposed date order for the basal sample. The probability distributions have been calculated following Stuiver and Reimer (1993)

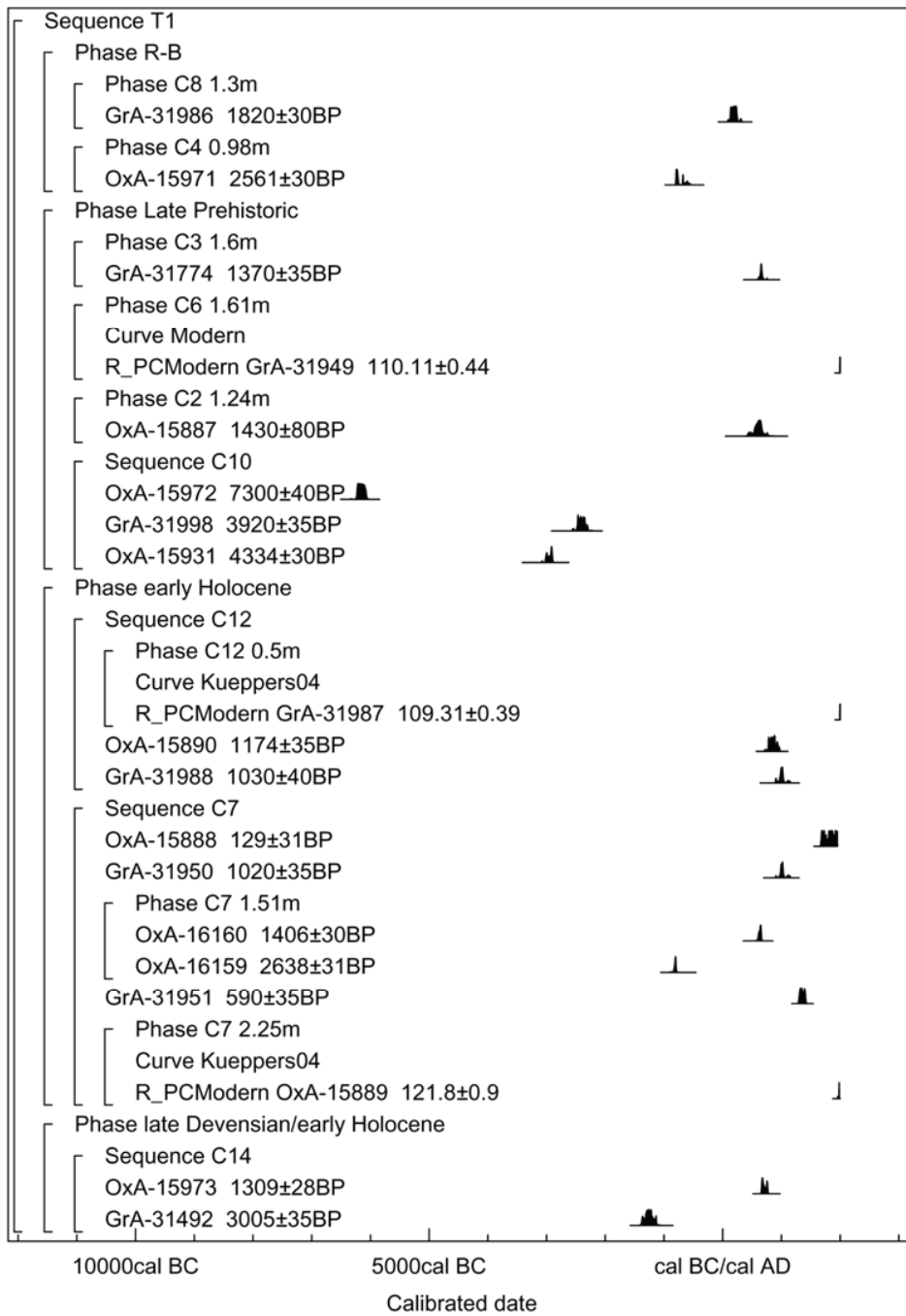


Figure 3: Calibrated radiocarbon dates from monoliths in the WQF series. The probability distributions have been calculated following Stuiver and Reimer (1993)

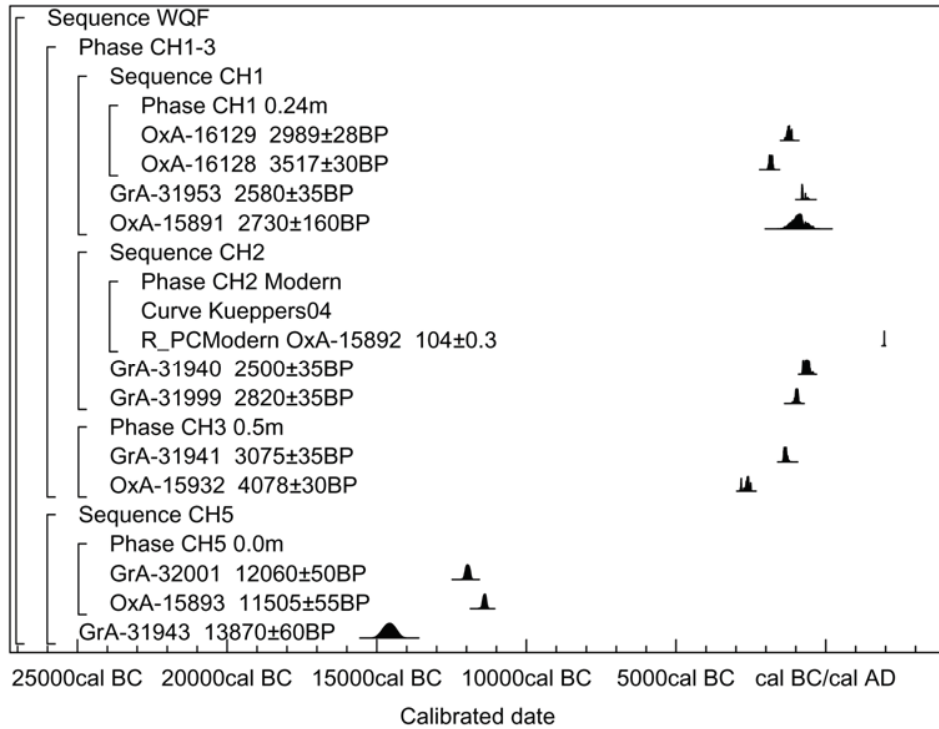
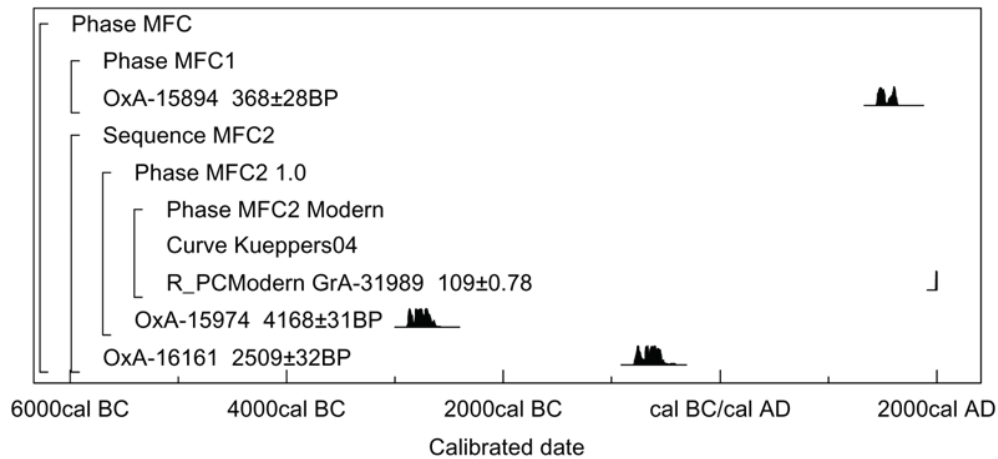


Figure 4: Calibrated radiocarbon dates from cores in the MFC series. The probability distributions have been calculated following Stuiver and Reimer (1993)



Works Cited

- Aerts-Bijma, A T, Meijer, H A J, and van der Plicht, J, 1997 AMS sample handling in Groningen, *Nuclear Instruments and Methods in Physics Research B*, **123**, 221–5
- Aerts-Bijma, A T, van der Plicht, J, and Meijer, H A J, 2001 Automatic AMS sample combustion and CO₂ collection, *Radiocarbon*, **43(2A)**, 293–8
- Blaauw, M, van der Plicht, J, and van Geel, B, 2004 Radiocarbon dating of bulk peat samples from raised bogs: non-existence of a previously reported ‘reservoir effect’?, *Quaternary Sci Rev*, **23**, 1537–42
- Bronk Ramsey, C, 1995 Radiocarbon calibration and analysis of stratigraphy, *Radiocarbon*, **36**, 425–30
- Bronk Ramsey, C, 1998 Probability and dating, *Radiocarbon*, **40**, 461–74
- Bronk Ramsey, C, 2001 Development of the radiocarbon calibration program, *Radiocarbon*, **43**, 355–63
- Bronk Ramsey, C, Higham, T, and Leach, P, 2004 Towards high precision AMS: progress and limitations, *Radiocarbon*, **46(1)**, 17–24
- Hamilton, W D, Marshall, P D, Brown, T, Allen, P, Meadows, I, and Cook G, forthcoming Radiocarbon dating, in *The Nene Valley Project*
- Hedges, R E M, Bronk, C R, and Housley, R A, 1989 The Oxford Accelerator Mass Spectrometry facility: technical developments in routine dating, *Archaeometry*, **31**, 99–113
- Kilian, M R, van der Plicht, J, and van Geel, B, 1995 Dating raised bogs: new aspects of AMS ¹⁴C wiggle matching, a reservoir effect and climatic change, *Quaternary Sci Rev*, **14**, 959–66
- Kilian, M R, van der Plicht, J, and van Geel, B, 2000 ¹⁴C wiggle matching of raised bog deposits and models of peat accumulation, *Quaternary Sci Rev*, **19**, 1011–33
- Mook, W G, 1986 Business meeting: Recommendations/Resolutions adopted by the Twelfth International Radiocarbon Conference, *Radiocarbon*, **28**, 799
- van der Plicht, J, Wijma, S, Aerts, A T, Pertuisot, M H, and Meijer, H A J, 2000 Status report: the Groningen AMS facility, *Nuclear Instruments and Methods in Physics Research B*, **172**, 58–65
- Reimer, P J, Baillie, M G L, Bard, E, Bayliss, A, Beck, J W, Bertrand, C J H, Blackwell, P G, Buck, C E, Burr, G S, Cutler, K B, Damon, P E, Edwards, R L, Fairbanks, R G, Friedrich, M, Guilderson, T P, Hogg, A G, Hughen, K A, Kromer, B, McCormac, G, Manning, S, Bronk Ramsey, C, Reimer, R W, Remmele, S, Southon, J R, Stuiver, M, Talamo, S, Taylor, F W, van der Plicht, J, and Weyhenmeyer, C E, 2004 IntCal04 Terrestrial radiocarbon age calibration, 0–26 Cal Kyr BP, *Radiocarbon*, **46**, 1029–58
- Scott, E M (ed), 2003 The Third International Radiocarbon Intercomparison (TIRI) and the Fourth International Radiocarbon Intercomparison (FIRI) 1990–2002: results, analysis, and conclusions, *Radiocarbon*, **45**, 135–408
- Shore, J S, Bartley, D D, and Harkness, D D, 1995 Problems encountered with the ¹⁴C dating of peat, *Quaternary Sci Rev*, **14**, 373–83
- Stuiver, M, and Kra, R S, 1986 Editorial comment, *Radiocarbon*, **28(2B)**, ii
- Stuiver, M, and Polach, H A, 1977 Reporting of ¹⁴C data, *Radiocarbon*, **19**, 355–63

Stuiver, M, and Reimer, P J, 1986 A computer program for radiocarbon age calculation, *Radiocarbon*, **28**, 1022–30

Stuiver, M, and Reimer, P J, 1993 Extended ^{14}C data base and revised CALIB 3.0 ^{14}C age calibration program, *Radiocarbon*, **35**, 215–30

Ward, G K, & Wilson, S R, 1978 Procedures for comparing and combining radiocarbon age determinations: a critique, *Archaeometry*, **20**, 19–31

Dendrochronology
Robert Howard

Figure x: Bar diagram of the samples in site chronology LOKQSQ01

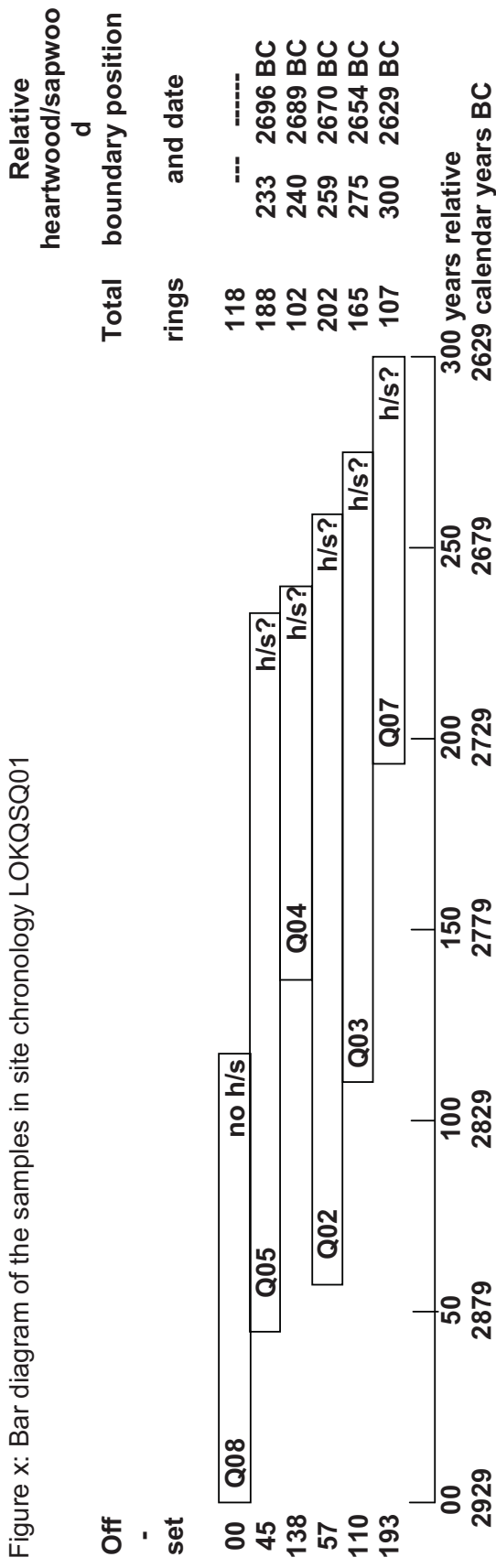


Table 1: Details of samples from Lockington Quarry on the river Trent in Leicestershire

Sample number	Sample location	Total rings	*Sapwood rings	First measured ring date	Last heartwood ring date	Last measured ring date
LOK-Q01	Quarry oak	84	h/s?	-----	-----	-----
LOK-Q02	Quarry oak	202	h/s?	2871 BC	2670 BC	2670 BC
LOK-Q03	Quarry oak	165	h/s?	2818 BC	2654 BC	2654 BC
LOK-Q04	Quarry oak	102	h/s?	2790 BC	2689 BC	2689 BC
LOK-Q05	Quarry oak	188	h/s?	2883 BC	2696 BC	2696 BC
LOK-Q06	Quarry oak	105	h/s?	2623 BC	2519 BC	2519 BC
LOK-Q07	Quarry oak	107	h/s?	2735 BC	2629 BC	2629 BC
LOK-Q08	Quarry oak	118	no h/s	2928 BC	-----	2811 BC

*h/s? = the last ring on the sample is at or approaching the heartwood/sapwood boundary

Table 2: Results of the cross-matching of site chronology LOKSQ01 and relevant reference chronologies when first ring date is 2928 BC and last ring date is 2629 BC

Reference chronology	Span of chronology	t-value
England National	^{4989 - 1661 BC}	12.5 (Hillam pers comm)
Shardlow Quarry, Derbys	2942 - 2610 BC	10.9 (Tyers 2000)
East Anglia: regional	3196 - 1681 BC	9.5 (Brown pers comm)
<small>Langford quarry, Notts</small>	2979 - 2125 BC	7.9 (Hillam unpubl)
Colwick Hall 1	3054 - 2697 BC	6.7 (Brown pers comm)
Stourport on Seven, Worcs	2869 - 2698 BC	6.5 (Hillam pers comm)

Table 3: Results of the cross-matching of sample LOK-Q06 and relevant reference chronologies when first ring date is 2623 BC and last ring date is 22519 BC

Reference chronology	Span of chronology	t-value
Wootton Quarry, Isle of Wight	3463 - 2557 BC	6.0 (Hillam 1994)
England National	^{4989 - 1661 BC}	5.8 (Hillam pers comm)
East Anglia: regional	3196 - 1681 BC	5.0 (Brown pers comm)
<small>Langford quarry, Notts</small>	2979 - 2125 BC	5.4 (Hillam unpubl)

Hillam J 1994, The dating of oak timbers from the Wootton Quarry Survey, Isle of Wight, Anc Mon Lab Rep 10/1994
 Tyers, I, 2000, Tree-ring analysis of prehistoric archaeological timbers from Shardlow Gravel Pit, Derbyshire, Anc Mon Lab Rep, **32/2000**

11.0 Bibliography

Aerts-Bijma, A T, Meijer, H A J, and van der Plicht, J. 1997. AMS sample handling in Groningen, *Nuclear Instruments and Methods in Physics Research B*, 123, 221–5

Aerts-Bijma, A T, van der Plicht, J, and Meijer, H A J. 2001. Automatic AMS sample combustion and CO₂ collection, *Radiocarbon*, 43(2A), 293–8

Andrew, R. 1984. *A Practical Pollen Guide to the British Flora*. QRA Technical Guide, No. 1, QRA.

Baker, S. 2003. *The Trent Valley: Palaeochannel Mapping from Aerial Photographs*. Trent Valley Geoarchaeology Research Report. Nottingham, Trent & Peak Archaeological Unit.

Barnes, I. 2003. Aerial remote-sensing techniques used in the management of archaeological monuments on the British army's Salisbury Plain training area, Wiltshire, UK'. *Archaeological Prospection*, 10, pp. 83-90.

Barton, R.N.E. 1992. *Hengistbury Head: The Late Upper Palaeolithic and Early Mesolithic sites*. Monograph Series. Oxford University Committee for Archaeology.

Barton, R.N.E. 1997. *Stone Age Britain*. Swindon: English Heritage.

Barton, R.N.E. Jacobi, R.M. Stapert, D. and Street M.J., 2003. The Late-glacial reoccupation of the British Isles and the Creswellian. *Journal of Quaternary Science*, 18(7), pp. 631-643.

Bates M. R. , Bates, R. C. and Whittaker, J. E. 2007. Mixed Method Approaches to the Investigation and Mapping of Buried Quaternary Deposits: Examples from Southern England. *Archaeological Prospection*. Archaeol. Prospect. (in press) Published online in Wiley InterScience (www.interscience.wiley.com) DOI: 10.1002/arp.303.

Bates, M.R. 2003. Visualising the subsurface: problems and procedures for areas of deeply stratified sediments. In: Howard, A.J. and Passmore, D. (eds) *The Alluvial Archaeology of Europe*. Balkema, Rotterdam. 277-289.

Beamish, M., Monckto, A., Brown, A.G., Greenwood, M.T. and Smith, D.N. 2002. Late Glacial, Neolithic, Bronze Age and medieval environments from Hemington Quarry (Eastern Extension), Castle Donington, Leicestershire. ULAS report 2002/166. Unpublished, deposited with Leics. SMR.

Bennett, K.D., Whittington, G. and Edwards, K.J. 1994. Plant nomenclatural changes and pollen morphology in the British Isles. *Quaternary Newsletter*, 73: 1-6.

Best, J. 1988. Sediment transport and bed morphology at river channel confluences. *Sedimentology* 35 (3): 481-98.

- Bewley, R. H.** 2003. Aerial survey for archaeology. *The Photogrammetric Record*, 18 (104), pp. 273-292.
- Bishop, M.** (2003). Issues and agenda in archaeological research and management: a case study from the Trent Valley, UK. In Howard, A.J., Macklin, M.G. and Passmore, D.G. (eds) *Alluvial Archaeology in Europe*. Lisse: Balkema: pp. 123-131.
- Blaauw, M, van der Plicht, J, and van Geel, B.** 2004 Radiocarbon dating of bulk peat samples from raised bogs: non-existence of a previously reported 'reservoir effect'?, *Quaternary Sci Rev*, 23, 1537-42
- Bridge, J., Collier, R. and Alexander, J.** 1998. Large-scale structure of structure of Calamas River deposits (Nebraska, USA) revealed using ground penetrating radar. *Sedimentology*, 45, 977 – 986.
- Bristow, C. S., Lancaster, N. and Duller, G. A. T.** 2005. Combining ground penetrating radar surveys and optical dating to determine dune migration in Namibia. *Journal of the Geological Society*, 162, pp. 315 – 321. London.
- Brock, J.** (eds.) *Research Problems in Zooarchaeology*. London: Institute of Archaeology, Occasional Publication 3. 25-38.
- Bronk Ramsey, C.** 1995 Radiocarbon calibration and analysis of stratigraphy, *Radiocarbon*, 36, 425-30
- Bronk Ramsey, C.** 1998 Probability and dating, *Radiocarbon*, 40, 461-74
- Bronk Ramsey, C.** 2001 Development of the radiocarbon calibration program, *Radiocarbon*, 43, 355-63
- Bronk Ramsey, C. Higham, T. and Leach, P.** 2004 Towards high precision AMS: progress and limitations, *Radiocarbon*, 46(1), 17-24
- Brophy, K. 1999. Seeing the cursus as a symbolic river, *British Archaeology*, 44.
- Brown, A.G., Carey, C., Challis, K., Howard, A. and Cooper, L.** 2005. *Predictive modelling of multi-period geoarchaeological resources at a river confluence*. Phase 1 Report for English Heritage. Universities of Exeter and Birmingham.
- Brown, A. G., Dinnin, M. and Toogood, T.** 2003 *Peat Wastage in the Somerset Levels A Study based on Field Evidence*. Report for Somerset County Council and the Environment Agency, 30p.
- Brown, A. G. and Salisbury, C. R.** in press. Geomorphology. In L. Cooper and S. Ripper (Eds.) *The Hemington Bridges Project*. English Heritage/ULAS, Leicester.
- Campbell, J.B.** 1977. *The Upper Palaeolithic of Britain: a Study of Man and Nature in the Late Ice Age*. 2 vols. Oxford. Clarendon Press.

Challis K.C. 2006. Airborne laser altimetry in alluviated landscapes. *Archaeological Prospection* 13: 103-127.

Challis, K., G. Priestnal, A. Gardener, J. Henderson & S. O'hara. 2004. Corona remotely sensed imagery in dryland archaeology: the Islamic City of al-Raqqqa, Syria. *Journal of Field Archaeology* 29, (1-2): 139-153.

Challis, K. & A.J. Howard, A.J. 2003. GIS-based modelling of sub-surface deposits for archaeological prospection in alluvial landscapes. In: Howard, A.J. and Passmore, D. (eds) *The Alluvial Archaeology of Europe*. Balkema, Rotterdam. 263-275.

Challis, K. 1995. *A564 Derby Southern Bypass Contract B. Rookery Lane: Archaeological assessment and evaluation*. Unpublished report, Nottingham University Consultants.

Clay 1985 A survey of two cropmark sites at Lockington-Hemington, Leicestershire, *Transactions of the Leicestershire Archaeological and Historical Society*, 59, pp. 17-26.

Clay, P. 1998. Neolithic/Early Bronze Age Pit Circles and their Environs at Burley Road, Oakham, Rutland. *Proceedings of the Prehistoric Society*, 64, pp. 293-330.

Clay, P. 2002. *The Prehistory of the East Midlands Claylands*, Leicester Archaeology Monographs No. 9. School of Archaeology and Ancient History, University of Leicester.

Clay, P. and Salisbury, C.R. 1990. A Norman mill dam and other sites at Hemington fields, Castle Donington, Leicestershire', *The Archaeological Journal*, 147, pp. 276-307.

Claerbout, J.F. and Muir, F. 1973. Robust modeling with erratic data. *Geophysics*, 38, 826-844.

Coope, G. R. & Osborne, P. J. (1968) Report on the Coleopterous fauna of a the Roman Well at Barnsley Park. *Transactions of the Bristol and Gloucestershire Archaeological Society* 86. 84-87

Cooper, L. 2001. The Glaston glutton and other strange beasts, *Rescue News*, 83, pp. 1-3.

Cooper, L. 2002a. 'A Creswellian campsite, Newtown Linford', *Transactions of the Leicestershire Archaeological and Historical Society*, 76, pp.

Cooper, L. 2002b. *The lithics in M. Beamish, Archaeology of the Wing to Whatborough Hill Trunk Main*, ULAS report 2002/099.

Cooper, L.P. 2003. Hemington Quarry, Castle Donington, Leicestershire, UK: a decade beneath the alluvium in the confluence zone, in A.J. Howard, M.G. Macklin and D.G. Passmore (eds), *Alluvial Archaeology in Europe*, A.A. Balkema, pp. 27-42.

- Cooper, L. and Jacobi, R.** 2001. Two Late Glacial finds from north-west Leicestershire, *Transactions of the Leicestershire Archaeological and Historical Society*, 75, pp. 118-121.
- Cooper, L., Ripper, S., & Clay, P.** 1994. The Hemington bridges, *Current Archaeology*, 140, pp. 316-21.
- Cooper, L. and Thomas, J.** 2001. Glaston, Grange Farm, *Transactions of the Leicestershire Archaeological and Historical Society*, 75, pp. 158-9.
- Cooper L. & Ripper, S.** 2000. Castle Donington, Hemington Quarry (SK 455 299), *Transactions of the Leicestershire Archaeological and Historical Society*, 74, pp. 233-5.
- Cooper L. & Ripper, S.** 2001. Castle Donington, Hemington Quarry (SK 455 299), *Transactions of the Leicestershire Archaeological and Historical Society*, 75, pp. 137-42.
- Cooper, L. and Ripper, S.** forthcoming a. *The Hemington Bridges*.
- Cooper, L. and Ripper, S.** forthcoming b. *Excavations at Hemington Quarry Western Extension*.
- Cooper, N.J.** (ed), 2006. *An Archaeological Resource Assessment and Research Agenda for the East Midlands*.
http://www.le.ac.uk/ar/east_midlands_research_framework.htm
- Courtney, P.** forthcoming. Hemington Bridge in its historical context, in L. Cooper & S. Ripper (eds) *The Hemington Bridges*.
- Coward, J. and Ripper, S.** 1999. *Castle Donington*. Willow Farm.
- Daniels F. and Albery R.A.** 1966. *Physical Chemistry*. John Wiley and Sons, Inc.
- Davis, R.** 1999. Bronze Age Metalwork from the Trent Valley, Newark, Notts, to Gainsborough, Lincs. *Transactions of the Thoroton Society*, 103, pp. 25-48.
- Deegan, A.** 1999. *The Nottinghamshire Mapping Project*, unpublished RCHME report.
- deGroot-Hedlin, C. and Constable, S.** 1990. Occam's inversion to generate smooth, two dimensional models from magnetotelluric data. *Geophysics*, 55, 1613-1624.
- Delcourt, P.A. and Delcourt, H.R.** 1980. Pollen preservation and quaternary environmental history in the south-eastern United States. *Palynology*, 4: 215-231.
- Dool, J.** 1985. 'Derby Racecourse; Excavations on the Roman industrial settlement, 1974', *Derbyshire Archaeological Journal*, 105, pp. 155-221.

Ekcs, C. and Friele, P. 2003. Sedimentary architecture and post-glacial evolution of Cheekye Fan, southwestern British Columbia, Canada, in, C. S. Bristow and H. M. Jol, *Ground Penetrating Radar in Sediments*, Geological Society Special Publications, pp. 87 - 98. London.

Elliott, L., and Knight, D. 1999. 'An Early Mesolithic and first millennium BC settlement and pit alignments at Swarkestone Lowes, Derbyshire', *Derbyshire Archaeological Journal*, 119, pp. 79-153.

Ellis, C. E. and Brown, A. G. 1999 Alluvial micro-fabrics, anisotropy of magnetic susceptibility and overbank processes. In A. G. Brown and T. A. Quine (Eds.), *Fluvial Processes and Environmental Change*. Wiley, Chichester, 181-206.

Elsdon, S.M. 1983. Iron Age and Roman sites at Red Hill, Ratcliffe on Soar, Nottinghamshire: excavations of E. Greenfield, 1963 and previous finds, *Transactions of the Thoroton Society*, 86, pp. 14-48.

Faegri, K. and Iversen, J. 1989. *Textbook of Pollen Analysis*. Chichester, John Wiley and Sons.

Fiedorczuk, J. and Schild, R. 2002. Wilczyce – a new late Magdalenian site in Poland in B.V. Eriksen and B. Bratlund (eds), *Recent Studies in the Final Palaeolithic of the European plain*, *Jutland Archaeological Society*, 91-100.

Field, D. 1999. *Bury the dead in a sacred landscape*. British Archaeology 43

Frere, S.S. and St. Joseph, J.K. 1983. *Roman Britain from the air*. Cambridge University Press.

Fyfe, R. M., Brown, A. G. and Coles, B. J. 2004 Vegetational change and human activity in the Exe Valley, Devon, UK. *Proceedings of the Prehistoric Society* 69, 161-182.

Garrod, D.A.E. 1926. *The Upper Palaeolithic Age in Britain*. Oxford. Clarendon Press.

Garton, D. 1993. 'A Late Upper Palaeolithic site near Newark, Nottinghamshire', *Transactions of the Thoroton Society*, 98, pp. 126-9.

Graf, A. 2002. Lower and Middle Palaeolithic Leicestershire and Rutland: progress and potential, *Transactions of the Leicestershire Archaeological and Historical Society*, 76, pp. 1-46.

Greenwood, M. T. Agnew, M. D. and Wood P. J. 2003. The use of caddisfly fauna (Insecta: Trichoptera) to characterise the Late-glacial River Trent, England. *Journal of Quaternary Science*, 18(7), pp. 645-661.

GSSI. 2004. *Radan 6.0 Users Manual*. New Hampshire, USA.

- Hall, A. R. & Kenward, H. K.** (1990) *Environmental Evidence from the Colonia*. The Archaeology of York. 14 (4). CBA.
- Hamilton, W. D., Marshall, P. D., Brown, T., Allen, P., Meadows, I. and Cook G.** forthcoming Radiocarbon dating, in *The Nene Valley Project*
- Hedges, R. E. M., Bronk, C. R. and Housley, R. A.** 1989 The Oxford Accelerator Mass Spectrometry facility: technical developments in routine dating, *Archaeometry*, 31, 99–113
- Heinz, J & T. Aiger.** 2003. Three dimensional GPR analysis of various Quaternary gravel-bed braided river deposits (southwestern Germany). In *Ground Penetrating Radar in Sediments*, Bristow CS, Jol HM (eds). Geological Society Special Publications: London. PP 99-110.
- Hey, G. & M. Lacey.** 2001. *Evaluation of archaeological decision making processes and sampling strategies*. Kent County Council: Oxford Archaeological Unit.
- Howard, A.J. & M.G. Macklin.** 1999. A generic geomorphological approach to archaeological interpretation in British river valleys: a guide for archaeologists investigating Holocene landscapes. *Antiquity* 73: 527-41.
- Hughes, G.** 2000. *The Lockington Gold hoard. An Earlier Bronze Age barrow cemetery at Lockington, Leicestershire*. Oxford: Oxbow Books.
- Hughes, G. and Roseff, R.** 1995. Excavations at Croft Quarry (SP 517 968), *Transactions of the Leicestershire Archaeological and Historical Society*, 69, pp. 100-108.
- Hughes, R.G.** 1999. Some unrecorded prehistoric tools from Derbyshire, *Derbyshire Archaeological Journal*, 119, pp. 5-11.
- Jacobi, R.M.** 1980 'The Upper Palaeolithic in Britain, with special reference to Wales', in J.A. Taylor (ed), *Culture and Environment in Prehistoric Wales*, BAR British Series 76, Oxford, pp. 15-99.
- Jacobi, R.M.** 1982. Later hunters in Kent: Tasmania and the earliest Neolithic, in P.E. Leach (ed), *Archaeology in Kent to AD 1500*. CBA Research Report No 48.
- Jacobi, R.** 1990 Leaf-points and the British Early Upper Palaeolithic in J.K. Kozłowski (ed) *Feuilles de Pierre: Les Industries à Pointes Foliacées du Paléolithique Supérieur Européen*. Études et Recherches Archéologiques de l'Université de Liège, 42, pp. 271-89.
- Jacobi, R.** 1991. The Creswellian, Creswell and Cheddar, in N. Barton, A.J. Roberts and D.A. Roe (eds), *The Late Glacial in north-west Europe: Human adaptation and environmental change at the end of the Pleistocene*. CBA Research Report 77.

- Jacobi, R.** 1997. 'The 'Creswellian' in Britain', in J.-P. Fagnart and A. Thévenin (eds), *Le Tardiglaciaire en Europe du Nord-Ouest*. Paris. Éditions du Comité des travaux historiques et scientifiques, pp. 497-505.
- Jacobi, R.M.** 1978a. Population and landscape in Mesolithic lowland Britain, in S. Limbrey and J.G. Evans (eds), *The Effect of Man on the Landscape*, CBA Research Report 21, pp. 77-85.
- Jacobi, R.M.** in press. The Late Upper Palaeolithic Lithic Collection from Gough's Cave, Cheddar, Somerset and Human Use of the Cave, *Proceedings of the Prehistoric Society*, 70, 1-92.
- Jacobi, R., Garton, D. and Brown, J.** 2001. Field-walking and the Late Upper Palaeolithic in Nottinghamshire, *Transactions of the Thoroton Society*, 105, pp. 17-22.
- Jol, H. M. and Bristow, C. S.** 2003. GPR in sediments: a guide to good practice, in, C. S. Bristow and H. M. Jol, *Ground Penetrating Radar in Sediments*, Geological Society Special Publications, pp. 9 - 27. London.
- Kenward, H. K.** (1974) Methods for palaeoentomology on site and in the laboratory. *Science and Archaeology* 13. 16-24
- Kenward, H. K.** (1975) Pitfalls in the environmental interpretation of insect death assemblages. *Journal of Archaeological Science* 2. 85-94.
- Kenward, H. K.** (1976) Reconstructing ancient ecological conditions from insect remains: some problems and an experimental approach. *Ecological Entomology* 1. 7-17
- Kenward, H. K.** (1978a) *The Analysis of Archaeological Insect Assemblages: a New Approach*. Archaeology of York, 19/1. Council for British Archaeology for York Archaeological Trust.
- Kenward, H. K.** (1978b) The value of insect remains as evidence of ecological conditions on archaeological sites. In Brothwell, D. R., Thomas, K. D., & Clutton-Brock, J. (eds.) *Research Problems in Zooarchaeology*. London: Institute of Archaeology, Occasional Publication 3. 25-38.
- Kenward, H. K.** (1982) Insect communities and death assemblages past and present in Hall, A. R. & Kenward, H. K. (eds.) *Environmental archaeology in the urban context*. CBA Research Report 43. 71-78
- Kenward, H. K. & Hall, A. R.** (1997) Enhancing bioarchaeological interpretation using indicator groups: stable manure as a paradigm. *Journal of Archaeological Science* 24. 663-673
- Kilian, M. R., van der Plicht, J. and van Geel, B.** 1995 Dating raised bogs: new aspects of AMS ¹⁴C wiggle matching, a reservoir effect and climatic change, *Quaternary Sci Rev*, 14, 959-66

Kilian, M. R., van der Plicht, J. and van Geel, B. 2000 ^{14}C wiggle matching of raised bog deposits and models of peat accumulation, *Quaternary Sci Rev*, 19, 1011–33

Knight, D., Marsden, P. and Carney, J. 2003. 'Local or non-local? Prehistoric granodiorite-tempered pottery in the East Midlands' in A. Gibson (ed) *Prehistoric Pottery. People, Pattern and Purpose*. Oxford: British Archaeological Reports International Series, 1156, pp. 111-125.

Knight, D., Malone, S., Howard, A.J. and Appleton, E. 1999. Chapel Farm, Shardlow, *Derbyshire, Archaeological Journal*, 119, pp. 286.

Knight, D. and Howard, A.J. 1994. 'The Trent Valley Survey', *Transactions of the Thoroton Society*, 99, pp. 126-9.

Knight, D. and Malone, S. 1997. Evaluation of a Late Iron Age and Romano-British Settlement and Palaeochannels of the Trent at Chapel Farm, Shardlow and Great Wilne, Derbyshire, *unpublished Trent and Peak Archaeological Trust Report* (Derbyshire SMR).

Knight, D. and Malone, S. 1998. Further evaluations of an Iron Age and Romano-British Settlement and Fluvial features at Chapel Farm, Shardlow and Great Wilne, Derbyshire, *unpublished Trent and Peak Archaeological Unit Report* (Derbyshire SMR).

Knox, R. 2005. An archaeological resource assessment of the Mesolithic in Leicestershire and Rutland, East Midlands Archaeological Research Framework, online paper. http://www.le.ac.uk/archaeology/pdf_files/08leicmeso.pdf

Leicestershire County Council. 1995. *Leicestershire Minerals Local Plan Review - Written Statement*.

Loke, M. H. 2000. Electrical imaging surveys for environmental and engineering studies. A practical guide to 2D and 3D surveys. Unpublished Guidebook available with Syscal Utilities.

Loveday, R. 2004. Contextualising monuments: the exceptional potential of the Middle Trent Valley, *Derbyshire Archaeological Journal*, 124, pp. 1-12.

Mangerud, J., Andersen, S.T., Berglund, B.E. and Dönnner, J.J. 1974. Quaternary stratigraphy of Norden, a proposal for terminology and classification, *Boreas*, 3, pp.109-127.

Margary, I. 1967. *Roman Roads in Britain*. London.

McNabb, J. forthcoming. 'An Archaeological Resource Assessment and Research Agenda for the Palaeolithic in the East Midlands (part of Western Doggerland)' in N. Cooper (ed.) forthcoming, *An Archaeological Resource Assessment and Research Agenda for the East Midlands*. http://www.le.ac.uk/archaeology/pdf_files/emidpal.pdf

McOmish, D. 2003. Cursus: solving a 6,000-year-old puzzle, *British Archaeology*, 69.

Meek, J. 1999. *Desk-based assessment of the proposed 'Fulcrum' site, Kegworth, Leicestershire*. Unpublished ULAS report 99/120.

Meek, J. 2000. *Archaeological desk-based assessment of Lockington barrow cemetery, Leicestershire*, Unpublished ULAS report 2000/162.

Moore, P.D., Webb, J.A. and Collinson, M.E. 1991. *Pollen Analysis*, (Second Edition). Oxford, Blackwell Science Publications.

Mook, W. G. 1986. Business meeting: Recommendations/Resolutions adopted by the Twelfth International Radiocarbon Conference, *Radiocarbon*, 28, 799

Myers, A.M. Forthcoming. An archaeological resource assessment and research agenda for the Mesolithic in the East Midlands, in N.J. Cooper (ed) forthcoming, *An Archaeological Resource Assessment and Research Agenda for the East Midlands*.http://www.le.ac.uk/archaeology/pdf_files/emidmeso.pdf

Optech. 2003. *ALTM 2033 Airborne Laser Terrain Mapper*. Optech, Toronto.

Palfreyman, A. and Ebbins, S. 2003. Redhill Iron Age and Romano-British site, Nottinghamshire: A new assessment, *Transactions of the Thoroton Society*, 107, pp. 17-40.

Passmore, D.G. C. Waddington & S.J. Houghton. 2002. Geoarchaeology of the Milfield Basin, Northern England; towards an integrated archaeological prospection, research and management framework. *Archaeological Prospection* 9: 71-91.

Passmore, D.G. C. Waddington & T. Van der Schriek. 2006. Enhancing the evaluation and management of river valley archaeology: geoarchaeology, in the Till-Tweed catchment, northern England. *Archaeological Prospection* 13: 269-81.

Pickering, J. and Hartley R.F. 1985. *Past Worlds in a Landscape, Leicestershire Museums, Art Galleries and Records Service Archaeological Reports Series 11*.

Posnansky, M. 1963. The Lower and Middle Palaeolithic industries of the English East Midlands, *Proceedings Prehistoric Society*, 29, pp. 357-94.

Prehistoric Society. 1999. *Research Frameworks for the Palaeolithic and Mesolithic of Britain and Ireland: A Report by the Working Party for the Palaeolithic and Mesolithic Day Meeting and the Council of the Prehistoric Society*. Prehistoric Society, Salisbury.

Reimer, P. J., Baillie, M. G. L., Bard, E., Bayliss, A., Beck, J. W., Bertrand, C. J. H., Blackwell, P. G., Buck, C. E., Burr, G. S., Cutler, K. B., Damon, P. E., Edwards, R. L., Fairbanks, R. G., Friedrich, M., Guilderson, T. P., Hogg, A. G., Hughen, K. A., Kromer, B., McCormac, G., Manning, S., Bronk Ramsey, C., Reimer, R. W., Remmele, S., Southon, J. R., Stuiver, M., Talamo, S., Taylor, F.

- W., van der Plicht, J. and Weyhenmeyer, C. E.** 2004 IntCal04 Terrestrial radiocarbon age calibration, 0–26 Cal Kyr BP, *Radiocarbon*, 46, 1029–58
- Riley, D.N.** 1987. *Air Photography and Archaeology*. London: Duckworth.
- Ripper, S.** 1997. *An archaeological evaluation of land west of Warren Farm, Lockington, Leicestershire (NGR SK477 296 and SK466 293)*. University of Leicester Archaeological Services.
- Ripper, S., and Butler, A.** 1999. Warren Farm, Lockington (SK 477 296 and SK 466 293), *Transactions of the Leicestershire Archaeological and Historical Society*, 73, pp. 101-4.
- Salisbury, C.R.** 1985. Taming the Trent. *East Midlands Archaeology*, 1, pp. 5-12.
- Salisbury, C.R.** 1991. Primitive British fish weirs, in G.L. Good, R.H. Jones, & M.W. Ponsford, (eds), *Waterfront Archaeology*, Proceedings of the Third International Conference 1988. CBA Research Report, 74, pp. 76-87. London: Council for British Archaeology.
- Salisbury, C.R.** 2004. *Bronze Age Lakes at Aston on Trent, Derbyshire*, page on Trent Valley GeoArchaeology website
http://www.nottingham.ac.uk/~aczkdc/TVG/aston_crs.html
- Salisbury, C.R., Whitley, P.J., Litton, C.D. and Fox, J.L.** 1984. Flandrian courses of the river Trent at Colwick, Nottinghamshire, *Mercian Geologist*, 9, pp. 189-207.
- Salisbury, C.R.** 1992. Archaeological evidence for palaeochannels in the Trent valley. In: Needham, S. and Macklin, M. 1992. *Alluvial Archaeology in Britain*. Oxbow Books, Oxford.
- Schwabedissen, S.H.** 1954 Die Federmesser-Gruppen des nordwesteuropäischen Flachlandes. *Zur Ausbreitung des Spät-Magdelénien*. Neumünster. Karl Wachholtz.
- Scott, E. M.** (ed), 2003 The Third International Radiocarbon Intercomparison (TIRI) and the Fourth International Radiocarbon Intercomparison (FIRI) 1990–2002: results, analysis, and conclusions, *Radiocarbon*, 45, 135–408
- Scurfield, C.J.** 1997. Bronze Age Metalwork from the River Trent in Nottinghamshire, *Transactions of the Thoroton Society*, 101, pp. 29-58.
- Shore, J. S., Bartley, D. D. and Harkness, D. D.** 1995 Problems encountered with the ¹⁴C dating of peat, *Quaternary Sci Rev*, 14, 373–83
- Smith, D. and Ripper, S.** 2000. *Building survey of Warren Farm farmhouse and farm buildings*. Unpublished ULAS report 2000/92.
- St Joseph, J.K., 1961. *Journal of Roman Studies*, XLI, pp. 133-4.
- St Joseph, J.K.** 1968. *Journal of Roman Studies*, XLVIII, pp. 128.

- Stringer, C., and Gamble, C.** 1993. *In search of the Neanderthals*. Thames & Hudson.
- Stringer, C.** 2002. The Ancient Human Occupation of Britain (AHOB) project. *Before Farming: the archaeology of Old World hunter-gatherers 2002/1*. Western Academic and Specialist Press. Online publication: <http://www.waspjournals.com/journal/news/occupation.php>
- Stockmarr, J.** 1971. Tablets with spores used in absolute pollen analysis. *Pollen et Spores*, 13: 615-621.
- Stuiver, M, and Kra, R S.** 1986. Editorial comment, *Radiocarbon*, 28(2B), ii
- Stuiver, M. and Polach, H. A.** 1977. Reporting of ¹⁴C data, *Radiocarbon*, 19, 355–63
- Stuiver, M. and Reimer, P. J.** 1986. A computer program for radiocarbon age calculation, *Radiocarbon*, 28, 1022–30
- Stuiver, M. and Reimer, P. J.** 1993 Extended ¹⁴C data base and revised CALIB 3.0 ¹⁴C age calibration program, *Radiocarbon*, 35, 215–30
- Taylor, J. 1997. Space and place: some thoughts on Iron Age and Romano-British landscapes, in A. Gwilt and C.C. Haselgrove (eds), *Reconstructing Iron Age Societies. New Approaches to the British Iron Age*, Oxbow Monograph 71, Oxbow: Oxford, pp.192-204.
- Takeshi, N. Brugiapaglia, E. Digerfeldt, G. Reille, M. De Beaulieu, JL. and Yasuda, Yoshinori.** 1998. Dense-media separation as a more efficient pollen extraction method for use with organic sediment/deposit samples: comparison with the conventional method. *Boreas* 27, 15-24.
- Thomas, J. and Jacobi, R.** 2001. Glaston, *Current Archaeology*, 173, pp.180-4.
- Tinsley, H.** 2004. *Monuments at Risk in Somerset Project (MARISP) Pollen Assessment*. Report for English Heritage.
- Van Dam, R. L., Van Den Berg, E. H., Schaap, M. G., Broekema, L. H. and Schlager, W.** 2003. Radar reflections from sedimentary structures in the vadose zone, in, C. S. Bristow and H. M. Jol, *Ground Penetrating Radar in Sediments*, Geological Society Special Publications, pp. 257 – 273. London.
- van der Plicht, J., Wijma, S., Aerts, A. T., Pertuisot, M. H. and Meijer, H. A. J.** 2000. Status report: the Groningen AMS facility, *Nuclear Instruments and Methods in Physics Research B*, 172, 58–65
- Vince, A.** forthcoming. An Archaeological Resource Assessment and Research Agenda for the Early and Middle Anglo-Saxon Period (c. 400-850) in the East Midlands, in N. Cooper, forthcoming

- Waddington, C. and Passmore, D.** 2006. *Planning for the future. Guidance for managing the archaeological and palaeoenvironmental resource in the Till-Tweed Valleys, Northumberland, UK.* Archaeological Research Services Ltd and English Heritage.
- Ward, G. K. & Wilson, S. R.** 1978 Procedures for comparing and combining radiocarbon age determinations: a critique, *Archaeometry*, 20, 19–31
- Watkin, J., Stead, I.M. and Palmer, S.** 1996. A decorated shield-boss from the River Trent, near Ratcliffeon-Soar, *The Antiquaries Journal*, 76, pp. 17-30.
- Wehr A & U. Lohr.** 1999. Airborne laser scanning – an introduction and overview. *Journal of Photogrammetry & Remote Sensing* 54: 68-82.
- Windell, D.** 1989. A Later Neolithic ‘Ritual Focus’ at West Cotton, Northamptonshire, in A. Gibson (ed), *Midlands Prehistory*, BAR (British Series), 204, pp. 85-94
- Wymer, J.** 1999. *The Lower Palaeolithic Occupation of Britain, Vols 1 and 2.* Salisbury: Wessex Archaeology and English Heritage.
- Wehr, A. and Lohr, U.** 1999. Airborne laser scanning – an introduction and overview. *ISPRS Journal of Photogrammetry & Remote Sensing*, 54, 68-82.
- Wilson, D.R.** (1982). *Air Photo Interpretation for Archaeologists.* London: Macmillan.
- Young, R.** 1988. Mixed lithic scatters and the Mesolithic-Neolithic transition in the north-east of England: a speculation, in I. Brooks and P. Philips (eds), *Breaking the Stony Silence: Papers from the Sheffield Lithics Conference.* Oxford: BAR (British Series), 213, pp. 161-86.